Links between the unfolded protein response and the DNA damage response in hypoxia

---



Tiffany See-ting Ma
St Cross College

Thesis submitted to the University of Oxford in accordance with the requirements for the degree of Doctor of Philosophy (DPhil)

Supervisor: Prof. Ester M. Hammond

University of Oxford
Department of Oncology
Michaelmas Term 2022

Abstract

Hypoxia is a common feature of solid tumours and is associated with poor patient prognosis, therapy resistance and metastasis. Severe hypoxia (<0.1% O_2) is one of the few physiologically relevant stresses that activates both the replication stress/DNA damage response (DDR) and the unfolded protein response (UPR). However, we carried out a systematic literature review using PRISMA guidelines and concluded that no previous mechanistic links were reported between the hypoxic DDR and UPR. We demonstrated for the first time that secondary structures called R-loops increase in hypoxia and contribute to hypoxia-induced replication stress. Interestingly, we found that the putative RNA/DNA helicase SETX, which resolves R-loops, is induced in hypoxic conditions and that this occurs in a UPR-dependent manner through the PERK/ATF4 axis. Upon depletion of SETX in hypoxia, R-loop levels increase, DNA damage accumulates and replication rates decrease. Therefore, these data establish SETX and R-loops as novel links between the UPR and DDR in hypoxia. These findings also led us to question both the mechanism and consequence of hypoxia-induced R-loops. Here, we show that hypoxia-induced R-loops regulate the nucleolar stress response. Specifically, R-loops accumulate on the rDNA in hypoxia and block rDNA transcription in hypoxic conditions. The nucleolar stress protein nucleolin translocates from the nucleolus to the nucleoplasm in hypoxia and this translocation is also dependent on R-loops. Furthermore, we determined that the accumulation of R-loops in hypoxia is dependent on reactive oxygen species (ROS) as ROS scavengers partially rescued rDNA transcription repression and nucleolin translocation. Together, these data led us to hypothesise that the hypoxic UPR, in an attempt to shut down protein synthesis, also downregulates the production of ribosomes, an energy-demanding process, through the ROS dependent accumulation of R-loops at the rDNA.

To my amazing parents

Acknowledgements

I have finally come to the most dreaded part of my DPhil where I have to write the acknowledgements – because this means that the four amazing years here are coming to an end. I will begrudgingly finish this thesis by thanking the incredible people who've made my Oxford experience nothing short of some of the most informative, phenomenal and iconic years of my life.

To Ester, the amazing ESFJ supervisor (now you'll never forget your Myers Briggs letters when I'm not in lab!) who can simultaneously make us laugh, align figures and learn yet another hilarious savage British phrase all in one sentence… Thank you for believing in me and always pushing me to strive for the best. I would not be the confident scientist I am today if you didn't teach me the important fundamentals of doing good research while giving me the encouragement and freedom to explore and develop my own ideas (#SecretExperiments). Thank you for helping me sharpen the invaluable skillsets of thinking critically for myself, questioning everything and asking great questions. I'll never forget the weekly meetings of intense science in your office where everything seemed to fall together on your whiteboard, relieving me of head-scratching from confusion/ trying to make sense of the data.

Thank you for always looking out for me even though you're a Stanford Tree and I'm an enemy Cal Bear who didn't know what a Christmas cracker was (see Hammond_Lab Twitter Christmas 2018 for evidence). I'll never forget how you were there for the whole lab when Anna gave us a scare, or when you offered to house me when I was potentially stranded in UK for the holidays. Thank you for making Teams calls work with the Hong Kong time zone during lockdown and making sure I didn't lose my mind during the 14-day hotel quarantine. I could write a whole thesis chapter/ appendix on the many hilarious conversations and 'Ester-isms' including cricket crash courses and rants about teenagers… but I'll leave those for the pub over our shared favourite beverage. All in all, thank you for being an incredible mentor and giving me countless opportunities to grow. You're the badass brilliant woman in science who encompasses passion for science, optimism, kindness, practicality, ambition and humour all in one. I couldn't have asked for a better DPhil supervisor or experience.

To the present members of the Hammond lab aka the loudest lab in the corridor, thank you for making research so much fun that it doesn't feel like work. Hannah(z), my maximum efficiency ENTJ Queen, you will always be my role model in science, you make it socially acceptable to have no inside-voice about our excitement for science. I'll never forget our drives to Nottingham, your incredible cooking/ tapas nights, and how you somehow know a bit about everything. Thanks for being one of my best friends here and I can't believe we screened 3000 papers together (never again…). Hala, I can't believe I got to sit next to the most popular person in the department who also happens to be brilliant and sweet – thank you for being a big sister to me, and for staying way past dinner time just to discuss abstract scientific models in the office together and calming spicy beans. Çağla, my fellow ENFJ, thank you for indulging in the Oxford/Hogwarts formal life with me with our countless Instagram photos and for your general Çağla-isms which we all love/ find entertaining #HighWycombe. Sophie, Ollie – you're unicorns who can do both chemistry/biology and 6 a.m. rowing/running so I envy you. Megan, Kat (乖/怪貓) and Conor (calm) – thanks for the constant reminder that I'm old, you disgusting millennium babies. Kat, I feel lucky that I get to work with a young, talented, passionate and empathetic scientist like you during my mini-postdoc year.

I would also like to thank past members of the Hammond lab who made my start in the lab incredibly enjoyable. Thank you Shaliny, for teaching me so much and being very patient with a starry-eyed first year. Anna, thanks for being my first friend in the department then almost dying on me (literally) and coming back to life, I still missing hearing your heels go click-clack in lab. Nat, you'll always be my *senpai*. Sam, thanks for teaching me qPCR and how not to limp in poker. Charlotte, everything is #SoChill. Many thanks to Kasia (WB queen), Ania (flips!), Joe, Ryan, Liz, Ming and Karen.

I would like to thank Val Macaulay for being one of my role models. Val, your kindness and scientific rigor are things I strive for. I would also like to thank Eric O'Neill for giving me extremely helpful career advice and for encouraging me to 'go for it'. Thank you to Ejung Moon and Andy Blackford for treating us to coffee/ a pint where we could talk about both science and life in general. Thank you to Natalia Gromak and Chiara Beghè for immense help on the DRIP protocol. Big thank you to Dr Monica Olcina and Prof Grant Stewart for an engaging and thought-provoking viva and that I thoroughly enjoyed.

I owe my thanks to many people in the Green Building and department: I've learned something from each of you and I'm grateful for your friendship. Thank you to Alice, Annamaria, Asmita, Bruno, Callum, David, Egon, Eliot, Florian, Ftoon, Gabrielle, Gwennie, Haonan, Hongbin, Hugo, Ignacio, Jack, James C., Jamie, Janine, Jen, John, Kay, Linda, Matt, May, Remko, Selena, Shahd, Shudong 哥, Sylvana, Tzveta, Wei, Xiaoning, YC, Yizhou and Yuri. Pauline, thanks for not crashing my car and for being the lit and savage Paris gal you are. Timo and Julia, thank you for being my adoptive German parents – I'll never forget dancing on rooftops with you two, Anjunadeep, the Museum Ball and the countless lunches at Richard Doll. Timo, thanks for showing me how to pipette with three hands. Anouk, thank you for living out the feminist dream of being a badass woman in radiation biology. SamJam, thank you for the late night science discussions and praying to the mini Buddha next to the qPCR machine with me as it runs. Ashwin, thanks (I think) for being an enabler since the first week of my DPhil – how many bops have we attended now? Was also super fun to organise student socials with you and less terrifying to dip into the biotech entrepreneurship world seeing you in the same competitions. Sophia, thank you for being the fun-loving and hilarious ball of sunshine you are. Bill 哥, thanks for teaching me bioinformatics where you could and I'll never forget when you bought all the beers off the undergrads at Uni Parks. Jonathan, you never cease to amaze me with how much you can juggle and I'm honoured to have been an extremely small part of Infinitopes – can't wait to see where this juggernaut goes.

Sovan, thank you for everything since day one. On top of being a fellow R-loop/transcription fanatic, I'm grateful for all the Bounty chocolate, jokes, Wagamama, kindness and generosity you and Lily have shown me the past 4 years. Pash, thank you for all the lovely conversations and always checking in on me as the first person in on Monday morning. Rhod, thank you for showing me (Jpeg) and Susan how to switch on the light in 780, the hilarious e-mail threads and saving us from microscopy-related disasters with your genius tricks and FIJI macros.

Cristiano, my CMO who's living life out as truly the Rickest Rick – thank you for always being there for me through the good and the bad, and going along with my crazy ideas even though you might not have felt like it. Thanks for being one of my BFFs here and I can't wait to see what intergalactic adventures we go on after the DPhil.

To my 56 Bartlemas gang, I couldn't have asked for better housemates. Eimear, you changed my life at Oxford and made it feel like home especially during the rough times in lockdown and

restrictions. You also showed me that law parties are just something else. Veit, thanks for enlightening us on Bayesian statistics, NIPS and intellectual podcasts. Ross and Jess, I'll always be your 'mom'.

To my friends back in Hong Kong and California, I'm incredibly grateful for your support especially during the first year in the UK when I was thousands of miles away from both homes. To my unwavering Peebles – Nat and Elizabeth – thank you for 16 years of friendship, visiting me in Oxford and cheering me on. Well done to us on that spontaneous Paris trip. To my CA>IL group, June and Jony Chan, thank you for being my family since 2009. To my Berkeley gang who visited, Shilin, Bonnie, Andrew, Sally – look at us struggling in organic chemistry in 2013 and now we're completing our PhDs/MDs around the world, we did it. Thank you to Val, Seth, Ashis, and the MFB group too.

To my best friend and soulmate, Susan Kilgas – thank you for making my years at Oxford unforgettable and undoubtedly some of the best in my life. From our TikTok stardom, 6 a.m. *Nature* papers, journal clubs over lockdown, Costa overdose, analysing IF images on Wine Wednesdays, 10-day marriage life to reciting pathways at BuzzGym, I've never met anyone else who loves science, dancing and life the same way you do. Thank you for inspiring me with your hard work, dedication to science, ambition and just zest for life in general. Even though we were inseparable, you've ditched me for Harvard (I'm still heartbroken), but it's okay because we'll do more UPR/ERAD experiments together once you start your own lab.

Jonny, thank you for your love, support and humour the past few years. Thank you for sitting through many biology presentations/ proofreading even though you're a yucky chemist, and for letting me win at Mario Kart every so often (though judging by your reaction, you didn't mean for it to happen). You've taught me a lot, everything from how to dance to Nicki Minaj, cricket rules, to how to open a bottle of wine using a shoe. You've made this DPhil incredibly fun and made me laugh whether it's a good or bad day. I'll never forget our days of being Bartlemas neighbours, when you would kindly cook for me after I've had a late night in lab. Or when you, as a 9 year Oxford veteran, showed me all the cool secret spots and short-cuts around the city. Thank you for being the most wonderful partner. I'll always be your most basic catalyst.

Finally, to my incredible family. Mom and Dad, you're both my inspiration and I can only hope to be half as cool and successful as you both. Mom, thank you for teaching me how to never hold back in life and to prioritise happiness. Dad, thank you for teaching me to think outside the box and to never give up, no matter how difficult something is. Thank you both for being the most loving, positive, inspiring and supportive parents to your 大頭妹. Oscar and Osborn, thank you for being the most supportive 細佬 s. Thank you to 爺爺, 嫲嫲 , Crystal and Auntie Susan for the unwavering love and encouragement.

Thank you all!

Table of contents

Abstract **1**

Acknowledgements **3**

Table of contents **6**

List of tables **10**

List of figures **12**

List of abbreviations **16**

Chapter 1 Introduction **24**

1.1 What is cancer? *24*
1.1.1 Hallmarks of Cancer 24
1.1.2 Tumour microenvironment 28

1.2 Hypoxia *32*
1.2.1 Defining hypoxia 32
1.2.2 Measuring hypoxia 33

1.3 Hypoxia and cancer *35*
1.3.1 Origins of tumour hypoxia 35
1.3.2 Types of tumour hypoxia (acute, chronic, cycling, mild, severe) 37
1.3.3 Tumour hypoxia and clinical importance 38
1.3.4 Hypoxia and radiotherapy resistance 40
1.3.5 Hypoxia and chemotherapy resistance 41

1.4 The biological response to hypoxia *44*
1.4.1 HIF 44
1.4.2 DNA damage response 47
1.4.3 DNA repair 54
1.4.4 Unfolded protein response 56
1.4.5 Reactive oxygen species (ROS) 60
1.4.6 Repression of global transcription 64

1.5 R-loops *66*
1.5.1 R-loops and their physiological functions 66
1.5.2 R-loops and genomic instability 69
1.5.3 R-loops in DNA repair and the DDR 71

1.6 Aims of this study *73*

Chapter 2 Methods and Materials **75**

2.1 Methods *75*
2.1.1 Cell culture 75

2.1.2 Cryopreservation of cell lines 75
2.1.3 Drug treatments 76
2.1.4 Short interfering RNA (siRNA) transfection 76
2.1.5 Bacterial transformation 77
2.1.6 Plasmid purification 78
2.1.7 DNA plasmid transfection 78
2.1.8 Hypoxia treatment 79
2.1.9 Cell lysis and protein sample preparation 79
2.1.10 Western blotting 79
2.1.11 Puromycin incorporation assay 80
2.1.12 Immunofluorescence microscopy 80
2.1.13 RNA extraction and purification 81
2.1.14 Complementary DNA (cDNA) synthesis through reverse transcription 82
2.1.15 Quantitative PCR (qPCR) 82
2.1.16 Click-iT nucleotide incorporation assay for EU and EdU 83
2.1.17 CellRox/MitoSox assay for measuring reactive oxygen species levels (ROS) 83
2.1.18 Fluorescence-activated cell sorting (FACS) using BrdU and PI 84
2.1.19 Clonogenic survival assay 85
2.1.20 R-loop detection by RNaseH1^{D210N} 85
2.1.21 DNA/RNA immunoprecipitation (DRIP) 86
2.1.22 DNA purification 87

2.2 Image analysis 88
2.2.1 Foci quantification 88
2.2.2 Nuclear intensity 88

2.3 Bioinformatics 88
2.3.1 Overlapping genes 88
2.3.2 Gene set enrichment analysis (GSEA) of hypoxia-induced UPR genes 89

2.4 Statistical analysis 89

2.5 Materials 90

Chapter 3 Links between the unfolded protein response and the DNA damage response in hypoxia 96

3.1 Introduction 96

3.2 Results 98
3.2.1 Pharmacological induction of replication stress does not induce the UPR 98
3.2.2 Pharmacological induction of the UPR does not induce replication stress 100
3.2.3 Induction of the UPR reduces Hu-induced DDR signalling 101
3.2.4 Protein translation is decreased in response to a Thaps-induced UPR 106
3.2.5 Thaps and Tuni-induced UPR reduces percentage of S phase cells 108
3.2.6 Systematic literature review using PRISMA guidelines: Search 110
3.2.7 Systematic literature review using PRISMA guidelines: Screen 112
3.2.8 Systematic literature review using PRISMA guidelines: Synthesis 115

3.3 Discussion 118

Chapter 4 Hypoxia-induced SETX links replication stress with the unfolded protein response 121

4.1 Introduction 121

4.2 Results 122
4.2.1 Collating available datasets 122
4.2.2 Identifying hypoxia-induced UPR genes 124
4.2.3 Hypoxia-induced UPR genes that play a role in the response to DNA damage 126
4.2.4 Hypoxia-induced UPR genes that regulate DNA synthesis 128
4.2.5 Hypoxia-induced UPR genes that are enriched on chromatin and/or stalled replication forks 130
4.2.6 Hypoxia-induced UPR genes that interact with RNA/DNA hybrids 131
4.2.7 SETX: a hypoxia-induced UPR gene that plays a role in multiple processes associated with replication stress 133
4.2.8 Exposure to hypoxia (<0.1% O_2) induces a DDR and UPR 135
4.2.9 The hypoxia induced DDR and UPR is oxygen dependent 136
4.2.10 The hypoxia-induced DDR is due to an accumulation of replication stress and not DNA damage 138
4.2.11 Hypoxia (<0.1% O_2) leads to an accumulation of R-loops 141
4.2.12 Hypoxia (<0.1% O_2) induced R-loops contribute to replication stress and DDR signalling 143
4.2.13 Hypoxia (<0.1% O_2) induces SETX in an oxygen dependent manner 144
4.2.14 SETX reduces R-loops and protects cells from DNA damage and cell death in hypoxia 145
4.2.15 SETX is induced through the UPR PERK/ATF4 arm in hypoxia (<0.1% O_2) 148
4.2.16 PERK inhibition in hypoxia leads to further increase in R-loops and the accumulation of DNA damage 151
4.2.17 UPR inhibition in hypoxia exacerbates replication stress 155
4.2.18 UPR inhibition in hypoxia further increases R-loops 158
4.2.19 Hypoxia-induced SETX links replication stress with the UPR 159

4.3 Discussion 161

Chapter 5 Hypoxia-induced R-loops and oxidative stress 163

5.1 Introduction 163

5.2 Results 164
5.2.1 UPR inducers Tuni and Thaps lead to an accumulation of R-loops 164
5.2.2 Hypoxia induces R-loops in an oxygen dependent manner 165
5.2.3 Hypoxia, Thaps and Tuni lead to repression of global transcription 166
5.2.4 ROS can lead to R-loops through DNA damage 169
5.2.5 Hypoxia leads to the accumulation of ROS in an oxygen dependent manner in the absence of DNA damage 171
5.2.6 Thaps and Tuni lead to an accumulation of ROS 174
5.2.7 Hypoxia-induced R-loops are ROS dependent 176
5.2.8 UPR induced R-loops are ROS dependent 177
5.2.9 Hypoxia-induced R-loops form on the rDNA 178
5.2.10 Hypoxia-induced R-loops block rDNA transcription 181

5.2.11 rDNA transcription repression in hypoxia is partially dependent on ROS..... 183
5.2.12 Hypoxia (<0.1% O_2) induces translocation of nucleolin in an oxygen dependent manner..... 185
5.2.13 Hypoxia-induced translocation of nucleolin is R-loops dependent..... 187
5.2.14 Hypoxia-induced translocation of nucleolin is ROS dependent..... 190

5.3 Discussion..... 191

Chapter 6 Final discussion 195

Chapter 7 References 202

Chapter 8 Appendix..... 247

8.1 FIJI scripts used for image analyses..... 247

8.2 Supplementary data..... 251

8.3 Presentations 259

8.4 Published papers from this thesis..... 260

List of tables

Table 1.1 Typical oxygen concentrations found in tumours and their respective healthy tissues 39

Table 2.1 Cell lines used in this study..... 90

Table 2.2 Chemicals and cell culture reagents..... 91

Table 2.3 Drugs used in this study 92

Table 2.4 Primary antibodies 93

Table 2.5 Secondary antibodies 94

Table 2.6 Primers for RT-qPCR 94

Table 2.7 Primers for DRIP-qPCR..... 95

Table 2.8 siRNA sequences 95

Table 2.9 Plasmids..... 95

Table 2.10 Components used to make up the reaction mix for reverse transcription 82

Table 2.11 Components used to make up the reaction mix for qPCR 95

Table 2.12 Cell lines and their plating efficiencies..... 95

Table 3.1 Search strategy for systematic literature review 111

Table 3.2 Coverage for truncations of search terms..... 112

Table 3.3 Eligibility criteria used to evaluate papers for inclusion or exclusion for review . 113

Table 3.4 Genes identified as potential links between the UPR and DDR in hypoxia 116

Table 4.1 Description of the data sets used in this study..... 123

Table 4.2 Description of the 5 genes from Figure 3.3 and the effects of their knockdown on BrdU incorporation. 130

Table 4.3 78 hypoxia-induced UPR genes that play a role in the response to DNA damage: replication stress associated processes. 133

Table S4.1 1113 hypoxia-induced UPR genes 251

Table S4.2 103 hypoxia-induced UPR genes that play a role in the response to DNA damage 255

Table S4.3 97 hypoxia-induced UPR genes whose proteins are enriched on chromatin, Hu-stalled replication forks or both 255

Table S4.4 79 hypoxia-induced UPR genes that are part of the RNA/DNA hybrid interactome 258

List of figures

Figure 1.1. Hallmarks of cancer, new dimensions. 26

Figure 1.2. Gradient of varying oxygen concentrations in the solid tumour. 36

Figure 1.3. HIF regulation under normoxic and hypoxic conditions. 46

Figure 1.4 Sources of replication stress. 49

Figure 1.5 The canonical DNA damage response. 51

Figure 1.6 Effects of hypoxia on the DNA repair pathways. 55

Figure 1.7 The unfolded protein response. 59

Figure 1.8 ROS inducers and scavengers, and cellular consequences of ROS. 63

Figure 1.9. R-loops form from transcription. 67

Figure 3.1. Hypoxia leads to the concurrent induction the UPR and DDR. 98

Figure 3.2. Pharmacological induction of replication stress does not a lead to a UPR. 99

Figure 3.3. Thaps and Tuni do not lead to replication stress. 101

Figure 3.4. Hu-induced phosphorylation of DDR proteins are reduced by concomitant Thaps treatment. 102

Figure 3.5. Hu-induced RPA foci are rescued by Thaps treatment. 103

Figure 3.6. Hu-induced phosphorylation of RPA and p53 are rescued by Thaps and Tuni treatment. 104

Figure 3.7. Hu-induced phosphorylation of RPA and p53 are PERK and IRE1α dependent. 105

Figure 3.8. Treatment with Thaps leads to decreased protein synthesis. 107

Figure 3.9. Treatment with Thaps leads to changes in the expression of CHK1 and p53. ... 108

Figure 3.10. Cell cycle profile of Thaps and Tuni treated cells. 109

Figure 3.11. Boolean strategy used for searching relevant papers. 111

Figure 3.12. PRISMA flow diagram of the systematic literature exclusion process. 114

Figure 4.1. Identifying and characterising the genes induced by the UPR in hypoxia (<0.1% O_2). 125

Figure 4.2. 103 UPR-induced genes in hypoxia (<0.1% O_2) play a role in the response to DNA damage. 127

Figure 4.3. 5 UPR-induced genes in hypoxia (<0.1% O_2) play a role in DNA synthesis. 129

Figure 4.4. 97 UPR-induced genes in hypoxia (<0.1% O_2) are enriched on chromatin and/or Hu-stalled replication forks. 131

Figure 4.5. 79 UPR-induced genes in hypoxia (<0.1% O_2) interact with R-loops. 132

Figure 4.6. Hypoxia (<0.1% O_2) leads to a concurrent DDR and UPR. 136

Figure 4.7. The hypoxia-induced UPR and DDR is oxygen dependent. 137

Figure 4.8. Hypoxia leads to replication stress but not DSBs. 138

Figure 4.9. Hypoxia leads to replication stress but not DSBs. 139

Figure 4.10. Hypoxia-induced replication stress is characterised by pan-nuclear γ-H2AX and RPA foci in the same cell. 141

Figure 4.11. R-loops accumulate in hypoxia (<0.1% O_2) 142

Figure 4.12. RNase H1 overexpression abrogates hypoxia-induced replication stress and DDR signalling. 144

Figure 4.13. SETX is induced in hypoxia (<0.1% O_2). 145

Figure 4.14. SETX reduces R-loops and protects from DNA damage and cell death in hypoxia. 147

Figure 4.15. SETX is induced through the PERK/ATF4 arm of the UPR. 150

Figure 4.16. PERK depletion or inhibition leads to a further accumulation of R-loops in hypoxia. 153

Figure 4.17. Inhibition of PERK in hypoxia leads to the accumulation of DNA damage..... 154

Figure 4.18. Inhibition of the UPR in hypoxia does not change the percentage of cells in S-phase..... 156

Figure 4.19. UPR inhibitors in hypoxia increase the average number of RPA foci per cell. . 158

Figure 4.20. UPR inhibition in hypoxia leads to a further increase in R-loops. 159

Figure 4.21. Hypoxia links the UPR with replication stress. 160

Figure 5.1. Conditions that induce the UPR lead to R-loop accumulation. 164

Figure 5.2. Hypoxia leads to the accumulation of R-loops in an oxygen dependent manner. 165

Figure 5.3. Hypoxia, Tuni and Thaps lead to global transcription repression. 167

Figure 5.4. Hypoxia leads to transcription repression in an oxygen dependent manner. ... 168

Figure 5.5. ROS leads to R-loops and DNA damage. 170

Figure 5.6. Hypoxia induces ROS in an oxygen dependent manner..... 172

Figure 5.7. Hypoxia does not lead to an increase in 8-oxoguanine..... 173

Figure 5.8. Thaps and Tuni lead to an increase in ROS. 174

Figure 5.9. Hypoxia-induced R-loops are ROS dependent. 177

Figure 5.10. UPR-induced R-loops are ROS dependent..... 178

Figure 5.11. Hypoxia-induced R-loops form in the nucleoli. 179

Figure 5.12. Hypoxia-induced R-loops form on the rDNA. 180

Figure 5.13. Hypoxia-induced R-loops block rDNA transcription. 182

Figure 5.14. Hypoxia-induced R-loops block global transcription. 183

Figure 5.15. Transcription repression in hypoxia is partially dependent on ROS..... 184

Figure 5.16. Nucleolin translocates in hypoxia in an oxygen dependent manner. 187

Figure 5.17. Nucleolin translocation in hypoxia is R-loop dependent..... 189

Figure 5.18. Nucleolin translocation in hypoxia is ROS dependent. 190

Figure 5.19. Hypoxia-induced ROS leads to the accumulation of R-loops in the absence of DNA damage. 194

Figure 6.1 Working model of how the UPR and DDR interact in hypoxia. 200

Figure S2.1 The script used in FIJI/ImageJ to quantify foci. 247

Figure S2.2. The algorithm used in FIJI/ImageJ to quantify nuclear intensity. 250

List of abbreviations

5'EU	5-ethynyluridine
8-oxoG	8-oxoguanine
18S	18S ribosomal RNA
47S	precursor rRNA
53BP1	p53 binding protein 1
% O_2	percentage of oxygen
°C	degree Celsius
ΔΔCt	delta delta Ct
γ-H2AX	phosphorylation of the serine-139 residue of H2AX histone family member X
AKT	protein kinase B
APE1	Apurinic/Apyrimidinic Endodeoxyribonuclease 1
APH	aphidicolin
APOBEC	Apolipoprotein B mRNA Editing Catalytic Polypeptide-like
AQR	Aquarius Intron-Binding Spliceosomal Factor
ARNT	Aryl hydrocarbon Receptor Nuclear Translocator
ATCC	American Type Culture Collection
ATF4	Activating Transcription Factor 4
ATF6	Activating Transcription Factor 6
ATF6i	ATF6 inhibitor
ATG12	Autophagy Related 12
atm	standard atmosphere
ATM	Ataxia Telangiectasia Mutated
ATMIN	ATM Interactor
ATR	Ataxia Telangiectasia mutated and Rad3-related protein
ATRIP	ATR-Interacting Protein
BCL-2	B-cell lymphoma 2
BCL-XL	B-cell lymphoma -extra large
BECN1	Beclin-1
BER	base excision repair
BRCA	BReast CAncer gene

BRCA1	Breast Cancer gene 1
BRCA2	Breast Cancer gene 2
BrdU	bromo-2'-deoxyuridine
CA-9	Carbonic Anhydrase 9
CAFs	cancer-associated fibroblasts
CBP	CREB-binding protein
C-D	co-directional
cDNA	complementary DNA
ChIP	chromatin immunoprecipitation
CHK1	Checkpoint Kinase 1
CHK1-S345	phosphorylation of CHK1 at serine 345
CHK2	Checkpoint Kinase 2
CHOP	C/EBP-Homologous Protein
CHX	cycloheximide
CPT	camptothecin
CO_2	carbon dioxide
COPD	chronic obstructive pulmonary disease
CSB	Cockayne syndrome group B
CSR	class switch recombination
Cu-ATSM	copper-complexed dithiosemicarbazone
DAPI	4',6-diamidino-2-phenylinodole
dC	deoxycytidine
DEPC water	Diethyl pyrocarbonate water
DDR	DNA damage response
DDX19	DEAD-Box Helicase 19B
DHX9	DExH-Box Helicase 9
DMEM	Dulbecco's modified Eagle's medium
DMSO	dimethylsulphoxide
DNA	deoxyribonucleic acid
DNA-PK	DNA-dependent protein kinase
DNA-PKcs	DNA-dependent protein kinase catalytic subunit
dNTP	deoxyribonucleotide

Dr1/DrAP1	negative factor 2
DRB	5,6-Dichlorobenzimidazole 1-β-D-ribofuranoside
DRIP	DNA/RNA immunoprecipitation
DSBs	double-strand breaks
dsDNA	double-stranded DNA
dU	deoxyuridine
E2F	E2 factor
ECM	extracellular matrix
EdU	5-ethynyl-2'-deoxyuridine
eIF2α	eukaryotic initiation factor 2 alpha
EMT	epithelial-mesenchymal transition
EPO	erythropoietin
ER	endoplasmic reticulum
ERAD	ER-associated degradation
ERCC1	Excision Repair Cross-Complementation Group 1
ERO-1α	endoplasmic reticulum oxidoredudctin-1 alpha
ETC	electron transport chain
ETP	etoposide
FACS	fluorescence-activated cell sorting
FANCD2	Fanconi anemia complementation group D2
FBS	foetal bovine serum
FDA	Food and Drug Administration
FIH	factor-inhibiting HIF
G_1 phase	growth 1 phase
G_2 phase	growth 2 phase
GADD45A	Growth Arrest and DNA Damage Inducible alpha
GLUT-1	Glucose Transporter Type 1
GRP78	Glucose Regulated Protein 78
h	hour(s)
H2AX	H2A histone family member X
H_2O_2	hydrogen peroxide
H3K9me3	trimethylation of the 9^{th} lysine residue on histone H3 protein

Hu	hydroxyurea
HCl	hydrochloric acid
HIF	Hypoxia-Inducible Factor
HIF-1	Hypoxia-Inducible Factor-1
HIF-2	Hypoxia-Inducible Factor-2
HIF-1α	Hypoxia-Inducible Factor-1 alpha
HIF-1β	Hypoxia-Inducible Factor-1 beta
HIF-2α	Hypoxia-Inducible factor-2 alpha
HIF-3α	Hypoxia-Inducible Factor-3 alpha
HO	head-on
HR	homologous recombination
HRE	Hypoxia Responsive Elements
IF	immunofluorescence
IGS	intergenic spacer
IP	immunoprecipitation
IRE1α	inositol-requiring enzyme 1 alpha
IRE1αi	IRE1α inhibitor
JNK	JUN N-terminal kinase
KAP1	KRAB-associated protein 1
kb	kilobase
KEAP1	Kelch Like ECH Associated Protein 1
kPa	kilopascal
LIG4	DNA Ligase IV
lncRNA	long non-coding RNA
MAPK	Mitogen-Activated Protein kinase
MDSC	myeloid derived stromal cell
MEM	Minimum Essential Media
miRNA	microRNA
MLH1	MutL protein homolog 1
mmHG	millimetre of mercury
MMR	mismatch repair
MRE11	Meiotic Recombination 11 Homolog 1

MRN	MRE11-RAD50-NBS1
MRP1	Multidrug Resistance-Associated Protein 1
mRNA	messenger RNA
MSH2	MutS homolog 2
MSH6	MutShomolog 6
MTH1	MutT Human Homolog 1
mTORC1	mammalian target of rapamycin complex 1
MYH1	myosin heavy chain 1
NaCl	Sodium chloride
NAC	*N*-acetylcysteine
NADPH	nicotinamide adenine dinucleotide phosphate
NBS1	nibrin
NCS	neocarzinostatin
NEIL2	Nei Like DNA Glycosylase 2
NER	nucleotide excision repair
NF-κB	nuclear factor-κB
NFY	nuclear factor-Y
NHEJ	non-homologous end-joining
NMP1	nucleophosmin
NORs	nucleolar organiser regions
NOX4	NADPH oxidase subunit 4
NRF2	Nuclear Factor Erythroid 2-Related Factor 2
OER	oxygen enhancement ratio
OGG1	8-oxogoaunine DNA glycosylase
P/S	penicillin-streptomycin
p300	histone acetyltransferase p300
p53	tumour protein p53
PARP1	poly(ADP-ribose) polymerase 1
PBS	phosphate buffer saline (PBS)
PCR	polymerase chain reaction
PDIs	protein disulfide isomerases
PERK	protein kinase RNA-like endoplasmic reticulum kinase

PERKi	PERK inhibitor
PET	positron emission tomography
PFA	paraformaldehyde
PHD	Prolyl-Hydroxylase Domain protein
Pi	protease inhibitor
PI	propidium iodide
PI3K	phosphatidylinositol-3 kinase
PIF1	Petite Integration Frequency 1
PIKK	phosphatidylinositol-3 kinase-like kinase
Pol ι	DNA polymerase iota
PQ	MitoPQ
PRISMA	Preferred Reporting Items for Systematic Reviews and Meta-Analyses
qPCR	quantitative polymerase chain reaction
RAD50	RAD50 Double Strand Break Repair Protein
RAD51	DNA repair protein RAD51 homolog 1
RAD52	RAD52 homolog
rDNA	ribosomal DNA
REDD1	Regulated in Development and DNA damage responses 1
REST	Repressor Element 1-Silencing Transcription factor
RIDD	IRE1-dependent decay
RNA	ribonucleic acid
RNA Pol I	RNA polymerase I
RNA Pol II	RNA polymerase II
RNase A	ribonuclease A
RNase H	ribonuclease H
RNaseH1	ribonuclease H1
$RNaseH1^{WT}$	wildtype RNaseH1
$RNaseH1^{D210N}$	RNaseH1 D210N mutant
$RNaseH1^{WKKD}$	RNaseH1 WKKD mutant
RNR	ribonucleotide reductase
ROS	reactive oxygen species
RPA	Replication Protein A

RPA-S33	phosphorylation of RPA at serine 33
rRNA	ribosomal RNA
RT	room temperature
RTE1	Repressor of Telomerase Expression 1
S phase	synthesis phase
SDS	sodium dodecyl sulphate
SERCA	sarco/endoplasmic reticulum Ca^{2+}-ATPase
SETX	senataxin
siRNA	small interfering RNA
SOD	superoxide dismutase
SSBs	single-strand breaks
ssDNA	single-stranded DNA
TAHHR	transcription-associated HR repair
TAM	tumour-associated macrophage
TARID	TCF21 Antisense RNA Inducing Promoter Demethylation
*t*BHP	*tert*-Butyl hydroperoxide
TBP	TATA-binding protein
TBS	Tris-Buffered Saline
TCF21	transcription factor 21
TC-NER	transcription-coupled nucleotide excision repair
TE	Tris-EDTA
Tempo	MitoTempo
TH-302	evofosfamide
Thaps	thapsigargin
TLS	translesion synthesis
TME	tumour microenvironment
TOP1	topoisomerase I
TopBP1	DNA topoisomerase II binding protein 1
TPZ	tirapazamine
TRCs	transcription-replication collisions
Treg	T-regulatory cells
Tuni	tunicamycin

UBF	Upstream Binding Factor
UPR	unfolded protein response
UTB	urea Tris buffer
UV	ultraviolet
VEGF	Vascular Endothelial Growth Factor A
VHL	von-Hippel-Lindau
VitC	vitamin C
WB	western blot
WEE1	WEE1 G2 Checkpoint Kinase
WHO	World Health Organisation
x *g*	times gravity
XRCC4	X-ray repair cross-complementing protein 4
XBP1	X-Box Binding Protein 1
XBP1u	unspliced X-Box Binding Protein 1
XBP1s	spliced X-Box Binding Protein 1
XPA	Xeroderma Pigmentosum Group A-Complementing Protein
XPB	Xeroderma Pigmentosum type B
XPD	Xeroderma Pigmentosum Group D-Complementing Protein
XPG	Xeroderma Pigmentosum Complementation Group G
XRN2	5’-3’ Exoribonuclease 2
YY1	Ying Yang 1

Chapter 1 Introduction

1.1 What is cancer?

1.1.1 Hallmarks of Cancer

Cancer is a group of more than 200 diseases that share the characteristics of uncontrolled cell proliferation, tissue invasion and potential spread through metastasis. According to the World Health Organisation (WHO), cancer is the second leading cause of death after cardiovascular diseases, having claimed approximately 10 million annual deaths worldwide or one in six deaths in 2020. Cancer can occur in almost any place in the human body, and is also widespread in the animal kingdom, affecting fish, birds, molluscs, reptiles and other mammals (Albuquerque *et al.*, 2018).

The earliest known documentation of cancer dates back to approximately 3000 BC in ancient Egypt as part of a trauma surgery textbook, where its author noted that 'there is no treatment' when describing cases of breast tumours (Kardinal & Yarbro, 1979). Greek physician Hippocrates described the finger-like projections from some cancers as crab-like, after which Roman physician Celsus translated the Greek terms into *cancer*, the Latin word for crab (Skuse, 2015). Another Greek physician, Galen, used the Greek word *oncos* meaning swelling to describe tumours, which led to the use of the word 'oncology' to describe the study of tumours (American Cancer Society).

Over the years, many theories formed with regards to what causes cancer. The humoral theory by Hippocrates proposed that the imbalance between the four different body fluids (humors) blood, phlegm, yellow bile and black bile, specifically an excess of black bile, caused

cancer; this hypothesis was passed on and unchallenged for 1,300 years (Weinstein & Case, 2008). Starting from the 17th century, other theories such as the lymph, blastema, chronic irritation, trauma and infectious disease theories emerged in an attempt to explain the cause of cancer (Blackadar, 2016). In 1858, Rudolf Virchow correctly hypothesised that cancer cells originate from the body's own cells (Hanselmann & Welter, 2016).

In the 20th century, researchers started making significant progress in cancer research, identifying the role of carcinogens in tumourigenesis, as well as developing chemo-, immuno- and radiation therapy (Sudhakar, 2009). Pivotal studies by Brookes and Lawley in the 1960s suggested that damage to DNA is the basic cause of cancer, turning the scientific community's attention to links between DNA damage and tumourigenesis (Institute of Cancer Research; Lawley and Brookes, 1965). In the 1970s, notable discoveries included identification of two classes of genes, oncogenes and tumour suppressor genes, which promote and prevent tumourigenesis, respectively (Sudhakar, 2009). Discoveries of mutations that produce gain of function oncogenes or loss of function tumour suppressor genes followed suit, laying the foundation of our current understanding of cancer biology, where we view cancer as a predominantly genetic disease.

In 2000, Hanahan and Weinberg published a seminal paper 'The Hallmarks of Cancer', describing the six alterations that, if acquired by normal cells, would allow transformation into cancer cells (Hanahan & Weinberg, 2000). The authors claim that the six hallmarks are shared by most if not all human cancer types and act as a conceptual scaffold for researchers to understand the multi-step and complex process of tumourigenesis, as well as the diverse range of phenotypes across tumour types. The paper has been cited 38,000 times and the

authors published an updated version 'Hallmarks of Cancer: The Next Generation' in 2011 where 'enabling characteristics' were added to hallmarks (Hanahan & Weinberg, 2011). More recently, Hanahan also published 'Hallmarks of Cancer: New Dimensions' (Hanahan, 2022). In Hanahan and Weinberg's model, hallmarks are functional capabilities whereas enabling characteristics are involved in activating hallmarks. The latest hallmarks and enabling characteristics as of 2022, synthesising new findings from the expanding cancer research literature, are shown in **Figure 1.1**.

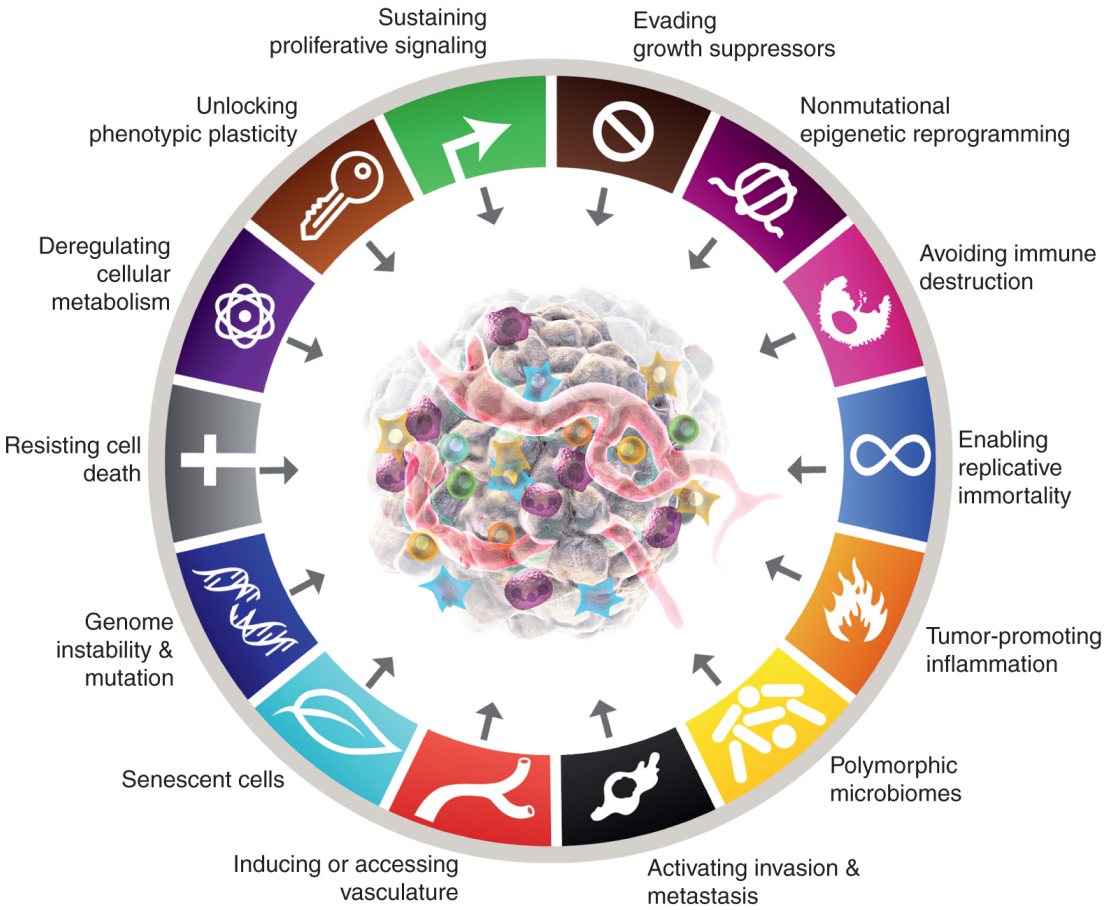


Figure 1.1. Hallmarks of cancer, new dimensions. Shown here are all hallmarks of cancer, except for 'genomic instability & mutation' and 'tumour-promoting inflammation' which were enabling characteristics added in 2011, and 'unlocking phenotypic plasticity' and 'senescent cells' which are new enabling characteristics added in 2022. 'Non-mutational epigenetic reprogramming' and 'polymorphic microbiomes' are two emerging hallmarks added in 2022. The rest are core hallmarks. Adapted and reprinted from Cancer Discovery, vol 12, issue 3, 12 January 2022, Hanahan, D. and Weinberg, R.A., Hallmarks of Cancer: New Dimensions, 31-46.

Copyright (2022) with permission from American Association for Cancer Research. License Number: 5338311426637

The authors noted that the most fundamental hallmark of cancer cells is arguably the ability to sustain chronic proliferation (Hanahan & Weinberg, 2011). This is consistent with how cancer typically causes death in patients: usually through organ failure, or through metastasis, both of which are propelled by tumour growth. For example, in brain cancer, patient death can be caused directly by tumour growth, resulting in brain herniation due to increasing pressure and lack of room for the brain, which is also termed the 'mass effect' (Silbergeld *et al.*, 1991). It has been shown that there is a positive correlation between tumour size and metastasis in a cohort of stage IV non-small cell lung cancer; patients with a tumour size of 3-7 cm or larger were more likely to develop brain and lung metastases than those with a tumour size of 3 cm or smaller (Shan *et al.*, 2019). A similar relationship has been observed in breast cancer patients (Liu *et al.*, 2021).

However, Hanahan marked that, hallmarks alone are not enough to address the complexities of cancer pathogenesis (Hanahan, 2022). The concept of enabling characteristics is needed to further explain how these hallmarks are established in the first place. Enabling characteristics result from neoplastic transformations and shed light on the molecular and cellular mechanisms that allow cancer cells and tumours to further adopt functional hallmark traits. Importantly, Hanahan and Weinberg state that 'genomic instability and mutation' is arguably the most prominent enabling characteristic (Hanahan & Weinberg, 2011). Genomic instability allows for mutations to accumulate and for the favourable mutations to be selected in a subpopulation of cells; these cells would go on to confer a survival advantage, proliferate and sustain tumourigenesis (Alexandrov *et al.*, 2013). Genomic instability leads to driver

mutations (such as mutations in the tumour suppressor gene *TP53*) as well as mutational signatures (combinations of mutation types) which if identified, could be useful in theranostics. Other forms of genomic instability include chromosomal instability, aneuploidy as well as microsatellite instability (Cortes-Ciriano *et al.*, 2017; Negrini *et al.*, 2010).

1.1.2 Tumour microenvironment

In addition to the hallmarks framework, the tumour microenvironment (TME) has become pivotal in characterising a cancer. Researchers now appreciate that the TME plays an integral role in tumourigenesis and malignant phenotype; this cannot be deduced by analysing biology at the level of a single cancer cell, but rather by taking into account the interactions between different groups of cells, metabolites, oxygen level, acidity, vasculature, extracellular matrix (ECM), exosomes and secreted factors that are all within the same vicinity (Petrova *et al.*, 2018).

A tumour is not only composed of cancer cells but is a heterogeneous collection of resident host cells, infiltrating cells, ECM and secreted factors (Anderson & Simon, 2020). Due to their pathological metabolic activity, tumour cells induce physical changes in their host tissues which frequently lead to the formation of a hypoxic and acidic TME with a chaotic vasculature of leaky blood vessels. Although the composition of the TME varies between tumour types, the key attributes are consistent, including immune cells, stromal cells, non-cellular components (ECM, exosomes and secreted factors), altered vasculature and altered physical conditions (oxygen, pH, nutrient levels) (Petrova *et al.*, 2018).

Importantly, the TME plays an important role in providing 'contextual synthetic lethality' for therapeutics (Chan *et al.*, 2010). Without further directly damaging DNA or causing mutations, the TME can still induce changes in cancer cells that make them more resistant or susceptible to chemo- and radiotherapy. For example, the TME can form an immune 'hot' or 'cold' tumour, which then determines the efficacy of chemo- and immunotherapies administered (Galon *et al.*, 2006; Galon & Bruni, 2019; Han *et al.*, 2016). Similarly, the stroma component of the TME can possess both tumour-suppressing and tumour-promoting actions, for example through the secretion of TGFβ and formation of cancer-associated fibroblasts (CAFs), respectively (Valkenburg *et al.*, 2018). Of note, TGFβ has pleiotropic effects and can contribute to both immune 'hot' and 'cold' phenotypes (Seoane & Gomis, 2017).

Therefore, it is also unsurprising that the TME is a major contributor to Hanahan and Weinberg's hallmarks of cancer, and their enabling characteristics. The TME can affect programming of invasiveness by facilitating epithelial-mesenchymal transition (EMT) or autocrine activation (Hanahan, 2022). The TME also contributes to the hallmark of activating invasion and metastasis through the CAFs component of the tumour stroma (Mao *et al.*, 2013). The 'tumour-promoting inflammation' enabling characteristic is rarely analysed outside of the TME context, as inflammation usually activates hallmarks by supplying bioactive molecules such as growth factors and proangiogenic factors to the microenvironment (Hanahan & Weinberg, 2011).

The TME may account for tumours where there are no genetic aberrations present to account for tumourigenesis. For example, two groups showed that in a subtype of ependymoma brain tumours, there were surprisingly no DNA mutations nor epigenetic aberrations, puzzling the

authors (Mack *et al.*, 2014; Parker *et al.*, 2014). Moreover, multiple groups have observed from sequencing studies that a notable fraction of tumours have zero mutations; for example, Greenman *et al.* reported that 73 out of 210 tumours had zero mutations in coding exons (Greenman *et al.*, 2007; Imielinski *et al.*, 2012; Kan *et al.*, 2010; Lawrence *et al.*, 2013). This implies that some cancer initiation mechanisms may be broader than we thought and go beyond the scope of gene mutations (Baker, 2014; Versteeg, 2014). Here, the TME becomes important in offering alternative explanations for how tumourigenesis is initiated and sustained without driver mutations. Such mechanisms may include aberrant alterations of the epigenome, regulatory RNA species or post-translational modifications (Dai *et al.*, 2019; Li *et al.*, 2021; Scholzová *et al.*, 2007; Thienpont, van Dyck, *et al.*, 2016). For example, as a key feature of the TME, hypoxia dynamically changes the methylation landscape controlling gene expression, namely by causing DNA hypermethylation (Kim & Park, 2020; Thienpont, Steinbacher, *et al.*, 2016). Hypoxia has also been associated with the dysregulation of microRNAs (miRNAs) across cancer types, with miR-210 functionally validated as a hypoxia-modulated miRNA (Bhandari *et al.*, 2019; Huang *et al.*, 2009; Ke *et al.*, 2017). Interestingly, hypoxia-induced metabolic and histone methylation changes have been recently linked to the tumourigenesis of the aforementioned mutation-free posterior fossa A ependymoma subset (Lin & Monje, 2020; Michealraj *et al.*, 2020).

Hypoxia is arguably one of the most prominent and important features of the TME (Petrova *et al.*, 2018; Singleton *et al.*, 2021). Firstly, subregions of hypoxia exist in approximately half of all solid tumours, making hypoxia a common feature of tumours regardless of tumour genotype and other variables of the TME (Blagosklonny, 2004; Dhani *et al.*, 2015; Vaupel *et al.*, 2001; Weber & Kuo, 2012). Secondly, hypoxia fuels multiple cancer hallmarks as well as

their enabling characteristics. Hypoxia has been established as a source of genomic instability, driving downregulation of DNA repair pathways while allowing cancer cells to accumulate replication stress (Luoto *et al.*, 2013; Ng *et al.*, 2018). Hypoxia induces VEGF and HIF signalling which contribute to pathogenic angiogenesis, opening new avenues for invasion. Hypoxia also upregulates glucose transporters and activates the glycolytic pathway (Carmeliet, 2005; Jones & Thompson, 2009; Semenza, 2010). The aberrant vascularisation induced by hypoxia in the TME can also induce immunosuppression, with immunosuppressive cells such as myeloid-derived suppressor cells (MDSCs), tumour-associated macrophages (TAMs) and T-regulatory (Treg) cells infiltrating hypoxic regions (Khouzam *et al.*, 2021). Thirdly, hypoxia provides a platform for understanding contextual synthetic lethality. For example, homologous recombination (HR) defects are genetically synthetic lethal with poly(ADP-ribose) polymerase 1 (PARP1) inhibition, therefore BReast CAncer gene (BRCA) deficient tumours are typically treated with PARP inhibitors. Hypoxia has been shown to decrease expression of HR proteins, and as such, PARP inhibitors increased clonogenic killing of hypoxic cells as hypoxia has provided 'contextual' synthetic lethality (Chan *et al.*, 2010).

The definition of hypoxia as well as ways to measure it will be discussed in the next section.

1.2 Hypoxia

1.2.1 Defining hypoxia

'Hypoxia' has been used to describe a state of insufficient oxygen in both normal and pathological tissues, as well as wounds (Hammond *et al.*, 2014). In normal tissues, hypoxia may serve a physiological function, for example through chemoreceptors to signal to the respiratory centre in the medulla and pons to increase pulmonary ventilation and cardiac output (Spyer *et al.*, 2006). However, hypoxia also plays a role in multiple human pathologies including cancer, myocardial ischemia, metabolic diseases and chronic heart and kidney diseases, and in reproductive diseases (such as preeclampsia and endometriosis) (Chen *et al.*, 2020).

It is important to define the different terms used in scientific and medical literature to describe oxygen levels. Firstly, **normoxia** refers to atmospheric levels of oxygen (21% O_2) which most researchers use to culture mammalian cells and perform experiments, including preclinical studies. Normoxia has sometimes been criticised as not being physiologically relevant enough for mammalian cell culture studies as actual oxygen levels inside the body are typically much lower than 21% O_2; this may hinder translation of findings into the clinic (Keeley & Mann, 2019). **Physoxia** or **physioxia** is the oxygen level in the normal tissue or organ, which varies widely inside the body. **Hypoxia** is any low or insufficient level of oxygen, specific to the tissue or organ of interest; under hypoxic conditions, the transcription factor hypoxia-inducible factor-1 (HIF) is stabilised (Hammond *et al.*, 2014). **Radiobiological hypoxia**, typically used in the context of cancer and radiotherapy, describes the level of hypoxia where significant resistance to cell death in response to radiation is observed (<0.13% O_2) (Hall &

Giaccia, 2012). **Anoxia** is used to describe a complete lack of oxygen, i.e., 0% O_2 (Wiebe & Machulla, 1999).

Therefore, the oxygen concentration that is considered 'hypoxia' is always relative to the normal oxygen level in the normal tissue or organ of interest. For example, the normal oxygen concentration in the kidney is 9.5% whereas in the dermal papillae of the skin it is 3.2%; what constitutes as hypoxia may be different for the two organs (Carreau *et al.*, 2011).

1.2.2 Measuring hypoxia

Two commonly used units to measure oxygen concentration are percentage of oxygen (% O_2) and millimetre of mercury (mmHg), where 1% O_2 is equivalent to 7.6 mmHg or 1.013 kPa (Hammond *et al.*, 2014). This conversion rate assumes the normal atmospheric pressure (1 atm or 101.325 kPa) and normal temperature (20 °C).

In laboratory settings, the level of oxygen dissolved inside cell culture media can be measured using a range of commercially available probes. In the clinic, blood oxygen can be measured using a pulse oximeter or a blood draw for a range of lung conditions (asthma, chronic obstructive pulmonary disease (COPD), cystic fibrosis, heart disease, pneumonia), viral infections and carbon monoxide poisoning (Cleveland Clinic).

In the clinic for oncology, pimonidazole, a nitroimidazole that binds to thiol-containing proteins in hypoxic cells, can be administered to patients and detected following tumour biopsy using an antibody specific to pimonidazole in immunohistochemistry (Varia *et al.*, 1998). Biopsies also allow for other hypoxia biomarkers to be measured, namely proteins such

as Carbonic Anhydrase 9 (CA-9) and Glucose Transporter Type 1 (GLUT-1) which are well-characterised targets of HIF which increase in hypoxia (Airley *et al.*, 2003; Hammond *et al.*, 2014).

In terms of non-invasive imaging of hypoxia, there are three main categories: radioisotope, resonance and optical techniques (Daimiel, 2019). The most widely established method is a radioisotope technique, nuclear based positron emission tomography (PET) imaging (Lopci *et al.*, 2014). PET is the main method used for assessing hypoxia clinically (Higgins & Hammond, 2022). Two main categories of radiotracers for PET imaging include nitroimidazole and copper-complexed dithiosemicarbazone (Cu-ATSM) derivatives, both of which are enzymatically reduced in hypoxic cells and subsequently retained in the cells (Hammond *et al.*, 2014). Resonance techniques include magnetic resonance imaging (MRI) based methods that are also being developed for imaging hypoxia, but they are less established than PET (Gérard *et al.*, 2019). Optical techniques for imaging hypoxia include bioluminescence, near-infrared spectroscopy and photo-acoustic imaging, which are still being developed and limited to use in research settings only (Bader *et al.*, 2020; Daimiel, 2019; Hammond *et al.*, 2014; Lopci *et al.*, 2014).

1.3 Hypoxia and cancer

1.3.1 Origins of tumour hypoxia

Areas of hypoxia occur in most of solid tumours, as well as in some liquid tumours (e.g., multiple myeloma) (Hu *et al.*, 2012). Not only is hypoxia a result of tumourigenesis, but hypoxia itself can also promote malignant progression by activating adaptive, pro-survival responses and angiogenesis, fuelling the vicious cycle. As a key part of the TME, hypoxia arises due to two main reasons: high metabolic demand of cancer cells from uncontrolled proliferation, as well as the malformed tumour vasculature (Wilson & Hay, 2011).

Firstly, the demand for oxygen from tumour cells outweighs the supply of oxygen from nearby blood vessels (Brown, 2002; Brown & Giaccia, 1998). As the tumour cells divide rapidly and the growth of new blood vessels lags behind, a gradient of oxygen concentration forms across cells surrounding the tumour blood vessel. As shown schematically in **Figure 1.2**, whereas cells near the blood vessel are well-oxygenated, cells further away from the blood vessel become increasing hypoxic, even anoxic. Hypoxia typically arises at a distance of approximately 150 μm away from a functional blood vessel in solid tumours (al Tameemi *et al.*, 2019; Bennewith & Dedhar, 2011; Helmlinger *et al.*, 1997). The cells that are extremely far away from any blood vessels may become necrotic (Pires *et al.*, 2010). However, peri-necrotic cells experiencing hypoxia (<1% O_2) are still able to survive (Hall & Giaccia, 2012). In essence, this type of hypoxia is deemed as diffusion-limited (Vaupel, 2001).

Secondly, the chaotic and malformed tumour vasculature is another source of hypoxia due to poor perfusion (Matsuo *et al.*, 2014). Although tumour blood vessels have the same components as normal blood vessels (including endothelial cells, mural cells and basement

membrane), all these components are abnormal in tumour blood vessels (Baluk *et al.*, 2005; Nagy *et al.*, 2010). The supply of oxygen is therefore unreliable and intermittent due to the random closing and opening of dysfunctional blood vessels, making this type of hypoxia perfusion-limited (Bader *et al.*, 2020; Chaplin *et al.*, 1987; Vaupel, 2001).

Ultimately, as mentioned previously, Hanahan and Weinberg stated that 'sustained chronic proliferation' is arguably the most fundamental hallmark of cancer cells (Hanahan & Weinberg, 2011); therefore unsurprisingly, tumour hypoxia is an almost universal feature of solid tumours, a natural consequence of uncontrolled cell growth.

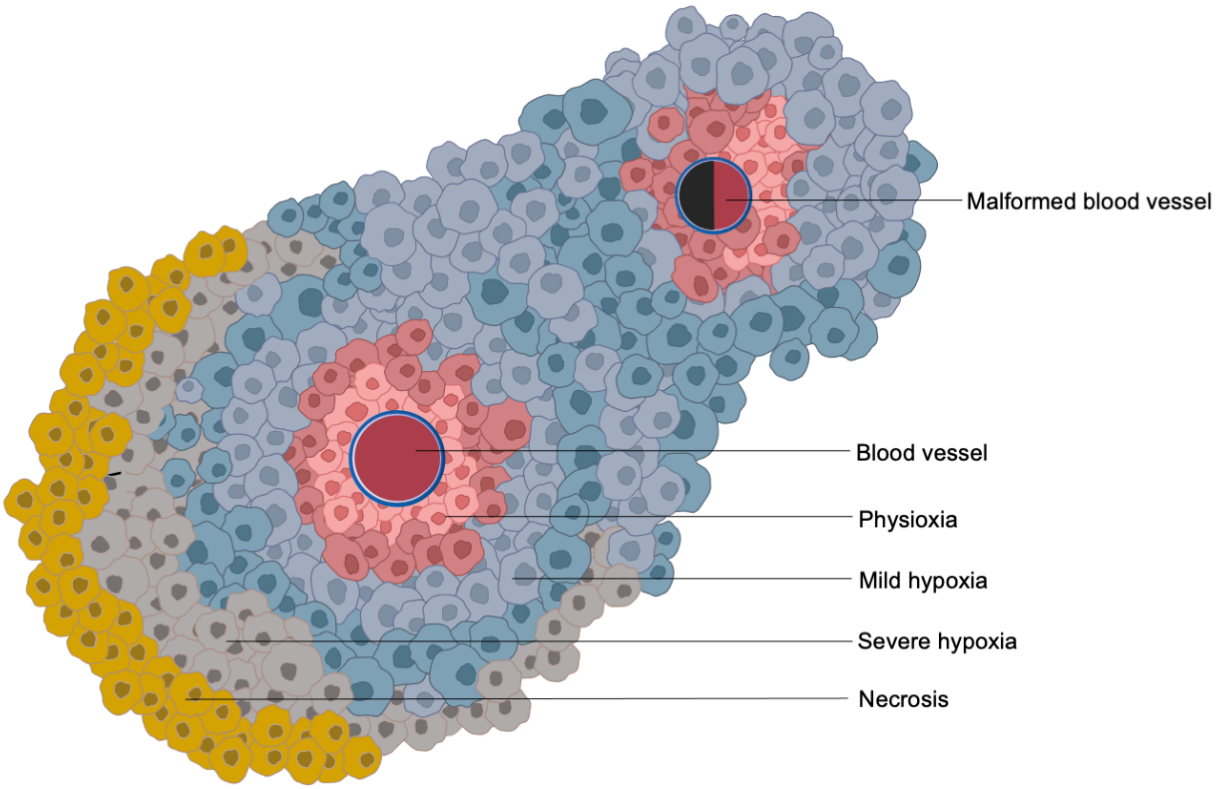


Figure 1.2. Gradient of varying oxygen concentrations in the solid tumour. Cells in the tumour surrounding blood vessels experience a range of oxygen concentrations. Those closest to the blood vessels (red cells) are well-oxygenated. At 70-150 µm away from the blood vessel, cells start to become mildly hypoxic (blue). Cells even further away become severely hypoxic (grey) but are still able to survive. Necrotic patches of cells (yellow) form in the hypoxic tumour. Cells surrounding the malformed blood vessel may experience acute hypoxia as the blood vessel may suddenly collapse or close.

1.3.2 Types of tumour hypoxia (acute, chronic, cycling, mild, severe)

Hypoxia can be sub-categorised based on duration or severity. Severity, as alluded to before in **1.2.1**, is measured using oxygen levels. Due to the heterogeneous TME, areas of both mild hypoxia (0.5-2% O_2) and severe levels of hypoxia, also referred to as radiobiological hypoxia (<0.1% O_2) can exist within the same tumour (Hammond *et al.*, 2014). Whereas both mild and severe hypoxia induce HIF-1 signalling, only severe hypoxia additionally induces other stress response pathways in the cell, such as the DNA damage response (DDR) and the unfolded protein response (UPR) (Olcina, Grand and Hammond, 2014; Bolland, Ma *et al.*, 2021). These oxygen level dependent pathways will be discussed in detail in **1.4**.

In terms of duration, hypoxia can be described as acute, chronic or cycling. Acute hypoxia is characterised by a sudden decrease in oxygen supply due to either malformed blood vessels collapsing and shutting off flow, or due to fluctuations in red blood cell flux (Horsman *et al.*, 1986). In contrast, chronic hypoxia exists because of diffusion-limited supply of oxygen over distances larger than 150 µm away from a functional blood vessel (Vaupel, 2001). The time frames for how long exactly 'acute' and 'chronic' hypoxia last are inconclusive as more data is needed from human tumours; however, there seems to be a general consensus that acute hypoxia contributes more to tumourigenic capacity and metastasis than chronic hypoxia does (Bayer & Vaupel, 2012; Bhaskara *et al.*, 2012; Martinive *et al.*, 2006; Rofstad *et al.*, 2010). One recent study showed that chronic hypoxic cells can survive beyond 96 hours and that acutely hypoxic cells start to die after 24 hours and were no longer detectable at 72 hours after labelling; both chronic and acutely hypoxic cells were shown to be equally radioresistant (Higgins & Hammond, 2022; Wadsworth *et al.*, 2022). Several studies have referred to timeframes under 48 hours of hypoxia as 'acute' and anything longer than 48 hours of hypoxia

as chronic (Dong *et al.*, 2019; Nejad *et al.*, 2021; Hussein *et al.*, 2006). Finally, cyclic hypoxia, also known as intermittent hypoxia, is characterised by dynamic cycles of hypoxia and reoxygenation due to changes in red blood cell flux and abnormal vasculature and is therefore associated with inefficient perfusion (Bader *et al.*, 2020; Michiels *et al.*, 2016). For example, cells in **Figure 1.2** surrounding the malformed blood vessel that may intermittently open and close can experience cyclic hypoxia. Cancer cells exposed to cyclic hypoxia may accumulate DNA damage as a result of increased levels of reactive oxygen species (ROS) damaging the DNA and contributing to replication catastrophe (Bader *et al.*, 2021).

1.3.3 Tumour hypoxia and clinical importance

Tumour hypoxia plays an important role in the clinic. In prognosis, patients with hypoxic tumours are predicted to have worse outcomes due to a higher likelihood of invasion and metastasis (Brown & Wilson, 2004). In treatments, hypoxia is a significant barrier to efficacy as hypoxic tumours are resistant to radiotherapy and can develop resistance to chemo- and immunotherapies (Graham & Unger, 2018; Hall & Giaccia, 2012; Minassian *et al.*, 2019; Rohwer & Cramer, 2011; Teicher, 1994). However, for the same reasons, hypoxia is also an attractive therapeutic target; radiosensitisers, angiogenesis inhibitors and hypoxia-activated prodrugs are just several of the hypoxia-targeting therapeutics in development in oncology (Ashton *et al.*, 2016; Mistry *et al.*, 2017; Wilson & Hay, 2011; Zannella *et al.*, 2013).

Table 1.1 shows differences in oxygen concentrations between tumour tissues and their respective normal tissues, as well as the impact of hypoxia on patient outcomes, demonstrating the importance of hypoxia in the clinic (McKeown, 2014; Walsh *et al.*, 2014).

Table 1.1 Typical oxygen concentrations found in tumours and their respective healthy tissues

Tumour Type	Normal tissue median O_2	Tumour tissue median O_2	Reference for median % O2 and number of patients (McKeown, 2014)	Fraction of hypoxic tumours among all tumours of this type (Walsh *et al.*, 2014)	Clinical outcomes for hypoxic vs. normoxic tumours (Walsh *et al.*, 2014)
Head and neck	40% (n=14)	1.6% (n=30)	Nordsmark, Bentzen and Overgaard, 1994	70% (median pO_2 <10 mm) (Brizel *et al.*, 1999)	Decreased 3-year survival rate (28% vs 38%) (Nordsmark *et al.*, 2005)
Lung	5.6% (N/A)	2.2% (n=20)	Le *et al.*, 2006	38% (HP2.5 >20%) (Graves *et al.*, 2010)	Decreased 2-year overall survival rate (17% vs 79%) (Le *et al.*, 2006)
Breast	6.8% (n=212)	1.3% (n=212)	Vaupel *et al.*, 2003, 2007	63% (pO_2 ≤2.5 mm Hg) (Vaupel *et al.*, 2003)	N/A
Pancreatic	6.8% (n=7)	0.4% (n=7)	Koong *et al.*, 200	100% (HP2.5 >20%) (Koong *et al.*, 2000)	N/A
Cervix	5.5% (N/A)	1.2% (n=730)	Sebestyén *et al.*, 2021; Vaupel *et al.*, 2007	48% (median pO_2 <10 mm) (Höckel *et al.*, 1993)	Decreased 6 year overall survival rate (29% vs 87%) (Lyng *et al.*, 2000)
Prostate	3.9% (n=59)	0.3% (n=59)	Movsas *et al.*, 2001	19% (Turaka *et al.*, 2012)	Decreased 8-year freedom from biochemical failure (46% vs 78%) (Turaka *et al.*, 2012)
Sarcoma	6.7% (n=283)	1.8% (n=283)	Vaupel *et al.*, 2007	45% (HP2.5>20%) (soft tissue) (Bentzen *et al.*, 2003)	Decreased 18-month disease free survival rates (35% vs 70%) (soft tissue) (Brizel *et al.*, 1996)
Brain tumour	3.4% (n=103)	1.7% (n=104)	Vaupel *et al.*, 2007	64% (HP2.5 >20%) (Collingridge *et al.*, 1999)	Decreased 3-year overall survival (25% vs 53%) (Lally *et al.*, 2006)
Rectal carcinoma	6.8% (N/A)	2.5% (n=15)	Mattern *et al.*, 1996	N/A	N/A

n= number of patients in brackets

1.3.4 Hypoxia and radiotherapy resistance

Radiotherapy is used in over half of cancer patients, including patients of breast, prostate, cervix, head and neck, lung, brain cancers as well as sarcomas. The goal of radiotherapy is to eradicate or diminish tumour growth by using high energy particles or waves to induce lethal double-strand breaks in the DNA of cancer cells while sparing normal cells; radiotherapy can be used in early-stage cancer as a localised standalone therapy as well as in combination with chemotherapy in advanced cancers (American Cancer Society; Jaffray and Gospodarowicz, 2015). Unfortunately, a significant portion of the cancers treated with radiotherapy also have regions of hypoxia (see **Table 1.1**) which makes the radiotherapy less effective (Brown & Giaccia, 1998). The oxygen enhancement ratio (OER) is the ratio of doses administered under hypoxic to aerobic conditions needed to achieve the same biological effect; the OER for ionising radiations range from 2.5-3.5 (Hall & Giaccia, 2012). In other words, hypoxia increases tumour resistance to radiotherapy by up to 3.5 times.

Although efforts in trying to increase oxygen delivery to tumours (either through administrating erythropoietin (EPO) or by allowing patients to breathe in high oxygen content gas) have failed to reach the clinic for various reasons, other strategies have shown promise (Horsman *et al.*, 2021). Food and Drug Administration (FDA) approved drugs including metformin, atovaquone and papaverine have been repurposed and used as effective radiosensitisers that increase oxygen delivery to hypoxic tumours by inhibiting mitochondrial respiration (Ashton *et al.*, 2016; Benej *et al.*, 2018; Skwarski *et al.*, 2021; Zhang *et al.*, 2013). Significant improvements in clinical outcomes have been shown in recent initial clinical trials (Skwarski *et al.*, 2021).

Another strategy is to use hypoxia activated bioreductive prodrugs. It was found that several different chemical moieties have the potential to be metabolised by enzymatic reduction specifically under hypoxic and not normoxic conditions, including nitro groups, quinones, aromatic *N*-oxides, aliphatic *N*-oxides and transition metals (Wigerup *et al.*, 2016). These highly electron-affinic compounds only become cytotoxic once reduced by enzymes in hypoxia and have little toxicity to normal tissues (Horsman *et al.*, 2021; Overgaard *et al.*, 1998). These compounds have also been shown to be radiosensitising to hypoxic and not normoxic cells as they can replace oxygen in ionising radiation to generate free radicals that can damage the DNA (Ahn, 2007; McKeown, 2014; McKeown *et al.*, 2007; Mistry *et al.*, 2017; Wilson & Hay, 2011). Therefore, due to their dual action through separate mechanisms, these compounds could be used as hypoxia activated pro-drugs alone, or in combination with radiotherapy as radiosensitisers (Wilson & Hay, 2011). The three most promising hypoxia activated prodrugs have been tirapazamine (TPZ), PR-104 and evofosfamide (TH-302). Unfortunately, despite showing promising results in preclinical, Phase I and Phase II studies, both TPZ and TH-302 failed to meet primary endpoints of improved survival in Phase III (Spiegelberg *et al.*, 2019). Researchers have mainly attributed this failure to poor stratification or selection of patients (patients would need to have hypoxic tumours) as well as varying levels of reductases in the tumours (Horsman *et al.*, 2021).

1.3.5 Hypoxia and chemotherapy resistance

Hypoxia promotes multiple pro-survival and adaptive responses in cancer cells which can mediate chemotherapy resistance (Kim & Lee, 2017). HIF signalling, in particular, promotes drug resistance in hypoxic tumours through multiple events, such as overexpressing drug

efflux proteins, inhibiting apoptosis, inducing autophagy, increasing angiogenesis through Vascular Endothelial Growth Factor A (VEGF) signalling, and regulating mitochondrial activities (Jing *et al.*, 2019; Lv *et al.*, 2015). Unfortunately, small molecule inhibitors targeting HIF-1α for cancer therapy have failed to progress to clinical trials due to a lack of efficacy *in vivo* (McAleese *et al.*, 2021). New avenues include evaluating HIF inhibitors with other anti-drugs as a combination chemotherapy.

Similarly, the DDR is also activated as an adaptive response in severe hypoxia and its pro-survival signalling contributes to drug resistance (Hammond *et al.*, 2002; Olcina *et al.*, 2010; Pires *et al.*, 2010). Components of the DDR can be inhibited in order to sensitise hypoxic cells to chemotherapy (Olcina *et al.*, 2010). Indeed, as supported by *in vitro* studies, inhibition of ATR, CHK1 and CHK2 checkpoint kinases of the DDR have been shown to sensitise cells exposed to hypoxia/ reoxygenation (Freiberg *et al.*, 2006; Hammond *et al.*, 2004, 2006; Leszczynska *et al.*, 2016; Pires *et al.*, 2012). Currently, there are multiple DDR inhibitors (targeting ATR, ATM, CHK1/2, WEE1 and DNA-PK) in clinical trial testing (Yap *et al.*, 2019).

Hypoxia also activates a major stress response pathway called the unfolded protein response (UPR), which can contribute to both oncogenesis and chemoresistance (Akman *et al.*, 2021; Avril *et al.*, 2017; Madden *et al.*, 2019; Reich *et al.*, 2020; Sisinni *et al.*, 2019). The UPR is described in detail in **1.4.4**. All three arms of the UPR pathway have been implicated in helping cancer cells ensure survival upon exposure to chemotherapeutic reagents. Knockdown of GRP78, ATF6, ATF4 or XBP1s has resensitised chemoresistant cells (Chen *et al.*, 2017; Kim *et al.*, 2016; Wang *et al.*, 2009). Moreover, XP1s has a role in promoting relapse of triple negative breast cancer *in vivo* (Chen *et al.*, 2014; Logue *et al.*, 2018). Interestingly, depending on the

chemotherapeutic reagent being used, cancer cells can switch between the arms of the UPR to avoid apoptotic signalling from the PERK/ CHOP arm and instead signal through the IRE1-XBP1s arm (Fujimoto *et al.*, 2016). On the other hand, colon cancer chemoresistant cells preferentially activate PERK/NRF2/MRP1 signalling, enhancing drug efflux (Salaroglio *et al.*, 2017). This demonstrates that cancer cells can selectively activate a specific UPR axis as their adaptive response to chemotherapy.

Despite designing small molecule inhibitors targeting hypoxia induced stress pathways to prevent chemotherapy resistance, a fundamental problem *in vivo* is the delivery of drugs to hypoxic tumours. As hypoxic regions exist due to a limited blood supply from an inefficient and chaotic vasculature, the delivery of therapeutic agents is also limited (Olcina *et al.*, 2010). One way to address this problem is to combine the drug with agents which normalise the tumour blood vessels transiently, to enhance the delivery both therapeutics (Jain, 2005).

1.4 The biological response to hypoxia

At the cellular level, hypoxia leads to the rapid activation of numerous transcription factors, resulting in multiple stress response pathways being activated (Schönenberger & Kovacs, 2015). Both mild and severe hypoxia activate the HIF signalling pathway, whereas only severe hypoxia activates the DDR and UPR pathways (Olcina, Grand and Hammond, 2014; Bolland, Ma *et al.*, 2021).

1.4.1 HIF

The hypoxia-inducible factor (HIF) family of transcription factors play an integral role in regulating the cellular response to hypoxia. With hundreds to thousands of targets, HIFs regulate genes that code for proteins involved in angiogenesis, energy metabolism, erythropoiesis, inflammation, immune regulation, pH regulation, and cell proliferation/survival and invasion/metastasis (Schödel & Ratcliffe, 2019; Semenza, 2003). Hypoxia-inducible factor-1 (HIF-1) and hypoxia-inducible factor-2 (HIF-2) expression up-regulate pathways that contribute to hallmarks of cancer, including angiogenesis, metastasis, cell proliferation and genomic instability (Pugh & Ratcliffe, 2003; Wigerup *et al.*, 2016).

The HIF transcription factor is a heterodimeric DNA-binding complex composed of two proteins: an oxygen labile α subunit (HIF-1α, HIF-2α or HIF-3α in humans) and a shared constitutively expressed HIF-1β/ARNT (aryl hydrocarbon receptor nuclear translocator) subunit (Schofield & Ratcliffe, 2004). HIF-1α, HIF-2α and HIF-3α when in complex with HIF-1β/ARNT are referred to as HIF-1, HIF-2 and HIF-3, respectively. The oxygen sensitive α subunit is inactivated and degraded under normoxic conditions (in the presence of oxygen) but stabilised under hypoxic conditions (Rankin & Giaccia, 2016).

Specifically, the proteolytic degradation of HIF-1α and HIF-2α is carried out by members of the prolyl-hydroxylase domain protein (PHD) family of enzymes as well as factor-inhibiting HIF (FIH), the asparaginyl hydroxylase (Choudhry & Harris, 2018). All 3 members of the PHD family and FIH belong to the non-haem, iron (II)-dependent and 2-oxoglutarate-dependent-oxygenase superfamily (Schofield & Ratcliffe, 2004). In the presence of oxygen, 2-oxoglutarate and iron (II), PHDs use oxygen as a substrate to hydroxylate conserved proline residues in HIF-1α and HIF-2α (Schofield & Ratcliffe, 2004). This hydroxylation allows the tumour suppressor protein von-Hippel-Lindau (VHL) to bind to HIF-α; as the recognition component of an E3 ubiquitin ligase complex, VHL targets the bound HIF-α for proteasomal degradation (Rankin & Giaccia, 2016).

In contrast, under hypoxic conditions (in the absence of oxygen), PHDs are inactivated, leading to HIF-α stabilisation and dimerisation with HIF-1β/ARNT. Upon dimerisation, HIF translocates to the nucleus where it binds to Hypoxia Responsive Elements (HRE) sequences (5'-[A/G]CGTG-3') in promoters of target genes (Choudhry & Harris, 2018). It is important to note that the recruitment of co-activators histone acetyltransferase p300 (p300) and CREB-binding protein (CBP) are required for transcriptional activation by HIF-α (Freedman *et al.*, 2002).

Under normoxic conditions and in the presence of iron (II) and 2-oxoglutarate, FIH hydroxylates an asparagine residue in HIF-α, blocking the recruitment of p300 co-activator and hence inactivating the transcriptional activity of HIF-α (Lando *et al.*, 2002). FIH is inactivated under hypoxic conditions.

Apart from hypoxia, other stimuli can also regulate HIF expression, including growth factor signalling (LaGory & Giaccia, 2016). Whereas hypoxia stabilises the protein expression of HIF (independent of cell type), growth factors increase HIF-α translation through activation of phosphatidylinositol-3 kinase (PI3K) or mitogen-activated protein kinase (MAPK) pathways in specific cell types (Patiar & Harris, 2006).

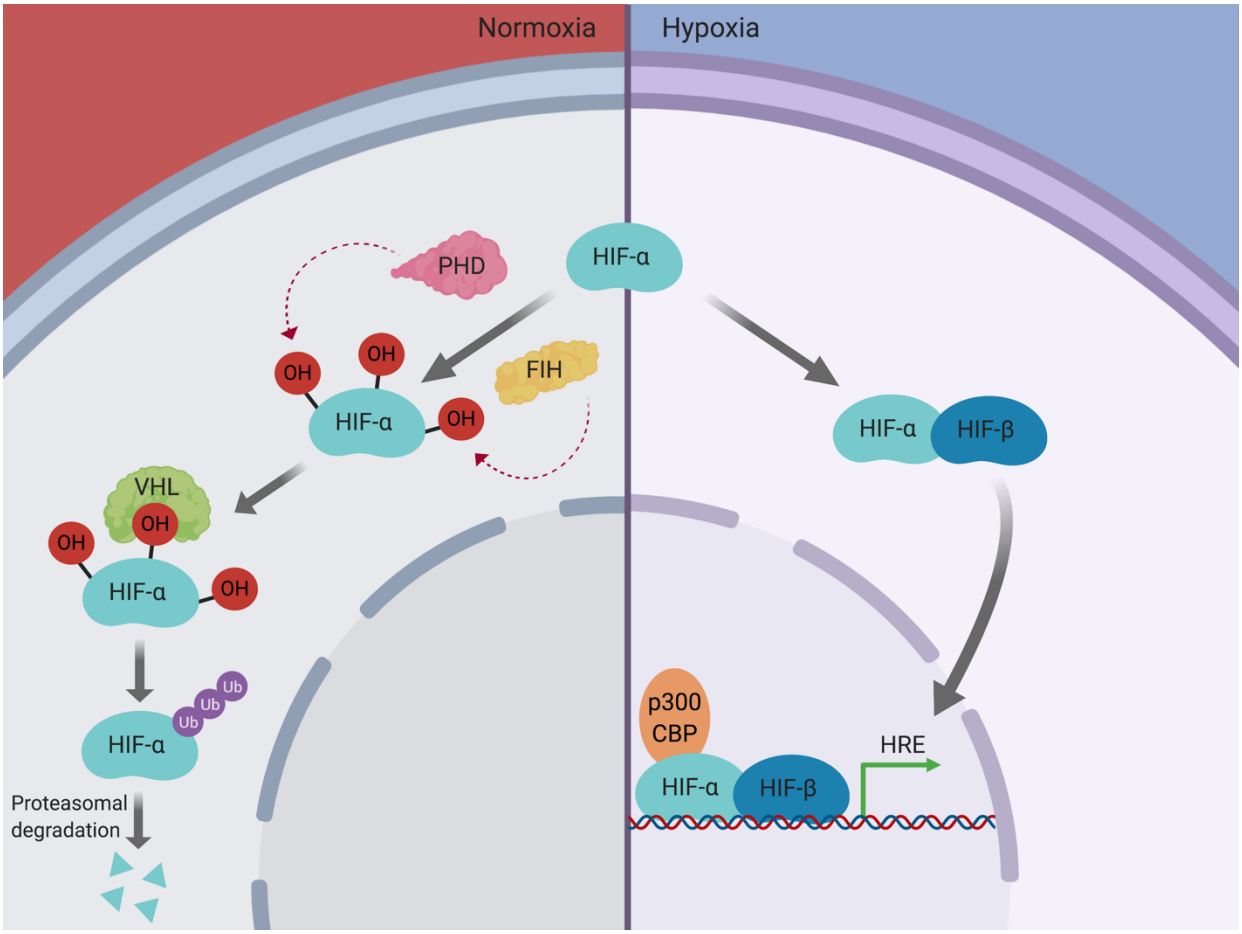


Figure 1.3. HIF regulation under normoxic and hypoxic conditions. Under normoxic conditions, PHD and FIH hydroxylate HIF-α in the presence of oxygen, iron (II) and 2-oxoglutarate. The hydroxylation allows VHL, which is the recognition component of an E3 ubiquitin ligase complex, to bind to HIF-α, targeting HIF-α for proteasomal degradation. In contrast, under hypoxic conditions, PHD and FIH are inactivated and do not hydroxylate HIF-α. HIF-α then binds with HIF-1β/ARNT and the complex formed translocates to the nucleus where it binds to the promoter of hypoxia responsive elements, and transcriptionally activates target genes. Figure created with BioRender.com.

Although HIF-1α and HIF-2α both lead to positive transcriptional responses in hypoxia, their transcriptional targets, kinetics of activation and oxygen-dependency differ (Schödel & Ratcliffe, 2019). Whereas HIF-1α is induced more by severe hypoxia, HIF-2α is induced more by moderate hypoxia (Holmquist-Mengelbier *et al.*, 2006). The induction of HIF-3α is less well understood due to its complex pattern of expression (Duan, 2016).

1.4.2 DNA damage response

It is important for a cell to pass on its genetic material, intact and undamaged, to the next generation during mitosis. This would ensure faithful inheritance of information needed for cellular functions, as well as prevention of neoplasia that stems from DNA mutations. However, DNA is constantly exposed to endogenous and environmental sources of mutagens, as well as errors from the cell's replication machinery (Jackson & Bartek, 2009). The DNA damage response (DDR) is the biological system that the cell has evolved to prevent, detect, and repair DNA damage (Blackford & Jackson, 2017; Pilié *et al.*, 2019). The DDR is controlled by the 'trinity' of kinases, namely ataxia telangiectasia mutated (ATM), ataxia telangiectasia and Rad3-related (ATR) and DNA-dependent protein kinase (DNA-PK). The three kinases are part of the phosphatidylinositol-3 kinase-like kinase (PIKK) family and are at the apex of a complex signal transduction pathway that ultimately leads to several possible cellular outcomes, including but not limited to DNA repair, cell cycle arrest, senescence and apoptosis (Abraham, 2004; Ciccia & Elledge, 2010). It has also been shown that other processes, such as DNA replication, repair to transcription, metabolic signalling and RNA splicing can also be regulated by ATM and ATR kinases (Bennetzen *et al.*, 2010; Matsuoka *et al.*, 2007; Paulsen *et al.*, 2009).

ATM is most well-characterised in the DDR for responding to double-strand breaks (DSBs) (Andegeko *et al.*, 2001; Harper & Elledge, 2007). Upon DNA damage that causes DSBs, such as ionising radiation, ATM binds to nibrin (NBS1), which is part of the MRE11-RAD50-NBS1 (MRN) complex found at DSBs (Carney *et al.*, 1998; Stewart *et al.*, 1999). This binding allows ATM to be activated and to phosphorylate downstream mediator proteins including KRAB-associated protein 1 (KAP1), checkpoint kinase 2 (CHK2) and tumour protein p53 (p53). These mediator proteins go on to activate effector proteins which mobilise the DDR machinery that executes cell cycle arrest, DNA repair, senescence, apoptosis etc. (van den Bosch *et al.*, 2003; White *et al.*, 2012). ATM phosphorylates serine 139 on histone H2AX in response to DSBs, and this phosphorylation, also known as gamma-H2AX (γ-H2AX), is a common marker of DNA damage as they form distinct foci on chromatin that can be quantified (Burma *et al.*, 2001). Another common DNA damage marker is the formation of p53 binding protein 1 (53BP1) foci which assemble at DSBs (Lee *et al.*, 2010; Mochan *et al.*, 2004; Shibata & Jeggo, 2020). The most direct method of detecting DSBs, however, is the neutral comet assay which measures damaged DNA fragments by looking at the length of the 'comet tail' (Calini *et al.*, 2002). Interestingly, there are also DSB-independent mechanisms of activating ATM, such as in response to chromatin changes or oxidative stress (e.g., hypoxia) (Kim *et al.*, 2009; Olcina *et al.*, 2013)

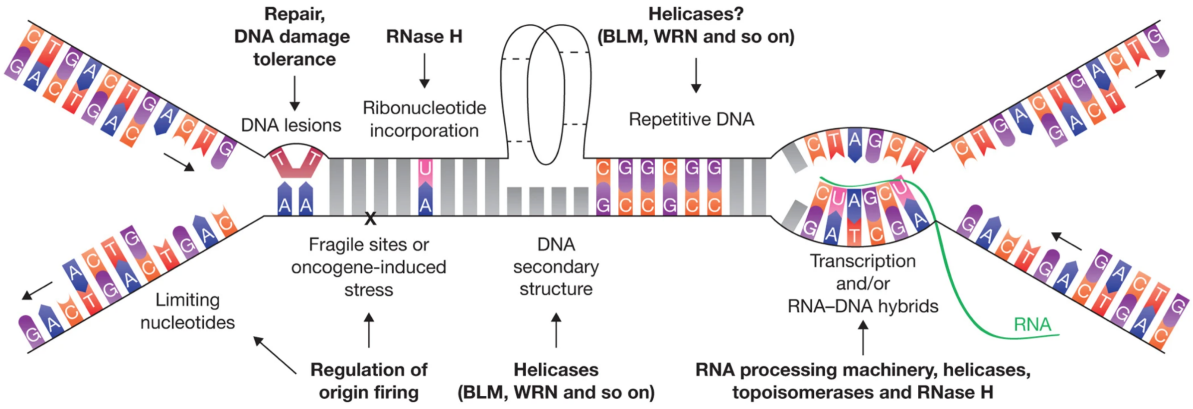


Figure 1.4 Sources of replication stress. A myriad of conditions can act as a barrier to the replication fork, causing replication stress and accumulation of ssDNA. These include reduced nucleotide pools, DNA lesions, repetitive sequences, RNA/DNA hybrids and transcription-replication collisions, oncogene-induced stress, ribonucleotide incorporation, DNA secondary structures and fragile sites. Known key resolution pathways for the respective sources of replication stress are shown in bold. Reprinted from (Zeman and Cimprich, 2014) with permission from Nature Publishing Group (license number 5390730989404).

In contrast, ATR is most well-known for responding to DNA replication stress (Blackford & Jackson, 2017). Although there is no unifying definition or molecular hallmarks, 'replication stress' generally refers to the slowing or stalling of replication fork progression or DNA synthesis (Zeman & Cimprich, 2014). Replication stress has been associated with expression of oncogenes, hypertranscription that causes replication-transcription conflicts, as well as other physical barriers that my hinder the DNA replication machinery and as a result form long stretches of single stranded DNA (ssDNA) (Bowry *et al.*, 2021; Kotsantis *et al.*, 2018; Zeman & Cimprich, 2014). The ssDNA results from when DNA helicases continuously unwind DNA despite DNA polymerase lagging and stalling (Pacek & Walter, 2004). Unlike ATM, ATR is essential for survival in replicating cells and responds to a wider range of genotoxic stresses compared to ATM (Brown & Baltimore, 2000; de Klein *et al.*, 2000; Zou & Elledge, 2003). ATR is recruited to ssDNA through ATRIP, which recognises replication protein A (RPA) that coats

the ssDNA (Zou & Elledge, 2003). On top of recruitment to ssDNA, other factors such as DNA topoisomerase II binding protein 1 (TopBP1) is needed to activate ATR, allowing ATR to phosphorylate key downstream targets such as CHK1 (Kumagai *et al.*, 2006; Liu *et al.*, 2000; Zhao & Piwnica-Worms, 2001). Like ATM, ATR also phosphorylates p53 and H2AX (Canman *et al.*, 1998; Liu *et al.*, 2000; Ward & Chen, 2001). Importantly, ATR phosphorylates RPA in response to replication stress in order to prevent further ssDNA accumulation and to stimulate DNA synthesis (Berti & Vindigni, 2016; Liu *et al.*, 2012; Vassin *et al.*, 2009). Therefore, phosphorylation of RPA and CHK1 by ATR are used as markers of replication stress. The ATR mediated response to replication stress ensures fork stabilisation, and fork restart once the source of replication stress has been resolved (Elvers *et al.*, 2011).

DNA-PK, also known as DNA-PKcs (DNA-dependent protein kinase catalytic subunit) is activated by DSBs; it is recruited to the damaged sites by Ku in order to promote the DNA repair pathway non-homologous end-joining (NHEJ) (Jette & Lees-Miller, 2015; Walker *et al.*, 2001). DNA-PK is responsible for repairing most of the DSBs in mammalian cells through NHEJ, except in the synthesis phase (S phase) of the cell cycle when the sister chromatid can act as a template for the DSB repair pathway HR (Davis *et al.*, 2014). DNA-PKcs kinase activity is essential for NHEJ and it can phosphorylate NHEJ factors including Ku70/80, X-ray repair cross-complementing protein 4 (XRCC4) and DNA Ligase IV (LIG4), as well as DDR factors like p53 and H2AX (Mahaney *et al.*, 2009; Wang & Lees-Miller, 2013).

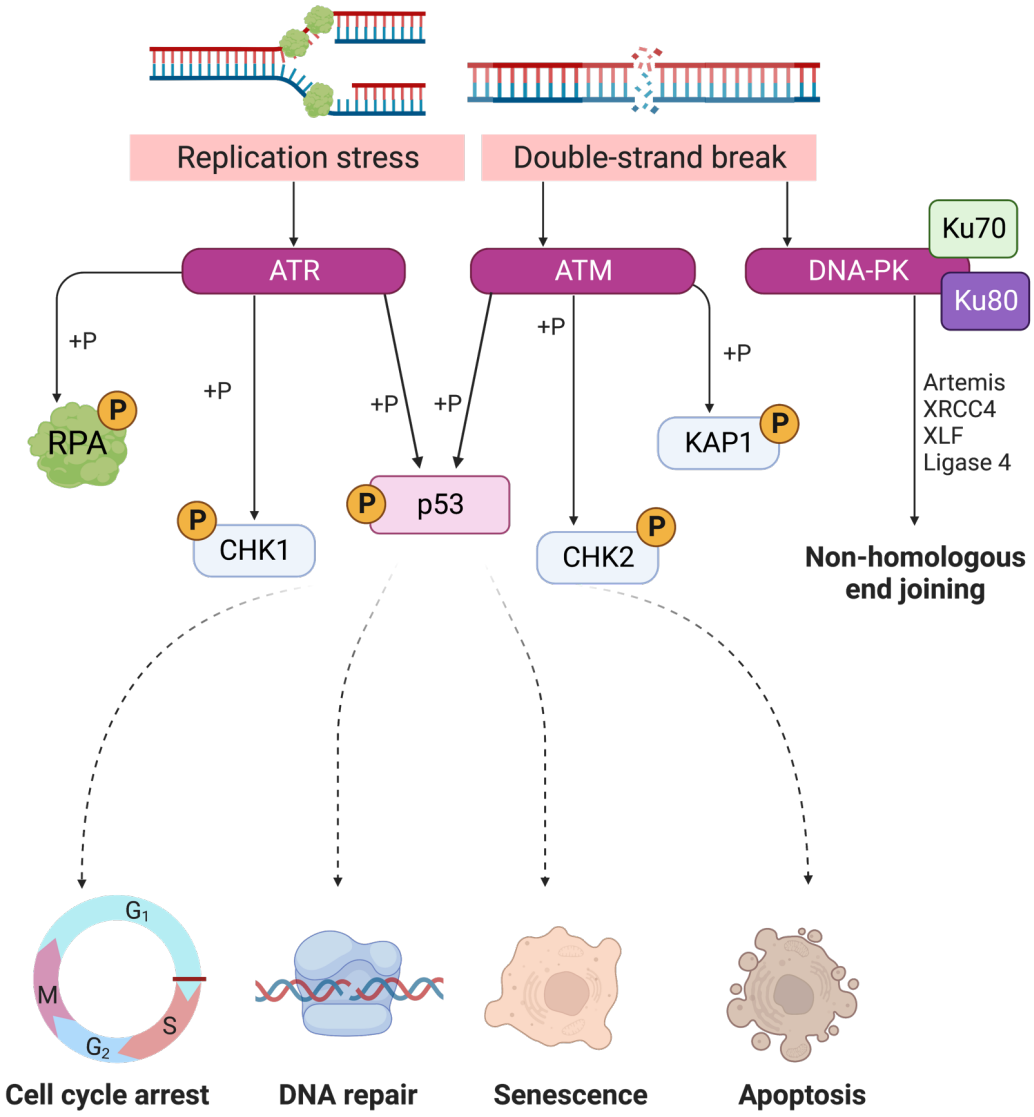


Figure 1.5 The canonical DNA damage response. In response to replication stress, ATR phosphorylates RPA, CHK1 and p53. In response to double strand breaks, ATM phosphorylates KAP1, CHK2 and p53. As a result, the DNA damage response leads to cell cycle arrest, DNA repair, senescence or apoptosis. In response to double strand breaks, DNA-PK can mediate the DNA repair pathway non-homologous end joining. Figure created with BioRender.com

Hypoxia (<0.1% O_2) activates the DDR. Interestingly, the hypoxic DDR occurs in the absence of detectable DNA damage and is an oxygen dependent response. ATM-dependent phosphorylation of CHK2 and KAP1, and ATR-dependent phosphorylation of RPA and CHK1 can be observed in hypoxia (Hammond *et al.*, 2002; Hammond *et al.*, 2003; Bencokova *et al.*,

2009). H2AX and p53, common downstream targets of ATM and ATR, are also phosphorylated. The hypoxic DDR is unlikely due to DNA damage because strikingly, there are no detectable SSBs or DSBs in hypoxia as visualised by the 53BP1 and comet assays (Hammond *et al.*, 2003; Bader, Dewhirst and Hammond, 2020; Ramachandran, Ma *et al.*, 2021). Instead, replication stress in a chromatin context where the 9th lysine residue on histone H3 protein is trimethylated (H3K9me3) in hypoxia activates the DDR (Olcina *et al.*, 2013).

The replication stress in hypoxia primarily stems from low deoxyribonucleotide (dNTP) levels, as ribonucleotide reductase (RNR), the bottleneck enzyme for synthesising dNTPs, requires oxygen as an essential cofactor (Foskolou *et al.*, 2017). Further support of replication stress in hypoxia includes the slowing of replication using the bromo-2'-deoxyuridine (BrdU) assay, as well as the DNA fibre assay (Hammond *et al.*, 2002; Pires *et al.*, 2010; Foskolou *et al.*, 2016). In hypoxia, the number of stalled replication forks increases, whereas new origin firing decreases; replication rates are reduced significantly but are not completely abrogated. The hypoxia-induced replication stress induced signalling can be detected by specific phosphorylations (RPA-S33, CHK1-S345 γ-H2AX). Interestingly, the hypoxia induced γ-H2AX appears as a pan-nuclear stain as opposed to forming foci which stem from SSBs or DSBs (Olcina *et al.*, 2013; Ramachandran, Ma *et al.*, 2021). Pan-nuclear γ-H2AX has been associated with replication stress (Moeglin *et al.*, 2019).

Whereas ATR signalling in hypoxia can be directly attributed to replication stress from depleted nucleotide pools, the origin of ATM signalling in hypoxia is less obvious when there is an absence of DSBs. ATM activation independent of DSBs has been observed in response to stresses such as heat, hypotonic stress, and agents that modify chromatin (Bakkenist &

Kastan, 2003; Guo *et al.*, 2010; Hunt *et al.*, 2007). Although replication stress definitely contributes to ATM signalling in hypoxia, as the ATR and ATM kinases share numerous common downstream targets and have been observed to activate each other under certain conditions, replication stress alone does not fully explain the activation of ATM in hypoxia (Cimprich & Cortez, 2008; Ng *et al.*, 2018; Olcina *et al.*, 2014). Olcina *et al.* found that the combination of replication stress and chromatin changes are required for ATM activation in hypoxia; specifically, both replication stress and hypoxia-induced H3K9me3 were found to be important for hypoxia-induced activation of ATM (Olcina *et al.*, 2013). H3K9me3 is a chromatin mark associated with heterochromatin and damage-induced ATM signalling and is induced in an oxygen dependent manner in hypoxia in the absence of damage (Goodarzi *et al.*, 2010; Olcina *et al.*, 2013; Sun *et al.*, 2009). In the absence of ATM, hypoxic cells experience a dramatic reduction in DNA replication rates, suggesting a role for ATM in maintaining DNA replication when replication stress and increases in heterochromatin co-exist (Olcina *et al.*, 2013).

DNA-PK is also activated in hypoxia (<0.1% O_2) but the activation is not followed by the recruitment of the XRCC4-LIG4 complex (Bouquet *et al.*, 2011). This suggests that DSBs are not the source of DNA-PK activation, which is unsurprising in hypoxia. Importantly, similar to ATM, DNA-PK is also activated by chromatin changes in hypoxia. Specifically, DNA-PK activation in hypoxic cells is associated with histone acetylation (Bouquet *et al.*, 2011). Additionally, DNA-PK has also been shown to respond to replication stress through phosphorylation and recruitment to stalled replication forks (Ying *et al.*, 2016). However, the direct relationship between replication stress and DNA-PK in hypoxia has yet to be reported.

Interestingly, crosstalk between the PIKK kinases and HIF-1α has been observed. ATM appears to stabilise HIF-1α in hypoxia by phosphorylating it at serine 696, which upregulates Regulated in Development and DNA damage responses 1 (REDD1), a negative regulator of mammalian target of rapamycin complex 1 (mTORC1) signalling (Cam *et al.*, 2010). Similarly, both ATR and DNA-PK also stabilise HIF-1α in hypoxia (Bouquet *et al.*, 2011; Fallone *et al.*, 2013; Pires *et al.*, 2012). The precise oxygen-dependency of the interaction between the PIKK kinases and HIF-1α, and whether this is a DDR-independent function of the kinases, have yet to be investigated.

1.4.3 DNA repair

Despite activating the DDR, hypoxia also leads to the general repression of DNA repair pathways including HR and mismatch repair (MMR) (Olcina *et al.*, 2010). However, the repression of DNA repair pathways has been observed in a range of oxygen concentrations (<0.1-2% O_2) and not just in severe hypoxia (<0.1% O_2) and is seen as an attempt by tumour cells to reduce high-energy consuming processes (Hammond *et al.*, 2014). The downregulation of key components of the DNA repair pathways in hypoxia contributes to the genomic instability feature observed in hypoxic tumours (Bristow & Hill, 2008).

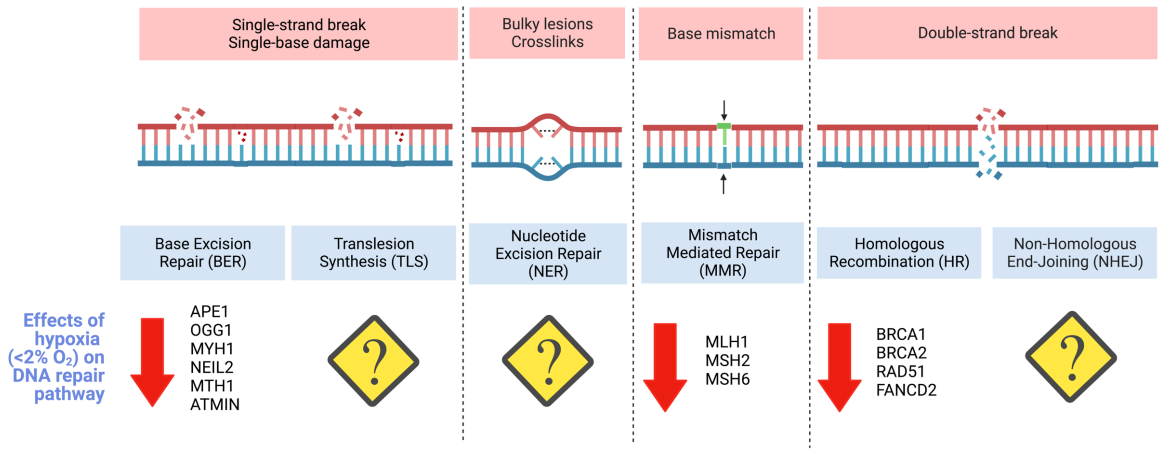


Figure 1.6 Effects of hypoxia on the DNA repair pathways. Hypoxia (<0.1-2% O_2) leads to the repression of base excision repair (BER), mismatch mediated repair (MMR) and homologous recombination (HR) pathways. The effects of hypoxia on translesion synthesis (TLS), nucleotide excision repair (NER) and non-homologous end-joining (NHEJ) are unclear. Figure created with BioRender.com

The inhibitory effects of hypoxia on HR and MMR are well-established (Scanlon & Glazer, 2015). Hypoxia transcriptionally downregulates key HR components including *BRCA1, RAD51* and *FANCD2* by the E2F transcription factor network (Bindra *et al.*, 2005; Bindra & Glazer, 2007; Scanlon & Glazer, 2014). Other HR components such as BRCA2 are also downregulated at the protein level in hypoxia (Fanale *et al.*, 2013). Additionally, as supported by increased microsatellite instability and frameshift mutations in hypoxia, hypoxia also reduces MMR capacity (Koshiji *et al.*, 2005; Mihaylova *et al.*, 2003; Rodríguez-Jiménez *et al.*, 2008). MMR genes such as *MLH1, MSH2* and *MSH6* are downregulated transcriptionally through different mechanisms. *MLH1* and *MSH2* are downregulated both at the mRNA and protein levels in severe hypoxia independently of HIF; *MSH2* and *MSH6* are repressed by HIF in mild hypoxia (Koshiji *et al.*, 2005; Mihaylova *et al.*, 2003).

The impact of hypoxia on nucleotide excision repair (NER) is less clear compared to HR and MMR. Severe hypoxia can reduce NER capacity as shown by decreased ability to repair UV irradiation-induced damage (Yuan *et al.*, 2000). However, one study showed that mild hypoxia (1.8% O_2) led to increased NER efficiency (Madan *et al.*, 2012). Moreover, it is unclear whether NER is repressed transcriptionally, as many NER genes have hypoxia HREs in their promoters (Rezvani *et al.*, 2010). The protein levels of XPA, XPB, XPD and XPG have been reported to be unchanged in hypoxia, whereas *ERRC1* is downregulated at both mRNA and protein levels in hypoxia (Dudás *et al.*, 2014; Mihaylova *et al.*, 2003; Yuan *et al.*, 2000).

How hypoxia affects NHEJ and translesion synthesis (TLS) is also less studied in comparison to HR and MMR pathways. Different studies claim that NHEJ factors increase, decrease or remain unchanged in hypoxia (Scanlon & Glazer, 2015). A proteomic study showed that NHEJ proteins increased in severe hypoxia, and another study showed that NHEJ repair efficiency increased in mild hypoxia (1.8% O_2) (Madan *et al.*, 2012; Ren *et al.*, 2013). On the other hand, one study showed that hypoxic cells have defective NHEJ (Kumareswaran *et al.*, 2012). As part of TLS, the DNA polymerase iota (Pol ι) is a low fidelity polymerase and has been observed to be upregulated by hypoxia via a HIF-1 binding site in its intron (Ito *et al.*, 2006). Interestingly, both NHEJ and TLS are error-prone repair pathways, therefore, if they are upregulated in hypoxia, and utilised more due to repression of HR, then they could contribute to increased mutagenesis.

Multiple genes involved in the base excision repair (BER) pathway have been shown to be repressed translationally in hypoxia, including *APE1, OGG1, MYH1, NEIL2* and *MTH1* (Chan *et al.*, 2014). Accordingly, the same study also showed that BER function is reduced in hypoxia. In addition, ATMIN, a protein that may play a role in the BER, is also repressed in hypoxic conditions (Kaplan & Glazer, 2020; Leszczynska *et al.*, 2016).

1.4.4 Unfolded protein response

The unfolded protein response (UPR) is a well-conserved intracellular pathway that maintains protein homeostasis (Hetz, 2012). This signalling response is activated upon detection of misfolded proteins in the endoplasmic reticulum (ER), the main site of folding and maturation for a range of proteins (transmembrane, secretory, cytosolic and ER-resident) (Liu & Kaufman,

2003). Once activated, the UPR leads to several outcomes, including global repression of translation to reduce protein-folding load, transcriptional induction of UPR genes to increase folding capacity, and ER-associated degradation (ERAD) to degrade any permanently damaged proteins (Cao & Kaufman, 2012; Trusina *et al.*, 2008; Tsai & Weissman, 2010; Walter & Ron, 2011; Wek & Cavener, 2007). Other notable downstream outcomes of the UPR include activating autophagy, apoptosis, as well as initiating an antioxidant response (Chandrika *et al.*, 2015; Cullinan & Diehl, 2004; Fribley *et al.*, 2009).

The UPR is divided into three distinct branches, each with their own transducer embedded in the ER membrane: inositol-requiring enzyme 1 (IRE1α), protein kinase R (PKR)-like endoplasmic reticulum kinase (PERK) and activating transcription factor 6 (ATF6). Each of these stress sensors are reversibly bound to UPR master regulator, glucose-regulated protein 78 (GRP78) under normal physiological conditions (Wang *et al.*, 2009). While bound to GRP78 via their luminal domains, the three UPR sensors are repressed and cannot be activated (Bertolotti *et al.*, 2000). Under conditions that induce ER stress, GRP78 disassociates from IRE1α, PERK and ATF6 to preferentially bind to unfolded proteins; this allows for the three sensors to be activated (Hetz, 2012). Both IRE1α and PERK activate by self-dimerising and autophosphorylating (Li *et al.*, 2010; Walter & Ron, 2011). Once activated, IRE1α triggers its RNase activity and characteristically splices X box-binding protein 1 (XBP1u) mRNA (Yoshida *et al.*, 2001). The spliced XBP1 (XBP1s) is translated into a protein transactivator of UPR genes involved in protein folding, glycosylation and ERAD (Lee *et al.*, 2003). In addition, activated IRE1α also degrades select mRNAs through IRE1-dependent decay (RIDD) and activates pathways such as those induced by JUN N-terminal kinase (JNK) and nuclear factor-κB (NF-κB) by binding to adaptor proteins (Hetz, 2012). When PERK is activated, it forms a dimer and

autophosphorylates, as identified by the formation of high molecular mass complexes of PERK (Bertolotti *et al.*, 2000). PERK is a well characterised member of the eIF2α kinase family; when activated PERK phosphorylates eIF2α, leading to attenuation of global translation (Trusina *et al.*, 2008). In response to phosphorylated eIF2α, the transcription factor activating transcription factor 4 (ATF4) is induced and upregulates the expression of ER stress response elements (Wortel *et al.*, 2017). GRP78 is thought to bind to ATF6 on its Golgi-localisation signal, hence masking its activation domain. Therefore, ATF6 activation leads to its transit to the Golgi apparatus, where it is cleaved (Ye *et al.*, 2000); the free ATF6 fragment (ATF6f) then translocates to the nucleus where it acts as a transcription factor upregulating GRP78 expression, as well as contributing to XBP1 splicing (Hillary & Fitzgerald, 2018). ATF6f also interacts with other transcription factors such as nuclear factor-Y (NF-Y), Ying Yang 1 (YY1), TATA-binding protein (TBP) and XBP1s (Hetz, 2012). It is worth noting that there is substantial crosstalk between the three branches of the UPR (Chang *et al.*, 2018).

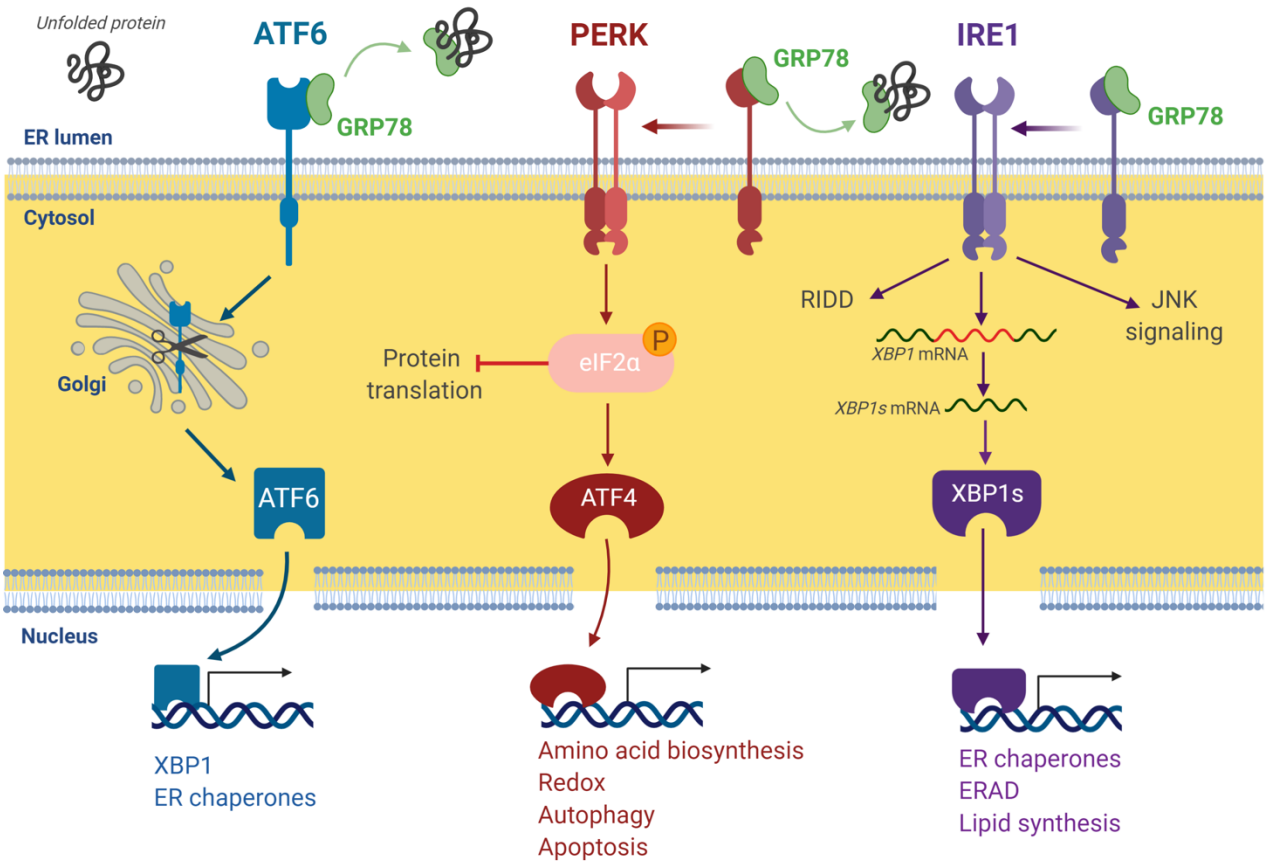


Figure 1.7 The unfolded protein response. Upon GRP78 disassociation, the activation of the three ER stress sensors (ATF6, PERK and IRE1) leads to a range of outcomes that restore protein homeostasis, including the transcriptional regulation of ER stress response genes in the nucleus. Figure created with BioRender.com.

Hypoxia leads to the accumulation of ER stress due to the reduction of disulfide bonds present in proteins (Koumenis *et al.*, 2007). It is estimated that one third of the eukaryotic proteome contains at least one disulfide bond; disulfide bonds exist in most secretory proteins and are absent in cytosolic proteins (Chang, 2016; Rajpal & Arvan, 2013). Most secretory proteins require disulfide bonds for folding and stability. Disulfide bonds introduced by protein disulfide isomerases (PDIs) during post-translational folding or isomerisation are oxygen dependent, as oxygen acts as the terminal electron acceptor in the redox relay reaction (Koritzinsky *et al.*, 2013). Once PDI has catalysed a disulfide bond formation, PDI itself must

be reoxidised by ER resident oxidases endoplasmic reticulum oxidoredudctin-1 alpha (ERO-1α) (Koritzinsky *et al.*, 2013).

Depending on the severity and duration of ER stress, the hypoxic UPR can lead to a myriad of outcomes. The transcription regulator C/EBP homologous protein (CHOP, also known as DDIT3) is induced in hypoxia downstream of the PERK/eIF2α/ATF4 arm and induces apoptosis in conditions of chronic or irreversible ER stress (Fels & Koumenis, 2006). NEF2-related factor-2 (NRF2) is induced downstream of PERK and mediates an antioxidant response to regulate redox homeostasis and contribute to cell survival (Cullinan & Diehl, 2004). Both PERK and IRE1α activate autophagy in response to hypoxia as a cytoprotective effect; IRE1α signalling may phosphorylate autophagy inhibitors BCL-2 and BCL-XL leading to their disassociation from autophagy inducer BECN1 and PERK/ATF4 induces the expression of ATG12 which induces autophagy (Akman *et al.*, 2021; Chipurupalli *et al.*, 2019). Importantly, the induction of the UPR in hypoxia is oxygen dependent as it is active in severe hypoxia (<0.1% O_2) and not in mild hypoxia (2% O_2) (Rzymski & Harris, 2007).

1.4.5 Reactive oxygen species (ROS)

One of the key consequences of hypoxia is the release and accumulation of reactive oxygen species (ROS) (Bell *et al.*, 2007; Brunelle *et al.*, 2005; Dirmeier *et al.*, 2002; Duranteau *et al.*, 1998; Guzy *et al.*, 2005; Killilea *et al.*, 2000; Mansfield *et al.*, 2005; Wood *et al.*, 1999). ROS is a broad term used to describe highly reactive chemical species that contain oxygen, including peroxides, superoxides, hydrogen peroxide (H_2O_2), hydroxyl radical, singlet oxygen and alpha-oxygen. Under normal physiological conditions, ROS are generated as a by-product of enzymatic reactions, such as those stemming from the NADPH oxidase complex, cytochrome

P450, lipoxygenase, cyclooxygenase, xanthine oxidase and peroxisomes (Galanis *et al.*, 2008). ROS can also be generated from the mitochondrial electron transport chain (ETC). Electrons generated from metabolic processes are funnelled into the mitochondrial ETC and accepted by oxygen, which can be converted into H_2O_2, diffusing into the cytoplasm where it can be partially reduced to form hydroxyl radicals, or fully reduced to form water (Turrens, 2003; Zhao *et al.*, 2019). Sometimes, electrons may also 'leak' from the ETC while being carried by ubiquinone, and their escape allow them to react with oxygen to form superoxides (Shields *et al.*, 2021). Finally, ROS can also be formed as a result of metal catalysed oxidation reactions (Collin, 2019).

ROS play roles in cell signalling, and can be generated in response to xenobiotics, cytokines and bacterial invasion (Ray *et al.*, 2012). ROS can contribute to signal transduction by modifying cysteine residues in redox-sensitive proteins; oxidation of specific reactive cysteine residues can subsequently lead to a change in enzymatic activity (Finkel, 2011). One such example is the activation of ATM in the absence of DSBs and the MRN complex, where oxidation of cysteine residues in ATM leads to a disulfide bond formation, allowing ATM to activate antioxidants such as superoxide dismutase (SOD) and catalase (Guo *et al.*, 2010). ROS have been observed to play cell signalling roles in programmed cell death, autophagy, mitochondrial fission and fusion, as well as proliferation. ROS can travel through cellular compartments such as through the mitochondria, nucleus, ER and peroxisomes; however, compartmentalisation of H_2O_2 can also occur upon stimuli e.g., growth factors, nutrients, by encapsulating the H_2O_2 in redoxsomes (Sinenko *et al.*, 2021). Of note, H_2O_2 is the most well-characterised ROS species in cell signalling, including its role in oxidising cysteine residues (Reczek & Chandel, 2017). However, ROS can also be deleterious to the cell. Oxidative stress

can result when there is an accumulation of ROS, either through an increase in ROS levels or a decrease in the antioxidant capacity of the cell (Galanis *et al.*, 2008). ROS are reactive due to the unpaired electron in the outer shell of oxygen. Therefore, an imbalance or excess ROS can lead to cellular insults where ROS can potentially damage macromolecules such as lipids, proteins and DNA (Thannickal & Fanburg, 2000). Specifically, oxidative damage includes lipid peroxidation, protein carbonylation, DSBs or conversion of guanine to 8-oxoguanine (8-oxoG) in the DNA, or damage to mitochondrial DNA (Massudi *et al.*, 2012; Moskalev *et al.*, 2013; Moskovitz & Oien, 2010; Park & Larsson, 2011). Hence, the cell has developed systems to tightly regulate the levels of ROS by quenching their reactivity through antioxidants such as glutathione, vitamin C and enzymes such as SOD and catalase. In addition, the Kelch Like ECH Associated Protein 1 (KEAP1)-NRF2 pathway has been established as the closest fit to a mammalian ROS receptor where NRF2 is the master regulator of the antioxidant response (D'Autréaux & Toledano, 2007).

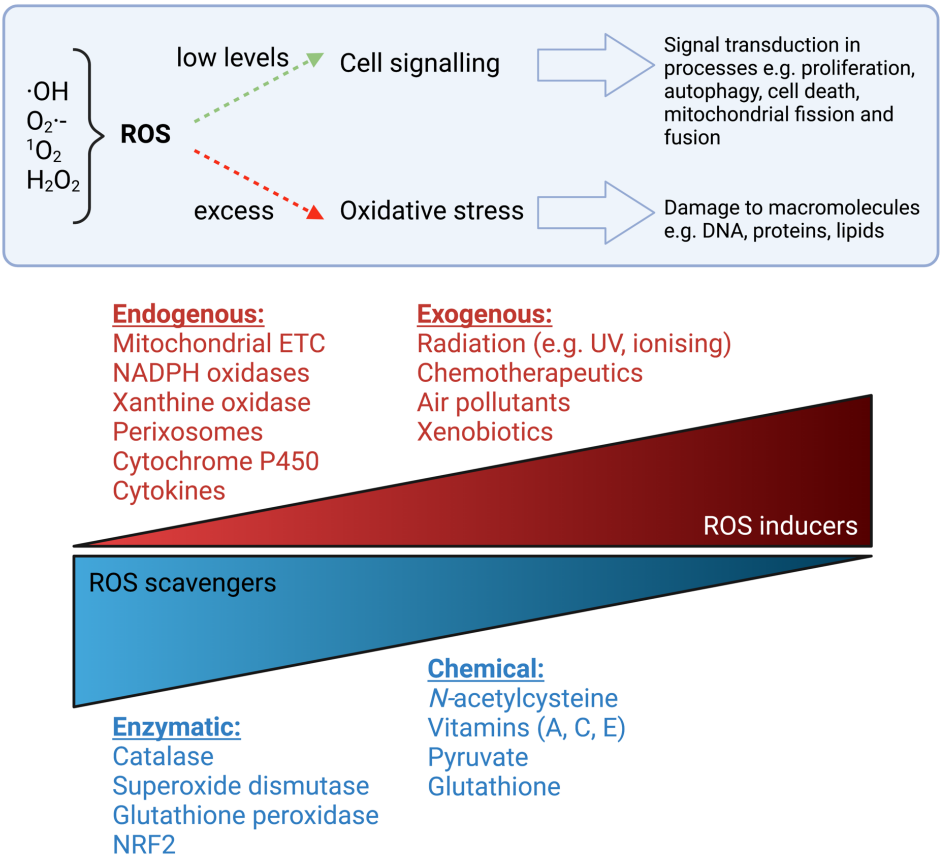


Figure 1.8 ROS inducers and scavengers, and cellular consequences of ROS. Different species of ROS can be generated in the cell; where low levels of ROS play a role in cell signalling, an excess of ROS leads to oxidative stress and damage of biomacromolecules. There are a range of ROS inducers (red) and ROS scavengers (blue). Figure created with BioRender.com

Paradoxically, ROS accumulates in hypoxia despite the reduced levels or absence of oxygen. The increase in ROS in hypoxia is primarily attributed to mitochondrial dysfunction, where electrons leak out of the mitochondrial ETC and generate ROS that contribute to the stabilisation of HIF-1α (Brunelle *et al.*, 2005; Chandel *et al.*, 1998; Guzy *et al.*, 2005; Mansfield *et al.*, 2005). Interestingly, hypoxia (1-2% O_2) requires mitochondrial ROS to stabilise HIF-1α whereas anoxia (0.0% O_2) stabilises HIF-1α by depriving PHD of its substrate, oxygen, without the need for mitochondrial ROS (Schroedl *et al.*, 2002). In addition, intracellular ROS is increased in an oxygen dose-dependent manner with lower oxygen levels inducing more ROS

(Bell *et al.*, 2007; Chandel *et al.*, 1998). Importantly, the increase in ROS is still observed in anoxia (0% O_2) (Dirmeier *et al.*, 2002; Zheng *et al.*, 2015).

Although not as well established, hypoxia also generates ROS through increasing the expression or activity of enzymes that generate ROS as a by-product. After the initial burst of mitochondrial ROS, which is curtailed after mitochondrial depolarisaton, hypoxia can induce ROS through the activity of xanthine oxidase (Abramov *et al.*, 2007). One study also showed that hypoxia induces the mRNA and protein levels of NADPH oxidase subunit 4 (NOX4), the activity of which contributes to an increase in ROS (Li *et al.*, 2008).

1.4.6 Repression of global transcription

Despite the activation of multiple stress pathways in severe hypoxia (<0.1% O_2), including the DDR, UPR and HIF-1α signalling, global transcription is repressed (Johnson, Denko and Barton, 2008; Ramachandran, Ma *et al.*, 2021). The global repression of RNA synthesis in hypoxia has been described as transcriptional stress. It has also been shown that hypoxia represses global transcription independently of HIF-1, and changes in global histone modifications may account for which genes are selectively activated and repressed (Johnson *et al.*, 2008). Mechanisms for how hypoxia represses the transcription of RNA polymerase II (RNA Pol II)-transcribed genes have been described. One study showed that Repressor Element 1-Silencing Transcription factor (REST) is induced in hypoxia and accounts for regulating 20% of hypoxia-repressed genes (Cavadas *et al.*, 2016). Another study showed that hypoxia induces the negative cofactor 2 (Dr1/DrAP1) which represses transcription by blocking the preinitiation complex assembly (Denko *et al.*, 2003).

However, most of the active transcription in the cell is attributed to RNA polymerase I (RNA Pol I)-mediated transcription of ribosomal DNA (rDNA) transcription into ribosomal RNA (rRNA) and not RNA Pol II mediated transcription. This is not surprising as the most abundant RNA species in the cell is rRNA (approximately 90% by mass), and the rDNA is the most actively transcribed region in the genome (Blobel & Potter, 1967; Duncan & Hershey, 1983; French *et al.*, 2003; Palazzo & Lee, 2015). The transcription of rDNA into rRNA is the first step in ribosome biogenesis, where a long precursor rRNA, known as the 47S, is transcribed. Transcription of rDNA occurs in the nucleolus where there are approximately 300 copies of the 13 kb rDNA sequence, interspaced with a 30 kb intergenic spacer (IGS). The tandem rDNA repeats are located on nucleolar organiser regions (NORs) distributed on the five acrocentric autosomes (chromosomes 13, 14, 15, 21, 22) in humans (van Sluis *et al.*, 2020). Interestingly, the rDNA repeats are one of the most unstable regions in the genomes due to deleterious recombination, therefore the rDNA genes have a unique amplification system to restore copy number (Kobayashi, 2014).

One study showed that under chronic hypoxic (1% O_2) conditions of 22 hours, rDNA transcription is repressed as levels of Upstream Binding Factor (UBF), which recruits RNA Pol I to rDNA promoter regions, are reduced, however this was dependent on acidic conditions concurrent with hypoxia treatment (Mekhail *et al.*, 2006). However, the mechanism of rDNA transcription repression in severe hypoxia (<0.1% O_2) at shorter or longer time points have yet to be studied.

1.5 R-loops

1.5.1 R-loops and their physiological functions

R-loops are three-stranded nucleic acid structures composed of a Watson-Crick RNA/DNA hybrid and a displaced non-hybridised ssDNA. R-loops were first described in 1976 by Thomas *et al.* and have become an increasingly popular area of research in the past decade as R-loops were found to be conserved structures in organisms ranging from bacteria to mammals and implicated in diseases such as cancer and neurodegeneration (Al-Hadid & Yang, 2016; Thomas *et al.*, 1976). While some use the terms RNA/DNA hybrids and R-loops interchangeably, others such as Santos-Pereira and Aguilera propose that RNA/DNA hybrids describe short structures that form transiently during lagging strand DNA synthesis or transcription at the active site of RNA polymerase during ribonucleotide triphosphate incorporation (Santos-Pereira & Aguilera, 2015). Instead, Santos-Pereira and Aguilera define R-loops as the longer form of RNA/DNA hybrids generated when the nascent RNA molecule hybridises with the template DNA in combination with the displaced ssDNA. Interestingly, RNA/DNA hybrids are more stable than double-stranded DNA (dsDNA) (Roberts & Crothers, 1992). Certain features on the DNA favour R-loop formation, including G-content, negative DNA supercoiling, DNA nicks, and the presence of G-quartets in the ssDNA (Duquette *et al.*, 2004; Roy *et al.*, 2010; Roy & Lieber, 2009; Santos-Pereira & Aguilera, 2015). R-loops also tend to form at repetitive sequences, such as transposable elements, rDNA, centromeres and telomeres (Arora *et al.*, 2014; Ginno *et al.*, 2012; Nadel *et al.*, 2015).

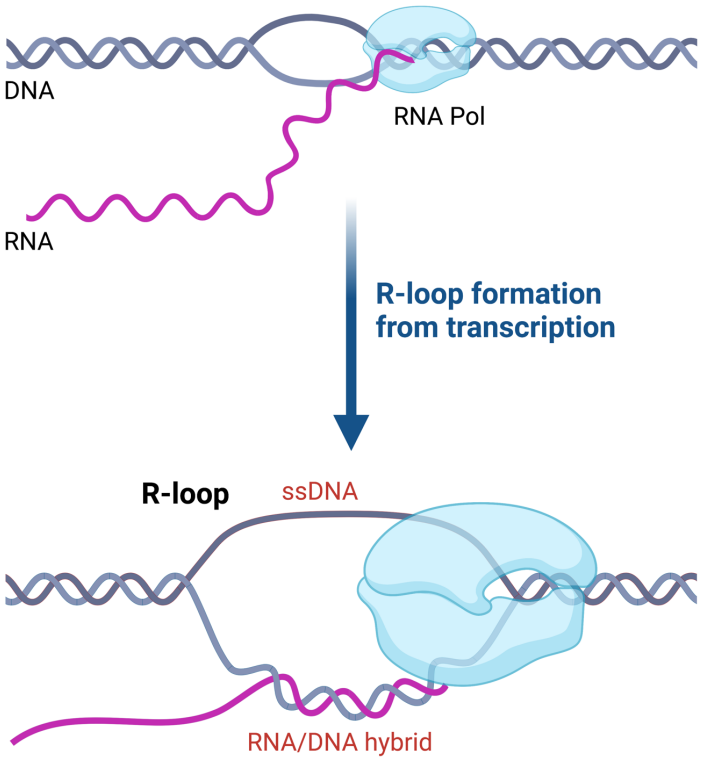


Figure 1.9. R-loops form from transcription. RNA polymerase generates a nascent RNA molecule from transcription. The RNA reanneals to the template strand from which it was transcribed. The resulting secondary structure is an R-loop, comprised of the RNA/DNA hybrid formed from Watson-Crick pairing and an exposed single-stranded DNA (ssDNA). Figure created with BioRender.com.

R-loops were found to play important physiological roles, including contributing to the mechanism behind class switch recombination (CSR). CSR, also known as antibody class switching, occurs in immunoglobulin genes of mature B cells in response to antigen stimulation signals (Stavnezer *et al.*, 2008). CSR allows the isotype of the immunoglobulin region to switch from μ (which corresponds to IgM) to other isotypes such as γ, α, or ε (which generate various IgG subtypes, IgA, or IgE) (Mackay *et al.*, 2020). Switch regions are required for CSR to occur; the switch regions share no consensus sequences but instead form R-loops

that exceed 1 kb. The R-loops formed on the switch regions do not lead to protein formation but are required to transcribe the gamma3 or gamma2b switch region needed for CSR (Stavnezer *et al.*, 2008).

Another physiological role that R-loops play is at promoters, where they can regulate gene expression. R-loops are abundant at promoters of genes transcribed by RNA Pol II (Chen *et al.*, 2017; Dumelie & Jaffrey, 2017; Nadel *et al.*, 2015; Sanz *et al.*, 2016). At promoters, R-loops may aid transcription by protecting the promoter DNA from methylation (Ginno *et al.*, 2012; Grunseich *et al.*, 2018). Promoter R-loops may also promote and inhibit binding of chromatin remodellers and transcription factors (Boque-Sastre *et al.*, 2015; Chen *et al.*, 2015). CpG islands in R-loop sequences have been shown to favour protein binding, however, the exact mechanism for distinguishing R-loops that recruit protein binding from those that inhibit protein binding is still unknown (Chen *et al.*, 2015). In addition, long non-coding RNA (lncRNA) may also form R-loops and bind to promoters. Clouetier *et al.* observed that the R-loops arising from lncRNA formed at promoters and coding regions, displaced repressors and promoted transcription (Cloutier *et al.*, 2016). Arab *et al.* found that antisense lncRNA TARID forms an R-loop at the TCF21 promoter; GADD45A acts as an epigenetic R-loop reader, reads the R-loop at TCF21 promoter, triggering local DNA demethylation and TCF21 expression (Arab *et al.*, 2019). Therefore, there are a myriad of mechanisms through which R-loops at promoters can regulate gene expression.

R-loops also play a role in mediating transcription termination. Studies have shown that R-loops are enriched at 3' end of select mammalian genes where they enable efficient termination of transcription (Skourti-Stathaki *et al.*, 2011, 2014; Zhang *et al.*, 2017). R-loops

at the 3’ end of the gene stall RNA Pol II downstream of the poly-adenylation sequence and require factors such as senataxin (SETX) and DExH-Box Helicase 9 (DHX9) to resolve them, and exonucleases such as 5’-3’ Exoribonuclease 2 (XRN2) to degrade the RNA, resulting in transcription termination. Loss of these factors, such as SETX, DHX9 and XRN2, lead to an accumulation in R-loops (Cristini *et al.*, 2018; Morales *et al.*, 2016; Skourti-Stathaki *et al.*, 2011).

1.5.2 R-loops and genomic instability

Despite the important roles of R-loops in normal physiology as described above, R-loops may become harmful if dysregulated. The dysregulation of R-loops has been linked to human diseases, especially cancer, neurological and autoimmune diseases (Richard & Manley, 2017). Mainly, R-loops can lead to genomic instability and DNA damage under certain contexts.

Firstly, R-loops may block replication. Transcription-replication collisions (TCRs) may occur as the transcription and replication machineries share the same DNA template. Therefore, it is unsurprising that R-loop mediated DNA damage seems to arise mainly during S phase (Gan *et al.*, 2011; Wellinger *et al.*, 2006). Interestingly, elegant studies in bacteria showed that when R-loops encountered replication forks in a head-on (HO) collision, the effects were more deleterious compared to when the collision was co-directional (C-D) (Lang *et al.*, 2017). HO collisions led to stalled replication, increased mutagenesis and prevented replication fork restart (Lang *et al.*, 2017). In human cells, Hamperl *et al.* found that HO TRCs induced ATR-CHK1 signalling, fork stalling and an increase in R-loop levels, whereas C-D TRCs induced ATM-CHK2 signalling, hybrid resolution and a decrease in R-loop levels (Hamperl *et al.*, 2017). In

addition, they found that replication stress and de-regulated origin firing induced HO TRCs and R-loops (Hamperl *et al.*, 2017).

Secondly, R-loops may also mediate transcriptional stress. Transcriptional stress can be described as excessive pausing, arrest or backtracking of RNA polymerases (Saponaro *et al.*, 2014). Paradoxically, although R-loops are often formed from transcription, they can also block transcription and further contribute to TRCs (Belotserkovskii *et al.*, 2017; Sollier & Cimprich, 2015). Whether R-loops are formed from RNA polymerases pausing, or R-loops themselves block upstream polymerases is unclear; however, both scenarios have been observed (Shivji *et al.*, 2018; X. Zhang *et al.*, 2017).

Ultimately, replication stress and transcriptional stress, both hallmarks of cancer, can contribute to and exacerbate TRCs (Bowry *et al.*, 2021). R-loops at TRCs can result in DSBs and replication fork collapse (Alzu *et al.*, 2012; Gan *et al.*, 2011; Tuduri *et al.*, 2009; Wahba *et al.*, 2011). Resolving R-loops through transcription-coupled nucleotide excision repair (TC-NER) pathway may also generate DSB in the process, which will be discussed below in **1.5.3**.

In addition, there are replication-independent mechanisms through which R-loops can cause pathologies or toxic effects. To start, the ssDNA portion of R-loops is prone to mutagenesis by xenobiotics and nucleases. For example, the Apolipoprotein B mRNA Editing Catalytic Polypeptide-like (APOBEC) family of enzymes bind to RNA and ssDNA and can deaminate deoxycytidine (dC) into deoxyuridine (dU) residues specifically on ssDNA (Sollier & Cimprich, 2015). Subsequently, BER enzyme DNA glycosylase may excise the uracil base, generating a DNA lesion. A mutational signature characterised by the activity of the APOBEC family of

cytidine deaminases is present in 14.4% of cancer samples (Alexandrov *et al.*, 2013). Interestingly, hypoxia, a hallmark TME trait of cancer, has been shown to induce APOBEC3B in cyclic conditions (Bader *et al.*, 2021). In a recent pre-print, APOBEC3B has been shown to bind to R-loops and contribute to R-loop mutagenesis (McCann *et al.*, 2021).

Another replication-independent manner through which R-loop dysregulation can cause defects is through transcription elongation. Co-transcriptionally formed RNA/DNA hybrids are needed to mediate elongation; when impaired, transcription elongation can lead to hyperrecombination (Huertas & Aguilera, 2003). R-loops are also implicated in DNA repair processes, and the inability to resolve R-loops can lead to accumulation of unrepaired DSBs (Cristini *et al.*, 2019). Finally, because R-loops are implicated in chromatin landscape and epigenetic signatures, their dysregulation can also lead to defective gene expression and regulation (Sanz *et al.*, 2016).

1.5.3 R-loops in DNA repair and the DDR

R-loops play a multifaceted role in DNA damage and repair, as they can cause DSBs through the mechanisms discussed, however, they may also partake in DNA repair pathways. Usually, DNA lesions that block transcription are repaired through TC-NER. Sollier *et al.* showed that when RNA/DNA hybrid processing factors such as Aquarius Intron-Binding Spliceosomal Factor (AQR) and SETX are depleted, or when topoisomerase I (TOP1) is inhibited, R-loops are induced; these R-loops are processed into DSBs by NER endonucleases XPF and XPG (Sollier *et al.*, 2014). Importantly, TC-NER factor Cockayne syndrome group B (CSB) is necessary for DSB formation (Sollier *et al.*, 2014). Whether generating DSBs to resolve R-loops through TC-NER is beneficial to the cell is still unclear.

Although R-loops are a potent source of DNA damage, they can also form after DNA damage, to either promote or inhibit DNA repair. Ohle *et al.* and Yashuara *et al.* show that R-loops promote DSB repair (Ohle *et al.*, 2016; Yasuhara *et al.*, 2018). In transcription-associated HR repair (TAHHR), RAD52 is recruited to the DSB in an R-loop dependent manner, and subsequent processing of the R-loop by XPG is required for repair by HR (Ohle *et al.*, 2016). Accurate repair of DSBs at transcriptionally active sites where R-loops serve as signal for the need for HR over NHEJ ensure that transcribed genes are protected from mutagenesis. Excessive removal of R-loops has been shown to reduce the efficiency of HR and NHEJ (Lu *et al.*, 2018). However, R-loops may also impede DNA repair. For example, persistent unscheduled R-loops may block the recruitment of DNA repair factors and affect the DNA flanking the DSB (Aguilera & Gómez-González, 2017). Unresolved R-loops at DSB sites can lead to chromosomal translocations and aberrant repair (Cohen *et al.*, 2018).

As previously mentioned, R-loops can lead to DDR signalling. Whereas R-loops from HO TCR induce ATR signalling, R-loops from C-D TCR leads to ATM signalling (Hamperl *et al.*, 2017). However, R-loops can also lead to non-canonical activation of ATM. In the absence of DSBs, blocking transcription can lead to R-loops that activate ATM (Tresini *et al.*, 2015). In addition, ssDNA binding protein RPA colocalises with R-loops throughout the whole cell cycle and not just in S phase (Nguyen *et al.*, 2017). Interestingly, R-loops at centromeres during mitosis can activate ATR in the absence of DNA damage, promoting faithful chromosome segregation (Kabeche *et al.*, 2018).

Conversely, the DDR can also mediate the resolution of R-loops. Interestingly, ATM, ATR and DNA-PK mediate the recruitment of SETX to TRC sites (Yüce & West, 2013). SETX was also found to interact with other DDR factors including MRE11, RAD50, and KAP1 (Yüce & West, 2013). Additionally, after DNA damage, ATR mediates the translocation of helicase DDX19 from the nuclear pore to the nucleus to resolve R-loops in an ATR/CHK1 dependent manner (Hodroj *et al.*, 2017).

It will be interesting to investigate how the cell distinguishes beneficial R-loops from harmful R-loops, and how different R-loops are read by the cell to carry out one of their many functions.

1.6 Aims of this study

To conclude, severe hypoxia (<0.1% O_2) leads to a unique stress response including the DDR, UPR and replication stress. Although the hypoxic induction of both the DDR and UPR had been reported, links between these two stress responses in hypoxia were not reported. Therefore, the first aim of this study was to investigate potential links between the DDR and UPR in hypoxia; do they interact in a way that promotes hypoxic cell survival?

In addition, at the start of this study hypoxia-induced replication stress had been described and attributed to reduced levels of nucleotides in these conditions (<0.1% O_2). We hypothesised that limited nucleotides were unlikely to be the only cause of hypoxia-induced replication stress and that given the significant impact on transcription observed in hypoxia, R-loops could also be relevant. At the time, R-loops in hypoxia had not been reported in the literature. Therefore, the second aim of this study was to investigate changes in R-loop levels

in hypoxia and determine if any changes observed were biologically significant to the hypoxic stress response.

Ultimately, the aim of this study was to deepen our understanding of the hypoxic stress response to allow for novel therapeutic strategies to be potentially identified in the future. For example, investigating potential links between the UPR and DDR may reveal UPR targets that can be inhibited in hypoxic tumours. Similarly, whether R-loops impact the hypoxic response may reveal another avenue for targeting hypoxic tumours beyond existing drugs that target replication stress.

Chapter 2 Methods and Materials

2.1 Methods

2.1.1 Cell culture

Cell lines listed were cultured in Dulbecco's modified Eagle's medium (DMEM) or Minimum Essential Media (MEM) supplemented with 10% foetal bovine serum (FBS) and 1% penicillin-streptomycin (P/S) solution. All cell lines were incubated in a humidified incubator at 37°C in 5% CO_2 and exponentially grown.

Mycoplasma testing of cells was routinely carried out using the HEK-Blue Detection kit (InvivoGen). Cells were grown in antibiotic free media for at least 48 hours before being harvested at 100% confluency. Cells were heated for 15 minutes at 100°C, 50 µL of which was added to 200 µL of HEK-Blue cells (1-3.5 x 10^5 cells/mL) in HEK-Blue detection medium (InvivoGen). Cells were plated in a 96 well plate along with positive and negative controls provided by the manufacturer and incubated for 24 under normal tissue culture conditions. Appearance of a pink colour indicated a negative result suggesting the absence of mycoplasma, whereas appearance of a blue colour indicated the presence of lipoprotein expressed by all types of bacteria and mycoplasma.

2.1.2 Cryopreservation of cell lines

Cells were grown until 70% confluence was reached. Cells were washed once with PBS, trypsinised, resuspended in 10 mL of fresh media and centrifuged at 150 x *g* for 5 minutes at RT (room temperature). The supernatant was removed, and the cell pellet was resuspended in 1-2 mL of media containing 10% FBS, 80% medium and 10% DMSO and placed in a 1.5 mL

cryovial (Thermo Scientific Nunc). The vial was placed in -80°C overnight in a Mr. Frosty container (Nalgene) before being stored in liquid nitrogen for long-term storage.

To recover cells, vials were removed from liquid nitrogen storage and thawed quickly in a 37°C water bath. Then, the thawed cells were transferred to 10 mL of pre-warmed media in a 15 mL falcon tube, centrifuged at 400 x *g* for 5 minutes at RT. The supernatant was removed, and the remaining cell pellet was resuspended in fresh media and placed in a 25 cm^2 flask.

2.1.3 Drug treatments

Drugs used for inducing DNA damage or replication stress include APH, ETP, Hu and NCS. Drugs used for inducing ER stress include Thaps and Tuni. Drugs used for inhibiting the UPR include AMG PERK 44 (PERKi), GSK2606414 (PERKi), 4μ8c (IRE1i), Ceapin-A7 (ATF6i). Drugs used for inducing ROS include H_2O_2, menadione, PQ and *t*BHP. Drugs used as ROS scavengers include catalase, NAC, Tempo and VitC. CPT was used to increase R-loops. DRB was used to decrease R-loops and transcription. CHX was used to inhibit translation. Supplier, stock and working concentrations can be found in **Table 2.3: Drugs**.

2.1.4 Short interfering RNA (siRNA) transfection

The Dharmafect-1 Transfection Reagent (Horizon Discovery) was used to transfect cells following the manufacturer's protocol. Cells were seeded in a 6-well plate using the appropriate cell density for the cell line and left overnight. The siRNA was incubated in FBS-free and antibiotic-free media. Separately, the Dharmafect-1 Transfection reagent was also incubated in FBS-free and antibiotic-free media. Both mixtures were left to incubate at RT for 5 minutes. The siRNA mixture was then mixed with the transfection reagent mixture and

incubated at RT for 20 minutes. The siRNA transfection mixture was then diluted in complete antibiotic-free media to a final concentration of 50 nM. The media on the seeded cells were discarded, and the siRNA transfection mixture was then added to the cells. Cells were incubated for 24 hours in a standard humified incubator at 37°C, after which the media was replaced with fresh complete antibiotic-free media. siRNA sequences can be found in **Table 2.8**.

2.1.5 Bacterial transformation

DH5α competent cells (Invitrogen) were thawed 20-30 minutes on ice from -80°C. 1-5 µL of plasmid DNA was gently mixed with 20-50 µL of competent cells in a microcentrifuge tube. Mixing was achieved by gently flicking the bottom of the tube. The plasmid DNA and competent cell mixture was incubated on ice for 20-30 minutes. The mixture was heat shocked at 42°C in a water bath for 45 seconds. The tube was incubated on ice again for 2 minutes. 800 µL of SOC media without antibiotic was added to the tube and incubated in a 37°C shaking incubator for 45 minutes. 100 µL of the transformation mixture was plated and spread onto 10 cm Luria broth (LB) agar plates containing the appropriate antibiotic and the plates were incubated upside down overnight at 37°C. The following day, a single colony was picked with a pipette tip and put into a 15 mL falcon containing 5 mL of LB supplemented with the appropriate antibiotic as a starter culture. The starter culture was incubated for 8 hours at 37°C in a shaker. Then, the 5 mL starter culture was propagated into 250 mL LB supplemented with the appropriate antibiotic in a 500 mL Erlenmeyer flask and incubated overnight at 37°C in a shaker. The bacterial cultures were ultra-centrifuged at 6000 x *g* at 4°C in ultra-centrifuge tubes. The pellets were stored long term at -20°C or purified on the same day.

2.1.6 Plasmid purification

The MaxiPrep Plasmid Purification kit (Qiagen) was used to purify the plasmids. Briefly, the bacterial pellets were lysed in buffer P1. Buffer P2 was added and mixed by inverting vigorously 4-6 times (not vortexed) and incubated at RT for 5 minutes. Chilled buffer P3 was added and mixed thoroughly by inverting vigorously 4-6 times and incubated on ice for 20 minutes. The mixture was then centrifuged at 20,000 x *g* for 30 minutes at 4°C. The supernatant was quickly collected, mixed, and centrifuged again at 20,000 x *g* for 15 minutes at 4°C. The supernatant was promptly added to a buffer QBT-equilibrated QIAGEN-tip 500, and the column was allowed to empty by gravity. The QIAGEN-tip was washed twice with buffer QC. The DNA was eluted with Buffer QF and precipitated by adding RT isopropanol, and centrifuged at 15,000 x *g* for 30 minutes at 4°C. The pellet was washed with RT 70% ethanol and centrifuged 15,000 x *g* for 10 minutes at 4°C. The pellet was left to air-dry at RT and was resuspended in Tris-EDTA (TE) buffer or diethyl pyrocarbonate (DEPC)-H_2O.

2.1.7 DNA plasmid transfection

Cells were transfected using jetPRIME® transfection reagent. Briefly, cells were seeded at 60-70% confluency and left overnight to attach on a 6 cm dish. The following day, 200 µL of jetPRIME® buffer was mixed with 2 µg of plasmid DNA in a microcentrifuge tube, vortexed for 10 seconds, and spun down. 4 µL of jetPRIME® reagent was added to the DNA/buffer mixture, vortexed for 10 seconds, and spun down. The transfection mixture was left to incubate at RT for 10 minutes. Then, cells were transfected by adding 200 µL of the transfection mixture directly onto 2 mL of media in the 6 cm dish of seeded cells in a drop-wise manner. The dish

was rocked gently back and forth. 16-20 hours post transfection, the media in the dish was replaced with fresh complete media.

2.1.8 Hypoxia treatment

Hypoxia treatments of <0.1% O_2 were carried out in a Bactron II anaerobic chamber (Shel Lab) and treatments of 2% O_2 in an M35 workstation (Don Whitley Ltd). For all hypoxia experiments, cells were plated on glass dishes except for colony survival assays, which were plated on 6-well plates. Oxygen concentrations were confirmed using an Oxylite probe (Oxford Optronix) and anaerobic indicator strips (Fisher Scientific).

2.1.9 Cell lysis and protein sample preparation

Cells were washed twice with PBS and harvested in UTB lysis buffer (9 M urea, 75 mM Tris-HCl pH 7.5, 0.15 M β-mercaptoethanol). Samples were sonicated for 20 seconds (s) twice with 10 s on ice in between before followed by centrifugation at 16000 x *g* for 10 minutes at 4°C.

2.1.10 Western blotting

10-100 µg of protein was mixed with sample buffer (3.3% SDS, 6 M urea, 17 mM Tris-HCl (pH 7.5), 0.07 M β-mercaptoethanol, 0.01% Bromophenol blue) and heated at 100°C for 10 minutes. 5 µL of protein ladder (Precision Plus Protein Standards, BioRad) was loaded for indication of molecular weight of the bands. Samples were electrophoresed in Tris-glycine running buffer (25 mM Tris base, 192 mM glycine, 0.1% (w/v) SDS) on 4-20% or 7.5% Mini-PROTEAN TGXTM pre-cast gels (BioRad) at 125 V for 75-120 minutes. Gels were electro-transferred onto a nitrocellulose membrane transblot (BioRad) on a Transblot-Turbo machine (BioRad) for 7 minutes in transfer buffer (25 mM Tris base, 150 mM glycine, 20% (v/v)

methanol). The membranes were placed in Intercept® Blocking Buffer (LI-COR) diluted 1:1 in Tris-Buffered Saline (TBS) (50 mM Tris-HCl, pH 7.6, 150 mM NaCl) for 1 hour of blocking. Membranes were probed with primary antibody (diluted in 1:1 of Intercept® Blocking Buffer (LI-COR):TBS-Tween) overnight at 4°C while shaking. Antibodies used are listed in **Table 2.4**. Membranes were washed 3 times in TBS-Tween for 10 minutes each time. Membranes were probed with IRDye 680/800 secondary antibody (diluted to 1:10000 in 1:1 Intercept® Blocking Buffer:TBSTween) for 1.5 hours at RT on a shaker. The membranes were then washed 3 times in TBS-Tween. The blots were developed using the Odyssey Infrared imaging system.

2.1.11 Puromycin incorporation assay

Cells were seeded and left to attach overnight. Puromycin was added to the cells at a final concentration of 1 μg/mL for 1 hour before being lysed in UTB buffer. Protein sample preparation was carried out as described in **2.1.9** and the samples were used in western blotting as described in **2.1.10**, using an anti-puromycin primary antibody (Kerafast) overnight at 4°C. Cells treated with 100 μM CHX for 1.5 hours as a positive control for significantly reducing puromycin incorporation.

2.1.12 Immunofluorescence microscopy

Cells on coverslips were washed once with PBS and fixed in 4% (w/v) paraformaldehyde in PBS for 10 minutes. The coverslips were washed 3 times with PBS to remove the paraformaldehyde. Cells were then permeabilised in 1% Triton-X-100 in PBS for 10 minutes, then blocked with 2% (w/v) BSA in 0.1% Tween-20 in PBS for 1 hour. Primary antibodies were incubated on coverslips for 2 hours at 37°C or overnight at 4°C. Coverslips were then washed 3 times with PBS before being incubated in secondary antibody for 1 hour at 37°C. Cells were

mounted onto slides using ProLong Gold Antifade Mountant with DAPI (Thermo Fisher). Cells were imaged using LSM710 confocal microscope (Carl Zeiss Microscopy Ltd). Antibodies used are listed in **Tables 2.4 and 2.5**.

For R-loop detection using S9.6 staining, coverslips were treated with RNase A for 1 hour at 37°C and, where indicated, with RNase H (NEB) for 24 hours at 37°C prior to blocking. Coverslips were then incubated with 1:100 diluted S9.6 antibody (Kerafast) for 36 hours at 4°C. Cells were mounted onto slides using ProLong Gold Antifade Mountant with DAPI (Thermo Fisher). Cells were imaged using LSM710 confocal microscope (Carl Zeiss Microscopy Ltd).

2.1.13 RNA extraction and purification

RNA was extracted using TRI reagent (Sigma) and purified with DNase I (NEB) treatment. At the end of treatment, cells were washed once with 2 mL of PBS before being scraped into 1 mL of TRI reagent (Sigma) and frozen at -20°C if needed. Samples were thawed on ice. 200 µL of 100% chloroform was added to each sample, vortexed for 15 s, incubated at RT for 2-3 minutes and centrifuged at 15000 x *g* for 15 minutes at 4°C. The supernatant was carefully removed and kept while the rest of the sample was discarded; 500 µL of 100% isopropanol was added to the supernatant. The samples were mixed and centrifuged at 15000 x *g* for 10 minutes at 4°C. The supernatant was discarded the pellet was resuspended in 1 mL of 70% ethanol, vortexed briefly, and centrifuged at 7500 x *g* for 5 minutes at 4°C. The supernatant was discarded, and the pellet was left to air dry for 20 minutes, resuspended in 60 µL of DEPC water (Fisher Scientific), heated in a 37°C oven for 3 minutes. The concentration of RNA was

measured using a NanoDrop™ spectrophotometer (Thermo Scientific) and the samples were frozen at -20°C if needed.

For DNase I (NEB) treatment, 1 µg of RNA was mixed with 0.2 units of DNase I and its reaction buffer, incubated at 37°C for 20 minutes. 1 µL of EDTA (0.5 M) was added to deactivate DNase I. Samples were incubated at 75°C for 10 minutes and RNA concentration was remeasured.

2.1.14 Complementary DNA (cDNA) synthesis through reverse transcription

500 ng of RNA was used to make cDNA using the Verso cDNA synthesis kit (Thermo Scientific). The RNA samples were mixed with cDNA synthesis buffer, dNTP mix, RNA primer, RT enhancer, Verso enzyme (Thermo Scientific) and DEPC water (Fisher Scientific) as shown in **Table 2.10**. The reaction was run in the PCR machine at 42°C for 60 minutes, 95°C for 2 minutes and held at 4°C. Samples were stored at -20°C if needed.

2.1.15 Quantitative PCR (qPCR)

Complementary DNA (cDNA) was prepared using the Verso cDNA synthesis kit (Thermo Scientific). SYBR Green PCR master mix (Applied Biosystems) and 7500 FAST Real-Time PCR machine (Applied Biosystems) were used. Forward and reverse primers (10 µM), SYBR Green PCR master mix, and DEPC water were added to cDNA samples as shown in **Table 2.11** in a 96 well plate. The run method was as follows: preparation at 50°C for 20 seconds and 95°C for 15 minutes; 40 cycles at 95°C for 15 seconds, 60°C for 30 seconds and 72°C for 30 seconds; melting curve at 95°C for 15 seconds, 60°C for 1 minute, 95°C for 30 seconds and 60°C for 15 seconds. The ΔΔCt method was used to determine relative mRNA fold change with 18S as the

reference gene. Primer sequences and working concentrations can be found in **Table 2.6: RT-qPCR primers**.

2.1.16 Click-iT nucleotide incorporation assay for EU and EdU

5-ethynyl uridine (0.5 mM) (Jena Bioscience) or EdU (10 µM) (Invitrogen/ Life Technologies) were added to cells on coverslips at the last hour or last 3 hours of treatment, respectively. After treatment, cells were washed once with PBS before being fixed in 4% (w/v) paraformaldehyde in PBS for 10 minutes at RT. Cells were washed twice with 3% BSA in PBS before being permeabilised with 0.1% Triton-X-100 in PBS for 15 minutes at RT. Cells were washed with 3% BSA in PBS before being incubated with 50 µL Click-iT buffer solution (Thermo Fisher) per coverslip for 30 minutes at RT in the dark. The coverslips were washed 3 times in PBS before being mounted onto slides with 25 µL of ProLong Gold Antifade Mountant with DAPI (Thermo Fisher). Cells were imaged using LSM710 confocal microscope (Carl Zeiss Microscopy Ltd) and a plug-in script on ImageJ was used to quantify the nuclear intensity. At least 100 cells were quantified per treatment.

2.1.17 CellRox/MitoSox assay for measuring reactive oxygen species levels (ROS)

During the last 30 minutes of treatment, cells were scraped, spun down and resuspended in 500 µL of complete media containing 5 µM CellRox Green (Invitrogen) or 5 µM MitoSox Red (Invitrogen) in a 1.5 mL microcentrifuge tube. The tubes were left on their side to incubate at 37°C in the dark. After 30 minutes, the cells were spun down, resuspended in 4% PFA, and incubated in the dark at RT for 10 minutes. After fixing, the cells were spun down, washed twice with PBS, then resuspended in 300 µL PBS. The samples were stored in the dark at 4°C and analysed within a day of fixing or were analysed immediately. Data acquisition was

carried out for 10,000 cells per experimental condition using the CytoFLEX flow cytometer (Beckman Coulter) and its respective CytExpert Software. Analysis after acquisition was carried out using the FlowJo software (BD Biosciences).

2.1.18 Fluorescence-activated cell sorting (FACS) using BrdU and PI

5 x 10^5 cells were seeded overnight and allowed to adhere. BrdU (20 µM) was added during the last hour of treatment and protected from light. Cells were trypsinised, resuspended in 2 mL of fresh media and centrifuged at 250 x g. The supernatant was removed, and the cell pellet was fixed in 1 mL of 70% ethanol while being vortexed and then chilled on ice for 30 minutes. For denaturation, samples were centrifuged at 250 x *g* for 5 minutes, had the ethanol supernatant removed and incubated in a HCl/ protease inhibitor mixture for 20 minutes at RT. For the first wash, samples were centrifuged at 2000 rpm for 5 minutes, had the HCl/ inhibitor supernatant removed, and resuspended in 2 mL PBS. For the second wash, samples were centrifuged at 450 x *g* for 5 minutes. The supernatant was removed, and the pellet was resuspended in 2 mL PBS containing 2% FBS. For antibody incubation, samples were centrifuged at 450 x *g* for 5 minutes; the supernatant was discarded, and the pellet was resuspended in 100 µL of BrdU antibody (1:50 in PBS 2% FBS) and incubated overnight at 4°C on a shaker in the dark. 2 mL of PBS was added to the samples, and they were centrifuged at 450 x *g* for 5 minutes. The samples were resuspended in secondary antibody solution (1:200 of Alexa Fluor 488- conjugated goat anti- mouse F(ab')2 fragment in PBS 2% FBS) for 60 minutes RT on a shaker in the dark. 1 mL of PBS was added before centrifugation at 450 x *g* for 5 minutes. The supernatant was removed, and the cell pellet was resuspended in propidium iodide (PI) staining solution containing PI (10 µg/ml) and RNase A (100 µg/ml) mixture and incubated at 37°C for 30 minutes. Data acquisition was carried out for 10,000

cells per experimental condition using Becton Dickinson FACSort flow cytometer and CellQuest Pro and ModFit LT software. Analysis after acquisition was carried out using the FlowJo software (BD Biosciences).

2.1.19 Clonogenic survival assay

Cells were trypsinised into a single-cell suspension and counted. 300-10,000 cells (depending on the plating efficiency of the cell line and whether the cells will be treated with ionising radiation) were plated into each well in 6-well plates, with 3 technical replicates per treatment. Cells were left to settle for 2-3 hours before drug treatment in combination with hypoxia treatment. After treatment, media containing the drug was replaced with fresh media and the cells were left to form colonies for 7-9 days in a humidified incubator at 37°C. The media was carefully removed, and crystal violet (0.5% w/v) in 50% methanol and 20% ethanol was added to the wells to stain and visualise the colonies. Colonies containing at least 50 cells were counted using a colony counter.

2.1.20 R-loop detection by RNaseH1^{D210N}

Cells were seeded and left overnight to attach. The following day, the RNaseH1^{D210N}-V5 plasmid (Addgene) DNA was transfected into the cells as described in **2.1.7**. 16-20 hours after transfection, the transfection mixture was replaced with fresh media. CPT (10 μM, 1 hour) and DRB (100 μM, 1 hour) treatments were used as controls to increase and decrease R-loops, respectively. At the end of treatment, cells were washed once with PBS, and incubated with ice-cold 0.2% Triton-X-100 for 2 minutes for pre-extraction. Cells were washed twice with PBS then fixed with 4% PFA for 10 minutes and washed 3 times with PBS. Immunofluorescence staining was carried out as described in 2.2.12 specifically with an anti-mouse V5 primary

antibody (Invitrogen) at 1:500 for 1 hour at RT, then with an Alexa Fluor 488- conjugated goat anti-mouse secondary antibody (Invitrogen) at 1:250 for 1 hour at RT. After microscopy, the nuclear intensity of V5 fluorescence was measured using ImageJ/ FIJI.

2.1.21 DNA/RNA immunoprecipitation (DRIP)

DNA/RNA immunoprecipitation (DRIP) was carried out as described in (Cristini *et al.*, 2018, 2019) with slight modifications. Isolated cell nuclei were harvested and lysed in nuclear lysis buffer (50 mM Tris-HCl pH 8.0, 5 mM EDTA, 1% SDS) on ice. Protein digestion was carried out for 3 hours at 55°C with 5 µL of 10 mg/mL proteinase K (Sigma Aldrich Aldrich). Genomic DNA was precipitated and resuspended in IP dilution buffer (16.7 mM Tris-HCl pH 8.0, 1.2 mM EDTA, 167 mM NaCl, 0.01% SDS, 1.1% Triton X-100). The samples were then treated with or without RNaseH (New England Biolabs) at 1.7 U/µg DNA for 2.5 hours at 37°C. Optimal DNA sonication conditions for each cell line were determined prior to the experiment. DNA was sonicated (Diagenode Bioruptor) at high frequency with each cycle being 1 minute (30 seconds on, 30 seconds off) for the optimal number of cycles. Sonication of DNA was confirmed by running 5 µL of the DNA on a 1.5% agarose gel. Once successful sonication was confirmed, the samples were pre-cleared using BSA-blocked DynaBeads Protein A (Thermo Fisher) for 1 hour at 4°C on a rotating wheel at 16 rpm. The beads were isolated using DynaMag (Thermo Fisher) and the supernatant containing genomic DNA was kept. Immunoprecipitation was carried out by incubating equal concentrations of genomic DNA with either S9.6 antibody (Kerafast) or IgG control overnight at 4°C on a rotating wheel at 16 rpm. The following day, BSA-blocked DynaBeads Protein A (Thermo Fisher) were used to pull down the immunoprecipitated complexes for 1.5 hours at 4°C on a rotating wheel at 16 rpm. The beads were washed for 5 minutes each at 4°C on a rotating wheel in wash buffer A (20

mM Tris-HCl pH 8.0, 2 mM EDTA, 150 mM NaCl, 0.1 % SDS, 1% Triton X-100), wash buffer B (20 mM Tris-HCl pH 8.0, 2 mM EDTA, 500 mM NaCl, 0.1% SDS, 1% Triton X-100), wash buffer C (10 mM Tris-HCl pH 8.0, 1 mM EDTA, 250 mM LiCl, 1% sodium deoxycholate (DOC), 1% IGEPAL®) and twice with wash buffer D (10 mM Tris-HCl pH 8.0, 1 mM EDTA). The DNA was then eluted with elution buffer (100 mM $NaHCO_3$, 1% SDS) at RT for 30 minutes on a rotating wheel and treated with 1.1 µL of 10 mg/ml proteinase K (Thermofisher) in digestion buffer (0.4M Tris-HCl pH 6.5, 0.1M EDTA) for 2 hours at 45°C. DNA purification was carried out as in **2.1.22**. Analysis was carried out using qPCR as described in **2.1.15**. The amount of immunoprecipitated material at a particular gene region was calculated as the percentage of input after subtracting the background signal (IgG control). The values were then normalised to the normoxic untreated condition of the promoter primer. Sequences of DRIP primers are available in **Table 2.7**.

2.1.22 DNA purification

The QIAquick PCR purification kit (Qiagen) was used to purify DNA from the DRIP protocol from 2.2.23. Briefly, 5 volumes of buffer PB was added to sample. If the mixture turned orange or violet, 10 µL of 3 M sodium acetate, pH 5, was added and mixed. The mixture was added to purification columns. Columns were centrifuged at 13,000 X *g* for 1 minute at RT and the effluent was discarded. The columns were washed with wash buffer PE and centrifuged at 13,000 X *g* for 1 minute at RT. The DNA bound to the column was eluted with 100 µL buffer EB and centrifuged at 13,000 X *g* for 1 minute at RT. DNA was stored at 4°C or -20°C for long term storage.

2.2 Image analysis

2.2.1 Foci quantification

The script in **Figure S2.1** was used in FIJI/ImageJ to quantify the number of foci per cell. 3 parameters were determined using the script to quantify each experiment, including: DAPI channel number, foci channel number, and prominence. The prominence value was determined by testing a range of prominence values. The prominence value which quantified none or very few foci in the negative control and a high number of foci in the positive control was picked. The prominence value was kept constant for analysing images from each experimental repeat.

2.2.2 Nuclear intensity

The ImageJ/FIJI algorithm in **Figure S2.2** was used as a plug-in to quantify the nuclear intensity of 5'EU, RNaseH1^{D210N}-V5 or 8-oxoguanine. The script required the user to specify which channel number was DAPI, and which channel number was the 5'EU, RNaseH1^{D210N}-V5 or 8-oxoguanine that needed to be quantified.

2.3 Bioinformatics

2.3.1 Overlapping genes

Lists of genes of interest were collated using RNA-seq datasets from our lab and other online datasets from published papers (Cristini *et al.*, 2018; Dungrawala *et al.*, 2015; Kavanaugh *et al.*, 2015; Luhr *et al.*, 2019; Olivieri *et al.*, 2020; Raina *et al.*, 2014; Sirbu *et al.*, 2013; Wang *et al.*, 2018). Hypoxia-induced genes and UPR-induced genes of interest were determined using the minimum two-fold increase cut-off. Two or more lists of genes were put into Microsoft

Excel. The 'highlight duplicates' function was used on the lists. The highlighted genes were identified as overlapping genes between the lists of genes of interest.

2.3.2 Gene set enrichment analysis (GSEA) of hypoxia-induced UPR genes

The GSEA analysis software was downloaded from the UC San Diego Broad Institute website https://www.gsea-msigdb.org/. The 'hallmark gene sets' was downloaded from the Molecular Signatures Database (MSigDB). Hypoxia-induced UPR genes were determined by overlapping gene lists using the method in **2.4.1**. The 4 files were prepared: expression dataset, phenotype labels, gene sets and chip annotations files. The files were uploaded onto the GSEA analysis software. The correct parameters were chosen, and the software was run, generating normalised enrichment score (NES) for the 'hallmark gene sets' pathways for the hypoxia-induced UPR genes.

2.4 Statistical analysis

Statistical tests were carried out using GraphPad Prism software (GraphPad Software Inc.) and include two-way ANOVA and 2-tailed Student's t test. *=p<0.05, **=p<0.01, ***=p<0.001 and ****=p<0.0001. Data shown from experiments with three independent repeats (n=3) represent mean ± standard error of the mean (SEM) unless stated otherwise.

2.5 Materials

Table 2.1 Cell lines used in this study

Cell line name	Tissue type	Growth media	Source of cells
A549	human lung adenocarcinoma	DMEM, 10% FBS, 1% P/S	American Type Culture Collection (ATCC)
RKO	human colorectal carcinoma	DMEM, 10% FBS, 1% P/S	American Type Culture Collection (ATCC)
HCT116	human colorectal carcinoma	DMEM, 10% FBS, 1% P/S	Gift from Professor Bert Vogelstein
MRC5	human foetal lung fibroblast	MEM, 10% FBS, 1% P/S	Gift from Professor Geoff Higgins

Table 2.2 Chemicals and cell culture reagents

Name	Producer/UK distributor
5-ethynyl-2'-deoxyuridine (EdU)	Invitrogen/ Life Technologies
5-ethynyl uridine (5' EU)	Jena Bioscience
β-mercaptoethanol	Fisher Scientific
Blocking Buffer LI-COR	LI-COR
Bromodeoxyuridine (BrdU)	Millipore
Dulbecco's modified Eagle's medium (DMEM)	Sigma-Aldrich UK
Diethyl pyrocarbonate water (DEPC water)	Fisher Scientific
Dimethylsulphoxide (DMSO)	Fisher Scientific
Ethanol	Fisher Scientific
Foetal bovine serum (FBS)	Autogen Bioscience
Formaldehyde	Sigma-Aldrich UK
Gel Loading Buffer II	Fisher Scientific
Glycerol	Fisher Scientific
Glycine	Sigma-Aldrich UK
Hydrochloride acid (HCl)	Sigma-Aldrich UK
Methanol	Fisher Scientific
Phosphate buffer saline (PBS)	Fisher Scientific
ProLong® Gold 4',6-diamidino-2-phenylinodole (DAPI)	Invitrogen/ Life Technologies
Propidium iodide (PI)	Sigma-Aldrich UK
Protease inhibitor (Pi)	Roche
RNAse A (ribonuclease A)	Sigma-Aldrich UK
RNase H (ribonuclease H)	New England Biolabs
Sodium dodecyl sulphate (SDS)	Fisher Scientific
Sodium chloride (NaCl)	Sigma-Aldrich UK
SYBR® Green	Applied Biosystems
Tris-Base	Sigma-Aldrich UK
Triton-X-100	Fisher Scientific
TRIzol®	Invitrogen/ Life Technologies
Trypan blue	Invitrogen
Trypsin 0.05% EDTA	Sigma-Aldrich UK
Tween 20	Fisher Scientific
Urea	Fisher Scientific

Table 2.3 Drugs used in this study

Name	Stock concentration and solvent; storage temperature	Final working concentration	Supplier
4μ8c (IRE1α inhibitor)	100 mM; DMSO; -20°C	20 μM	Sigma
5,6-Dichlorobenzimidazole 1-β-D-ribofuranoside (DRB)	100 mM; DMSO; -20°C	100 μM	Sigma
AMG PERK 44 (PERK inhibitor)	100 mM; DMSO; -20°C	20 μM	Tocris Bioscience
Aphidicolin (APH)	10 mM; DMSO; -20°C	30 μM	MedChemExpress
Camptothecin (CPT)	12 mM; DMSO; -20°C	10 μM	Sigma
Catalase from bovine liver	Powder, -20°C	2000 units/mg	Sigma
Ceapin-A7 (ATF6 inhibitor)	10 mM; DMSO; -20°C	10 μM	Sigma
Cycloheximide (CHX)	100 mg/mL; DMSO; -20°C	100 μM	Sigma
Etoposide (ETP)	25 mM; DMSO; -20°C	25 μM	Sigma
GSK2606414 (PERK inhibitor)	100 mM; DMSO; -20°C	10 μM	Calbiochem
Hydrogen peroxide (H_2O_2)	30% w/w in water	5 mM	Sigma
Hydroxyurea (Hu)	1 M; water; -20°C	2 mM	Sigma
Menadione	100 mM; DMSO; -20°C	100 μM	Sigma
MitoPQ (PQ)	10 mM; DMSO; -20°C	10 μM	Cayman Chemical
MitoTempo (Tempo)	10 mM; DMSO; -20°C	10 μM	Sigma
N-acetylcysteine (NAC)	100 mM; PBS; -20°C; pH 7.4	5 mM or 20 mM	Sigma
Neocarzinostatin (NCS)	500 μg/mL; none; 4°C	200 ng/mL	Sigma
Puromycin	5 mg/ mL; water; -20°C	5 μg/ mL	Fisher Scientific
Tert-Butyl hydroperoxide (*t*BHP)	70% w/w; water; 4°C	20 μM	Sigma
Thapsigargin (Thaps)	2 mM; DMSO; -20°C	2 μM	MP Biomedicals
Tunicamycin (Tuni)	5 mg/mL; DMSO; -20°C	5 μg/mL	MP Biomedicals
Vitamin C (VitC)	50 mM; water; -20°C	2 mM	Sigma

Table 2.4 Primary antibodies

Name	Species	Dilution	Application	Producer	Product code
53BP1	Rabbit	1:500	IF	Novus Biologicals	NB100-305
β-Actin	Mouse	1:10000	WB	Santa Cruz	AC-15
β-Tubulin	Rabbit	1:10000	WB	Cell Signaling	2146S
ATF4	Rabbit	1:50	IP	Cell Signaling	D4B8
ATM	Rabbit	1:1000	WB	Cell Signaling	2873
ATR	Mouse	1:1000	WB	Santa Cruz	sc-515173
CHK1	Mouse	1:1000	WB	Santa Cruz	sc-8408
CHK1-S345	Rabbit	1:1000	WB	Cell Signaling	2348
CHK2	Mouse	1:1000	WB	Millipore	05-649
CHK2-T68	Rabbit	1:1000	WB	Cell Signaling	2661
Fibrillarin	Mouse	1:100	IF	Abcam	ab-4566
GRP78	Mouse	1:1000	WB	BD Biosciences	610979
H2AX	Rabbit	1:1000	WB	Millipore	07-627
γ-H2AX	Mouse	1:250/1:1000	IF/WB	Millipore	05-636
HIF-1α	Mouse	1:500	WB	BD Biosciences	NB100-105
IgG	Mouse	1:100	IP	Invitrogen	10400C
KAP1	Rabbit	1:1000	WB	Bethyl Laboratories	A300-274A
KAP1-S824	Rabbit	1:1000	WB	Cell Signaling	4127S
Lamin B2	Rabbit	1:1000	WB	Abcam	ab-97513
Nucleolin	Rabbit	1:100/1:1000	IF/WB	Abcam	ab-50279
p53 (DO-1)	Mouse	1:2000	WB	Santa Cruz	sc-126
p53-S15	Rabbit	1:1000	WB	Cell Signaling	12571
PERK	Rabbit	1:1000	WB	Cell Signaling	3192
Puromycin	Mouse	1:1000	WB	Kerafast	3RH11
RPA32	Rat	1:250/1:1000	IF/WB	Cell Signaling	2208
RPA32 S4/8	Rabbit	1:1000	WB	Bethyl Laboratories	A300-245A
S9.6	Rabbit	1:100/10 μg: 20 μg	IF/DRIP	Kerafast	Kf-Ab01137-23.0
SETX	Rabbit	1:1000	WB	Bethyl Laboratories	A301-105A
V5	Mouse	1:500	IF	Invitrogen	46-0705

Table 2.5 Secondary antibodies

Name	Species	Dilution	Application	Producer	Product code
IRDye 800CW donkey anti-mouse IgG	Mouse	1:10000	WB	LI-COR	926-32212
IRDye 680RD Goat anti-Mouse IgG	Mouse	1:10000	WB	LI-COR	926-68070
IRDye 800CW donkey anti-rabbit IgG	Rabbit	1:10000	WB	LI-COR	926-32213
IRDye 680RD Goat anti-Rabbit IgG	Rabbit	1:10000	WB	LI-COR	926-68071
IRDye 800CW Goat anti-Rabbit IgG	Rabbit	1:10000	WB	LI-COR	926-32211
Alexa Fluor 488-conjugated goat anti-rabbit IgG	Rabbit	1:250	IF	Invitrogen	A32731
Alexa Fluor 594-conjugated goat anti-rat IgG	Rat	1:250	IF	Invitrogen	A11007
Alexa Fluor 488-conjugated goat anti-mouse F(ab')2 fragment	Mouse	1:250	IF	Invitrogen	A11017
Alexa Fluor 488-conjugated goat anti Rat	Rat	1:250	IF	Invitrogen	A11006

Table 2.6 Primers for RT-qPCR

Gene	Forward	Reverse
18S	GCCCGAAGCGTTTACTTTGA	TCCATTATTCCTAGCTGCGGTATC
AQR	GGCGGCATTAGCTGAAACTG	CAGCTGTAAGCCCATCCACA
DHX9	GCCAATTTCTGGCCAAAGCA	CGAGGCTCAATGGGGAGTTT
PIF1	CGAGCCTAGCACAGAAGCC	CCCAGGATTCGCTTTAGCAG
Primer set 1	ACCTGTCGTCGGAGAGGTTG	GTCACCGTGAGGCCAGAG
RNaseH1	CCTGTACTTACTGGTGTGGA	CCGTGTGAAAGACGCATCTG
RNaseH2B	GCATCTTGTTGCTGAAACTTC	TCCTTGTCAGTGGAAGCTTG
RTE1L	GGACTTGGTCAAGAGCGGAA	AGTCAGGTCAAAGGATGCCG
SETX	CTTCATCCTCGGACATTTGAG	TTAATAATGGCACCACGCTTC

Table 2.7 Primers for DRIP-qPCR

Gene	Forward	Reverse
D1	GGTATATCTTTCGCTCCGAGTC	ACAGGTCGCCAGAGGACAG
D2	TGGCGCTAAACCATTCGTAG	GTCGAGGGCTGACTTTCAATAG

Table 2.8 siRNA sequences

Name of siRNA	Target sequence(s)	Company
siATF4	CCACGUUGGAUGACACUUGdTdT	Dharmacon
siPERK	CCAAUGGGAUAGUGACGAA, GGUAGGAUCUGAUGAAUUU, GCAAUUAGCCUUAAGUUGU, AAAUUUGGCUGAAAGAUGA	Dharmacon
siSETX	CCAAUUGCUCCUUUCAGGUGUUUGA	Dharmacon

Table 2.9 Plasmids

Name of plasmid	Source
pHyPer-Nuc	Evrogen
RNaseH1^{D210N}-V5	Addgene #111904
RNaseH1^{WT}-GFP	Gift from Professor Natalia Gromak
RNaseH1^{WT}-V5	Addgene #111906
RNaseH1^{WKKD}-V5	Addgene #111905

Table 2.10 Components used to make up the reaction mix for reverse transcription

Reagent	Volume/well (µL)
RNA sample	5
cDNA synthesis buffer	2
dNTP mix	1
RNA primer	0.5
RT enhancer	0.5
Verso enzyme	0.5
DEPC water	0.5

Table 2.11 Components used to make up the reaction mix for qPCR

Reagent	Volume/well (µL)
SYBR Green PCR Master Mix (Applied Biosystems)	12.5
Forward primer	2.5
Reverse primer	2.5
DEPC water (Fisher Scientific)	2.5
cDNA	5

Table 2.12 Cell lines and their plating efficiencies

Cell line	Seeding density of cells		Plating efficiency
A549	250	6-well plate	80%

Chapter 3 Links between the unfolded protein response and the DNA damage response in hypoxia

3.1 Introduction

As radiobiological hypoxia (<0.1% O_2) is a unique stress response that induces both the UPR and DDR, we asked whether there are genes upregulated by one stress pathway that can affect the other, and potentially contribute to the pro-survival phenotypes of hypoxic tumours. Potential synergy between the two stress pathways may allow hypoxic tumours to confer resistance to therapy and malignant progression. While inhibiting the DDR is a well-established strategy for sensitising cancer cells to radiation or chemotherapy, targeting the UPR for the same purpose has not been explored to the same extent, much less in hypoxia.

Firstly, because hypoxia induces both stress responses (UPR and DDR) we made use of the combination of pharmacological agents to induce one response and not the other as a means to identify links. Thapsigargin (Thaps) and tunicamycin (Tuni) are pharmacological UPR inducers that cause ER stress by blocking the SERCA calcium pump on the ER membrane and by blocking N-linked glycosylation, respectively (Doan *et al.*, 2015, Wyszynski *et al.*, 2012). Hu depletes dNTP pools by inhibiting RNR, Aphidicolin (APH) generates long stretches of ssDNA by inhibiting DNA polymerases α, ε and δ; both lead to stalled replication forks (Vesela *et al.*, 2017).

Secondly, we designed and conducted a systematic review to determine what links have already been reported between the UPR and DDR in hypoxia in literature. This approach ensured that we did not omit any pivotal studies that might have already identified genes that connect the UPR with the DDR in hypoxic conditions.

Given that both the UPR and DDR are major transcriptional responses, we hypothesised that the combination of our approaches would identify genes that may warrant follow-up investigation in the lab.

3.2 Results

3.2.1 Pharmacological induction of replication stress does not induce the UPR

To begin investigating the potential links between the DDR and UPR in hypoxia (<0.1 O_2), we needed to separate the two pathways because concurrent induction of both makes it difficult to study their interactions without confounding effects. The concurrent induction of both pathways can be observed on a western blot; we treated human lung adenocarcinoma A549 cells to a time course in hypoxia (<0.1% O_2) and as expected, saw an increase in levels of UPR master regulator GRP78, as well as that of DDR marker γ-H2AX (**Figure 3.1**). We also observed the UPR transmembrane sensor PERK being activated, as indicated by an electrophoretic shift on a western blot as a result of autophosphorylation (DuRose *et al.*, 2006).

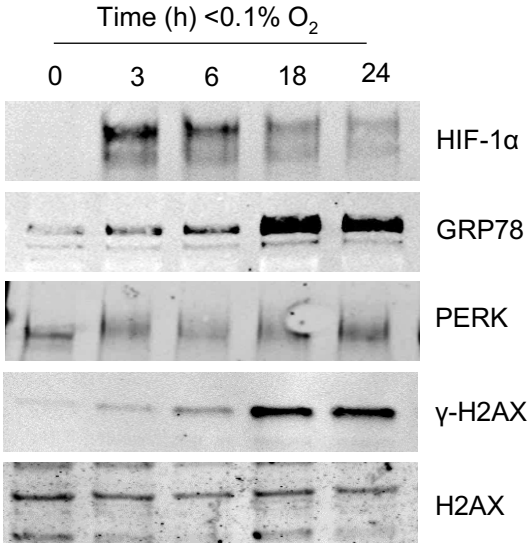


Figure 3.1. Hypoxia leads to the concurrent induction the UPR and DDR. A549 cells were exposed to a time course in hypoxia (<0.1% O_2). Whole cell lysates were collected for western blotting of UPR and DDR proteins. Increased GRP78 and shift in PERK are indicative of a UPR. Phosphorylation of H2AX (γ-H2AX) signify a DDR. H2AX was used as a loading control. n=3

One method to separate the two pathways is to use pharmacological agents as our tools to induce only one stress response and not the other. Therefore, as a first step it was important to determine if these agents did indeed induce either a DDR or UPR or, if like hypoxia, they induced both pathways (which would render them as unsuitable tools in our study). Whether replication stress alone in the absence of DSBs leads to ER stress and a UPR has not been explicitly investigated. Therefore, we treated A549 cells with established replication stress inducing agents Hu or APH in normoxia (21% O_2) and blotted for the transmembrane sensor PERK. As expected, Hu and APH led to replication stress as confirmed by phosphorylation of RPA and p53. The positive control Thaps led to a UPR, as shown by PERK shifting on the western blot. PERK did not appear to be autophosphorylated in Hu- and APH- treated cells (**Figure 3.2**).

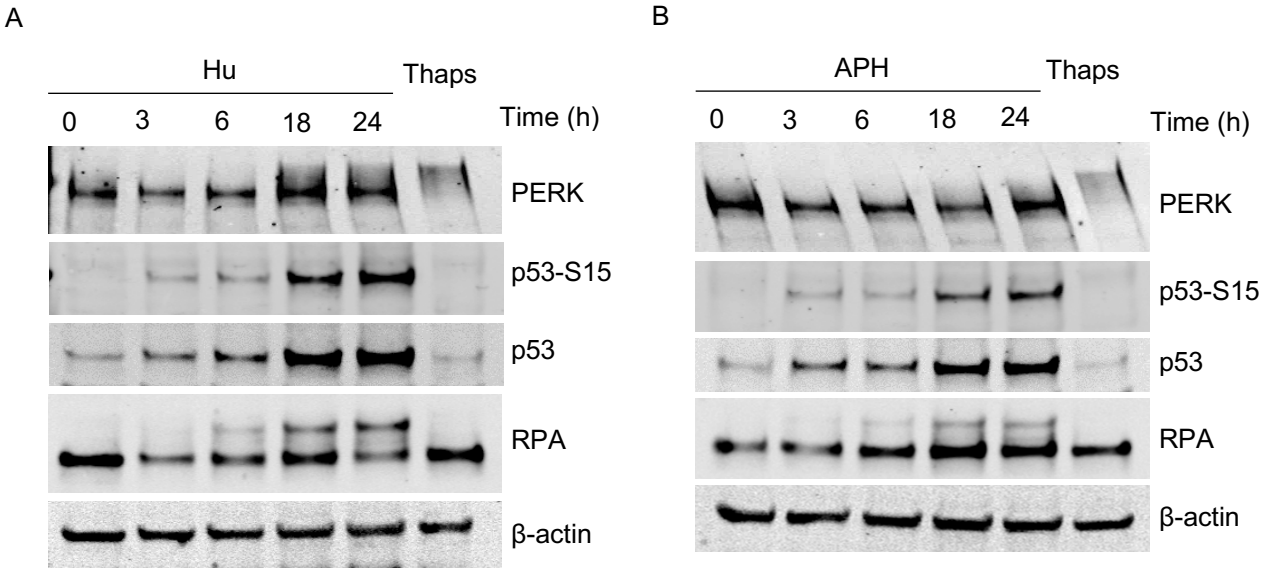


Figure 3.2. Pharmacological induction of replication stress does not a lead to a UPR. A549 cells were exposed to **A.** hydroxyurea (Hu) (2 mM) or **B.** aphidicolin (APH) (30 µM) for the times indicated. Thapsigargin (Thaps) (2 µM for 6 hours) was used as a positive control to induce a UPR. Whole cell lysates were collected for western blotting of UPR and DDR proteins. The levels of β-actin are shown as a loading control. n=3

Therefore, these pharmacological inducers of replication stress did not appear lead to unfolded proteins and a UPR and can be used in our study as tools that only lead to a replication stress-induced DDR.

3.2.2 Pharmacological induction of the UPR does not induce replication stress

Conversely, we asked whether agents which induce a UPR also lead to replication stress. Therefore, we treated A549 cells with Thaps and Tuni in normoxia (21% O_2). We probed for markers of replication stress and found that neither RPA nor CHK1 at serine 345 were phosphorylated in response to UPR induction, indicating that UPR induction does not lead to replication stress (**Figure 3.3A**). To further support this finding, we showed that RPA foci were not formed in response to 24 hours of Thaps treatment (**Figure 3.3B, C**). In contrast, Hu treatment, our positive control for replication stress, led to phosphorylation of RPA and CHK1 and the formation of RPA foci. Notably, once again we saw that Hu treatment does not lead to a UPR as Hu treatment did not increase GRP78 (**Figure 3.3A**). Therefore, these pharmacological inducers of ER stress did not lead to replication stress and can be used in our study as tools that only lead to a UPR.

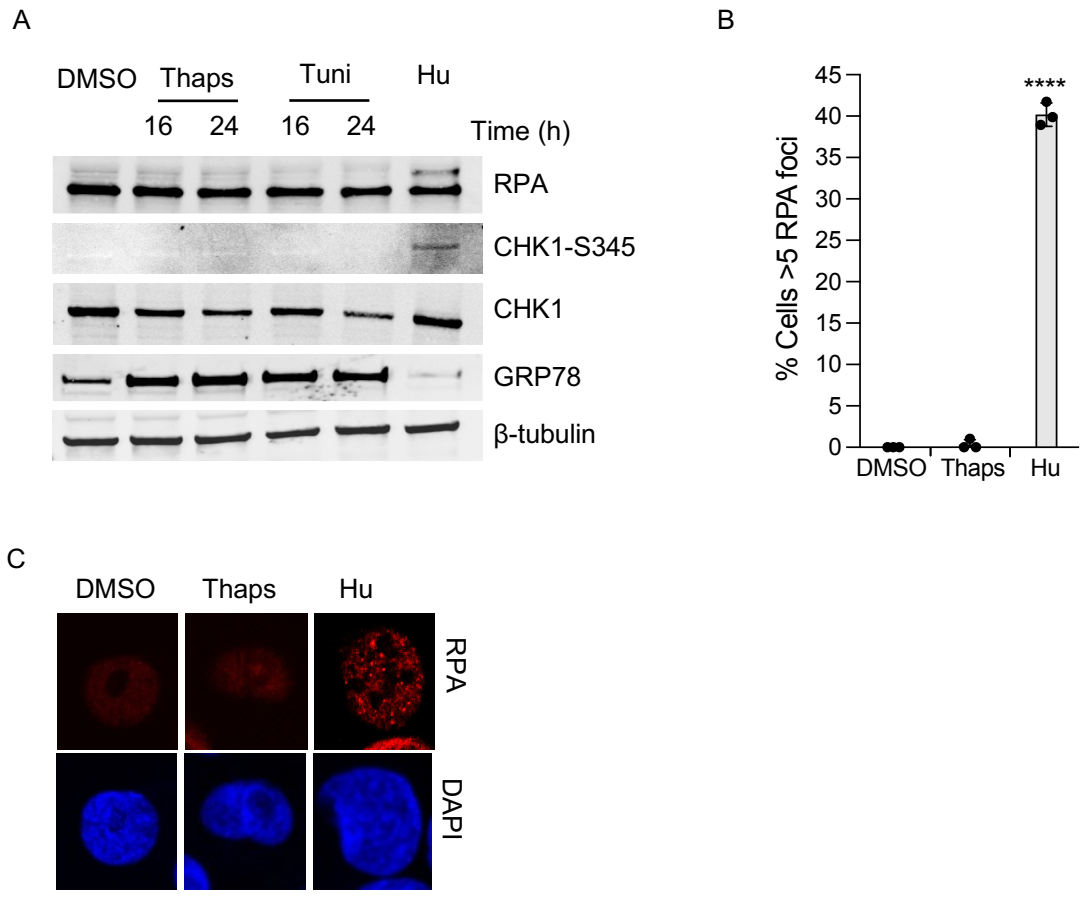


Figure 3.3. Thaps and Tuni do not lead to replication stress. A. A549 cells were treated for 16 and 24 hours with Thaps (2 µM) or Tuni (5 µg/mL). Whole-cell lysates were collected for western blotting. Hu (2 mM, 6 hours) was used as a positive control. The bottom RPA band shows the total level of RPA32 protein, and the upper band shows its phosphorylation. **B.** Quantification of the proportion of cells with >5 RPA foci in A549 cells treated with Thaps (2 µM, 24 hours) or Hu (2 mM, 6 hours). The two-tailed Student's *t*-test was used: ****$p < 0.0001$. **C.** Representative images of part B from immunofluorescent staining for RPA foci. n=3

3.2.3 Induction of the UPR reduces Hu-induced DDR signalling

So far, we found that our conditions for inducing replication stress do not activate the UPR and that conversely, agents for inducing ER stress do not activate the DDR (**Figures 3.2, 3.3**). Therefore, they are suitable pharmacological tools for separating the DDR and UPR. How the DDR and UPR affect one another when both are activated has not been fully investigated previously.

Pharmacological induction of the DDR, UPR or both in normoxia allows us to make comparisons between conditions. Therefore, we used Hu to induce replication stress and Thaps to induce the UPR. We treated A549 cells with Hu, Thaps, or both. Once again, we saw that Hu treatment does not lead to a UPR as PERK is not activated. As expected, Hu led to a replication stress response as shown by phosphorylation of DDR proteins and Thaps led to a UPR as shown by phosphorylation of PERK. Strikingly, when both pathways were activated, DDR signalling was reduced. Specifically, Hu-induced phosphorylation of RPA, p53, CHK1 and KAP1 were reduced when Thaps was added (**Figure 3.4**).

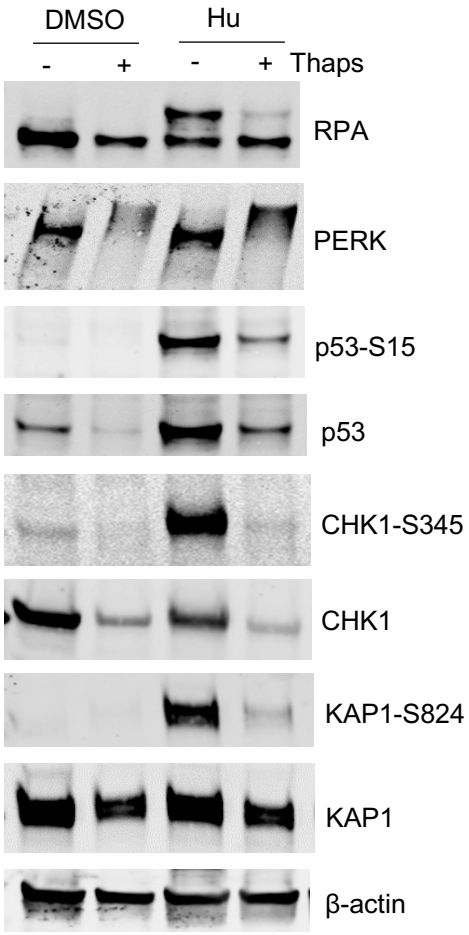


Figure 3.4. Hu-induced phosphorylation of DDR proteins are reduced by concomitant Thaps treatment. A549 cells were treated with Hu (2 mM) with or without Thaps (2 µM) for 24 hours. Whole cell lysates were collected for western blotting of DDR proteins. The levels of β-actin are shown as a loading control. n=3

Although total p53 and CHK1 levels decreased in response to Thaps alone, total RPA and KAP1 levels remained stable; all DDR phosphorylations were rescued despite this difference. Therefore, we concluded that the rescue of Hu-induced phosphorylations of DDR proteins by Thaps was not dependent on decreased expression of the DDR protein.

As we observed a clear decrease in Hu-induced RPA phosphorylation by western blot when Thaps was added, we next investigated the number of RPA foci. We carried out immunofluorescence staining for RPA. We found that Hu-induced RPA foci were significantly reduced by Thaps treatment. The rescue was significant as the percentage of cells with >5 RPA foci decreased from approximately 50% to 10% (**Figure 3.5**).

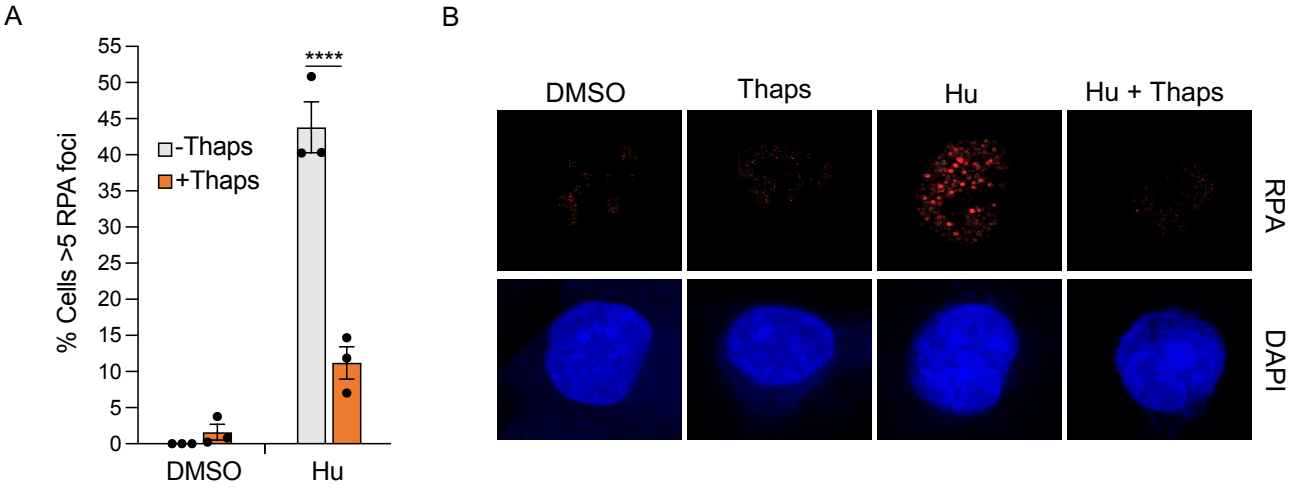


Figure 3.5. Hu-induced RPA foci are rescued by Thaps treatment. A. A549 cells were treated with Hu (2 mM) with or without Thaps (2 µM) for 24 hours and then stained for RPA. The percentage of cells with more than >5 RPA foci was quantified. The two-tailed Student's *t*-test was used: ****$p < 0.0001$. **B.** Representative images of RPA from part A. n=3

To ensure that the rescue was not cell line or drug dependent, we repeated the experiment adding another cell line and an alternative UPR inducer. Although Thaps and Tuni both induce

a UPR, they do so through different mechanisms. We treated RKO and A549 cells with Hu with or without Thaps or Tuni. We found that both Thaps and Tuni rescued Hu-induced DDR signalling in both cell lines (**Figure 3.6**). Furthermore, we observed multiple bands indicative of phosphorylated RPA, which are likely due to DDR kinases phosphorylating RPA at different sites (serines 33, 4, and 8) (Liu *et al.*, 2012). Multiple phosphorylation events are detected by the 'RPA' antibody whereas phosphorylation of RPA at serines 4 and 8 detected by the 'RPA S4/8' antibody. The Hu-induced phosphorylation of RPA was rescued by both Thaps and Tuni. Hence, we concluded that pharmacological induction of the UPR (through two different mechanisms) rescued Hu-induced DDR signalling.

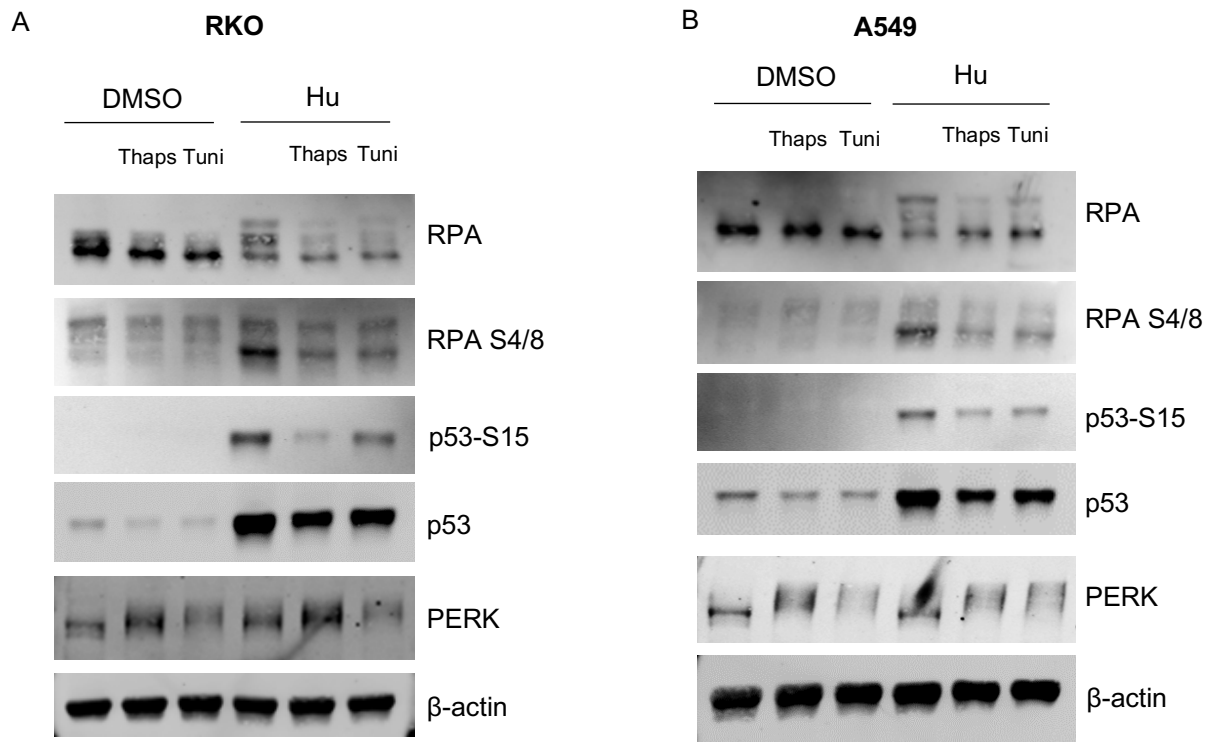


Figure 3.6. Hu-induced phosphorylation of RPA and p53 are rescued by Thaps and Tuni treatment. Western blots with **A.** RKO and **B.** A549 cell lysates following 24-hour treatments with Thaps (2 µM) and Tuni (5 µg/mL), with or without Hu (2 mM). n=3

Tuni treatment alone reduced total p53 levels but did not affect total RPA levels, as we have previously demonstrated with Thaps (**Figures 3.4**). Therefore, we also conclude that the loss

of some DDR proteins in response to an activated UPR is consistent amongst different UPR-inducing agents and likely related to protein half-life.

Next, we investigated whether the rescue of Hu-induced DDR signalling by UPR induction was dependent on a specific branch of the UPR. As previously introduced, there are 3 branches (PERK, IRE1α and ATF6) to the UPR and a number of inhibitors available to inhibit signalling under each branch. We treated A549 cells with Hu with or without Thaps, with or without PERK inhibitor (PERKi) or IRE1α inhibitor (IRE1αi). As expected, Thaps reduced Hu-induced phosphorylation of RPA and p53. Interestingly, when PERKi or IRE1αi was added, the phosphorylation of RPA and p53 were partially restored (**Figure 3.7**). These preliminary findings suggest that both the PERK and IRE1α arms of the UPR have downstream effects that can rescue Hu-induced DDR signalling. However, the effect observed is not dramatic and the experiment was only performed once; the inhibitory effects of the IRE1αi was also not confirmed.

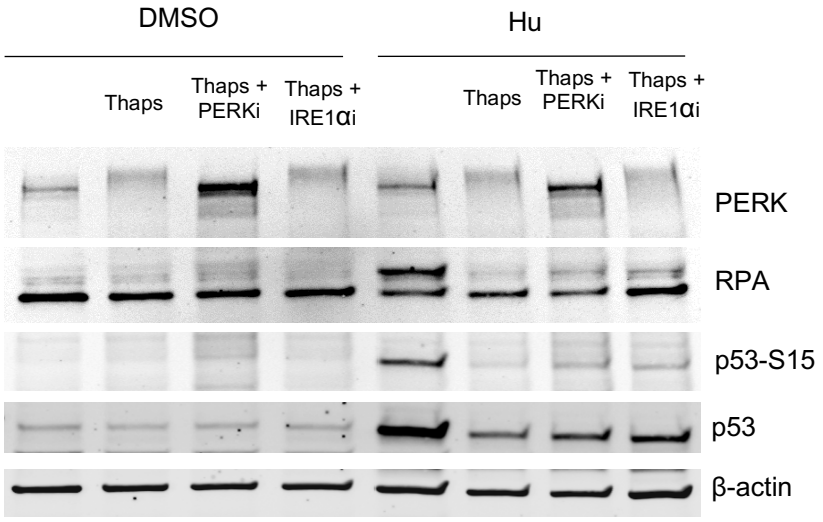


Figure 3.7. Hu-induced phosphorylation of RPA and p53 are PERK and IRE1α dependent. A549 cells were treated with Hu (2 mM) with or without Thaps (2 μM) for 24 hours. Thaps

was added with or without PERK inhibitor AMG PERK 44 (PERKi) (10 μM) or IRE1α inhibitor 4μ8c (IRE1αi) (10 μM). Whole cell lysates were collected for western blotting. The levels of β-actin are shown as a loading control. n=1

3.2.4 Protein translation is decreased in response to a Thaps-induced UPR

We have demonstrated Hu-induced DDR signalling can be significantly reduced by concomitant pharmacological induction of the UPR (**Figures 3.4, 3.6, 3.7**). One hypothesis that must be considered is that the induction of a UPR blocks translation and as a result some of the markers of the response to replication stress are decreased as opposed to replication stress *per se*. It is well-characterised that one of the outcomes of UPR signalling is the inhibition of translation in an eIF2α dependent manner (Guan *et al.*, 2014). Reduced translation rates have significant and rapid impact on the expression levels of proteins and of short-lived proteins in particular. A number of stress-responsive proteins, including those involved in the DDR, are known to have short half-lives, for example p53 (Giaccia & Kastan, 1998). Therefore, this raises the possibility that our investigation of links between the UPR and DDR could be complicated by the loss of key DDR proteins due to reduced translation rates. To confirm the inhibition of global protein synthesis upon UPR signalling and to investigate its effects on DDR proteins, we treated A549 cells with Thaps and added puromycin before harvesting the cells. The incorporation of puromycin into elongating peptides in the last hour of treatment acts a read-out for protein synthesis rate (Kelleher *et al.*, 2013). We found that Thaps treatment led to a prominent decrease in global translation rate by 3 hours and that protein synthesis began recovering by 6 hours but did not return to normal levels over a 24-hour period (**Figure 3.8**). These changes in protein translation kinetics are similar to those observed previously where, in response to Thaps, there is an initial steep

decrease in protein synthesis in the first 2-3 hours and subsequent slow recovery over the course of 24 hours (Guan *et al.*, 2014).

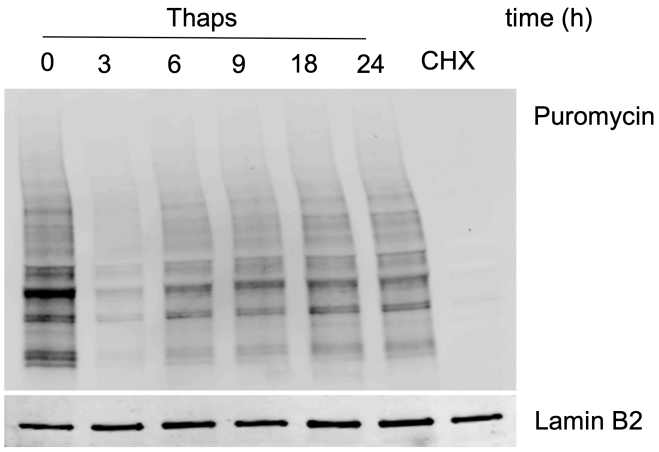


Figure 3.8. Treatment with Thaps leads to decreased protein synthesis. A549 cells were treated with Thaps (2 µM) for the times indicated or cycloheximide (CHX) (100 µM, 90 minutes). Puromycin (1 µg/mL) was added for the last hour of treatment to all samples. Puromycin containing proteins were then visualised using an anti-puromycin antibody. The levels of Lamin B2 are shown as a loading control. n=2

Next, we looked at the expression of key DDR proteins in response to Thaps. The levels of p53, which has a short half-life of 20 minutes, decreased as expected. Similarly, CHK1, which has a half-life of 8 hours, also decreased (Gong *et al.*, 2018). However, the levels of other key DDR proteins appeared to remain stable, including H2AX, RPA, ATM and ATR (**Figure 3.9**).

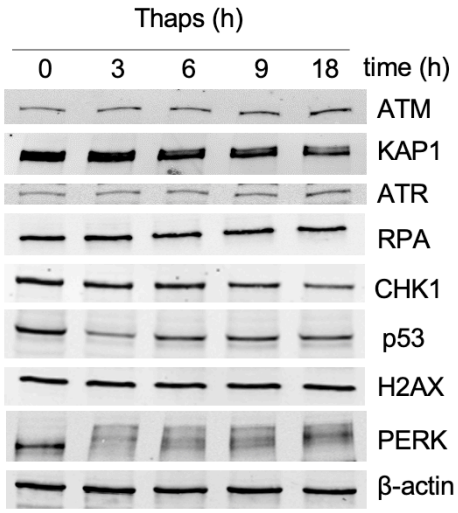


Figure 3.9. Treatment with Thaps leads to changes in the expression of CHK1 and p53. A549 cells were treated with Thaps (2 μM) for the times indicated followed by western blotting. The levels of β-actin are shown as a loading control. The clear shift in PERK mobility demonstrates a Thaps-induced UPR. n=3

Therefore, we have verified that when investigating links between the UPR and DDR it is important to not focus on proteins with short half-lives such as p53 and CHK1 as these are lost likely due to reduced translation. However, total levels of RPA remained stable in response to Thaps, indicating that phosphorylation/localisation of RPA is an appropriate DDR marker to use when studying the effects of the UPR on replication stress *per se* and not on markers of replication stress.

3.2.5 Thaps and Tuni-induced UPR reduces percentage of S phase cells

Apart from global translation inhibition, we must also consider the effects of the UPR on the cell cycle. One obvious hypothesis to test out is that the UPR might be increasing the percentage of cells in the G_1 phase of the cell cycle and reducing the percentage of cells in S phase i.e., the cells that can undergo replication stress. Studies have shown that the UPR can cause growth arrest in G_1, as PERK activation leads to the loss of cyclin D1 which is needed for the G_1/S transition (Brewer & Diehl, 2000; Hamanaka *et al.*, 2005; Zhang *et al.*, 2006).

Therefore, we exposed A549 cells to 6 or 18 hours of Thaps and Tuni treatment and stained with PI to analyse the cell cycle profile. At 6 hours, there were no apparent effects; at 18 hours, however, Thaps and Tuni both led to an increase in the percentage of cells in G_1 phase and a decrease of those in S phase (**Figure 3.10**). The increase in the percentage of cells in G_1 phase in response to Thaps and Tuni is consistent with what has been reported in the literature.

These preliminary data suggest that when we study the effects of the UPR on replication stress in hypoxia, we also need to take into account cell cycle dynamics.

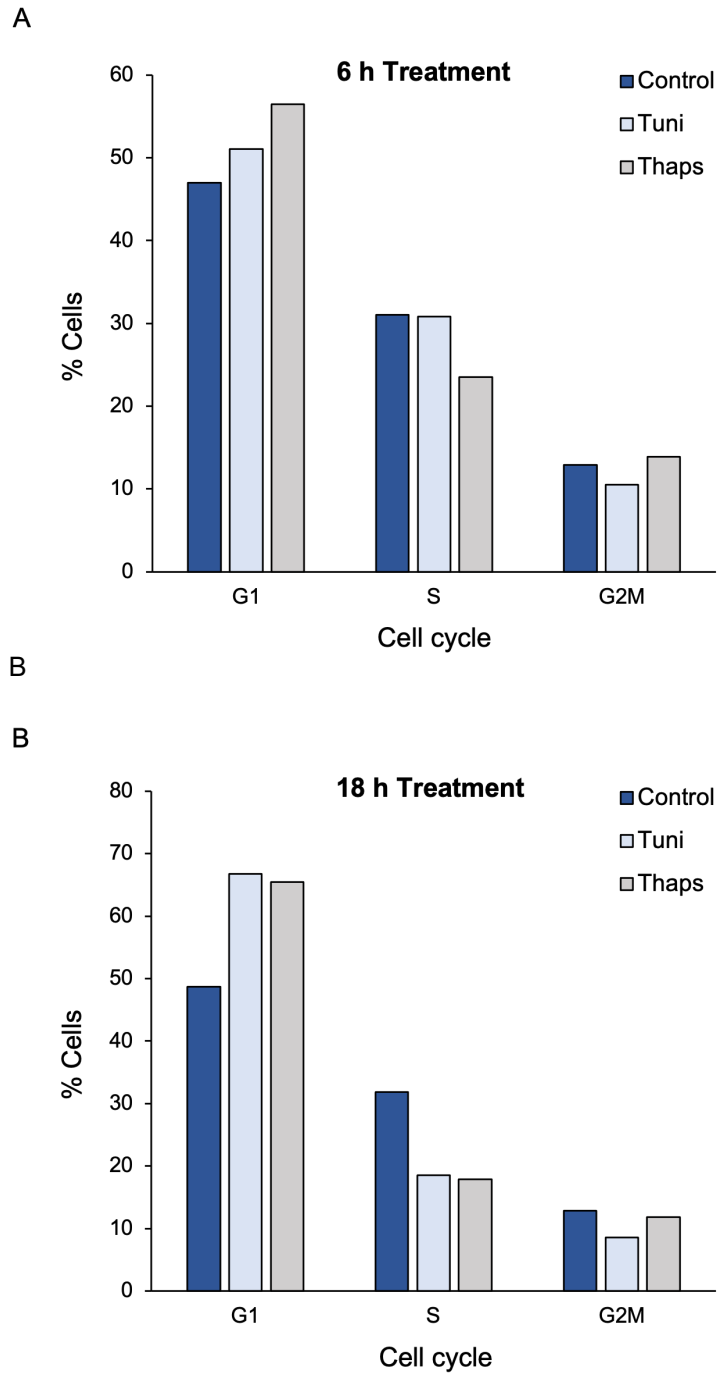


Figure 3.10. Cell cycle profile of Thaps and Tuni treated cells. A549 cells were treated with Thaps (2 µM) or Tuni (5 µg/mL) for **A.** 6 hours or **B.** 18 hours before being fixed and stained with PI and analysed by FACS. n=1 for Tuni, n=2 for Thaps

Together, using this approach of separating the pathways in normoxia, our data suggest links between the UPR and DDR which could be significant in the biological response to hypoxia.

3.2.6 Systematic literature review using PRISMA guidelines: Search

Thus far, we have shown that there are clear links between the UPR and DDR in normoxia: UPR can reduce replication stress induced DDR signalling although this is complicated by effects on both the cell cycle and protein translation. This prompted us to ask whether or not the UPR and DDR interact in a similar manner in hypoxia. However, before performing wet-lab experiments to investigate, we decided to check whether potential links between the UPR and DDR in hypoxia had already been identified in the literature.

We carried out a systematic literature review using standards set by PRISMA (Preferred Reporting Items for Systematic Reviews and Meta-Analyses) guidelines (Page *et al.*, 2021). We designed the search to have 3 areas of interest: DDR under hypoxia, UPR under hypoxia, and UPR and DDR under hypoxia. The search terms for each area of interest are shown in **Figure 3.11**: relevant and closely related terms were determined and truncated to account for derivational affixes to increase the sensitivity of our search. We retrieved literature *via* Ovid MEDLINE following an electronic search restricted to publications from between January 1, 2010 to October 9, 2020 to ensure that the most recent publications were reviewed. The detailed search strategy is shown in **Table 3.1** and the coverage for the truncation of search terms are shown in **Table 3.2**.

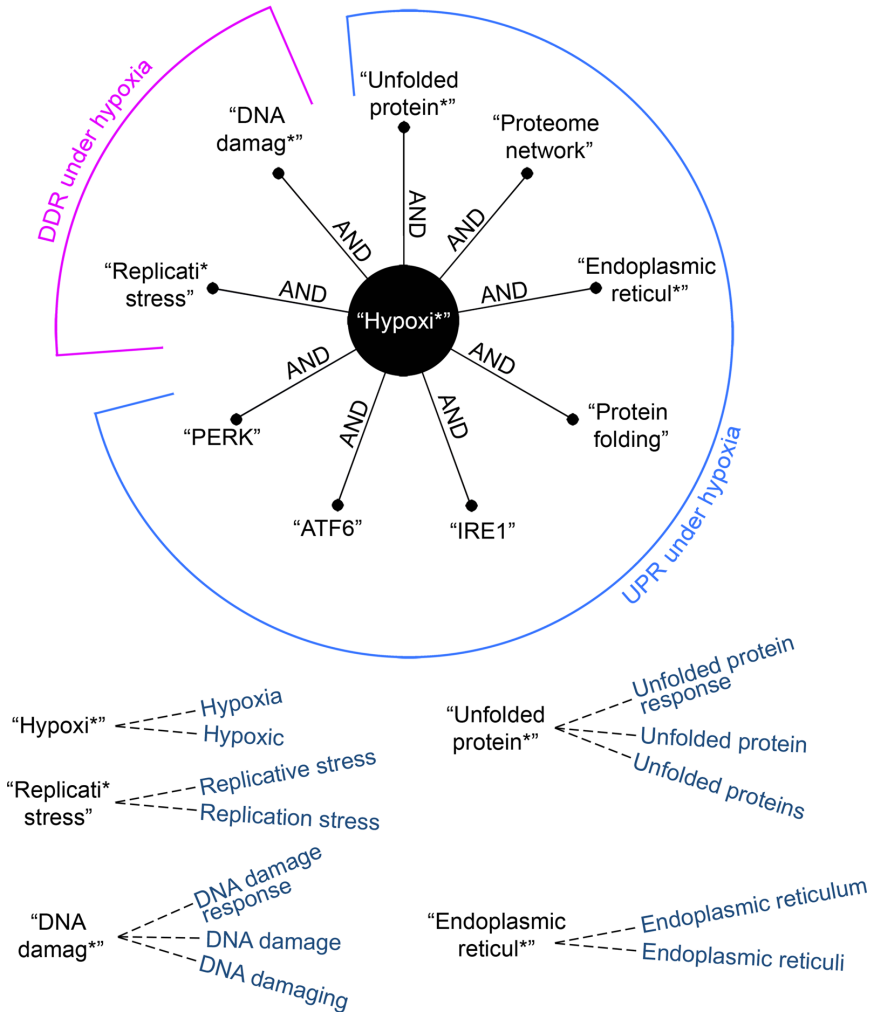


Figure 3.11. Boolean strategy used for searching relevant papers. Relevant and closely related terms were determined and appropriately truncated to account for derivational affixes.

Table 3.1 Search strategy for systematic literature review

	Area of Interest		
	DDR under hypoxia	**UPR under hypoxia**	**UPR, DDR under hypoxia**
Search Input	*DNA damag** + *hypoxi**	*Unfolded protein** + *hypoxi**	*Unfolded protein** + *DNA damag** + *hypoxi**
	Replicati stress* + *hypoxi**	*Proteome network* + *hypoxi**	
		*Endoplasmic reticul** + *hypoxi**	

		IRE1 *+* *hypoxi**	
		ATF6 *+* *hypoxi**	
		PERK *+* *hypoxi**	
		Protein folding *+* *hypoxi**	

Table 3.2 Coverage for truncations of search terms

Search term	Word Coverage
*Hypoxi**	Hypoxia Hypoxic
Replicati stress*	Replicative stress Replication stress
*DNA damag**	DNA damage DNA damage response DNA damage response (DDR) DNA damaging
*Unfolded protein**	Unfolded protein Unfolded proteins Unfolded protein response Unfolded protein response (UPR) Unfolded protein load
*Endoplasmic reticul**	Endoplasmic reticulum Endoplasmic reticulum (ER) Endoplasmic reticuli Endoplasmic reticuli (ER)

3.2.7 Systematic literature review using PRISMA guidelines: Screen

After retrieving the literature, duplicates of publications were deleted; remaining materials were then evaluated for suitability at the title, abstract and full-text levels. Two reviewers, myself and Dr Hannah Bolland, used the eligibility criteria shown in **Table 3.3** to independently screen for papers to be included in the systematic review, and the process was reviewed by a third reviewer, Syafiq Ramlee. The inclusion and exclusion criteria were

determined based on the SPIDER (sample, phenomenon of interest, design, evaluation, research type) framework. Importantly, we chose to include papers using hypoxic conditions within the range of <2% O_2 as the reported O_2 level rarely reflects the actual O_2 concentration in the cell culture dish, as in some cases (e.g., after prolonged exposure), the O_2 concentration may be significantly lower than reported and lead to a UPR/DDR. Moreover, certain cell lines may have a UPR/DDR at O_2 concentrations higher than <0.1% O_2. After independent screening, discrepancies between the results of the screens were resolved through discussion between the reviewers.

Table 3.3 Eligibility criteria used to evaluate papers for inclusion or exclusion for review

	Inclusion criteria	Exclusion criteria
Sample	Human cell model	Non-human cell model
Phenomenon of Interest	Activation of DDR and/or UPR (proteins, genes, transcripts) under hypoxia	Study not relevant to UPR and/or DDR and/or hypoxia
Design	Cell lines exposed to hypoxia at <2% O_2 concentration	Cell lines not exposed to relevant oxygen concentration (>2% O_2); Exact oxygen concentration not reported
Evaluation	Link between UPR and DDR (alluded or explicit)	Inexplicit link between UPR and DDR; Pathways discussed separately in paper
Research type	Empirical research	Secondary sources and non-empirical texts (i.e., review papers, textbook chapters, conference proceedings); Non-English texts

The search yielded 2,490 articles for review and, following exclusion, 202 articles remained for further analysis (**Figure 3.12**).

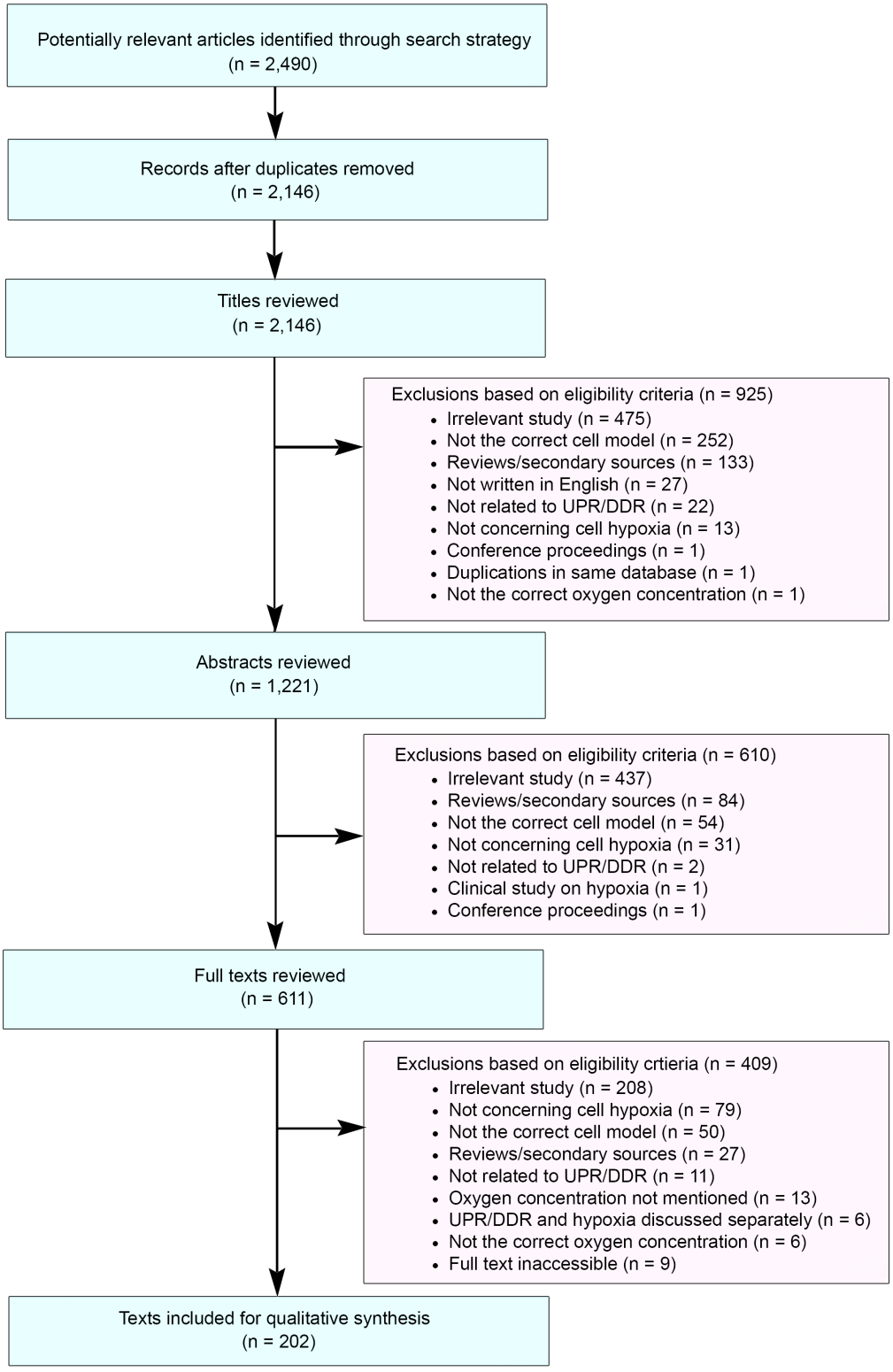


Figure 3.12. PRISMA flow diagram of the systematic literature exclusion process. The 2,490 studies retrieved from the Ovid MEDLINE database published between January 1, 2010 and October 9, 2020 had duplicates removed, then were excluded at the level of the title, abstract, then full text.

3.2.8 Systematic literature review using PRISMA guidelines: Synthesis

From the 202 studies remaining after exclusion, we extracted relevant data by assessing study methodology (oxygen concentration and cell lines used), reported observations and identified biological regulators. In conclusion, our systematic approach identified no published studies that have explicitly investigated the links between the UPR and DDR in hypoxia (<2% O_2). However, we noted that it was clear the UPR, and DDR interact with many of the same pathways in hypoxia, including autophagy, HIF regulation, immune signalling, metabolic reprogramming, antioxidant response and PI3K/Akt/mTOR signalling.

Importantly, however, we noted that links between the UPR and DDR in normoxia are not unprecedented. For example, Nagelkerke *et al.* showed that the PERK/ATF/LAMP3 arm of the UPR affects radio-resistance by interfering with the DDR (Nagelkerke *et al.*, 2013). Yamamori *et al.* showed that ER stress can suppress DSB repair by degrading Rad51 (Yamamori *et al.*, 2013). One report showed that DSB-inducing agent etoposide (ETP) activates IRE1α activity in the absence of ER stress markers; specifically, there is no spliced XBP activity 1 and instead there is RIDD activation (Dufey *et al.*, 2020).

Therefore, papers which only described genes, proteins, or findings as part of the hypoxic DDR or hypoxic UPR but not both (since there were none) were further investigated to determine if, by searching for and including studies carried out in normoxia conditions, links between the UPR and DDR could be extrapolated. Through systematic review, we identified 23 genes (**Table 3.4**) which although not linked directly to both the hypoxia-induced DDR and UPR, may represent a credible link between the two pathways. We identified these genes because even though they have only been described to play a role in either the hypoxic UPR

or hypoxic DDR, by including studies of these genes under normoxic conditions, we found evidence that the genes play roles in both stress response pathways (Bolland, Ma *et al.*, 2021).

Table 3.4 Genes identified as potential links between the UPR and DDR in hypoxia
From the systematic review, a list of genes was identified as playing key roles in the hypoxia-induced UPR (coloured in green) or the hypoxia-induced DDR (blue). Each gene has previously been linked to the other stress pathway in normoxia, for example LAMP3 was highlighted in the systematic review as being involved in the hypoxic UPR, but it has also been linked to the DDR in normoxia. Conversely, JMJD2B was highlighted in the systematic review as being involved in the hypoxic DDR but has only been linked to the UPR in normoxia.

Gene	Regulation by the UPR	Oxygen concentration investigated (% O_2)	References
LAMP3	PERK/eIF2α/ATF4	0.1, 1.0	(Mujcic *et al.*, 2013; Nagelkerke, Bussink, Mujcic, *et al.*, 2013; Nagelkerke *et al.*, 2015)
ULK1	PERK/eIF2α/ATF4	<0.02	(Schaaf *et al.*, 2013)
TRIB3	PERK/eIF2α/ATF4	0.1 0.2, 0.5	(Wennemers *et al.*, 2011)
CHOP	PERK/eIF2α/ATF4	1.0	(Jeong *et al.*, 2014; Mujcic *et al.*, 2013; Petry *et al.*, 2019; Pi *et al.*, 2014; Rouschop *et al.*, 2013; Vandewynckel *et al.*, 2015; Xu *et al.*, 2016; Yoo *et al.*, 2016; N. Zhang *et al.*, 2015; H. Zheng *et al.*, 2020)
NOXA	PERK/eIF2α/ATF4	1.0	(Sermeus *et al.*, 2012)
NORAD	PERK/eIF2α/ATF4	1.0	(X. Zhao *et al.*, 2020)
SIAH1/2	PERK/eIF2α/ATF4 and IRE1α/XBP1	1.0	(Adam *et al.*, 2015; García-Limones *et al.*, 2016; Moehlenbrink *et al.*, 2010; Pérez *et al.*, 2012)
DYRK2	PERK/eIF2α/ATF4	1.0	(Pérez *et al.*, 2012)
HIPK2	PERK/eIF2α/ATF4	0.2, 1.0, 2.0	(Moehlenbrink *et al.*, 2010; Tong *et al.*, 2013)
CREB	PERK/eIF2α/ATF4	1.0	(Kikuchi *et al.*, 2016)
NUPR1	PERK/eIF2α/ATF4	0.2	(Hamidi *et al.*, 2012)
NRF2	PERK/eIF2α/ATF4	0, 1.0	(Elanchezhian *et al.*, 2012; Grandi *et al.*, 2016; Miyamoto *et al.*, 2011; Xia *et al.*, 2020; X.-Y. Zheng *et al.*, 2015)
GSK-3B	PERK/eIF2α/ATF4	1.0	(Hotokezaka *et al.*, 2015)

STAU1	PERK/eIF2α/ATF4 and interacts with XBP1	1.0	(Bonnet-Magnaval *et al.*, 2016)
GADD45B	PERK/eIF2α/ATF4	1.0	(Ma *et al.*, 2016)
C-SRC	IRE1α/XBP1	1.0	(Torrisi *et al.*, 2020)
HK2	IRE1α/XBP1	1.0	(Y. Liu *et al.*, 2016)
CAV1	IRE1α/XBP1	1.0	(Díaz *et al.*, 2020)
CYPB	ATF6	0.1	(Jeong *et al.*, 2014, 2015)
CLU	GRP78 binding	1.0	(Alnasser *et al.*, 2016)
IGFBP-3	GRP78 binding	1.0	(Grkovic *et al.*, 2013)
SP1	General ER stress induced	1.0	(Koizume *et al.*, 2015)
Gene	**Regulation by the DDR**	**Oxygen concentration investigated (% O_2)**	**References**
JMJD2B	Activates hypoxic DDR *via* ATM-RAD3 pathway	1.0	(L. Chen *et al.*, 2014)

3.3 Discussion

Here, we investigated the links between the UPR and DDR in normoxia using an approach to separate the two pathways, followed by a systematic literature review to search for any studies linking the UPR and DDR in hypoxia (Bolland, Ma *et al.*, 2021).

To investigate how the UPR and DDR interact in normoxia, we used pharmacological reagents which only induce one or the other pathway. We show that these pharmacological reagents are appropriate tools for our study as UPR inducers do not lead to replication stress, and replication stress inducers do not lead to a UPR (**Figures 3.2, 3.3**). Interestingly and strikingly, we demonstrate that Hu-induced DDR signalling is reduced by activating the UPR (**Figures 3.4, 3.6**).

To our knowledge, this is the first time these reagents have been used together to show an interaction between the two pathways. Most existing studies linking the UPR and DDR in normoxia have focused on how the PERK and IRE1α arms of the UPR, or their downstream factors, have a functional relationship with specific DDR proteins (González-Quiroz *et al.*, 2020). For example, silencing of XBP1s downstream of IRE1α has been shown to increase γ-H2AX foci formation and to reduce the expression of MRN complex proteins (Lyu *et al.*, 2019). Another example is that downregulation of PERK correlates with increased phosphorylation of ATM and CHK2, as well as an increase in γ-H2AX (Bobrovnikova-Marjon *et al.*, 2010). Here, our results seem to be consistent with several findings in literature as they suggest the same pattern, i.e., the UPR can reduce DDR signalling, possibly by reducing or preventing DNA damage. However, our results do not indicate whether UPR activation is affecting DDR signalling or replication stress and DNA damage *per se*. Future studies to interrogate the levels

of DNA damage (comet assays) and replication fork dynamics (DNA fibre assays) would likely be informative.

We considered the hypothesis that the UPR is affecting the activity of DDR proteins because of global translation inhibition. A canonical function of the UPR is to halt global protein synthesis in response to proteotoxic stress, specifically through the phosphorylation of eIF2α which is downstream of the PERK arm (Guan *et al.*, 2014; Koumenis *et al.*, 2002). Therefore, UPR induction through Thaps could be reducing DDR signalling by halting the translation of DDR players. We found that, however, the total levels of multiple DDR proteins in response to Thaps remain unchanged, including that of RPA, ATM, ATR and KAP1 (**Figure 3.9**).

The effects of the UPR on the cell cycle must also be considered. As activating the UPR can lead to a G_1 cell cycle arrest due to cyclin D1 loss through the PERK/eIF2α arm, we considered the hypothesis that the UPR can rescue replication stress signalling by limiting the proportion of cells that can enter S phase i.e., the cells that can experience replication stress (Brewer & Diehl, 2000; Hamanaka *et al.*, 2005; Zhang *et al.*, 2006). Indeed, we observed that Thaps and Tuni treatment over 18 hours led to an increase in the percentage of cells in the G_1 phase of the cell cycle, and a significant reduction in the percentage of cells in S phase (**Figure 3.10**). This suggests that we must take cell cycle dynamics into account when studying how the UPR may affect replication stress in hypoxia in Chapter 4.

Given the striking phenotype where activating the UPR can abrogate Hu-induced DDR signalling and existing studies supporting interactions between the UPR and DDR in normoxia, we next sought to investigate links between the UPR and DDR in hypoxia, as hypoxia is known

to activate both pathways. We decided to perform a systematic literature review using PRISMA guidelines to thoroughly search for any existing studies that may have already identified genes or mechanisms through which the UPR and DDR interact in hypoxia. However, we found that no such studies exist. We identified a number of genes as potential links between the UPR and DDR in hypoxia; these genes have been observed to play a role in one pathway in hypoxia, and to also play a role in the other pathway but in normoxia (**Table 3.4**).

In particular, one of the genes identified in **Table 3.4** is NRF2, the master antioxidant regulator. Paradoxically, in hypoxia there is a release of mitochondrial ROS which allows NRF2 to dissociate from its negative regulator KEAP1 and to bind to antioxidant response elements (ARE) in the nucleus (Chandel *et al.*, 2000; Nguyen *et al.*, 2009). NRF2 has been shown to protect epithelial cells from ionising radiation by enhancing DDR signalling in normoxia and to activate ABCB1 mediated chemoresistance *via* an increase in drug efflux in hypoxia (Kim *et al.*, 2012; Xia *et al.*, 2020). NRF2 has been identified as novel prognostic biomarker in colorectal cancer, and four lead clinical compounds have been shown to target NRF2 signalling (O'Cathail *et al.*, 2020; Yagishita *et al.*, 2020).

In conclusion, our data suggest there are links, but these have not been reported in the response to hypoxia likely because both stress responses are concurrently induced, making it difficult to study. In the next chapter, we will investigate specific links between the UPR and DDR in hypoxia as we confirmed with the systematic literature review that this has not been reported previously.

Chapter 4 Hypoxia-induced SETX links replication stress with the unfolded protein response

4.1 Introduction

The focus of this chapter is the impact the DDR and UPR have on each other in hypoxia.

Here, we plan to use a bioinformatic approach to look for genes potentially involved in the DDR/replication stress that are regulated by the UPR. There are numerous datasets available online from researchers who study either the UPR or DDR, especially RNA-sequencing (RNA-seq) datasets. Our lab also has multiple RNA-seq datasets generated from hypoxia-treated cells. By overlapping these datasets, we hope to see which genes are common between these transcriptional responses.

In this chapter, we will also study the role of putative RNA/DNA helicase senataxin (SETX) in hypoxia, as SETX was one of the genes identified from our bioinformatic analyses to be a hypoxia-induced UPR gene that may play a role in the DDR.

4.2 Results

4.2.1 Collating available datasets

Numerous RNA-seq datasets are available, which characterise the gene expression changes associated with both hypoxia and the UPR. In this study, we have made use of both our own datasets and those available for download. Similarly, screens which identify genes and proteins involved in DNA replication and in the response to DNA damage as well as proteins associated with the replication fork are also available for download (**Table 4.1**).

Table 4.1 Description of the data sets used in this study

Data set number	Data set source	Data type	Experimental conditions	Cell line
1	Hammond lab resource	RNA-seq	Hypoxia (<0.1% O_2) for 6 hours	RKO (colorectal)
2	Hammond lab resource	RNA-seq	Hypoxia (<0.1% O_2) for 6 hours N.B 2% O_2 also available (6 hours)	U87 (glioblastoma)
3	(Luhr *et al.*, 2019) https://pubmed.ncbi.nlm.nih.gov/30926605/	RNA-seq	Tunicamycin (Tuni) (2.5 µg/mL) for 18 hours Tuni + siControl Tuni + PERKi (GSK2606414) Tuni + siPERK-1 Tuni + siPERK-2 Tuni + siATF-1 Tuni + siATF-2	LNCaP (prostate)
4a	(Raina *et al.*, 2014) https://www.ncbi.nlm.nih.gov/pmc/articles/PMC4324732/	RNA-seq (up-regulated genes available only)	Tunicamycin (Tuni) (5 µg/mL) for 2 and 10 hours	HEK293 (kidney, embryonic)
4b			Thapsigargin (Thaps) (5 nM) for 2 and 10 hours	
5	(Olivieri *et al.*, 2020) https://pubmed.ncbi.nlm.nih.gov/32649862/	Hits from CRISPR-Cas9 screens measuring viability	27 genotoxic agents against CRISPR-knockouts	RPE1 (retinal pigment epithelium)
6	(Kavanaugh *et al.*, 2015) https://www.ncbi.nlm.nih.gov/pmc/articles/PMC4651756/	Hits from RNAi screen measuring DNA replication	RNAi knockdowns	U2OS cells (osteosarcoma)
7	(Dungrawala *et al.*, 2015) https://www.ncbi.nlm.nih.gov/pmc/articles/PMC4575883/	iPOND-SILAC-MS identifying enriched proteins at replication fork	Hu N.B Hu+ATRi also available	HEK293 (kidney, embryonic)
8	(Sirbu *et al.*, 2013) https://pubmed.ncbi.nlm.nih.gov/24047897/	iPOND-MS identifying enriched proteins at replication fork	Hu N.B Hu+ATRi also available	HEK293 (kidney, embryonic)
9	(Cristini *et al.*, 2018) https://pubmed.ncbi.nlm.nih.gov/29742442/	S9.6 IP-MS identifying RNA/DNA hybrid Interactome	N/A	HeLa (cervical adenocarcinoma)
10	(Wang *et al.*, 2018) https://pubmed.ncbi.nlm.nih.gov/30108179/	S9.6 IP-MS identifying RNA/DNA hybrid Interactome	N/A	Human B-cells

4.2.2 Identifying hypoxia-induced UPR genes

In order to determine which specific UPR genes are upregulated in hypoxia (<0.1% O_2), genes that are upregulated by pharmacological induction of the UPR were overlapped with genes induced in hypoxia (<0.1% O_2). 9530 genes up-regulated by pharmacological induction of the UPR by either Thaps or Tuni were compared to 1636 genes up-regulated by hypoxia (<0.1% O_2); we found that the two groups shared 1113 genes in common (**Figure 4.1A**). The 1113 genes can be found in **Table S4.1**.

To characterise the potentially 1113 hypoxia-induced and UPR regulated genes, we used the gene set enrichment analysis (GSEA) tool to identify shared biological functions amongst these genes. Specifically, we used the 50 'hallmark' gene sets from the Molecular Signatures Database to categorise the 1113 genes as the hallmark gene sets cover a large range of well-defined biological states or processes, reduce redundancy and produce robust enrichment results (Liberzon *et al.*, 2015). As expected, hallmark pathways such as 'hypoxia', 'unfolded protein response' and 'p53' were identified as enriched pathways in the analysis of the 1113 genes (**Figure 4.1B**).

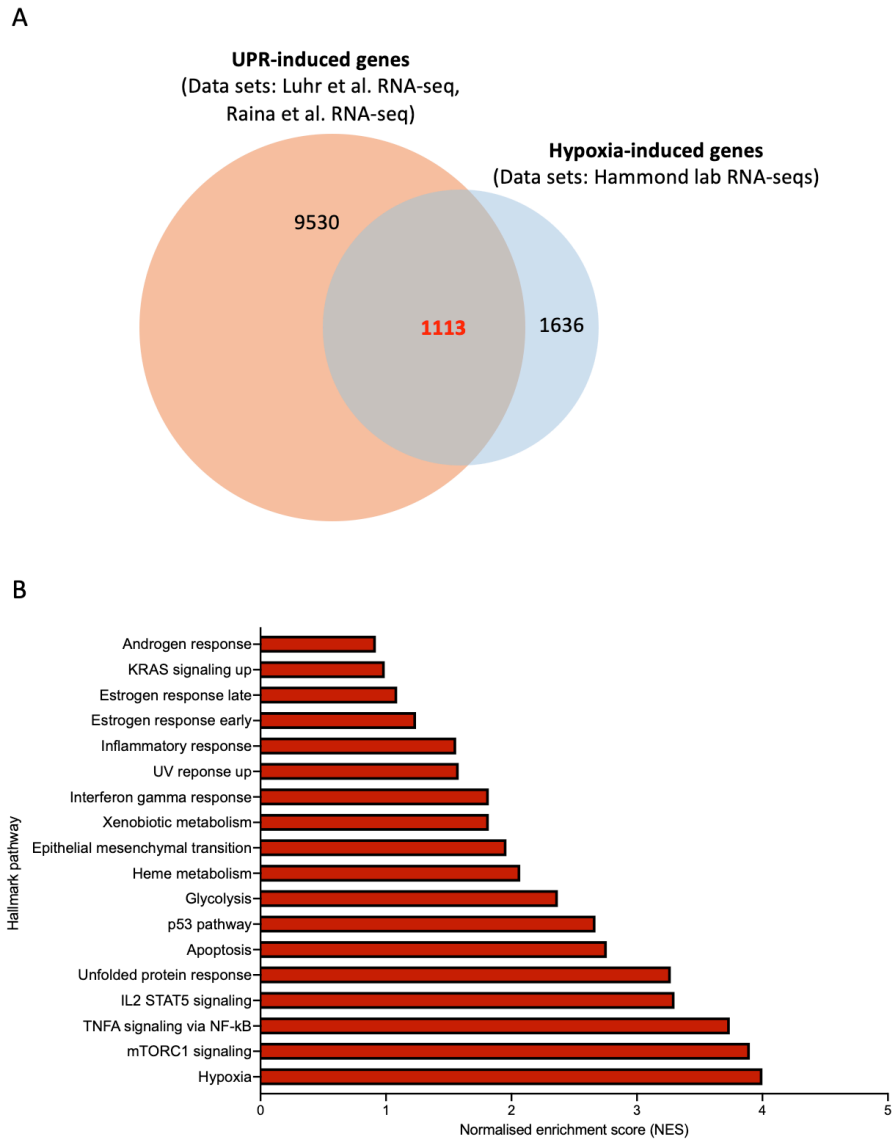


Figure 4.1. Identifying and characterising the genes induced by the UPR in hypoxia (<0.1% O_2). A. Overlap between genes up-regulated by pharmacological induction of the UPR (orange) and genes up-regulated by hypoxia (<0.1% O_2) (blue) identified 1113 genes (red). Data sets are described in Table 4.1. **B.** Gene set enrichment analysis (GSEA) of the 1113 genes from A using hallmark gene sets. UPR-induced genes are from 3 RNA-seq datasets: LNCaP cells treated with tunicamycin (2.5 µg/mg) for 18 hours(Luhr *et al.*, 2019; Raina *et al.*, 2014), HEK293 cells treated with thapsigargin (5 nM) for 2 and 10 hours and HEK293 cells treated with tunicamycin (5 µg/mL) for 2 and 10 hours (Raina *et al.*, 2014). Hypoxia-induced genes are from 2 RNA-seq datasets: RKO cells in 6 hours of <0.1% O_2 (Ramachandran, Ma *et al.*, 2021) and U87 cells in 6 hours of <0.1% O_2 (Hammond lab, unpublished).

Encouragingly, out of the 28 genes identified in the systematic literature review as genes that are potential links between the UPR and DDR in hypoxia (**Table 3.4**), 6 of them are also part

of the 1113 hypoxia induced UPR genes (**Figure 4.1, Table S4.1**). The 6 genes are LAMP3, TRIB3, CHOP, NUPR1, GADD45B and HK2.

4.2.3 Hypoxia-induced UPR genes that play a role in the response to DNA damage

After identifying the 1113 hypoxia-induced UPR genes, we next asked whether any of them play a role in the response to DNA damage. To do this, we used the CRISPR screen data set from Olivieri *et al.* which identified 1133 hits (before FDR correction) as genes whose loss led to sensitivity or resistance to at least one of the 27 genotoxic agents used (Olivieri *et al.*, 2020). The 27 genotoxic agents used led to a wide range of stresses including SSBs, DSBs and replication stress. We overlapped the data sets and found that out of the 1113 hypoxia-induced UPR genes, 103 of them were also hits in the Olivieri *et al.* CRISPR screen against genotoxic agents (**Figure 4.2A**). The 103 genes are listed in **Table S4.2**.

To characterise the 103 hypoxia-induced UPR genes that play a role in the response to DNA damage, we grouped them into their respective 'classical' DNA repair pathways using the same categorisation criteria as Olivieri *et al.* We found that while 20 of the 103 genes could be categorised as a member of a classical DNA repair pathway such as HR or MMR, 83 of the genes were 'non-classical' DDR genes as they did not fit into an established pathway (**Figure 4.2B**). This may not be surprising as Olivieri *et al.* also noted that DNA repair terms only covered 398 out of the 841 hits (after FDR correction) and that their CRISPR screen identified many genes that were not previously associated with the response to DNA damage. To further investigate the 83 non-classical DDR genes, we analysed their GO biological processes using the bioinformatic web-tool GeneCodis and found that the most commonly annotated terms

included positive and negative regulation of transcription by RNA polymerase II and apoptotic process (**Figure 4.2C**).

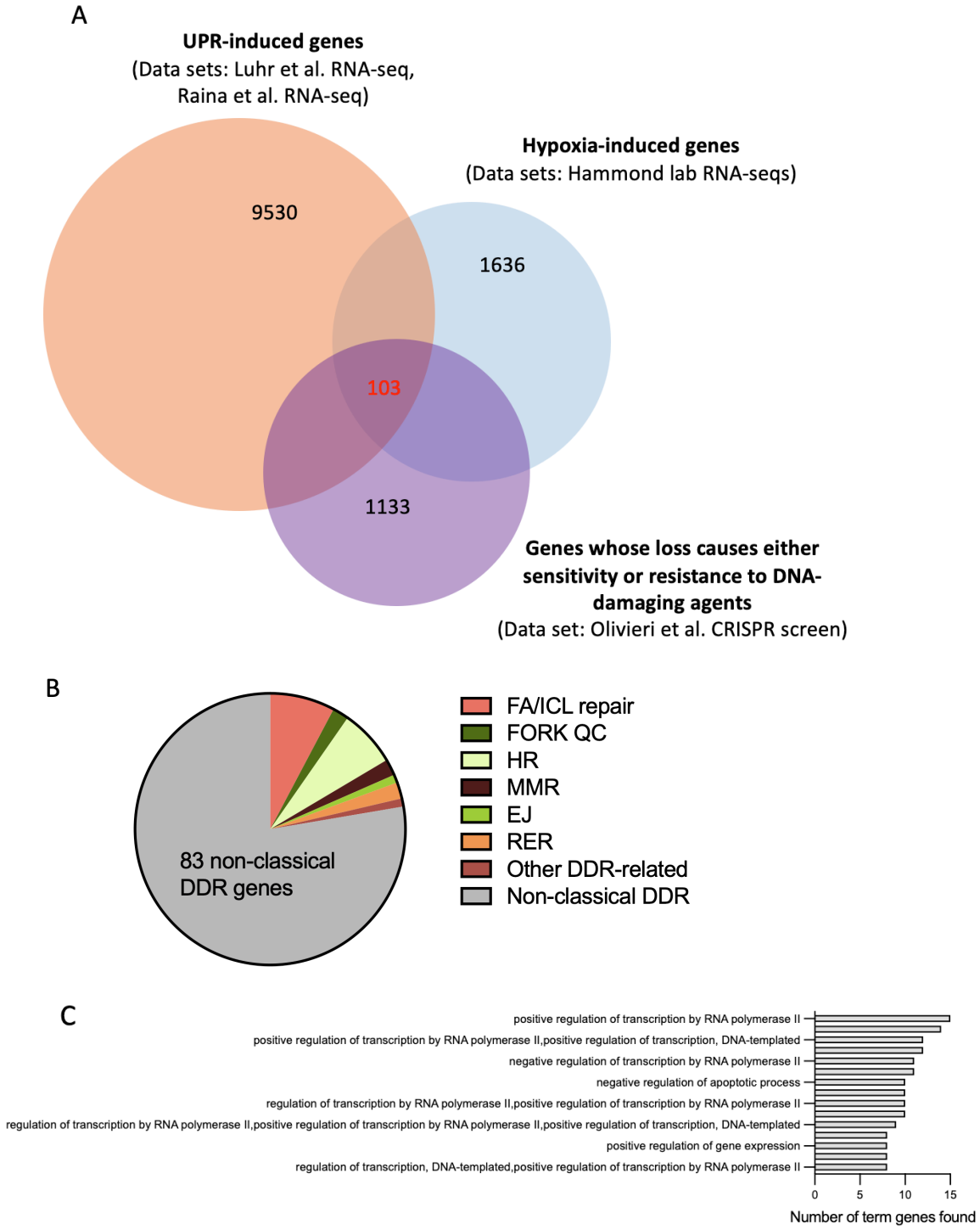


Figure 4.2. 103 UPR-induced genes in hypoxia (<0.1% O_2) play a role in the response to DNA damage. A. Overlap between genes up-regulated by pharmacological induction of the unfolded protein response (UPR) (orange), genes up-regulated by hypoxia (<0.1% O_2) (blue) and genes whose loss causes either sensitivity or resistance to DNA-damaging agents (purple)

identified 103 genes (red). Data sets are described in **Table 4.1**. **B.** Analysis of the 103 genes from A categorised the genes into their respective DNA repair pathways including 83 non-classical DDR genes. C. Enriched GO biological processes of the 83 non-classical DDR genes from B. The 1133 genes whose loss causes either sensitivity or resistance to DNA-damaging agents are from a CRISPR-Cas9 screen in RPE1 cells (Olivieri *et al.*, 2020).

Interestingly, out of the 28 genes identified in the systematic literature review as genes that are potential links between the UPR and DDR in hypoxia (**Table 3.4**), one of them, TRIB3, is also part of the 103 UPR-induced genes in hypoxia that play a role in the response to DNA damage (**Figure 4.2, Table S4.2**). TRIB3 is a putative kinase and an NF-κB target, induced by ATF4/CHOP under ER stress, has a role in regulating the integrated stress response, inhibits CHOP-dependent cell death during ER stress, and can inhibit APOBEC3A editing of nuclear DNA (Aynaud *et al.*, 2012; Wennemers *et al.*, 2011, 2012). Depletion of TRIB3 was shown to reduce hypoxic cell survival (Wennemers *et al.*, 2011). Interestingly, mass spectrometry data shows that TRIB3 binds to DNA damage related proteins HMG1, TOP1, Ku80 and multiple members of the DDX family of RNA/DNA helicases (Lee *et al.*, 2019). Therefore, as TRIB3 has been identified by both systematic literature review and bioinformatic approaches to be a potential link between the hypoxic UPR and DDR, it warrants further investigation in the lab.

4.2.4 Hypoxia-induced UPR genes that regulate DNA synthesis

Hypoxia (<0.1% O_2) is known to significantly reduce DNA synthesis rates (Foskolou *et al.*, 2016). Therefore, we next asked whether any of the hypoxia-induced UPR genes (**Figure 4.1A, Table S4.1**) also played a role in DNA synthesis. Using an RNAi screen, Kavanaugh *et al.* identified 949 hits, genes whose knockdown resulted in a DNA synthesis rate at least two standard deviations above or below the untreated control (Kavanaugh *et al.*, 2015). We overlapped the Kavanaugh *et al.* RNAi data set with the 1113 hypoxia-induced UPR genes and identified 5

genes whose knockdown results in a significant increase or decrease in DNA synthesis (**Figure 4.3**).

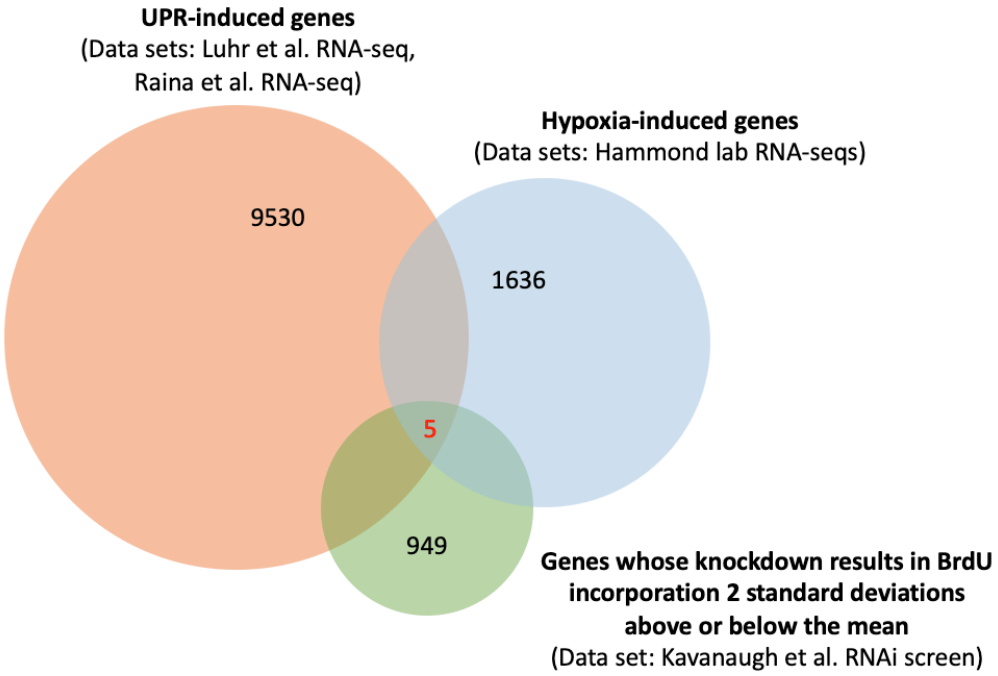


Figure 4.3. 5 UPR-induced genes in hypoxia (<0.1% O_2) play a role in DNA synthesis. Overlap between genes up-regulated by pharmacological induction of the UPR (orange), genes up-regulated by hypoxia (<0.1% O_2) (blue) and genes whose knockdown results in BrdU incorporation 2 standard deviations above or below the mean (green) identified 5 genes (red). Data sets are described in **Table 4.1**.

Descriptions of the 5 genes and the effect of their knockdown on DNA synthesis are shown in **Table 4.2**. Whereas knockdown of 3 of the 5 genes resulted in an increase in DNA synthesis, knockdown of 2 of the 5 genes resulted in a decrease in DNA synthesis. Notably, SDCBP was also a hit in the Olivieri *et al.* CRISPR screen against genotoxic agents and is the only hypoxia-induced UPR gene that is a hit in both screens. Additionally, one of the 5 hits is RRM2; in our lab, we found that RNR switches subunit from RRM2 to RMM2B in order to maintain DNA replication in hypoxia (Foskolou *et al.*, 2017). Overall, this indicates that hypoxia-induced UPR genes include those that both promote and inhibit S phase progression.

Table 4.2 Description of the 5 genes from Figure 3.3 and the effects of their knockdown on BrdU incorporation.

The 949 genes whose knockdown results in BrdU incorporation 2 standard deviations above or below the mean re from an RNAi screen in U2OS cells (Kavanaugh *et al.*, 2015).

Gene	Gene card description	BrdU incorporation when gene is knocked down
RLF	RLF (RLF Zinc Finger) is a Protein Coding gene that may be involved in transcriptional regulation.	Increased 38.1%
CYLD	Encodes a cytoplasmic protein with three cytoskeletal-associated protein-glycine-conserved (CAP-GLY) domains that functions as a deubiquitinating enzyme. Mutations in this gene have been associated with cylindromatosis, multiple familial trichoepithelioma, and Brooke-Spiegler syndrome.	Increased 41.7%
FBXW7	This gene encodes a member of the F-box protein family which is characterized by an approximately 40 amino acid motif, the F-box. The F-box proteins constitute one of the four subunits of ubiquitin protein ligase complex called SCFs (SKP1-cullin-F-box), which function in phosphorylation-dependent ubiquitination.	Increased 41.7%
RRM2	This gene encodes one of two non-identical subunits for ribonucleotide reductase. This reductase catalyses the formation of deoxyribonucleotides from ribonucleotides. Synthesis of the encoded protein (M2) is regulated in a cell-cycle dependent fashion.	Decreased 3.8%
SDCBP	The protein encoded by this gene was initially identified as a molecule linking syndecan-mediated signalling to the cytoskeleton. The syntenin protein contains tandemly repeated PDZ domains that bind the cytoplasmic, C-terminal domains of a variety of transmembrane proteins. This protein may also affect cytoskeletal-membrane organization, cell adhesion, protein trafficking, and the activation of transcription factors. The protein is primarily localized to membrane-associated adherens junctions and focal adhesions but is also found at the endoplasmic reticulum and nucleus	Decreased 8.7%
Average BrdU incorporation in untreated cells: 23.9% +/- 6.6% (S.D.)		

4.2.5 Hypoxia-induced UPR genes that are enriched on chromatin and/or stalled replication forks

As hypoxia (<0.1% O_2) induces a replication stress response, we next asked whether the proteins of any of the hypoxia-induced UPR genes are enriched on chromatin, stalled replication forks or both. Using an Isolation of Proteins on Nascent DNA (iPOND)-Mass

Spectrometry approach, Dungrawala *et al.* and Sirbu *et al.* identified proteins enriched at unperturbed chromatin and Hu-stalled replication forks (Dungrawala *et al.*, 2015; Sirbu *et al.*, 2013). We overlapped both iPOND-MS data sets with the 1113 hypoxia-induced UPR genes and identified 97 genes whose proteins are enriched on chromatin, Hu-stalled replication forks, or both (**Figure 4.4**). The list of 97 proteins can be found in **Table S4.3**.

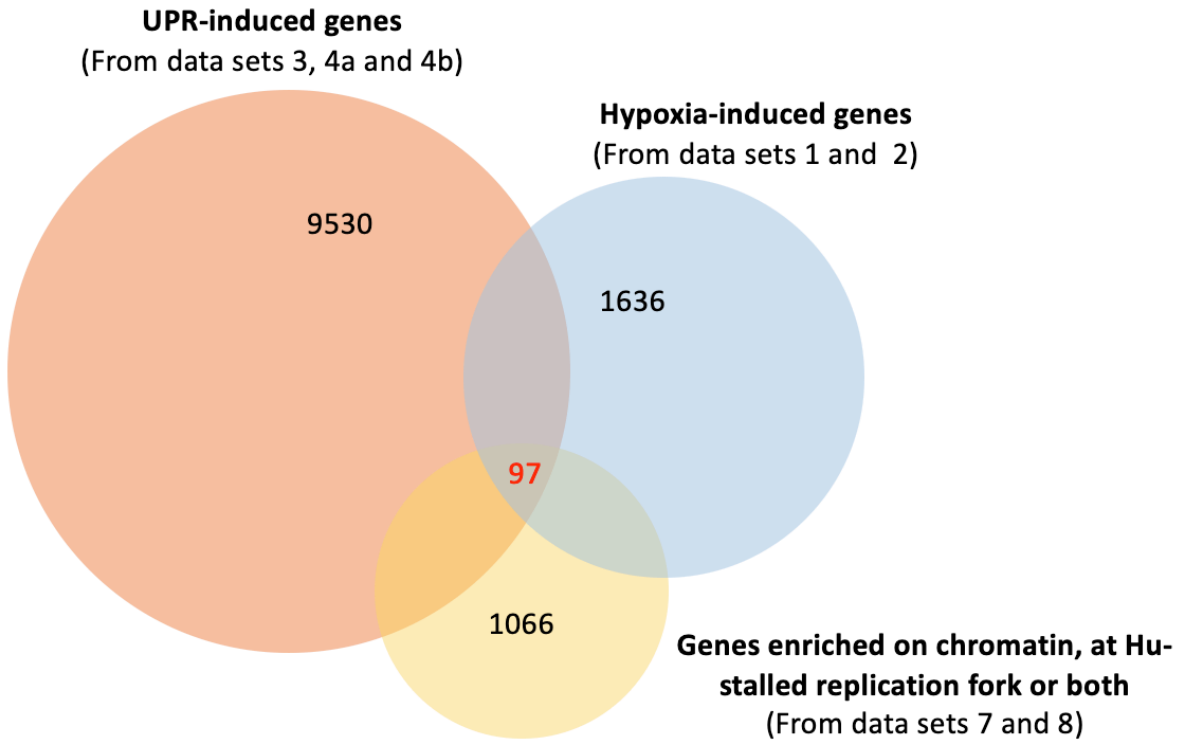


Figure 4.4. 97 UPR-induced genes in hypoxia (<0.1% O_2) are enriched on chromatin and/or Hu-stalled replication forks. Overlap between genes up-regulated by pharmacological induction of the UPR (orange), genes up-regulated by hypoxia (<0.1% O_2) (blue) and genes whose proteins are enriched at chromatin and/or Hu-stalled replication forks (yellow) identified 97 genes (red). Data sets are described in **Table 4.1**.

4.2.6 Hypoxia-induced UPR genes that interact with RNA/DNA hybrids

Noting that many transcription-associated processes are part of the enriched GO biological processes of the 103 hypoxia-induced UPR genes that play a role in the response to DNA

damage (**Figure 4.2C**), we asked whether transcription-associated structures, RNA/DNA hybrids or R-loops, may interact with hypoxia-induced UPR genes. Therefore, we used 2 data sets from Cristini *et al.* and Wang *et al.* which used S9.6 IP-MS to identify the RNA/DNA hybrid interactome (Cristini *et al.*, 2018; Wang *et al.*, 2018). We overlapped the RNA/DNA hybrid interactome with hypoxia-induced UPR genes (**Figure 4.1A, Table S4.1**) and found 79 genes, which are listed in **Table S4.4**.

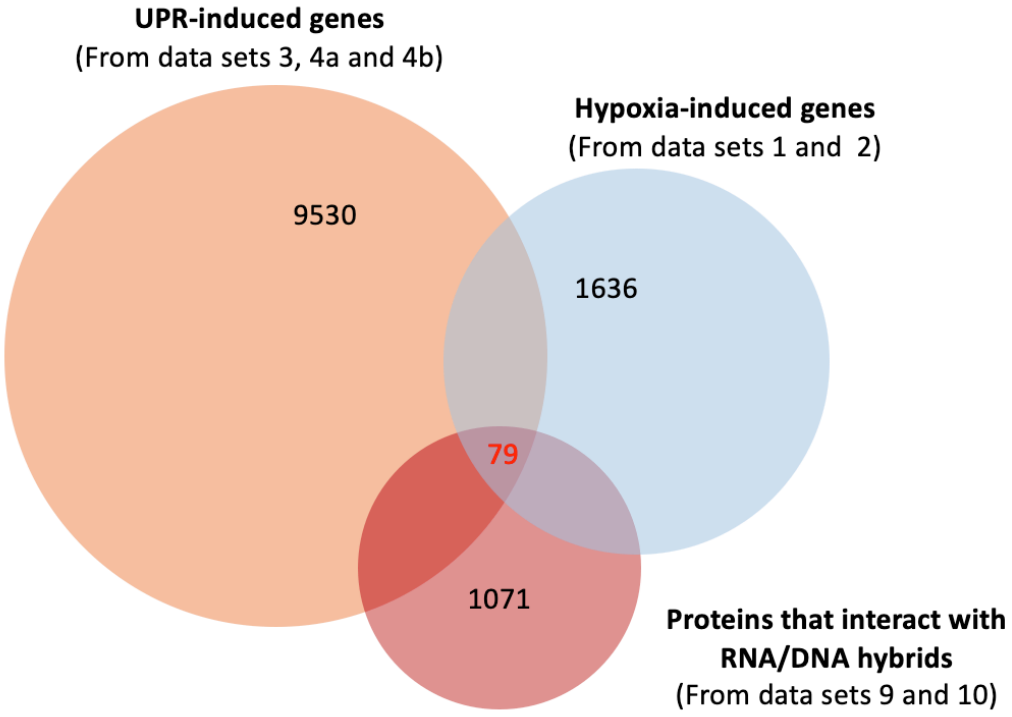


Figure 4.5. 79 UPR-induced genes in hypoxia (<0.1% O_2) interact with R-loops. Overlap between genes up-regulated by pharmacological induction of the UPR (orange), genes up-regulated by hypoxia (<0.1% O_2) (blue) and proteins that interact with RNA/DNA hybrids (yellow) identified 79 genes (red). Data sets are described in **Table 4.1**.

4.2.7 SETX: a hypoxia-induced UPR gene that plays a role in multiple processes associated with replication stress

To narrow down to a potential gene of interest that could link the UPR and DDR in hypoxia, we collated the data from **Figures 4.2-4.5** in **Table 4.3**. Out of the 103 hypoxia-induced UPR genes that play a role in the response to DNA damage (**Table S4.2**), 78 are involved in at least one of the following replication stress associated processes: DNA synthesis, enrichment on chromatin, enrichment on Hu-stalled replication forks, and interaction with R-loops. We found that the gene involved in the highest number of these replication stress associated processes is senataxin (SETX), a putative RNA/DNA helicase well characterised for resolving R-loops (Cohen *et al.*, 2018; Hasanova *et al.*, 2022).

Table 4.3 78 hypoxia-induced UPR genes that play a role in the response to DNA damage: replication stress associated processes.
Hypoxia-induced UPR genes that play a role in the DDR (grey column) were identified in Table S4.2; these are the genes we would like to further investigate. To narrow down to a specific gene, we looked at whether these 103 genes are involved in replication stress associated processes (yellow columns) by collating information from **Tables 4.2, S4.3 and S4.4**. The total number of processes each gene is involved in is tallied up in the green column. The SETX gene 'scored' the highest.

Hypoxia induced UPR gene that plays a role in the DDR	Affects DNA synthesis when knocked down	Enriched on chromatin	Enriched at Hu-stalled replication fork	Interacts with RNA/DNA hybrids	Number of processes gene is involved in
SETX		✓	✓	✓	3
BRCA1		✓	✓		2
FANCA		✓	✓		2
FANCD2		✓	✓		2
FANCI		✓	✓		2
MCM6		✓		✓	2
RAD9A		✓	✓		2

RBM39		✓		✓	2
RNASEH2A		✓		✓	2
SART1		✓		✓	2
SDCBP	✓	✓			2
STAG1		✓	✓		2
ACTA2			✓		1
ARIH2			✓		1
ATXN2L				✓	1
BTAF1		✓			1
CDCA5		✓			1
CYLD	✓				1
FBXW7	✓				1
GATA6		✓			1
GOT1			✓		1
GZF1		✓			1
MCM8		✓			1
MND1				✓	1
ORC6		✓			1
PRIM1		✓			1
RAD54L			✓		1
RB1				✓	1
RLF	✓				1
RMI1			✓		1
RRM2	✓				1
TP53		✓			1
USP1		✓			1
USP37		✓			1
VAC14			✓		1

From **Table 4.3**, SETX looks particularly interesting to study: not only is it the gene that 'scored' the highest in terms of being involved in the most replication stress associated processes, SETX is also the only R-loop interacting protein that is also enriched at Hu-stalled replication forks. Given that SETX has an established role in resolving R-loops, is a putative hypoxia-

induced UPR gene that might play in the DDR, and that R-loops have not been studied in hypoxia before, we next investigated R-loops and SETX in hypoxia to see if they have a role in linking the UPR and DDR in hypoxia.

4.2.8 Exposure to hypoxia (<0.1% O_2) induces a DDR and UPR

In order to formally demonstrate that hypoxia induces the DDR and UPR concurrently, we exposed human lung adenocarcinoma A549 cells to <0.1% O_2. As expected, hypoxia led to the stabilisation of HIF-1α. Evidence of a hypoxia-induced DDR included phosphorylation of H2AX (γ-H2AX), p53 (p53-S15) and KAP1 (KAP1-S824). Etoposide (ETP), a topoisomerase II inhibitor, was used as a positive control for DNA damage. Hu, an inhibitor of RNR, was used as a positive control for replication stress (**Figure 4.6A**). In the same samples, we also observed an increase in GRP78, the UPR master regulator, in response to hypoxia (<0.1% O_2) indicating a concurrent UPR (**Figure 4.6B**). Therefore, as predicted we demonstrated that these cells underwent both a DDR and UPR in a similar time frame after exposure to hypoxic conditions (<0.1% O_2).

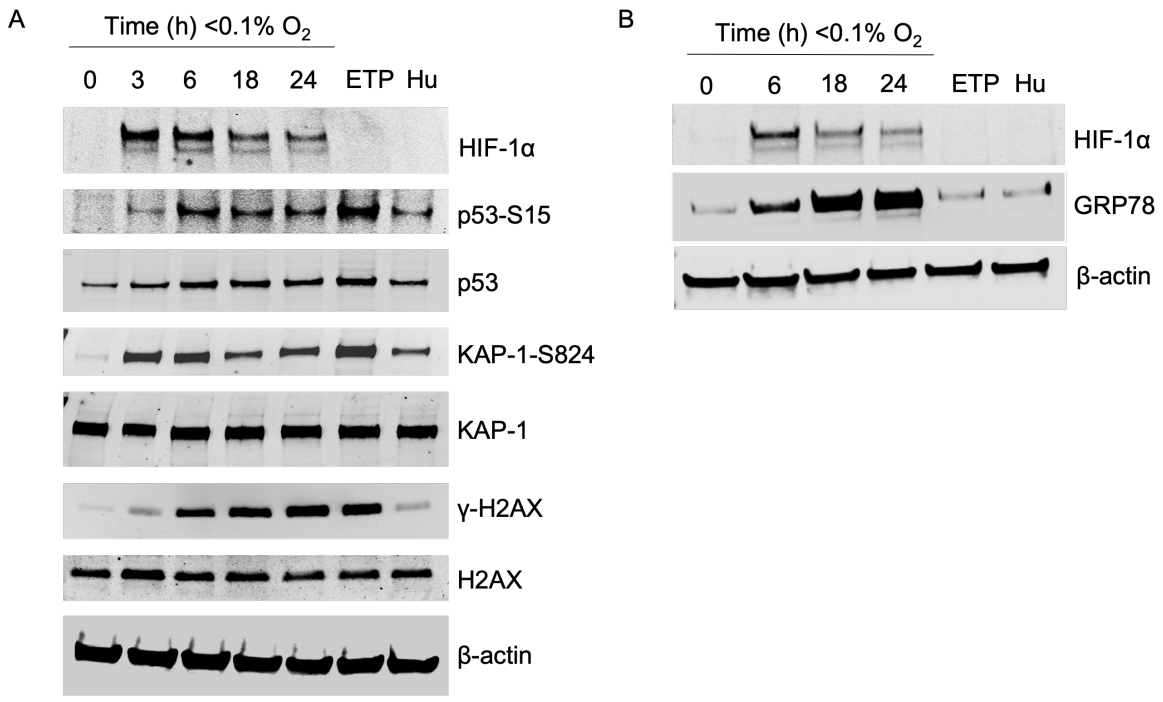


Figure 4.6. Hypoxia (<0.1% O_2) leads to a concurrent DDR and UPR. A. A549 cells were exposed to <0.1% O_2 for the times indicated and whole cell lysates were collected for western blotting. Etoposide (ETP) (25 μM for 6 hours) and hydroxyurea (Hu) (2 mM for 6 hours) were used as positive controls. β-actin was used as a loading control. **B.** Western blot showing hypoxic (<0.1% O_2) activation of the UPR in A549 cells. ETP (25 μM for 6 hours) and Hu (2 mM for 6 hours) were used as controls. β-actin was used as a loading control. n=3

4.2.9 The hypoxia induced DDR and UPR is oxygen dependent

We next investigated the oxygen dependency of the hypoxia-induced DDR and UPR. The DDR and UPR have been reported to have similar oxygen dependencies but have rarely been investigated in the same model (Koumenis *et al.*, 2002; Bi *et al.*, 2005; Koumenis *et al.*, 2007; Bencokova *et al.*, 2009). Therefore, we exposed A549 cells to a range of low oxygen tensions where HIF-1α is stabilised and found that the DDR and UPR occur specifically at <0.1% O_2 and not at 2% O_2 (**Figure 4.7**).

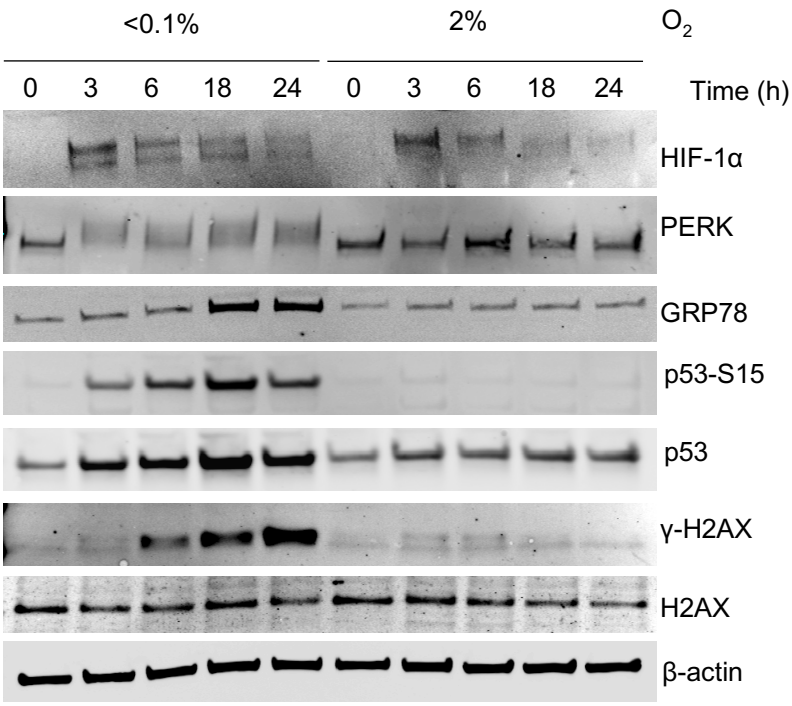


Figure 4.7. The hypoxia-induced UPR and DDR is oxygen dependent. A549 cells were exposed to hypoxic conditions (2 or <0.1% O_2) for the times indicated followed by western blotting using the antibodies shown. Increased GRP78 and a shift in PERK are indicative of a UPR. Phosphorylation of p53 (p53-S15) and H2AX (γ-H2AX) signify a DDR. β-actin was used as a loading control. n=3

At <0.1% O_2, p53 and H2AX were, again, phosphorylated and the UPR master regulator GRP78 was upregulated. Moreover, PERK showed an electrophoretic shift on the western blot, consistent with autophosphorylation as reported (Koumenis *et al.*, 2002). These indications of either an activated DDR or UPR were absent at 2% O_2. Therefore, both pathways appear to share the same oxygen dependency; they are activated at severe hypoxia (<0.1% O_2) but not mild hypoxia (2% O_2). These data also suggest that neither the DDR nor UPR is dependent on the stabilisation of HIF-1α, which occurs at both <0.1 and 2% O_2.

4.2.10 The hypoxia-induced DDR is due to an accumulation of replication stress and not DNA damage

Although hypoxia (<0.1% O_2) leads to DDR signalling (**Figure 4.7**), it is important to note that this signalling is a result of replication stress and not DNA damage (Hammond *et al.*, 2002; Hammond *et al.*, 2003). To firmly establish that hypoxia leads to replication stress and not DSBs, we exposed A549 cells to <0.1% O_2 and carried out immunofluorescence staining for markers of replication stress and DNA damage (**Figure 4.8**). As expected, the proportion of cells undergoing replication stress, as indicated by the formation of >5 RPA foci in the nucleus, increased up to approximately 40%, which likely reflects the proportion of A549 cells in S phase. However, the proportion of cells with 53BP1 foci (blue bars), a marker of DNA damage from DSBs, showed no significant increase during exposure to hypoxia (<0.1% O_2). In comparison, the DNA damaging drug neocarzinostatin (NCS) led to formation of RPA, γ-H2AX and 53BP1 foci in over 60% of cells after 6 hours of treatment.

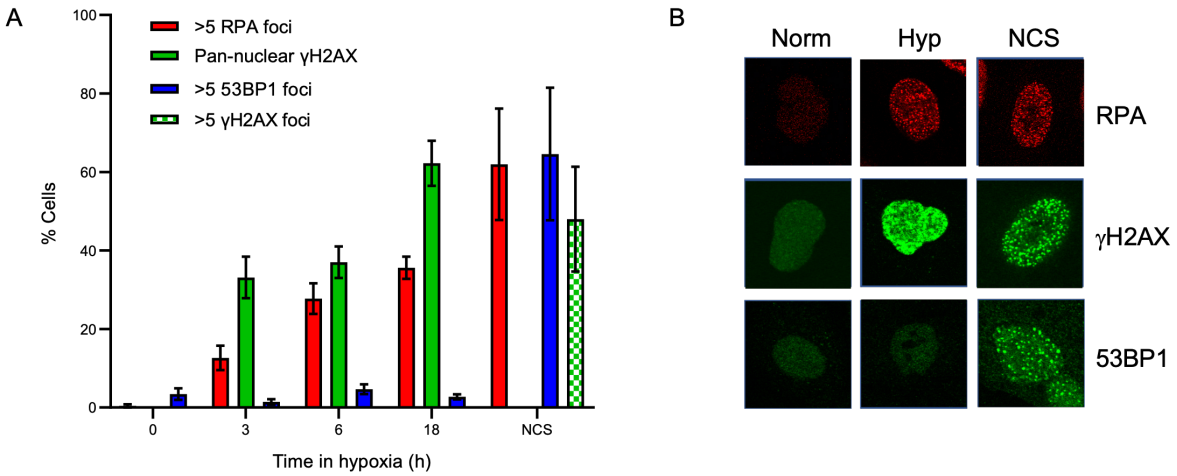


Figure 4.8. Hypoxia leads to replication stress but not DSBs. A. A549 cells were exposed to <0.1% O_2 for the times indicated and then co-stained for RPA and γ-H2AX and for 53BP1. The DNA damaging agent neocarzinostatin (NCS) (200 ng/µL for 6 hours) was used as a positive control for DNA damage. A representative plot of 3 independent experiments is shown here where error bars represent S.D. from fields of view. **B.** Representative images of RPA (red), γ-H2AX (green) and 53BP1 (green) staining in A549 cells exposed to 0, 6 hours of <0.1% O_2 and NCS from part A. n=3

It is important to note that in contrast to cells with γ-H2AX foci, the proportion of cells with pan-nuclear γ-H2AX (green bars) staining did increase in hypoxia. This pan-nuclear stain is characteristic of hypoxic cells and has been associated with replication stress (Bencokova *et al.*, 2009; Hammond *et al.*, 2003). In comparison, NCS formed distinct nuclear γ-H2AX foci (**Figure 4.8**).

To demonstrate that the lack of DSBs in hypoxic (<0.1% O_2) cells despite the accumulation of replication stress was not a cell line dependent observation, a second cell line, human colorectal cancer RKO cell, was investigated. As previously, when RKO cells were exposed to <0.1% O_2, there was an increase in the proportion of cells undergoing replication stress (positive for RPA foci) but the proportion of cells with 53BP1 foci did not significantly increase (**Figure 4.9**).

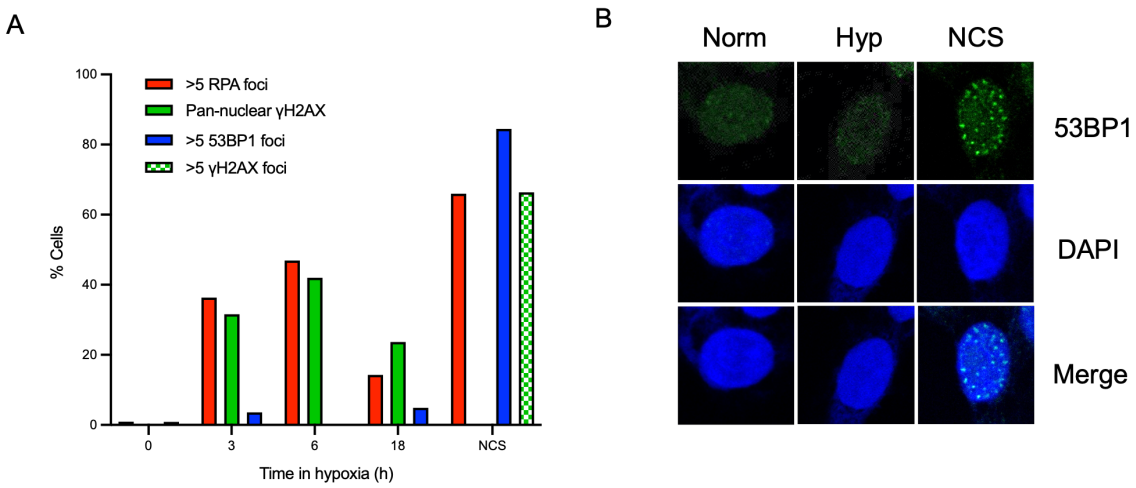


Figure 4.9. Hypoxia leads to replication stress but not DSBs. A. RKO cells were exposed to <0.1% O_2 for the times indicated and then co-stained for RPA and γ-H2AX and for 53BP1. Neocarzinostatin (200 ng/μL for 6 hours) was used as a positive control for DNA damage. Error bars showing S.D. are from at least 5 fields of view from a representative experiment. **B.** Representative images of 53BP1 (green) staining in A549 cells from part A. n=2

Next, we asked whether the cells that formed RPA foci in response to hypoxia were the same cells that had pan-nuclear γ-H2AX staining. Although both markers are characteristic of hypoxic cells, whether they form in the same cells has not been formally verified. The use of pan-nuclear γ-H2AX is less well-established as a marker of replication stress compared to RPA foci. Therefore, in RKO cells exposed to <0.1% O_2, we quantified the number of RPA foci/cell and recorded whether or not there was also pan-nuclear γ-H2AX staining (**Figure 4.10A**). We found that the cells positive for pan-nuclear γ-H2AX had a higher average number of RPA foci per cell compared to pan-nuclear γ-H2AX negative cells at every time point; the difference at each hypoxic time point was statistically significant. This indicates that the hypoxia-induced replication stress is characterised by pan-nuclear γ-H2AX staining and RPA foci in the same cell. Furthermore, this was the first time we quantified the number of RPA foci per cell in addition to quantifying the percentage of cell population with >5 RPA foci. Previous reports demonstrated that in response to hypoxia, the number of cells with >5 RPA foci increases rapidly but then decreases with longer exposure to hypoxia (Pires *et al.*, 2010). Now, by analysing the number of RPA foci/cell in hypoxia we have determined a similar pattern. The average number of RPA foci/cell increased significantly but decreased at a later time point (**Figure 4.10A**). The number of detected foci per cell ranged from 0 to 38.

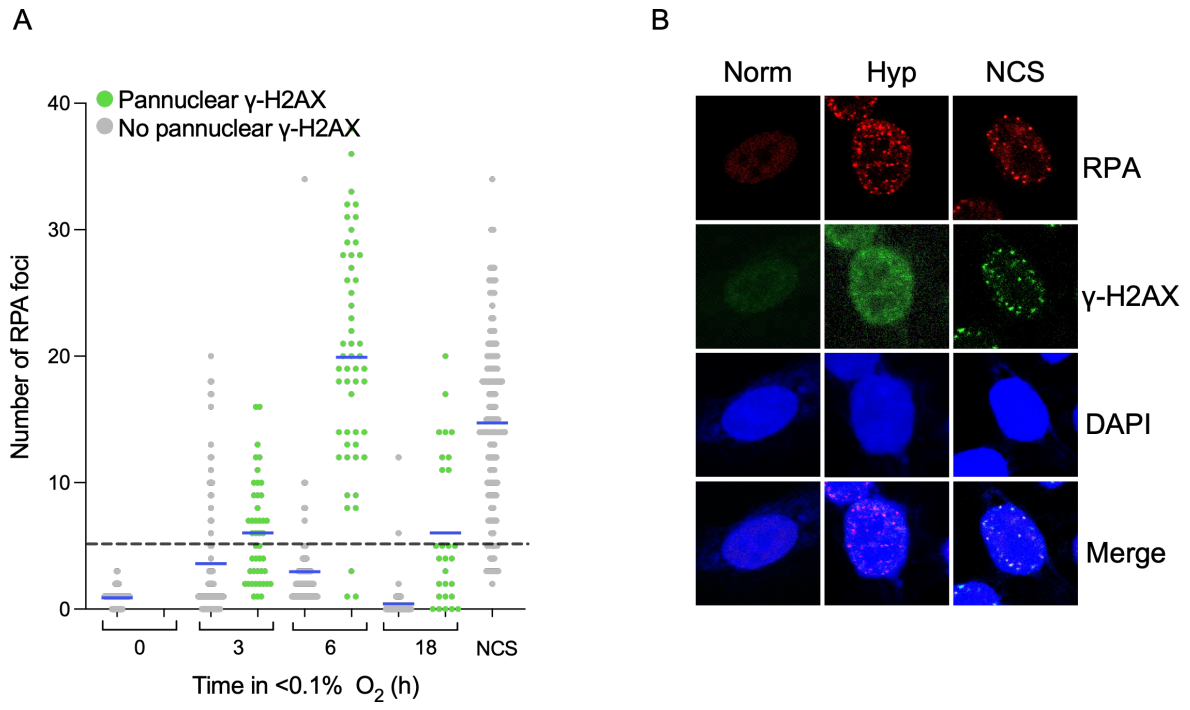


Figure 4.10. Hypoxia-induced replication stress is characterised by pan-nuclear γ-H2AX and RPA foci in the same cell. A. RKO cells were exposed to hypoxia (<0.1% O_2) for the times indicated and then co-stained for RPA and γ-H2AX. Neocarzinostatin (NCS) (200 ng/µL for 6 hours) was used as a positive control for DNA damage. The number of RPA foci/cell are shown in the γ-H2AX positive (green circles) and negative (grey circles) cells. The γ-H2AX positive cells had a higher average number of RPA foci per cell as shown by the blue line. Cells above the black dotted line would be characterised as experiencing replication stress as they have > 5 RPA foci/nuclei. At least 100 cells were quantified for each timepoint. **B.** Representative images of RPA (red) and γ-H2AX (green) staining in RKO cells exposed to 0, 6 hours of <0.1% O_2 and NCS from part A. n=2

4.2.11 Hypoxia (<0.1% O_2) leads to an accumulation of R-loops

As we previously identified SETX as a hypoxia-induced UPR gene of interest and SETX is known to resolve R-loops, we asked whether or not R-loop levels changed in hypoxia. R-loops, 3-stranded nucleic acid structures, are comprised of an RNA/DNA hybrid and an exposed ssDNA (Crossley *et al.*, 2019). The wild-type RNaseH1 enzyme binds to and resolves RNA/DNA hybrids. To measure R-loops, we transfected A549 cells with mutant RNaseH1^{D210N}-V5, a catalytically dead mutant of RNaseH1 that can only bind to R-loops but not resolve them.

Visualising this mutant has been routinely used as a method in the R-loop field to quantify R-loop levels (Chen *et al.*, 2017; Nowotny *et al.*, 2007). CPT and DRB were used as positive controls for increasing and decreasing R-loop levels, respectively (Chen *et al.*, 2017; Cristini *et al.*, 2019; Makharashvili *et al.*, 2018; Sanz *et al.*, 2016). We exposed the transfected A549 cells to a time course in hypoxia and stained the cells for V5. Strikingly, we observed a robust accumulation of R-loops in hypoxia (<0.1% O_2) by up to approximately 3.5 times the normoxic levels (**Figure 4.11**).

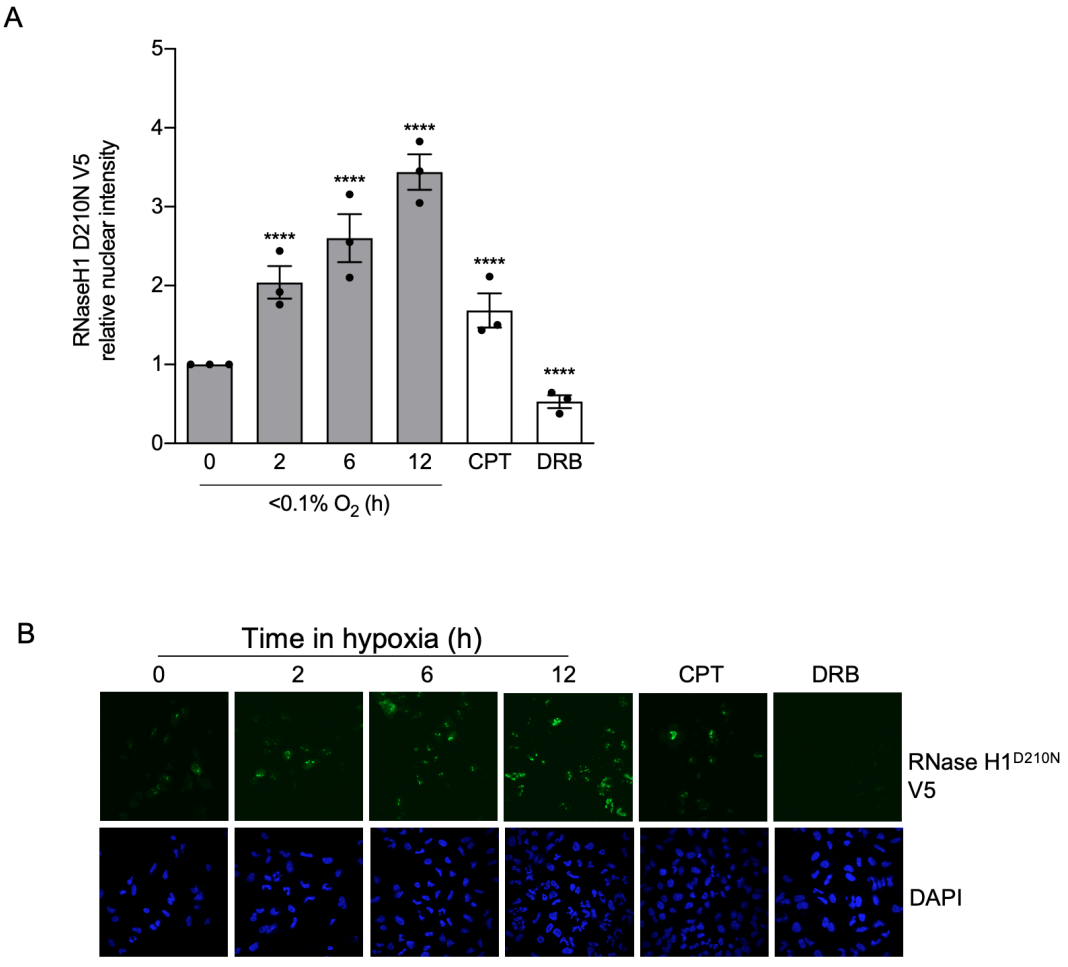


Figure 4.11. R-loops accumulate in hypoxia (<0.1% O_2). A. A549 cells were transfected with RNaseH1^{D210N}-V5 and exposed to hypoxia (<0.1% O_2), CPT (10 µM, 20 min), or DRB (100 µM, 1 hour). Staining for V5 was then carried out and the nuclear intensity determined, normalised to the normoxic control. The two-tailed Student's *t*-test was used: ****$p < 0.0001$. **B.** Representative images of Part A. n=3

4.2.12 Hypoxia (<0.1% O_2) induced R-loops contribute to replication stress and DDR signalling

To our knowledge, we observed for the first time that R-loops accumulate in severe hypoxia (**Figure 4.11**). As we know that replication stress accumulates in hypoxia, and R-loops can contribute to replication stress, we next asked whether R-loops contribute to replication stress signalling in hypoxia. We transfected the human colorectal cancer cell line, HCT116, with mock or wildtype RNaseH1 plasmid and exposed them to 6 hours of hypoxia (<0.1% O_2). Interestingly, we observed that replication stress markers in hypoxia were indeed reduced upon wildtype RNaseH1 overexpression; hypoxia-induced phosphorylation of RPA and CHK1 were reduced (**Figure 4.12A**) and hypoxia-induced RPA foci were reduced by approximately 40% (**Figure 4.12B**). Next, we asked whether or not R-loops also contribute to DDR signalling. Again, we transfected HCT116 cells with wildtype RNaseH1 plasmid and exposed them to 6 hours of hypoxia (<0.1% O_2). Consistent with what we observed with replications stress markers, hypoxia-induced DDR signalling was also abrogated upon RNaseH1 overexpression (**Figure 4.12C**). Phosphorylation of KAP1, p53 and H2AX were reduced. Interestingly, HIF-1α levels were also reduced when R-loops levels were reduced.

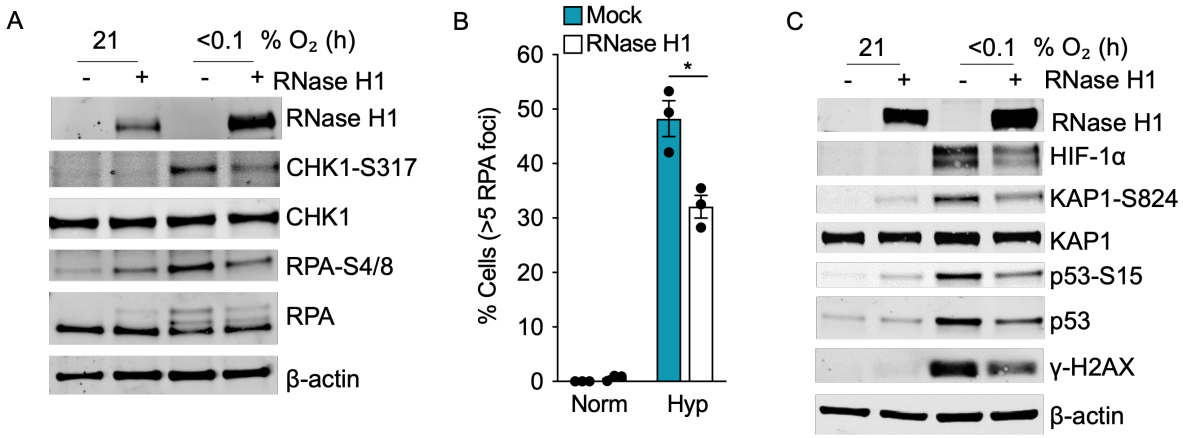


Figure 4.12. RNaseH1 overexpression abrogates hypoxia-induced replication stress and DDR signalling. HCT116 cells were transfected with wildtype RNaseH1 and exposed to hypoxia (<0.1% O_2) for 6 hours and followed by **A.** western blotting with the antibodies against replication stress markers shown, where β-actin was used as a loading control **B.** immunofluorescence staining for RPA where the two-tailed Student's *t*-test was used (**p*= 0.0142) or **C.** western blotting with the antibodies against DDR markers shown where β-actin was used as a loading control. n=3 *All data from Figure 4.12 was generated by Dr Shaliny Ramachandran.*

4.2.13 Hypoxia (<0.1% O_2) induces SETX in an oxygen dependent manner

As our bioinformatic analyses pinpointed SETX as a hypoxia-induced UPR gene of interest that is known to resolve R-loops, and we observed a striking increase in R-loop levels in hypoxia (<0.1% O_2) (**Figure 4.11**), we next asked whether or not the levels of SETX also increased in hypoxia. We exposed a panel of human cancer cell lines to a time course in hypoxia (<0.1% O_2) and observed that SETX protein levels indeed increased, especially at the later time points (**Figure 4.13A, B, C**).

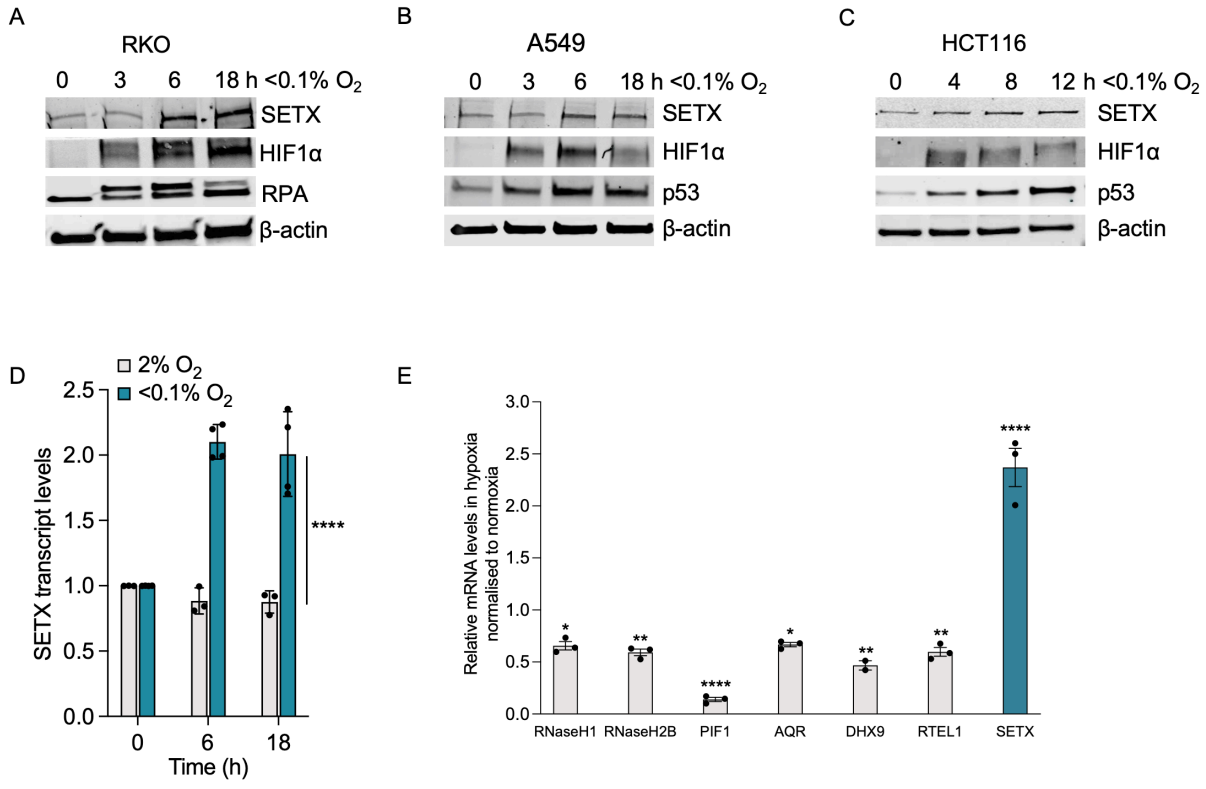


Figure 4.13. SETX is induced in hypoxia (<0.1% O_2). Western blots of lysates from **A.** RKO, **B.** A549 and **C.** HCT116 cells exposed to <0.1% O_2 for the time shown. β-Actin was used as a loading control. **D.** A549 cells exposed to hypoxia, 2% O_2 or <0.1% O_2 for the times indicated and the relative mRNA levels of SETX to 18S were determined. The two-way ANOVA was used: ****p< 0.0001. **E.** RKO cells were exposed to 6 hours of hypoxia (<0.1% O_2) followed by RT-qPCR for the mRNAs indicated relative to the normoxic control normalised to 18S. One-way ANOVA Dunnett's multiple comparisons test was used: RNaseH1 (p = 0.0162), RNaseH2B (p = 0.0042), PIF1 (p < 0.0001), AQR (p = 0.0207), DHX9 (p = 0.0010), RTEL1 (p= 0.0046), SETX (p < 0.0001). n=3 All *the data from Figure 4.14 were generated by Dr Shaliny Ramachandran.*

In addition to the increase at protein level, we saw that SETX was also transcriptionally induced by hypoxia (<0.1% O_2) with an approximately two-fold increase. Importantly, SETX induction in hypoxia is oxygen dependent as we only observed an increase in SETX mRNA levels in severe hypoxia (<0.1% O_2) and not in mild hypoxia (2% O_2) (**Figure 4.13D**). We next asked whether or not other well-established R-loop resolving factors, including RNaseH1, RNaseH2B, PIF1, AQR, DHX9 and RTEL1, are also induced in hypoxia (<0.1% O_2) like SETX. Strikingly, the other R-loop resolving factors were not induced after 6 hours of hypoxia (<0.1% O_2) and were in fact repressed at the mRNA level (**Figure 4.13E**). This finding makes SETX even more interesting to study as it stands out as the only gene out of the panel of R-loop resolving factors to be induced in hypoxia (<0.1% O_2).

4.2.14 SETX reduces R-loops and protects cells from DNA damage and cell death in hypoxia

Next, we asked whether or not hypoxia-induced SETX has a role to play in resolving R-loops in hypoxia. Here, we used the S9.6 antibody which recognises the RNA/DNA hybrid portion of an R-loop and is widely used in the R-loop field to measure R-loop levels (Boguslawski *et al.*, 1986; Bou-Nader *et al.*, 2022). RNase H treatment to resolve R-loops was used as a control in S9.6 immunofluorescence, to show the specificity of the S9.6 antibody to R-loops. We transfected A549 cells with mock or siRNA to SETX and exposed them to hypoxia (<0.1% O_2). As expected, we saw an increase in R-loop levels from normoxia to hypoxia in mock-

transfected cells, consistent with what we observed using the orthogonal mutant RNaseH1 assay from **Figure 4.11**. Excitingly, there was a further increase in R-loop levels in SETX depleted cells in both normoxia and hypoxia (**Figure 4.14A**), indicating that SETX reduces R-loops in both normoxia and hypoxia. This is consistent with studies characterising SETX as a putative RNA/DNA helicase that can resolve RNA/DNA hybrids (Cohen *et al.*, 2018).

Next, we asked whether or not the further increase in R-loops in SETX depleted cells would lead to DNA damage. Unresolved R-loops are known to lead to genomic instability and potentially SSBs and DSBs (Crossley *et al.*, 2019). Therefore, we fixed SETX depleted cells exposed to hypoxia and stained for DNA damage marker 53BP1 foci. As expected, there was no increase in DNA damage in mock transfected cells exposed to hypoxia. However, there was a striking increase in DNA damage in SETX depleted cells in hypoxia (**Figure 4.14B**), indicating that SETX protects hypoxic cells from DNA damage, possibly through reducing R-loops that accumulate in hypoxia.

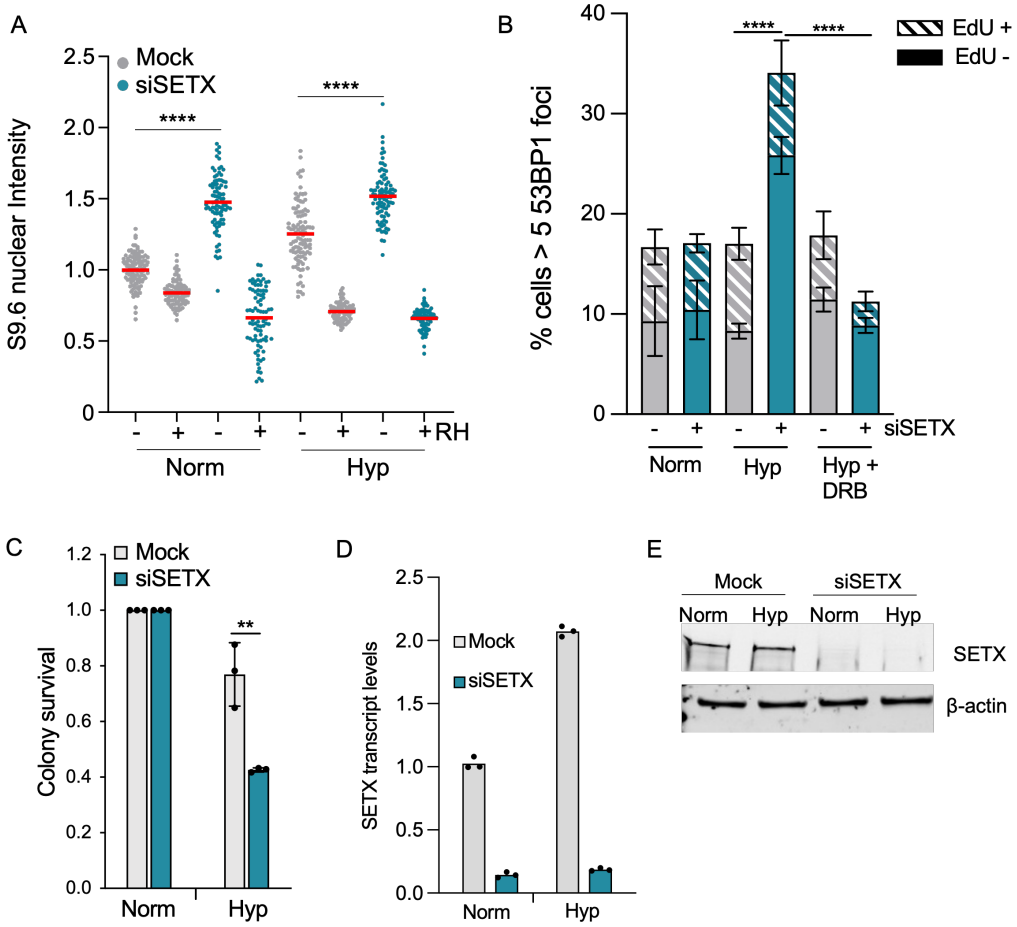


Figure 4.14. SETX reduces R-loops and protects from DNA damage and cell death in hypoxia. **A.** A549 cells were transfected with mock (grey) or SETX siRNA (green) and exposed to 21% O_2 or <0.1% O_2 for 12 hours. Cells were fixed and stained with S9.6 antibody and DAPI and treated with RNase H prior to staining where indicated. The nuclear intensity of S9.6 was quantified. **B.** A549 cells that were either mock-transfected (grey) or transfected with SETX siRNA (green) were pulsed with EdU (10 µM) for 1 h then and exposed to 21% O_2 (Norm), <0.1% O_2 (Hyp) for 6 h or treated with DRB (100 µM) in <0.1% O_2 for 6 h (Hyp + DRB). The percentage of cells displaying 53BP1 (>5 per nucleus) is shown. The two-tailed Student's *t*-test was used: ****$p < 0.0001$. **C.** Colony survival of A549 cells with either mock treatment or SETX siRNA after 0 and 18 h of hypoxia (Hyp) (<0.1% O_2) treatment. The two-tailed Student's *t*-test was used: **p = 0.0068. **D.** RT-qPCR for SETX normalised to 18S in cells from A, representative of n=2. **E.** Western blotting for SETX using cells from B. n=3 except for D which is n=2. *Data in panels A and D of Figure 4.15 were generated by Dr Shaliny Ramachandran.*

Interestingly, we were able to rescue the DNA damage by adding DRB, an RNA pol II inhibitor that reduces transcription; this implies that the DNA damage that accumulates in SETX depleted hypoxic cells may be transcription-associated. Moreover, to see whether or not the increase in DNA damage is S phase specific, we pulsed the cells with EdU before fixing.

Surprisingly, the DNA damage observed in SETX-depleted cells occurred mainly in non-S phase (EdU negative) cells, suggesting that SETX is resolving hypoxic R-loops that do not result from transcription-replication conflicts (**Figure 4.14B**). The precise mechanism for which SETX depleted cells in hypoxia accumulate DNA damage therefore warrants further investigation.

Finally, to see whether or not the increase in DNA damage in SETX depleted cells affects survival, we carried out a colony survival assay. Unsurprisingly, SETX depleted cells in hypoxia had reduced survival compared to cells exposed to hypoxia alone (**Figure 4.14C**), indicating that SETX protects hypoxic cells from cell death.

4.2.15 SETX is induced through the UPR PERK/ATF4 arm in hypoxia (<0.1% O_2)

Next, we investigated the mechanism through which SETX is induced in hypoxia. As SETX was identified as a hypoxia-induced UPR gene from our bioinformatic analyses (**Figure 4.1A, Table S4.1**), we expected SETX to be induced downstream of at least one of the 3 arms of the UPR. Encouragingly, we found predicted binding sites for the UPR transcription factor ATF4 (downstream of PERK) in the GeneHancer identifiers GH09J132349 and GH09J132944 corresponding to the *SETX* promoter region (Fishilevich *et al.*, 2017).

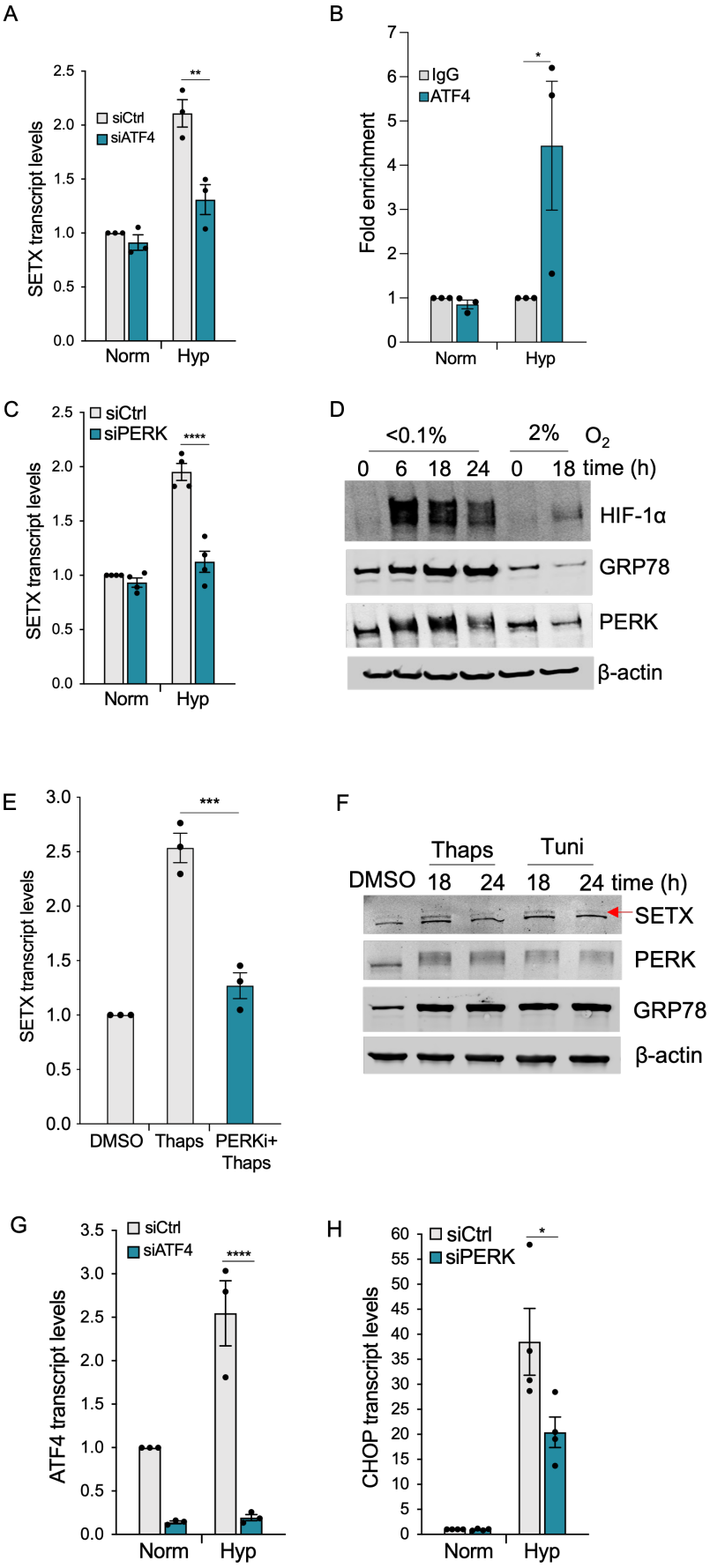

A
SETX transcript levels
siCtrl
siATF4
**
Norm
Hyp
B
Fold enrichment
IgG
ATF4
*
Norm
Hyp
C
SETX transcript levels
siCtrl
siPERK
****
Norm
Hyp
D
<0.1%
2%
O2
0 6 18 24 0 18 time (h)
HIF-1α
GRP78
PERK
β-actin
E
SETX transcript levels
***
DMSO
Thaps
PERKi+ Thaps
F
Thaps
Tuni
DMSO 18 24 18 24 time (h)
SETX
PERK
GRP78
β-actin
G
ATF4 transcript levels
siCtrl
siATF4
****
Norm
Hyp
H
CHOP transcript levels
siCtrl
siPERK
*
Norm
Hyp

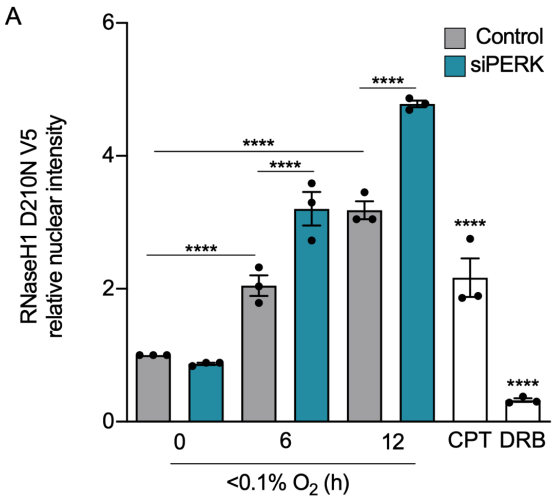
Figure 4.15. SETX is induced through the PERK/ATF4 arm of the UPR. A. A549 cells were transfected with mock (grey) or ATF4 siRNA (green) and exposed to 21% O_2 or <0.1% O_2 for 16 hours. SETX transcript levels were determined with RT-qPCR. One-way ANOVA Tukey's multiple comparisons test was used: ** p = 0.0023. **B.** A549 cells were exposed to 21% O_2 or <0.1% O_2 for 4 hours, and fold enrichment of ATF4 on the SETX promoter relative to IgG control was determined using ChIP-qPCR. One-way ANOVA Tukey's multiple comparisons test was used: * p = 0.0416. **C.** A549 cells were transfected with mock (grey) or PERK siRNA (green) and exposed to 21% O_2 or <0.1% O_2 for 16 hours. SETX transcript levels were determined with RT-qPCR. One-way ANOVA Tukey's multiple comparisons test was used: **** p < 0.0001. **D.** Western blots of lysates from A549 cells exposed to hypoxia (<0.1% O_2 or 2% O_2) for the times shown. β-actin was used as a loading control. **E.** A549 cells were treated with or without GSK2606414 (10 μM) (PERKi) and exposed to DMSO or Thaps (2 μM) for 6 hours. SETX transcript levels were determined with RT-qPCR. One-way ANOVA Tukey's multiple comparisons test was used: *** p = 0.0003. **F.** Western blot lysates from A549 cells treated with Thaps (2 μM) or Tuni (5 μg/mL) for the times shown. β-actin was used as a loading control. **G.** RT-qPCR for ATF4 normalised to 18S using cells from A. One-way ANOVA Tukey's multiple comparisons test was used: **** p < 0.0001. **H.** RT-qPCR for CHOP normalised to 18S to confirm knockdown of PERK using cells from C. One-way ANOVA Tukey's multiple comparisons test was used: * p = 0.0206. n=3, n=1 for F. *Data in panels A, B, C, G and H in Figure 4.15 were generated by Dr Shaliny Ramachandran.*

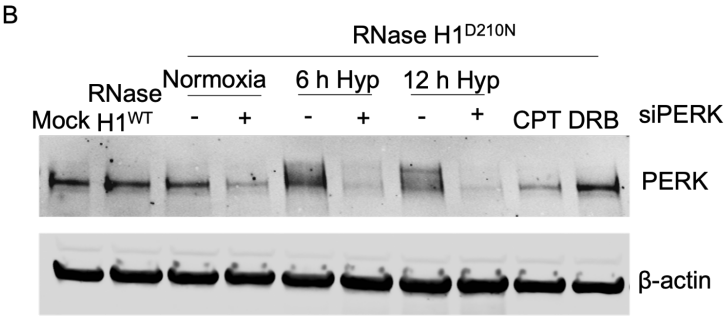
To confirm that SETX is induced through the PERK/ATF4 branch of the UPR in hypoxia, we depleted the transcription factor ATF4 with siRNA. Indeed, we saw that the induction of SETX transcripts was abrogated in ATF4 depleted cells in hypoxia (**Figure 4.15A**). In addition, we used chromatin immunoprecipitation qPCR (ChIP-qPCR) to directly show that ATF4 binds on the SETX promoter in hypoxia (**Figure 4.15B**). As ATF4 is a transcription factor induced downstream of PERK, we expected that SETX would also be induced in a PERK dependent manner. Therefore, we depleted cells of PERK using siRNA, and indeed observed that SETX induction in hypoxia was reduced (**Figure 4.15C**). In hypoxia (<0.1% O_2) where the UPR is active, other signalling pathways such as HIF-1α are also active (**Figure 4.15D**). To formally demonstrate that it is specifically the UPR that induces SETX, we used the UPR inducer Thaps, and showed that SETX is induced in response to Thaps in a PERK dependent manner (**Figure 4.15E**). The transcriptional induction of SETX by Thaps and Tuni is also reflected in the bioinformatic datasets listed in **Table 4.1** (Luhr *et al.*, 2019; Raina *et al.*, 2014). Finally, to

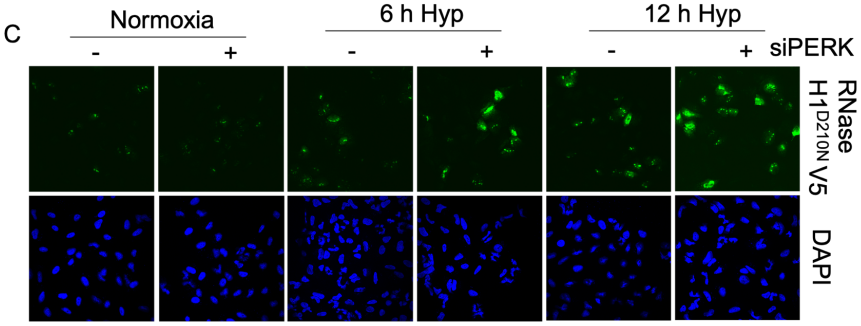
confirm that the UPR inducers can also induce SETX protein levels, we indeed saw that Thaps and Tuni treatment led to an increase in SETX levels on a western blot (**Figure 4.15F**). These data, in combination with our bioinformatic analyses showing that SETX is a hypoxia-induced UPR gene (**Figure 4.1A, Table S4.1**), strongly support that SETX is induced through the PERK/ATF4 arm of the UPR in hypoxia.

4.2.16 PERK inhibition in hypoxia leads to further increase in R-loops and the accumulation of DNA damage

After establishing that SETX is induced through the PERK/ATF4 arm of the UPR, we next asked whether depletion or inhibition of PERK would phenocopy SETX depletion in hypoxia i.e., result in a further increase in R-loops and an accumulation of DNA damage in hypoxia. Therefore, we depleted A549 cells of PERK using siRNA, exposed them to 6 and 12 hours of hypoxia (<0.1% O_2) and measured R-loop levels. Strikingly, there was a significant further increase in R-loop levels at each time point in hypoxia where PERK was depleted (**Figure 4.16A-C**). Where 6 hours of hypoxia (<0.1% O_2) led to an approximate 2-fold increase in R-loop levels, PERK depletion further increased that to approximately 3-fold. The same pattern was observed at 12 hours of hypoxia where the 3-fold increase in R-loop levels was further increased to almost 5-fold upon PERK depletion. In addition to genetic depletion of PERK, we also treated A549 cells with PERK inhibitor (PERKi) GSK2606414 and measured R-loop levels after exposure to hypoxia. Consistently, we saw the same pattern as with the PERK siRNA: inhibiting PERK at each time point in hypoxia clearly led to a further increase in R-loops (**Figure 4.16D**).


A
RNaseH1 D210N V5
relative nuclear intensity
Control
siPERK
****
0
6
12
CPT
DRB
<0.1% O2 (h)


B
RNase H1D210N
Normoxia
6 h Hyp
12 h Hyp
RNase
Mock
H1WT
CPT
DRB
siPERK
PERK
β-actin


C
Normoxia
6 h Hyp
12 h Hyp
siPERK
RNase H1D210N V5
DAPI

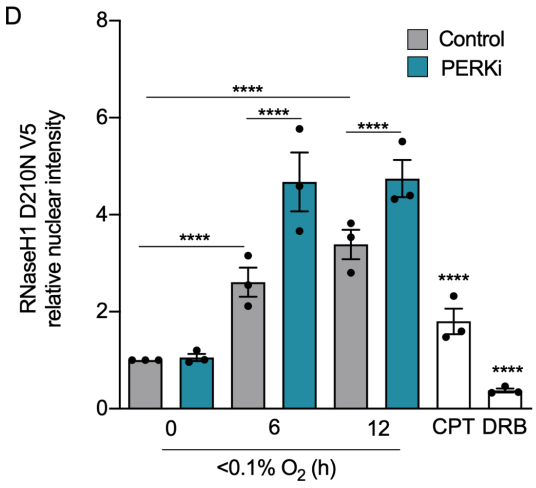

D
RNaseH1 D210N V5
relative nuclear intensity
Control
PERKi
****
0
6
12
CPT
DRB
<0.1% O2 (h)

Figure 4.16. PERK depletion or inhibition leads to a further accumulation of R-loops in hypoxia. A. A549 cells were transfected with mock (grey) or PERK siRNA (green), then transfected with RNaseH1^{D210N}-V5 and exposed to hypoxia (<0.1% O_2) for the times shown, CPT (10 μM, 20 min), or DRB (100 μM, 1 h). Staining for V5 was then carried out and the nuclear intensity determined, normalised to normoxic control. The two-tailed Student's *t*-test was used: ****p < 0.0001. **B.** Western blot of lysates from part A to confirm PERK knockdown. **C.** Representative images of part A. **D.** A549 cells were transfected with RNaseH1^{D210N}-V5, treated with or without GSK2606414 (10 μM) (PERKi) and exposed to hypoxia (<0.1% O_2) for the times shown, CPT (10 μM, 20 min), or DRB (100 μM, 1 h). Staining for V5 was then carried out and the nuclear intensity determined, normalised to normoxic control. The two-tailed Student's *t*-test was used: ****p < 0.0001. n=3

Next, we asked whether PERK inhibition could lead to an accumulation in DNA damage in hypoxia. We exposed A549 cells to hypoxia (<0.1% O_2) with or without PERK inhibitor and carried out immunofluorescence staining for the DSB marker 53BP1. As expected, cells exposed to hypoxia (<0.1% O_2) alone did not accumulate DSBs. Strikingly, PERK inhibition in hypoxia led to a significant increase in DSBs as measured by the percentage of cells with >5 53BP1 foci (**Figure 4.17A**). Interestingly, we were able to rescue the PERKi-induced increase in DSBs with the transcription inhibitor DRB (**Figure 4.17A, B**), suggesting that the DNA damage accumulated may be transcription associated.

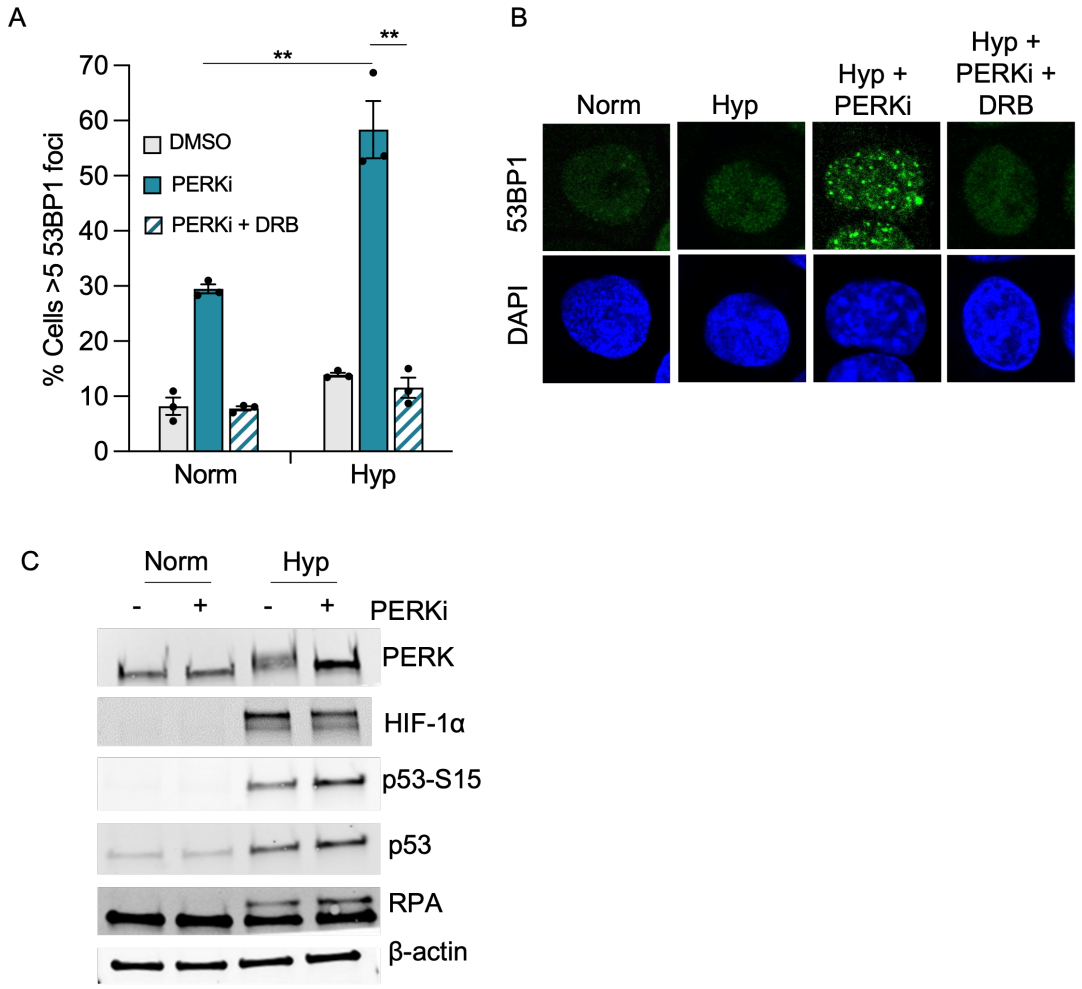


Figure 4.17. Inhibition of PERK in hypoxia leads to the accumulation of DNA damage. A. The percentage of cells displaying 53BP1 foci (>5 per nucleus) as determined by immunofluorescence, in A549 cells exposed to 21% O_2 (Norm) or 6 hours of <0.1% O_2 (Hyp). Cells were treated with DMSO, PERK inhibitor GSK2606414 (10 µM) (PERKi), or DRB (100 µM) and PERK inhibitor (10 µM), (PERKi + DRB). The two-tailed Student's *t*-test was used: Norm PERKi versus Hyp + PERKi (***p* = 0.0067), Hyp + PERKi versus Hyp + PERKi + DRB (***p* = 0.0068). **B.** Representative images of part A. **C.** Western blot of A549 cell lysates from part A to confirm PERK inhibition. β-actin was used as a loading control. n=3

In addition, we also asked whether the increase in R-loops and DNA damage from PERK inhibition in hypoxia affected DDR signalling. Unsurprisingly, we saw a further increase in hypoxia-induced DDR signalling upon PERK inhibition as phosphorylation of p53 and RPA are further increased (**Figure 4.17C**).

4.2.17 UPR inhibition in hypoxia exacerbates replication stress

As we saw that inhibiting the PERK arm of the UPR led to an accumulation of DSBs and increased DDR signalling in hypoxia (**Figure 4.17**), we next asked whether inhibiting PERK would increase phosphorylated RPA bound on chromatin, a canonical marker of replication stress. Here, we also tested an alternative UPR inhibitor, 4μ8c, which inhibits IRE1α; this allows us to investigate whether inhibiting another arm of the UPR would also affect replication stress.

Before we explored the impact of the UPR inhibitors on replication stress, however, we asked whether these inhibitors had an effect on cell cycle distribution in hypoxia. As replication stress can only occur in S phase cells, any changes to the percentage of cells in S phase could affect the number of cells experiencing replication stress (those with >5 RPA foci) (Gelot *et al.*, 2015). Therefore, we exposed A549 cells to hypoxia (<0.1% O_2) with or without one of the UPR inhibitors, GSK2606414 (PERKi) or 4μ8c (IRE1αi), and added EdU, which was incorporated into replicating cells in S phase (**Figure 4.18A**). We carried out immunofluorescence staining for EdU and found that as expected, hypoxia (<0.1% O_2) alone led to a decrease in the percentage of S phase cells undergoing DNA synthesis. We found that there was no change in the percentage of S phase cells in hypoxia (<0.1% O_2) when UPR inhibitors were added (**Figure 4.18B**). Although only preliminary data was generated (n=1), we were confident enough to proceed to the analysis of replication stress. We verified that the UPR inhibitors had no significant effect on cell cycle distribution. To conclusively rule out a role for the UPR in cell cycle distribution, further analysis would be required, potentially including the use of DNA fibres.

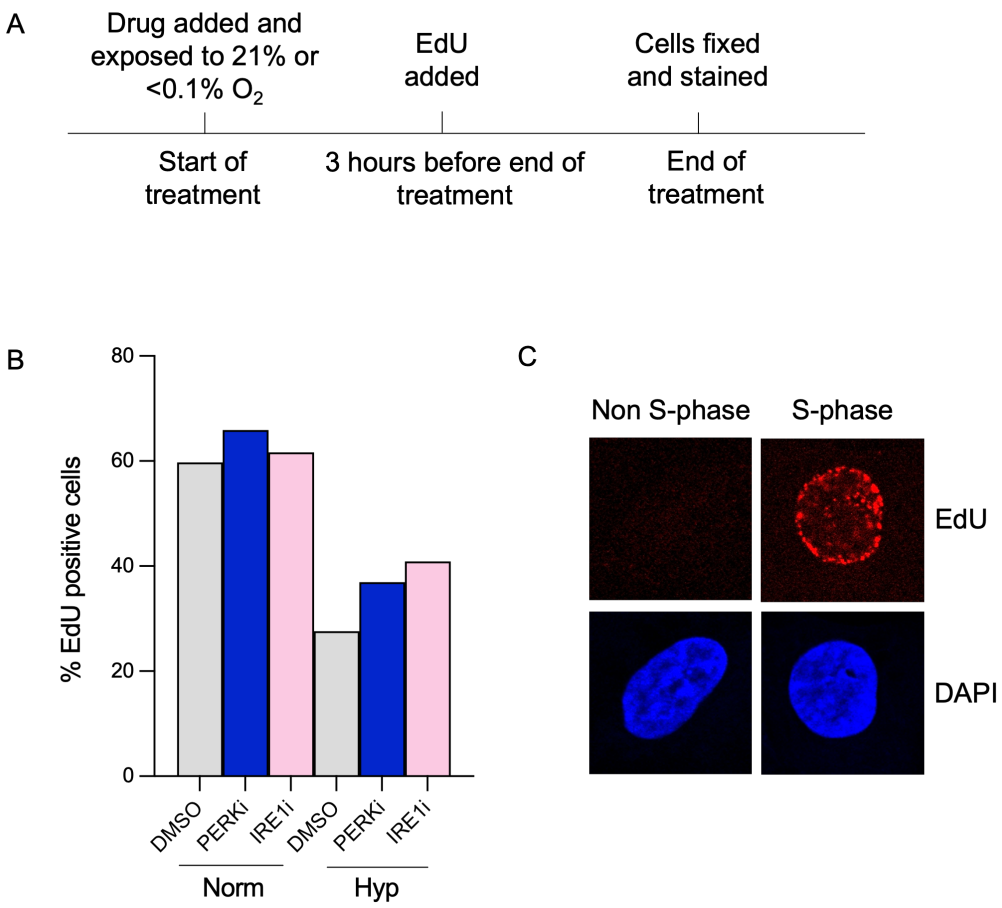


Figure 4.18. Inhibition of the UPR in hypoxia does not change the percentage of cells in S-phase. A. A schematic representation of the experiment. **B.** A549 cells were exposed to 0 and 6 hours of hypoxia (<0.1% O_2) with or without a UPR inhibitor: PERK inhibitor (GSK2606414) (10 µM) or IRE1α inhibitor (4µ8c) (10 µM). EdU (10 µM) was added during the last 3 hours of treatment; cells were fixed and stained for EdU. The percentage of EdU positive cells were quantified. **C.** Representative images of A549 cells labelled with EdU from part B. n=1

Next, we proceeded to ask whether or not UPR inhibition in hypoxia affects replication stress. We exposed A549 cells to hypoxia with or without one of the UPR inhibitors and carried out staining for RPA. As expected, hypoxia (<0.1% O_2) led to a significant increase in the percentage of cells with >5 RPA foci. However, PERK or IRE1α inhibition in hypoxia had no significant effect on the percentage of cells with >5 RPA foci (**Figure 4.19A**). This was perhaps unsurprising given that inhibition of the UPR was unlikely to impact nucleotide levels and therefore the primary source of replication stress in hypoxia (Foskolou *et al.*, 2017). This is also consistent with what we observed in **Figure 4.18B**, where UPR inhibition did not change

the percentage of cells in S phase in hypoxia that could experience replication stress. This led us to consider a more refined assay; we quantified the number of RPA foci per cell. We found that the average number of RPA foci per cell in hypoxia (<0.1% O_2) increased significantly when either PERK inhibitor or IRE1α inhibitor was added, from 27 to 35 or 34, respectively (**Figure 4.19B, C**). To see if we can observe the same phenotype from genetic depletion of PERK, we transfected A549 cells with siRNA to PERK, exposed them to 6 hours of hypoxia (<0.1% O_2), and quantified the number of RPA foci per cell. Consistently, we once again observed a significant increase in the number of RPA foci per cell upon PERK depletion in hypoxia (**Figure 4.19D**).

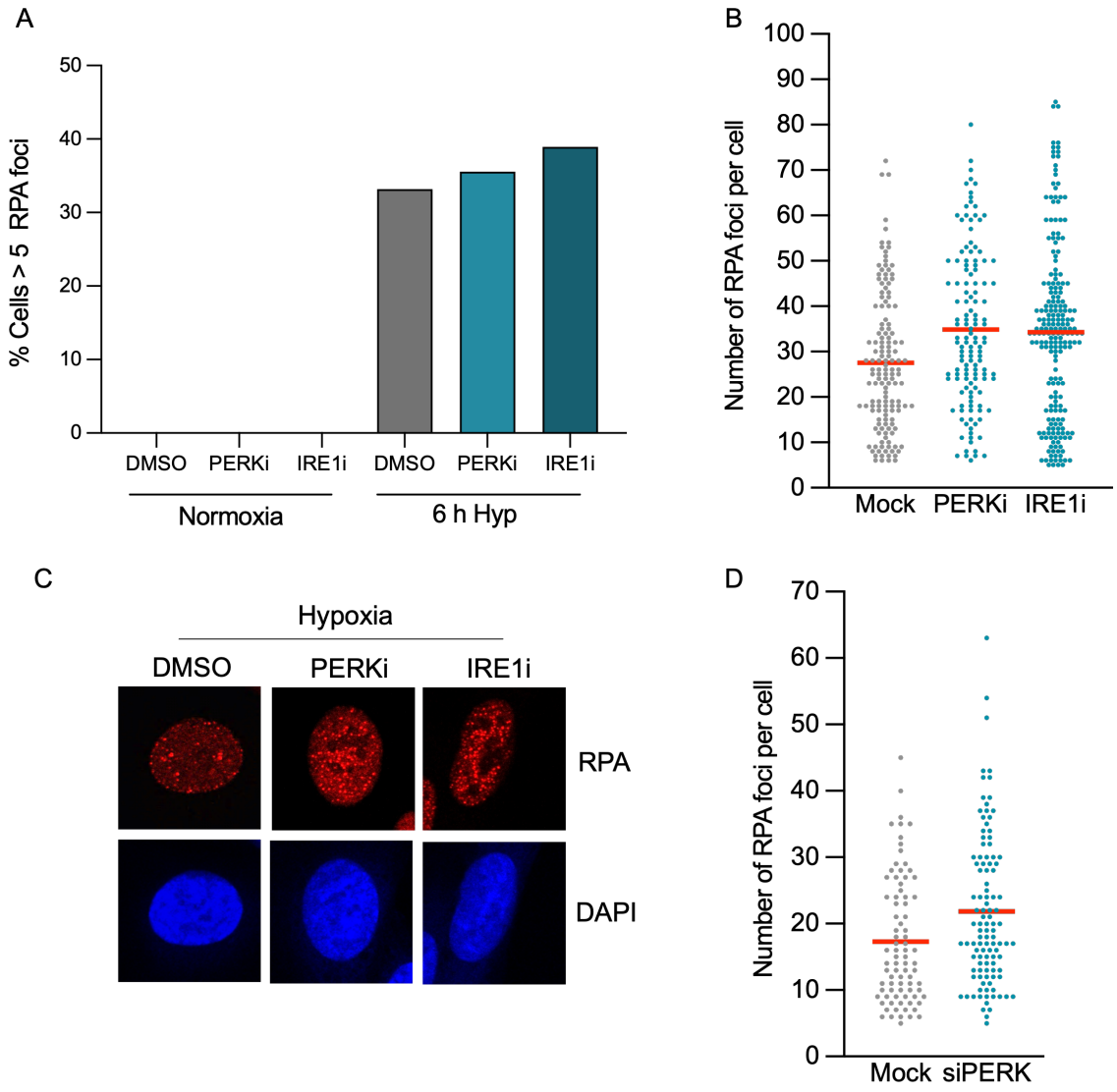


Figure 4.19. UPR inhibitors in hypoxia increase the average number of RPA foci per cell. A. A549 cells were exposed to 0 and 6 hours of Hypoxia (Hyp) <0.1% O_2 with or without a UPR inhibitor: PERK inhibitor (GSK2606414) (10 μM) or IRE1α inhibitor (4μ8c) (10 μM). Cells were fixed and stained for RPA. **B.** The number of RPA foci per cell in 6 hours of hypoxia (<0.1% O_2) from part A quantified. **C.** Representative images of hypoxic cells from part B. **D.** A549 cells were transfected with mock (grey) or PERK siRNA (green) and exposed to 6 hours of <0.1% O_2; cells were fixed and stained for RPA. n=2 with at least 100 cells imaged per condition per repeat.

Consequently, the increase in the number of RPA foci per cell upon UPR inhibition supports our hypothesis that inhibiting the UPR in hypoxia (<0.1 O_2) exacerbates existing replication stress. These data support the model that the UPR might have a role in reducing replication stress in hypoxia, and interestingly, that at least both the PERK and IRE1α arms of the pathway are involved. Although the percentage of hypoxic (<0.1% O_2) cells undergoing replication stress remains the same (**Figure 4.19A**), the average amount of replication stress in those cells increased in response to UPR inhibition.

4.2.18 UPR inhibition in hypoxia further increases R-loops

We observed that inhibition of the PERK and IRE1α arms of the UPR led to a further increase in hypoxia-induced replication stress per cell (**Figure 4.18**). We also noted that hypoxia-induced R-loops contribute to replication stress (**Figure 4.12**). Consistently, we saw that depleting or inhibiting PERK led to a further increase in hypoxic R-loops (**Figure 4.16**). Therefore, we next asked whether inhibiting the other two arms of the UPR, namely the IRE1α and ATF6 branches, would also increase R-loops. We treated A549 cells with IRE1α inhibitor (4μ8c), ATF6 inhibitor (Ceapin-A7) or another PERK inhibitor that we had not previously used (AMG PERK 44) and exposed them to 6 hours of hypoxia (<0.1% O_2). As expected, R-loop levels increased with hypoxia alone. Consistently, PERK inhibition in hypoxia using the AMG PERK 44 inhibitor repeated the same result we observed using the GSK2606414 PERK inhibitor, i.e.,

a further increase in hypoxic R-loop levels. Excitingly, we found that inhibiting the IRE1α arm in hypoxia also further increased R-loops (**Figure 4.20**), indicating that the PERK arm may not be the only UPR arm that regulates R-loops in hypoxia. Inhibiting the ATF6 arm also led to a further increase in hypoxic R-loop levels, however, this was not statistically significant (**Figure 4.20**).

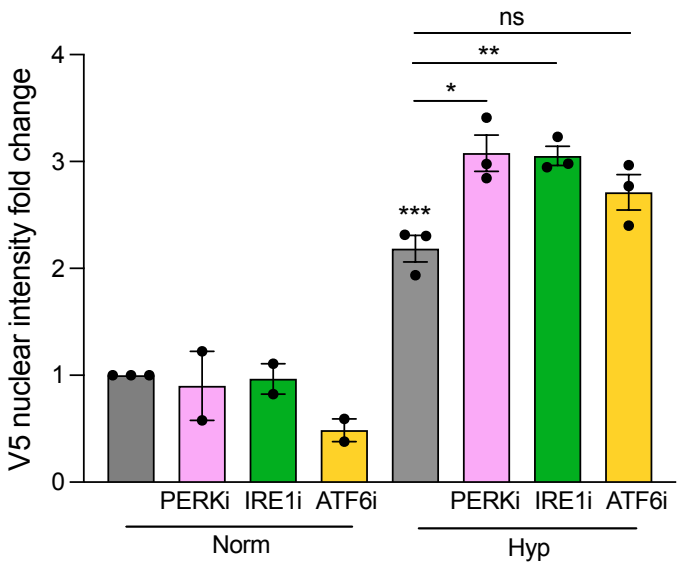


Figure 4.20. UPR inhibition in hypoxia leads to a further increase in R-loops. A549 cells were transfected with RNaseH1^{D210N}-V5 and exposed to 0 and 6 hours of hypoxia (<0.1% O_2) with or without a UPR inhibitor: PERK inhibitor (AMG PERK 44) (20 µM), IRE1α inhibitor (4µ8c) (20 µM) or ATF6 inhibitor (Ceapin-A7). Staining for V5 was then carried out and the nuclear intensity determined, normalised to the normoxic control. The two-tailed Student's *t*-test was used: Hyp ***$p < 0.0007$, Hyp versus Hyp + PERKi *$p < 0.0133$, Hyp versus Hyp + IRE1i **$p < 0.0048$, Hyp versus Hyp + ATF6i $p = 0.0634$. n=3

4.2.19 Hypoxia-induced SETX links replication stress with the UPR

The data in Chapter 4 support the model that the UPR and DDR interact with each other in hypoxia. We saw for the first time that R-loops accumulate in hypoxia (<0.1% O_2), and that they contribute to both DDR and replication stress signalling. We also showed that the UPR signals through the PERK/ATF4 arm to induce the expression of putative RNA/DNA helicase SETX. Importantly, we found that SETX plays a role in reducing hypoxic R-loops; therefore,

unsurprisingly, upon SETX depletion, we observed a further increase in R-loops, an accumulation of DNA damage and reduced hypoxic survival. A schematic of our model is shown in **Figure 4.21** (Ramachandran, Ma *et al.*, 2021).

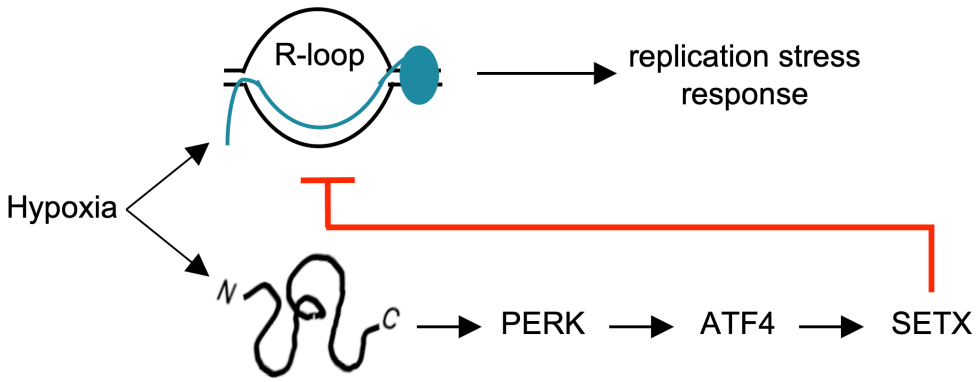


Figure 4.21. Hypoxia links the UPR with replication stress. Hypoxia leads to the activation of the UPR and replication stress. In addition to a shortage of nucleotide pools, R-loops accumulate in hypoxia and contribute to replication stress. The PERK branch of the UPR signals trough transcription factor ATF4 to increase SETX expression hypoxia. Hypoxia-induced SETX reduces R-loop accumulation and subsequent replication stress-mediated signalling.

4.3 Discussion

In Chapter 4, we started with a bioinformatic approach to look for genes potentially involved in the DDR/replication stress that are regulated by the UPR in hypoxia. Using datasets available online as well as from our lab, we generated a list of 1113 hypoxia-induced UPR genes (**Table S4.1**). Out of the 1113 genes, 103 of them are hypoxia-induced UPR genes that may play a role in the DDR (**Table S4.3**). Out of the 103 genes, 78 genes (**Table 4.3**) were involved in a replication stress associated process: DNA synthesis, enrichment on chromatin, enrichment on Hu-stalled replication forks, and interactions with R-loops. We were particularly interested in replication stress and not in other types of genotoxic stresses because hypoxia (<0.1% O_2) activates the DDR through replication stress in the absence of SSBs and DSBs (**Figures 4.7, 4.8, 4.9, 4.10**). Out of the 78 genes, SETX stood out as the most interesting gene to study as a potential link between the UPR and DDR in hypoxia. Not only was it the gene that 'scored' the highest in terms of being involved in the most replication stress associated processes, SETX was also the only R-loop interacting protein that is also enriched at Hu-stalled replication forks.

Excitingly, we showed with wet lab experiments that indeed, SETX plays an important and novel role in hypoxia. We found that R-loops accumulate in radiobiological hypoxia (<0.1% O_2), contribute to DDR and replication stress signalling, and that SETX reduces these hypoxic R-loops. When SETX was depleted, DNA damage accumulated, the levels of hypoxic R-loops further increased, and there was reduced hypoxic cell survival. We confirmed that SETX is indeed induced through the UPR in hypoxia, specifically through the PERK/ATF4 arm; the increased expression of SETX through the activation of the UPR is consistent with our

bioinformatic analyses. In summary, hypoxia-induced SETX links two major transcriptional responses, the DDR and UPR, in hypoxia in a novel manner i.e., through R-loops.

R-loops have not been studied in the physiological context of tumour hypoxia, and they have become increasingly implicated in genome instability and replication stress in the last two decades (Crossley *et al.*, 2019). Excitingly, we observed for the first time here that R-loops accumulate robustly in hypoxia (<0.1% O_2). However, many questions remain despite our findings in Chapter 4: we still do not know how and where R-loops form in hypoxia, and whether they play a functional role as part of a stress response. In addition, why is SETX induced through the UPR, and not the DDR, to resolve hypoxic R-loops? Furthermore, we identified other hypoxia-induced UPR genes that are part of the RNA/DNA hybrid interactome (**Table S4.4**); do they play a similar role to SETX?

Finally, we have focused on the PERK arm of the UPR in Chapter 4. We showed that depleting or inhibiting PERK in hypoxia led to the accumulation of DNA damage and a further increase in R-loops and replication stress. Although we have started to investigate how the IRE1α and ATF6 arms of the UPR may impact the DDR and replication stress in hypoxia in a similar manner to the PERK arm, these preliminary experiments warrant further investigation. Together, these data suggest that SETX may not be the only link between the UPR and DDR in hypoxia.

Chapter 5 Hypoxia-induced R-loops and oxidative stress

5.1 Introduction

We previously determined a link between the UPR and R-loops in hypoxia in Chapter 4 (Ramachandran, Ma *et al.*, 2021). The focus of this chapter is to investigate the mechanism through which these R-loops form, where they form on the genome, and what functions they may serve, if any, as part of the hypoxic stress response.

In this chapter, we will investigate the mechanism of R-loop formation firstly by determining whether or not R-loop induction is oxygen dependent. As R-loops are tightly associated with transcription, we will also measure changes in transcription in hypoxia. In addition, we will investigate oxidative stress as a potential mechanism for R-loop formation. Here, we define oxidative stress as the accumulation of reactive oxygen species (ROS) (Pizzino *et al.*, 2017).

As the R-loop signal in hypoxia seems to originate mainly from the nucleoli (observed qualitatively), we will investigate whether or not R-loops are forming on genes transcribed in the nucleoli. Finally, we will also explore the functional roles of R-loops in hypoxia, including their effects on the nucleolar stress response as well as global transcription repression.

5.2 Results

5.2.1 UPR inducers Tuni and Thaps lead to an accumulation of R-loops

Previously, we found that there are links between the UPR and R-loops in hypoxia. This suggested that other methods to induce a UPR would also lead to R-loop accumulation. Therefore, we treated A549 cells with pharmacological reagents which induce the UPR, Tuni and Thaps, and measured R-loop levels. Indeed, both Tuni and Thaps led to a robust accumulation of R-loops; there was an increase of at least 2-fold after 6 hours of treatment (**Figure 5.1**). This suggested that conditions which lead to a UPR (i.e., hypoxia, Tuni and Thaps) all lead to an increase in R-loops. Notably, two other recent studies have reported findings consistent with our result; Choo *et al.* and Bruno *et al.* observed that Thaps treatment increases S9.6 signal (Bruno *et al.*, 2022; Choo *et al.*, 2020).

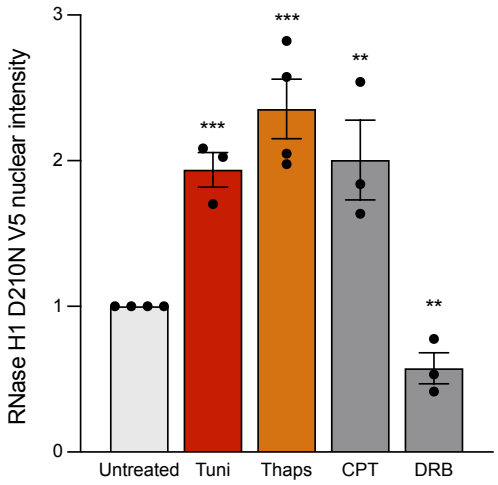


Figure 5.1. Conditions that induce the UPR lead to R-loop accumulation. A549 cells were transfected with RNaseH1^{D210N}-V5 and exposed to tunicamycin (Tuni, 5 µg/mL) or thapsigargin (Thaps, 2 µM) for 6 hours. CPT (10 µM, 1 h) and DRB (100 µM, 1 h) were used as controls for increasing and decreasing R-loops, respectively. Staining for V5 was then carried out and the nuclear intensity determined, normalised to the untreated control. The two-tailed Student's *t*-test was used to compare against untreated control: Tuni ***p = 0.0002, Thaps ***p = 0.0006, CPT **p = 0.0071, DRB **p = 0.0049. n=3/4

5.2.2 Hypoxia induces R-loops in an oxygen dependent manner

Next, we investigated the oxygen dependency of R-loop induction in hypoxia. We confirmed in **Figure 4.7** that the induction of the UPR is oxygen dependent; the UPR is only activated in severe hypoxia (<0.1% O_2) and not in mild hypoxia (2% O_2). Therefore, we exposed A549 cells to both severe and mild hypoxia and measured R-loop levels. Supportively, we found that mild hypoxia (2% O_2) which does not induce a UPR also does not induce R-loop accumulation (**Figure 5.2**). This further suggests that R-loop accumulation is not associated with HIF signalling, which is stabilised in both severe and mild hypoxia (Hammond *et al.*, 2014).

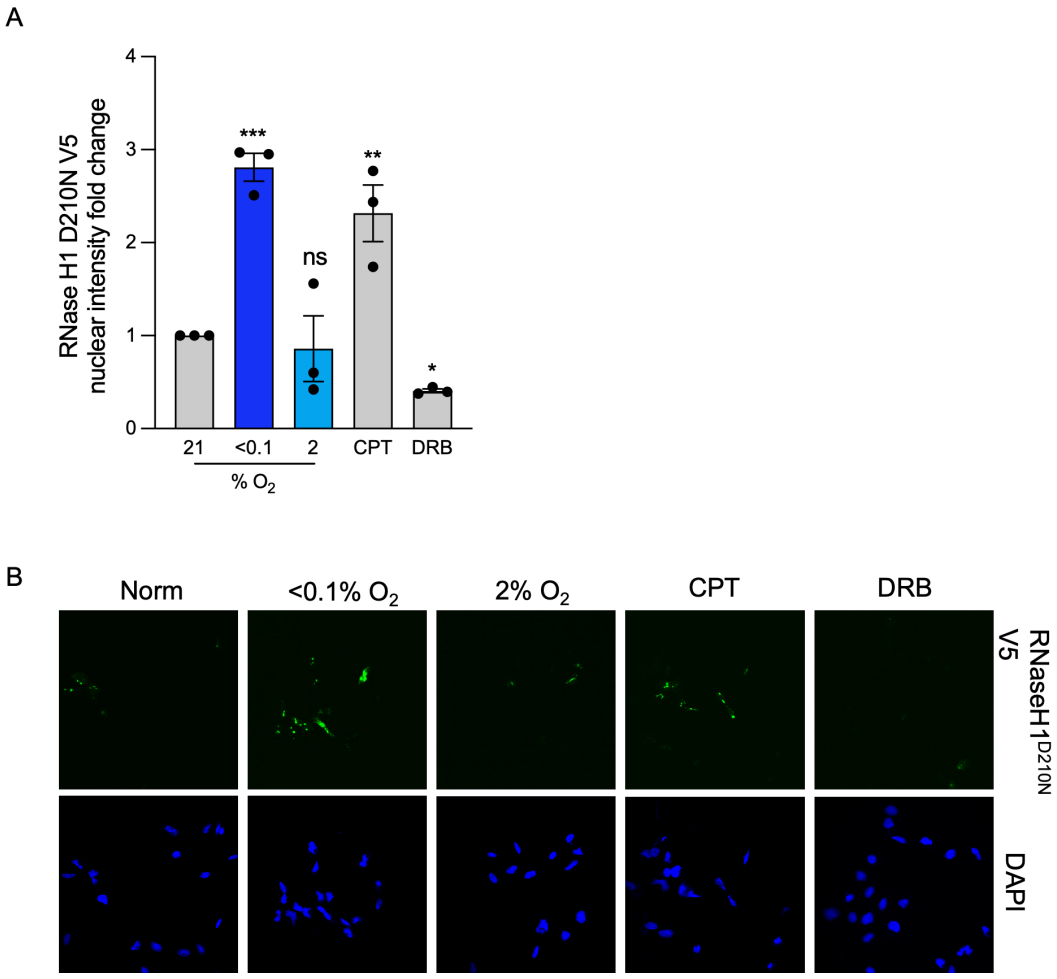


Figure 5.2. Hypoxia leads to the accumulation of R-loops in an oxygen dependent manner. **A.** A549 cells were transfected with RNaseH1^{D210N}-V5 and exposed to 21, <0.1 or 2% O_2 for 6 hours. CPT (10 µM, 1 h) and DRB (100 µM, 1 h) were used as controls. Staining for V5 was then carried out and the nuclear intensity determined, normalised to normoxic control. The

Student's *t*-test was used to control against the normoxic control: <0.1% O_2 ***p = 0.0003, 2% O_2 p = 0.7139, CPT *p = 0.0123, DRB ****p < 0.0001. **B.** Representative images of part A. n=3

5.2.3 Hypoxia, Thaps and Tuni lead to repression of global transcription

Next, we started investigating mechanisms by which R-loops could form in response to conditions which induce a UPR (hypoxia, Tuni, Thaps). In literature, active transcription that may cause transcription-replication collisions (TRCs) is often cited as a source of R-loops (Belotserkovskii *et al.*, 2018; Crossley *et al.*, 2019; Rinaldi *et al.*, 2021). Another potential source of R-loops is DNA damage, where break sites have been identified as potential R-loop initiation zones (Roy *et al.*, 2010). However, as there are no detectable SSBs or DSBs in hypoxia, we focused on investigating transcriptional changes.

We treated A549 cells with 6 hours of hypoxia (<0.1% O_2), Tuni or Thaps and measured global transcription using 5-ethynyl-uridine (5'EU) labelling, where 5'EU is incorporated into nascent transcripts. 5'EU can be visualised in immunofluorescence using click chemistry and its fluorescent intensity is used as a readout for tracking transcription (Jao & Salic, 2008; Mannack *et al.*, 2016; Wissink *et al.*, 2019). We found that all 3 conditions which lead to a UPR led to global transcription inhibition (**Figure 5.3**); hypoxia, Tuni and Thaps treatment led to a similar reduction in 5'EU incorporation fold change.

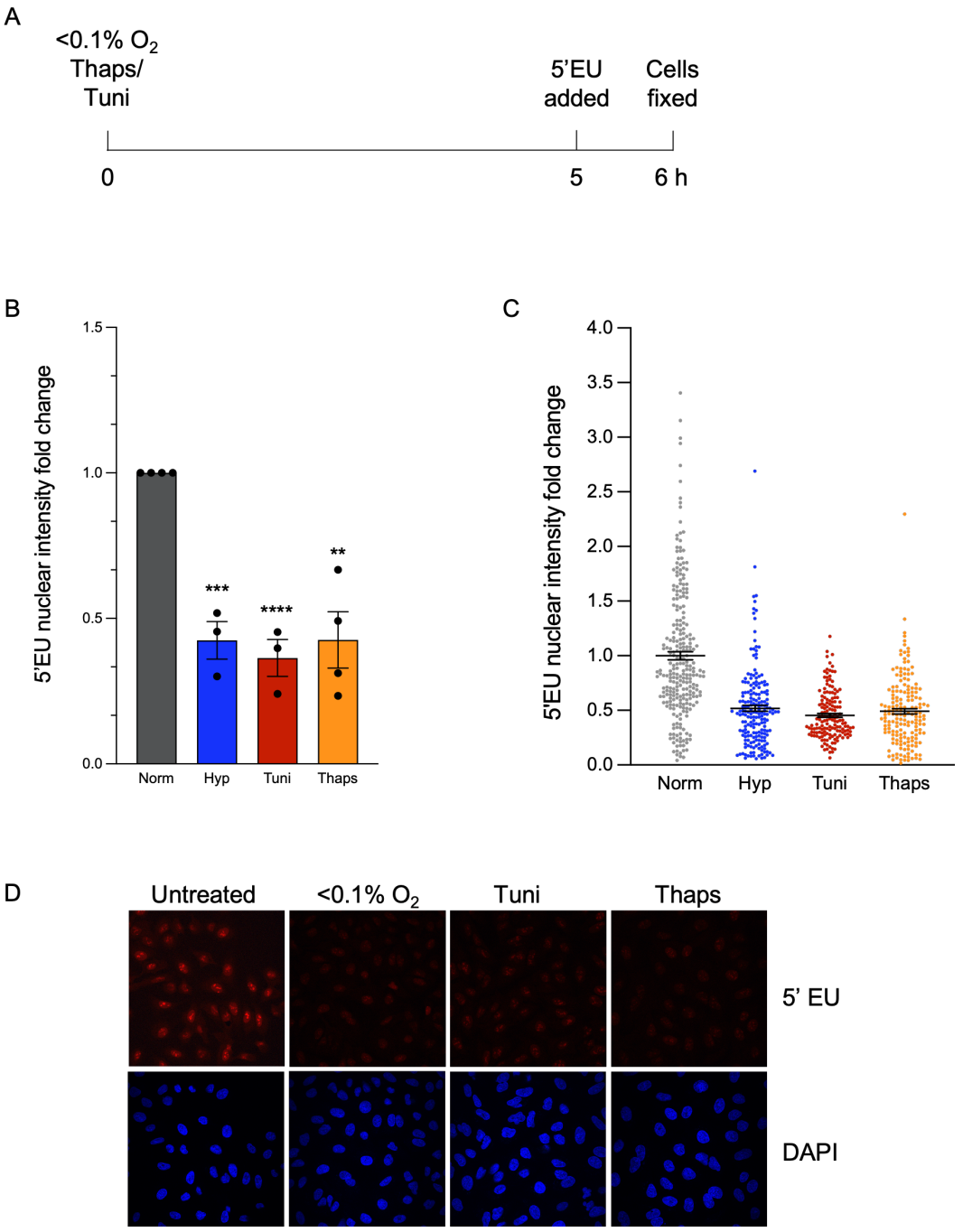


Figure 5.3. Hypoxia, Tuni and Thaps lead to global transcription repression. A549 cells were exposed to <0.1% O_2, tunicamycin (Tuni, 5 µg/mL) or thapsigargin (Thaps, 2 µM) for 6 hours with 5'EU (0.5 mM) added during the final 1 hour. **A.** Schematic representation of the experiment. **B.** Quantification of mean 5'EU fold change from 3 independent experiments, normalised to normoxic control. The two-tailed Student's *t*-test was used to compare to normoxic control: Hyp ***p = 0.0001, Tuni ****p < 0.0001, Thaps **p = 0.001. **C.** Representative plot of one experiment where each dot represents a single cell. **D.** Representative images of part C. n=3

To confirm if repression of global transcription shares the same oxygen dependency as the UPR in hypoxia, we exposed a panel of cell lines to both severe (<0.1% O_2) and mild (2% O_2) hypoxia and measured global transcription. This includes human colorectal cancer cell lines HCT116 and RKO, as well as the normal (non-cancerous) lung fibroblast cell line MRC5. Consistently, severe hypoxia (<0.1% O_2) led to transcription repression in all 3 cell lines (**Figure 5.4**). In contrast, we found that mild hypoxia (2% O_2) did not lead to transcription repression in any of the 3 cell lines; interestingly, there was even a slight increase in transcription in HCT116 cells exposed to mild hypoxia (**Figure 5.4A**). These data confirm that global transcription repression and UPR share the same oxygen dependency in hypoxia and that this phenomenon is not restricted to cancer cells.

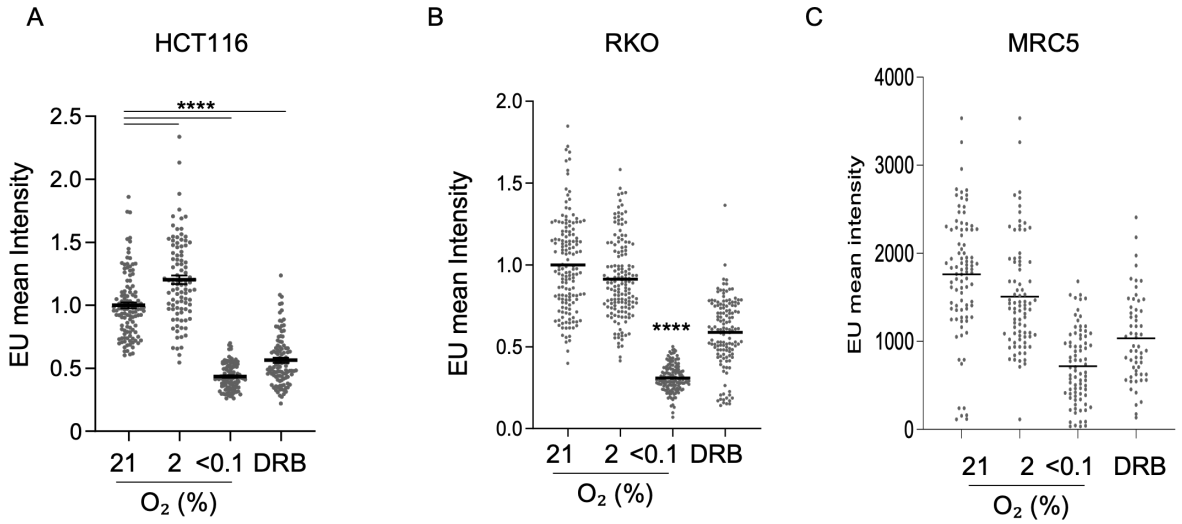


Figure 5.4. Hypoxia leads to transcription repression in an oxygen dependent manner. A. HCT116, **B.** RKO or **C.** MRC5 cells were exposed to 6 hours of 21%, 2% or <0.1% O_2 with 5'EU (0.5 mM) added during the final 6 hours. DRB (100 μM, 6 hours) was used as a positive control for reducing global transcription. The two-tailed Student's *t*-test was used, ****$p < 0.0001$. n=3 *All data in Figure 5.4 was generated by Dr Natalie Ng.*

Therefore, it is tempting to hypothesise that perhaps it is global transcription repression that may lead to the accumulation of R-loops in hypoxia; after all, R-loops have been associated

with transcription repression (Drolet *et al.*, 1994; Niehrs & Luke, 2020). However, we reasoned that not all forms of transcription repression lead to R-loop accumulation; for example, the transcription inhibitor DRB is used as a positive control for reducing R-loops (**Figure 5.1A**) as well as a positive control for reducing transcription (**Figure 5.4**). These data suggest that R-loops accumulate in conditions which include decreased transcription however this is challenging to interrogate further. Specifically, as we do not know the precise mechanism of transcription repression in hypoxia, we have no method to rescue transcription repression in hypoxia and then measure the impact on R-loops. Therefore, we decided to consider other mechanisms through which R-loops could be accumulating in hypoxia or conditions that lead to a UPR.

5.2.4 ROS can lead to R-loops through DNA damage

Another potential source of R-loops in hypoxia is ROS. Many studies have shown that hypoxia leads to the release of ROS (Bell *et al.*, 2007; Brunelle *et al.*, 2005; Dirmeier *et al.*, 2002; Duranteau *et al.*, 1998; Guzy *et al.*, 2005; Killilea *et al.*, 2000; Mansfield *et al.*, 2005; Wood *et al.*, 1999). In addition, recent studies have shown that ROS can induce R-loops (Bauer *et al.*, 2020; Lee *et al.*, 2021; Renaudin *et al.*, 2021; Tan, Duan, *et al.*, 2020; Tan, Wang, *et al.*, 2020; Teng *et al.*, 2018). Firstly, to confirm that ROS can lead to R-loops in our cell line, we treated A549 cells with ROS-inducing pharmacological reagents, *tert*-Butyl hydroperoxide (*t*BHP) and MitoPQ (PQ), with and without their respective ROS scavengers *N*-acetylcysteine (NAC) and MitoTempo (Tempo). Whereas *t*BHP and NAC are used as a universal ROS inducer and scavenger, respectively, PQ and Tempo are widely used as a mitochondrial ROS inducer and scavenger. We found that indeed, ROS inducers *t*BHP and PQ both led to a robust accumulation of R-loops, to an approximate 3-fold and almost 4-fold increase, respectively

(**Figure 5.5A**). The increase in R-loop levels by the ROS inducers was rescued by their respective scavengers, NAC and Tempo. These data suggest that we are able to reproduce the ROS-induced R-loops that others have observed.

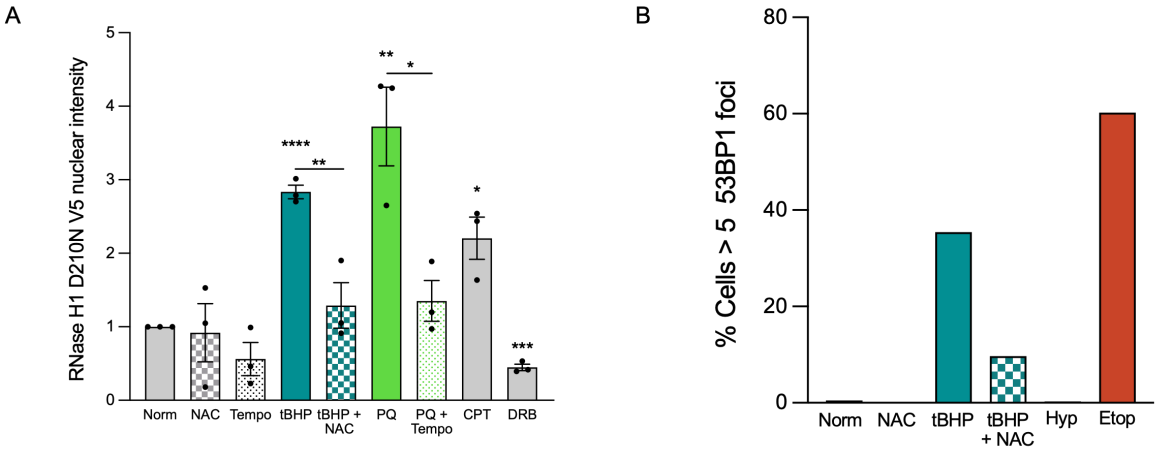


Figure 5.5. ROS leads to R-loops and DNA damage. A. A549 cells were transfected with RNaseH1^{D210N}-V5 and exposed to 6 hours of tert-Butyl hydroperoxide (tBHP, 20 µM) with and without N-acetyl-cysteine (NAC, 20 mM) or MitoPQ (PQ, 10 µM) with and without MitoTempo (Tempo, 10 µM). CPT (10 µM, 1 h) and DRB (100 µM, 1 h) were used as controls. Staining for V5 was then carried out and the nuclear intensity determined, normalised to normoxic control. The two-tailed Student's *t*-test was used. **B.** A549 cells were treated with *t*BHP (20 µM) with or without NAC (20 mM) or hypoxia (<0.1% O_2). Etoposide (20 or etoposide (Etop, 20 µM, 6 hours) was used as a positive control. Cells were fixed and stained for DNA damage marker 53BP1. n=3 for part A, n=1 for part B

However, the studies demonstrating that ROS can lead to R-loops usually identify DNA damage as the underlying mechanism. ROS can cause SSBs, DSBs or oxidised bases which lead to an accumulation of R-loops, especially if transcription is occurring at the sites of damage (Lee *et al.*, 2021; Tan, Duan, *et al.*, 2020; Teng *et al.*, 2018). Therefore, to confirm that the conditions we used to show that ROS-inducers increase R-loop levels can also lead to DNA damage, we treated A549 cells with *t*BHP with and without NAC and measured the DNA damage marker 53BP1. We used hypoxia (<0.1% O_2) as a negative control and ETP as a positive control. As expected, hypoxia did not increase DNA damage, whereas ETP led to a

robust accumulation of DSBs. Consistent with literature, we observed a clear increase in the percentage of cells with >5 53BP1 by 40% from *t*BHP treatment (**Figure 5.5B**). The ROS-induced DNA damage was rescued when the scavenger NAC was added, indicating that the damage is ROS-specific. This preliminary experiment is supportive of previous reports suggesting that ROS can induce R-loops in a DNA damage dependent manner.

5.2.5 Hypoxia leads to the accumulation of ROS in an oxygen dependent manner in the absence of DNA damage

Many studies have shown that hypoxia leads to the release of ROS (Bell *et al.*, 2007; Brunelle *et al.*, 2005; Dirmeier *et al.*, 2002; Duranteau *et al.*, 1998; Guzy *et al.*, 2005; Killilea *et al.*, 2000; Mansfield *et al.*, 2005; Wood *et al.*, 1999). To confirm that hypoxia can induce ROS in our cell line, we treated A549 cells with 6 hours of severe (<0.1% O_2) or mild (2% O_2) hypoxia and added the fluorescent ROS probe CellRox during the last 30 minutes of treatment. The cells were fixed and the intensity of CellRox was measured, which detects total intracellular ROS. We observed that there was a consistent increase in intracellular ROS in <0.1% O_2, and no increase in 2% O_2 (**Figure 5.6A**). This is perhaps not surprising as there have been reports of how intracellular ROS is increased in an oxygen dose-dependent manner with lower oxygen levels inducing more ROS (Bell *et al.*, 2007; Chandel *et al.*, 1998).

To use an orthogonal assay to measure ROS levels, as well as to check if nuclear ROS levels correlate with total intracellular ROS levels, we transfected A549 cells with the pHyPer-Nuc plasmid and exposed them to hypoxia. The pHyPer-Nuc plasmid is a nuclear-targeted fluorescent hydrogen peroxide (H_2O_2) sensor (Fischer-Fantuzzi & Vesco, 1988; Haas *et al.*, 1996). We observed an increased in nuclear H_2O_2 in cells exposed to severe hypoxia (<0.1%

O_2), but no increase in cells exposed to mild hypoxia (2% O_2) (Figure 5.6B). The increase in nuclear H_2O_2 in cells exposed to <0.1% O_2 was rescued with catalase treatment to confirm specificity of the fluorescent signal to H_2O_2. Interestingly, this preliminary data suggests that H_2O_2 levels can increase in the nuclei of severely hypoxic cells; this is important as we will have to confirm that ROS is present in the nucleus if they are potentially causing R-loops.

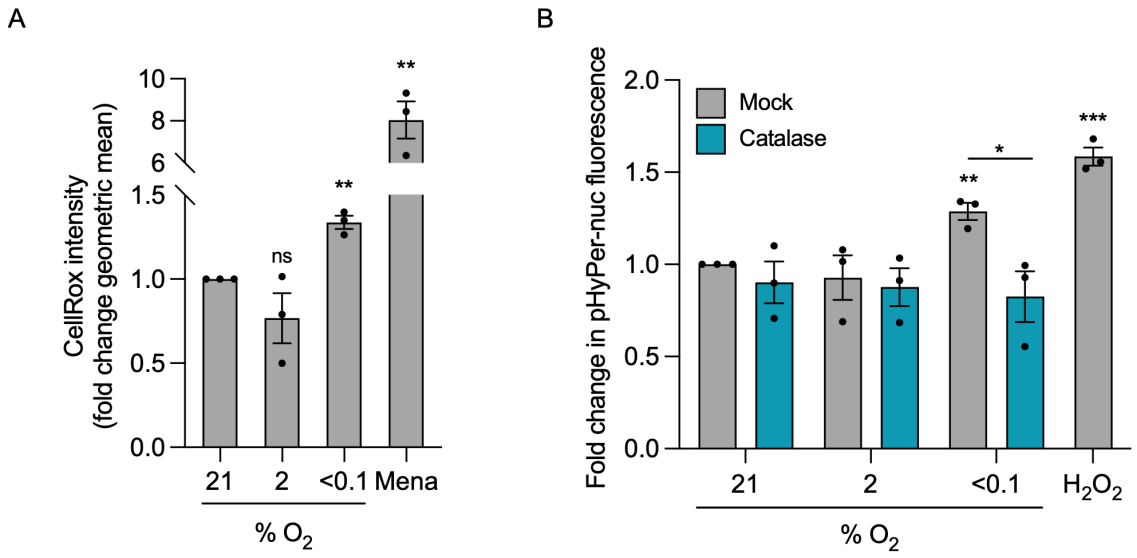


Figure 5.6. Hypoxia induces ROS in an oxygen dependent manner. A. A549 cells were exposed to 6 hours of <0.1% or 2% O_2, with CellRox (5 µM) added during the last 30 minutes of treatment. Menadione (100 µM, 6 hours) was used as a positive control. Cells were fixed and CellRox intensity was measured, normalised to 21% O_2. The two-tailed Student's *t*-test was used. **B.** A549 cells were transfected with pHyPer-Nuc and exposed to 6 hours of <0.1% or 2% O_2 with and without catalase (2000 U/mg). H_2O_2 (5 mM, 3 hours) was used as a positive control. Cells were fixed and nuclear intensity was measured, normalised to 21% O_2. The two-tailed Student's *t*-test was used. n=3

Studies that show ROS leading to R-loops usually pinpoint DNA damage as the mechanism for R-loop formation, as ROS can damage the DNA in the form of SSBs, DSBs or oxidised bases at transcribed sites. However, despite increasing intracellular ROS levels, hypoxia (<0.1% O_2) does not lead to an increase in DNA damage, as demonstrated with comet and 53BP1 foci assays (Hammond & Giaccia, 2004; Olcina *et al.*, 2013). To confirm that there is no DNA

damage in hypoxic conditions where ROS levels are elevated, we extended our previous studies and investigated the levels of 8-oxoguanine (8-oxoG), one of the most common DNA lesions caused by ROS. Therefore, we exposed A549 cells to a time course in hypoxia (<0.1% O_2) and measured 8-oxoG levels using immunofluorescence intensity. Interestingly, there was no increase in 8-oxoG over 24 hours of hypoxia (<0.1% O_2) treatment (**Figure 5.7**). Ultimately, the hypoxic increase in ROS does not seem to lead to detectable DNA damage.

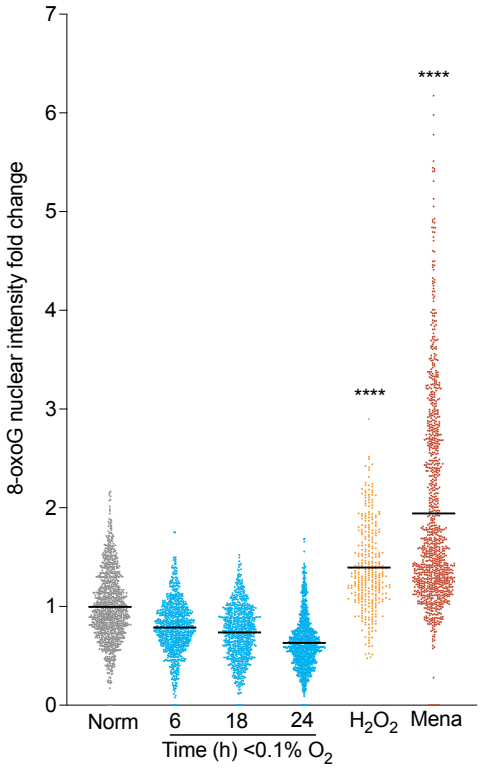


Figure 5.7. Hypoxia does not lead to an increase in 8-oxoguanine. A549 cells were exposed to <0.1% for the times shown. Cells were fixed and stained for 8-oxoguanine (8-oxoG), and the nuclear intensity was determined, normalised to normoxic control. H_2O_2 (5 mM, 3 hours) and menadione (100 µM, 3 hours) were used as positive controls for inducing 8-oxoG. The two-tailed Student's *t*-test was used. n=3

5.2.6 Thaps and Tuni lead to an accumulation of ROS

Although the release of ROS in hypoxia is established in literature, less is known about ROS and the response to UPR inducers. Therefore, we treated A549 cells with Thaps and Tuni, and measured total intracellular ROS levels with CellRox. We found that consistently, both Thaps and Tuni led to a robust increase in intracellular ROS over the course of 6 hours of treatment (**Figure 5.8A**).

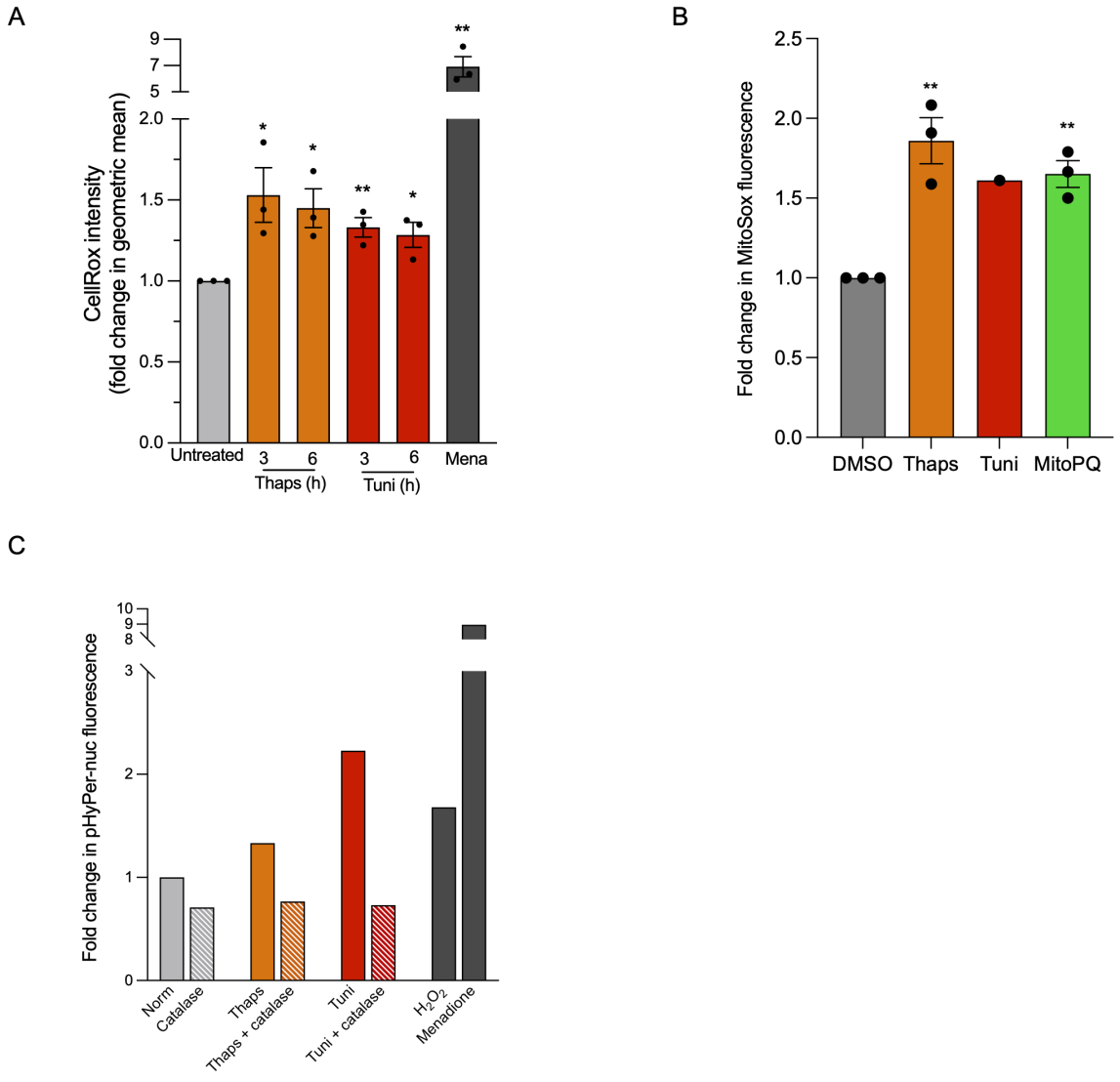


Figure 5.8. Thaps and Tuni lead to an increase in ROS. A. A549 cells were exposed to tunicamycin (Tuni, 5 µg/mL) or thapsigargin (Thaps, 2 µM) for the times shown, with CellRox (5 µM) added during the last 30 minutes of treatment. Menadione (100 µM, 6 hours) was used as a positive control. Cells were fixed and CellRox intensity was measured, normalised to untreated control. The two-tailed Student's *t*-test was used. **B**. A549 cells were exposed to Tuni (5 µg/mL) or Thaps (2 µM) for 6 hours, with MitoSox (5 µM) added during the last 30

minutes of treatment. Cells were fixed and MitoSox intensity was measured, normalised to DMSO control. MitoPQ (10 µM, 6 hours) was used as a positive control. The two-tailed Student's *t*-test was used. **C.** A549 cells were transfected with pHyPer-Nuc and exposed to 6 hours of Thaps (2 µM) or Tuni (5 µg/mL) with and without catalase (2000 U/mg). Menadione (100 µm, 3 hours) and H_2O_2 (5 mM, 3 hours) were used as positive controls. Cells were fixed and nuclear intensity was measured. n=3 for parts A and B, n=1 for part C

In hypoxia, the consensus is that ROS is released from the mitochondria (Bell *et al.*, 2007; Bell, Klimova, Eisenbart, Schumacker, *et al.*, 2007; Brunelle *et al.*, 2005; Chandel *et al.*, 1998; Guzy *et al.*, 2005). Therefore, we asked whether the increase in UPR-induced ROS is also mitochondrial. Here, we used a similar fluorescent probe to CellRox called MitoSox, which is a fluorescent ROS sensor that specifically detects superoxide and is targeted to the mitochondria. We treated A549 cells with Thaps and Tuni and observed that, indeed, both pharmacological UPR inducers led to an increase in mitochondrial ROS (**Figure 5.8B**). The fold change increase of 1.5 is approximately the same as the fold change increase in total intracellular ROS (**Figure 5.8A**).

Finally, we asked whether the UPR induced ROS is able to travel into the nucleus. Here, we transfected A549 cells with the pHyPer-Nuc plasmid then added Thaps and Tuni. Consistently, our preliminary results showed that both Thaps and Tuni led to an increase in nuclear H_2O_2, both of which could be rescued with catalase treatment (**Figure 5.8C**). Excitingly, although the UPR is known to have crosstalk with redox signalling through positive and negative regulations (e.g., through NRF2, ERO1α), it has not been shown before that UPR induced ROS are located inside the nucleus. These data would need repeating to draw a firm conclusion.

5.2.7 Hypoxia-induced R-loops are ROS dependent

Thus far, we have shown that hypoxia leads to an increase in ROS and R-loops (**Figures 5.2, 5.6**), and that ROS can lead to R-loops (**Figure 5.5A**). Therefore, we asked whether hypoxia-induced R-loops are ROS dependent. We transfected A549 cells with RNaseH1^{D210N}-V5 and exposed them to <0.1% O_2 with and without one of the ROS scavengers: NAC, vitamin C or catalase. Strikingly, we found that the increase in hypoxia-induced R-loops was significantly rescued by all 3 different ROS scavengers (**Figure 5.9A**).

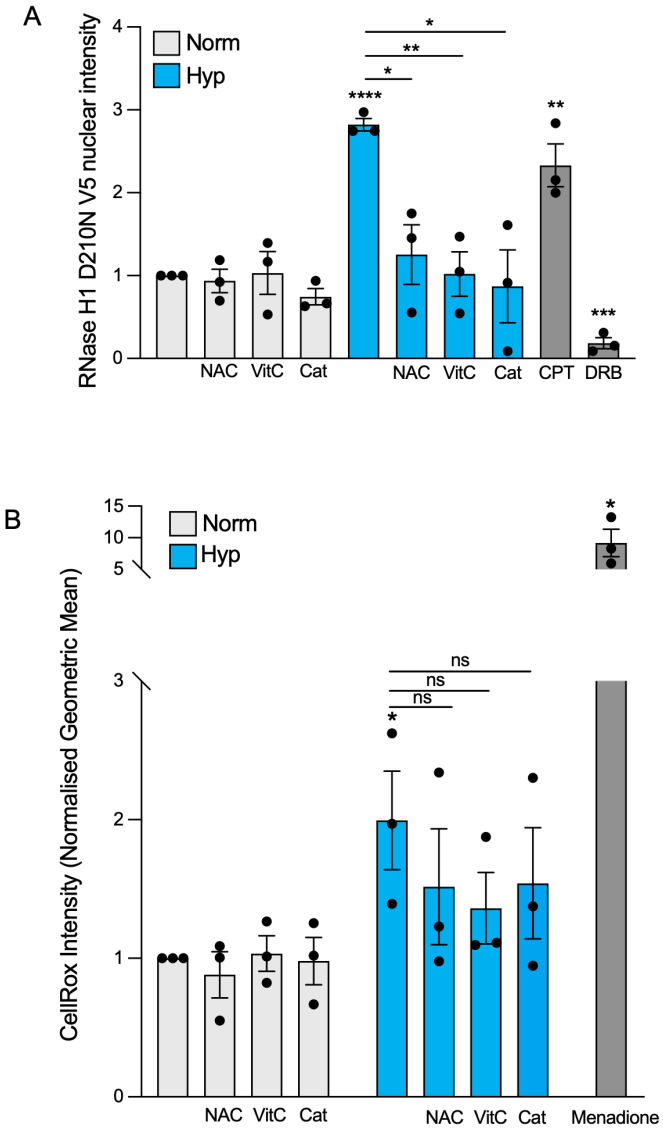


Figure 5.9. Hypoxia-induced R-loops are ROS dependent. A549 cells were transfected with RNaseH1^{D210N}-V5, treated with NAC (5 mM), Vitamin C (2 mM) or catalase (2000 U/mg) then exposed to 6 hours of 21 or <0.1% O_2. **A.** Cells were fixed and stained for V5, where CPT (10 μM) and DRB (100 μM) were used as positive controls or **B.** cells were incubated with CellRox Green (5 uM) during the final 30 minutes of treatment and fixed, where menadione (100 μM, 6 hours) was used as a positive control. Measurements were normalised to the normoxic control and the two-tailed Student's *t*-test was used. n=3

To ensure that intracellular ROS levels were indeed reduced by the scavengers and that the rescue was not an off-target phenotype, we concurrently measured CellRox intensity while performing the experiments in **Figure 5.9A**. We observed that in each independent experiment, hypoxia-induced ROS levels were accordingly reduced by the scavengers (**Figure 5.9B**). However, due to variation between repeats, the average reduction in hypoxia-induced ROS by the scavengers was not statistically significant.

Excitingly, our data so far suggests that hypoxia-induced R-loops are ROS dependent, and that they occur independently of DNA damage. This is in contrast to other studies that show that ROS usually leads to R-loops through SSBs, DSBs or oxidised bases (Bauer *et al.*, 2020; Lee *et al.*, 2021; Renaudin *et al.*, 2021; Tan, Duan, *et al.*, 2020; Tan, Wang, *et al.*, 2020; Teng *et al.*, 2018).

5.2.8 UPR induced R-loops are ROS dependent

In parallel to hypoxia, we saw that pharmacological UPR inducers are also able to increase R-loop and ROS levels (**Figures 5.1, 5.8**). Therefore, to support our hypoxia studies we asked whether or not UPR induced R-loops are ROS dependent. We transfected A549 cells with RNaseH1^{D210N}-V5 and exposed them to Tuni and Thaps with and without one of the ROS scavengers: NAC and Tempo. Strikingly, both Tuni and Thaps induced R-loops were

significantly rescued by both total ROS scavenger NAC, and mitochondrial ROS scavenger, Tempo (**Figure 5.10**). These data suggest that there is crosstalk between the UPR, R-loops and redox signalling, possibly through the mitochondria.

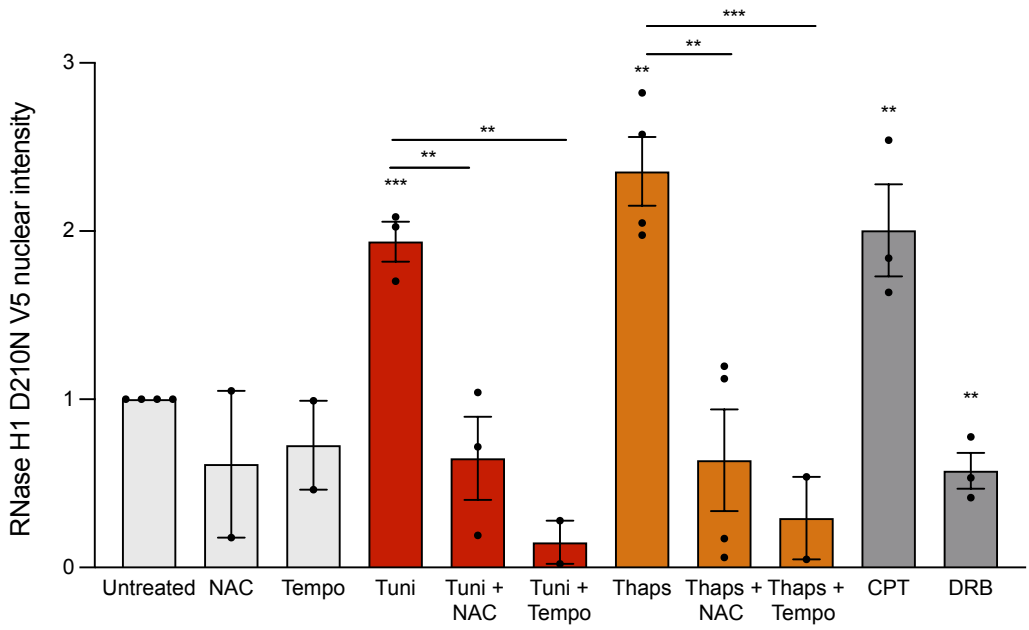


Figure 5.10. UPR-induced R-loops are ROS dependent. A549 cells were transfected with RNaseH1^{D210N}-V5, treated with NAC (5 mM) or Tempo (10 μM) then exposed to 6 hours of Tuni (5 μg/mL) or Thaps (2 μM). Cells were fixed and stained for V5, where CPT (10 μM) and DRB (100 μM) were used as positive controls. The nuclear intensity was quantified and normalised to the untreated control. The two-tailed Student's *t*-test was used. n=3

5.2.9 Hypoxia-induced R-loops form on the rDNA

Next, we asked where the R-loops are forming in hypoxia. From our previous experiments measuring R-loop levels in hypoxia where we used immunofluorescence imaging to visualise the intensity of RNaseH1^{D210N}-V5 (**Figures 5.2, 5.9**), we observed that the most prominent R-loop signal consistently originated from the nucleoli of the cells. The V5 signal usually overlapped with where DAPI staining was weak, i.e., the regions which appear as black cavities in the nucleus. The consensus in literature is that these structures are the nucleoli due to there being a 3-fold lower concentration of DNA for DAPI to stain (Pontvianne *et al.*,

2016). Therefore, we hypothesised that R-loops may be forming in the nucleoli in hypoxia. To verify this, we transfected A549 cells with RNaseH1^{D210N}-V5, exposed them to 6 hours of hypoxia (<0.1% O_2), co-stained for V5 and the nucleolar marker, fibrillarin, and found a complete overlap (**Figure 5.11A, B**).

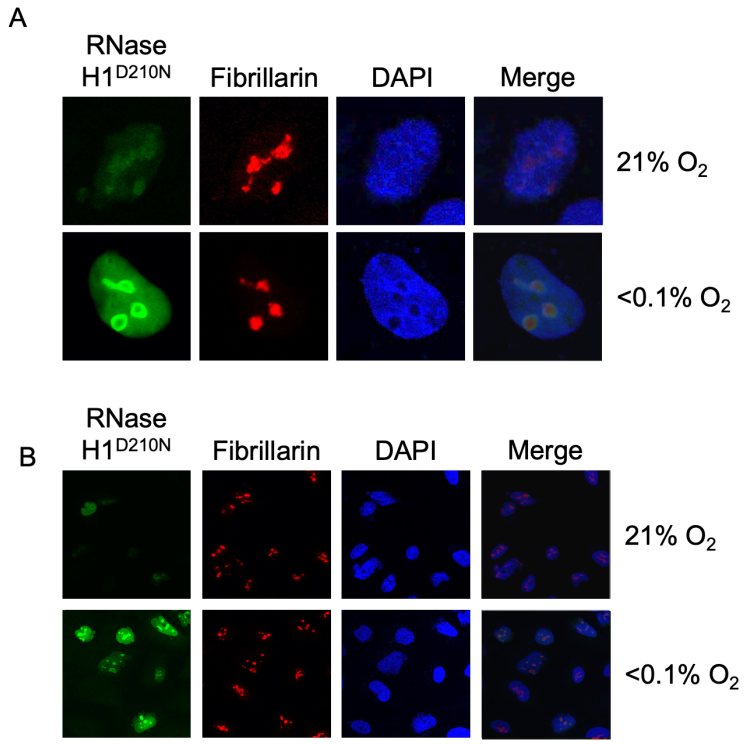


Figure 5.11. Hypoxia-induced R-loops form in the nucleoli. A. Representative images of A549 cells transfected with RNaseH1^{D210N}-V5, exposed to 6 hours of <0.1% O_2, fixed and stained for V5 and fibrillarin. **B.** For clarity a zoomed out image is shown. n=1

The main genes transcribed in the nucleolus are rDNA genes encoding pre-cursor 47S rRNA transcript which is cleaved into smaller subunits that will become part of the ribosome. As rDNA genes are the most highly transcribed genes in eukaryotic cells and are prone to R-loop formation due to G-richness, we predict that R-loops form on rDNA genes in hypoxia (Santos-Pereira & Aguilera, 2015). To formally test the hypothesis, we carried out RNA/DNA immunoprecipitation for regions on the ribosomal DNA (rDNA). We designed primers for two regions of the rDNA: upstream of the main promoter (D1) and in the 28S region (D2) (**Figure**

5.12A). Then, we exposed A549 cells to 6 hours of hypoxia (<0.1% O_2), with and without the ROS scavenger NAC. As most of the hypoxic R-loops seemed to form in the nucleoli, and we established that hypoxic R-loops are ROS dependent, we expected NAC to reduce R-loop induction. Strikingly, we saw a significant increase in R-loops at both D1 and D2 in hypoxia (**Figure 5.12B, C**). In support of our hypothesis, NAC treatment significantly rescued R-loops induced at D2 and partially rescued R-loops at D1. Therefore, our data suggest that hypoxia-induced R-loops are forming on the rDNA, and that this occurs in a ROS dependent manner.

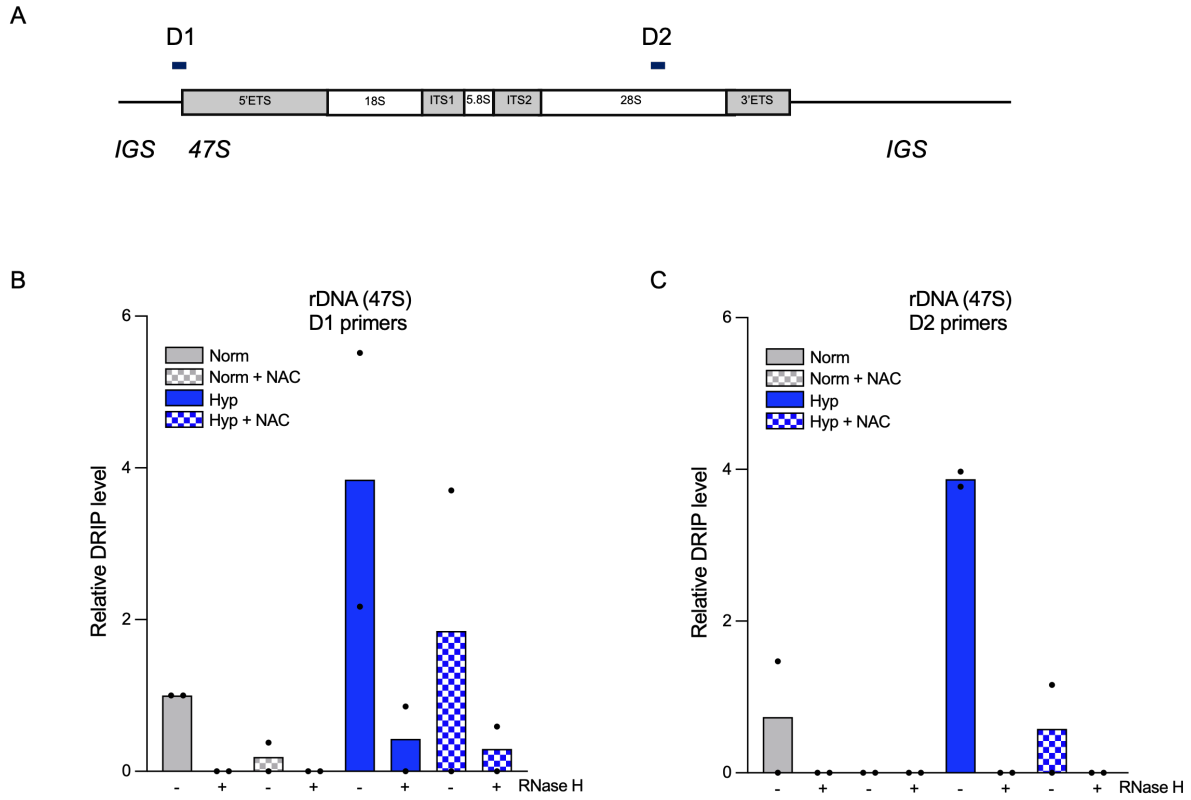


Figure 5.12. Hypoxia-induced R-loops form on the rDNA. A. Schematic of product of RNA polymerase I transcription, long precursor rRNA, 47S. Location of primers D1 and D2 are shown. **B.** DNA/RNA-immunoprecipitation of D1 qPCR (DRIP-qPCR) analysis of A549 cells exposed to 6 hours of <0.1% O_2 with and without NAC (20 mM). RNase H was used to decrease DRIP signal. Values were normalised to normoxic control of D1. Each sample subtracted the beads only (no antibody) control. **C.** Same as part B but for DRIP-qPCR analysis of D2 instead of D1. n=2 for parts B and C

5.2.10 Hypoxia-induced R-loops block rDNA transcription

Next, we asked whether hypoxic R-loops on the rDNA serve a function. As global transcription is repressed in hypoxia (**Figures 5.3B, 5.4**), it is unlikely that increased R-loops are a result of increased transcription. To confirm this, we designed qPCR primers 'primer set 1' to the 5'ETS region of 47S, to determine the relative levels of nascent 47S precursor rRNA, the version of the transcript before any cleavage occurs for rDNA processing (**Figure 5.12A**). We exposed HCT116 cells to a time course in hypoxia (<0.1% O_2) and observed that, unsurprisingly, there was a rapid repression in the transcription of nascent rRNA (**Figure 5.12B**). Next, we asked whether or not R-loops affect the transcription of rDNA in hypoxia, as we previously observed that they form on the rDNA (**Figure 5.12B, C**). Therefore, we overexpressed wildtype RNaseH1 ($RNaseH1^{WT}$) in HCT116 cells in order to remove R-loops, then exposed them to 6 hours of hypoxia (<0.1% O_2). Excitingly, we saw an increase in rDNA transcription in hypoxic cells expressing $RNaseH1^{WT}$, suggesting that R-loops may be blocking rDNA transcription (**Figure 5.12C**). To see if we can observe the same phenotype in another cell line, we used A549 cells and exposed them to the same conditions. Excitingly, we also observed a clear rescue in the repression of rDNA transcription in hypoxic A549 cells upon $RNaseH1^{WT}$ overexpression (**Figure 5.12D**).

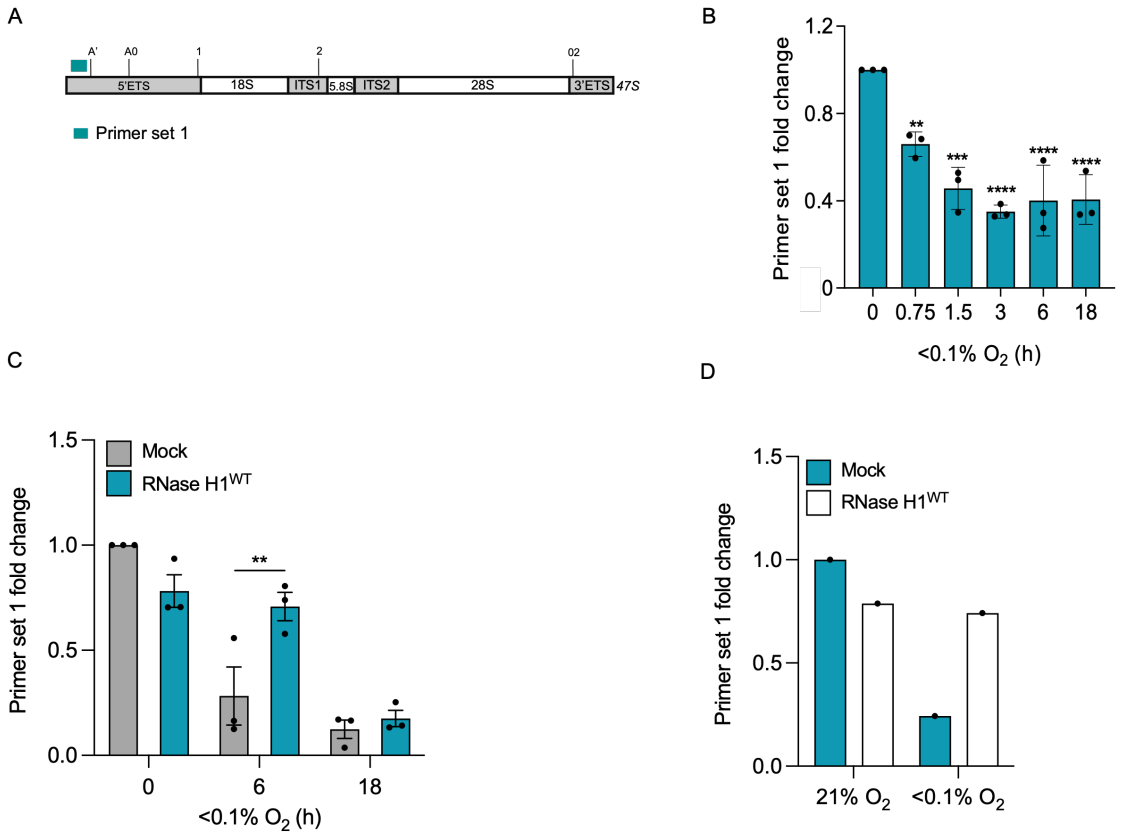


Figure 5.13. Hypoxia-induced R-loops block rDNA transcription. A. Schematic of product of RNA polymerase I transcription, long precursor rRNA, 47S. Location of primer 1 is shown. **B.** HCT116 cells were exposed to <0.1% O_2 for the times shown followed by RT-qPCR for primer set 1 measuring nascent 47S rRNA precursor. The two-tailed Student's *t*-test was used. **C.** HCT116 cells were transfected with mock (grey) or RNaseH1^{WT} (blue), exposed to 6 hours of <0.1% O_2 followed by RT-qPCR for primer set 1. The two-tailed Student's *t*-test was used. **D.** A549 cells were transfected with mock (blue) or RNaseH1^{WT} (white), exposed to 6 hours of <0.1% O_2 followed by RT-qPCR for primer set 1. n=3 for parts B and C, n=1 for part D. *Figure 5.13B was generated by Dr Natalie Ng.*

Next, to use an orthogonal assay to look at transcription, we transfected HCT116 cells with mock or wildtype RNaseH1, exposed them to 6 hours of hypoxia (<0.1% O_2) and measured 5'EU incorporation. As expected, both hypoxia (<0.1% O_2) and DRB treatments led to a decrease in global transcription. Strikingly, this preliminary experiment showed that global transcription repression was significantly rescued upon RNaseH1^{WT} overexpression (**Figure 5.14A, B**). This may not be surprising as most of the RNA species in the cell are rRNA

(approximately 90% by mass), and rDNA are the most abundant genes in the eukaryotic genome; therefore, most global transcription may be attributed to rDNA transcription (Kobayashi, 2011; Palazzo & Lee, 2015).

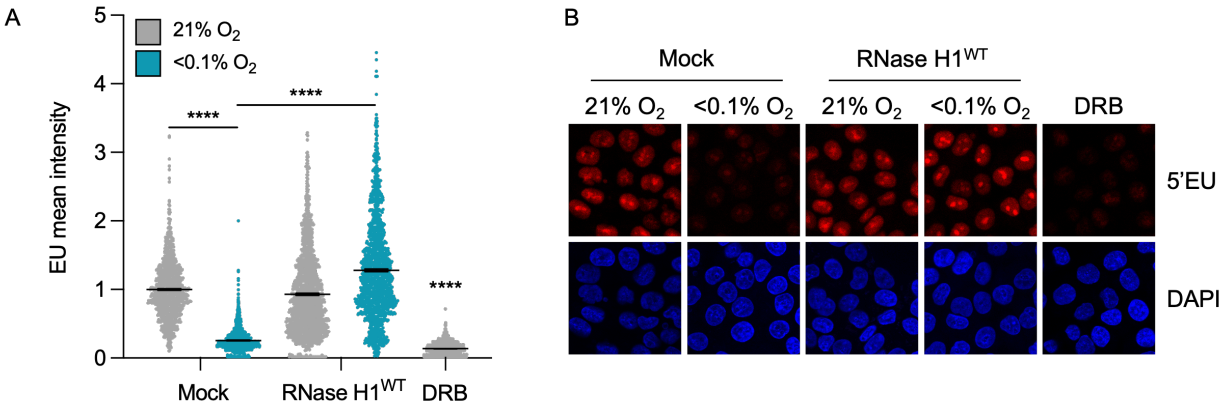


Figure 5.14. Hypoxia-induced R-loops block global transcription. A. HCT cells were transfected with mock (grey) or RNaseH1^{WT} (blue), exposed to 6 hours of <0.1% O_2 with 5'EU (0.5 mM) added during the final 1 hour. DRB (100 µM, 6 hours) was used as a control. The nuclear intensity was quantified and normalised to normoxic mock control. The two-tailed Student's *t*-test was used. **B.** Representative images from A. n=3

5.2.11 rDNA transcription repression in hypoxia is partially dependent on ROS

So far, our data suggests that hypoxic R-loops are ROS-induced, form on the rDNA, and block rDNA transcription. Therefore, we hypothesised that the repression of rDNA transcription in hypoxia may also be ROS dependent. We treated A549 cells with and without a range of ROS scavengers and exposed them to 6 hours of hypoxia (<0.1% O_2) and measured nascent rDNA transcription. We found that, the panel of ROS scavengers was able to rescue the transcription repression of primer set 1 in hypoxia (**Figure 5.15A**). These data support our model that in hypoxia, the release of ROS leads to accumulation of R-loops on the rDNA that can block transcription.

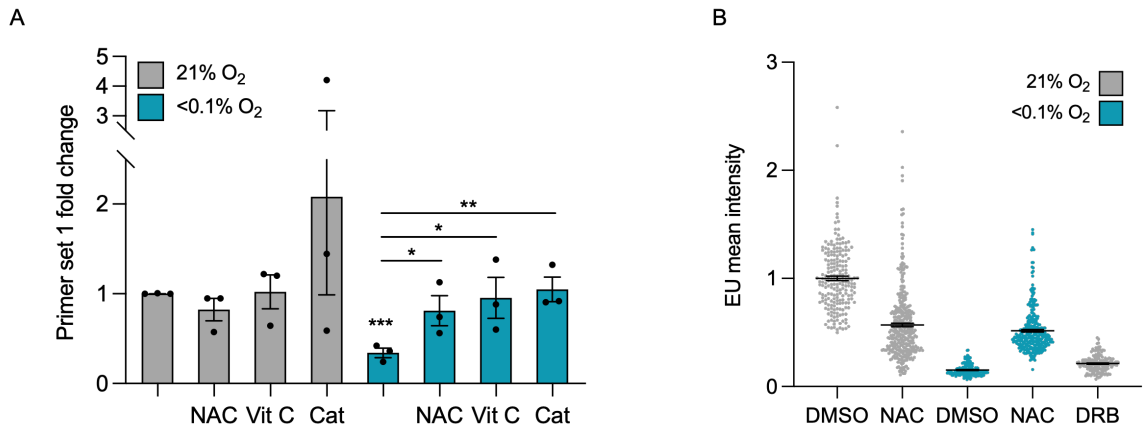


Figure 5.15. Transcription repression in hypoxia is partially dependent on ROS. A. A549 cells were treated with or without NAC (20 mM), vitamin C (VitC, 2 mM) and catalase (2000 U/mg) and exposed to 6 hours of 21% O_2 or <0.1% O_2 followed by RT-qPCR for primer set 1 normalised to 18S, measuring nascent rDNA transcription. The two-tailed Student's *t*-test was used. **B.** A549 cells were treated with or without NAC (20 mM) and exposed to 6 hours of 21% O_2 or <0.1% O_2 with 5'EU (0.5 mM) added during the final 1 hour. The nuclear intensity was quantified. DRB (100 µM, 6 hours) was used as a control. n=3 for part A, n=1 for part B.

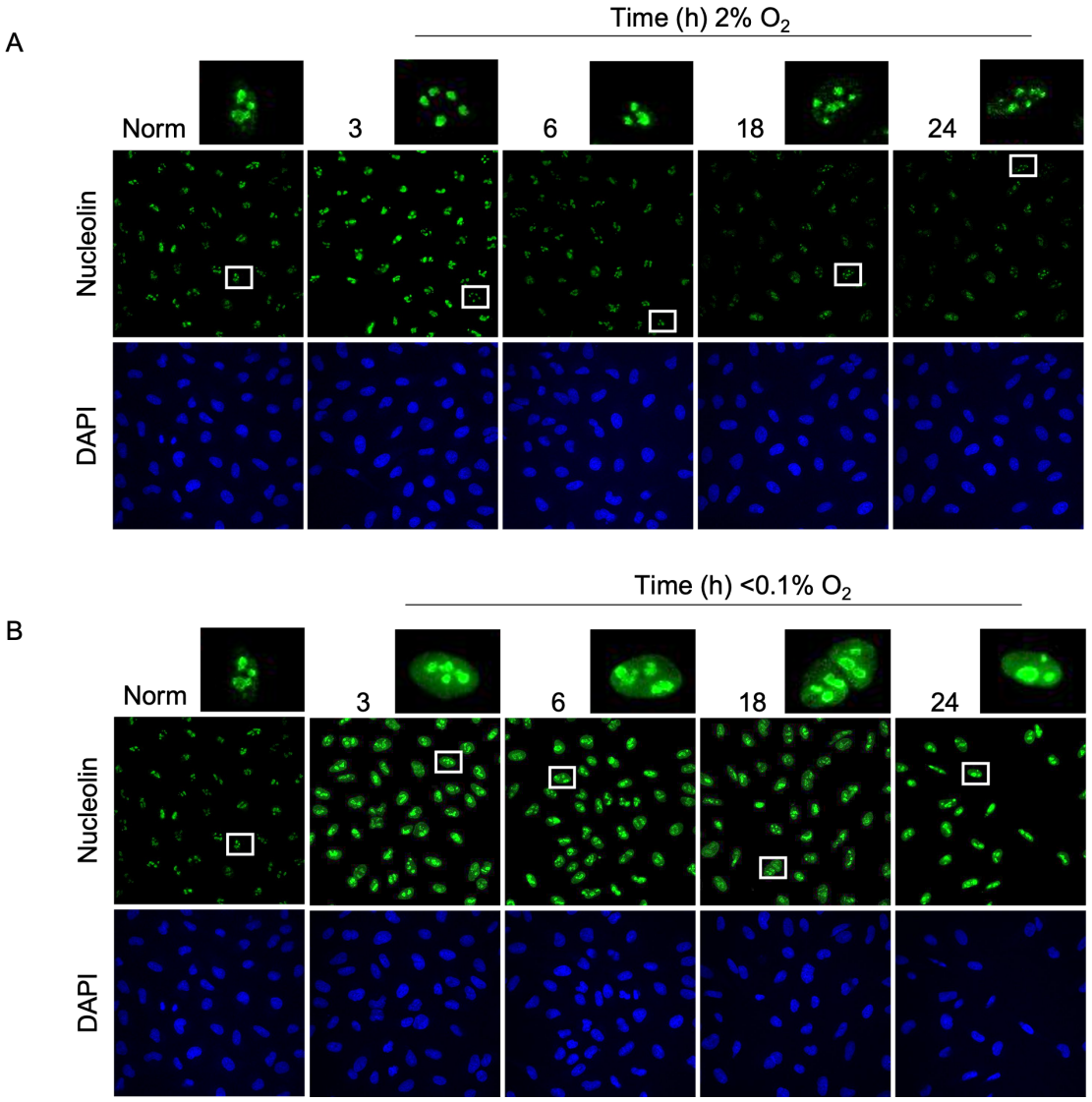
Next, to use an orthogonal assay to look at transcription, we exposed A549 cells to hypoxia (<0.1% O_2) with and without the scavenger NAC and measured 5'EU incorporation. As expected, both hypoxia and DRB led to a significant reduction in global transcription. However, upon addition of ROS scavenger NAC, there was a clear partial rescue of global transcription (**Figure 5.15B**). In support of our data in **Figure 5.15A**, ROS scavenger NAC can also rescue global transcription repression in hypoxia (**Figure 5.15B**); this is again not surprising as most of global transcription can be attributed to transcription of rDNA (Albert *et al.*, 2012; Conconi *et al.*, 1989). Therefore, using two assays, our findings indicate that ROS scavengers are able to at least partially rescue transcription repression in hypoxia. In the future as we repeat experiments, it will be important to use a panel of ROS scavengers as NAC, although widely used as an antioxidant, has other mechanisms of actions unrelated to scavenging ROS (Pedre *et al.*, 2021).

5.2.12 Hypoxia (<0.1% O_2) induces translocation of nucleolin in an oxygen dependent manner

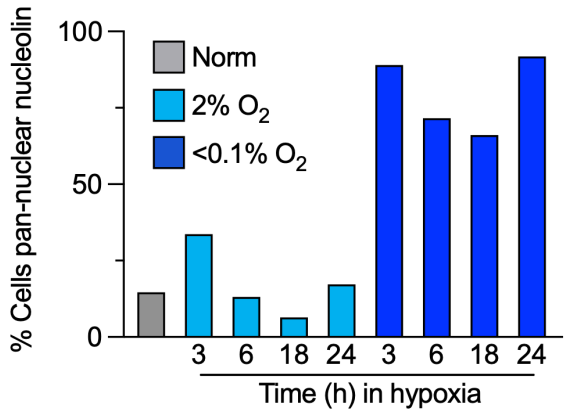
Thus far, our data suggests that hypoxic R-loops play a clear role in the nucleolus: they form on the rDNA and block rDNA transcription. As the nucleolus is the site of rDNA synthesis, which can consume roughly 80% of the cellular energy, it is unsurprising that a resource scarce setting induced by hypoxia would lead cells to shut down processes in the nucleolus (Dubois & Boisvert, 2016). As such, nucleolar proteins such as nucleolin are interesting to study under hypoxic conditions (Fähling *et al.*, 2007; Mekhail *et al.*, 2006). Nucleolin was the first identified metazoan factor that interacts directly with pre-rRNA, and this interaction is necessary for subsequent rRNA processing and ribosome biogenesis (Ginisty, 1998). Interestingly, nucleolin has also been identified as a protein that binds RNA/DNA hybrids and can participate in the DDR (Kobayashi *et al.*, 2012; Wang *et al.*, 2018). In addition, nucleolin also directly interacts with RPA and SETX, both of which bind to R-loops (Daniely & Borowiec, 2000; Suraweera *et al.*, 2009).

Therefore, we investigated how nucleolin expression changes in hypoxia. We exposed A549 cells to mild (2% O_2) and severe (<0.1% O_2) hypoxia and stained for nucleolin using fluorescent microscopy. As expected, nucleolin in untreated normoxic cells was located mainly in the nucleoli. We observed that exposure to 2% O_2 did not lead to significant changes in the localisation of nucleolin (**Figure 5.16A**). However, we found that exposure to <0.1% O_2 led to a striking translocation of nucleolin from the nucleolus to the nucleoplasm in a high percentage of cells (**Figure 5.16B**). We quantified this and found that this 'pan-nuclear' nucleolin phenotype was consistent across all time points in <0.1% O_2 (**Figure 5.16B, C**). To check whether total nucleolin levels are changing when this translocation occurs, we exposed

A549 cells to a time course in hypoxia (<0.1% O_2). We observed that nucleolin protein levels remained unchanged from whole cell lysates (**Figure 5.16D**). These preliminary data indicate that the translocation of nucleolin in response to hypoxia is oxygen dependent, and shares the same oxygen dependency as the UPR, DDR and R-loop and ROS inductions in hypoxia.



C



D

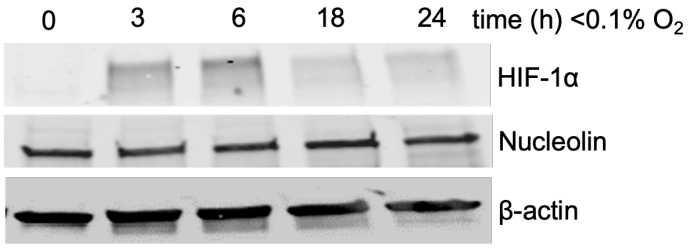


Figure 5.16. Nucleolin translocates in hypoxia in an oxygen dependent manner. A. A549 cells were exposed to 2% O_2 for the times shown. Cells were fixed and stained for nucleolin. **B.** A549 cells were exposed to <0.1% O_2 for the times shown. Cells were fixed and stained for nucleolin. **C.** Quantification of pan-nuclear nucleolin from parts A and B. Error bars represent S.E.M. from more than 5 fields of view per condition. **D.** Western blotting of whole cell lysates from A549 cells were exposed <0.1% O_2 for the times shown. β-actin was used as a loading control. n=1

5.2.13 Hypoxia-induced translocation of nucleolin is R-loops dependent

Given that nucleolin translocation shares the same oxygen-dependency as R-loop induction in hypoxia, and that nucleolin has been characterised to bind to RPA and SETX, both of which bind to R-loops, we next investigated whether nucleolin translocation is R-loop dependent in hypoxia. We transfected A549 cells with mock or RNaseH1^{WT}-V5 and exposed them to 6 hours of hypoxia (<0.1% O_2). As expected, nucleolin translocated from the nucleolus to the

nucleoplasm in around 60-90% of hypoxic cells (**Figure 5.17A**). Strikingly, removal of R-loops through wildtype RNaseH1 overexpression significantly rescued nucleolin translocation by approximately two-thirds (**Figure 5.17B**). To ensure that the hypoxic pan-nuclear nucleolin rescue phenotype was specific to R-loops, and not due to transfection of plasmids, we repeated the experiment but additionally transfected in the catalytically- and binding-dead mutant of RNaseH1, RNaseH1^{WKKD} as well as luciferase as extra controls. We also performed this experiment in two cell lines, A549 and HCT116, to confirm whether or not the phenotype was cell line specific. As expected, 6 hours of hypoxia (<0.1% O_2) led to nucleolin translocation in both mock-transfected A549 and HCT116 cells (**Figure 5.17C, D**). Once again, we found that wildtype RNaseH1 overexpression significantly reduced nucleolin translocation in hypoxic cells in both cell lines. Importantly, we found that cells transfected with the functionally dead RNaseH1^{WKKD} mutant or luciferase did not rescue hypoxia-induced translocation of nucleolin (**Figure 5.17C, D**). Excitingly, these preliminary data suggest that R-loops mediate the response of nucleolin to hypoxia.

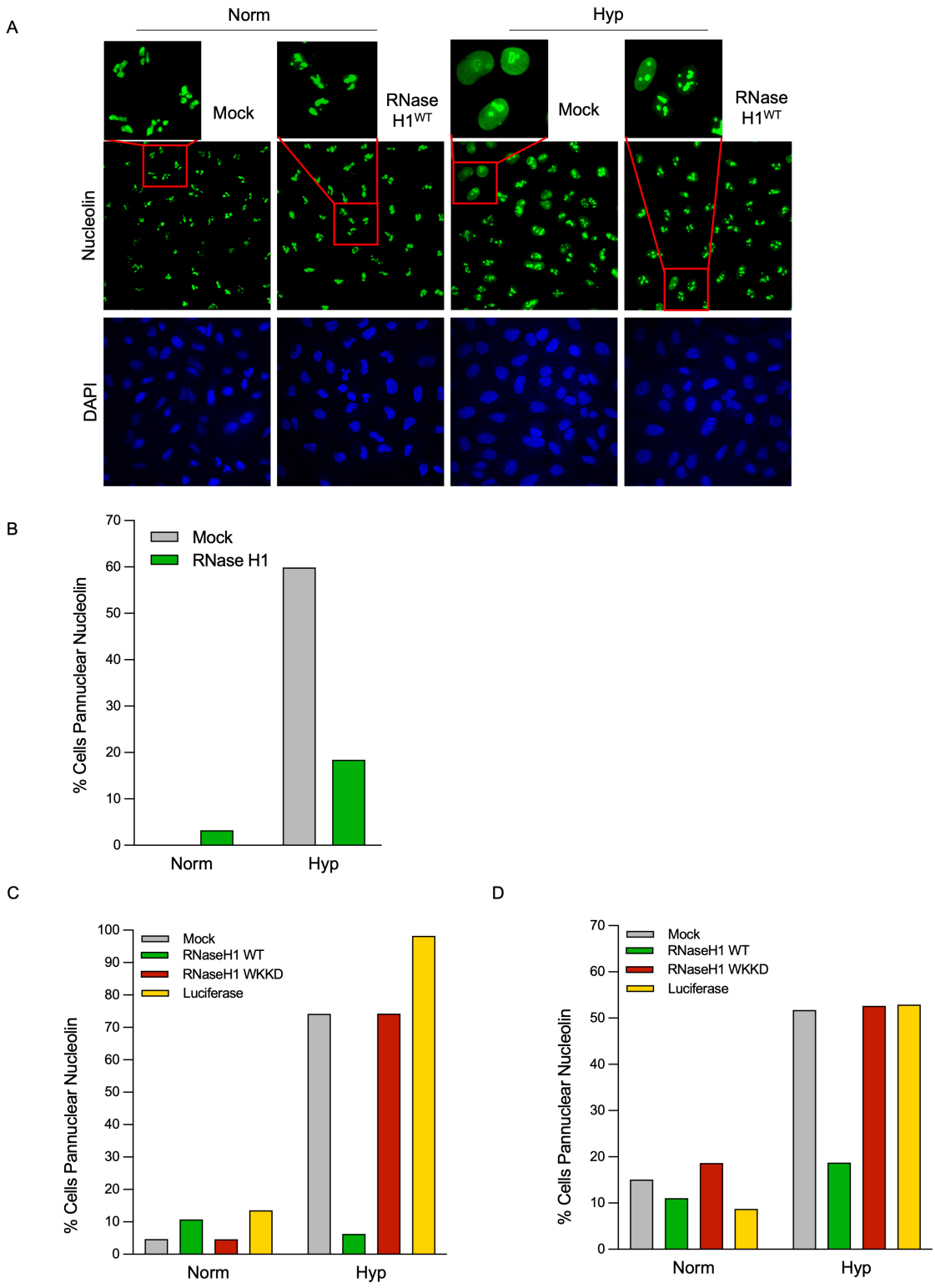


Figure 5.17. Nucleolin translocation in hypoxia is R-loop dependent. A. A549 cells were transfected with RNaseH1^{WT}-V5 and exposed to 21% O_2 or <0.1% O_2 for 6 hours. Cells were fixed and stained for nucleolin. **B.** Quantification of pan-nuclear nucleolin from part A. **C.** A549 cells were transfected with mock, RNaseH1^{WT}-V5, RNaseH1^{WKKD} or luciferase and exposed to 21% O_2 or <0.1% O_2 for 6 hours. Cells were fixed and stained for nucleolin and pan-nuclear nucleolin was quantified. **D.** Same as part C but for HCT116 cells instead of A549 cells. n=1

5.2.14 Hypoxia-induced translocation of nucleolin is ROS dependent

So far, our data showed that in hypoxia, R-loops are ROS dependent, and nucleolin translocation is dependent on R-loops. Therefore, we expect that nucleolin translocation in hypoxia should also be ROS dependent. To test out our hypothesis, we treated A549 cells with and without a panel of ROS scavengers (NAC, vitamin C or catalase) and exposed them to 6 hours of hypoxia (<0.1% O_2), and quantified pan-nuclear nucleolin. As expected, hypoxia (<0.1% O_2) treatment led to a clear increase in the percentage of cells with pan-nuclear nucleolin. Strikingly, NAC, vitamin C or catalase treatment led to a significant reduction in the proportion of cells with pan-nuclear nucleolin (**Figure 5.18**). This preliminary experiment suggests that our ROS-induced R-loops model in hypoxia upholds for R-loops that affect nucleolin translocation.

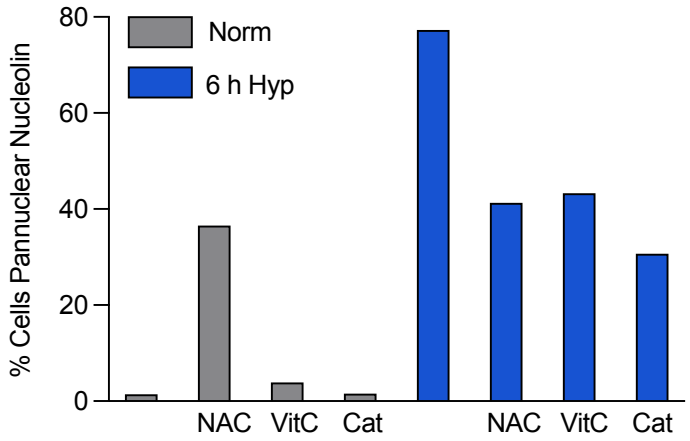


Figure 5.18. Nucleolin translocation in hypoxia is ROS dependent. A549 cells were treated with NAC (20 mM), Vitamin C (2 mM) or catalase (2000 U/mg) then exposed to 21% O_2 or <0.1% O_2 for 6 hours. Cells were fixed and stained for nucleolin. More than 100 cells were counted in each condition, n=1.

5.3 Discussion

We began Chapter 5 by shifting our focus onto R-loops in hypoxia. We asked: how do hypoxic R-loops form, where on the genome do they accumulate, and do they serve any cellular functions as part of the hypoxia-induced stress response?

How do R-loops form in hypoxia? Excitingly, we found that R-loop formation in hypoxia is ROS dependent (**Figure 5.9**), and that this occurs in the absence of DNA damage despite the release of ROS that could potentially cause SSBs, DSBs or oxidised bases (**Figure 5.7**). In addition, we observed many parallels between hypoxia and the UPR. Pharmacological reagents which induce the UPR, Tuni and Thaps, as well as hypoxia, all lead to an increase in ROS, and subsequent accumulation in ROS-induced R-loops. Key questions remain, including: which specific ROS species lead to an increase in R-loops? Do Thaps and Tuni-induced ROS overlap with hypoxia-induced ROS species; do they originate from the mitochondria then travel to the nucleus? Moreover, although we pinpointed ROS as an upstream contributor to R-loop accumulation in hypoxia, how ROS mechanistically leads to R-loops in the absence of DNA damage is still unknown. One study has shown that low levels of H_2O_2 that do not lead to detectable DNA damage cause RNA polymerase II to stall; pausing of RNA polymerase is associated with R-loops (Allison & Wang, 2019; Nilson *et al.*, 2017). Therefore, a plausible hypothesis is that hypoxia-induced ROS can cause RNA polymerase to pause and stall, which induces R-loops. Another study showed that in *BRCA2* deficient cells, elevated levels of ROS impair RNaseH1, which leads to an accumulation of R-loops on the mitochondrial DNA (Renaudin *et al.*, 2021). Therefore, restoring the function of R-loop resolving factors that are repressed in hypoxia (**Figure 4.13E**) such as RNaseH1, RNaseH2B, PIF1, AQR, DHX9 and RTEL1 would be interesting to study; would doing so reduce R-loop levels in hypoxia?

Where do hypoxic R-loops form? We have shown for the first time that R-loops accumulate on the rDNA in hypoxia (**Figure 5.10**). This is not surprisingly as nucleoli are naturally enriched in R-loops, and other studies have shown that in response to other stresses e.g., hypoosomotic stress, R-loops accumulate on the rDNA (Santos-Pereira & Aguilera, 2015; Velichko *et al.*, 2019). However, many interesting questions remain, including: do R-loops also accumulate at UPR or DDR targets in hypoxia? This would be expected as numerous UPR and several selective DDR targets are being actively transcribed in a background of transcriptional repression as part of the stress response to hypoxia. Our hypothesis is that R-loops do not form at HIF target genes in hypoxia as we see no accumulation of R-loops in 2% O_2 (where HIF is stabilised and active), although this remains to be formally verified.

Do R-loops serve any cellular functions in hypoxia? Indeed, we found evidence that R-loops may serve a role in halting an energy-consuming processes in hypoxia. As ribosome biogenesis consumes approximately 80% of cellular energy, it would be imperative to halt the process in the hypoxic tumour microenvironment, where nutrients are scarce (Dubois & Boisvert, 2016). The first step in ribosome biogenesis is rDNA transcription, therefore by blocking transcription of pre-cursor 47S rRNA in hypoxia, R-loops could help the cell conserve energy earlier rather than later in the ribosome biogenesis process. An interesting question to ask here is how the cell is able to differentiate between R-loops that arise from active transcription versus R-loops that halt the transcription machinery as a signal. There have been recent attempts to categorise R-loops into different classes: promoter-paused (Class I) R-loops vs elongation-associated (Class II) R-loops, and R-loops where RPA binds to both DNA strands vs R-loops where RPA only binds to the template strand (Castillo-Guzman & Chédin, 2021; Chen *et al.*,

2022). Alternatively, the class of R-loops that accumulate in hypoxia may not matter; the R-loops may simply be a result of polymerase pausing. For example, a study showed that BRCA1-associated breast tumours accumulate R-loops due to promoter-proximal RNA polymerase II pausing (Zhang *et al.*, 2017).

Apart from blocking rDNA transcription, R-loops also mediate the nucleolar stress response to hypoxia. Nucleolin is a nucleolar protein required for the first step of rDNA transcription as well as rRNA processing (Ginisty, 1998). Interestingly, nucleolin binds to both RPA and SETX, both of which are associated with R-loops (Daniely & Borowiec, 2000; Suraweera *et al.*, 2009). We found that, hypoxia leads to the translocation of nucleolin from the nucleolus to the nucleoplasm in an oxygen and R-loop dependent manner (**Figures 5.14, 5.15**). Interestingly, one study has shown that in response to heat shock, nucleolin also translocates to the nucleoplasm in a p53-dependent manner, where it sequesters RPA from sites of ongoing DNA synthesis (Daniely & Borowiec, 2000). It would be interesting to see whether nucleolin also translocates in response to Tuni and Thaps, to check whether this is a UPR dependent mechanism. Finally, it would also be interesting to see how R-loops regulate the expression of other nucleolar stress response genes, as well as UPR and DDR genes in hypoxia.

Further work will be needed to confirm the findings in the latter parts of Chapter 5. However, an exciting model that connects R-loops, oxidative stress and nucleolar stress in hypoxia has been developed as a result (**Figure 5.19**).

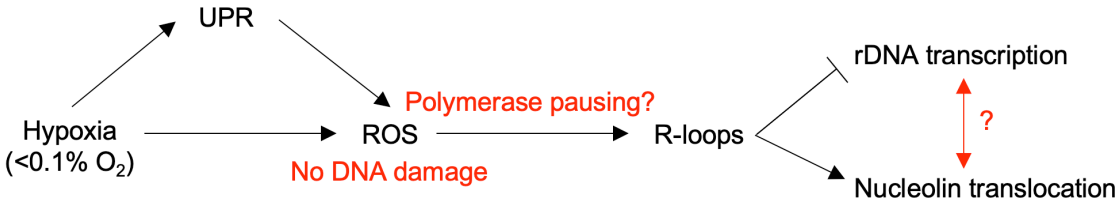


Figure 5.19. Hypoxia-induced ROS leads to the accumulation of R-loops in the absence of DNA damage. Hypoxia (<0.1% O_2) or the UPR leads to an increase in ROS. Despite the increase in hypoxia-induced ROS, there is no detectable DNA damage in the form SSBs, DSBs or 8-oxoguanine. Hypoxia-induced ROS leads to the accumulation of R-loops on the rDNA, which blocks rDNA transcription. The hypoxia-induced R-loops also mediate nucleolin translocation from the nucleoli to the nucleoplasm. The potential link between nucleolin translocation and rDNA transcription repression warrants further investigation.

Chapter 6 Final discussion

Hypoxia is a common trait of tumours and is associated with metastasis, resistance to chemo- and radiotherapy, and poor patient prognosis (Graham & Unger, 2018; Hammond *et al.*, 2014; Teicher, 1994). It is therefore important to understand the molecular mechanisms underlying the poor clinical outcomes of patients with hypoxic tumours in order to develop targeted therapeutics and more accurate diagnostic and prognostic tools.

The UPR and DDR are major stress response pathways in the cell that protect proteome and genome integrity, respectively; how the two pathways contribute to tumourigenesis and therapy resistance independently of each other has been studied extensively in the cancer biology field. Hypoxia (<0.1% O_2) is one of the few physiologically relevant stresses to simultaneously activate the UPR and DDR. Therefore, it is important to study how the two pathways interact and potentially synergise in hypoxic tumours to promote survival and therapy resistance.

Hypoxia is intriguing in that it can activate the DDR in the absence of DNA damage. The hypoxia-induced DDR is mainly activated by replication stress, which can contribute to genome instability by increasing mutagenesis by exposing ssDNA to mutagens e.g., chemical species or nucleases, and increasing the likelihood of chromosomal breakage and rearrangements at fragile sites (Luoto *et al.*, 2013). Hypoxia provides an ideal condition for tumours: they benefit from increased potential for mutagenesis from replication stress, are protected from the potential deleterious effects of replication stress due to activated ATM and ATR signalling, and do not experience DSBs which is the most lethal type of DNA lesions. By performing a systematic literature review, we found that no previous links between the

UPR and DDR in hypoxia have been reported; however, such links are likely to exist, as supported by studies reporting interactions between UPR and DDR proteins in normoxia (Bolland, Ma *et al.*, 2021). Therefore, our investigation focused on exploring links between the UPR and DDR in hypoxia.

Interestingly, in our studies we found that hypoxic tumours are able to escape from DSBs due to the simultaneous activation of the UPR. We found that the hypoxic UPR plays a non-canonical role in protecting hypoxic cells from lethal DSBs. Importantly, the interaction we found between the UPR and DDR in hypoxia is based on R-loops. R-loops are structures that may contribute to genome instability, e.g., through transcription-replication collisions (TRCs). We showed for the first time that the level of R-loops increases in hypoxia. Interestingly, the hypoxic UPR induces RNA/DNA helicase SETX in hypoxia to resolve these R-loops. As R-loops are able to contribute to replication stress and potentially lead to DSBs if unresolved, the UPR thereby protects hypoxic cells from DNA damage by resolving R-loops. Although SETX is induced through the PERK/ATF arm of the UPR, we found that inhibiting other arms of the UPR also led to a further increase in hypoxic R-loops. Alternative mechanisms through which the other arms of the UPR protect hypoxic cells from DNA damage therefore warrant further investigation. Moreover, we identified other hypoxia-induced UPR genes that bind RNA/DNA hybrids that may serve a similar role to SETX; it would be interesting to see whether depletion of those genes also phenocopies SETX depletion in hypoxia.

We found that both hypoxia and pharmacological inducers of the UPR lead to an accumulation of R-loops. Therefore, we asked whether these R-loops may be serving a biological function in response to hypoxic or proteomic stress. Indeed, we found that hypoxic

R-loops form on the rDNA and block transcription of long pre-rRNA, 47S. This is unsurprising as one of the canonical roles of the UPR is to reduce protein synthesis. As ribosome biogenesis uses approximately 80% of cellular energy, the UPR may halt protein synthesis most efficiently by blocking the first step of ribosome biogenesis, the transcription of rDNA (Blobel & Potter, 1967).

Nucleolin is a key protein in ribosome biogenesis and is required for the first processing step of pre-rRNA (Ginisty, 1998). In this study, we report for the first time that nucleolin translocates from the nucleolus to the nucleoplasm in severe hypoxia (<0.1% O_2) and not in mild hypoxia (2% O_2); therefore, nucleolin translocation also shares the same oxygen dependency as R-loop and UPR induction in hypoxia. Indeed, we found that nucleolin translocation in hypoxia is dependent on R-loops, as abrogating R-loops with wildtype RNaseH1 overexpression rescued the translocation. Supportively, heat stress and chemotoxic stress, both known to induce the UPR, has been reported to induce nucleolin translocation (Morfoisse *et al.*, 2016). In addition, nucleolin has previously been identified as a protein that binds to RNA/DNA hybrids and RPA (Daniely & Borowiec, 2000; Wang *et al.*, 2018). One hypothesis is that nucleolin may be binding to R-loops or RPA outside of the nucleolus in response to hypoxia; however, how nucleolin differentiates between R-loops inside and outside the nucleolus is unknown. Nucleolin is a multifunctional protein and can play different roles depending on subcellular localisation. In particular, nucleolin in the nucleoplasm has been associated with favourable expression of proliferative, anti-apoptotic and angiogenic genes (Berger *et al.*, 2015). Moreover, nucleolin regulates the balance between DNA replication and repair. The role of nucleolin in hypoxia therefore warrants further investigation.

Interestingly, we found that both hypoxia and pharmacological UPR inducers increase R-loops in a ROS dependent manner. Existing studies reporting ROS-induced R-loops attribute R-loop formation to DNA damage, as ROS can oxidise bases and cause SSBs and DSBs and hinder transcription. However, ROS-induced R-loops in hypoxia accumulate in the absence of DNA damage. This suggests that ROS may serve as a regulator of intracellular signalling in hypoxia. Indeed, scavenging ROS in hypoxia also rescued repression of rDNA transcription and nucleolin translocation, supporting our model of the ROS-R-loop axis in hypoxia.

It will be interesting to investigate the mechanism through which ROS leads to R-loops without DNA damage. One study has shown that low-dose H_2O_2 treatment that does not lead to DNA damage can cause RNA Pol II pausing; therefore, a plausible hypothesis is that hypoxia-induced ROS leads to RNA Pol I pausing, which can lead to formation of R-loops (Nilson *et al.*, 2017; Zhang *et al.*, 2017). Hence, a future experiment to carry out is RNA Pol I ChIP to see which genes RNA Pol I is enriched on hypoxia, or a nuclear run-on assay to identify where RNA Pol I is active and inactive in hypoxia.

One study showed that a redox mechanism underlies nucleolar stress sensing by nucleolar protein nucleophosmin (NMP1), where oxidation of a cysteine residue in NMP1 mediates its dissociation from rRNA/rDNA and translocation from the nucleolus to the nucleoplasm (Yang *et al.*, 2016). That study used hypoxia (<0.1% O_2), heat shock (which is known to induce the UPR) and actinomycin D (transcription inhibitor) as examples of stresses that increased ROS and caused NPM1 translocation (Yang *et al.*, 2016). Therefore, another working hypothesis is that hypoxia-induced ROS mediate the translocation of nucleolar proteins where it can bind

to ROS-induced R-loops in the nucleoplasm as opposed to those in the nucleolus. Encouraging, NPM1 has also been identified as a protein that binds RNA/DNA hybrids (Wang *et al.*, 2018). To confirm this hypothesis, it would be interesting to co-immunoprecipitate nucleolin and R-loops in hypoxia to see if nucleolin is binding to R-loops specifically in the nucleoplasm fraction of the cell.

From our studies, we hypothesise the following working model which is summarised in **Figure 6.1**. We propose that the UPR and DDR interact in hypoxia to protect hypoxic cells from DNA damage. Specifically, the UPR induces SETX through the PERK/ATF4 arm to resolve hypoxic R-loops in hypoxia. In the absence of PERK or SETX in hypoxia, DNA damage accumulates. Other arms of the UPR may also protect hypoxic cells from DNA damage, possibly through resolving R-loops; however, this warrants further investigation. We also propose that R-loops in hypoxia are induced in a ROS dependent manner in the absence of DNA damage. We hypothesise that the R-loops may serve a functional role in the nucleolar stress response in hypoxia where they block rDNA transcription and mediate nucleolin translocation from the nucleolus to the nucleoplasm. Distinguishing between the different types of R-loops – the ones that the UPR resolves, and the ones that contribute to the nucleolar stress response – will be useful in the future development of this working model.

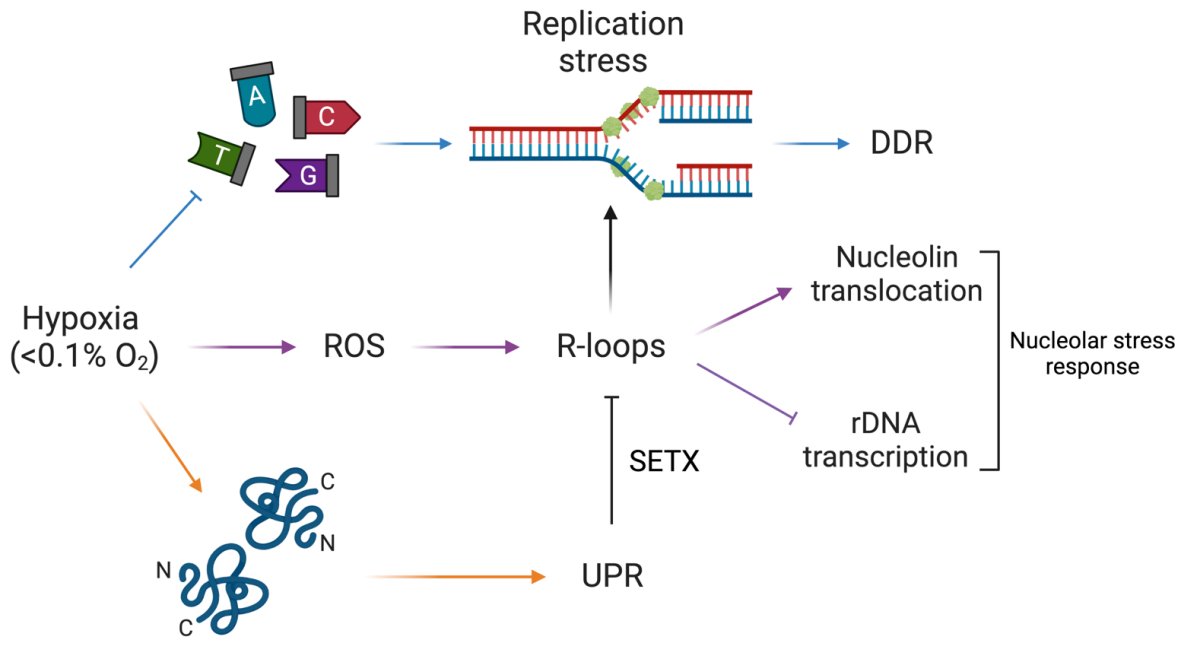


Figure 6.1 Working model of how the UPR and DDR interact in hypoxia. Blue arrows: hypoxia leads to the depletion of nucleotide pools, causing replication forks to stall; the replication stress leads to activation of the DDR. Orange arrows: hypoxia reduces disulfide bonds within proteins and leads to the accumulation of misfolded proteins in the ER, which activates the UPR. Purple arrows: Hypoxia leads to the release and accumulation of ROS which increases R-loops; the R-loops block rDNA transcription and contribute to nucleolin translocation which is R-loop dependent. Black arrow/line: R-loops contribute to replication stress and DDR signalling in hypoxia; if unresolved, R-loops can lead to DNA damage. The UPR resolves R-loops by inducing factors such as SETX.

Ultimately, to address the first aim of this study in **1.6**, we found that indeed, there are links between the UPR and DDR in hypoxia. The UPR protects hypoxic cells from DNA damage through the resolution of R-loops, making the PERK/ATF4/SETX axis an attractive therapeutic target in hypoxic tumours that could be potentially used in conjunction with radiotherapy or drugs that target the DDR. Similarly, other components of the UPR such as IRE1α and ATF6 or their downstream targets may also be potential therapeutic targets in hypoxic tumours, though this requires more data to conclude. To address the second aim of the study, we found that hypoxia increases R-loops which contribute to replication stress but also mediate the

nucleolar stress response. Therefore, disrupting R-loop homeostasis may be another potential therapeutic strategy for hypoxic tumours.

Chapter 7 References

Abou Khouzam, R., Brodaczewska, K., Filipiak, A., Zeinelabdin, N. A., Buart, S., Szczylik, C., Kieda, C., & Chouaib, S. (2021). Tumor Hypoxia Regulates Immune Escape/Invasion: Influence on Angiogenesis and Potential Impact of Hypoxic Biomarkers on Cancer Therapies. *Frontiers in Immunology*, *11*. https://doi.org/10.3389/fimmu.2020.613114

Abraham, R. T. (2004). PI 3-kinase related kinases: 'big' players in stress-induced signaling pathways. *DNA Repair*, *3*(8–9), 883–887. https://doi.org/10.1016/j.dnarep.2004.04.002

Abramov, A. Y., Scorziello, A., & Duchen, M. R. (2007). Three distinct mechanisms generate oxygen free radicals in neurons and contribute to cell death during anoxia and reoxygenation. *The Journal of Neuroscience : The Official Journal of the Society for Neuroscience*, *27*(5), 1129–1138. https://doi.org/10.1523/JNEUROSCI.4468-06.2007

Adam, M. G., Matt, S., Christian, S., Hess-Stumpp, H., Haegebarth, A., Hofmann, T. G., & Algire, C. (2015). SIAH ubiquitin ligases regulate breast cancer cell migration and invasion independent of the oxygen status. *Cell Cycle*, *14*(23), 3734–3747. https://doi.org/10.1080/15384101.2015.1104441

Aguilera, A., & Gómez-González, B. (2017). DNA–RNA hybrids: the risks of DNA breakage during transcription. *Nature Structural & Molecular Biology*, *24*(5), 439–443. https://doi.org/10.1038/nsmb.3395

Ahn, G.-O. (2007). Targeting tumors with hypoxia-activated cytotoxins. *Frontiers in Bioscience*, *12*(8–12), 3483. https://doi.org/10.2741/2329

Airley, R. E., Loncaster, J., Raleigh, J. A., Harris, A. L., Davidson, S. E., Hunter, R. D., West, C. M. L., & Stratford, I. J. (2003). GLUT-1 and CAIX as intrinsic markers of hypoxia in carcinoma of the cervix: Relationship to pimonidazole binding. *International Journal of Cancer*, *104*(1), 85–91. https://doi.org/10.1002/ijc.10904

Akman, M., Belisario, D. C., Salaroglio, I. C., Kopecka, J., Donadelli, M., de Smaele, E., & Riganti, C. (2021). Hypoxia, endoplasmic reticulum stress and chemoresistance: dangerous liaisons. *Journal of Experimental & Clinical Cancer Research*, *40*(1), 28. https://doi.org/10.1186/s13046-020-01824-3

al Tameemi, W., Dale, T. P., Al-Jumaily, R. M. K., & Forsyth, N. R. (2019). Hypoxia-Modified Cancer Cell Metabolism. *Frontiers in Cell and Developmental Biology*, *7*. https://doi.org/10.3389/fcell.2019.00004

Albert, B., Perez-Fernandez, J., Léger-Silvestre, I., & Gadal, O. (2012). Regulation of Ribosomal RNA Production by RNA Polymerase I: Does Elongation Come First? *Genetics Research International*, *2012*, 1–13. https://doi.org/10.1155/2012/276948

Albuquerque, T. A. F., Drummond do Val, L., Doherty, A., & de Magalhães, J. P. (2018). From humans to hydra: patterns of cancer across the tree of life. *Biological Reviews*, *93*(3), 1715–1734. https://doi.org/10.1111/brv.12415

Alexandrov, L. B., Nik-Zainal, S., Wedge, D. C., Aparicio, S. A. J. R., Behjati, S., Biankin, A. v., Bignell, G. R., Bolli, N., Borg, A., Børresen-Dale, A.-L., Boyault, S., Burkhardt, B., Butler, A. P., Caldas, C., Davies, H. R., Desmedt, C., Eils, R., Eyfjörd, J. E., Foekens, J. A., … Stratton, M. R. (2013). Signatures of mutational processes in human cancer. *Nature*, *500*(7463), 415–421. https://doi.org/10.1038/nature12477

Al-Hadid, Q., & Yang, Y. (2016). R-loop: an emerging regulator of chromatin dynamics. *Acta Biochimica et Biophysica Sinica*, *48*(7), 623–631. https://doi.org/10.1093/abbs/gmw052

Allison, D. F., & Wang, G. G. (2019). R-loops: formation, function, and relevance to cell stress. *Cell Stress*, *3*(2), 38–46. https://doi.org/10.15698/cst2019.02.175

Alnasser, H. A., Guan, Q., Zhang, F., Gleave, M. E., Nguan, C. Y. C., & Du, C. (2016). Requirement of clusterin expression for prosurvival autophagy in hypoxic kidney tubular epithelial cells. *American Journal of Physiology-Renal Physiology*, *310*(2), F160–F173. https://doi.org/10.1152/ajprenal.00304.2015

Alzu, A., Bermejo, R., Begnis, M., Lucca, C., Piccini, D., Carotenuto, W., Saponaro, M., Brambati, A., Cocito, A., Foiani, M., & Liberi, G. (2012). Senataxin Associates with Replication Forks to Protect Fork Integrity across RNA-Polymerase-II-Transcribed Genes. *Cell*, *151*(4), 835–846. https://doi.org/10.1016/j.cell.2012.09.041

American Cancer Society. (n.d.-a). *How Radiation Therapy Is Used to Treat Cancer*.

American Cancer Society. (n.d.-b). *Understanding What Cancer Is: Ancient Times to Present*. Retrieved 30 June 2022, from https://www.cancer.org/treatment/understanding-your-diagnosis/history-of-cancer/what-is-cancer.html

Andegeko, Y., Moyal, L., Rotman, G., Shiloh, Y., Mittelman, L., & Tsarfaty, I. (2001). Nuclear Retention of ATM at Sites of DNA Double Strand Breaks. *Journal of Biological Chemistry*, *276*(41), 38224–38230. https://doi.org/10.1074/jbc.M102986200

Anderson, N. M., & Simon, M. C. (2020). The tumor microenvironment. *Current Biology*, *30*(16), R921–R925. https://doi.org/10.1016/j.cub.2020.06.081

Arab, K., Karaulanov, E., Musheev, M., Trnka, P., Schäfer, A., Grummt, I., & Niehrs, C. (2019). GADD45A binds R-loops and recruits TET1 to CpG island promoters. *Nature Genetics*, *51*(2), 217–223. https://doi.org/10.1038/s41588-018-0306-6

Arora, R., Lee, Y., Wischnewski, H., Brun, C. M., Schwarz, T., & Azzalin, C. M. (2014). RNaseH1 regulates TERRA-telomeric DNA hybrids and telomere maintenance in ALT tumour cells. *Nature Communications*, *5*(1), 5220. https://doi.org/10.1038/ncomms6220

Ashton, T. M., Fokas, E., Kunz-Schughart, L. A., Folkes, L. K., Anbalagan, S., Huether, M., Kelly, C. J., Pirovano, G., Buffa, F. M., Hammond, E. M., Stratford, M., Muschel, R. J., Higgins, G. S., & McKenna, W. G. (2016). The anti-malarial atovaquone increases radiosensitivity by alleviating tumour hypoxia. *Nature Communications*, *7*(1), 12308. https://doi.org/10.1038/ncomms12308

Avril, T., Vauléon, E., & Chevet, E. (2017). Endoplasmic reticulum stress signaling and chemotherapy resistance in solid cancers. *Oncogenesis*, *6*(8), e373–e373. https://doi.org/10.1038/oncsis.2017.72

Aynaud, M.-M., Suspène, R., Vidalain, P.-O., Mussil, B., Guétard, D., Tangy, F., Wain-Hobson, S., & Vartanian, J.-P. (2012). Human Tribbles 3 Protects Nuclear DNA from Cytidine Deamination by APOBEC3A. *Journal of Biological Chemistry*, *287*(46), 39182–39192. https://doi.org/10.1074/jbc.M112.372722

Bader, S. B., Dewhirst, M. W., & Hammond, E. M. (2020). Cyclic Hypoxia: An Update on Its Characteristics, Methods to Measure It and Biological Implications in Cancer. *Cancers*, *13*(1), 23. https://doi.org/10.3390/cancers13010023

Bader, S. B., Ma, T. S., Simpson, C. J., Liang, J., Maezono, S. E. B., Olcina, M. M., Buffa, F. M., & Hammond, E. M. (2021). Replication catastrophe induced by cyclic hypoxia leads to increased APOBEC3B activity. *Nucleic Acids Research*, *49*(13), 7492–7506. https://doi.org/10.1093/nar/gkab551

Baker, S. G. (2014). A Cancer Theory Kerfuffle Can Lead to New Lines of Research. *JNCI Journal of the National Cancer Institute*, *107*(2), dju405–dju405. https://doi.org/10.1093/jnci/dju405

Bakkenist, C. J., & Kastan, M. B. (2003). DNA damage activates ATM through intermolecular autophosphorylation and dimer dissociation. *Nature*, *421*(6922), 499–506. https://doi.org/10.1038/nature01368

Baluk, P., Hashizume, H., & McDonald, D. M. (2005). Cellular abnormalities of blood vessels as targets in cancer. *Current Opinion in Genetics & Development*, *15*(1), 102–111. https://doi.org/10.1016/j.gde.2004.12.005

Bauer, M., Nascakova, Z., Mihai, A.-I., Cheng, P. F., Levesque, M. P., Lampart, S., Hurwitz, R., Pfannkuch, L., Dobrovolna, J., Jacobs, M., Bartfeld, S., Dohlman, A., Shen, X., Gall, A. A., Salama, N. R., Töpfer, A., Weber, A., Meyer, T. F., Janscak, P., & Müller, A. (2020). The ALPK1/TIFA/NF-κB axis links a bacterial carcinogen to R-loop-induced replication stress. *Nature Communications*, *11*(1), 5117. https://doi.org/10.1038/s41467-020-18857-z

Bayer, C., & Vaupel, P. (2012). Acute versus chronic hypoxia in tumors. *Strahlentherapie Und Onkologie*, *188*(7), 616–627. https://doi.org/10.1007/s00066-012-0085-4

Bell, E. L., Klimova, T. A., Eisenbart, J., Moraes, C. T., Murphy, M. P., Budinger, G. R. S., & Chandel, N. S. (2007). The Qo site of the mitochondrial complex III is required for the transduction of hypoxic signaling via reactive oxygen species production. *Journal of Cell Biology*, *177*(6), 1029–1036. https://doi.org/10.1083/jcb.200609074

Bell, E. L., Klimova, T. A., Eisenbart, J., Schumacker, P. T., & Chandel, N. S. (2007). Mitochondrial Reactive Oxygen Species Trigger Hypoxia-Inducible Factor-Dependent Extension of the Replicative Life Span during Hypoxia. *Molecular and Cellular Biology*, *27*(16), 5737–5745. https://doi.org/10.1128/MCB.02265-06

Belotserkovskii, B. P., Soo Shin, J. H., & Hanawalt, P. C. (2017). Strong transcription blockage mediated by R-loop formation within a G-rich homopurine–homopyrimidine sequence localized in the vicinity of the promoter. *Nucleic Acids Research*, *45*(11), 6589–6599. https://doi.org/10.1093/nar/gkx403

Belotserkovskii, B. P., Tornaletti, S., D'Souza, A. D., & Hanawalt, P. C. (2018). R-loop generation during transcription: Formation, processing and cellular outcomes. *DNA Repair*, *71*, 69–81. https://doi.org/10.1016/j.dnarep.2018.08.009

Bencokova, Z., Kaufmann, M. R., Pires, I. M., Lecane, P. S., Giaccia, A. J., & Hammond, E. M. (2009). ATM Activation and Signaling under Hypoxic Conditions. *Molecular and Cellular Biology*, *29*(2), 526–537. https://doi.org/10.1128/MCB.01301-08

Benej, M., Hong, X., Vibhute, S., Scott, S., Wu, J., Graves, E., Le, Q.-T., Koong, A. C., Giaccia, A. J., Yu, B., Chen, C.-S., Papandreou, I., & Denko, N. C. (2018). Papaverine and its derivatives radiosensitize solid tumors by inhibiting mitochondrial metabolism. *Proceedings of the National Academy of Sciences*, *115*(42), 10756–10761. https://doi.org/10.1073/pnas.1808945115

Bennetzen, M. v., Larsen, D. H., Bunkenborg, J., Bartek, J., Lukas, J., & Andersen, J. S. (2010). Site-specific Phosphorylation Dynamics of the Nuclear Proteome during the DNA Damage Response. *Molecular & Cellular Proteomics*, *9*(6), 1314–1323. https://doi.org/10.1074/mcp.M900616-MCP200

Bennewith, K. L., & Dedhar, S. (2011). Targeting hypoxic tumour cells to overcome metastasis. *BMC Cancer*, *11*(1), 504. https://doi.org/10.1186/1471-2407-11-504

Bentzen, L., Keiding, S., Nordsmark, M., Falborg, L., Hansen, S. B., Keller, J., Nielsen, O. S., & Overgaard, J. (2003). Tumour oxygenation assessed by 18F-fluoromisonidazole PET and polarographic needle electrodes in human soft tissue tumours. *Radiotherapy and Oncology*, *67*(3), 339–344. https://doi.org/10.1016/S0167-8140(03)00081-1

Berger, C. M., Gaume, X., & Bouvet, P. (2015). The roles of nucleolin subcellular localization in cancer. *Biochimie*, *113*, 78–85. https://doi.org/10.1016/j.biochi.2015.03.023

Berti, M., & Vindigni, A. (2016). Replication stress: getting back on track. *Nature Structural & Molecular Biology*, *23*(2), 103–109. https://doi.org/10.1038/nsmb.3163

Bertolotti, A., Zhang, Y., Hendershot, L. M., Harding, H. P., & Ron, D. (2000). Dynamic interaction of BiP and ER stress transducers in the unfolded-protein response. *Nature Cell Biology*, *2*(6), 326–332. https://doi.org/10.1038/35014014

Bhandari, V., Hoey, C., Liu, L. Y., Lalonde, E., Ray, J., Livingstone, J., Lesurf, R., Shiah, Y.-J., Vujcic, T., Huang, X., Espiritu, S. M. G., Heisler, L. E., Yousif, F., Huang, V., Yamaguchi, T. N., Yao, C. Q., Sabelnykova, V. Y., Fraser, M., Chua, M. L. K., … Bristow, R. G. (2019). Molecular landmarks of tumor hypoxia across cancer types. *Nature Genetics*, *51*(2), 308–318. https://doi.org/10.1038/s41588-018-0318-2

Bhaskara, V. K., Mohanam, I., Rao, J. S., & Mohanam, S. (2012). Intermittent Hypoxia Regulates Stem-like Characteristics and Differentiation of Neuroblastoma Cells. *PLoS ONE*, *7*(2), e30905. https://doi.org/10.1371/journal.pone.0030905

Bi, M., Naczki, C., Koritzinsky, M., Fels, D., Blais, J., Hu, N., Harding, H., Novoa, I., Varia, M., Raleigh, J., Scheuner, D., Kaufman, R. J., Bell, J., Ron, D., Wouters, B. G., & Koumenis, C. (2005). ER stress-regulated translation increases tolerance to extreme hypoxia and promotes tumor growth. *The EMBO Journal*, *24*(19), 3470–3481. https://doi.org/10.1038/sj.emboj.7600777

Bindra, R. S., Gibson, S. L., Meng, A., Westermark, U., Jasin, M., Pierce, A. J., Bristow, R. G., Classon, M. K., & Glazer, P. M. (2005). Hypoxia-Induced Down-regulation of BRCA1 Expression by E2Fs. *Cancer Research*, *65*(24), 11597–11604. https://doi.org/10.1158/0008-5472.CAN-05-2119

Bindra, R. S., & Glazer, P. M. (2007). Repression of RAD51 gene expression by E2F4/p130 complexes in hypoxia. *Oncogene*, *26*(14), 2048–2057. https://doi.org/10.1038/sj.onc.1210001

Blackadar, C. B. (2016). Historical review of the causes of cancer. *World Journal of Clinical Oncology*, *7*(1), 54–86. https://doi.org/10.5306/wjco.v7.i1.54

Blackford, A. N., & Jackson, S. P. (2017). ATM, ATR, and DNA-PK: The Trinity at the Heart of the DNA Damage Response. *Molecular Cell*, *66*(6), 801–817. https://doi.org/10.1016/j.molcel.2017.05.015

Blagosklonny, M. v. (2004). Antiangiogenic therapy and tumor progression. *Cancer Cell*, *5*(1), 13–17. https://doi.org/10.1016/S1535-6108(03)00336-2

Blobel, G., & Potter, V. R. (1967). Studies on free and membrane-bound ribosomes in rat liver. *Journal of Molecular Biology*, *26*(2), 279–292. https://doi.org/10.1016/0022-2836(67)90297-5

Bobrovnikova-Marjon, E., Grigoriadou, C., Pytel, D., Zhang, F., Ye, J., Koumenis, C., Cavener, D., & Diehl, J. A. (2010). PERK promotes cancer cell proliferation and tumor growth by limiting oxidative DNA damage. *Oncogene*, *29*(27), 3881–3895. https://doi.org/10.1038/onc.2010.153

Boguslawski, S. J., Smith, D. E., Michalak, M. A., Mickelson, K. E., Yehle, C. O., Patterson, W. L., & Carrico, R. J. (1986). Characterization of monoclonal antibody to DNA · RNA and its application to immunodetection of hybrids. *Journal of Immunological Methods*, *89*(1), 123–130. https://doi.org/10.1016/0022-1759(86)90040-2

Bolland, H., Ma, T. S., Ramlee, S., Ramadan, K., & Hammond, E. M. (2021). Links between the unfolded protein response and the DNA damage response in hypoxia: a systematic review. *Biochemical Society Transactions*, *49*(3), 1251–1263. https://doi.org/10.1042/BST20200861

Bonnet-Magnaval, F., Philippe, C., van den Berghe, L., Prats, H., Touriol, C., & Lacazette, E. (2016). Hypoxia and ER stress promote Staufen1 expression through an alternative translation mechanism. *Biochemical and Biophysical Research Communications*, *479*(2), 365–371. https://doi.org/10.1016/j.bbrc.2016.09.082

Boque-Sastre, R., Soler, M., Oliveira-Mateos, C., Portela, A., Moutinho, C., Sayols, S., Villanueva, A., Esteller, M., & Guil, S. (2015). Head-to-head antisense transcription and R-loop formation promotes transcriptional activation. *Proceedings of the National Academy of Sciences*, *112*(18), 5785–5790. https://doi.org/10.1073/pnas.1421197112

Bou-Nader, C., Bothra, A., Garboczi, D. N., Leppla, S. H., & Zhang, J. (2022). Structural basis of R-loop recognition by the S9.6 monoclonal antibody. *Nature Communications*, *13*(1), 1641. https://doi.org/10.1038/s41467-022-29187-7

Bouquet, F., Ousset, M., Biard, D., Fallone, F., Dauvillier, S., Frit, P., Salles, B., & Muller, C. (2011). A DNA-dependent stress response involving DNA-PK occurs in hypoxic cells and contributes to cellular adaptation to hypoxia. *Journal of Cell Science*, *124*(11), 1943–1951. https://doi.org/10.1242/jcs.078030

Bowry, A., Kelly, R. D. W., & Petermann, E. (2021). Hypertranscription and replication stress in cancer. *Trends in Cancer*, *7*(9), 863–877. https://doi.org/10.1016/j.trecan.2021.04.006

Brewer, J. W., & Diehl, J. A. (2000). PERK mediates cell-cycle exit during the mammalian unfolded protein response. *Proceedings of the National Academy of Sciences*, *97*(23), 12625–12630. https://doi.org/10.1073/pnas.220247197

Bristow, R. G., & Hill, R. P. (2008). Hypoxia, DNA repair and genetic instability. *Nature Reviews Cancer*, *8*(3), 180–192. https://doi.org/10.1038/nrc2344

Brizel, D. M., Dodge, R. K., Clough, R. W., & Dewhirst, M. W. (1999). Oxygenation of head and neck cancer: changes during radiotherapy and impact on treatment outcome. *Radiotherapy and Oncology*, *53*(2), 113–117. https://doi.org/10.1016/S0167-8140(99)00102-4

Brizel, D. M., Scully, S. P., Harrelson, J. M., Layfield, L. J., Bean, J. M., Prosnitz, L. R., & Dewhirst, M. W. (1996). Tumor oxygenation predicts for the likelihood of distant metastases in human soft tissue sarcoma. *Cancer Research*, *56*(5), 941–943.

Brown, E. J., & Baltimore, D. (2000). ATR disruption leads to chromosomal fragmentation and early embryonic lethality. *Genes & Development*, *14*(4), 397–402.

Brown, J. M. (2002). Tumor Microenvironment and the Response to Anticancer Therapy. *Cancer Biology & Therapy*, *1*(5), 453–458. https://doi.org/10.4161/cbt.1.5.157

Brown, J. M., & Giaccia, A. J. (1998). The unique physiology of solid tumors: opportunities (and problems) for cancer therapy. *Cancer Research*, *58*(7), 1408–1416.

Brown, J. M., & Wilson, W. R. (2004). Exploiting tumour hypoxia in cancer treatment. *Nature Reviews Cancer*, *4*(6), 437–447. https://doi.org/10.1038/nrc1367

Brunelle, J. K., Bell, E. L., Quesada, N. M., Vercauteren, K., Tiranti, V., Zeviani, M., Scarpulla, R. C., & Chandel, N. S. (2005). Oxygen sensing requires mitochondrial ROS but not oxidative phosphorylation. *Cell Metabolism*, *1*(6), 409–414. https://doi.org/10.1016/j.cmet.2005.05.002

Bruno, T., Corleone, G., Catena, V., Cortile, C., de Nicola, F., Fabretti, F., Gumenyuk, S., Pisani, F., Mengarelli, A., Passananti, C., & Fanciulli, M. (2022). AATF/Che-1 localizes to paraspeckles and suppresses R-loops accumulation and interferon activation in Multiple Myeloma. *The EMBO Journal*. https://doi.org/10.15252/embj.2021109711

Burma, S., Chen, B. P., Murphy, M., Kurimasa, A., & Chen, D. J. (2001). ATM Phosphorylates Histone H2AX in Response to DNA Double-strand Breaks. *Journal of Biological Chemistry*, *276*(45), 42462–42467. https://doi.org/10.1074/jbc.C100466200

Calini, V., Urani, C., & Camatini, M. (2002). Comet assay evaluation of DNA single- and double-strand breaks induction and repair in C3H10T1/2 cells. *Cell Biology and Toxicology*, *18*(6), 369–379. https://doi.org/10.1023/A:1020811522100

Cam, H., Easton, J. B., High, A., & Houghton, P. J. (2010). mTORC1 Signaling under Hypoxic Conditions Is Controlled by ATM-Dependent Phosphorylation of HIF-1α. *Molecular Cell*, *40*(4), 509–520. https://doi.org/10.1016/j.molcel.2010.10.030

Canman, C. E., Lim, D.-S., Cimprich, K. A., Taya, Y., Tamai, K., Sakaguchi, K., Appella, E., Kastan, M. B., & Siliciano, J. D. (1998). Activation of the ATM Kinase by Ionizing Radiation and Phosphorylation of p53. *Science*, *281*(5383), 1677–1679. https://doi.org/10.1126/science.281.5383.1677

Cao, S. S., & Kaufman, R. J. (2012). Unfolded protein response. *Current Biology*, *22*(16), R622–R626. https://doi.org/10.1016/j.cub.2012.07.004

Carmeliet, P. (2005). VEGF as a Key Mediator of Angiogenesis in Cancer. *Oncology*, *69*(Suppl. 3), 4–10. https://doi.org/10.1159/000088478

Carney, J. P., Maser, R. S., Olivares, H., Davis, E. M., le Beau, M., Yates, J. R., Hays, L., Morgan, W. F., & Petrini, J. H. J. (1998). The hMre11/hRad50 Protein Complex and Nijmegen Breakage Syndrome: Linkage of Double-Strand Break Repair to the Cellular DNA Damage Response. *Cell*, *93*(3), 477–486. https://doi.org/10.1016/S0092-8674(00)81175-7

Carreau, A., Hafny-Rahbi, B. el, Matejuk, A., Grillon, C., & Kieda, C. (2011). Why is the partial oxygen pressure of human tissues a crucial parameter? Small molecules and hypoxia. *Journal of Cellular and Molecular Medicine*, *15*(6), 1239–1253. https://doi.org/10.1111/j.1582-4934.2011.01258.x

Castillo-Guzman, D., & Chédin, F. (2021). Defining R-loop classes and their contributions to genome instability. *DNA Repair*, *106*, 103182. https://doi.org/10.1016/j.dnarep.2021.103182

Cavadas, M. A. S., Mesnieres, M., Crifo, B., Manresa, M. C., Selfridge, A. C., Keogh, C. E., Fabian, Z., Scholz, C. C., Nolan, K. A., Rocha, L. M. A., Tambuwala, M. M., Brown, S., Wdowicz, A.,

Corbett, D., Murphy, K. J., Godson, C., Cummins, E. P., Taylor, C. T., & Cheong, A. (2016). REST is a hypoxia-responsive transcriptional repressor. *Scientific Reports*, *6*(1), 31355. https://doi.org/10.1038/srep31355

Chan, N., Ali, M., McCallum, G. P., Kumareswaran, R., Koritzinsky, M., Wouters, B. G., Wells, P. G., Gallinger, S., & Bristow, R. G. (2014). Hypoxia Provokes Base Excision Repair Changes and a Repair-Deficient, Mutator Phenotype in Colorectal Cancer Cells. *Molecular Cancer Research*, *12*(10), 1407–1415. https://doi.org/10.1158/1541-7786.MCR-14-0246

Chan, N., Pires, I. M., Bencokova, Z., Coackley, C., Luoto, K. R., Bhogal, N., Lakshman, M., Gottipati, P., Oliver, F. J., Helleday, T., Hammond, E. M., & Bristow, R. G. (2010). Contextual Synthetic Lethality of Cancer Cell Kill Based on the Tumor Microenvironment. *Cancer Research*, *70*(20), 8045–8054. https://doi.org/10.1158/0008-5472.CAN-10-2352

Chandel, N. S., Maltepe, E., Goldwasser, E., Mathieu, C. E., Simon, M. C., & Schumacker, P. T. (1998). Mitochondrial reactive oxygen species trigger hypoxia-induced transcription. *Proceedings of the National Academy of Sciences*, *95*(20), 11715–11720. https://doi.org/10.1073/pnas.95.20.11715

Chandel, N. S., McClintock, D. S., Feliciano, C. E., Wood, T. M., Melendez, J. A., Rodriguez, A. M., & Schumacker, P. T. (2000). Reactive Oxygen Species Generated at Mitochondrial Complex III Stabilize Hypoxia-inducible Factor-1α during Hypoxia. *Journal of Biological Chemistry*, *275*(33), 25130–25138. https://doi.org/10.1074/jbc.M001914200

Chandrika, B. B., Yang, C., Ou, Y., Feng, X., Muhoza, D., Holmes, A. F., Theus, S., Deshmukh, S., Haun, R. S., & Kaushal, G. P. (2015). Endoplasmic Reticulum Stress-Induced Autophagy Provides Cytoprotection from Chemical Hypoxia and Oxidant Injury and Ameliorates Renal Ischemia-Reperfusion Injury. *PLOS ONE*, *10*(10), e0140025. https://doi.org/10.1371/journal.pone.0140025

Chang, T. K., Lawrence, D. A., Lu, M., Tan, J., Harnoss, J. M., Marsters, S. A., Liu, P., Sandoval, W., Martin, S. E., & Ashkenazi, A. (2018). Coordination between Two Branches of the Unfolded Protein Response Determines Apoptotic Cell Fate. *Molecular Cell*. https://doi.org/10.1016/j.molcel.2018.06.038

Chang, Z. (2016). Biogenesis of Secretory Proteins. In *Encyclopedia of Cell Biology* (pp. 535–544). Elsevier. https://doi.org/10.1016/B978-0-12-394447-4.10065-3

Chaplin, D. J., Olive, P. L., & Durand, R. E. (1987). Intermittent blood flow in a murine tumor: radiobiological effects. *Cancer Research*, *47*(2), 597–601.

Chen, D., Rauh, M., Buchfelder, M., Eyupoglu, I. Y., & Savaskan, N. (2017). The oxido-metabolic driver ATF4 enhances temozolamide chemo-resistance in human gliomas. *Oncotarget*, *8*(31), 51164–51176. https://doi.org/10.18632/oncotarget.17737

Chen, J.-Y., Lim, D.-H., Chen, L., Zhou, Y., Zhang, F., Shao, C., Zhang, X., Li, H., Wang, D., Zhang, D.-E., & Fu, X.-D. (2022). *Systematic Evaluation of Different R-loop Mapping Methods:*

Achieving Consensus, Resolving Discrepancies and Uncovering Distinct Types of RNA:DNA Hybrids.

Chen, L., Chen, J.-Y., Zhang, X., Gu, Y., Xiao, R., Shao, C., Tang, P., Qian, H., Luo, D., Li, H., Zhou, Y., Zhang, D.-E., & Fu, X.-D. (2017). R-ChIP Using Inactive RNase H Reveals Dynamic Coupling of R-loops with Transcriptional Pausing at Gene Promoters. *Molecular Cell*, *68*(4), 745-757.e5. https://doi.org/10.1016/j.molcel.2017.10.008

Chen, L., Fu, L., Kong, X., Xu, J., Wang, Z., Ma, X., Akiyama, Y., Chen, Y., & Fang, J. (2014). Jumonji domain-containing protein 2B silencing induces DNA damage response via STAT3 pathway in colorectal cancer. *British Journal of Cancer*, *110*(4), 1014–1026. https://doi.org/10.1038/bjc.2013.808

Chen, P. B., Chen, H. v, Acharya, D., Rando, O. J., & Fazzio, T. G. (2015). R loops regulate promoter-proximal chromatin architecture and cellular differentiation. *Nature Structural & Molecular Biology*, *22*(12), 999–1007. https://doi.org/10.1038/nsmb.3122

Chen, P.-S., Chiu, W.-T., Hsu, P.-L., Lin, S.-C., Peng, I.-C., Wang, C.-Y., & Tsai, S.-J. (2020). Pathophysiological implications of hypoxia in human diseases. *Journal of Biomedical Science*, *27*(1), 63. https://doi.org/10.1186/s12929-020-00658-7

Chen, X., Iliopoulos, D., Zhang, Q., Tang, Q., Greenblatt, M. B., Hatziapostolou, M., Lim, E., Tam, W. L., Ni, M., Chen, Y., Mai, J., Shen, H., Hu, D. Z., Adoro, S., Hu, B., Song, M., Tan, C., Landis, M. D., Ferrari, M., … Glimcher, L. H. (2014). XBP1 promotes triple-negative breast cancer by controlling the HIF1α pathway. *Nature*, *508*(7494), 103–107. https://doi.org/10.1038/nature13119

Chipurupalli, S., Kannan, E., Tergaonkar, V., D'Andrea, R., & Robinson, N. (2019). Hypoxia Induced ER Stress Response as an Adaptive Mechanism in Cancer. *International Journal of Molecular Sciences*, *20*(3), 749. https://doi.org/10.3390/ijms20030749

Choo, J. A. M. Y., Schlösser, D., Manzini, V., Magerhans, A., & Dobbelstein, M. (2020). The integrated stress response induces R-loops and hinders replication fork progression. *Cell Death & Disease*, *11*(7), 538. https://doi.org/10.1038/s41419-020-2727-2

Choudhry, H., & Harris, A. L. (2018). Advances in Hypoxia-Inducible Factor Biology. In *Cell Metabolism*. https://doi.org/10.1016/j.cmet.2017.10.005

Ciccia, A., & Elledge, S. J. (2010). The DNA Damage Response: Making It Safe to Play with Knives. *Molecular Cell*, *40*(2), 179–204. https://doi.org/10.1016/j.molcel.2010.09.019

Cimprich, K. A., & Cortez, D. (2008). ATR: an essential regulator of genome integrity. *Nature Reviews Molecular Cell Biology*, *9*(8), 616–627. https://doi.org/10.1038/nrm2450

Cleveland Clinic. (n.d.). *Blood Oxygen Level*. Retrieved 2 July 2022, from https://my.clevelandclinic.org/health/diagnostics/22447-blood-oxygen-level

Cloutier, S. C., Wang, S., Ma, W. K., al Husini, N., Dhoondia, Z., Ansari, A., Pascuzzi, P. E., & Tran, E. J. (2016). Regulated Formation of lncRNA-DNA Hybrids Enables Faster

Transcriptional Induction and Environmental Adaptation. *Molecular Cell*, *61*(3), 393–404. https://doi.org/10.1016/j.molcel.2015.12.024

Cohen, S., Puget, N., Lin, Y.-L., Clouaire, T., Aguirrebengoa, M., Rocher, V., Pasero, P., Canitrot, Y., & Legube, G. (2018). Senataxin resolves RNA:DNA hybrids forming at DNA double-strand breaks to prevent translocations. *Nature Communications*, *9*(1), 533. https://doi.org/10.1038/s41467-018-02894-w

Collin, F. (2019). Chemical Basis of Reactive Oxygen Species Reactivity and Involvement in Neurodegenerative Diseases. *International Journal of Molecular Sciences*, *20*(10), 2407. https://doi.org/10.3390/ijms20102407

Collingridge, D. R., Piepmeier, J. M., Rockwell, S., & Knisely, J. P. S. (1999). Polarographic measurements of oxygen tension in human glioma and surrounding peritumoural brain tissue. *Radiotherapy and Oncology*, *53*(2), 127–131. https://doi.org/10.1016/S0167-8140(99)00121-8

Conconi, A., Widmer, R. M., Koller, T., & Sogo, JoséM. (1989). Two different chromatin structures coexist in ribosomal RNA genes throughout the cell cycle. *Cell*, *57*(5), 753–761. https://doi.org/10.1016/0092-8674(89)90790-3

Cortes-Ciriano, I., Lee, S., Park, W.-Y., Kim, T.-M., & Park, P. J. (2017). A molecular portrait of microsatellite instability across multiple cancers. *Nature Communications*, *8*(1), 15180. https://doi.org/10.1038/ncomms15180

Cristini, A., Groh, M., Kristiansen, M. S., & Gromak, N. (2018). RNA/DNA Hybrid Interactome Identifies DXH9 as a Molecular Player in Transcriptional Termination and R-Loop-Associated DNA Damage. *Cell Reports*, *23*(6), 1891–1905. https://doi.org/10.1016/j.celrep.2018.04.025

Cristini, A., Ricci, G., Britton, S., Salimbeni, S., Huang, S. N., Marinello, J., Calsou, P., Pommier, Y., Favre, G., Capranico, G., Gromak, N., & Sordet, O. (2019). Dual Processing of R-Loops and Topoisomerase I Induces Transcription-Dependent DNA Double-Strand Breaks. *Cell Reports*, *28*(12), 3167-3181.e6. https://doi.org/10.1016/j.celrep.2019.08.041

Crossley, M. P., Bocek, M., & Cimprich, K. A. (2019). R-Loops as Cellular Regulators and Genomic Threats. *Molecular Cell*, *73*(3), 398–411. https://doi.org/10.1016/j.molcel.2019.01.024

Cullinan, S. B., & Diehl, J. A. (2004). PERK-dependent Activation of Nrf2 Contributes to Redox Homeostasis and Cell Survival following Endoplasmic Reticulum Stress. *Journal of Biological Chemistry*, *279*(19), 20108–20117. https://doi.org/10.1074/jbc.M314219200

Dai, X., Kaushik, A. C., & Zhang, J. (2019). The Emerging Role of Major Regulatory RNAs in Cancer Control. *Frontiers in Oncology*, *9*, 920. https://doi.org/10.3389/fonc.2019.00920

Daimiel, I. (2019). Insights into Hypoxia: Non-invasive Assessment through Imaging Modalities and Its Application in Breast Cancer. *Journal of Breast Cancer*, *22*(2), 155. https://doi.org/10.4048/jbc.2019.22.e26

Daniely, Y., & Borowiec, J. A. (2000). Formation of a Complex between Nucleolin and Replication Protein a after Cell Stress Prevents Initiation of DNA Replication. *Journal of Cell Biology*, *149*(4), 799–810. https://doi.org/10.1083/jcb.149.4.799

D'Autréaux, B., & Toledano, M. B. (2007). ROS as signalling molecules: mechanisms that generate specificity in ROS homeostasis. *Nature Reviews Molecular Cell Biology*, *8*(10), 813–824. https://doi.org/10.1038/nrm2256

Davis, A. J., Chen, B. P. C., & Chen, D. J. (2014). DNA-PK: A dynamic enzyme in a versatile DSB repair pathway. *DNA Repair*, *17*, 21–29. https://doi.org/10.1016/j.dnarep.2014.02.020

de Klein, A., Muijtjens, M., van Os, R., Verhoeven, Y., Smit, B., Carr, A. M., Lehmann, A. R., & Hoeijmakers, J. H. J. (2000). Targeted disruption of the cell-cycle checkpoint gene ATR leads to early embryonic lethality in mice. *Current Biology*, *10*(8), 479–482. https://doi.org/10.1016/S0960-9822(00)00447-4

Denko, N., Wernke-Dollries, K., Johnson, A. B., Hammond, E., Chiang, C.-M., & Barton, M. C. (2003). Hypoxia Actively Represses Transcription by Inducing Negative Cofactor 2 (Dr1/DrAP1) and Blocking Preinitiation Complex Assembly. *Journal of Biological Chemistry*, *278*(8), 5744–5749. https://doi.org/10.1074/jbc.M212534200

Dhani, N., Fyles, A., Hedley, D., & Milosevic, M. (2015). The Clinical Significance of Hypoxia in Human Cancers. *Seminars in Nuclear Medicine*, *45*(2), 110–121. https://doi.org/10.1053/j.semnuclmed.2014.11.002

Díaz, M. I., Díaz, P., Bennett, J. C., Urra, H., Ortiz, R., Orellana, P. C., Hetz, C., & Quest, A. F. G. (2020). Caveolin-1 suppresses tumor formation through the inhibition of the unfolded protein response. *Cell Death & Disease*, *11*(8), 648. https://doi.org/10.1038/s41419-020-02792-4

Dirmeier, R., O'Brien, K. M., Engle, M., Dodd, A., Spears, E., & Poyton, R. O. (2002). Exposure of Yeast Cells to Anoxia Induces Transient Oxidative Stress. *Journal of Biological Chemistry*, *277*(38), 34773–34784. https://doi.org/10.1074/jbc.M203902200

Doan, N. T. Q., Paulsen, E. S., Sehgal, P., Møller, J. V., Nissen, P., Denmeade, S. R., Isaacs, J. T., Dionne, C. A., & Christensen, S. B. (2015). Targeting thapsigargin towards tumors. In *Steroids*. https://doi.org/10.1016/j.steroids.2014.07.009

Dong, G., Lin, X., Liu, H., Gao, D., Cui, J., Ren, Z., & Chen, R. (2019). Intermittent hypoxia alleviates increased VEGF and pro-angiogenic potential in liver cancer cells. *Oncology Letters*. https://doi.org/10.3892/ol.2019.10486

Drolet, M., Bi, X., & Liu, L. F. (1994). Hypernegative supercoiling of the DNA template during transcription elongation in vitro. *The Journal of Biological Chemistry*, *269*(3), 2068–2074.

Duan, C. (2016). Hypoxia-inducible factor 3 biology: Complexities and emerging themes. *American Journal of Physiology - Cell Physiology*. https://doi.org/10.1152/ajpcell.00315.2015

Dubois, M.-L., & Boisvert, F.-M. (2016). The Nucleolus: Structure and Function. In *The Functional Nucleus* (pp. 29–49). Springer International Publishing. https://doi.org/10.1007/978-3-319-38882-3_2

Dudás, J., Schartinger, V. H., Romani, A., Schweigl, G., Kordsmeyer, K., Marta, P. I., Url, C., Kral, F., & Riechelmann, H. (2014). Cell cycle association and hypoxia regulation of excision repair cross complementation group 1 protein (ERCC1) in tumor cells of head and neck cancer. *Tumor Biology*, *35*(8), 7807–7819. https://doi.org/10.1007/s13277-014-2001-2

Dufey, E., Bravo-San Pedro, J. M., Eggers, C., González-Quiroz, M., Urra, H., Sagredo, A. I., Sepulveda, D., Pihán, P., Carreras-Sureda, A., Hazari, Y., Sagredo, E. A., Gutierrez, D., Valls, C., Papaioannou, A., Acosta-Alvear, D., Campos, G., Domingos, P. M., Pedeux, R., Chevet, E., … Hetz, C. (2020). Genotoxic stress triggers the activation of IRE1α-dependent RNA decay to modulate the DNA damage response. *Nature Communications*, *11*(1), 2401. https://doi.org/10.1038/s41467-020-15694-y

Dumelie, J. G., & Jaffrey, S. R. (2017). Defining the location of promoter-associated R-loops at near-nucleotide resolution using bisDRIP-seq. *ELife*, *6*. https://doi.org/10.7554/eLife.28306

Duncan, R., & Hershey, J. W. (1983). Identification and quantitation of levels of protein synthesis initiation factors in crude HeLa cell lysates by two-dimensional polyacrylamide gel electrophoresis. *The Journal of Biological Chemistry*, *258*(11), 7228–7235.

Dungrawala, H., Rose, K. L., Bhat, K. P., Mohni, K. N., Glick, G. G., Couch, F. B., & Cortez, D. (2015). The Replication Checkpoint Prevents Two Types of Fork Collapse without Regulating Replisome Stability. *Molecular Cell*, *59*(6), 998–1010. https://doi.org/10.1016/j.molcel.2015.07.030

Duquette, M. L., Handa, P., Vincent, J. A., Taylor, A. F., & Maizels, N. (2004). Intracellular transcription of G-rich DNAs induces formation of G-loops, novel structures containing G4 DNA. *Genes & Development*, *18*(13), 1618–1629. https://doi.org/10.1101/gad.1200804

Duranteau, J., Chandel, N. S., Kulisz, A., Shao, Z., & Schumacker, P. T. (1998). Intracellular Signaling by Reactive Oxygen Species during Hypoxia in Cardiomyocytes. *Journal of Biological Chemistry*, *273*(19), 11619–11624. https://doi.org/10.1074/jbc.273.19.11619

DuRose, J. B., Tam, A. B., & Niwa, M. (2006). Intrinsic Capacities of Molecular Sensors of the Unfolded Protein Response to Sense Alternate Forms of Endoplasmic Reticulum Stress. *Molecular Biology of the Cell*, *17*(7), 3095–3107. https://doi.org/10.1091/mbc.e06-01-0055

Elanchezhian, R., Palsamy, P., Madson, C. J., Mulhern, M. L., Lynch, D. W., Troia, A. M., Usukura, J., & Shinohara, T. (2012). Low glucose under hypoxic conditions induces unfolded protein response and produces reactive oxygen species in lens epithelial cells. *Cell Death & Disease*, *3*(4), e301–e301. https://doi.org/10.1038/cddis.2012.40

Elvers, I., Johansson, F., Groth, P., Erixon, K., & Helleday, T. (2011). UV stalled replication forks restart by re-priming in human fibroblasts. *Nucleic Acids Research*, *39*(16), 7049–7057. https://doi.org/10.1093/nar/gkr420

Emami Nejad, A., Najafgholian, S., Rostami, A., Sistani, A., Shojaeifar, S., Esparvarinha, M., Nedaeinia, R., Haghjooy Javanmard, S., Taherian, M., Ahmadlou, M., Salehi, R., Sadeghi, B., & Manian, M. (2021). The role of hypoxia in the tumor microenvironment and development of cancer stem cell: a novel approach to developing treatment. *Cancer Cell International*, *21*(1), 62. https://doi.org/10.1186/s12935-020-01719-5

Fähling, M., Mrowka, R., Steege, A., Martinka, P., Perlewitz, A., Persson, P. B., & Thiele, B. J. (2007). Translational control of hypoxia sensitive genes by nucleolin. *The FASEB Journal*, *21*(6). https://doi.org/10.1096/fasebj.21.6.A1402

Fallone, F., Britton, S., Nieto, L., Salles, B., & Muller, C. (2013). ATR controls cellular adaptation to hypoxia through positive regulation of hypoxia-inducible factor 1 (HIF-1) expression. *Oncogene*, *32*(37), 4387–4396. https://doi.org/10.1038/onc.2012.462

Fanale, D., Bazan, V., Caruso, S., Castiglia, M., Bronte, G., Rolfo, C., Cicero, G., & Russo, A. (2013). Hypoxia and Human Genome Stability: Downregulation of BRCA2 Expression in Breast Cancer Cell Lines. *BioMed Research International*, *2013*, 1–8. https://doi.org/10.1155/2013/746858

Fels, D. R., & Koumenis, C. (2006). The PERK/eIF2α/ATF4 module of the UPR in hypoxia resistance and tumor growth. *Cancer Biology & Therapy*, *5*(7), 723–728. https://doi.org/10.4161/cbt.5.7.2967

Finkel, T. (2011). Signal transduction by reactive oxygen species. *Journal of Cell Biology*, *194*(1), 7–15. https://doi.org/10.1083/jcb.201102095

Fischer-Fantuzzi, L., & Vesco, C. (1988). Cell-dependent efficiency of reiterated nuclear signals in a mutant simian virus 40 oncoprotein targeted to the nucleus. *Molecular and Cellular Biology*, *8*(12), 5495–5503. https://doi.org/10.1128/mcb.8.12.5495-5503.1988

Fishilevich, S., Nudel, R., Rappaport, N., Hadar, R., Plaschkes, I., Iny Stein, T., Rosen, N., Kohn, A., Twik, M., Safran, M., Lancet, D., & Cohen, D. (2017). GeneHancer: genome-wide integration of enhancers and target genes in GeneCards. *Database*, *2017*. https://doi.org/10.1093/database/bax028

Foskolou, I. P., Biasoli, D., Olcina, M. M., & Hammond, E. M. (2016). *Measuring DNA Replication in Hypoxic Conditions* (pp. 11–25). https://doi.org/10.1007/978-3-319-26666-4_2

Foskolou, I. P., Jorgensen, C., Leszczynska, K. B., Olcina, M. M., Tarhonskaya, H., Haisma, B., D'Angiolella, V., Myers, W. K., Domene, C., Flashman, E., & Hammond, E. M. (2017). Ribonucleotide Reductase Requires Subunit Switching in Hypoxia to Maintain DNA Replication. *Molecular Cell*, *66*(2), 206-220.e9. https://doi.org/10.1016/j.molcel.2017.03.005

Freedman, S. J., Sun, Z. Y. J., Poy, F., Kung, A. L., Livingston, D. M., Wagner, G., & Eck, M. J. (2002). Structural basis for recruitment of CBP/p300 by hypoxia-inducible factor-1α. *Proceedings of the National Academy of Sciences of the United States of America*. https://doi.org/10.1073/pnas.082117899

Freiberg, R. A., Krieg, A. J., Giaccia, A. J., & Hammond, E. M. (2006). Checking in on Hypoxia/Reoxygenation. *Cell Cycle*, *5*(12), 1304–1307. https://doi.org/10.4161/cc.5.12.2811

French, S. L., Osheim, Y. N., Cioci, F., Nomura, M., & Beyer, A. L. (2003). In Exponentially Growing Saccharomyces cerevisiae Cells, rRNA Synthesis Is Determined by the Summed RNA Polymerase I Loading Rate Rather than by the Number of Active Genes. *Molecular and Cellular Biology*, *23*(5), 1558–1568. https://doi.org/10.1128/MCB.23.5.1558-1568.2003

Fribley, A., Zhang, K., & Kaufman, R. J. (2009). *Regulation of Apoptosis by the Unfolded Protein Response* (pp. 191–204). https://doi.org/10.1007/978-1-60327-017-5_14

Fujimoto, A., Kawana, K., Taguchi, A., Adachi, K., Sato, M., Nakamura, H., Ogishima, J., Yoshida, M., Inoue, T., Nishida, H., Tomio, K., Yamashita, A., Matsumoto, Y., Arimoto, T., Wada-Hiraike, O., Oda, K., Nagamatsu, T., Osuga, Y., & Fujii, T. (2016). Inhibition of endoplasmic reticulum (ER) stress sensors sensitizes cancer stem-like cells to ER stress-mediated apoptosis. *Oncotarget*, *7*(32), 51854–51864. https://doi.org/10.18632/oncotarget.10126

Galanis, A., Pappa, A., Giannakakis, A., Lanitis, E., Dangaj, D., & Sandaltzopoulos, R. (2008). Reactive oxygen species and HIF-1 signalling in cancer. *Cancer Letters*, *266*(1), 12–20. https://doi.org/10.1016/j.canlet.2008.02.028

Galon, J., & Bruni, D. (2019). Approaches to treat immune hot, altered and cold tumours with combination immunotherapies. *Nature Reviews Drug Discovery*, *18*(3), 197–218. https://doi.org/10.1038/s41573-018-0007-y

Galon, J., Costes, A., Sanchez-Cabo, F., Kirilovsky, A., Mlecnik, B., Lagorce-Pagès, C., Tosolini, M., Camus, M., Berger, A., Wind, P., Zinzindohoué, F., Bruneval, P., Cugnenc, P.-H., Trajanoski, Z., Fridman, W.-H., & Pagès, F. (2006). Type, Density, and Location of Immune Cells Within Human Colorectal Tumors Predict Clinical Outcome. *Science*, *313*(5795), 1960–1964. https://doi.org/10.1126/science.1129139

Gan, W., Guan, Z., Liu, J., Gui, T., Shen, K., Manley, J. L., & Li, X. (2011). R-loop-mediated genomic instability is caused by impairment of replication fork progression. *Genes & Development*, *25*(19), 2041–2056. https://doi.org/10.1101/gad.17010011

García-Limones, C., Lara-Chica, M., Jiménez-Jiménez, C., Pérez, M., Moreno, P., Muñoz, E., & Calzado, M. A. (2016). CHK2 stability is regulated by the E3 ubiquitin ligase SIAH2. *Oncogene*, *35*(33), 4289–4301. https://doi.org/10.1038/onc.2015.495

Gelot, C., Magdalou, I., & Lopez, B. S. (2015). Replication stress in mammalian cells and its consequences for mitosis. In *Genes*. https://doi.org/10.3390/genes6020267

Gérard, M., Corroyer-Dulmont, A., Lesueur, P., Collet, S., Chérel, M., Bourgeois, M., Stefan, D., Limkin, E. J., Perrio, C., Guillamo, J.-S., Dubray, B., Bernaudin, M., Thariat, J., & Valable, S. (2019). Hypoxia Imaging and Adaptive Radiotherapy: A State-of-the-Art Approach in the Management of Glioma. *Frontiers in Medicine*, *6*. https://doi.org/10.3389/fmed.2019.00117

Giaccia, A. J., & Kastan, M. B. (1998). The complexity of p53 modulation: Emerging patterns from divergent signals. In *Genes and Development*. https://doi.org/10.1101/gad.12.19.2973

Ginisty, H. (1998). Nucleolin functions in the first step of ribosomal RNA processing. *The EMBO Journal*, *17*(5), 1476–1486. https://doi.org/10.1093/emboj/17.5.1476

Ginno, P. A., Lott, P. L., Christensen, H. C., Korf, I., & Chédin, F. (2012). R-Loop Formation Is a Distinctive Characteristic of Unmethylated Human CpG Island Promoters. *Molecular Cell*, *45*(6), 814–825. https://doi.org/10.1016/j.molcel.2012.01.017

Gong, E. Y., Hernández, B., Nielsen, J. H., Smits, V. A. J., Freire, R., & Gillespie, D. A. (2018). Chk1 KA1 domain auto-phosphorylation stimulates biological activity and is linked to rapid proteasomal degradation. *Scientific Reports*. https://doi.org/10.1038/s41598-018-35616-9

González-Quiroz, M., Blondel, A., Sagredo, A., Hetz, C., Chevet, E., & Pedeux, R. (2020). When Endoplasmic Reticulum Proteostasis Meets the DNA Damage Response. *Trends in Cell Biology*, *30*(11), 881–891. https://doi.org/10.1016/j.tcb.2020.09.002

Goodarzi, A. A., Jeggo, P., & Lobrich, M. (2010). The influence of heterochromatin on DNA double strand break repair: Getting the strong, silent type to relax. *DNA Repair*, *9*(12), 1273–1282. https://doi.org/10.1016/j.dnarep.2010.09.013

Graham, K., & Unger, E. (2018). Overcoming tumor hypoxia as a barrier to radiotherapy, chemotherapy and immunotherapy in cancer treatment. *International Journal of Nanomedicine*, *Volume 13*, 6049–6058. https://doi.org/10.2147/IJN.S140462

Grandi, A., Santi, A., Campagnoli, S., Parri, M., de Camilli, E., Song, C., Jin, B., Lacombe, A., Castori-Eppenberger, S., Sarmientos, P., Grandi, G., Viale, G., Terracciano, L., Chiarugi, P., Pileri, P., & Grifantini, R. (2016). ERMP1, a novel potential oncogene involved in UPR and oxidative stress defense, is highly expressed in human cancer. *Oncotarget*, *7*(39), 63596–63610. https://doi.org/10.18632/oncotarget.11550

Graves, E. E., Vilalta, M., Cecic, I. K., Erler, J. T., Tran, P. T., Felsher, D., Sayles, L., Sweet-Cordero, A., Le, Q.-T., & Giaccia, A. J. (2010). Hypoxia in Models of Lung Cancer: Implications for Targeted Therapeutics. *Clinical Cancer Research*, *16*(19), 4843–4852. https://doi.org/10.1158/1078-0432.CCR-10-1206

Greenman, C., Stephens, P., Smith, R., Dalgliesh, G. L., Hunter, C., Bignell, G., Davies, H., Teague, J., Butler, A., Stevens, C., Edkins, S., O'Meara, S., Vastrik, I., Schmidt, E. E., Avis, T., Barthorpe, S., Bhamra, G., Buck, G., Choudhury, B., … Stratton, M. R. (2007). Patterns

of somatic mutation in human cancer genomes. *Nature*, *446*(7132), 153–158. https://doi.org/10.1038/nature05610

Grkovic, S., O'Reilly, V. C., Han, S., Hong, M., Baxter, R. C., & Firth, S. M. (2013). IGFBP-3 binds GRP78, stimulates autophagy and promotes the survival of breast cancer cells exposed to adverse microenvironments. *Oncogene*, *32*(19), 2412–2420. https://doi.org/10.1038/onc.2012.264

Grunseich, C., Wang, I. X., Watts, J. A., Burdick, J. T., Guber, R. D., Zhu, Z., Bruzel, A., Lanman, T., Chen, K., Schindler, A. B., Edwards, N., Ray-Chaudhury, A., Yao, J., Lehky, T., Piszczek, G., Crain, B., Fischbeck, K. H., & Cheung, V. G. (2018). Senataxin Mutation Reveals How R-Loops Promote Transcription by Blocking DNA Methylation at Gene Promoters. *Molecular Cell*, *69*(3), 426-437.e7. https://doi.org/10.1016/j.molcel.2017.12.030

Guan, B.-J., Krokowski, D., Majumder, M., Schmotzer, C. L., Kimball, S. R., Merrick, W. C., Koromilas, A. E., & Hatzoglou, M. (2014). Translational Control during Endoplasmic Reticulum Stress beyond Phosphorylation of the Translation Initiation Factor eIF2α. *Journal of Biological Chemistry*, *289*(18), 12593–12611. https://doi.org/10.1074/jbc.M113.543215

Guo, Z., Kozlov, S., Lavin, M. F., Person, M. D., & Paull, T. T. (2010). ATM Activation by Oxidative Stress. *Science*, *330*(6003), 517–521. https://doi.org/10.1126/science.1192912

Guzy, R. D., Hoyos, B., Robin, E., Chen, H., Liu, L., Mansfield, K. D., Simon, M. C., Hammerling, U., & Schumacker, P. T. (2005). Mitochondrial complex III is required for hypoxia-induced ROS production and cellular oxygen sensing. *Cell Metabolism*, *1*(6), 401–408. https://doi.org/10.1016/j.cmet.2005.05.001

Haas, J., Park, E. C., & Seed, B. (1996). Codon usage limitation in the expression of HIV-1 envelope glycoprotein. *Current Biology : CB*, *6*(3), 315–324. https://doi.org/10.1016/s0960-9822(02)00482-7

Hall, E. J., & Giaccia, A. J. (2012). Oxygen Effect and Reoxygenation. In *Radiobiology for the Radiologist* (7th ed., pp. 86–103). Wolters Kluwer Health/Lippincott Williams & Wilkins.

Hamanaka, R. B., Bennett, B. S., Cullinan, S. B., & Diehl, J. A. (2005). PERK and GCN2 Contribute to eIF2α Phosphorylation and Cell Cycle Arrest after Activation of the Unfolded Protein Response Pathway. *Molecular Biology of the Cell*, *16*(12), 5493–5501. https://doi.org/10.1091/mbc.e05-03-0268

Hamidi, T., Cano, C. E., Grasso, D., Garcia, M. N., Sandi, M. J., Calvo, E. L., Dagorn, J.-C., Lomberk, G., Urrutia, R., Goruppi, S., Carracedo, A., Velasco, G., & Iovanna, J. L. (2012). Nupr1-Aurora Kinase A Pathway Provides Protection against Metabolic Stress-Mediated Autophagic-Associated Cell Death. *Clinical Cancer Research*, *18*(19), 5234–5246. https://doi.org/10.1158/1078-0432.CCR-12-0026

Hammond, E. (2003). Comparison of hypoxia-induced replication arrest with hydroxyurea and aphidicolin-induced arrest. *Mutation Research/Fundamental and Molecular*

Mechanisms of Mutagenesis, *532*(1–2), 205–213. https://doi.org/10.1016/j.mrfmmm.2003.08.017

Hammond, E. M., Asselin, M.-C., Forster, D., O'Connor, J. P. B., Senra, J. M., & Williams, K. J. (2014). The Meaning, Measurement and Modification of Hypoxia in the Laboratory and the Clinic. *Clinical Oncology*, *26*(5), 277–288. https://doi.org/10.1016/j.clon.2014.02.002

Hammond, E. M., Denko, N. C., Dorie, M. J., Abraham, R. T., & Giaccia, A. J. (2002). Hypoxia Links ATR and p53 through Replication Arrest. *Molecular and Cellular Biology*, *22*(6), 1834–1843. https://doi.org/10.1128/MCB.22.6.1834-1843.2002

Hammond, E. M., Dorie, M. J., & Giaccia, A. J. (2003). ATR/ATM Targets Are Phosphorylated by ATR in Response to Hypoxia and ATM in Response to Reoxygenation. *Journal of Biological Chemistry*, *278*(14), 12207–12213. https://doi.org/10.1074/jbc.M212360200

Hammond, E. M., Dorie, M. J., & Giaccia, A. J. (2004). Inhibition of ATR Leads to Increased Sensitivity to Hypoxia/Reoxygenation. *Cancer Research*, *64*(18), 6556–6562. https://doi.org/10.1158/0008-5472.CAN-04-1520

Hammond, E. M., Freiberg, R. A., & Giaccia, A. J. (2006). The roles of Chk 1 and Chk 2 in hypoxia and reoxygenation. *Cancer Letters*, *238*(2), 161–167. https://doi.org/10.1016/j.canlet.2005.06.029

Hammond, E. M., & Giaccia, A. J. (2004). The role of ATM and ATR in the cellular response to hypoxia and re-oxygenation. *DNA Repair*, *3*(8–9), 1117–1122. https://doi.org/10.1016/j.dnarep.2004.03.035

Hamperl, S., Bocek, M. J., Saldivar, J. C., Swigut, T., & Cimprich, K. A. (2017). Transcription-Replication Conflict Orientation Modulates R-Loop Levels and Activates Distinct DNA Damage Responses. *Cell*, *170*(4), 774-786.e19. https://doi.org/10.1016/j.cell.2017.07.043

Han, H. D., Byeon, Y., Kang, T. H., Jung, I. D., Lee, J.-W., Shin, B. C., Lee, Y. J., Sood, A. K., & Park, Y.-M. (2016). Toll-like receptor 3-induced immune response by poly(D,L-lactide-co-glycolide) nanoparticles for dendritic cell-based cancer immunotherapy. *International Journal of Nanomedicine*, *Volume 11*, 5729–5742. https://doi.org/10.2147/IJN.S109001

Hanahan, D. (2022). Hallmarks of Cancer: New Dimensions. *Cancer Discovery*, *12*(1), 31–46. https://doi.org/10.1158/2159-8290.CD-21-1059

Hanahan, D., & Weinberg, R. A. (2000). The hallmarks of cancer. *Cell*, *100*(1), 57–70. https://doi.org/10.1016/s0092-8674(00)81683-9

Hanahan, D., & Weinberg, R. A. (2011). Hallmarks of cancer: the next generation. *Cell*, *144*(5), 646–674. https://doi.org/10.1016/j.cell.2011.02.013

Hanselmann, R. G., & Welter, C. (2016). Origin of Cancer: An Information, Energy, and Matter Disease. *Frontiers in Cell and Developmental Biology*, *4*. https://doi.org/10.3389/fcell.2016.00121

Harper, J. W., & Elledge, S. J. (2007). The DNA Damage Response: Ten Years After. *Molecular Cell*, *28*(5), 739–745. https://doi.org/10.1016/j.molcel.2007.11.015

Hasanova, Z., Klapstova, V., Porrua, O., Stefl, R., & Sebesta, M. (2022). *Human senataxin is a bona fide R-loop resolving enzyme and transcription termination factor*.

Helmlinger, G., Yuan, F., Dellian, M., & Jain, R. K. (1997). Interstitial pH and pO2 gradients in solid tumors in vivo: High-resolution measurements reveal a lack of correlation. *Nature Medicine*, *3*(2), 177–182. https://doi.org/10.1038/nm0297-177

Hetz, C. (2012). The unfolded protein response: controlling cell fate decisions under ER stress and beyond. *Nature Reviews Molecular Cell Biology*, *13*(2), 89–102. https://doi.org/10.1038/nrm3270

Higgins, G. S., & Hammond, E. M. (2022). Elucidating the role of transiently hypoxic tumour cells on radiation resistance. *British Journal of Cancer*, *126*(7), 971–972. https://doi.org/10.1038/s41416-022-01741-6

Hillary, R. F., & Fitzgerald, U. (2018). A lifetime of stress: ATF6 in development and homeostasis. In *Journal of Biomedical Science*. https://doi.org/10.1186/s12929-018-0453-1

Höckel, M., Knoop, C., Schlenger, K., Vorndran, B., Bauβnann, E., Mitze, M., Knapstein, P. G., & Vaupel, P. (1993). Intratumoral pO2 predicts survival in advanced cancer of the uterine cervix. *Radiotherapy and Oncology*, *26*(1), 45–50. https://doi.org/10.1016/0167-8140(93)90025-4

Hodroj, D., Recolin, B., Serhal, K., Martinez, S., Tsanov, N., Abou Merhi, R., & Maiorano, D. (2017). An ATR-dependent function for the Ddx19 RNA helicase in nuclear R-loop metabolism. *The EMBO Journal*, *36*(9), 1182–1198. https://doi.org/10.15252/embj.201695131

Holmquist-Mengelbier, L., Fredlund, E., Löfstedt, T., Noguera, R., Navarro, S., Nilsson, H., Pietras, A., Vallon-Christersson, J., Borg, Å., Gradin, K., Poellinger, L., & Påhlman, S. (2006). Recruitment of HIF-1α and HIF-2α to common target genes is differentially regulated in neuroblastoma: HIF-2α promotes an aggressive phenotype. *Cancer Cell*. https://doi.org/10.1016/j.ccr.2006.08.026

Horsman, M. R., Siemann, D. W., Nordsmark, M., Khalil, A. A., Overgaard, J., & Chaplin, D. J. (1986). The Combination of Nicotinamide and Carbogen Breathing to Improve Tumour Oxygenation Prior to Radiation Treatment. In *Advances in Experimental Medicine and Biology* (Vol. 361).

Horsman, M. R., Sørensen, B. S., Busk, M., & Siemann, D. W. (2021). Therapeutic Modification of Hypoxia. *Clinical Oncology*, *33*(11), e492–e509. https://doi.org/10.1016/j.clon.2021.08.014

Hotokezaka, Y., Katayama, I., van Leyen, K., & Nakamura, T. (2015). GSK-3β-dependent downregulation of γ-taxilin and αNAC merge to regulate ER stress responses. *Cell Death & Disease*, *6*(4), e1719–e1719. https://doi.org/10.1038/cddis.2015.90

Hu, J., van Valckenborgh, E., Menu, E., de Bruyne, E., & Vanderkerken, K. (2012). Understanding the hypoxic niche of multiple myeloma: therapeutic implications and contributions of mouse models. *Disease Models & Mechanisms*, *5*(6), 763–771. https://doi.org/10.1242/dmm.008961

Huang, X., Ding, L., Bennewith, K. L., Tong, R. T., Welford, S. M., Ang, K. K., Story, M., Le, Q.-T., & Giaccia, A. J. (2009). Hypoxia-Inducible mir-210 Regulates Normoxic Gene Expression Involved in Tumor Initiation. *Molecular Cell*, *35*(6), 856–867. https://doi.org/10.1016/j.molcel.2009.09.006

Huertas, P., & Aguilera, A. (2003). Cotranscriptionally Formed DNA:RNA Hybrids Mediate Transcription Elongation Impairment and Transcription-Associated Recombination. *Molecular Cell*, *12*(3), 711–721. https://doi.org/10.1016/j.molcel.2003.08.010

Hunt, C. R., Pandita, R. K., Laszlo, A., Higashikubo, R., Agarwal, M., Kitamura, T., Gupta, A., Rief, N., Horikoshi, N., Baskaran, R., Lee, J.-H., Löbrich, M., Paull, T. T., Roti Roti, J. L., & Pandita, T. K. (2007). Hyperthermia Activates a Subset of Ataxia-Telangiectasia Mutated Effectors Independent of DNA Strand Breaks and Heat Shock Protein 70 Status. *Cancer Research*, *67*(7), 3010–3017. https://doi.org/10.1158/0008-5472.CAN-06-4328

Hussein, D., Estlin, E. J., Dive, C., & Makin, G. W. J. (2006). Chronic hypoxia promotes hypoxia-inducible factor-1α–dependent resistance to etoposide and vincristine in neuroblastoma cells. *Molecular Cancer Therapeutics*, *5*(9), 2241–2250. https://doi.org/10.1158/1535-7163.MCT-06-0145

Imielinski, M., Berger, A. H., Hammerman, P. S., Hernandez, B., Pugh, T. J., Hodis, E., Cho, J., Suh, J., Capelletti, M., Sivachenko, A., Sougnez, C., Auclair, D., Lawrence, M. S., Stojanov, P., Cibulskis, K., Choi, K., de Waal, L., Sharifnia, T., Brooks, A., … Meyerson, M. (2012). Mapping the hallmarks of lung adenocarcinoma with massively parallel sequencing. *Cell*, *150*(6), 1107–1120. https://doi.org/10.1016/j.cell.2012.08.029

Institute of Cancer Research. (n.d.). *DNA damage and cancer*. Retrieved 30 June 2022, from https://www.icr.ac.uk/about-us/our-achievements/our-scientific-discoveries/dna-damage-and-cancer

Ito, A., Koshikawa, N., Mochizuki, S., Omura, K., & Takenaga, K. (2006). Hypoxia-inducible factor-1 mediates the expression of DNA polymerase ι in human tumor cells. *Biochemical and Biophysical Research Communications*, *351*(1), 306–311. https://doi.org/10.1016/j.bbrc.2006.10.048

Jackson, S. P., & Bartek, J. (2009). The DNA-damage response in human biology and disease. *Nature*, *461*(7267), 1071–1078. https://doi.org/10.1038/nature08467

Jaffray, D. A., & Gospodarowicz, M. K. (2015). Radiation Therapy for Cancer. In *Cancer: Disease Control Priorities* (3rd ed., Vol. 3). The International Bank for Reconstruction and Development / The World Bank.

Jain, R. K. (2005). Normalization of Tumor Vasculature: An Emerging Concept in Antiangiogenic Therapy. *Science*, *307*(5706), 58–62. https://doi.org/10.1126/science.1104819

Jao, C. Y., & Salic, A. (2008). Exploring RNA transcription and turnover in vivo by using click chemistry. *Proceedings of the National Academy of Sciences*, *105*(41), 15779–15784. https://doi.org/10.1073/pnas.0808480105

Jeong, K., Kim, H., Kim, K., Kim, S.-J., Hahn, B.-S., Jahng, G.-H., Yoon, K.-S., Kim, S. S., Ha, J., Kang, I., & Choe, W. (2014). Cyclophilin B is involved in p300-mediated degradation of CHOP in tumor cell adaptation to hypoxia. *Cell Death & Differentiation*, *21*(3), 438–450. https://doi.org/10.1038/cdd.2013.164

Jeong, K., Kim, K., Kim, H., Oh, Y., Kim, S., Jo, Y., & Choe, W. (2015). Hypoxia induces cyclophilin B through the activation of transcription factor 6 in gastric adenocarcinoma cells. *Oncology Letters*, *9*(6), 2854–2858. https://doi.org/10.3892/ol.2015.3102

Jette, N., & Lees-Miller, S. P. (2015). The DNA-dependent protein kinase: A multifunctional protein kinase with roles in DNA double strand break repair and mitosis. *Progress in Biophysics and Molecular Biology*, *117*(2–3), 194–205. https://doi.org/10.1016/j.pbiomolbio.2014.12.003

Jing, X., Yang, F., Shao, C., Wei, K., Xie, M., Shen, H., & Shu, Y. (2019). Role of hypoxia in cancer therapy by regulating the tumor microenvironment. *Molecular Cancer*, *18*(1), 157. https://doi.org/10.1186/s12943-019-1089-9

Johnson, A. B., Denko, N., & Barton, M. C. (2008). Hypoxia induces a novel signature of chromatin modifications and global repression of transcription. *Mutation Research/Fundamental and Molecular Mechanisms of Mutagenesis*, *640*(1–2), 174–179. https://doi.org/10.1016/j.mrfmmm.2008.01.001

Jones, R. G., & Thompson, C. B. (2009). Tumor suppressors and cell metabolism: a recipe for cancer growth. *Genes & Development*, *23*(5), 537–548. https://doi.org/10.1101/gad.1756509

Kabeche, L., Nguyen, H. D., Buisson, R., & Zou, L. (2018). A mitosis-specific and R loop–driven ATR pathway promotes faithful chromosome segregation. *Science*, *359*(6371), 108–114. https://doi.org/10.1126/science.aan6490

Kan, Z., Jaiswal, B. S., Stinson, J., Janakiraman, V., Bhatt, D., Stern, H. M., Yue, P., Haverty, P. M., Bourgon, R., Zheng, J., Moorhead, M., Chaudhuri, S., Tomsho, L. P., Peters, B. A., Pujara, K., Cordes, S., Davis, D. P., Carlton, V. E. H., Yuan, W., … Seshagiri, S. (2010). Diverse somatic mutation patterns and pathway alterations in human cancers. *Nature*, *466*(7308), 869–873. https://doi.org/10.1038/nature09208

Kaplan, A. R., & Glazer, P. M. (2020). Impact of hypoxia on DNA repair and genome integrity. *Mutagenesis*, *35*(1), 61–68. https://doi.org/10.1093/mutage/gez019

Kardinal, C. G., & Yarbro, J. W. (1979). A conceptual history of cancer. *Seminars in Oncology*, *6*(4), 396–408.

Kavanaugh, G., Ye, F., Mohni, K. N., Luzwick, J. W., Glick, G., & Cortez, D. (2015). A whole genome RNAi screen identifies replication stress response genes. *DNA Repair*, *35*, 55–62. https://doi.org/10.1016/j.dnarep.2015.09.024

Ke, H.-L., Li, W.-M., Lin, H.-H., Hsu, W.-C., Hsu, Y.-L., Chang, L.-L., Huang, C.-N., Li, C.-C., Chang, H.-P., Yeh, H.-C., Li, C.-F., & Wu, W.-J. (2017). Hypoxia-regulated MicroRNA-210 Overexpression is Associated with Tumor Development and Progression in Upper Tract Urothelial Carcinoma. *International Journal of Medical Sciences*, *14*(6), 578–584. https://doi.org/10.7150/ijms.15699

Keeley, T. P., & Mann, G. E. (2019). Defining Physiological Normoxia for Improved Translation of Cell Physiology to Animal Models and Humans. *Physiological Reviews*, *99*(1), 161–234. https://doi.org/10.1152/physrev.00041.2017

Kelleher, A. R., Kimball, S. R., Dennis, M. D., Schilder, R. J., & Jefferson, L. S. (2013). The mTORC1 signaling repressors REDD1/2 are rapidly induced and activation of p70S6K1 by leucine is defective in skeletal muscle of an immobilized rat hindlimb. *American Journal of Physiology - Endocrinology and Metabolism*. https://doi.org/10.1152/ajpendo.00409.2012

Kikuchi, D., Tanimoto, K., & Nakayama, K. (2016). CREB is activated by ER stress and modulates the unfolded protein response by regulating the expression of IRE1α and PERK. *Biochemical and Biophysical Research Communications*, *469*(2), 243–250. https://doi.org/10.1016/j.bbrc.2015.11.113

Killilea, D. W., Hester, R., Balczon, R., Babal, P., & Gillespie, M. N. (2000). Free radical production in hypoxic pulmonary artery smooth muscle cells. *American Journal of Physiology-Lung Cellular and Molecular Physiology*, *279*(2), L408–L412. https://doi.org/10.1152/ajplung.2000.279.2.L408

Kim, I., & Park, J.-W. (2020). Hypoxia-driven epigenetic regulation in cancer progression: A focus on histone methylation and its modifying enzymes. *Cancer Letters*, *489*, 41–49. https://doi.org/10.1016/j.canlet.2020.05.025

Kim, J. K., Kang, K. A., Piao, M. J., Ryu, Y. S., Han, X., Fernando, P. M. D. J., Oh, M. C., Park, J. E., Shilnikova, K., Boo, S. J., Na, S.-Y., Jeong, Y. J., Jeong, S. U., & Hyun, J. W. (2016). Endoplasmic reticulum stress induces 5-fluorouracil resistance in human colon cancer cells. *Environmental Toxicology and Pharmacology*, *44*, 128–133. https://doi.org/10.1016/j.etap.2016.05.005

Kim, J. Y., & Lee, J. Y. (2017). Targeting tumor adaption to chronic hypoxia: Implications for drug resistance, and how it can be overcome. In *International Journal of Molecular Sciences*. https://doi.org/10.3390/ijms18091854

Kim, S. B., Pandita, R. K., Eskiocak, U., Ly, P., Kaisani, A., Kumar, R., Cornelius, C., Wright, W. E., Pandita, T. K., & Shay, J. W. (2012). Targeting of Nrf2 induces DNA damage signaling and protects colonic epithelial cells from ionizing radiation. *Proceedings of the National Academy of Sciences*, *109*(43). https://doi.org/10.1073/pnas.1207718109

Kim, Y.-C., Gerlitz, G., Furusawa, T., Catez, F., Nussenzweig, A., Oh, K.-S., Kraemer, K. H., Shiloh, Y., & Bustin, M. (2009). Activation of ATM depends on chromatin interactions occurring before induction of DNA damage. *Nature Cell Biology*, *11*(1), 92–96. https://doi.org/10.1038/ncb1817

Kobayashi, J., Fujimoto, H., Sato, J., Hayashi, I., Burma, S., Matsuura, S., Chen, D. J., & Komatsu, K. (2012). Nucleolin Participates in DNA Double-Strand Break-Induced Damage Response through MDC1-Dependent Pathway. *PLoS ONE*, *7*(11), e49245. https://doi.org/10.1371/journal.pone.0049245

Kobayashi, T. (2011). Regulation of ribosomal RNA gene copy number and its role in modulating genome integrity and evolutionary adaptability in yeast. *Cellular and Molecular Life Sciences*, *68*(8), 1395–1403. https://doi.org/10.1007/s00018-010-0613-2

Kobayashi, T. (2014). Ribosomal RNA gene repeats, their stability and cellular senescence. *Proceedings of the Japan Academy, Series B*, *90*(4), 119–129. https://doi.org/10.2183/pjab.90.119

Koizume, S., Ito, S., Nakamura, Y., Yoshihara, M., Furuya, M., Yamada, R., Miyagi, E., Hirahara, F., Takano, Y., & Miyagi, Y. (2015). Lipid starvation and hypoxia synergistically activate ICAM1 and multiple genes in an Sp1-dependent manner to promote the growth of ovarian cancer. *Molecular Cancer*, *14*(1), 77. https://doi.org/10.1186/s12943-015-0351-z

Koong, A. C., Mehta, V. K., Le, Q. T., Fisher, G. A., Terris, D. J., Brown, J. M., Bastidas, A. J., & Vierra, M. (2000). Pancreatic tumors show high levels of hypoxia. *International Journal of Radiation Oncology*Biology*Physics*, *48*(4), 919–922. https://doi.org/10.1016/S0360-3016(00)00803-8

Koritzinsky, M., Levitin, F., van den Beucken, T., Rumantir, R. A., Harding, N. J., Chu, K. C., Boutros, P. C., Braakman, I., & Wouters, B. G. (2013). Two phases of disulfide bond formation have differing requirements for oxygen. *Journal of Cell Biology*, *203*(4), 615–627. https://doi.org/10.1083/jcb.201307185

Koshiji, M., To, K. K.-W., Hammer, S., Kumamoto, K., Harris, A. L., Modrich, P., & Huang, L. E. (2005). HIF-1α Induces Genetic Instability by Transcriptionally Downregulating MutSα Expression. *Molecular Cell*, *17*(6), 793–803. https://doi.org/10.1016/j.molcel.2005.02.015

Kotsantis, P., Petermann, E., & Boulton, S. J. (2018). Mechanisms of Oncogene-Induced Replication Stress: Jigsaw Falling into Place. *Cancer Discovery*, *8*(5), 537–555. https://doi.org/10.1158/2159-8290.CD-17-1461

Koumenis, C., Bi, M., Ye, J., Feldman, D., & Koong, A. C. (2007). *Hypoxia and the Unfolded Protein Response* (pp. 275–293). https://doi.org/10.1016/S0076-6879(07)35014-3

Koumenis, C., Naczki, C., Koritzinsky, M., Rastani, S., Diehl, A., Sonenberg, N., Koromilas, A., & Wouters, B. G. (2002). Regulation of Protein Synthesis by Hypoxia via Activation of the Endoplasmic Reticulum Kinase PERK and Phosphorylation of the Translation Initiation Factor eIF2α. *Molecular and Cellular Biology*, *22*(21), 7405–7416. https://doi.org/10.1128/MCB.22.21.7405-7416.2002

Kumagai, A., Lee, J., Yoo, H. Y., & Dunphy, W. G. (2006). TopBP1 Activates the ATR-ATRIP Complex. *Cell*, *124*(5), 943–955. https://doi.org/10.1016/j.cell.2005.12.041

Kumareswaran, R., Ludkovski, O., Meng, A., Sykes, J., Pintilie, M., & Bristow, R. G. (2012). Chronic hypoxia compromises repair of DNA double-strand breaks to drive genetic instability. *Journal of Cell Science*, *125*(1), 189–199. https://doi.org/10.1242/jcs.092262

LaGory, E. L., & Giaccia, A. J. (2016). The ever-expanding role of HIF in tumour and stromal biology. In *Nature Cell Biology*. https://doi.org/10.1038/ncb3330

Lally, B. E., Rockwell, S., Fischer, D. B., Collingridge, D. R., Piepmeier, J. M., & Knisely, J. P. S. (2006). The Interactions of Polarographic Measurements of Oxygen Tension and Histological Grade in Human Glioma. *The Cancer Journal*, *12*(6), 461–466. https://doi.org/10.1097/00130404-200611000-00005

Lando, D., Peet, D. J., Whelan, D. A., Gorman, J. J., & Whitelaw, M. L. (2002). Asparagine hydroxylation of the HIF transactivation domain: A hypoxic switch. *Science*. https://doi.org/10.1126/science.1068592

Lang, K. S., Hall, A. N., Merrikh, C. N., Ragheb, M., Tabakh, H., Pollock, A. J., Woodward, J. J., Dreifus, J. E., & Merrikh, H. (2017). Replication-Transcription Conflicts Generate R-Loops that Orchestrate Bacterial Stress Survival and Pathogenesis. *Cell*, *170*(4), 787-799.e18. https://doi.org/10.1016/j.cell.2017.07.044

Lawley, P. D., & Brookes, P. (1965). Molecular Mechanism of the Cytotoxic Action of Difunctional Alkylating Agents and of Resistance to this Action. *Nature*, *206*(4983), 480–483. https://doi.org/10.1038/206480a0

Lawrence, M. S., Stojanov, P., Polak, P., Kryukov, G. v, Cibulskis, K., Sivachenko, A., Carter, S. L., Stewart, C., Mermel, C. H., Roberts, S. A., Kiezun, A., Hammerman, P. S., McKenna, A., Drier, Y., Zou, L., Ramos, A. H., Pugh, T. J., Stransky, N., Helman, E., … Getz, G. (2013). Mutational heterogeneity in cancer and the search for new cancer-associated genes. *Nature*, *499*(7457), 214–218. https://doi.org/10.1038/nature12213

Le, Q.-T., Chen, E., Salim, A., Cao, H., Kong, C. S., Whyte, R., Donington, J., Cannon, W., Wakelee, H., Tibshirani, R., Mitchell, J. D., Richardson, D., O'Byrne, K. J., Koong, A. C., & Giaccia, A. J. (2006). An Evaluation of Tumor Oxygenation and Gene Expression in Patients with Early Stage Non–Small Cell Lung Cancers. *Clinical Cancer Research*, *12*(5), 1507–1514. https://doi.org/10.1158/1078-0432.CCR-05-2049

Lee, A.-H., Iwakoshi, N. N., & Glimcher, L. H. (2003). XBP-1 Regulates a Subset of Endoplasmic Reticulum Resident Chaperone Genes in the Unfolded Protein Response. *Molecular and Cellular Biology*. https://doi.org/10.1128/mcb.23.21.7448-7459.2003

Lee, J.-H., Goodarzi, A. A., Jeggo, P. A., & Paull, T. T. (2010). 53BP1 promotes ATM activity through direct interactions with the MRN complex. *The EMBO Journal*, *29*(3), 574–585. https://doi.org/10.1038/emboj.2009.372

Lee, J.-H., Ryu, S. W., Ender, N. A., & Paull, T. T. (2021). Poly-ADP-ribosylation drives loss of protein homeostasis in ATM and Mre11 deficiency. *Molecular Cell*, *81*(7), 1515-1533.e5. https://doi.org/10.1016/j.molcel.2021.01.019

Lee, Y.-C., Wang, W.-L., Chang, W.-C., Huang, Y.-H., Hong, G.-C., Wang, H.-L., Chou, Y.-H., Tseng, H.-C., Lee, H.-T., Li, S.-T., Chen, H.-L., Wu, C.-C., Yang, H.-F., Wang, B.-Y., & Chang, W.-W. (2019). Tribbles Homolog 3 Involved in Radiation Response of Triple Negative Breast Cancer Cells by Regulating Notch1 Activation. *Cancers*, *11*(2), 127. https://doi.org/10.3390/cancers11020127

Leszczynska, K. B., Dobrynin, G., Leslie, R. E., Ient, J., Boumelha, A. J., Senra, J. M., Hawkins, M. A., Maughan, T., Mukherjee, S., & Hammond, E. M. (2016). Preclinical testing of an ATR inhibitor demonstrates improved response to standard therapies for esophageal cancer. *Radiotherapy and Oncology*, *121*(2), 232–238. https://doi.org/10.1016/j.radonc.2016.10.023

Leszczynska, K. B., Göttgens, E.-L., Biasoli, D., Olcina, M. M., Ient, J., Anbalagan, S., Bernhardt, S., Giaccia, A. J., & Hammond, E. M. (2016). Mechanisms and consequences of ATMIN repression in hypoxic conditions: roles for p53 and HIF-1. *Scientific Reports*, *6*(1), 21698. https://doi.org/10.1038/srep21698

Li, H., Korennykh, A. v., Behrman, S. L., & Walter, P. (2010). Mammalian endoplasmic reticulum stress sensor IRE1 signals by dynamic clustering. *Proceedings of the National Academy of Sciences*, *107*(37), 16113–16118. https://doi.org/10.1073/pnas.1010580107

Li, S., Tabar, S. S., Malec, V., Eul, B. G., Klepetko, W., Weissmann, N., Grimminger, F., Seeger, W., Rose, F., & Hänze, J. (2008). NOX4 Regulates ROS Levels Under Normoxic and Hypoxic Conditions, Triggers Proliferation, and Inhibits Apoptosis in Pulmonary Artery Adventitial Fibroblasts. *Antioxidants & Redox Signaling*, *10*(10), 1687–1698. https://doi.org/10.1089/ars.2008.2035

Li, W., Li, F., Zhang, X., Lin, H.-K., & Xu, C. (2021). Insights into the post-translational modification and its emerging role in shaping the tumor microenvironment. *Signal Transduction and Targeted Therapy*, *6*(1), 422. https://doi.org/10.1038/s41392-021-00825-8

Liberzon, A., Birger, C., Thorvaldsdóttir, H., Ghandi, M., Mesirov, J. P., & Tamayo, P. (2015). The Molecular Signatures Database Hallmark Gene Set Collection. *Cell Systems*. https://doi.org/10.1016/j.cels.2015.12.004

Lin, G. L., & Monje, M. (2020). Understanding the Deadly Silence of Posterior Fossa A Ependymoma. *Molecular Cell*, *78*(6), 999–1001. https://doi.org/10.1016/j.molcel.2020.05.020

Liu, C. Y., & Kaufman, R. J. (2003). The unfolded protein response. In *Journal of Cell Science*. https://doi.org/10.1242/jcs.00408

Liu, Q., Guntuku, S., Cui, X. S., Matsuoka, S., Cortez, D., Tamai, K., Luo, G., Carattini-Rivera, S., DeMayo, F., Bradley, A., Donehower, L. A., & Elledge, S. J. (2000). Chk1 is an essential kinase that is regulated by Atr and required for the G(2)/M DNA damage checkpoint. *Genes & Development*, *14*(12), 1448–1459.

Liu, S., Opiyo, S. O., Manthey, K., Glanzer, J. G., Ashley, A. K., Amerin, C., Troksa, K., Shrivastav, M., Nickoloff, J. A., & Oakley, G. G. (2012). Distinct roles for DNA-PK, ATM and ATR in RPA phosphorylation and checkpoint activation in response to replication stress. *Nucleic Acids Research*, *40*(21), 10780–10794. https://doi.org/10.1093/nar/gks849

Liu, Y., He, M., Zuo, W.-J., Hao, S., Wang, Z.-H., & Shao, Z.-M. (2021). Tumor Size Still Impacts Prognosis in Breast Cancer With Extensive Nodal Involvement. *Frontiers in Oncology*, *11*. https://doi.org/10.3389/fonc.2021.585613

Liu, Y., Hou, X., Liu, M., Yang, Z., Bi, Y., Zou, H., Wu, J., Che, H., Li, C., Wang, X., Wang, K., Zhong, C., Zhang, J., Yu, T., Bian, Q., Chai, S., Liu, H., Ai, J., & Zhao, S. (2016). XBP1 silencing decreases glioma cell viability and glycolysis possibly by inhibiting HK2 expression. *Journal of Neuro-Oncology*, *126*(3), 455–462. https://doi.org/10.1007/s11060-015-2003-y

Logue, S. E., McGrath, E. P., Cleary, P., Greene, S., Mnich, K., Almanza, A., Chevet, E., Dwyer, R. M., Oommen, A., Legembre, P., Godey, F., Madden, E. C., Leuzzi, B., Obacz, J., Zeng, Q., Patterson, J. B., Jäger, R., Gorman, A. M., & Samali, A. (2018). Inhibition of IRE1 RNase activity modulates the tumor cell secretome and enhances response to chemotherapy. *Nature Communications*, *9*(1), 3267. https://doi.org/10.1038/s41467-018-05763-8

Lopci, E., Grassi, I., Chiti, A., Nanni, C., Cicoria, G., Toschi, L., Fonti, C., Lodi, F., Mattioli, S., & Fanti, S. (2014). PET radiopharmaceuticals for imaging of tumor hypoxia: a review of the evidence. *American Journal of Nuclear Medicine and Molecular Imaging*, *4*(4), 365–384.

Lu, W.-T., Hawley, B. R., Skalka, G. L., Baldock, R. A., Smith, E. M., Bader, A. S., Malewicz, M., Watts, F. Z., Wilczynska, A., & Bushell, M. (2018). Drosha drives the formation of DNA:RNA hybrids around DNA break sites to facilitate DNA repair. *Nature Communications*, *9*(1), 532. https://doi.org/10.1038/s41467-018-02893-x

Luhr, M., Torgersen, M. L., Szalai, P., Hashim, A., Brech, A., Staerk, J., & Engedal, N. (2019). The kinase PERK and the transcription factor ATF4 play distinct and essential roles in autophagy resulting from tunicamycin-induced ER stress. *Journal of Biological Chemistry*, *294*(20), 8197–8217. https://doi.org/10.1074/jbc.RA118.002829

Luoto, K. R., Kumareswaran, R., & Bristow, R. G. (2013). Tumor hypoxia as a driving force in genetic instability. *Genome Integrity*, *4*(1), 5. https://doi.org/10.1186/2041-9414-4-5

Lv, Y., Zhao, S., Han, J., Zheng, L., Yang, Z., & Zhao, L. (2015). Hypoxia-inducible factor-1α induces multidrug resistance protein in colon cancer. *OncoTargets and Therapy*, 1941. https://doi.org/10.2147/OTT.S82835

Lyng, H., Sundfør, K., Tropé, C., & Rofstad, E. K. (2000). Disease control of uterine cervical cancer: relationships to tumor oxygen tension, vascular density, cell density, and frequency of mitosis and apoptosis measured before treatment and during radiotherapy. *Clinical Cancer Research : An Official Journal of the American Association for Cancer Research*, *6*(3), 1104–1112.

Lyu, X., Zhang, M., Li, G., Cai, Y., Li, G., & Qiao, Q. (2019). Interleukin-6 production mediated by the IRE1-XBP1 pathway confers radioresistance in human papillomavirus-negative oropharyngeal carcinoma. *Cancer Science*, *110*(8), 2471–2484. https://doi.org/10.1111/cas.14094

Ma, D., Shen, B., Seewoo, V., Tong, H., Yang, W., Cheng, X., Jin, Z., Peng, C., & Qiu, W. (2016). GADD45β induction by S-adenosylmethionine inhibits hepatocellular carcinoma cell proliferation during acute ischemia-hypoxia. *Oncotarget*, *7*(24), 37215–37225. https://doi.org/10.18632/oncotarget.9295

Mack, S. C., Witt, H., Piro, R. M., Gu, L., Zuyderduyn, S., Stütz, A. M., Wang, X., Gallo, M., Garzia, L., Zayne, K., Zhang, X., Ramaswamy, V., Jäger, N., Jones, D. T. W., Sill, M., Pugh, T. J., Ryzhova, M., Wani, K. M., Shih, D. J. H., … Taylor, M. D. (2014). Epigenomic alterations define lethal CIMP-positive ependymomas of infancy. *Nature*, *506*(7489), 445–450. https://doi.org/10.1038/nature13108

Mackay, R. P., Xu, Q., & Weinberger, P. M. (2020). R-Loop Physiology and Pathology: A Brief Review. *DNA and Cell Biology*, *39*(11), 1914–1925. https://doi.org/10.1089/dna.2020.5906

Madan, E., Gogna, R., & Pati, U. (2012). p53 Ser15 phosphorylation disrupts the p53–RPA70 complex and induces RPA70-mediated DNA repair in hypoxia. *Biochemical Journal*, *443*(3), 811–820. https://doi.org/10.1042/BJ20111627

Madden, E., Logue, S. E., Healy, S. J., Manie, S., & Samali, A. (2019). The role of the unfolded protein response in cancer progression: From oncogenesis to chemoresistance. *Biology of the Cell*, *111*(1), 1–17. https://doi.org/10.1111/boc.201800050

Mahaney, B. L., Meek, K., & Lees-Miller, S. P. (2009). Repair of ionizing radiation-induced DNA double-strand breaks by non-homologous end-joining. *Biochemical Journal*, *417*(3), 639–650. https://doi.org/10.1042/BJ20080413

Makharashvili, N., Arora, S., Yin, Y., Fu, Q., Wen, X., Lee, J.-H., Kao, C.-H., Leung, J. W., Miller, K. M., & Paull, T. T. (2018). Sae2/CtIP prevents R-loop accumulation in eukaryotic cells. *ELife*, *7*. https://doi.org/10.7554/eLife.42733

Mannack, L. V. J. C., Eising, S., & Rentmeister, A. (2016). Current techniques for visualizing RNA in cells. *F1000Research*, *5*, 775. https://doi.org/10.12688/f1000research.8151.1

Mansfield, K. D., Guzy, R. D., Pan, Y., Young, R. M., Cash, T. P., Schumacker, P. T., & Simon, M. C. (2005). Mitochondrial dysfunction resulting from loss of cytochrome c impairs cellular oxygen sensing and hypoxic HIF-α activation. *Cell Metabolism*, *1*(6), 393–399. https://doi.org/10.1016/j.cmet.2005.05.003

Mao, Y., Keller, E. T., Garfield, D. H., Shen, K., & Wang, J. (2013). Stromal cells in tumor microenvironment and breast cancer. *Cancer and Metastasis Reviews*, *32*(1–2), 303–315. https://doi.org/10.1007/s10555-012-9415-3

Martinive, P., Defresne, F., Bouzin, C., Saliez, J., Lair, F., Grégoire, V., Michiels, C., Dessy, C., & Feron, O. (2006). Preconditioning of the Tumor Vasculature and Tumor Cells by Intermittent Hypoxia: Implications for Anticancer Therapies. *Cancer Research*, *66*(24), 11736–11744. https://doi.org/10.1158/0008-5472.CAN-06-2056

Massudi, H., Grant, R., Braidy, N., Guest, J., Farnsworth, B., & Guillemin, G. J. (2012). Age-Associated Changes In Oxidative Stress and NAD+ Metabolism In Human Tissue. *PLoS ONE*, *7*(7), e42357. https://doi.org/10.1371/journal.pone.0042357

Matsuo, M., Matsumoto, S., Mitchell, J. B., Krishna, M. C., & Camphausen, K. (2014). Magnetic Resonance Imaging of the Tumor Microenvironment in Radiotherapy: Perfusion, Hypoxia, and Metabolism. *Seminars in Radiation Oncology*, *24*(3), 210–217. https://doi.org/10.1016/j.semradonc.2014.02.002

Matsuoka, S., Ballif, B. A., Smogorzewska, A., McDonald, E. R., Hurov, K. E., Luo, J., Bakalarski, C. E., Zhao, Z., Solimini, N., Lerenthal, Y., Shiloh, Y., Gygi, S. P., & Elledge, S. J. (2007). ATM and ATR Substrate Analysis Reveals Extensive Protein Networks Responsive to DNA Damage. *Science*, *316*(5828), 1160–1166. https://doi.org/10.1126/science.1140321

Mattern, J., Kallinowski, F., Herfarth, C., & Volm, M. (1996). Association of resistance-related protein expression with poor vascularization and low levels of oxygen in human rectal cancer. *International Journal of Cancer*, *67*(1), 20–23. https://doi.org/10.1002/(SICI)1097-0215(19960703)67:1<20::AID-IJC5>3.0.CO;2-1

McAleese, C. E., Choudhury, C., Butcher, N. J., & Minchin, R. F. (2021). Hypoxia-mediated drug resistance in breast cancers. *Cancer Letters*, *502*, 189–199. https://doi.org/10.1016/j.canlet.2020.11.045

McCann, J. L., Cristini, A., Law, E. K., Lee, S. Y., Tellier, M., Carpenter, M. A., Beghè, C., Kim, J. J., Jarvis, M. C., Stefanovska, B., Temiz, N. A., Bergstrom, E. N., Salamango, D. J., Brown, M. R., Murphy, S., Alexandrov, L. B., Miller, K. M., Gromak, N., & Harris, R. S. (2021). *R-loop homeostasis and cancer mutagenesis promoted by the DNA cytosine deaminase APOBEC3B*.

McKeown, S. R. (2014). Defining normoxia, physoxia and hypoxia in tumours—implications for treatment response. *The British Journal of Radiology*, *87*(1035), 20130676. https://doi.org/10.1259/bjr.20130676

McKeown, S. R., Cowen, R. L., & Williams, K. J. (2007). Bioreductive Drugs: from Concept to Clinic. *Clinical Oncology*, *19*(6), 427–442. https://doi.org/10.1016/j.clon.2007.03.006

Mekhail, K., Rivero-Lopez, L., Khacho, M., & Lee, S. (2006). Restriction of rRNA Synthesis by VHL Maintains Energy Equilibrium under Hypoxia. *Cell Cycle*, *5*(20), 2401–2413. https://doi.org/10.4161/cc.5.20.3387

Michealraj, K. A., Kumar, S. A., Kim, L. J. Y., Cavalli, F. M. G., Przelicki, D., Wojcik, J. B., Delaidelli, A., Bajic, A., Saulnier, O., MacLeod, G., Vellanki, R. N., Vladoiu, M. C., Guilhamon, P., Ong, W., Lee, J. J. Y., Jiang, Y., Holgado, B. L., Rasnitsyn, A., Malik, A. A., … Taylor, M. D. (2020). Metabolic Regulation of the Epigenome Drives Lethal Infantile Ependymoma. *Cell*, *181*(6), 1329-1345.e24. https://doi.org/10.1016/j.cell.2020.04.047

Michiels, C., Tellier, C., & Feron, O. (2016). Cycling hypoxia: A key feature of the tumor microenvironment. *Biochimica et Biophysica Acta (BBA) - Reviews on Cancer*, *1866*(1), 76–86. https://doi.org/10.1016/j.bbcan.2016.06.004

Mihaylova, V. T., Bindra, R. S., Yuan, J., Campisi, D., Narayanan, L., Jensen, R., Giordano, F., Johnson, R. S., Rockwell, S., & Glazer, P. M. (2003). Decreased Expression of the DNA Mismatch Repair Gene *Mlh1* under Hypoxic Stress in Mammalian Cells. *Molecular and Cellular Biology*, *23*(9), 3265–3273. https://doi.org/10.1128/MCB.23.9.3265-3273.2003

Minassian, L. M., Cotechini, T., Huitema, E., & Graham, C. H. (2019). *Hypoxia-Induced Resistance to Chemotherapy in Cancer* (pp. 123–139). https://doi.org/10.1007/978-3-030-12734-3_9

Mistry, I. N., Thomas, M., Calder, E. D. D., Conway, S. J., & Hammond, E. M. (2017). Clinical Advances of Hypoxia-Activated Prodrugs in Combination With Radiation Therapy. *International Journal of Radiation Oncology*Biology*Physics*, *98*(5), 1183–1196. https://doi.org/10.1016/j.ijrobp.2017.03.024

Miyamoto, N., Izumi, H., Miyamoto, R., Bin, H., Kondo, H., Tawara, A., Sasaguri, Y., & Kohno, K. (2011). Transcriptional Regulation of Activating Transcription Factor 4 under Oxidative Stress in Retinal Pigment Epithelial ARPE-19/HPV-16 Cells. *Investigative Opthalmology & Visual Science*, *52*(3), 1226. https://doi.org/10.1167/iovs.10-5775

Mochan, T. A., Venere, M., DiTullio, R. A., & Halazonetis, T. D. (2004). 53BP1, an activator of ATM in response to DNA damage. *DNA Repair*, *3*(8–9), 945–952. https://doi.org/10.1016/j.dnarep.2004.03.017

Moeglin, E., Desplancq, D., Conic, S., Oulad-Abdelghani, M., Stoessel, A., Chiper, M., Vigneron, M., Didier, P., Tora, L., & Weiss, E. (2019). Uniform Widespread Nuclear Phosphorylation of Histone H2AX Is an Indicator of Lethal DNA Replication Stress. *Cancers*, *11*(3), 355. https://doi.org/10.3390/cancers11030355

Moehlenbrink, J., Bitomsky, N., & Hofmann, T. G. (2010). Hypoxia suppresses chemotherapeutic drug-induced p53 Serine 46 phosphorylation by triggering HIPK2 degradation. *Cancer Letters*, *292*(1), 119–124. https://doi.org/10.1016/j.canlet.2009.11.016

Morales, J. C., Richard, P., Patidar, P. L., Motea, E. A., Dang, T. T., Manley, J. L., & Boothman, D. A. (2016). XRN2 Links Transcription Termination to DNA Damage and Replication Stress. *PLOS Genetics*, *12*(7), e1006107. https://doi.org/10.1371/journal.pgen.1006107

Morfoisse, F., Tatin, F., Hantelys, F., Adoue, A., Helfer, A.-C., Cassant-Sourdy, S., Pujol, F., Gomez-Brouchet, A., Ligat, L., Lopez, F., Pyronnet, S., Courty, J., Guillermet-Guibert, J., Marzi, S., Schneider, R. J., Prats, A.-C., & Garmy-Susini, B. H. (2016). Nucleolin Promotes Heat Shock–Associated Translation of VEGF-D to Promote Tumor Lymphangiogenesis. *Cancer Research*, *76*(15), 4394–4405. https://doi.org/10.1158/0008-5472.CAN-15-3140

Moskalev, A. A., Shaposhnikov, M. v., Plyusnina, E. N., Zhavoronkov, A., Budovsky, A., Yanai, H., & Fraifeld, V. E. (2013). The role of DNA damage and repair in aging through the prism of Koch-like criteria. *Ageing Research Reviews*, *12*(2), 661–684. https://doi.org/10.1016/j.arr.2012.02.001

Moskovitz, J., & Oien, D. B. (2010). Protein Carbonyl and the Methionine Sulfoxide Reductase System. *Antioxidants & Redox Signaling*, *12*(3), 405–415. https://doi.org/10.1089/ars.2009.2809

Movsas, B., Chapman, J. D., Hanlon, A. L., Horwitz, E. M., Pinover, W. H., Greenberg, R. E., Stobbe, C., & Hanks, G. E. (2001). Hypoxia in Human Prostate Carcinoma. *American Journal of Clinical Oncology*, *24*(5), 458–461. https://doi.org/10.1097/00000421-200110000-00009

Mujcic, H., Nagelkerke, A., Rouschop, K. M. A., Chung, S., Chaudary, N., Span, P. N., Clarke, B., Milosevic, M., Sykes, J., Hill, R. P., Koritzinsky, M., & Wouters, B. G. (2013). Hypoxic Activation of the PERK/eIF2α Arm of the Unfolded Protein Response Promotes Metastasis through Induction of LAMP3. *Clinical Cancer Research*, *19*(22), 6126–6137. https://doi.org/10.1158/1078-0432.CCR-13-0526

Nadel, J., Athanasiadou, R., Lemetre, C., Wijetunga, N. A., Ó Broin, P., Sato, H., Zhang, Z., Jeddeloh, J., Montagna, C., Golden, A., Seoighe, C., & Greally, J. M. (2015). RNA:DNA hybrids in the human genome have distinctive nucleotide characteristics, chromatin composition, and transcriptional relationships. *Epigenetics & Chromatin*, *8*(1), 46. https://doi.org/10.1186/s13072-015-0040-6

Nagelkerke, A., Bussink, J., Mujcic, H., Wouters, B. G., Lehmann, S., Sweep, F. C., & Span, P. N. (2013). Hypoxia stimulates migration of breast cancer cells via the PERK/ATF4/LAMP3-arm of the unfolded protein response. *Breast Cancer Research*, *15*(1), R2. https://doi.org/10.1186/bcr3373

Nagelkerke, A., Bussink, J., van der Kogel, A. J., Sweep, F. C. G. J., & Span, P. N. (2013). The PERK/ATF4/LAMP3-arm of the unfolded protein response affects radioresistance by interfering with the DNA damage response. *Radiotherapy and Oncology*, *108*(3), 415–421. https://doi.org/10.1016/j.radonc.2013.06.037

Nagelkerke, A., Sweep, F. C. G. J., Stegeman, H., Grénman, R., Kaanders, J. H. A. M., Bussink, J., & Span, P. N. (2015). Hypoxic regulation of the PERK/ATF4/LAMP3-arm of the

unfolded protein response in head and neck squamous cell carcinoma. *Head & Neck*, *37*(6), 896–905. https://doi.org/10.1002/hed.23693

Nagy, J., Chang, S.-H., Shih, S.-C., Dvorak, A., & Dvorak, H. (2010). Heterogeneity of the Tumor Vasculature. *Seminars in Thrombosis and Hemostasis*, *36*(03), 321–331. https://doi.org/10.1055/s-0030-1253454

Negrini, S., Gorgoulis, V. G., & Halazonetis, T. D. (2010). Genomic instability — an evolving hallmark of cancer. *Nature Reviews Molecular Cell Biology*, *11*(3), 220–228. https://doi.org/10.1038/nrm2858

Ng, N., Purshouse, K., Foskolou, I. P., Olcina, M. M., & Hammond, E. M. (2018). Challenges to DNA replication in hypoxic conditions. *The FEBS Journal*, *285*(9), 1563–1571. https://doi.org/10.1111/febs.14377

Nguyen, H. D., Yadav, T., Giri, S., Saez, B., Graubert, T. A., & Zou, L. (2017). Functions of Replication Protein A as a Sensor of R Loops and a Regulator of RNaseH1. *Molecular Cell*, *65*(5), 832-847.e4. https://doi.org/10.1016/j.molcel.2017.01.029

Nguyen, T., Nioi, P., & Pickett, C. B. (2009). The Nrf2-Antioxidant Response Element Signaling Pathway and Its Activation by Oxidative Stress. *Journal of Biological Chemistry*, *284*(20), 13291–13295. https://doi.org/10.1074/jbc.R900010200

Niehrs, C., & Luke, B. (2020). Regulatory R-loops as facilitators of gene expression and genome stability. *Nature Reviews Molecular Cell Biology*, *21*(3), 167–178. https://doi.org/10.1038/s41580-019-0206-3

Nilson, K. A., Lawson, C. K., Mullen, N. J., Ball, C. B., Spector, B. M., Meier, J. L., & Price, D. H. (2017). Oxidative stress rapidly stabilizes promoter-proximal paused Pol II across the human genome. *Nucleic Acids Research*, *45*(19), 11088–11105. https://doi.org/10.1093/nar/gkx724

Nordsmark, M., Bentzen, S. M., & Overgaard, J. (1994). Measurement of Human Tumour Oxygenation Status by a Polarographic Needle Electrode: An analysis of inter- and intratumour heterogeneity. *Acta Oncologica*, *33*(4), 383–389. https://doi.org/10.3109/02841869409098433

Nordsmark, M., Bentzen, S. M., Rudat, V., Brizel, D., Lartigau, E., Stadler, P., Becker, A., Adam, M., Molls, M., Dunst, J., Terris, D. J., & Overgaard, J. (2005). Prognostic value of tumor oxygenation in 397 head and neck tumors after primary radiation therapy. An international multi-center study. *Radiotherapy and Oncology*, *77*(1), 18–24. https://doi.org/10.1016/j.radonc.2005.06.038

Nowotny, M., Gaidamakov, S. A., Ghirlando, R., Cerritelli, S. M., Crouch, R. J., & Yang, W. (2007). Structure of Human RNase H1 Complexed with an RNA/DNA Hybrid: Insight into HIV Reverse Transcription. *Molecular Cell*, *28*(2), 264–276. https://doi.org/10.1016/j.molcel.2007.08.015

O'Cathail, S. M., Wu, C.-H., Lewis, A., Holmes, C., Hawkins, M. A., & Maughan, T. (2020). NRF2 metagene signature is a novel prognostic biomarker in colorectal cancer. *Cancer Genetics*, *248–249*, 1–10. https://doi.org/10.1016/j.cancergen.2020.08.006

Ohle, C., Tesorero, R., Schermann, G., Dobrev, N., Sinning, I., & Fischer, T. (2016). Transient RNA-DNA Hybrids Are Required for Efficient Double-Strand Break Repair. *Cell*, *167*(4), 1001-1013.e7. https://doi.org/10.1016/j.cell.2016.10.001

Olcina, M., Lecane, P. S., & Hammond, E. M. (2010). Targeting Hypoxic Cells through the DNA Damage Response. *Clinical Cancer Research*, *16*(23), 5624–5629. https://doi.org/10.1158/1078-0432.CCR-10-0286

Olcina, M. M., Foskolou, I. P., Anbalagan, S., Senra, J. M., Pires, I. M., Jiang, Y., Ryan, A. J., & Hammond, E. M. (2013). Replication Stress and Chromatin Context Link ATM Activation to a Role in DNA Replication. *Molecular Cell*, *52*(5), 758–766. https://doi.org/10.1016/j.molcel.2013.10.019

Olcina, M. M., Grand, R. J., & Hammond, E. M. (2014). ATM activation in hypoxia - causes and consequences. *Molecular & Cellular Oncology*, *1*(1), e29903. https://doi.org/10.4161/mco.29903

Olivieri, M., Cho, T., Álvarez-Quilón, A., Li, K., Schellenberg, M. J., Zimmermann, M., Hustedt, N., Rossi, S. E., Adam, S., Melo, H., Heijink, A. M., Sastre-Moreno, G., Moatti, N., Szilard, R. K., McEwan, A., Ling, A. K., Serrano-Benitez, A., Ubhi, T., Feng, S., … Durocher, D. (2020). A Genetic Map of the Response to DNA Damage in Human Cells. *Cell*, *182*(2), 481-496.e21. https://doi.org/10.1016/j.cell.2020.05.040

Overgaard, J., Sand Hansen, H., Overgaard, M., Bastholt, L., Berthelsen, A., Specht, L., Lindeløv, B., & Jørgensen, K. (1998). A randomized double-blind phase III study of nimorazole as a hypoxic radiosensitizer of primary radiotherapy in supraglottic larynx and pharynx carcinoma. Results of the Danish Head and Neck Cancer Study (DAHANCA) Protocol 5-85. *Radiotherapy and Oncology*, *46*(2), 135–146. https://doi.org/10.1016/S0167-8140(97)00220-X

Pacek, M., & Walter, J. C. (2004). A requirement for MCM7 and Cdc45 in chromosome unwinding during eukaryotic DNA replication. *The EMBO Journal*, *23*(18), 3667–3676. https://doi.org/10.1038/sj.emboj.7600369

Page, M. J., McKenzie, J. E., Bossuyt, P. M., Boutron, I., Hoffmann, T. C., Mulrow, C. D., Shamseer, L., Tetzlaff, J. M., Akl, E. A., Brennan, S. E., Chou, R., Glanville, J., Grimshaw, J. M., Hróbjartsson, A., Lalu, M. M., Li, T., Loder, E. W., Mayo-Wilson, E., McDonald, S., … Moher, D. (2021). The PRISMA 2020 statement: an updated guideline for reporting systematic reviews. *BMJ*, n71. https://doi.org/10.1136/bmj.n71

Palazzo, A. F., & Lee, E. S. (2015). Non-coding RNA: what is functional and what is junk? *Frontiers in Genetics*, *6*. https://doi.org/10.3389/fgene.2015.00002

Park, C. B., & Larsson, N.-G. (2011). Mitochondrial DNA mutations in disease and aging. *Journal of Cell Biology*, *193*(5), 809–818. https://doi.org/10.1083/jcb.201010024

Parker, M., Mohankumar, K. M., Punchihewa, C., Weinlich, R., Dalton, J. D., Li, Y., Lee, R., Tatevossian, R. G., Phoenix, T. N., Thiruvenkatam, R., White, E., Tang, B., Orisme, W., Gupta, K., Rusch, M., Chen, X., Li, Y., Nagahawhatte, P., Hedlund, E., … Gilbertson, R. J. (2014). C11orf95–RELA fusions drive oncogenic NF-κB signalling in ependymoma. *Nature*, *506*(7489), 451–455. https://doi.org/10.1038/nature13109

Patiar, S., & Harris, A. L. (2006). Role of hypoxia-inducible factor-1α as a cancer therapy target. *Endocrine-Related Cancer*. https://doi.org/10.1677/erc.1.01290

Paulsen, R. D., Soni, D. v., Wollman, R., Hahn, A. T., Yee, M.-C., Guan, A., Hesley, J. A., Miller, S. C., Cromwell, E. F., Solow-Cordero, D. E., Meyer, T., & Cimprich, K. A. (2009). A Genome-wide siRNA Screen Reveals Diverse Cellular Processes and Pathways that Mediate Genome Stability. *Molecular Cell*, *35*(2), 228–239. https://doi.org/10.1016/j.molcel.2009.06.021

Pedre, B., Barayeu, U., Ezeriņa, D., & Dick, T. P. (2021). The mechanism of action of N-acetylcysteine (NAC): The emerging role of H2S and sulfane sulfur species. *Pharmacology & Therapeutics*, *228*, 107916. https://doi.org/10.1016/j.pharmthera.2021.107916

Pérez, M., García-Limones, C., Zapico, I., Marina, A., Schmitz, M. L., Muñoz, E., & Calzado, M. A. (2012). Mutual regulation between SIAH2 and DYRK2 controls hypoxic and genotoxic signaling pathways. *Journal of Molecular Cell Biology*, *4*(5), 316–330. https://doi.org/10.1093/jmcb/mjs047

Petrova, V., Annicchiarico-Petruzzelli, M., Melino, G., & Amelio, I. (2018). The hypoxic tumour microenvironment. *Oncogenesis*, *7*(1), 10. https://doi.org/10.1038/s41389-017-0011-9

Petry, A., Zhang, Z., Trautz, B., Rieß, F., & Görlach, A. (2019). Cross Talk Between p22phox and ATF4 in the Endothelial Unfolded Protein Response. *Antioxidants & Redox Signaling*, *30*(1), 40–55. https://doi.org/10.1089/ars.2017.7481

Pi, L., Li, X., Song, Q., Shen, Y., Lu, X., & Di, B. (2014). Knockdown of glucose-regulated protein 78 abrogates chemoresistance of hypopharyngeal carcinoma cells to cisplatin induced by unfolded protein in response to severe hypoxia. *Oncology Letters*, *7*(3), 685–692. https://doi.org/10.3892/ol.2013.1753

Pilié, P. G., Tang, C., Mills, G. B., & Yap, T. A. (2019). State-of-the-art strategies for targeting the DNA damage response in cancer. *Nature Reviews Clinical Oncology*, *16*(2), 81–104. https://doi.org/10.1038/s41571-018-0114-z

Pires, I. M., Bencokova, Z., McGurk, C., & Hammond, E. M. (2010). Exposure to acute hypoxia induces a transient DNA damage response which includes Chk1 and TLK1. *Cell Cycle*, *9*(13), 2502–2507. https://doi.org/10.4161/cc.9.13.12059

Pires, I. M., Bencokova, Z., Milani, M., Folkes, L. K., Li, J.-L., Stratford, M. R., Harris, A. L., & Hammond, E. M. (2010). Effects of Acute versus Chronic Hypoxia on DNA Damage Responses and Genomic Instability. *Cancer Research*, *70*(3), 925–935. https://doi.org/10.1158/0008-5472.CAN-09-2715

Pires, I. M., Olcina, M. M., Anbalagan, S., Pollard, J. R., Reaper, P. M., Charlton, P. A., McKenna, W. G., & Hammond, E. M. (2012). Targeting radiation-resistant hypoxic tumour cells through ATR inhibition. *British Journal of Cancer*, *107*(2), 291–299. https://doi.org/10.1038/bjc.2012.265

Pizzino, G., Irrera, N., Cucinotta, M., Pallio, G., Mannino, F., Arcoraci, V., Squadrito, F., Altavilla, D., & Bitto, A. (2017). Oxidative Stress: Harms and Benefits for Human Health. *Oxidative Medicine and Cellular Longevity*, *2017*, 1–13. https://doi.org/10.1155/2017/8416763

Pontvianne, F., Carpentier, M.-C., Durut, N., Pavlištová, V., Jaške, K., Schořová, Š., Parrinello, H., Rohmer, M., Pikaard, C. S., Fojtová, M., Fajkus, J., & Sáez-Vásquez, J. (2016). Identification of Nucleolus-Associated Chromatin Domains Reveals a Role for the Nucleolus in 3D Organization of the A. thaliana Genome. *Cell Reports*, *16*(6), 1574–1587. https://doi.org/10.1016/j.celrep.2016.07.016

Pugh, C. W., & Ratcliffe, P. J. (2003). Regulation of angiogenesis by hypoxia: role of the HIF system. *Nature Medicine*, *9*(6), 677–684. https://doi.org/10.1038/nm0603-677

Raina, K., Noblin, D. J., Serebrenik, Y. v, Adams, A., Zhao, C., & Crews, C. M. (2014). Targeted protein destabilization reveals an estrogen-mediated ER stress response. *Nature Chemical Biology*, *10*(11), 957–962. https://doi.org/10.1038/nchembio.1638

Rajpal, G., & Arvan, P. (2013). Disulfide Bond Formation. In *Handbook of Biologically Active Peptides* (pp. 1721–1729). Elsevier. https://doi.org/10.1016/B978-0-12-385095-9.00236-0

Ramachandran, S., Ma, T. S., Griffin, J., Ng, N., Foskolou, I. P., Hwang, M.-S., Victori, P., Cheng, W.-C., Buffa, F. M., Leszczynska, K. B., El-Khamisy, S. F., Gromak, N., & Hammond, E. M. (2021). Hypoxia-induced SETX links replication stress with the unfolded protein response. *Nature Communications*, *12*(1), 3686. https://doi.org/10.1038/s41467-021-24066-z

Rankin, E. B., & Giaccia, A. J. (2016). Hypoxic control of metastasis. In *Science*. https://doi.org/10.1126/science.aaf4405

Ray, P. D., Huang, B.-W., & Tsuji, Y. (2012). Reactive oxygen species (ROS) homeostasis and redox regulation in cellular signaling. *Cellular Signalling*, *24*(5), 981–990. https://doi.org/10.1016/j.cellsig.2012.01.008

Reczek, C. R., & Chandel, N. S. (2017). The Two Faces of Reactive Oxygen Species in Cancer. *Annual Review of Cancer Biology*, *1*(1), 79–98. https://doi.org/10.1146/annurev-cancerbio-041916-065808

Reich, S., Nguyen, C. D. L., Has, C., Steltgens, S., Soni, H., Coman, C., Freyberg, M., Bichler, A., Seifert, N., Conrad, D., Knobbe-Thomsen, C. B., Tews, B., Toedt, G., Ahrends, R., & Medenbach, J. (2020). A multi-omics analysis reveals the unfolded protein response regulon and stress-induced resistance to folate-based antimetabolites. *Nature Communications*, *11*(1), 2936. https://doi.org/10.1038/s41467-020-16747-y

Ren, Y., Hao, P., Dutta, B., Cheow, E. S. H., Sim, K. H., Gan, C. S., Lim, S. K., & Sze, S. K. (2013). Hypoxia Modulates A431 Cellular Pathways Association to Tumor Radioresistance and Enhanced Migration Revealed by Comprehensive Proteomic and Functional Studies. *Molecular & Cellular Proteomics*, *12*(2), 485–498. https://doi.org/10.1074/mcp.M112.018325

Renaudin, X., Lee, M., Shehata, M., Surmann, E.-M., & Venkitaraman, A. R. (2021). BRCA2 deficiency reveals that oxidative stress impairs RNaseH1 function to cripple mitochondrial DNA maintenance. *Cell Reports*, *36*(5), 109478. https://doi.org/10.1016/j.celrep.2021.109478

Rezvani, H. R., Mahfouf, W., Ali, N., Chemin, C., Ged, C., Kim, A. L., de Verneuil, H., Taïeb, A., Bickers, D. R., & Mazurier, F. (2010). Hypoxia-inducible factor-1α regulates the expression of nucleotide excision repair proteins in keratinocytes. *Nucleic Acids Research*, *38*(3), 797–809. https://doi.org/10.1093/nar/gkp1072

Richard, P., & Manley, J. L. (2017). R Loops and Links to Human Disease. *Journal of Molecular Biology*, *429*(21), 3168–3180. https://doi.org/10.1016/j.jmb.2016.08.031

Rinaldi, C., Pizzul, P., Longhese, M. P., & Bonetti, D. (2021). Sensing R-Loop-Associated DNA Damage to Safeguard Genome Stability. *Frontiers in Cell and Developmental Biology*, *8*. https://doi.org/10.3389/fcell.2020.618157

Roberts, R. W., & Crothers, D. M. (1992). Stability and Properties of Double and Triple Helices: Dramatic Effects of RNA or DNA Backbone Composition. *Science*, *258*(5087), 1463–1466. https://doi.org/10.1126/science.1279808

Rodríguez-Jiménez, F. J., Moreno-Manzano, V., Lucas-Dominguez, R., & Sánchez-Puelles, J.-M. (2008). Hypoxia Causes Downregulation of Mismatch Repair System and Genomic Instability in Stem Cells. *Stem Cells*, *26*(8), 2052–2062. https://doi.org/10.1634/stemcells.2007-1016

Rofstad, E. K., Gaustad, J.-V., Egeland, T. A. M., Mathiesen, B., & Galappathi, K. (2010). Tumors exposed to acute cyclic hypoxic stress show enhanced angiogenesis, perfusion and metastatic dissemination. *International Journal of Cancer*, *127*(7), 1535–1546. https://doi.org/10.1002/ijc.25176

Rohwer, N., & Cramer, T. (2011). Hypoxia-mediated drug resistance: Novel insights on the functional interaction of HIFs and cell death pathways. *Drug Resistance Updates*, *14*(3), 191–201. https://doi.org/10.1016/j.drup.2011.03.001

Rouschop, K. M., Dubois, L. J., Keulers, T. G., van den Beucken, T., Lambin, P., Bussink, J., van der Kogel, A. J., Koritzinsky, M., & Wouters, B. G. (2013). PERK/eIF2α signaling protects therapy resistant hypoxic cells through induction of glutathione synthesis and protection against ROS. *Proceedings of the National Academy of Sciences*, *110*(12), 4622–4627. https://doi.org/10.1073/pnas.1210633110

Roy, D., & Lieber, M. R. (2009). G Clustering Is Important for the Initiation of Transcription-Induced R-Loops In Vitro, whereas High G Density without Clustering Is Sufficient

Thereafter. *Molecular and Cellular Biology*, *29*(11), 3124–3133. https://doi.org/10.1128/MCB.00139-09

Roy, D., Zhang, Z., Lu, Z., Hsieh, C.-L., & Lieber, M. R. (2010). Competition between the RNA Transcript and the Nontemplate DNA Strand during R-Loop Formation In Vitro: a Nick Can Serve as a Strong R-Loop Initiation Site. *Molecular and Cellular Biology*, *30*(1), 146–159. https://doi.org/10.1128/MCB.00897-09

Rzymski, T., & Harris, A. L. (2007). The Unfolded Protein Response and Integrated Stress Response to Anoxia. *Clinical Cancer Research*, *13*(9), 2537–2540. https://doi.org/10.1158/1078-0432.CCR-06-2126

Salaroglio, I. C., Panada, E., Moiso, E., Buondonno, I., Provero, P., Rubinstein, M., Kopecka, J., & Riganti, C. (2017). PERK induces resistance to cell death elicited by endoplasmic reticulum stress and chemotherapy. *Molecular Cancer*, *16*(1), 91. https://doi.org/10.1186/s12943-017-0657-0

Santos-Pereira, J. M., & Aguilera, A. (2015). R loops: new modulators of genome dynamics and function. *Nature Reviews Genetics*, *16*(10), 583–597. https://doi.org/10.1038/nrg3961

Sanz, L. A., Hartono, S. R., Lim, Y. W., Steyaert, S., Rajpurkar, A., Ginno, P. A., Xu, X., & Chédin, F. (2016). Prevalent, Dynamic, and Conserved R-Loop Structures Associate with Specific Epigenomic Signatures in Mammals. *Molecular Cell*, *63*(1), 167–178. https://doi.org/10.1016/j.molcel.2016.05.032

Saponaro, M., Kantidakis, T., Mitter, R., Kelly, G. P., Heron, M., Williams, H., Söding, J., Stewart, A., & Svejstrup, J. Q. (2014). RECQL5 Controls Transcript Elongation and Suppresses Genome Instability Associated with Transcription Stress. *Cell*, *157*(5), 1037–1049. https://doi.org/10.1016/j.cell.2014.03.048

Scanlon, S. E., & Glazer, P. M. (2014). Hypoxic Stress Facilitates Acute Activation and Chronic Downregulation of Fanconi Anemia Proteins. *Molecular Cancer Research*, *12*(7), 1016–1028. https://doi.org/10.1158/1541-7786.MCR-13-0628

Scanlon, S. E., & Glazer, P. M. (2015). Multifaceted control of DNA repair pathways by the hypoxic tumor microenvironment. *DNA Repair*, *32*, 180–189. https://doi.org/10.1016/j.dnarep.2015.04.030

Schaaf, M. B. E., Cojocari, D., Keulers, T. G., Jutten, B., Starmans, M. H., de Jong, M. C., Begg, A. C., Savelkouls, K. G. M., Bussink, J., Vooijs, M., Wouters, B. G., & Rouschop, K. M. A. (2013). The autophagy associated gene, ULK1, promotes tolerance to chronic and acute hypoxia. *Radiotherapy and Oncology*, *108*(3), 529–534. https://doi.org/10.1016/j.radonc.2013.06.015

Schödel, J., & Ratcliffe, P. J. (2019). Mechanisms of hypoxia signalling: new implications for nephrology. *Nature Reviews Nephrology*, *15*(10), 641–659. https://doi.org/10.1038/s41581-019-0182-z

Schofield, C. J., & Ratcliffe, P. J. (2004). Oxygen sensing by HIF hydroxylases. In *Nature Reviews Molecular Cell Biology*. https://doi.org/10.1038/nrm1366

Scholzová, E., Malík, R., Ševčík, J., & Kleibl, Z. (2007). RNA regulation and cancer development. *Cancer Letters*, *246*(1–2), 12–23. https://doi.org/10.1016/j.canlet.2006.03.021

Schönenberger, M. J., & Kovacs, W. J. (2015). Hypoxia signaling pathways: Modulators of oxygen-related organelles. In *Frontiers in Cell and Developmental Biology*. https://doi.org/10.3389/fcell.2015.00042

Schroedl, C., McClintock, D. S., Budinger, G. R. S., & Chandel, N. S. (2002). Hypoxic but not anoxic stabilization of HIF-1α requires mitochondrial reactive oxygen species. *American Journal of Physiology-Lung Cellular and Molecular Physiology*, *283*(5), L922–L931. https://doi.org/10.1152/ajplung.00014.2002

Sebestyén, A., Kopper, L., Dankó, T., & Tímár, J. (2021). Hypoxia Signaling in Cancer: From Basics to Clinical Practice. *Pathology and Oncology Research*, *27*. https://doi.org/10.3389/pore.2021.1609802

Semenza, G. L. (2003). Targeting HIF-1 for cancer therapy. *Nature Reviews Cancer*, *3*(10), 721–732. https://doi.org/10.1038/nrc1187

Semenza, G. L. (2010). HIF-1: upstream and downstream of cancer metabolism. *Current Opinion in Genetics & Development*, *20*(1), 51–56. https://doi.org/10.1016/j.gde.2009.10.009

Seoane, J., & Gomis, R. R. (2017). TGF-β Family Signaling in Tumor Suppression and Cancer Progression. *Cold Spring Harbor Perspectives in Biology*, *9*(12), a022277. https://doi.org/10.1101/cshperspect.a022277

Sermeus, A., Genin, M., Maincent, A., Fransolet, M., Notte, A., Leclere, L., Riquier, H., Arnould, T., & Michiels, C. (2012). Hypoxia-Induced Modulation of Apoptosis and BCL-2 Family Proteins in Different Cancer Cell Types. *PLoS ONE*, *7*(11), e47519. https://doi.org/10.1371/journal.pone.0047519

Shan, Q., Fan, Y., Guo, J., Han, X., Wang, H., & Wang, Z. (2019). Relationship between tumor size and metastatic site in patients with stage IV non-small cell lung cancer: A large SEER-based study. *PeerJ*, *7*, e7822. https://doi.org/10.7717/peerj.7822

Shibata, A., & Jeggo, P. A. (2020). Roles for 53BP1 in the repair of radiation-induced DNA double strand breaks. *DNA Repair*, *93*, 102915. https://doi.org/10.1016/j.dnarep.2020.102915

Shields, H. J., Traa, A., & van Raamsdonk, J. M. (2021). Beneficial and Detrimental Effects of Reactive Oxygen Species on Lifespan: A Comprehensive Review of Comparative and Experimental Studies. *Frontiers in Cell and Developmental Biology*, *9*. https://doi.org/10.3389/fcell.2021.628157

Shivji, M. K. K., Renaudin, X., Williams, Ç. H., & Venkitaraman, A. R. (2018). BRCA2 Regulates Transcription Elongation by RNA Polymerase II to Prevent R-Loop Accumulation. *Cell Reports*, *22*(4), 1031–1039. https://doi.org/10.1016/j.celrep.2017.12.086

Silbergeld, D. L., Rostomily, R. C., & Alvord, E. C. (1991). The cause of death in patients with glioblastoma is multifactorial: *Journal of Neuro-Oncology*, *10*(2), 179–185. https://doi.org/10.1007/BF00146880

Sinenko, S. A., Starkova, T. Yu., Kuzmin, A. A., & Tomilin, A. N. (2021). Physiological Signaling Functions of Reactive Oxygen Species in Stem Cells: From Flies to Man. *Frontiers in Cell and Developmental Biology*, *9*. https://doi.org/10.3389/fcell.2021.714370

Singleton, D. C., Macann, A., & Wilson, W. R. (2021). Therapeutic targeting of the hypoxic tumour microenvironment. *Nature Reviews Clinical Oncology*, *18*(12), 751–772. https://doi.org/10.1038/s41571-021-00539-4

Sirbu, B. M., McDonald, W. H., Dungrawala, H., Badu-Nkansah, A., Kavanaugh, G. M., Chen, Y., Tabb, D. L., & Cortez, D. (2013). Identification of Proteins at Active, Stalled, and Collapsed Replication Forks Using Isolation of Proteins on Nascent DNA (iPOND) Coupled with Mass Spectrometry. *Journal of Biological Chemistry*, *288*(44), 31458–31467. https://doi.org/10.1074/jbc.M113.511337

Sisinni, L., Pietrafesa, M., Lepore, S., Maddalena, F., Condelli, V., Esposito, F., & Landriscina, M. (2019). Endoplasmic Reticulum Stress and Unfolded Protein Response in Breast Cancer: The Balance between Apoptosis and Autophagy and Its Role in Drug Resistance. *International Journal of Molecular Sciences*, *20*(4), 857. https://doi.org/10.3390/ijms20040857

Skourti-Stathaki, K., Kamieniarz-Gdula, K., & Proudfoot, N. J. (2014). R-loops induce repressive chromatin marks over mammalian gene terminators. *Nature*, *516*(7531), 436–439. https://doi.org/10.1038/nature13787

Skourti-Stathaki, K., Proudfoot, N. J., & Gromak, N. (2011). Human Senataxin Resolves RNA/DNA Hybrids Formed at Transcriptional Pause Sites to Promote Xrn2-Dependent Termination. *Molecular Cell*, *42*(6), 794–805. https://doi.org/10.1016/j.molcel.2011.04.026

Skuse, A. (2015). What Was Cancer? Definition, Diagnosis and Cause. In *Constructions of Cancer in Early Modern England* (pp. 20–39). Palgrave Macmillan UK. https://doi.org/10.1057/9781137487537_2

Skwarski, M., McGowan, D. R., Belcher, E., di Chiara, F., Stavroulias, D., McCole, M., Derham, J. L., Chu, K.-Y., Teoh, E., Chauhan, J., O'Reilly, D., Harris, B. H. L., Macklin, P. S., Bull, J. A., Green, M., Rodriguez-Berriguete, G., Prevo, R., Folkes, L. K., Campo, L., … Higgins, G. S. (2021). Mitochondrial Inhibitor Atovaquone Increases Tumor Oxygenation and Inhibits Hypoxic Gene Expression in Patients with Non–Small Cell Lung Cancer. *Clinical Cancer Research*, *27*(9), 2459–2469. https://doi.org/10.1158/1078-0432.CCR-20-4128

Sollier, J., & Cimprich, K. A. (2015). Breaking bad: R-loops and genome integrity. *Trends in Cell Biology*, *25*(9), 514–522. https://doi.org/10.1016/j.tcb.2015.05.003

Sollier, J., Stork, C. T., García-Rubio, M. L., Paulsen, R. D., Aguilera, A., & Cimprich, K. A. (2014). Transcription-Coupled Nucleotide Excision Repair Factors Promote R-Loop-Induced Genome Instability. *Molecular Cell*, *56*(6), 777–785. https://doi.org/10.1016/j.molcel.2014.10.020

Spiegelberg, L., Houben, R., Niemans, R., de Ruysscher, D., Yaromina, A., Theys, J., Guise, C. P., Smaill, J. B., Patterson, A. v., Lambin, P., & Dubois, L. J. (2019). Hypoxia-activated prodrugs and (lack of) clinical progress: The need for hypoxia-based biomarker patient selection in phase III clinical trials. *Clinical and Translational Radiation Oncology*, *15*, 62–69. https://doi.org/10.1016/j.ctro.2019.01.005

Spyer, K. M., Ackland, G. L., & Gourine, A. V. (2006). NEUROPHYSIOLOGY | Overview. In *Encyclopedia of Respiratory Medicine* (pp. 131–138). Elsevier. https://doi.org/10.1016/B0-12-370879-6/00500-7

Stavnezer, J., Guikema, J. E. J., & Schrader, C. E. (2008). Mechanism and Regulation of Class Switch Recombination. *Annual Review of Immunology*, *26*(1), 261–292. https://doi.org/10.1146/annurev.immunol.26.021607.090248

Stewart, G. S., Maser, R. S., Stankovic, T., Bressan, D. A., Kaplan, M. I., Jaspers, N. G. J., Raams, A., Byrd, P. J., Petrini, J. H. J., & Taylor, A. M. R. (1999). The DNA Double-Strand Break Repair Gene hMRE11 Is Mutated in Individuals with an Ataxia-Telangiectasia-like Disorder. *Cell*, *99*(6), 577–587. https://doi.org/10.1016/S0092-8674(00)81547-0

Sudhakar, A. (2009). History of Cancer, Ancient and Modern Treatment Methods. *Journal of Cancer Science & Therapy*, *01*(02), i–iv. https://doi.org/10.4172/1948-5956.100000e2

Sun, Y., Jiang, X., Xu, Y., Ayrapetov, M. K., Moreau, L. A., Whetstine, J. R., & Price, B. D. (2009). Histone H3 methylation links DNA damage detection to activation of the tumour suppressor Tip60. *Nature Cell Biology*, *11*(11), 1376–1382. https://doi.org/10.1038/ncb1982

Suraweera, A., Lim, Y., Woods, R., Birrell, G. W., Nasim, T., Becherel, O. J., & Lavin, M. F. (2009). Functional role for senataxin, defective in ataxia oculomotor apraxia type 2, in transcriptional regulation. *Human Molecular Genetics*, *18*(18), 3384–3396. https://doi.org/10.1093/hmg/ddp278

Tan, J., Duan, M., Yadav, T., Phoon, L., Wang, X., Zhang, J.-M., Zou, L., & Lan, L. (2020). An R-loop-initiated CSB–RAD52–POLD3 pathway suppresses ROS-induced telomeric DNA breaks. *Nucleic Acids Research*, *48*(3), 1285–1300. https://doi.org/10.1093/nar/gkz1114

Tan, J., Wang, X., Phoon, L., Yang, H., & Lan, L. (2020). Resolution of ROS-induced G-quadruplexes and R-loops at transcriptionally active sites is dependent on BLM helicase. *FEBS Letters*, *594*(9), 1359–1367. https://doi.org/10.1002/1873-3468.13738

Teicher, B. A. (1994). Hypoxia and drug resistance. *Cancer and Metastasis Reviews*, *13*(2), 139–168. https://doi.org/10.1007/BF00689633

Teng, Y., Yadav, T., Duan, M., Tan, J., Xiang, Y., Gao, B., Xu, J., Liang, Z., Liu, Y., Nakajima, S., Shi, Y., Levine, A. S., Zou, L., & Lan, L. (2018). ROS-induced R loops trigger a transcription-coupled but BRCA1/2-independent homologous recombination pathway through CSB. *Nature Communications*, *9*(1), 4115. https://doi.org/10.1038/s41467-018-06586-3

Thannickal, V. J., & Fanburg, B. L. (2000). Reactive oxygen species in cell signaling. *American Journal of Physiology-Lung Cellular and Molecular Physiology*, *279*(6), L1005–L1028. https://doi.org/10.1152/ajplung.2000.279.6.L1005

Thienpont, B., Steinbacher, J., Zhao, H., D'Anna, F., Kuchnio, A., Ploumakis, A., Ghesquière, B., van Dyck, L., Boeckx, B., Schoonjans, L., Hermans, E., Amant, F., Kristensen, V. N., Koh, K. P., Mazzone, M., Coleman, M. L., Carell, T., Carmeliet, P., & Lambrechts, D. (2016). Tumour hypoxia causes DNA hypermethylation by reducing TET activity. *Nature*, *537*(7618), 63–68. https://doi.org/10.1038/nature19081

Thienpont, B., van Dyck, L., & Lambrechts, D. (2016). Tumors smother their epigenome. *Molecular & Cellular Oncology*, *3*(6), e1240549. https://doi.org/10.1080/23723556.2016.1240549

Thomas, M., White, R. L., & Davis, R. W. (1976). Hybridization of RNA to double-stranded DNA: formation of R-loops. *Proceedings of the National Academy of Sciences*, *73*(7), 2294–2298. https://doi.org/10.1073/pnas.73.7.2294

Tong, Y., Li, Q.-G., Xing, T.-Y., Zhang, M., Zhang, J.-J., & Xia, Q. (2013). HIF1 regulates WSB-1 expression to promote hypoxia-induced chemoresistance in hepatocellular carcinoma cells. *FEBS Letters*, *587*(16), 2530–2535. https://doi.org/10.1016/j.febslet.2013.06.017

Torrisi, F., Minafra, L., Cammarata, F. P., Savoca, G., Calvaruso, M., Vicario, N., Maccari, L., Pérès, E. A., Özçelik, H., Bernaudin, M., Botta, L., Russo, G., Parenti, R., & Valable, S. (2020). SRC Tyrosine Kinase Inhibitor and X-rays Combined Effect on Glioblastoma Cell Lines. *International Journal of Molecular Sciences*, *21*(11), 3917. https://doi.org/10.3390/ijms21113917

Tresini, M., Warmerdam, D. O., Kolovos, P., Snijder, L., Vrouwe, M. G., Demmers, J. A. A., van IJcken, W. F. J., Grosveld, F. G., Medema, R. H., Hoeijmakers, J. H. J., Mullenders, L. H. F., Vermeulen, W., & Marteijn, J. A. (2015). The core spliceosome as target and effector of non-canonical ATM signalling. *Nature*, *523*(7558), 53–58. https://doi.org/10.1038/nature14512

Trusina, A., Papa, F. R., & Tang, C. (2008). Rationalizing translation attenuation in the network architecture of the unfolded protein response. *Proceedings of the National Academy of Sciences*, *105*(51), 20280–20285. https://doi.org/10.1073/pnas.0803476105

Tsai, Y. C., & Weissman, A. M. (2010). The Unfolded Protein Response, Degradation from the Endoplasmic Reticulum, and Cancer. *Genes & Cancer*, *1*(7), 764–778. https://doi.org/10.1177/1947601910383011

Tuduri, S., Crabbé, L., Conti, C., Tourrière, H., Holtgreve-Grez, H., Jauch, A., Pantesco, V., de Vos, J., Thomas, A., Theillet, C., Pommier, Y., Tazi, J., Coquelle, A., & Pasero, P. (2009). Topoisomerase I suppresses genomic instability by preventing interference between replication and transcription. *Nature Cell Biology*, *11*(11), 1315–1324. https://doi.org/10.1038/ncb1984

Turaka, A., Buyyounouski, M. K., Hanlon, A. L., Horwitz, E. M., Greenberg, R. E., & Movsas, B. (2012). Hypoxic Prostate/Muscle Po2 Ratio Predicts for Outcome in Patients With Localized Prostate Cancer: Long-Term Results. *International Journal of Radiation Oncology*Biology*Physics*, *82*(3), e433–e439. https://doi.org/10.1016/j.ijrobp.2011.05.037

Turrens, J. F. (2003). Mitochondrial formation of reactive oxygen species. *The Journal of Physiology*, *552*(2), 335–344. https://doi.org/10.1113/jphysiol.2003.049478

Valkenburg, K. C., de Groot, A. E., & Pienta, K. J. (2018). Targeting the tumour stroma to improve cancer therapy. *Nature Reviews Clinical Oncology*, *15*(6), 366–381. https://doi.org/10.1038/s41571-018-0007-1

van den Bosch, M., Bree, R. T., & Lowndes, N. F. (2003). The MRN complex: coordinating and mediating the response to broken chromosomes. *EMBO Reports*, *4*(9), 844–849. https://doi.org/10.1038/sj.embor.embor925

van Sluis, M., van Vuuren, C., Mangan, H., & McStay, B. (2020). NORs on human acrocentric chromosome p-arms are active by default and can associate with nucleoli independently of rDNA. *Proceedings of the National Academy of Sciences*, *117*(19), 10368–10377. https://doi.org/10.1073/pnas.2001812117

Vandewynckel, Y.-P., Laukens, D., Bogaerts, E., Paridaens, A., van den Bussche, A., Verhelst, X., van Steenkiste, C., Descamps, B., Vanhove, C., Libbrecht, L., de Rycke, R., Lambrecht, B. N., Geerts, A., Janssens, S., & van Vlierberghe, H. (2015). Modulation of the unfolded protein response impedes tumor cell adaptation to proteotoxic stress: a PERK for hepatocellular carcinoma therapy. *Hepatology International*, *9*(1), 93–104. https://doi.org/10.1007/s12072-014-9582-0

Varia, M. A., Calkins-Adams, D. P., Rinker, L. H., Kennedy, A. S., Novotny, D. B., Fowler, W. C., & Raleigh, J. A. (1998). Pimonidazole: A Novel Hypoxia Marker for Complementary Study of Tumor Hypoxia and Cell Proliferation in Cervical Carcinoma. *Gynecologic Oncology*, *71*(2), 270–277. https://doi.org/10.1006/gyno.1998.5163

Vassin, V. M., Anantha, R. W., Sokolova, E., Kanner, S., & Borowiec, J. A. (2009). Human RPA phosphorylation by ATR stimulates DNA synthesis and prevents ssDNA accumulation during DNA-replication stress. *Journal of Cell Science*, *122*(22), 4070–4080. https://doi.org/10.1242/jcs.053702

Vaupel, P. (2001). Oxygenation status of malignant tumors: Pathogenesis of hypoxia and significance for tumor therapy. *Seminars in Oncology*, *28*, 29–35. https://doi.org/10.1016/S0093-7754(01)90210-6

Vaupel, P., Höckel, M., & Mayer, A. (2007). Detection and Characterization of Tumor Hypoxia Using pO 2 Histography. *Antioxidants & Redox Signaling*, *9*(8), 1221–1236. https://doi.org/10.1089/ars.2007.1628

Vaupel, P., Mayer, A., Briest, S., & Höckel, M. (2003). Oxygenation gain factor: a novel parameter characterizing the association between hemoglobin level and the oxygenation status of breast cancers. *Cancer Research*, *63*(22), 7634–7637.

Vaupel, P., Thews, O., & Hoeckel, M. (2001). Treatment Resistance of Solid Tumors. *Medical Oncology*, *18*(4), 243–260. https://doi.org/10.1385/MO:18:4:243

Velichko, A. K., Petrova, N. v, Luzhin, A. v, Strelkova, O. S., Ovsyannikova, N., Kireev, I. I., Petrova, N. v, Razin, S. v, & Kantidze, O. L. (2019). Hypoosmotic stress induces R loop formation in nucleoli and ATR/ATM-dependent silencing of nucleolar transcription. *Nucleic Acids Research*, *47*(13), 6811–6825. https://doi.org/10.1093/nar/gkz436

Versteeg, R. (2014). Tumours outside the mutation box. *Nature*, *506*(7489), 438–439. https://doi.org/10.1038/nature13061

Vesela, E., Chroma, K., Turi, Z., & Mistrik, M. (2017). Common chemical inductors of replication stress: Focus on cell-based studies. In *Biomolecules*. https://doi.org/10.3390/biom7010019

Wadsworth, B. J., Lee, C.-M., & Bennewith, K. L. (2022). Transiently hypoxic tumour cell turnover and radiation sensitivity in human tumour xenografts. *British Journal of Cancer*, *126*(11), 1616–1626. https://doi.org/10.1038/s41416-021-01691-5

Wahba, L., Amon, J. D., Koshland, D., & Vuica-Ross, M. (2011). RNase H and Multiple RNA Biogenesis Factors Cooperate to Prevent RNA:DNA Hybrids from Generating Genome Instability. *Molecular Cell*, *44*(6), 978–988. https://doi.org/10.1016/j.molcel.2011.10.017

Walker, J. R., Corpina, R. A., & Goldberg, J. (2001). Structure of the Ku heterodimer bound to DNA and its implications for double-strand break repair. *Nature*, *412*(6847), 607–614. https://doi.org/10.1038/35088000

Walsh, J. C., Lebedev, A., Aten, E., Madsen, K., Marciano, L., & Kolb, H. C. (2014). The Clinical Importance of Assessing Tumor Hypoxia: Relationship of Tumor Hypoxia to Prognosis and Therapeutic Opportunities. *Antioxidants & Redox Signaling*, *21*(10), 1516–1554. https://doi.org/10.1089/ars.2013.5378

Walter, P., & Ron, D. (2011). The Unfolded Protein Response: From Stress Pathway to Homeostatic Regulation. *Science*, *334*(6059), 1081–1086. https://doi.org/10.1126/science.1209038

Wang, C., & Lees-Miller, S. P. (2013). Detection and Repair of Ionizing Radiation-Induced DNA Double Strand Breaks: New Developments in Nonhomologous End Joining. *International Journal of Radiation Oncology*Biology*Physics*, *86*(3), 440–449. https://doi.org/10.1016/j.ijrobp.2013.01.011

Wang, I. X., Grunseich, C., Fox, J., Burdick, J., Zhu, Z., Ravazian, N., Hafner, M., & Cheung, V. G. (2018). Human proteins that interact with RNA/DNA hybrids. *Genome Research*, *28*(9), 1405–1414. https://doi.org/10.1101/gr.237362.118

Wang, J., Yin, Y., Hua, H., Li, M., Luo, T., Xu, L., Wang, R., Liu, D., Zhang, Y., & Jiang, Y. (2009). Blockade of GRP78 sensitizes breast cancer cells to microtubules-interfering agents that induce the unfolded protein response. *Journal of Cellular and Molecular Medicine*, *13*(9b), 3888–3897. https://doi.org/10.1111/j.1582-4934.2009.00873.x

Wang, M., Wey, S., Zhang, Y., Ye, R., & Lee, A. S. (2009). Role of the unfolded protein response regulator GRP78/BiP in development, cancer, and neurological disorders. In *Antioxidants and Redox Signaling*. https://doi.org/10.1089/ars.2009.2485

Ward, I. M., & Chen, J. (2001). Histone H2AX Is Phosphorylated in an ATR-dependent Manner in Response to Replicational Stress. *Journal of Biological Chemistry*, *276*(51), 47759–47762. https://doi.org/10.1074/jbc.C100569200

Weber, C. E., & Kuo, P. C. (2012). The tumor microenvironment. *Surgical Oncology*, *21*(3), 172–177. https://doi.org/10.1016/j.suronc.2011.09.001

Weinstein, I. B., & Case, K. (2008). The History of Cancer Research: Introducing an AACR Centennial Series. *Cancer Research*, *68*(17), 6861–6862. https://doi.org/10.1158/0008-5472.CAN-08-2827

Wek, R. C., & Cavener, D. R. (2007). Translational Control and the Unfolded Protein Response. *Antioxidants & Redox Signaling*, *9*(12), 2357–2372. https://doi.org/10.1089/ars.2007.1764

Wellinger, R. E., Prado, F., & Aguilera, A. (2006). Replication Fork Progression Is Impaired by Transcription in Hyperrecombinant Yeast Cells Lacking a Functional THO Complex. *Molecular and Cellular Biology*, *26*(8), 3327–3334. https://doi.org/10.1128/MCB.26.8.3327-3334.2006

Wennemers, M., Bussink, J., Scheijen, B., Nagtegaal, I. D., van Laarhoven, H. W., Raleigh, J. A., Varia, M. A., Heuvel, J. J., Rouschop, K. M., Sweep, F. C., & Span, P. N. (2011). Tribbles homolog 3 denotes a poor prognosis in breast cancer and is involved in hypoxia response. *Breast Cancer Research*, *13*(4), R82. https://doi.org/10.1186/bcr2934

Wennemers, M., Bussink, J., van den Beucken, T., Sweep, F. C. G. J., & Span, P. N. (2012). Regulation of TRIB3 mRNA and Protein in Breast Cancer. *PLoS ONE*, *7*(11), e49439. https://doi.org/10.1371/journal.pone.0049439

White, D., Rafalska-Metcalf, I. U., Ivanov, A. v., Corsinotti, A., Peng, H., Lee, S.-C., Trono, D., Janicki, S. M., & Rauscher, F. J. (2012). The ATM Substrate KAP1 Controls DNA Repair in Heterochromatin: Regulation by HP1 Proteins and Serine 473/824 Phosphorylation. *Molecular Cancer Research*, *10*(3), 401–414. https://doi.org/10.1158/1541-7786.MCR-11-0134

Wiebe, L. I., & Machulla, H.-J. (1999). Hypoxia: an Introduction. In *Imaging of Hypoxia* (pp. 1–18). Springer Netherlands. https://doi.org/10.1007/978-94-017-1828-8_1

Wigerup, C., Påhlman, S., & Bexell, D. (2016). Therapeutic targeting of hypoxia and hypoxia-inducible factors in cancer. *Pharmacology & Therapeutics*, *164*, 152–169. https://doi.org/10.1016/j.pharmthera.2016.04.009

Wilson, W. R., & Hay, M. P. (2011). Targeting hypoxia in cancer therapy. *Nature Reviews Cancer*, *11*(6), 393–410. https://doi.org/10.1038/nrc3064

Wissink, E. M., Vihervaara, A., Tippens, N. D., & Lis, J. T. (2019). Nascent RNA analyses: tracking transcription and its regulation. *Nature Reviews Genetics*, *20*(12), 705–723. https://doi.org/10.1038/s41576-019-0159-6

Wood, J. G., Johnson, J. S., Mattioli, L. F., & Gonzalez, N. C. (1999). Systemic hypoxia promotes leukocyte-endothelial adherence via reactive oxidant generation. *Journal of Applied Physiology*, *87*(5), 1734–1740. https://doi.org/10.1152/jappl.1999.87.5.1734

Wortel, I. M. N., van der Meer, L. T., Kilberg, M. S., & van Leeuwen, F. N. (2017). Surviving Stress: Modulation of ATF4-Mediated Stress Responses in Normal and Malignant Cells. In *Trends in Endocrinology and Metabolism*. https://doi.org/10.1016/j.tem.2017.07.003

Wyszynski, F. J., Lee, S. S., Yabe, T., Wang, H., Gomez-Escribano, J. P., Bibb, M. J., Lee, S. J., Davies, G. J., & Davis, B. G. (2012). Biosynthesis of the tunicamycin antibiotics proceeds via unique exo-glycal intermediates. *Nature Chemistry*. https://doi.org/10.1038/nchem.1351

Xia, X., Wang, Q., Ye, T., Liu, Y., Liu, D., Song, S., & Zheng, C. (2020). NRF2 ABCB1-mediated efflux and PARP1-mediated dampening of DNA damage contribute to doxorubicin resistance in chronic hypoxic HepG2 cells. *Fundamental & Clinical Pharmacology*, *34*(1), 41–50. https://doi.org/10.1111/fcp.12505

Xu, M., Bi, X., He, X., Yu, X., Zhao, M., & Zang, W. (2016). Inhibition of the mitochondrial unfolded protein response by acetylcholine alleviated hypoxia/reoxygenation-induced apoptosis of endothelial cells. *Cell Cycle*, *15*(10), 1331–1343. https://doi.org/10.1080/15384101.2016.1160985

Yagishita, Y., Gatbonton-Schwager, T. N., McCallum, M. L., & Kensler, T. W. (2020). Current Landscape of NRF2 Biomarkers in Clinical Trials. *Antioxidants*, *9*(8), 716. https://doi.org/10.3390/antiox9080716

Yamamori, T., Meike, S., Nagane, M., Yasui, H., & Inanami, O. (2013). ER stress suppresses DNA double-strand break repair and sensitizes tumor cells to ionizing radiation by stimulating proteasomal degradation of Rad51. *FEBS Letters*, *587*(20), 3348–3353. https://doi.org/10.1016/j.febslet.2013.08.030

Yang, K., Wang, M., Zhao, Y., Sun, X., Yang, Y., Li, X., Zhou, A., Chu, H., Zhou, H., Xu, J., Wu, M., Yang, J., & Yi, J. (2016). A redox mechanism underlying nucleolar stress sensing by

nucleophosmin. *Nature Communications*, *7*(1), 13599. https://doi.org/10.1038/ncomms13599

Yap, T. A., Plummer, R., Azad, N. S., & Helleday, T. (2019). The DNA Damaging Revolution: PARP Inhibitors and Beyond. *American Society of Clinical Oncology Educational Book*, *39*, 185–195. https://doi.org/10.1200/EDBK_238473

Yasuhara, T., Kato, R., Hagiwara, Y., Shiotani, B., Yamauchi, M., Nakada, S., Shibata, A., & Miyagawa, K. (2018). Human Rad52 Promotes XPG-Mediated R-loop Processing to Initiate Transcription-Associated Homologous Recombination Repair. *Cell*, *175*(2), 558-570.e11. https://doi.org/10.1016/j.cell.2018.08.056

Ye, J., Rawson, R. B., Komuro, R., Chen, X., Davé, U. P., Prywes, R., Brown, M. S., & Goldstein, J. L. (2000). ER stress induces cleavage of membrane-bound ATF6 by the same proteases that process SREBPs. *Molecular Cell*. https://doi.org/10.1016/S1097-2765(00)00133-7

Ying, S., Chen, Z., Medhurst, A. L., Neal, J. A., Bao, Z., Mortusewicz, O., McGouran, J., Song, X., Shen, H., Hamdy, F. C., Kessler, B. M., Meek, K., & Helleday, T. (2016). DNA-PKcs and PARP1 Bind to Unresected Stalled DNA Replication Forks Where They Recruit XRCC1 to Mediate Repair. *Cancer Research*, *76*(5), 1078–1088. https://doi.org/10.1158/0008-5472.CAN-15-0608

Yoo, J.-J., Lee, D. H., Cho, Y., Cho, E. J., Lee, J.-H., Yu, S. J., Kim, Y. J., Kim, C. Y., & Yoon, J.-H. (2016). Differential sensitivity of hepatocellular carcinoma cells to suppression of hepatocystin transcription under hypoxic conditions. *Journal of Bioenergetics and Biomembranes*, *48*(6), 581–590. https://doi.org/10.1007/s10863-016-9677-5

Yoshida, H., Matsui, T., Yamamoto, A., Okada, T., & Mori, K. (2001). XBP1 mRNA is induced by ATF6 and spliced by IRE1 in response to ER stress to produce a highly active transcription factor. *Cell*. https://doi.org/10.1016/S0092-8674(01)00611-0

Yuan, J., Narayanan, L., Rockwell, S., & Glazer, P. M. (2000). Diminished DNA repair and elevated mutagenesis in mammalian cells exposed to hypoxia and low pH. *Cancer Research*, *60*(16), 4372–4376.

Yüce, Ö., & West, S. C. (2013). Senataxin, Defective in the Neurodegenerative Disorder Ataxia with Oculomotor Apraxia 2, Lies at the Interface of Transcription and the DNA Damage Response. *Molecular and Cellular Biology*, *33*(2), 406–417. https://doi.org/10.1128/MCB.01195-12

Zannella, V. E., Dal Pra, A., Muaddi, H., McKee, T. D., Stapleton, S., Sykes, J., Glicksman, R., Chaib, S., Zamiara, P., Milosevic, M., Wouters, B. G., Bristow, R. G., & Koritzinsky, M. (2013). Reprogramming Metabolism with Metformin Improves Tumor Oxygenation and Radiotherapy Response. *Clinical Cancer Research*, *19*(24), 6741–6750. https://doi.org/10.1158/1078-0432.CCR-13-1787

Zeman, M. K., & Cimprich, K. A. (2014). Causes and consequences of replication stress. *Nature Cell Biology*, *16*(1), 2–9. https://doi.org/10.1038/ncb2897

Zhang, F., Hamanaka, R. B., Bobrovnikova-Marjon, E., Gordan, J. D., Dai, M.-S., Lu, H., Simon, M. C., & Diehl, J. A. (2006). Ribosomal Stress Couples the Unfolded Protein Response to p53-dependent Cell Cycle Arrest. *Journal of Biological Chemistry*, *281*(40), 30036–30045. https://doi.org/10.1074/jbc.M604674200

Zhang, N., Ji, N., Jiang, W.-M., Li, Z.-Y., Wang, M., Wen, J.-M., Li, Y., Chen, X., & Chen, J.-M. (2015). Hypoxia-induced autophagy promotes human prostate stromal cells survival and ER-stress. *Biochemical and Biophysical Research Communications*, *464*(4), 1107–1112. https://doi.org/10.1016/j.bbrc.2015.07.086

Zhang, P., Li, H., Tan, X., Chen, L., & Wang, S. (2013). Association of metformin use with cancer incidence and mortality: A meta-analysis. *Cancer Epidemiology*, *37*(3), 207–218. https://doi.org/10.1016/j.canep.2012.12.009

Zhang, X., Chiang, H.-C., Wang, Y., Zhang, C., Smith, S., Zhao, X., Nair, S. J., Michalek, J., Jatoi, I., Lautner, M., Oliver, B., Wang, H., Petit, A., Soler, T., Brunet, J., Mateo, F., Angel Pujana, M., Poggi, E., Chaldekas, K., … Li, R. (2017). Attenuation of RNA polymerase II pausing mitigates BRCA1-associated R-loop accumulation and tumorigenesis. *Nature Communications*, *8*(1), 15908. https://doi.org/10.1038/ncomms15908

Zhao, H., & Piwnica-Worms, H. (2001). ATR-Mediated Checkpoint Pathways Regulate Phosphorylation and Activation of Human Chk1. *Molecular and Cellular Biology*, *21*(13), 4129–4139. https://doi.org/10.1128/MCB.21.13.4129-4139.2001

Zhao, R., Jiang, S., Zhang, L., & Yu, Z. (2019). Mitochondrial electron transport chain, ROS generation and uncoupling (Review). *International Journal of Molecular Medicine*. https://doi.org/10.3892/ijmm.2019.4188

Zhao, X., Wei, X., Wang, X., & Qi, G. (2020). Long non-coding RNA NORAD regulates angiogenesis of human umbilical vein endothelial cells via miR-590-3p under hypoxic conditions. *Molecular Medicine Reports*. https://doi.org/10.3892/mmr.2020.11064

Zheng, H., Wu, Y., Guo, T., Liu, F., Xu, Y., & Cai, S. (2020). Hypoxia Induces Growth Differentiation Factor 15 to Promote the Metastasis of Colorectal Cancer via PERK-eIF2α Signaling. *BioMed Research International*, *2020*, 1–12. https://doi.org/10.1155/2020/5958272

Zheng, X.-Y., Xu, J., Chen, X., Li, W., & Wang, T. (2015). Attenuation of oxygen fluctuation-induced endoplasmic reticulum stress in human lens epithelial cells. *Experimental and Therapeutic Medicine*, *10*(5), 1883–1887. https://doi.org/10.3892/etm.2015.2725

Zou, L., & Elledge, S. J. (2003). Sensing DNA Damage Through ATRIP Recognition of RPA-ssDNA Complexes. *Science*, *300*(5625), 1542–1548. https://doi.org/10.1126/science.1083430

Chapter 8 Appendix

8.1 FIJI scripts used for image analyses

```
//Requires LOCI Plugin

dir = getDirectory("Choose a Directory");
list = getFileList(dir);
run("Input/Output...", "jpeg=100 gif=-1 file=.csv copy_column copy_row save_column save_row");

setBatchMode(true);

for (loop=0; loop<lengthOf(list);loop++){
if(endsWith(list[loop],".czi")){ //Edit File format for images i.e. czi or nd2
//open(dir+list[loop]);

updateResults();
run("Clear Results");
IJ.renameResults("Results","Final");

run("Bio-Formats", "open=["+dir+list[loop]+"] color_mode=Default rois_import=[ROI manager] view=Hyperstack stack_order=XYCZT series_2");

Title = getTitle();

//run("Smooth", "stack");
run("Split Channels");

selectWindow("C2-"+Title); // Dapi Channel Number
run("Smooth");
setAutoThreshold("Otsu dark");
//run("Threshold...");
setOption("BlackBackground", false);
run("Convert to Mask");
run("Fill Holes");
run("Watershed");
run("Set Measurements...", "area redirect=None decimal=3");
run("Analyze Particles...", "size=50-300 exclude clear add");
num_Cells = roiManager("Count");
roiManager("Measure");
IJ.renameResults("Results","Final");
run("Flatten");
rename("flat");

run("ROI Map");
roiManager("Reset");

selectWindow("C1-"+Title); //Foci Channel Number
run("Smooth");
run("Find Maxima...", "prominence=50 strict output=[Point Selection]"); // Alter prominence for Foci
//run("Find Maxima...", "noise=15 output=[Point Selection]"); // Alter noise parameter to find foci, test with process>find maxima
roiManager("Add");
selectWindow("flat");
roiManager("select", 0);
run("Flatten");
saveAs("Jpeg", dir+Title+".jpg");
close();

selectWindow("Roi Map");
roiManager("select", 0);
run("Set Measurements...", "min redirect=None decimal=3");
run("Measure");

for (i=1; i<num_Cells+1; i++){
    foci = 0;
    for (j=0; j<nResults; j++) {
        cell = getResult("Min", j);
        if(cell == i){
            foci++;
        }
    }
IJ.renameResults("Results","Temp");
IJ.renameResults("Final","Results");
setResult("Foci", i-1, foci);
IJ.renameResults("Results","Final");
IJ.renameResults("Temp","Results");
}
close("Results");
IJ.renameResults("Final","Results");

saveAs("Results", dir+Title+"_Results.csv");
run("Close All");
close("Results");
roiManager("Reset");
}
}

setBatchMode(false);
```

Figure S2.1 The script used in FIJI/ImageJ to quantify foci. The script was written by Dr Rhodri Wilson, University of Oxford.

```java
import java.awt.Color;

import ij.IJ;
import ij.ImagePlus;
import ij.gui.GenericDialog;
import ij.gui.Overlay;
import ij.gui.Roi;
import ij.measure.ResultsTable;
import ij.plugin.PlugIn;
import ij.plugin.filter.EDM;
import ij.plugin.filter.MaximumFinder;
import ij.plugin.filter.RankFilters;
import ij.plugin.filter.ThresholdToSelection;
import ij.process.AutoThresholder;
import ij.process.Blitter;
import ij.process.ByteProcessor;
import ij.process.FloatProcessor;
import ij.process.FloodFiller;
import ij.process.ImageProcessor;
import ij.process.ShortProcessor;

public class Measuring_Rings implements PlugIn {

    private String threshold = "Huang";
    private double openingRadius = 10;
    private double ringGap = 2;
    private double ringWidth = 15;
    private boolean showImages = false;
    private boolean showROIs = true;
    private boolean showLabels = true;
    private boolean showTouchingBorder = false;


    @Override
    public void run(String arg) {
        ImagePlus imp = IJ.getImage();
        if (imp == null)
            return;


        GenericDialog gd = new GenericDialog(getClass().getSimpleName().replace("_", " "));

        String[] methods = AutoThresholder.getMethods();
        gd.addChoice("Threshold method", methods, threshold);
        gd.addNumericField("Nucleus_cleanup_radius", openingRadius, 1);
        gd.addNumericField("Gap_to_ring", ringGap, 1);
        gd.addNumericField("Ring_width", ringWidth, 1);
        gd.addCheckbox("Show_overlay", showROIs);
        gd.addCheckbox("Show_cell_names", showLabels);
        gd.addCheckbox("Show_labelled_images", showImages);
        gd.addCheckbox("Show_touching_border", showTouchingBorder);
        gd.showDialog();
        if (gd.wasCanceled())
            return;
        threshold = gd.getNextChoice();
        openingRadius = gd.getNextNumber();
        ringGap = gd.getNextNumber();
        ringWidth = gd.getNextNumber();
        showROIs = gd.getNextBoolean();
        showLabels = gd.getNextBoolean();
        showImages = gd.getNextBoolean();
        showTouchingBorder = gd.getNextBoolean();



        int width = imp.getWidth();
        int height = imp.getHeight();


        ImageProcessor ipNuclei = imp.getStack().getProcessor(1).duplicate();
        ImageProcessor ipCytoplasm = imp.getStack().getProcessor(2).duplicate();

        ipNuclei.blurGaussian(1);
        ipNuclei.setAutoThreshold(threshold, true, ImageProcessor.NO_LUT_UPDATE);
        ByteProcessor bp = new ByteProcessor(width, height);
        float threshold = (float)ipNuclei.getMinThreshold();
        for (int i = 0; i < width*height; i++) {
            if (ipNuclei.getf(i) > threshold)
                bp.setf(i, 255f);
        }

        RankFilters rf = new RankFilters();
        rf.rank(bp, openingRadius, RankFilters.MIN);
        //rf.rank(bp, openingRadius, RankFilters.MAX);

        EDM edm = new EDM();
        edm.toWatershed(bp);


        // Determine Voronoi separation lines
        int backgroundValue = (byte)255;
        FloatProcessor fpEDM = edm.makeFloatEDM(bp, backgroundValue, false);
        fpEDM.multiply(-1);
```

```
        int maxOutputType = MaximumFinder.SEGMENTED;
        boolean isEDM = false;
        ByteProcessor bpSeparation = new MaximumFinder().findMaxima(fpEDM, 0.5, ImageProcessor.NO_THRESHOLD, maxOutputType, false, isEDM);
    bpSeparation.invert();

        // Expand the nuclei to have a bit of gap
        ByteProcessor bpGap = (ByteProcessor)bp.duplicate();
        rf.rank(bpGap, ringGap, RankFilters.MAX);

        // Expand the nuclei to compute the ring
        ByteProcessor bpRing = (ByteProcessor)bpGap.duplicate();
        rf.rank(bpRing, ringWidth, RankFilters.MAX);

        // Subtract the separation lines
        bpRing.copyBits(bpSeparation, 0, 0, Blitter.SUBTRACT);

        // Create a labelled image of the expanded nuclei
        ShortProcessor ipLabels = labelImage(bpRing, true);

        // Subtract the nuclei from the ring image
        bpRing.copyBits(bpGap, 0, 0, Blitter.SUBTRACT);

        // Measure intensities & areas
        int nCells = (int)(ipLabels.getStatistics().max);
        double[] nPixelsNuclei = new double[nCells];
        double[] nPixelsRing = new double[nCells];
        double[] sumNuclei = new double[nCells];
        double[] sumRing = new double[nCells];
        boolean[] touchesBorder = new boolean[nCells];
        for (int y = 0; y < height; y++) {
            for (int x = 0; x < width; x++) {
                int label = (int)(ipLabels.getf(x, y));
                if (label == 0)
                    continue;
                int ind = label-1;
                if (bp.getf(x, y) != 0f) {
                    nPixelsNuclei[ind]++;
                    sumNuclei[ind] += ipCytoplasm.getf(x, y);
                }
                if (bpRing.getf(x, y) != 0f) {
                    nPixelsRing[ind]++;
                    sumRing[ind] += ipCytoplasm.getf(x, y);
                }
                // Check if touching the border
                if (x == 0 || x == width-1 || y == 0 || y == height-1)
                    touchesBorder[ind] = true;
            }
        }

        // Show the results
        ResultsTable rt = ResultsTable.getResultsTable();
        if (rt == null)
            rt = new ResultsTable();

        for (int i = 0; i < nCells; i++) {
            if (!showTouchingBorder && touchesBorder[i])
                continue;

            rt.incrementCounter();
            rt.addLabel(imp.getShortTitle());
            rt.addValue("Cell", i + 1);
            rt.addValue("Nucleus num pixels", nPixelsNuclei[i]);
            rt.addValue("Nucleus mean intensity", sumNuclei[i] / nPixelsNuclei[i]);
            rt.addValue("Cytoplasm ring num pixels", nPixelsRing[i]);
            rt.addValue("Cytoplasm ring mean intensity", sumRing[i] / nPixelsRing[i]);
            if (showTouchingBorder)
                rt.addValue("Touching border", touchesBorder[i] ? "True" : "");
        }
        rt.show("Results");

        if (!showImages && !showROIs)
            return;

        // Create labelled images
        bp.max(1);
        bpRing.max(1);
        ImageProcessor ipNucleiLabels = ipLabels.duplicate();
        ipNucleiLabels.copyBits(bp, 0, 0, Blitter.MULTIPLY);
        ImageProcessor ipRingLabels = ipLabels.duplicate();
        ipRingLabels.copyBits(bpRing, 0, 0, Blitter.MULTIPLY);

        ThresholdToSelection tts = new ThresholdToSelection();
        if (showROIs) {
            Overlay overlay = new Overlay();
            for (int label = 1; label <= nCells; label++) {
                ipNucleiLabels.setThreshold(label, label, ImageProcessor.NO_LUT_UPDATE);
                Roi roiNucleus = tts.convert(ipNucleiLabels);
                roiNucleus.setStrokeColor(Color.RED);

                ipRingLabels.setThreshold(label, label, ImageProcessor.NO_LUT_UPDATE);
                Roi roiRing = tts.convert(ipRingLabels);
                roiRing.setStrokeColor(Color.YELLOW);
```

```
                roiRing.setStrokeColor(Color.YELLOW);


                if (showLabels) {
                    roiNucleus.setName("Cell_" + label);
                    roiRing.setName("");
                } else {
                    roiNucleus.setName("Nucleus_" + label);
                    roiRing.setName("Ring_" + label);
                }

                overlay.add(roiNucleus);
                overlay.add(roiRing);
            }
            overlay.drawNames(true);
            imp.setOverlay(overlay);
        }




        if (showImages) {
            ImagePlus impNuclei = new ImagePlus("Nucleus labels", ipNucleiLabels);
            IJ.run(impNuclei, "Glasbey", null);
            ipNucleiLabels.setMinAndMax(0, 255);
            impNuclei.show();
            ImagePlus impRing = new ImagePlus("Nucleus ring labels", ipRingLabels);
            IJ.run(impRing, "Glasbey", null);
            ipRingLabels.setMinAndMax(0, 255);
            impRing.show();
        }

    }




    public static ShortProcessor labelImage(ByteProcessor bp, boolean conn8) {
        int w = bp.getWidth();
        int h = bp.getHeight();
        short shortMax = (short)65535;
        ShortProcessor sp = new ShortProcessor(w, h);
        byte[] pxByte = (byte[])bp.getPixels();
        short[] pxShort = (short[])sp.getPixels();
        for (int i = 0; i < pxByte.length; i++) {
            if (pxByte[i] != 0)
                pxShort[i] = shortMax;
        }
        // Loop through and flood fill
        FloodFiller ff = new FloodFiller(sp);
        double label = 0;
        for (int i = 0; i < pxShort.length; i++) {
            if (pxShort[i] == shortMax) {
                label++;
                sp.setValue(label);
                if (conn8)
                    ff.fill8(i % w, i / w);
                else
                    ff.fill(i % w, i / w);
            }
        }
        sp.setMinAndMax(0, label);
        return sp;
    }


}
```

Figure S2.2. The algorithm used in FIJI/ImageJ to quantify nuclear intensity. The script was written by Dr Kienan Savage, Queen's University Belfast.

8.2 Supplementary data

Table S4.1 1113 hypoxia-induced UPR genes

AACS	CDK4	FAM210A	KLF11	P4HA2	RRM2B	TMEM241
AADAT	CDKAL1	FAM215A	KLF4	P4HB	RSL24D1	TMEM263
AAED1	CDKL5	FAM219A	KLF5	PACSIN2	RSPH3	TMEM39A
AAK1	CDKN1A	FAM220A	KLF7	PADI1	RSRC2	TMEM41B
AARS	CDKN1B	FAM222A	KLHDC10	PAG1	RUFY3	TMEM45A
ABCA5	CDON	FAM3C	KLHDC7B	PAICS	RUNX1	TMEM50B
ABCB6	CDT1	FAM43A	KLHL28	PAN2	RYBP	TMEM98
ABHD1	CEBPB	FAM53C	KLHL29	PANX1	SAP30	TNFAIP3
ABL2	CEBPG	FAM84B	KRBOX4	PARD3B	SARAF	TNFRSF10B
ABLIM3	CENPM	FANCA	KRCC1	PARP16	SARS	TNFRSF9
ABTB1	CENPQ	FANCC	LACC1	PARP2	SART1	TNFSF9
ABTB2	CEP120	FANCD2	LAMB3	PATL1	SAT1	TP53
ACAP1	CEP128	FANCG	LAMP3	PAWR	SAV1	TP53BP2
ACBD3	CEP135	FANCI	LARP1B	PCBP3	SCAND2P	TP53I3
ACD	CEP57	FAS	LARP6	PCGF5	SCAPER	TPBG
ACER2	CEP85L	FBXL3	LBH	PCIF1	SCN9A	TPCN2
ACTA2	CGGBP1	FBXL6	LCA5	PCK2	SDC4	TPD52
ADAM17	CGRRF1	FBXO16	LDLRAD3	PCSK5	SDCBP	TPP2
ADAMTS1	CHAC1	FBXO32	LDLRAD4	PDCD10	SDF2L1	TRAF1
ADCK2	CHCHD3	FBXO4	LGALS8	PDCD4	SDSL	TRAM1
ADM	CHD1L	FBXO42	LHFPL2	PDE4D	SEC11C	TRIB3
ADM2	CHD2	FBXW7	LHX9	PDGFC	SEC23B	TRIM16
ADPRHL2	CHEK1	FDXR	LIMS1	PDIA3	SEC24A	TRIM16L
AEN	CHMP4C	FEM1C	LIN54	PDIA4	SEC24D	TRIM27
AFF3	CHSY1	FIBIN	LINC00313	PDIA6	SEC61A1	TRIM36
AGPAT5	CISD2	FKBP14	LINC00319	PDK1	SEC61G	TRIM38
AIFM2	CITED2	FKBP2	LINC00471	PDK3	SEL1L	TRIM5
AKAP17A	CLGN	FLYWCH1	LINC00511	PEA15	SELK	TRIM65
AKAP3	CLIC4	FNBP1	LINC00649	PEAR1	SEPHS2	TRIM9
AKNA	CLIP4	FNDC3B	LINC00662	PELI1	SERINC1	TRIQK
AKTIP	CLK1	FOS	LINC00909	PER1	SERINC3	TRIT1
ALDH16A1	CLK3	FOSL2	LINC00963	PER2	SERPINB8	TRMT1
ALDH1A3	CMSS1	FOXC1	LMO4	PFKFB4	SERPINI1	TRNAU1AP
ALDH1L2	CNOT8	FOXO6	LONP1	PFKP	SERTAD1	TSC22D3
ALDH4A1	COG3	FOXP2	LPO	PGF	SESN1	TSLP
ALG12	COMTD1	FOXRED1	LRAT	PGM1	SESN2	TSPAN5
ALG2	COPG1	FRRS1	LRRC42	PHGDH	SETX	TSPYL2
ALKBH5	CORO1A	FYN	LRRC49	PHLDA3	SFI1	TSTD2
ALPK1	COX19	FZD7	LRRC8E	PI4K2A	SGK1	TTLL7

AMPH	CPEB2	FZD8	LRRFIP1	PIGA	SGK3	TUBE1
AMZ2P1	CPM	GABARAPL1	LUCAT1	PIM1	SGPL1	TUFT1
ANG	CREB3L2	GADD45A	LURAP1L	PIP5KL1	SGTB	TULP3
ANK2	CREB3L4	GADD45B	LYSMD3	PJA2	SH2D4A	TVP23B
ANKMY2	CREB5	GARS	MAFA	PKIA	SH2D5	TWIST1
ANKRD37	CRELD1	GAS5	MAFF	PLAGL1	SH3BGR	TXNDC11
ANO6	CRELD2	GATA6	MAGI1	PLCD1	SH3BP4	TXNIP
ANXA1	CRYBB2P1	GATM	MAGT1	PLCH1	SHB	TYK2
ANXA5	CSF1	GBE1	MAMDC4	PLCXD2	SHCBP1	TYMS
ANXA6	CSGALNACT2	GCC1	MANF	PLEKHA2	SHMT2	TYRO3
AP1AR	CSRNP1	GCH1	MAP1LC3B	PLEKHA8	SIAH1	UAP1
AP3D1	CSRP2	GCLC	MAP1LC3B2	PLEKHF1	SIAH2	UBA6
APAF1	CTAGE5	GDF15	MAP2K1	PLEKHG1	SIRT2	UBA6-AS1
APBB3	CTBP2	GFPT1	MAP3K8	PLK2	SLC10A7	UBALD2
APLF	CTDP1	GLRX	MAP4K5	PLK3	SLC16A1	UBC
APOBEC3C	CTH	GLYCTK	MAPK7	PLXNA2	SLC16A3	UBE2J1
APOL6	CTNS	GMDS-AS1	MARS	PMAIP1	SLC1A4	UBN2
APTR	CYLD	GMNN	MAST4	PNLIPRP3	SLC22A15	UBTD2
ARC	DAB2	GMPPA	MBNL2	PNPLA8	SLC25A10	UFM1
ARF4	DACT1	GMPPB	MBNL3	PNRC1	SLC25A29	UGCG
ARFGAP2	DARS	GNA13	MCC	PNRC2	SLC25A36	UGDH
ARFGAP3	DCLK1	GOLGA1	MCF2L	POLA1	SLC25A45	UGP2
ARG2	DCLK2	GOLGA4	MCM2	POLD1	SLC2A1	ULBP1
ARHGAP28	DDB2	GOLGA5	MCM3	POLH	SLC2A3	ULBP2
ARHGAP35	DDIT3	GOLGA8A	MCM4	POLI	SLC30A1	ULK3
ARHGEF2	DDIT4	GOLPH3L	MCM5	POLL	SLC30A4	UNC13B
ARHGEF7	DDR2	GOLT1B	MCM6	PPIL1	SLC33A1	UNC5B
ARID3A	DDX41	GORAB	MCM7	PPIL3	SLC35B1	UPF3A
ARID5A	DDX50	GOT1	MCM8	PPIP5K1	SLC38A1	UPP1
ARIH2	DDX59	GPNMB	MDM2	PPM1D	SLC38A2	UPRT
ARL5B	DENND2A	GPR1	MDM4	PPME1	SLC39A14	USO1
ARL6IP6	DERL2	GPRC5A	MEF2A	PPP1R13B	SLC3A2	USP1
ARMCX3	DERL3	GPT2	MET	PPP1R15A	SLC41A2	USP31
ARRDC2	DESI2	GRB10	METRNL	PPP1R16A	SLC6A9	USP37
ARRDC3	DHRS3	GRPEL2	MEX3C	PPP1R3B	SLC7A1	VAC14
ARRDC4	DHX32	GRSF1	MIIP	PPP1R3E	SLC7A11	VEGFA
ARVCF	DIRC2	GTF2IRD1	MIR22HG	PPP2R5B	SLC7A11-AS1	VEPH1
ASCC3	DLC1	GTPBP2	MIR3189	PPP3CC	SLC7A5	VIMP
ASNS	DLGAP1-AS2	GXYLT1	MIR503HG	PREB	SLC9A1	VLDLR
ATAD3A	DLL4	GXYLT2	MIS12	PREP	SLCO1B3	VPS35
ATAD3B	DNAJB11	GYG1	MKRN2	PREPL	SLCO5A1	VPS37C

ATF2	DNAJB2	GZF1	MKS1	PRIM1	SLFN11	WARS
ATF3	DNAJB4	HAUS6	MLH1	PRIM2	SLFN13	WBP4
ATF4	DNAJB5	HAX1	MME	PRIMPOL	SLFN5	WDR19
ATG13	DNAJB9	HBEGF	MMS19	PRKAA2	SLIT3	WDR25
ATL1	DNAJC1	HBP1	MND1	PRKAB2	SMAD9	WDR45B
ATP1A2	DNAJC25	HDAC9	MOAP1	PRKCA	SMAP1	WDR54
ATP2A2	DNAJC3	HECA	MOCOS	PRKCE	SMG6	WDR76
ATP2A3	DNAJC3-AS1	HERC3	MOSPD2	PRKD1	SMOX	WDR90
ATP6V1C2	DNAJC6	HERPUD1	MOV10L1	PRPF19	SMS	WDTC1
ATP8B2	DNMT1	HEY1	MRPL12	PRSS16	SMYD3	WIPF2
ATXN1	DNTTIP1	HGS	MSC	PSAT1	SNHG1	XBP1
ATXN2L	DOCK7	HID1	MSH4	PSG4	SNHG15	XIAP
AVPI1	DPYSL4	HINFP	MSMO1	PSMG1	SNHG7	XPNPEP1
AZI2	DTL	HIST3H2BB	MSTO1	PSPH	SNHG8	XPOT
B4GALT1	DUS3L	HK2	MSTO2P	PTHLH	SNRPA	YARS
BBC3	DUSP1	HKDC1	MTFP1	PTPN14	SNX18P7	YEATS2
BCL10	DUSP10	HMOX1	MTHFD1	PTPRB	SNX22	YEATS4
BEST1	DUSP16	HNRNPL	MTHFD1L	PTPRH	SOS2	YIPF5
BET1	DUSP28	HOXB9	MTHFD2	PUS7	SOWAHC	YPEL2
BEX2	DUSP3	HRASLS	MTMR4	PXK	SOX4	YPEL3
BHLHA15	DUSP6	HS1BP3	MTR	RAB1A	SOX9	YPEL5
BHLHE40	DUSP8	HSF2BP	MUTYH	RAB20	SPATA4	ZBTB17
BIRC2	DYRK1B	HSP90B1	MXD1	RAB33B	SPCS2	ZBTB34
BLOC1S2	DYRK3	HSPA13	MXI1	RAB39B	SPCS3	ZBTB38
BLOC1S3	DYRK4	HSPA5	MYBL1	RAB3GAP2	SPIRE1	ZBTB41
BLOC1S6	E2F1	HSPA9	MYBL2	RAB5A	SPIRE2	ZBTB5
BLZF1	E2F7	HSPBAP1	MYC	RAB5B	SPRY1	ZBTB8A
BNIP3L	EAF2	HSPBP1	MYCL	RABL2B	SRD5A3	ZCWPW1
BRCA1	ECSIT	HYOU1	MYO1E	RAD51	SREBF1	ZDBF2
BRWD3	EDA2R	IARS	MZF1	RAD51AP1	SRP68	ZEB2
BTAF1	EDEM1	IBA57	N4BP2	RAD54L	SSR1	ZFAND2A
BTBD10	EDEM3	IBTK	N4BP3	RAD9A	STAC3	ZFP69B
BTBD11	EEFSEC	ICK	NANS	RAI14	STAG1	ZFYVE1
BTG1	EFCAB2	ID2	NBAS	RALA	STAMBP	ZGLP1
BTG2	EFNA3	IER5	NBR2	RAP2A	STARD4	ZHX2
C10orf10	EFNA5	IFRD1	NCAPH2	RAPGEF2	STARD5	ZKSCAN1
C10orf25	EFNB1	IGFBP3	NCBP1	RASGEF1B	STAT2	ZMAT3
C12orf73	EGLN1	IKBIP	NCKAP5L	RASSF1	STC2	ZNF165
C14orf28	EGLN3	IL1RAP	NCOA7	RB1	STK10	ZNF22
C16orf72	EGR1	IL20RB	NDEL1	RBM39	STK32A	ZNF292
C19orf48	EHD4	IL23A	NDNF	RBMS3	STOM	ZNF367
C20orf194	EIF1	IL6ST	NDOR1	RCBTB2	STX3	ZNF432

C21orf2	EIF1B	ING1	NDRG1	RCC1	STX5	ZNF536
C3orf67	EIF2AK3	ING3	NDUFA4L2	RDH10	SUCO	ZNF555
C6orf48	EIF2S2	INHBE	NECAB1	RECQL4	SUSD6	ZNF596
C6orf62	EIF3D	INPP5B	NEDD4	RELB	SYBU	ZNF621
C7orf57	EIF4EBP1	INSIG1	NEDD4L	RELT	SYNE1	ZNF627
C8orf58	EIF5	INSIG2	NELFB	REPS2	SYT5	ZNF653
C9orf72	ELL2	INTS7	NFIL3	RETSAT	SYTL1	ZNF654
CA13	EMC9	IPMK	NFKB2	RFC1	SYTL2	ZNF697
CADPS2	EML2	IQCB1	NFKBIA	RFC2	SYVN1	ZNF699
CALCOCO1	ENOSF1	IQGAP3	NFKBIB	RFC4	TARS	ZNF70
CALCOCO2	ENTPD7	IRAK1	NFKBIE	RFX2	TAX1BP1	ZNF770
CALR	EPC1	IRAK2	NFKBIL1	RGS20	TBX3	ZNF773
CALU	EPC2	IRF1	NFX1	RHBDF2	TCP11L2	ZNF787
CAMK1D	EPHB3	IRF2BP2	NGLY1	RHEBL1	TELO2	ZNF79
CARS	EPRS	IRS2	NPHP4	RHOB	TENM4	ZNF804A
CATSPER2P1	ERICH2	IRX6	NPIPP1	RIMKLA	TEP1	ZNF841
CBX4	ERMAP	ISG20	NR1D2	RIMS3	TERC	ZSCAN12P1
CCDC163P	ERO1A	ITCH	NR2C2AP	RIOK3	TET2	ZSWIM6
CCDC171	ERO1B	ITPR1	NR3C1	RLF	TFG	ZW10
CCDC174	ERO1L	JDP2	NR4A1	RMI1	TGDS	
CCDC18	ERP44	JHDM1D-AS1	NR4A2	RMND1	TGFBR1	
CCDC186	ERRFI1	JMJD6	NR4A3	RNASE4	TGIF1	
CCDC34	ESCO1	JOSD1	NRBF2	RNASEH2A	THAP1	
CCDC59	ESRP1	JUND	NSMAF	RND1	THAP10	
CCDC86	ESYT1	KANSL3	NT5DC3	RNF122	THAP2	
CCDC9	ETS2	KCMF1	NUCB1	RNF185	THAP5	
CCNG2	EVI5L	KCNJ3	NUCB2	RNF19A	THAP9-AS1	
CCNO	EXO1	KCNK1	NUPR1	RNF19B	THOP1	
CCPG1	EXOC6B	KCTD5	OAS3	RNF24	TIFA	
CCSAP	EXOSC6	KCTD9	OLMALINC	RNMT	TIGAR	
CD83	EYA1	KDM3A	OPTN	RNU5E-1	TIMELESS	
CDC42EP3	EZH2	KDM4A	ORC6	ROCK1P1	TIMM17A	
CDC45	F3	KDM4B	OS9	RPL23AP7	TIMM44	
CDC6	FAM107B	KDM4C	OSBP	RPS6KA2	TIMP3	
CDCA2	FAM110A	KDM7A	OSBPL10	RPS6KA4	TJP2	
CDCA5	FAM129A	KIAA1211	OSBPL6	RPS6KA5	TLN2	
CDCA7L	FAM13A	KIAA1324L	OSER1	RPTOR	TMCO4	
CDH15	FAM167A	KIAA1841	OSGIN1	RRAGC	TMED7	
CDH3	FAM189A1	KIF5A	OSTC	RRBP1	TMEM170A	
CDK2AP2	FAM207A	KLF10	P4HA1	RRM2	TMEM2	

Table S4.2 103 hypoxia-induced UPR genes that play a role in the response to DNA damage

ACTA2	ESCO1	KCTD5	PRIM1	SHLD1	YPEL5
ARIH2	EXO1	KDM4A	PRIMPOL	SHLD2	ZBTB17
ATG13	FANCA	MCM6	PTPN14	SLC10A7	ZNF367
ATXN2L	FANCC	MCM8	RAD51	SLC25A36	
BBC3	FANCD2	MLH1	RAD51AP1	SLFN11	
BIRC2	FANCG	MMS19	RAD54L	SNRPA	
BRCA1	FANCI	MND1	RAD9A	SOX9	
BTAF1	FBXO32	MOSPD2	RB1	STAG1	
C16orf72	FBXO42	MYBL1	RBM39	SYNE1	
CCNG2	FBXW7	NFKBIA	RLF	TAX1BP1	
CDC6	FNDC3B	ORC6	RMI1	TMEM2	
CDCA2	GATA6	OSTC	RNASEH2A	TP53	
CDCA5	GNA13	PAN2	RNF185	TRNAU1AP	
CDH3	GOT1	PATL1	RRAGC	UFM1	
CDKN1B	GZF1	PAWR	RRM2	UGP2	
CEBPB	IBTK	PDCD10	RUNX1	USP1	
CLK3	IL6ST	POLH	SART1	USP37	
CYLD	IRX6	POLL	SDC4	VAC14	
DNTTIP1	JMJD6	PPIL1	SDCBP	VPS37C	
EPC1	KANSL3	PPP1R3B	SETX	YIPF5	

Table S4.3 97 hypoxia-induced UPR genes whose proteins are enriched on chromatin, Hu-stalled replication forks or both

	Enriched on unperturbed chromatin	Enriched at Hu-stalled replication forks
BRCA1	✓	✓
CDCA7L	✓	✓
FANCA	✓	✓
FANCD2	✓	✓
FANCI	✓	✓
PDCD4	✓	✓
POLD1	✓	✓
RAD9A	✓	✓
SETX	✓	✓
STAG1	✓	✓
UBC	✓	✓

ZNF22	✓	✓
ALKBH5	✓	
ARID3A	✓	
BTAF1	✓	
CCDC86	✓	
CDC45	✓	
CDCA5	✓	
CGGBP1	✓	
CHD1L	✓	
CHD2	✓	
CTBP2	✓	
DDX41	✓	
DNMT1	✓	
DTL	✓	
DUS3L	✓	
EEFSEC	✓	
EXO1	✓	
FLYWCH1	✓	
GATA6	✓	
GZF1	✓	
HNRNPL	✓	
HOXB9	✓	
HSPBP1	✓	
IRF2BP2	✓	
MCM2	✓	
MCM3	✓	
MCM4	✓	
MCM5	✓	
MCM6	✓	
MCM7	✓	
MCM8	✓	
NCBP1	✓	
NELFB	✓	
ORC6	✓	
PARP2	✓	
POLA1	✓	
PPM1D	✓	
PPME1	✓	
PRIM1	✓	

PRIM2	✓	
PSMG1	✓	
PUS7	✓	
RBM39	✓	
RCC1	✓	
RECQL4	✓	
RFC1	✓	
RFC2	✓	
RFC4	✓	
RNASEH2A	✓	
RNMT	✓	
SART1	✓	
SDCBP	✓	
TELO2	✓	
TIGAR	✓	
TIMELESS	✓	
TP53	✓	
TRMT1	✓	
UAP1	✓	
UBN2	✓	
UGDH	✓	
USP1	✓	
USP37	✓	
WDR76	✓	
XPOT	✓	
YEATS4	✓	
ZHX2	✓	
ZNF787	✓	
ZNF79	✓	
ACTA2		✓
ARIH2		✓
ASCC3		✓
CALR		✓
DDB2		✓
EIF3D		✓
FAM3C		✓
GOT1		✓
HMOX1		✓
MAPK7		✓

NANS		✓
NGLY1		✓
P4HB		✓
PCK2		✓
RAD54L		✓
RMI1		✓
SAP30		✓
VAC14		✓

Table S4.4 79 hypoxia-induced UPR genes that are part of the RNA/DNA hybrid interactome

AARS	DDX50	MCM4	PRPF19
ACAP1	DNMT1	MCM5	RAB1A
AKAP17A	EEFSEC	MCM6	RB1
ANXA6	EHD4	MCM7	RBM39
AP3D1	EIF2S2	MND1	RFC1
APOBEC3C	EIF3D	MRPL12	RFC4
ARF4	EPRS	MTHFD1	RNASEH2A
ARHGEF2	EXOSC6	MTHFD1L	RRBP1
ASCC3	FNBP1	MYO1E	RSL24D1
ASNS	GARS	NCBP1	SARS
ATAD3A	GFPT1	NFKB2	SART1
ATP2A2	HNRNPL	OAS3	SETX
ATXN2L	HYOU1	P4HB	SRP68
CCDC59	IARS	PAICS	STK10
CCDC86	KCNK1	PARP2	TARS
CLIC4	LONP1	PCBP3	TFG
CORO1A	LRRFIP1	PDIA6	TRAF1
DARS	MARS	PFKP	WARS
DDB2	MCM2	PHGDH	YARS
DDX41	MCM3	POLD1	

8.3 Presentations

UK DNA Replication Conference, Biochemical Society, University of Birmingham – 2022 (Elevated Oral Presentation) 'Hypoxia-induced R-loops and oxidative stress'

Oncology Departmental Seminar Series, University of Oxford – 2022 (Oral Presentation) 'Hypoxia-induced R-loops and oxidative stress'

Invited Talk, Max Planck Institute for Biology of Ageing, Cologne – 2021 (Oral Presentation) 'Hypoxia-induced SETX links replication stress with the unfolded protein response'

Oncology Departmental Seminar Series, University of Oxford – 2021 (Oral Presentation) 'Hypoxia-induced SETX links replication stress with the unfolded protein response'

Department of Oncology Annual Student Symposium, University of Oxford – 2020 (Oral Presentation)

Department of Oncology Annual Student Symposium, University of Oxford – 2019 (Poster)

8.4 Published papers from this thesis

Hypoxia-induced SETX links replication stress with the unfolded protein response. Ramachandran S*, **Ma TS***, Griffin J, Ng N, Foskolou IP, Hwang MS, Victori P, Cheng WC, Buffa FM, Leszczynska KB, El-Khamisy SF, Gromak N, Hammond EM. Nat Commun. 2021 Jun 17;12(1):3686.

Links between the unfolded protein response and the DNA damage response in hypoxia: a systematic review. Bolland H*, **Ma TS***, Ramlee S, Ramadan K, Hammond EM. Biochem Soc Trans. 2021 Jun 30;49(3):1251-1263.

Replication catastrophe induced by cyclic hypoxia leads to increased APOBEC3B activity. Bader SB, **Ma TS**, Simpson CJ, Liang J, Maezono SEB, Olcina MM, Buffa FM, Hammond EM**.** Nucleic Acids Res. 2021 Jul 21;49(13):7492-7506.

*indicates shared first authorship

nature COMMUNICATIONS

ARTICLE

https://doi.org/10.1038/s41467-021-24066-z OPEN

Hypoxia-induced SETX links replication stress with the unfolded protein response

Shaliny Ramachandran[1,7], Tiffany S. Ma[1,7], Jon Griffin[2,3], Natalie Ng[1], Iosifina P. Foskolou[1], Ming-Shih Hwang[1], Pedro Victori[1], Wei-Chen Cheng[1], Francesca M. Buffa[1], Katarzyna B. Leszczynska[1,6], Sherif F. El-Khamisy[2,4], Natalia Gromak[5] & Ester M. Hammond[1✉]

Tumour hypoxia is associated with poor patient prognosis and therapy resistance. A unique transcriptional response is initiated by hypoxia which includes the rapid activation of numerous transcription factors in a background of reduced global transcription. Here, we show that the biological response to hypoxia includes the accumulation of R-loops and the induction of the RNA/DNA helicase SETX. In the absence of hypoxia-induced SETX, R-loop levels increase, DNA damage accumulates, and DNA replication rates decrease. Therefore, suggesting that, SETX plays a role in protecting cells from DNA damage induced during transcription in hypoxia. Importantly, we propose that the mechanism of SETX induction in hypoxia is reliant on the PERK/ATF4 arm of the unfolded protein response. These data not only highlight the unique cellular response to hypoxia, which includes both a replication stress-dependent DNA damage response and an unfolded protein response but uncover a novel link between these two distinct pathways.

[1] Department of Oncology, Oxford Institute for Radiation Oncology, University of Oxford, Oxford, UK. [2] Department of Molecular Biology and Biotechnology, Healthy Lifespan and Neuroscience Institute, Firth Court, University of Sheffield, Sheffield, UK. [3] Department of Histopathology, Sheffield Teaching Hospitals NHS Foundation Trust, Sheffield, UK. [4] Institute of Cancer Therapeutics, University of Bradford, Bradford, UK. [5] Sir William Dunn School of Pathology, University of Oxford, Oxford, UK. [6] Present address: Laboratory of Molecular Neurobiology, Neurobiology Center, Nencki Institute of Experimental Biology, Polish Academy of Sciences, Warsaw, Poland. [7] These authors contributed equally: Shaliny Ramachandran, Tiffany S. Ma. ✉email: ester.hammond@oncology.ox.ac.uk

The microenvironment of the majority of solid tumours is characterised by regions of low oxygen (hypoxia), which result from abnormal vasculature and increased oxygen demand. Tumour hypoxia plays a pivotal role in tumorigenesis and has been associated with increased aggressiveness, metastasis, resistance to radiotherapy, and poor patient prognosis[1]. The level of hypoxia associated with radiation resistance (<0.13% O_2) is characterised by a rapid induction of replication stress, which is defined as the slowing or stalling of replication forks. We have attributed hypoxia-induced replication stress to decreased nucleotide availability[2–4]. Hypoxia-induced replication stress leads to the induction of an ATR- and ATM-dependent DNA damage response (DDR), although hypoxia-induced replication stress is insufficient to induce ATM-mediated signalling and increased levels of heterochromatic histone marks, notably H3K9me3 are also required[5–7]. Importantly, both hypoxia-induced ATR and ATM activity occur in the absence of detectable DNA damage[8]. Transcriptional stress, defined as global repression of RNA synthesis, has also been identified in the hypoxic conditions which lead to a DDR[9].

R-loops are 3–stranded nucleic acid structures that are linked to transcription and can contribute to replication stress[10]. R-loops are comprised of an RNA/DNA hybrid and a displaced single-stranded DNA (ssDNA), for recent reviews see[11–13]. R-loops form within the genome at actively transcribed genes preferentially occurring at gene promoters and terminators. R-loop homoeostasis is regulated through several pathways including mRNA processing, RNA modifications, DNA topology, single-stranded DNA-binding proteins and by specialised R-loop processing enzymes such as RNase H, RNA/DNA hybrid helicases and DNA nucleases[14–17]. R-loops regulate gene expression but can also lead to genome instability, which is particularly apparent in cells with deficiencies in R-loop processing and binding factors, including for example BRCA1[18–22]. Recently, a role for R-loops has been described in the regulation of RNA polymerase I (Pol I) activity by RNA polymerase II (Pol II)[23]. R-loops have not been studied in the context of hypoxia however, hypoxia initiates a significant change to cellular transcription suggesting there may be an impact on R-loop formation and resolution[9,24]. Despite a reduction in global levels of transcription, a number of transcriptional pathways are induced in hypoxia including the hypoxia-inducible factors (HIF1-3), p53 and those initiated by the unfolded protein response (UPR)[25–27]. The UPR is an ER stress-response pathway that leads to global translation inhibition while upregulating selective genes including those involved in protein folding, redox homoeostasis and protein degradation[28]. In contrast to the DDR, which is activated by ssDNA in hypoxia, the UPR is activated by misfolded proteins. Notably, the DNA repair pathways, including critical R-loop associated factors such as BRCA1 and Rad51, have been shown to be repressed through a variety of mechanisms in response to hypoxia[29–31].

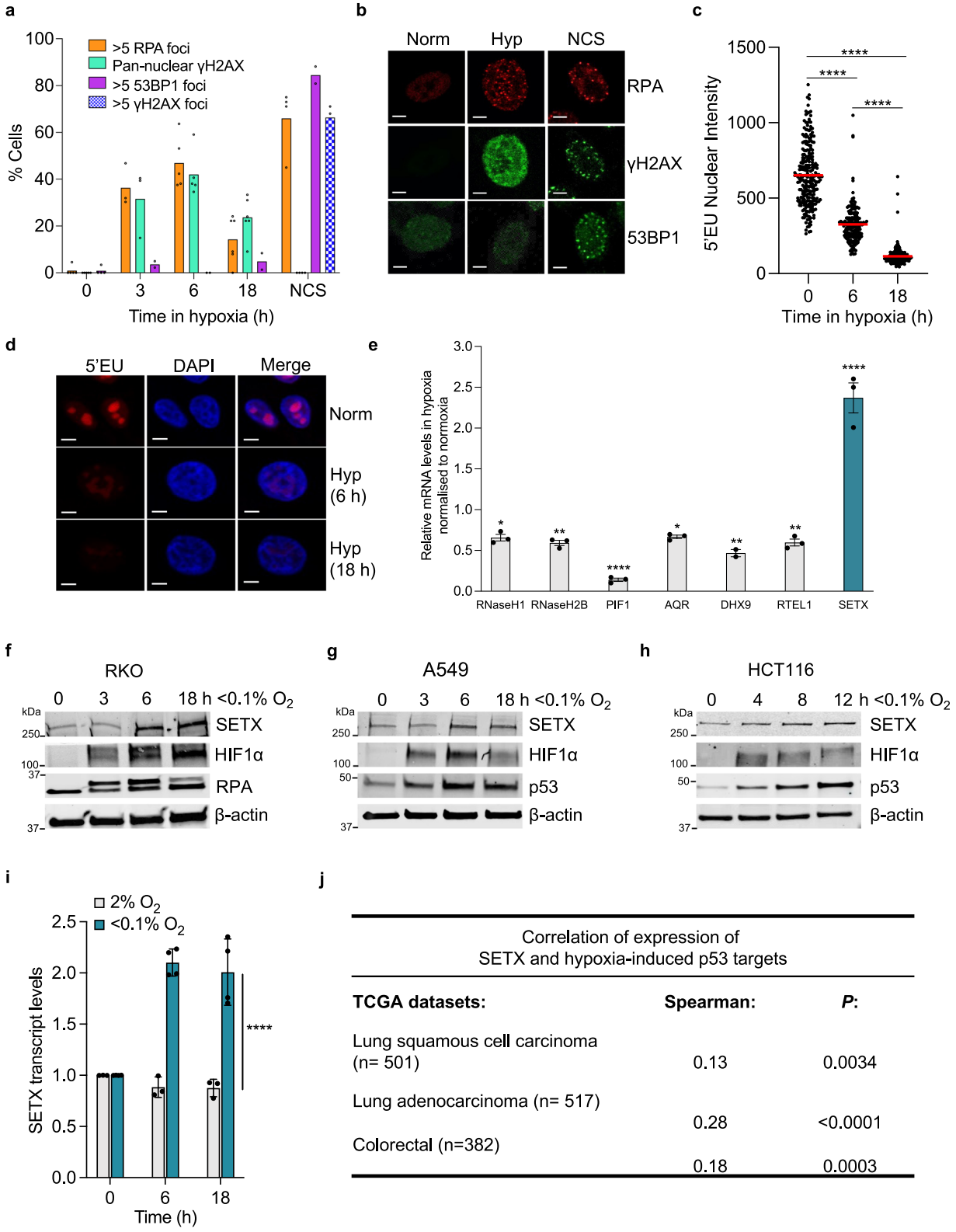
Senataxin (SETX) is a putative RNA/DNA helicase that can facilitate transcription termination and gene transcription of a subset of genes[32–36]. The yeast homologue of SETX, Sen1, was shown to be involved in transcription-coupled repair and protect cells from transcription-associated recombination[37–39]. In addition, Sen1 has been shown to act at the replication fork and facilitate replication at highly transcribed genes[40]. SETX has also been linked to R-loops at transcription–replication collisions and to participate in the antiviral response[39,41]. Mutations in *SETX* have been associated with two neurodegenerative diseases, ataxia with oculomotor apraxia type 2 (AOA2) and amyotrophic lateral sclerosis type 4 (ALS4)[42,43].

The role of R-loops and factors involved in R-loop processing including RNA/DNA helicases have not been investigated in response to hypoxia. We show that in hypoxia, which includes transcriptional and replication stress, R-loops increase. The majority of the factors investigated associated with R-loops were found to be repressed with the notable exception of SETX, which was induced in hypoxia, prompting us to focus on the role of SETX in hypoxia. We found that the loss of SETX leads to an accumulation of R-loops, and that hypoxia-induced SETX protected cells from replication stress, transcription-dependent DNA damage and apoptosis. Most importantly, hypoxia-induced SETX was dependent on the PERK branch of the UPR, suggestive of a link between the UPR and replication stress in hypoxia.

Results

SETX is induced in an oxygen-dependent manner. Exposure to hypoxia (<0.1% O_2) led to the rapid accumulation of RPA foci and pan-nuclear γH2AX in the absence of 53BP1 foci. Importantly, the cells that had pan-nuclear γH2AX also had RPA foci which indicate a replication stress-dependent DDR in the absence of detectable DNA damage (Fig. 1a, b and Supplementary Fig. 1a). This hypoxia-induced DDR occurred in a background of decreased global transcription rates as shown by quantification of 5-ethynyluridine (5′EU) incorporation (Fig. 1c, d and Supplementary Fig. 1b). In these same conditions (<0.1% O_2), the transcript levels of a number of R-loop processing factors including RNase H1, RNase H2B, PIF1, DHX9, RTEL1, and AQR, were significantly repressed, in contrast, SETX was upregulated (Fig. 1e). As SETX has not previously been shown to be stress-responsive at the transcriptional level, we verified that hypoxia-mediated induction of SETX was evident in a number of cell lines (Supplementary Fig. 1c–e). SETX protein levels were also upregulated in hypoxia in the cell lines tested (Fig. 1f–h). To determine oxygen dependency, we compared expression levels in <0.1% O_2 to 2% O_2 and found that SETX was specifically induced at <0.1% O_2 (Fig. 1i). Next, we looked for evidence of links between hypoxia and SETX in cancer patients, using The Cancer Genome Atlas (TCGA) colorectal and lung cancers datasets. Here, we compared SETX expression with both, a validated hypoxia signature and with a group of genes that, like SETX, we have previously shown are induced at <0.1% O_2 but not 2% O_2[25,44]. As we saw no indication of SETX induction in 2% O_2, we were not surprised to find that SETX expression did not correlate with the hypoxia signature (Supplementary Fig. 1f). However, in agreement with the SETX induction at <0.1% O_2, SETX expression showed a positive correlation with the group of genes we have identified as induced at <0.1% O_2 (Fig. 1j)[25]. Therefore, it seems likely that SETX expression is increased in patient samples with tumours experiencing hypoxia-induced replication stress, lending further support to our novel finding that SETX is induced in an oxygen-dependent manner.

Loss of SETX leads to changes in gene expression in hypoxia. SETX has been suggested to affect Pol II binding at certain genes and to facilitate transcriptional termination of a number of genes[34,35,45]. Under normoxic conditions SETX knockdown led to a significant decrease in 5′EU incorporation and given that the majority of transcriptional output is rRNA, this agrees with the recent report demonstrating that SETX supports rRNA transcription[23]. In hypoxia where transcription rates are reduced, there was a modest, further decrease in 5′EU incorporation upon SETX depletion (Fig. 2a). A previous study identified changes in the expression of 36 genes in response to SETX depletion, and 60 genes changing in a SETX-dependent manner in response to viral infection[41]. We carried out RNA-seq, which confirmed that SETX was induced in hypoxia by approximately 3-fold and found that SETX depletion affected a small subset of genes (17 increasing and 48 decreasing) in normoxia, and of these genes, 5 were



j

Correlation of expression of SETX and hypoxia-induced p53 targets

TCGA datasets:	Spearman:	P:
Lung squamous cell carcinoma (n= 501)	0.13	0.0034
Lung adenocarcinoma (n= 517)	0.28	<0.0001
Colorectal (n=382)	0.18	0.0003

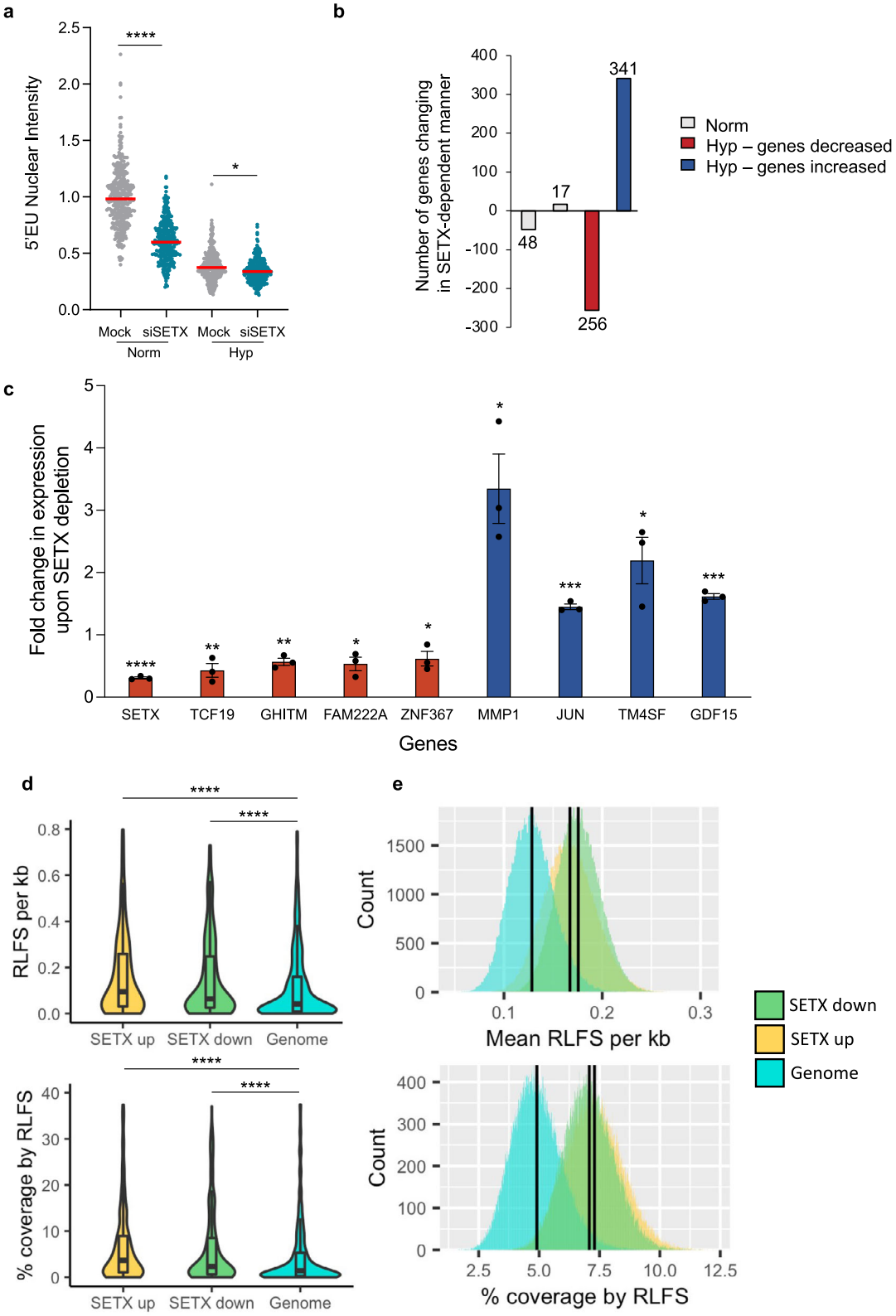
previously identified as regulated in a SETX-dependent manner. In contrast, SETX depletion in hypoxia caused 341 genes to increase and 256 genes to decrease in expression (Fig. 2b). These changes were also validated by RT-qPCR (Fig. 2c). We asked whether the differentially expressed genes shared any common features by gene ontology analysis and found that approximately 20% of genes upregulated in SETX-depleted hypoxic cells were involved in rRNA processing, nucleolus and ribosome biogenesis (Supplementary Fig. 2a). In addition, hypoxia-induced genes that had increased expression in SETX-depleted cells had a slightly shorter gene length compared to the hypoxia-induced genes that were unaffected or had decreased expression upon SETX depletion (Supplementary Fig. 2b). Differentially expressed genes had similar numbers of exons, G4 quadruple structures or GC per

Fig. 1 SETX is induced in an oxygen-dependent manner. a RKO cells were exposed to <0.1% O_2 for 0, 3, 6 and 18 h or to NCS (200 ng/μL) for 6 h. Cells were fixed and stained for γH2AX, RPA and 53BP1. The percentage of cells stained with each marker in each condition is shown, individual data points represent the average in separate fields of view. More than 100 cells were counted in each condition. A representative plot (of 2 independent) experiments is shown. **b** Representative images from **a** (scale bar: 5 μm). NCS = neocarzinostatin. **c** RKO cells were exposed to <0.1% O_2 for 0, 6 and 18 h with 5′EU (0.5 mM) added for the final 6 h. Representative of 3 independent experiments ($n = 3$). Each dot represents a cell and a minimum of 100 cells was imaged per treatment. One-way ANOVA Tukey's multiple comparisons test was used, ****$p < 0.0001$. **d** Representative images from **c** (scale bar: 5 μm). **e** RKO cells were exposed to <0.1% O_2 for 6 h followed by RT-qPCR for the mRNAs indicated relative to the normoxic control. The dashed line indicates normoxic expression levels. One-way ANOVA Dunnett's multiple comparisons test was used: RNase H1 ($p = 0.0162$), RNase H2B ($p = 0.0042$), PIF1 ($p < 0.0001$), AQR ($p = 0.0207$), DHX9 ($p = 0.0010$), RTEL1 ($p = 0.0046$), SETX ($p < 0.0001$). **f** RKO cells were treated for 0, 3, 6, and 18 h of <0.1% O_2. The levels of SETX, HIF1α and RPA are shown. β-actin is the loading control. **g** A549 cells were treated for 0, 3, 6, and 18 h of <0.1% O_2. The levels of SETX, HIF1α, and p53 are shown. β-actin is the loading control. **h** HCT116 cells at 0, 4, 8, and 12 h of treatment with <0.1% O_2. The levels of SETX, HIF1α, p53 and the loading control β-actin, are shown. **i** A549 cells were exposed to hypoxia, 2% O_2 or <0.1% O_2 for the times indicated and the relative mRNA levels of SETX determined. Two-way ANOVA was used ($p < 0.0001$). **j** To examine *SETX* expression against tumour-associated hypoxia-induced p53 activity (referred to as hypoxia-induced p53 targets), raw data for each sequenced gene were rescaled to set the median equal to 1, and hypoxic p53 targets were determined by quantifying the median expression of 6 p53 target genes associated with hypoxia-induced p53 activity (encoding *BTG2, CYFIP2, INPP5D, KANK3, PHLDA3,* and *SULF2*)[25]. Correlations and statistical significance were determined by calculating Spearman's rho rank correlation coefficient (*r*) and two-tailed *P*-value using Hmisc package in RStudio: Lung squamous cell carcinoma ($p = 0.0034$), lung adenocarcinoma ($p < 0.0001$), Colorectal ($p = 0.0003$). **a–i** Data from three independent experiments ($n = 3$), mean ± standard error of the mean (SEM) are displayed unless otherwise indicated.

cent (Supplementary Fig. 2c–e). Next, we investigated the prevalence of R-loop forming sequences (RLFS) in the genes altered in a SETX-dependent manner using a validated prediction tool[46,47] There was no difference in the RLFS density between up and downregulated genes, however, both gene sets have significantly more RLFS than genes randomly selected from all protein-coding genes (Fig. 2d, e). Together these analyses suggest that SETX has a role in regulating gene expression which is hypoxia specific and is likely linked to a role in R-loop resolution as the affected genes all have high levels of RLFS.

R-loops accumulate in response to hypoxia. To determine the impact of loss of SETX in hypoxia on R-loops, we used the S9.6 antibody, which specifically recognises RNA/DNA hybrids. The nuclear intensity of S9.6 increased in response to hypoxia and importantly, this was ablated by treatment with RNase H, an endonuclease that degrades the RNA component of R-loops (Fig. 3a, b). A slot blot using the S9.6 antibody in normoxic and hypoxic conditions also demonstrated an increase in S9.6 staining in hypoxia (Supplementary Fig. 3a). Importantly, an orthogonal assay using the catalytic-dead mutant RNase $H1^{D210N}$ to visualise R-loops also determined an accumulation in R-loops in response to hypoxia (Fig. 3c, d)[48,49]. Together, these findings demonstrate that R-loop levels increase in response to hypoxia. To further investigate this surprising finding, we asked how decreasing R-loops in hypoxia through overexpression of RNase H1 would impact the biological response to hypoxia. R-loops can lead to a localised increase in H3K9me2 and to replication stress, both of which are part of the hypoxic response[50,51]. Overexpression of RNase H1 leads to a decrease in H3K9me2 (3-fold) and H3K9me3 (3-fold) in hypoxia but had no significant impact on the levels of these marks in normoxic conditions (Fig. 3e). As expected, exposure to hypoxia led to phosphorylation of RPA and Chk1, confirming replication stress. However, cells overexpressing RNase H1 showed decreased levels of hypoxic RPA and Chk1 phosphorylation, and RPA foci in comparison to the mock-treated cells (Fig. 3f, g). It has been previously shown that the combination of replication stress and a heterochromatic environment lead to an ATM-dependent DDR in hypoxia[5]. Overexpression of RNase H1 led to a decrease in ATM signalling, including reduced KAP1-S824, p53-S15, and γH2AX in hypoxia (Fig. 3h). Together, these data demonstrate that overexpression of RNase H1 significantly impacts both replication stress and the DDR in hypoxia (<0.1% O_2) supporting that the biological response is affected by the accumulation of R-loops in hypoxia.

Loss of SETX leads to DNA damage and decreased viability in hypoxia. Next, we investigated the role of SETX and found that siRNA mediated depletion of SETX led to an increase in the levels of R-loops in both normoxia and hypoxia, and again, this increase was ablated with RNase H treatment (Fig. 4a and Supplementary Fig. 3b–f). As R-loops can contribute to replication stress, we asked if SETX had a role to play in replication in hypoxia. Depletion of SETX led to a significant increase in stalled replication forks in normoxic conditions (Supplementary Fig. 3g). However, no changes were detected in hypoxic conditions, likely because hypoxia alone induced high levels of stalled forks (Supplementary Fig. 3h). However, SETX depletion also decreased replication rates and this was more significant in hypoxic compared to normoxic conditions (Fig. 4b and Supplementary Fig. 3i, j). Given that unresolved R-loops have been associated with DNA damage, we asked whether depleting SETX would lead to DNA damage in hypoxia. As expected, there was no increase in DNA damage in hypoxia but upon SETX depletion there was a significant increase in DNA damage as determined by increased numbers of cells with 53BP1 foci (Fig. 4c and validated with a second siRNA Supplementary Fig. 4a). To test whether the DNA damage observed in the SETX-depleted hypoxic cells was linked to transcription, we treated cells with dichloro-beta-D-ribofuranosylbenzimidazole (DRB), which inhibits Pol II-mediated transcription. DRB rescued the DNA damage observed in the SETX-depleted hypoxic cells suggesting that the damage observed in SETX-depleted hypoxic cells was transcription-dependent (Fig. 4c). We confirmed that DRB did not rescue DNA damage non-specifically by demonstrating that DRB did not rescue Adriamycin-induced DNA damage (Supplementary Fig. 4b). It should be noted that by inhibiting transcription, DRB led to a decrease in R-loop levels, suggesting that SETX may be protecting the hypoxic cells from co-transcriptional R-loop associated DNA damage (Supplementary Fig. 4c–e). Interestingly, the DNA damage observed in SETX-depleted hypoxic cells occurred in non-S-phase cells, suggesting that the role of SETX in hypoxia is not to mediate transcription–replication conflicts (Fig. 4D). DNA damage, if unrepaired, can lead to increased apoptosis and reduced survival. In hypoxia, SETX depletion led to decreased colony survival when compared to control cells, suggesting that SETX function contributes to hypoxic cell viability (Fig. 4e). SETX depletion also led to a significant increase in apoptosis compared to the control cells specifically in hypoxia and again, this was found to be transcription-dependent as the addition of DRB rescued the apoptosis induced by SETX loss (Fig. 4f and



Supplementary Fig. 4f). Taken together, SETX protects hypoxic cells from transcription linked DNA damage and apoptosis.

SETX upregulation is dependent on the UPR. SETX has not previously been shown to be stress-responsive, to investigate the mechanism of SETX induction in hypoxia, A549 cells were used as these showed the most robust transcriptional induction of SETX in hypoxia. Multiple candidate transcription factors are active at the oxygen level (<0.1% O_2) shown to induce SETX, including HIF, p53 and those involved in the UPR (ATF3, ATF4, ATF5 and CHOP) (Supplementary Fig. 5a, b). Given that SETX was not induced at 2% O_2 where HIF is active, and SETX expression did not correlate with a hypoxia signature, it seemed unlikely that SETX induction was dependent on HIF. However, to

Fig. 2 Gene expression changes in response to the loss of SETX. a RKO control cells or SETX-depleted cells were exposed to 21% and <0.1% O_2 for 6 h in the presence of 5′EU. Cells were fixed, stained and quantified for 5′EU (0.5 mM) incorporation. Cells treated with siRNA to SETX are shown in green. Data from three independent experiments ($n = 3$) where each dot represents a cell and a minimum of 100 cells were imaged per treatment. One-way ANOVA Tukey's multiple comparisons test was used: ****$p < 0.0001$, *$p = 0.0146$. **b** RNA-seq results comparing RKO cells treated with control siRNA or SETX siRNA in 21% O_2 (Norm, grey) and <0.1% O_2 (Hyp). Genes with a decreased expression upon SETX depletion in hypoxia shown in red, and genes with an increased expression upon SETX depletion in hypoxia shown in blue. RNA-seq was carried out in 3 biological replicates ($n = 3$). **c** RKO cells were treated with control siRNA or SETX siRNA and exposed to <0.1% O_2 for 6 h followed by RT-qPCR. For each gene, relative mRNA levels were determined using 18S as the reference gene. The fold change in expression upon SETX depletion in hypoxia as compared to the control siRNA in hypoxia are shown. Genes in red were repressed in SETX-depleted hypoxic cells, while genes in blue were induced, according to the RNA-seq results. The dotted line indicates no change in expression upon SETX depletion. Data from three independent experiments ($n = 3$), mean ± standard error of the mean (SEM) are displayed. Two-tailed Student's *t*-test was used: SETX ($p < 0.0001$), TCF19 ($p = 0.0066$), GHITM ($p = 0.0017$), FAM222A ($p = 0.0128$), ZNF367 ($p = 0.0305$), MMP1 ($p = 0.0135$), JUN ($p = 0.0006$), TM4SF ($p = 0.0331$), GDF15 ($p = 0.0002$). **d** R-loop forming sequence (RLFS) density measured as RLFS per kb of gene length (upper panel) and % coverage of gene by RLFS (lower panel). The genome plot represents one random sample of all protein-coding genes ($n = 500$). Centre line = median; upper and lower bounds of box = 75th and 25th percentiles (3rd and 1st quartiles); upper and lower bounds of the whiskers = 1.5 times the interquartile range from the corresponding 'hinge' where the line originates from the box; minima and maxima are given by the top and bottom of the overlaid violin plot. $n = 500$ represents the number of protein-coding genes randomly selected to create the null genome distribution shown in light blue. The SETX up and SETX down violin plots used all of the differentially expressed in the corresponding group. Two-tailed Student's *t*-test was used: *p*-value = **** = 2.2×10^{-16}. **e** Resampling of RLFS densities used to calculate *p*-values shown in **d**. Black vertical lines represent the mean of each distribution.

formally test this, we depleted HIF1α and asked whether this affected SETX induction in hypoxia. As expected SETX induction in hypoxia was not affected by HIF1α siRNA in contrast to the control gene VEGF, confirming that SETX is not induced by HIF1α in hypoxia (Supplementary Fig. 5c, d). We also demonstrated that SETX expression was not induced with the hypoxia mimetic desferrioxamine (DFO) and 2% O_2, which lead to HIF stabilisation (Supplementary Fig. 5e, f). Next, we found that SETX induction in hypoxia was not affected by p53 siRNA, suggesting that p53 signalling does not contribute to SETX induction in hypoxia (Fig. 5a and Supplementary Fig. 5g). In support of this conclusion, we and others have found no evidence of a functional p53 response element in the SETX promoter[52]. Next, we investigated whether SETX induction could be linked to the UPR. Predicted binding sites were identified for the UPR transcription factor ATF4 in the GeneHancer identifier GH09J132349 corresponding to the *SETX* promoter region. We depleted ATF4 using siRNA and demonstrated that ATF4 is responsible for the induction of SETX in hypoxia (Fig. 5b and Supplementary Fig. 6a). The transcript levels of the ATF4 target CHOP were tested in parallel to confirm ATF4 knockdown (Supplementary Fig. 6b). ChIP was used to determine direct ATF4-mediated transactivation of SETX and demonstrated that ATF4 was enriched at the SETX promoter specifically in hypoxia (Fig. 5c). ATF4 enrichment at the CHOP gene was used as a positive control (Supplementary Fig. 6c). To further investigate whether SETX is a UPR target, we exposed cells to a range of stresses including tunicamycin and thapsigargin, both of which are known to induce the UPR, and found that both led to a significant increase in SETX mRNA similar to the induction observed in hypoxia (<0.1% O_2) (Fig. 5d, Supplementary Fig. 6d). Consistent with this, SETX was found to be upregulated in published RNA sequencing datasets upon tunicamycin or thapsigargin treatment[53,54]. We considered that SETX might be responsive to replication stress and that tunicamycin and thapsigargin could induce replication stress. However, hydroxyurea (Hu) did not induce SETX (Fig. 5d) and we saw no evidence of replication stress-induced in response to either thapsigargin or tunicamycin (Fig. 5e and Supplementary Fig. 6e, f). The data presented so far suggest that the hypoxia-induced UPR reduces replication stress through PERK/ATF4-dependent induction of SETX. To interrogate the relationship between the UPR and replication stress we made use of agents which, unlike hypoxia, induce either a UPR or replication stress but not both (Fig. 5e). Cells were treated with Hu, to induce replication stress, with or without thapsigargin and the number of cells with RPA foci determined in each condition. The number of cells with Hu-induced RPA foci were significantly reduced by thapsigargin treatment (Fig. 5f, g). Importantly, we determined that this was not due to decreased expression of RPA which could have occurred due to reduced translation rates induced by the UPR (Supplementary Fig. 6g). Signalling to ATF4 in hypoxia is primarily mediated by the protein kinase R (PKR)-like endoplasmic reticulum kinase (PERK)[55,56] which led us to the hypothesis that the reduction in Hu-induced replication stress observed in the presence of thapsigargin could be PERK-mediated. In support of this hypothesis, we demonstrated again that adding thapsigargin to Hu-treated cells reduced RPA phosphorylation (Fig. 5h) but that this effect was abrogated if a PERK inhibitor GSK2606414 (PERKi) was also included (Fig. 5i).

The UPR is linked with replication stress in hypoxia. As expected, depleting PERK using siRNA abrogated the hypoxia-mediated induction of SETX (Fig. 6a and Supplementary Fig. 6h). In addition, PERKi led to a significant decrease in SETX mRNA levels in hypoxia as compared to the control cells (Supplementary Fig. 6i, j). We also verified that pre-treating cells with PERKi abrogated thapsigargin-mediated SETX induction, again demonstrating that SETX induction during the UPR is downstream of PERK (Fig. 6b and Supplementary Fig. 6k).

Since SETX depletion led to an increase in R-loops, we hypothesised that PERK depletion would have a similar effect. To test our hypothesis, we used both S9.6 and $RNaseH1^{D210N}$ to determine changes in R-loop levels with siRNA to PERK or PERKi. siRNA mediated PERK depletion and PERKi led to an increase in R-loop levels in hypoxia using both detection methods suggesting that, like SETX, PERK signalling negatively regulates R-loops in hypoxia (Fig. 6c and Supplementary Fig. 7a–e). As SETX depletion led to an increase in transcription-dependent DNA damage, we asked whether PERK inhibition showed a similar effect. Akin to SETX depletion, PERK inhibition led to an accumulation of DNA damage which was more significant under hypoxic conditions and dependent on transcription (Fig. 6d). Together, these data suggest a role for PERK in reducing replication stress and DNA damage in hypoxia. In agreement with this conclusion, when PERK was inhibited in hypoxia we saw an increase in both phosphorylations of p53 and RPA indicating an exacerbation of the DDR and replication stress (Fig. 6e). To investigate further, we determined the number of

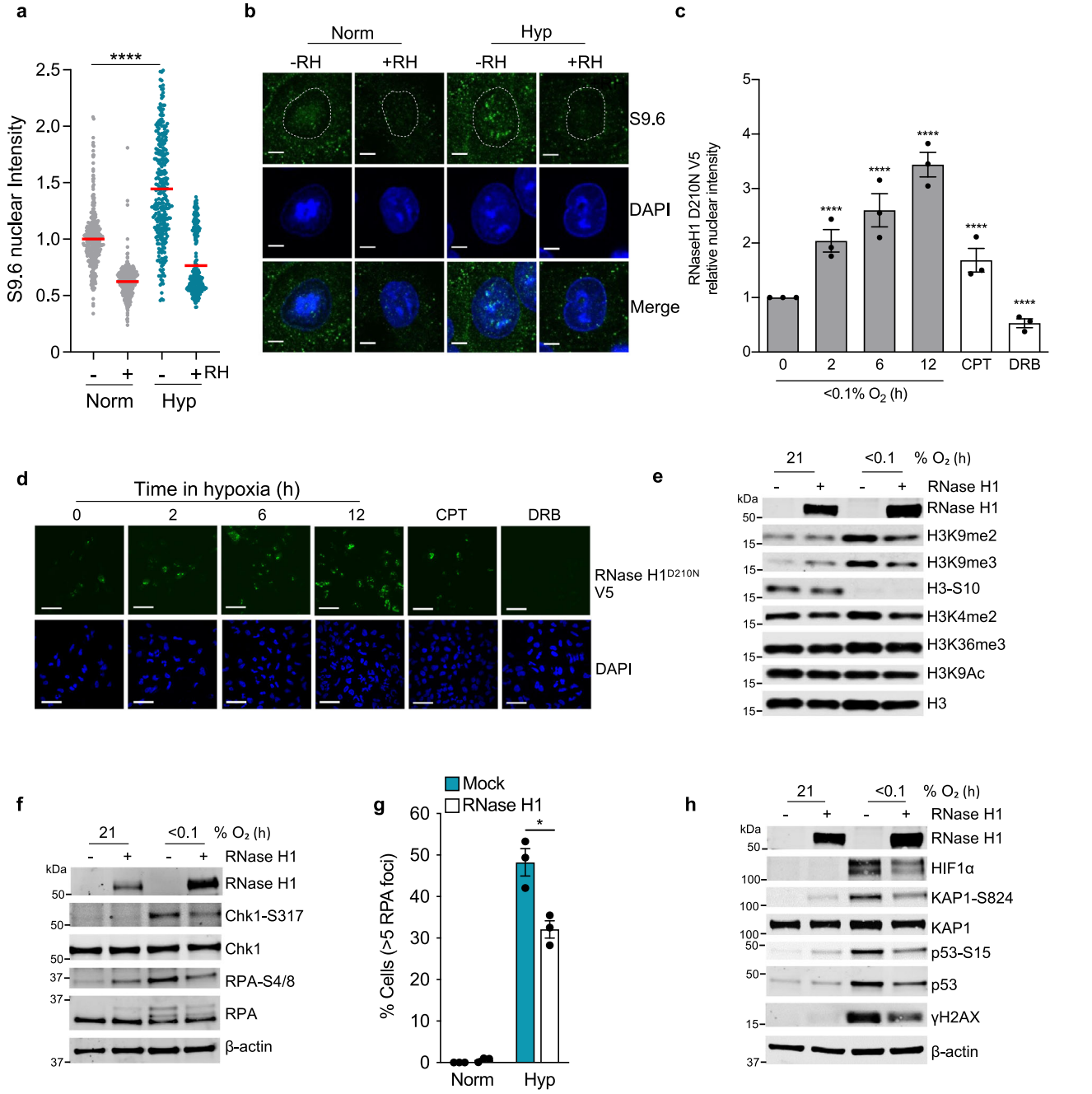


Fig. 3 Accumulation of R-loops in hypoxia (<0.1% O2). a A549 cells were exposed to 21% O_2 or <0.1% O_2 (shown in green) for 12 h, fixed and stained with the S9.6 antibody and DAPI. Where indicated, coverslips were treated with RNase H prior to staining. Data from three independent experiments ($n = 3$) where each dot represents a cell and a minimum of 100 cells were imaged per treatment. One-way ANOVA Tukey's multiple comparisons test was used, $^{****}p < 0.0001$. **b** Representative images from **a** (scale bar: 5 μm). A dashed white line indicates a nuclear outline based on a DAPI stain that was used to measure the nuclear S9.6 intensity. **c** A549 cells were transfected with RNase $HI^{D210N}V5$ and exposed to hypoxia (<0.1% O_2), CPT (10 μM, 20 min), or DRB (100 μM, 1 h). Staining for V5 was then carried out and the nuclear intensity determined. The two-tailed Student's *t*-test was used: $^{****}p < 0.0001$. **d** Representative images from part **c** are shown (scale bar: 30 μm). V5 staining is green, DAPI to show the nucleus is blue. **e** HCT116 cells were transfected with mock or RNase H1 plasmid and exposed to 21% O_2 or <0.1% O_2 for 6 h. RNase H1 overexpression was confirmed by western blot analysis. Changes in chromatin modifications H3K9me2, H3K9me3, H3-S10, H3K4me2, H3K36me3, and H3K9Ac are shown. Total H3 was included as a loading control. **f** HCT116 cells were treated as in part **e** (<0.1% O_2 for 6 h). The levels of RPA-S4/8 and Chk1-S317 are shown. RPA, Chk1, and β-actin controls were included. **g** HCT116 cells transfected with mock or RNase H1 plasmid and exposed to 21% O_2 (Norm) or <0.1% O_2 (Hyp) for 6 h were stained for RPA and the % of cells with >5 RPA foci determined. Two-tailed Student's *t*-test was used: $p = 0.0142$. **h** Western blotting was carried out on cells treated as in part **g**. ATM activation was detected using KAP1-S824, p53-S15, and γH2AX. Total KAP1, p53, H3 and β-actin control westerns were included. **a**–**h** Data from three independent experiments ($n = 3$), mean ± standard error of the mean (SEM) are displayed unless otherwise indicated.

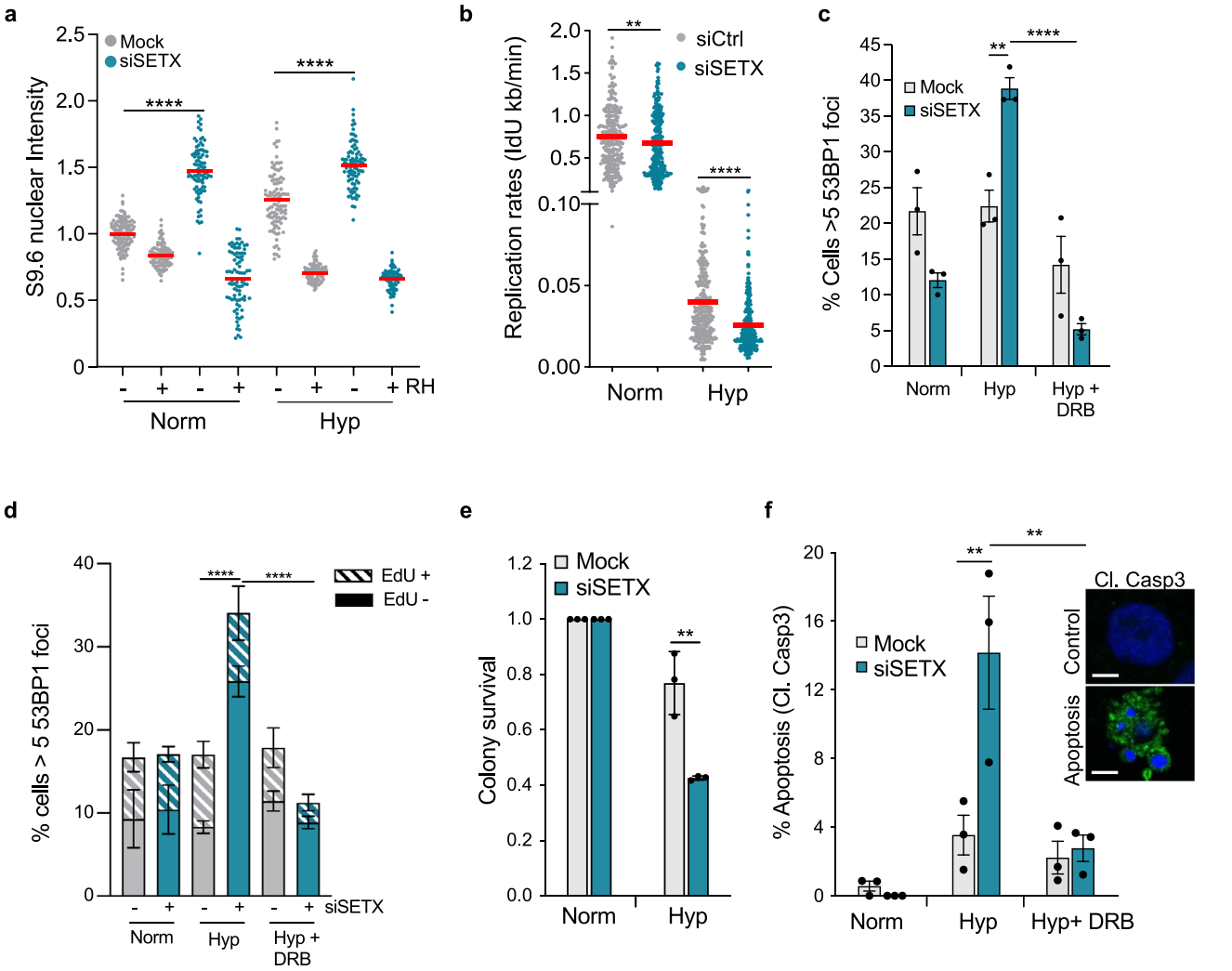
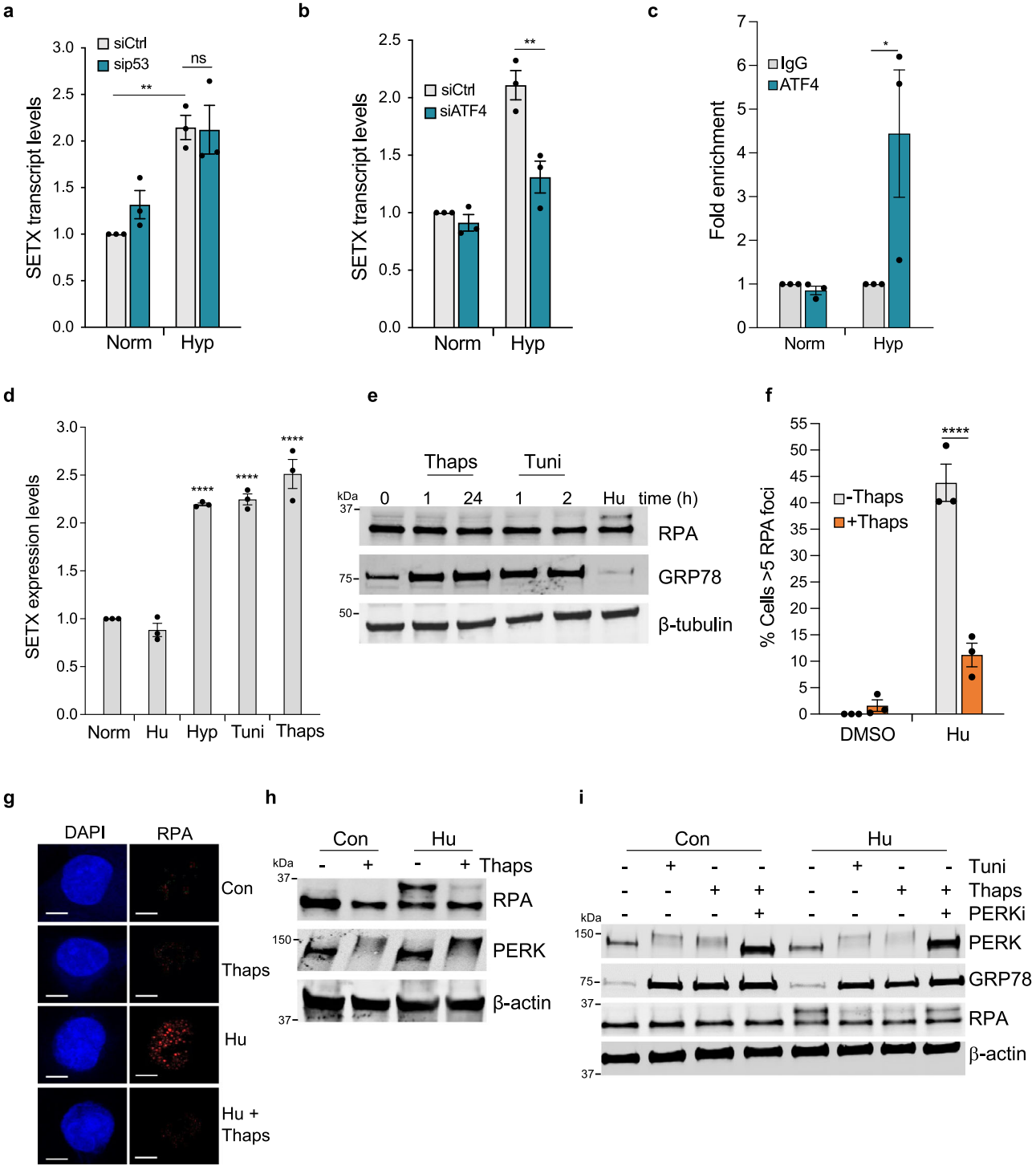


Fig. 4 SETX reduces R-loops and protects from DNA damage and cell death in hypoxia. a A549 cells that were either mock-transfected (grey) or transfected with SETX siRNA (green), were exposed to 21% O_2 or <0.1% O_2 for 12 h. Cells were fixed and stained with the S9.6 antibody and DAPI. Where indicated, coverslips were treated with RNase H prior to staining. Data from one independent experiment ($n = 1$) where each dot represents a cell and a minimum of 100 cells were imaged per treatment. **b** Replication rates, as determined by IdU incorporation rates, of RKO cells transfected with control siRNA versus SETX siRNA exposed to 21% O_2 (Norm) or <0.1% O_2 (Hyp) for 6 h. Data from three independent experiments ($n = 3$) where each dot represents a fibre and a minimum of 100 fibres were analysed per treatment. Two-tailed Mann–Whitney *U* test was used: $^{****}p < 0.0001$, $^{*}p = 0.0068$. **c** Percentage of cells displaying 53BP1 foci (>5 per nucleus) in RKO cells with either mock-treated or treated with SETX siRNA. Cells were exposed to 21% O_2 (Norm), 6 h of <0.1% O_2 (Hyp) or pre-treated with DRB (100 μM) followed by 6 h of <0.1% O_2 (Hyp + DRB). One-way ANOVA Tukey's multiple comparisons test was used: $^{ns}p = 0.1240$, $^{**}p = 0.0046$, $^{****}p < 0.0001$. **d** A549 cells that were either mock-transfected (grey) or transfected with SETX siRNA (green) were pulsed with EdU (10 μM) for 1 h then and exposed to 21% O_2 (Norm), <0.1% O_2 (Hyp) for 6 h or treated with DRB (100 μM) in <0.1% O_2 for 6 h (Hyp + DRB). The percentage of cells displaying 53BP1 (>5 per nucleus) is shown. Two-tailed Student's *t*-test was used: $^{****}p \leq 0.0001$. **e** Colony survival of A549 cells with either mock treatment or SETX siRNA after 0 and 18 h of hypoxia (Hyp) (<0.1% O_2) treatment. Two-tailed Student's *t*-test was used: $p = 0.0065$. **f** A549 cells were mock-treated or treated with SETX siRNA and exposed to 21% O_2 (Norm), <0.1% O_2 (Hyp) for 24 h or pre-treated with DRB (100 μM) followed by 24 h of <0.1% O_2 (Hyp + DRB). The percentage of cells positive for cleaved caspase 3 (Cl. Casp3) is shown. Representative images of a normal and apoptotic cell are included (scale bar: 5 μm). One-way ANOVA Tukey's multiple comparisons test was used: Hyp Mock versus Hyp siSETX ($^{**}p = 0.0035$), Hyp siSETX versus Hyp+ DRB siSETX ($^{**}p = 0.0020$). **a**–**f** Data from three independent experiments ($n = 3$), mean ± SEM are displayed unless otherwise indicated. Source data for **d** is provided as a Source Data file.

cells experiencing replication stress as measured by those with RPA foci when PERK was lost and found that the percentage of cells experiencing replication stress in hypoxia did not change with PERK depletion (Supplementary Fig. 7f). This was not entirely surprising as cells exposed to hypoxia (<0.1% O_2) demonstrate high levels of replication stress due to reduced dNTP levels. However, it was apparent that the cells with reduced PERK activity had increased numbers of RPA foci per cell in hypoxia suggesting again that hypoxia cells with reduced PERK activity have increased levels of replication stress (Fig. 6f, g and Supplementary Fig. 7g). Finally, we tested whether PERK inhibition led to increased replication stress in hypoxia using the DNA fibre assay. Inhibition of PERK led to decreased replication rates in both normoxia and hypoxia, suggesting that PERK signalling acts to alleviate replication stress (Fig. 6h). Taken together, our data suggest that in hypoxia, the PERK branch of



the UPR signals through SETX and potentially other unidentified factors to reduce R-loops, replication stress, DNA damage and apoptosis (Fig. 6i).

Discussion

Our study suggests that R-loops accumulate in response to hypoxia and that this biological response includes induction of the RNA/DNA helicase SETX. Hypoxia-induced SETX reduces replication stress and protects hypoxic cells from transcription-associated DNA damage and apoptosis. Importantly, SETX induction is dependent on the PERK branch of the UPR. PERK inhibition increased R-loops and replication stress, uncovering an entirely novel aspect of PERK function in hypoxia.

The accumulation of R-loops in hypoxia may act as a signal of transcriptional stress to the cell, leading to a further cascade of stress-response signalling pathways. R-loops have previously been shown to activate non-canonical ATM signalling through spliceosomal displacement[57]. Our data show that by reducing R-loops through the overexpression of RNase H1 in hypoxia, both the DDR and replication stress responses are alleviated. The reduction in replication stress in hypoxia upon RNase H1 overexpression could be due to less R-loops forming barriers to replication fork progression[58]. Together, these data highlight

Fig. 5 SETX upregulation is dependent on the PERK branch of the UPR. a A549 cells were treated with either control siRNA or p53 siRNA and exposed to 21% O_2 (Norm) or <0.1% O_2 (Hyp) for 6 h. SETX mRNA levels were determined by RT-qPCR. One-way ANOVA Tukey's multiple comparisons test was used: $^{ns}p = 0.9996$, $^{**}p = 0.0050$. **b** A549 cells were treated with either control siRNA or ATF4 siRNA and exposed to 21% O_2 (Norm) or <0.1% O_2 (Hyp) for 16 h. SETX mRNA levels were determined by RT-qPCR. One-way ANOVA Tukey's multiple comparisons test was used: $^{**}p = 0.0023$. **c** A549 cells were exposed to 21% O_2 (Norm) or <0.1% O_2 (Hyp) for 4 h, and ChIP-qPCR experiments were performed to determine fold enrichment of ATF4 at the SETX promoter relative to IgG control. One-way ANOVA Tukey's multiple comparisons test was used: $^{*}p = 0.0416$. **d** SETX mRNA levels in non-treated A549 cells (Norm), Hu (1 mM), <0.1% O_2 (Hyp), tunicamycin (Tuni, 5 μg/mL) or thapsigargin (Thaps, 2 μM) for 16 h. One-way ANOVA Dunnett's multiple comparisons test was used: $^{****}p < 0.0001$. **e** A549 cells were exposed to Thapsigargin (Thaps) (2 μM) or Tunicamycin (Tuni) (5 μg/mL) for the times indicated, or to Hu (2 mM, 8 h) followed by western blotting. **f** Percentage of cells displaying RPA foci (>5 per nucleus) in A549 control or Hu (2 mM) treated cells that were also treated with or without Thaps (2 μM) for 24 h. The two-tailed Student's *t*-test was used: $^{****}p < 0.0001$. **g** Representative images from **f** (scale bar: 5 μm). **h** A549 control or Hu (2 mM) treated cells were also treated with or without Thaps (2 μM) for 24 h followed by western blotting. β-actin was used as the loading control. **i** A549 control or Hu (2 mM) treated cells were also treated with DMSO, Tuni (5 μg/mL), Thaps (2 μM) or Thaps (2 μM) and PERKi (10 μM) for 24 h followed by western blotting. β-actin was used as the loading control. **a**–**i** Data from three independent experiments ($n = 3$), mean ± SEM are displayed unless otherwise indicated.

transcriptional stress as an additional signal to nucleotide depletion in the induction of ATM/ATR signalling in hypoxia. R-loops are therefore implicated as making a significant contribution to the biological response to hypoxia.

While the DDR and UPR are both active in hypoxia, the DDR is restricted to S phase cells[5]. The UPR/PERK dependency of SETX induction ensures that cells in all phases of the cell cycle increase SETX levels in hypoxia. Combined with our findings using an inhibitor of transcription, this suggests a role for SETX in resolving co-transcriptional R-loops. We hypothesise that these hypoxia-induced R-loops occur at stress-responsive genes which are induced in response to hypoxia, for example, HIF targets. Previous reports have demonstrated that an accumulation of R-loops can lead to an increase in DNA damage. However, hypoxia does not lead to an accumulation of DNA damage even after extended periods of time, suggesting that the hypoxia-induced R-loops are distinct to those induced by other genotoxic stresses such as camptothecin and G-quadruplex ligands[59,60]. The DNA damage we observed in SETX-depleted hypoxic cells is transcription-dependent, supporting the hypothesis that the role of hypoxia-induced SETX is to resolve the co-transcriptional R-loops that are prone to DNA damage and therefore reduce genomic instability.

Lending support to our finding that SETX is induced by the UPR in hypoxia, RNA-sequencing showed that SETX knockdown led to increased transcription of rRNA processing, nucleolar and ribosome biogenesis genes in hypoxia. Given that the UPR is known to inhibit rRNA transcription and protein translation, it is possible that one of the mechanisms that contribute to these functions of the UPR is through the induction of SETX. A role for SETX in hypoxia-induced UPR-mediated repression of rRNA and translation warrants further investigation.

Interestingly, a previous report showed that in response to a short exposure (1 h) of thapsigargin or DTT, PERK inhibits replication fork progression, and origin firing through a Claspin/Chk1 pathway[61]. While it is challenging to interpret these seemingly contradictory findings with those presented here, this does further support a role for the UPR in replication stress. Differences likely arise from the use of chemically induced UPR signalling and the hypoxia-induced UPR and the timeframe of the experiments carried out[62].

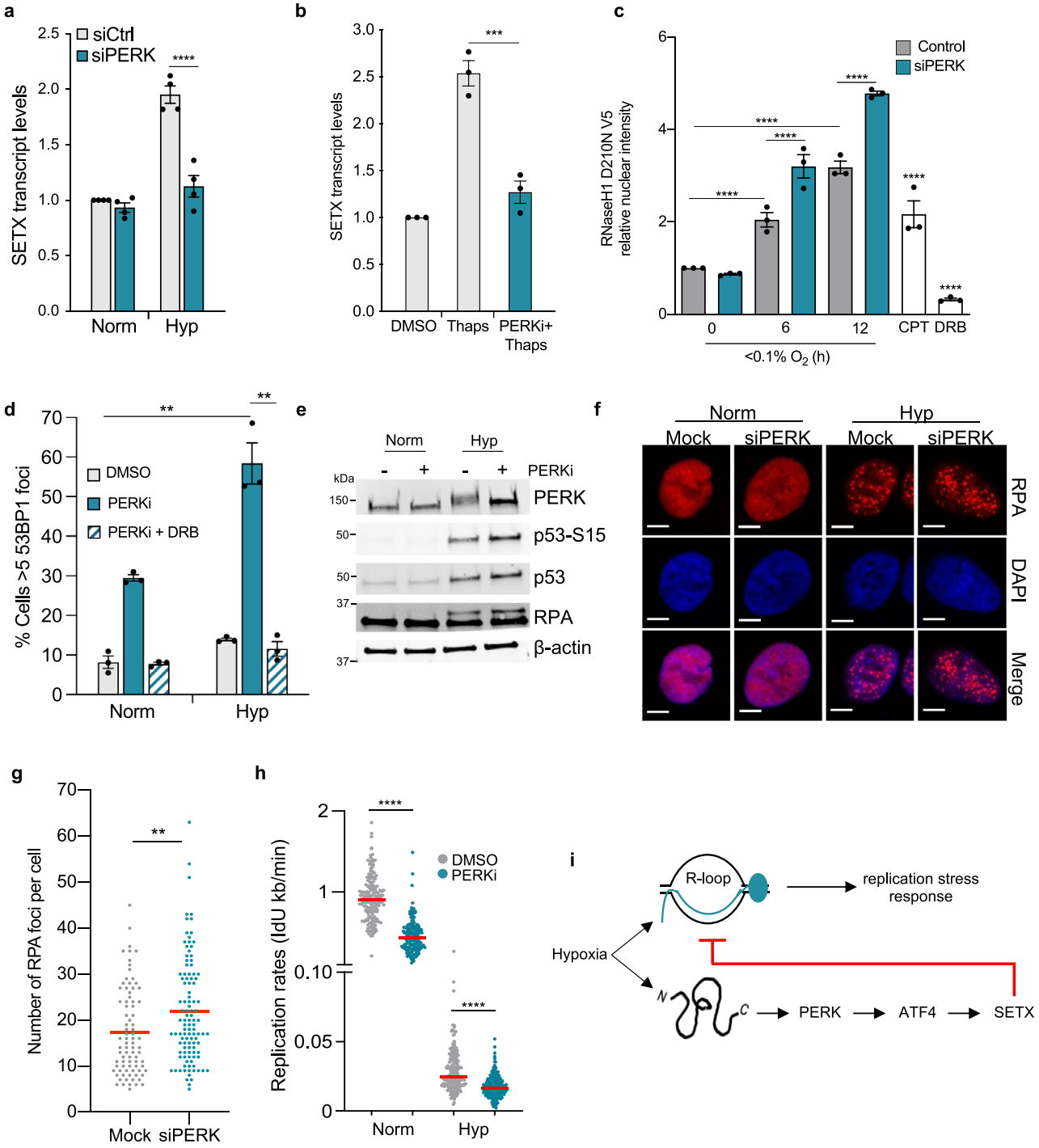
SETX has been identified as a potential tumour suppressor[63] and in support of this, SETX expression was found to be reduced in a number of cancers compared to normal tissue controls[43]. However, AOA2 patients do not present with increased cancer susceptibility suggesting a level of redundancy with other R-loop resolution mechanisms exists to protect genome stability. In this study, SETX depletion increased R-loops, replication stress, DNA damage and apoptosis in hypoxia suggesting that SETX may promote hypoxic tumour growth, and hence be a potential therapeutic target. Interestingly, *SETX* was recently identified as a gene whose knockout increases sensitivity to cisplatin in a set of genome-wide CRISPR-Cas9 screens[64]. It is possible that in the hypoxic microenvironment in which multiple pathways including DNA repair and potentially R-loop resolution factors are repressed, loss of SETX function would not be readily compensated by other mechanisms in a manner similar to its deficiency in the cerebellum. In addition, this study demonstrates that inhibiting PERK leads to increased R-loops, DNA damage and replication stress in hypoxia, and therefore PERK could also be a potential therapeutic target. Targeting PERK in cancer has been controversial as PERK has demonstrated both tumours promoting and suppressive activities depending on the type of cancer and intensity of stress[65]. However, in hypoxia, PERK supports tumour survival and growth, therefore suggesting PERK as a potential therapeutic target specifically for hypoxic tumours[66,67]. Since PERK inhibition also increased replication stress in hypoxic conditions, we postulate that using PERK inhibitors in conjunction with replication stress inducers such as ATR inhibitors may be beneficial in solid tumours.

Methods

Cell lines and reagents. RKO, HCT116 and A549 (ATCC) were grown in DMEM supplemented with 10% FBS and cultured in humidified incubators at 37 °C and 5% CO_2. Cells were routinely tested for mycoplasma and found to be negative. For plasmid transfections, JetPrime (Polyplus transfection) was used. ppyCAG_RNaseH1_WT (#111906) and ppyCAG_RNaseH1_D210N (#111904) were supplied by Addgene. siRNA transfections were performed using Dharma-FECT-1 (Thermo-Fisher Scientific), sequences are available in the SI. siSETX-A siRNA was used for Figs. 2d–f, 3b and Supplementary Figs. 2D–G, 3, 4, 5A, G. siSETX-B siRNA was used for Figs. 2c, 3a, c–f and Supplementary Figs. 2B, C and 5F. AllStars negative control siRNA (Qiagen) and ON-TARGETplus non-targeting pool (Dharmacon) were used as control siRNA. Specific siRNA sequences are shown in Supplementary Table S2. Drugs used were the radiomimetic neocarzinostatin (NCS), DRB, Camptothecin (CPT), Hydroxyurea, hypoxia mimetic DFO, Adriamycin (Sigma), tunicamycin and thapsigargin (MP Biomedicals), and PERK inhibitor GSK2606414 (Calbiochem). Irradiations were performed using a Gamma Service GSR D1 Cs137 irradiator.

Hypoxia treatment. Bactron II and BactronEZ anaerobic chambers (Shel Lab) were used for <0.1% O_2. An M35 hypoxia work station (Don Whitley Ltd) was used for 2% O_2. All experiments at <0.1% O_2 were plated in glass dishes, except for colony survival assays, which were plated in 6 well plates. All hypoxic treatments were harvested within the chamber using equilibrated buffers. Oxygen tensions were confirmed with the Oxylite probe (Oxford Optronix).

Immunoblotting. Cells were harvested in UTB lysis buffer (9 M Urea, 75 mM Tris-HCl pH 7.5, 0.15 M β-mercaptoethanol). Blots were visualised using the Odyssey Infrared imaging system. Antibodies used were SETX, KAP1 (Bethyl); GRP78, HIF1α, (BD Biosciences); ATM-S1981, RPA-S4/8, β-Tubulin (Abcam); ATM, RPA, KAP1-S824, p53-S15, H3K9me2, H3K4me2, H3K9Ac, H3-S10, H3, H3K36me3, Chk1-S317, PERK (Cell Signaling); p53, β-actin, RNase H1, Chk1 (Santa Cruz); and H3K9me3, γH2AX, H2AX (Millipore).



RT-qPCR. RNA was extracted using TRI reagent (Sigma), treated with DNase I (NEB) and cDNA prepared using the Verso cDNA synthesis kit (Thermo-Scientific). SYBR Green PCR master mix (Applied Biosystems) and 7500 FAST Real-Time PCR machine (Applied Biosystems) were used. The ΔΔCt method was used to determine relative mRNA fold change with 18S as the reference gene. Primer sequences can be found in Table S1.

Chromatin immunoprecipitation (ChIP) - qPCR. Treated cells were fixed with 1% formaldehyde and quenched in 125 mM glycine. Cells were lysed with SDS lysis buffer (0.5% SDS, 10 mM EDTA, 50 mM tris pH 8.1). After sonication with Diagenode Bioruptor, samples were precleared with protein A agarose beads and subsequently incubated with ATF4 antibody (Cell Signaling) overnight. Antibody–antigen complexes were then pulled down with agarose beads and washed with the following buffers—low salt wash buffer (0.1% SDS, 1% Triton-X 100, 2 mM EDTA, 20 mM Tris pH 8.1, 150 mM NaCl), high salt wash (0.1% SDS, 1% Triton-X 100, 2 mM EDTA, 20 mM Tris pH 8.1, 500 mM NaCl), LiCl wash buffer (1% Igepal, 10 mM Tris pH 8.1, 250 mM LiCl, 1 mM EDTA, 1% sodium deoxycholate), TE wash buffer (10 mM Tris pH 8.0, 1 mM EDTA). DNA was eluted with 0.1 M $NaHCO_3$ and 1% SDS, cross-linking reversed and treated with proteinase K. DNA was purified with Qiagen PCR purification kits and qPCR was carried out using the following primers: SETX For: CTCAGGTGTCT-CAGCGGATG, SETX Rev: CGCATTGTTCGCAAGACCTA, CHOP For: AAG AGGCTCACGACCGACTA and CHOP Rev: ATGATGCAATGTTTGGCAAC. The amount of immunoprecipitated material was calculated as the fold enrichment over IgG control.

Fig. 6 Hypoxia links the UPR with replication stress. a A549 cells were treated with either control siRNA or PERK siRNA and exposed to 21% O_2 (Norm) or <0.1% O_2 (Hyp) for 16 h. SETX mRNA levels were determined by RT-qPCR. One-way ANOVA Tukey's multiple comparisons test was used: $^{****}p < 0.0001$. **b** A549 cells were treated with or without PERKi (10 μM) and exposed to DMSO or Thaps (2 μM) for 6 h. SETX mRNA levels were determined by RT-qPCR. One-way ANOVA Tukey's multiple comparisons test was used: $^{***}p = 0.0003$. **c** A549 cells were either mock-treated or treated with PERK siRNA, transfected with RNase HI^{D210N}V5 and exposed to hypoxia (<0.1% O_2), CPT (10 μM, 20 min) or DRB (100 μM, 1 h). Staining for V5 was then carried out and the nuclear intensity determined. The two-tailed Student's *t*-test was used: $^{****}p < 0.0001$. **d** The percentage of cells displaying 53BP1 foci (>5 per nucleus) as determined by immunofluorescence, in A549 cells exposed to 21% O_2 (Norm) or 6 h of <0.1% O_2 (Hyp). Cells were treated with DMSO, PERKi (10 μM), or DRB (100 μM) and PERKi (10 μM) (PERKi + DRB). The two-tailed Student's *t*-test was used: Norm PERKi versus Hyp PERKi ($^{**}p = 0.0067$), Hyp + PERKi versus Hyp+ PERKi + DRB ($^{**}p = 0.0068$). **e** A549 cells were treated with DMSO or PERKi (10 μM) and exposed to normoxia or hypoxia (<0.1% O_2) for 6 h followed by western blotting as indicated. PERK inhibition was confirmed by the absence in the electrophoretic mobility shift of PERK on the western blot. **f** A549 cells with either mock treatment or PERK siRNA were exposed to hypoxia (<0.1% O_2) for 6 h, cells were fixed and stained for RPA by immunofluorescence assays. Representative images are shown (scale bar: 5 μm). **g** Quantification of the number of RPA foci per cell from **f**. Treatment with siRNA PERK is indicated in green. Data from two independent experiments ($n = 2$) where each dot represents a cell and a minimum of 100 cells were imaged per treatment. Two-tailed Mann–Whitney *U* test was used: $^{**}p = 0.0024$. **h** Replication rates, as determined by IdU incorporation rates, of A549 cells treated with DMSO or PERKi (10 μM) and exposed to 21% O_2 (Norm) or <0.1% O_2 (Hyp) for 6 h. Data from two independent experiments ($n = 2$) where each dot represents a fibre and a minimum of 100 fibres were analysed per treatment. Two-tailed Mann–Whitney *U* test was used: $^{****}p < 0.0001$. **i** Hypoxia leads to the activation of the UPR and replication stress. In addition to a shortage of nucleotides, R-loops accumulate in hypoxia and contribute to replication stress. The PERK branch of the UPR signals through ATF4 to increase SETX expression in hypoxia. Hypoxia-induced SETX reduces R-loop accumulation and subsequent replication stress-mediated signalling. **a**–**h** Data from three independent experiments ($n = 3$), mean ± SEM are displayed unless otherwise indicated.

Immunofluorescence and confocal microscopy. Cells were fixed in 4% (w/v) paraformaldehyde in PBS, permeabilised in 1% Triton-X 100 in PBS and blocked with 2% (w/v) BSA in 0.1% Tween-20 in PBS. Primary antibodies 53BP1 (Novus Biologicals), RPA (Cell Signaling) and cleaved caspase 3 (Cell Signaling) were used. For 5′EU staining, cells were incubated with 5′ethynyluridine (EU) (0.5 mM) (Jena Bioscience) and Click-iT Alexa Fluor 647 labelling kit (ThermoFisher) was used to measure nascent transcription in the entire nucleus. For EdU staining, cells were incubated with EdU (10 μM) and Click-iT Alexa Fluor 647 labelling kit (ThermoFisher) was used to measure replication. The S9.6 staining protocol used was as previously described[14]. Coverslips were treated with RNase A (Fermentas) for 1 h at 37 °C and where indicated with RNase H (NEB) for 24 h at 37 °C prior to blocking. Coverslips were then incubated with 1:100 diluted S9.6 antibody (Kerafast) for 36 h at 4 °C. Cells were mounted and the entire nucleus imaged using LSM780 or LSM710 confocal microscope (Carl Zeiss, Germany), using a ×63/1.40 Oil DIC M27 Plan-ApoChromat objective. Detection of R-loops using RNase $H1^{D210N}$-V5 was carried out as previously described[68]. In brief, cells transfected with RNase $H1^{D210N}$-V5 were pre-extracted in ice-cold PBS/0.2% Triton-X 100 for 2 min, fixed in 4% (w/v) paraformaldehyde, permeabilised in 0.1% Triton-X 100, blocked with 1% (w/v) BSA in 1% (w/v) FBS in PBS, incubated with 1:500 diluted V5 antibody (ThermoFisher Scientific) for 1 h at room temperature before confocal imaging. DAPI was excited with laser line 405 nm and emission collected between 410 and 495 nm. Alexa-fluor 488 was excited with laser line 488 nm and emission collected between 495 and 596 nm. Alexa-fluor 594 was excited with laser line 594 nm and emission collected between 599 and 734 nm. Alexa-fluor 647 was excited with laser line 633 nm and emission collected between 638 and 755 nm. The 5′EU, S9.6 and V5 mean nuclear intensity signal (including the nucleolus) was determined using the ImageJ plugin/algorithm kindly provided by Dr Kienan Savage, Queen's University Belfast[69]. A minimum of 100 cells was included per treatment.

RNA-seq. RNA was extracted using TRI reagent (Sigma) and treated with DNase I (NEB). The samples were purified using the RNeasy MinElute Clean-up kit (Qiagen) and purity confirmed using a Bioanalyzer. The mRNA fraction was selected for reverse transcription to cDNA. The cDNA generated was end-repaired, A-tailed and adaptor-ligated. cDNA libraries were size selected, multiplexed, tested for quality and subjected to paired-end sequencing in one lane of a flow cell. Accession for RNA-seq data is GSE157371.

RNA-seq differential expression analysis. The analyses were run through an established RNA-seq pipeline by the Buffa lab. The technical adaptors in the pair-end raw reads were trimmed out by trimmomatic-0.32 and the clear reads were aligned to human genome version GRCh38 release 82 using tophat v2.0.13. The mapped reads from each gene were counted and normalised to fragments per kilobase of transcript per million (FPKM) using Cuffdiff-2.2.1. Fragments from PCR duplication were removed by Picard 1.124. The significance of fold changes of genes among samples was estimated by the nonparametric method Rank Product 3.3, a package in R[70–75].

Correlation of SETX expression with TCGA RNA-seq data. RNA-seq data (RNA Seq V2 RSEM) for 382 colorectal adenocarcinoma tumours, 501 lung squamous cell carcinomas and 517 lung adenocarcinomas were downloaded from the TCGA project (accessed through cBioportal: http://www.cbioportal.org/ on the 12th April 2017). To examine *SETX* expression against hypoxia, a validated hypoxia metagene signature was used[44]. To examine *SETX* expression against tumour-associated, hypoxia-induced p53 activity (referred to as hypoxic p53 targets in the figure), raw data for each sequenced gene were rescaled to set the median equal to 1, and hypoxic p53 targets were determined by quantifying the median expression of 6 p53 target genes associated with hypoxia-induced p53 activity (encoding *BTG2, CYFIP2, INPP5D, KANK3, PHLDA3,* and *SULF2*)[25].

Prediction of RLFS sequences. The quantitative model of R-loop forming sequences (qm-RLFS) was used to predict RLFS from fasta files of the human genome build GRCh38.p13 (accessed from https://www.gencodegenes.org/human/ on 23rd March 2020) using default settings. Bedtools[76] was used to merge RLFS with at least 1 base pair overlap and these merged regions were used for subsequent analysis.

Gene coordinates were accessed via BiomaRt using the Ensembl hg38 build version 100[77] and tested for overlaps with the coordinates of genes in the up and downregulated groups. Two kb flanks were added at the transcription start transcription termination sites to include promoter and terminator regions respectively. Only co-transcriptional RLFS were assessed. Custom R scripts were then used to quantify and plot RLFS per kilobase of gene length and per cent of a gene covered by RLFS. For senataxin knockdown vs. genome comparisons, each set of genes (up or downregulated by SETX KD vs. all protein-coding genes) was sampled 100,000 times, drawing 20% of the number of genes in the SETX KD group with each iteration. The mean of each RLFS metric was calculated for each iteration and the values plotted as probability densities and compared using two-tailed Student's *t*-tests.

DNA fibre analysis. For normoxic (21% O_2) treatments, cells were pulse-labelled with CldU (25 mM) for 20 min, washed once with fresh media, followed by the second label IdU (250 mM) for 20 min. For hypoxic (<0.1% O_2) treatments, cells were incubated in hypoxia for 3 h before being pulse-labelled with CldU (25 mM) for 2 h, washed once with fresh media, then followed by IdU (250 mM) for 1 h[78]. Fibres were spread, stained and mounted (Invitrogen) and imaged using LSM780 confocal microscope (Carl Zeiss Microscopy Ltd) using a ×63/1.40 Oil DIC M27 Plan-ApoChromat objective. Alexa-fluor 488 was excited with laser line 488 nm and emission collected between 493 and 551 nm. Alexa-fluor 555 was excited with laser line 543 nm and emission collected between 559 and 659 nm. Replication rates were calculated as V_{IdU} (kb/min) = $[(x * 0.132\ \mu m) * 2.59\ kb/\mu m]/t$ (min), where x = length of IdU.

Statistical analysis. Statistical tests were performed using GraphPad Prism software (GraphPad Software Inc.) and include one-way ANOVA, two-way ANOVA, two-tailed Student's *t*-test and Mann–Whitney *U* tests. ns = non-significant, $^{*}p \le 0.05$, $^{**}p \le 0.01$, $^{***}p \le 0.001$, $^{****}p \le 0.0001$.

Reporting summary. Further information on research design is available in the Nature Research Reporting Summary linked to this article.

Data availability

The sequencing data that support the findings reported in this study have been deposited in the National Center for Biotechnology Information Gene Expression Omnibus (GEO)

and are accessible through the GEO Series accession number GSE157371. All other relevant data are available from the corresponding author upon request. Source data are provided with this paper.

Received: 12 May 2020; Accepted: 31 May 2021;
Published online: 17 June 2021

References

1. Hammond, E. M. et al. The meaning, measurement and modification of hypoxia in the laboratory and the clinic. *Clin. Oncol.* **26**, 277–288 (2014).
2. Foskolou, I. P. et al. Ribonucleotide reductase requires subunit switching in hypoxia to maintain DNA replication. *Mol. Cell* **66**, 206–220.e9 (2017).
3. Pires, I. M. et al. Effects of acute versus chronic hypoxia on DNA damage responses and genomic instability. *Cancer Res.* **70**, 925–935 (2010).
4. Ng, N. et al. Challenges to DNA replication in hypoxic conditions. *FEBS J.* **285**, 1563–1571 (2018).
5. Olcina, M. M. et al. Replication stress and chromatin context link ATM activation to a role in DNA replication. *Mol. Cell* **52**, 758–766 (2013).
6. Dobrynin, G. et al. KDM4A regulates HIF-1 levels through H3K9me3. *Sci. Rep.* **7**, 11094 (2017).
7. Olcina, M. M. et al. H3K9me3 facilitates hypoxia-induced p53-dependent apoptosis through repression of APAK. *Oncogene* **35**, 793–799 (2016).
8. Bencokova, Z. et al. ATM activation and signaling under hypoxic conditions. *Mol. Cell Biol.* **29**, 526–537 (2009).
9. Johnson, A. B., Denko, N. & Barton, M. C. Hypoxia induces a novel signature of chromatin modifications and global repression of transcription. *Mutat. Res.* **640**, 174–179 (2008).
10. Zeman, M. K. & Cimprich, K. A. Causes and consequences of replication stress. *Nat. Cell Biol.* **16**, 2–9 (2014).
11. Marnef, A. & Legube, G. R-loops as Janus-faced modulators of DNA repair. *Nat. Cell Biol.* **23**, 305–313 (2021).
12. García-Muse, T. & Aguilera, A. R loops: from physiological to pathological roles. *Cell* **179**, 604–618 (2019).
13. Crossley, M. P., Bocek, M. & Cimprich, K. A. R-loops as cellular regulators and genomic threats. *Mol. Cell* **73**, 398–411 (2019).
14. Hamperl, S. et al. Transcription-replication conflict orientation modulates R-loop levels and activates distinct DNA damage responses. *Cell* **170**, 774–786. e19 (2017).
15. Santos-Pereira, J. M. & Aguilera, A. R loops: new modulators of genome dynamics and function. *Nat. Rev. Genet.* **16**, 583–597 (2015).
16. Sollier, J. & Cimprich, K. A. Breaking bad: R-loops and genome integrity. *Trends Cell Biol.* **25**, 514–522 (2015).
17. Niehrs, C. & Luke, B. Regulatory R-loops as facilitators of gene expression and genome stability. *Nat. Rev. Mol. Cell Biol.* **21**, 167–178 (2020).
18. Li, X. & Manley, J. L. Inactivation of the SR protein splicing factor ASF/SF2 results in genomic instability. *Cell* **122**, 365–378 (2005).
19. Wahba, L. et al. RNase H and multiple RNA biogenesis factors cooperate to prevent RNA:DNA hybrids from generating genome instability. *Mol. Cell* **44**, 978–988 (2011).
20. Huertas, P. & Aguilera, A. Cotranscriptionally formed DNA:RNA hybrids mediate transcription elongation impairment and transcription-associated recombination. *Mol. Cell* **12**, 711–721 (2003).
21. Hamperl, S. & Cimprich, K. A. The contribution of co-transcriptional RNA: DNA hybrid structures to DNA damage and genome instability. *DNA Repair* **19**, 84–94 (2014).
22. Hatchi, E. et al. BRCA1 recruitment to transcriptional pause sites is required for R-loop-driven DNA damage repair. *Mol. Cell* **57**, 636–647 (2015).
23. Abraham, K. J. et al. Nucleolar RNA polymerase II drives ribosome biogenesis. *Nature* **585**, 298–302 (2020).
24. Denko, N. et al. Hypoxia actively represses transcription by inducing negative cofactor 2 (Dr1/DrAP1) and blocking preinitiation complex assembly. *J. Biol. Chem.* **278**, 5744–5749 (2003).
25. Leszczynska, K. B. et al. Hypoxia-induced p53 modulates both apoptosis and radiosensitivity via AKT. *J. Clin. Invest.* **125**, 2385–2398 (2015).
26. Rzymski, T. et al. Regulation of autophagy by ATF4 in response to severe hypoxia. *Oncogene* **29**, 4424–4435 (2010).
27. Koumenis, C. et al. Regulation of protein synthesis by hypoxia via activation of the endoplasmic reticulum kinase PERK and phosphorylation of the translation initiation factor eIF2alpha. *Mol. Cell Biol.* **22**, 7405–7416 (2002).
28. Koumenis, C. & Wouters, B. G. "Translating" tumor hypoxia: unfolded protein response (UPR)-dependent and UPR-independent pathways. *Mol. Cancer Res.* **4**, 423–436 (2006).
29. Scanlon, S. E. & Glazer, P. M. Multifaceted control of DNA repair pathways by the hypoxic tumor microenvironment. *DNA Repair* **32**, 180–189 (2015).
30. Chan, N. et al. Contextual synthetic lethality of cancer cell kill based on the tumor microenvironment. *Cancer Res.* **70**, 8045–8054 (2010).
31. Leszczynska, K. B. et al. Mechanisms and consequences of ATMIN repression in hypoxic conditions: roles for p53 and HIF-1. *Sci. Rep.* **6**, 21698 (2016).
32. Martin-Tumasz, S. & Brow, D. A. *Saccharomyces cerevisiae* Sen1 helicase domain exhibits 5′- to 3′-helicase activity with a preference for translocation on DNA rather than RNA. *J. Biol. Chem.* **290**, 22880–22889 (2015).
33. Kim, H. D., Choe, J. & Seo, Y. S. The sen1(+) gene of *Schizosaccharomyces pombe*, a homologue of budding yeast SEN1, encodes an RNA and DNA helicase. *Biochemistry* **38**, 14697–14710 (1999).
34. Skourti-Stathaki, K., Proudfoot, N. J. & Gromak, N. Human senataxin resolves RNA/DNA hybrids formed at transcriptional pause sites to promote Xrn2-dependent termination. *Mol. Cell* **42**, 794–805 (2011).
35. Suraweera, A. et al. Functional role for senataxin, defective in ataxia oculomotor apraxia type 2, in transcriptional regulation. *Hum. Mol. Genet.* **18**, 3384–3396 (2009).
36. Fogel, B. L. et al. Mutation of senataxin alters disease-specific transcriptional networks in patients with ataxia with oculomotor apraxia type 2. *Hum. Mol. Genet.* **23**, 4758–4769 (2014).
37. Mischo, H. E. et al. Yeast Sen1 helicase protects the genome from transcription-associated instability. *Mol. Cell* **41**, 21–32 (2011).
38. Li, W. et al. Sen1, the yeast homolog of human senataxin, plays a more direct role than Rad26 in transcription coupled DNA repair. *Nucleic Acids Res.* **44**, 6794–6802 (2016).
39. Yuce, O. & West, S. C. Senataxin, defective in the neurodegenerative disorder ataxia with oculomotor apraxia 2, lies at the interface of transcription and the DNA damage response. *Mol. Cell Biol.* **33**, 406–417 (2013).
40. Alzu, A. et al. Senataxin associates with replication forks to protect fork integrity across RNA-polymerase-II-transcribed genes. *Cell* **151**, 835–846 (2012).
41. Miller, M. S. et al. Senataxin suppresses the antiviral transcriptional response and controls viral biogenesis. *Nat. Immunol.* **16**, 485–494 (2015).
42. Bennett, C. L. & La, A. R. Spada, Unwinding the role of senataxin in neurodegeneration. *Discov. Med.* **19**, 127–136 (2015).
43. Groh, M. et al. Senataxin: genome guardian at the interface of transcription and neurodegeneration. *J. Mol. Biol.* **429**, 3181–3195 (2017).
44. Buffa, F. M. et al. Large meta-analysis of multiple cancers reveals a common, compact and highly prognostic hypoxia metagene. *Br. J. Cancer* **102**, 428–435 (2010).
45. Steinmetz, E. J. et al. Genome-wide distribution of yeast RNA polymerase II and its control by Sen1 helicase. *Mol. Cell* **24**, 735–746 (2006).
46. Jenjaroenpun, P. et al. QmRLFS-finder: a model, web server and stand-alone tool for prediction and analysis of R-loop forming sequences. *Nucleic Acids Res.* **43**, 10081 (2015).
47. Kuznetsov, V. A. et al. Toward predictive R-loop computational biology: genome-scale prediction of R-loops reveals their association with complex promoter structures, G-quadruplexes and transcriptionally active enhancers. *Nucleic Acids Res.* **46**, 7566–7585 (2018).
48. Chen, L. et al. R-ChIP using inactive rnase h reveals dynamic coupling of R-loops with transcriptional pausing at gene promoters. *Mol. Cell* **68**, 745–757.e5 (2017).
49. Barroso, S. et al. The DNA damage response acts as a safeguard against harmful DNA-RNA hybrids of different origins. *EMBO Rep.* **20**, e47250 (2019).
50. Groh, M. et al. R-loops associated with triplet repeat expansions promote gene silencing in Friedreich ataxia and fragile X syndrome. *PLoS Genet.* **10**, e1004318 (2014).
51. Skourti-Stathaki, K., Kamieniarz-Gdula, K. & Proudfoot, N. J. R-loops induce repressive chromatin marks over mammalian gene terminators. *Nature* **516**, 436–439 (2014).
52. Tebaldi, T. et al. Whole-genome cartography of p53 response elements ranked on transactivation potential. *BMC Genomics* **16**, 464 (2015).
53. Luhr, M. et al. The kinase PERK and the transcription factor ATF4 play distinct and essential roles in autophagy resulting from tunicamycin-induced ER stress. *J. Biol. Chem.* **294**, 8197–8217 (2019).
54. Raina, K. et al. Targeted protein destabilization reveals an estrogen-mediated ER stress response. *Nat. Chem. Biol.* **10**, 957–962 (2014).
55. Rzymski, T. & Harris, A. L. The unfolded protein response and integrated stress response to anoxia. *Clin. Cancer Res.* **13**, 2537–2540 (2007).
56. Cojocari, D. et al. New small molecule inhibitors of UPR activation demonstrate that PERK, but not IRE1alpha signaling is essential for promoting adaptation and survival to hypoxia. *Radiother. Oncol.* **108**, 541–547 (2013).
57. Tresini, M. et al. The core spliceosome as target and effector of non-canonical ATM signalling. *Nature* **523**, 53–58 (2015).
58. Gan, W. et al. R-loop-mediated genomic instability is caused by impairment of replication fork progression. *Genes Dev.* **25**, 2041–2056 (2011).

59. De Magis, A. et al. DNA damage and genome instability by G-quadruplex ligands are mediated by R loops in human cancer cells. *Proc. Natl Acad. Sci. USA* **116**, 816–825 (2019).
60. Sordet, O. et al. Ataxia telangiectasia mutated activation by transcription- and topoisomerase I-induced DNA double-strand breaks. *EMBO Rep.* **10**, 887–893 (2009).
61. Cabrera, E. et al. PERK inhibits DNA replication during the unfolded protein response via Claspin and Chk1. *Oncogene* **36**, 678–686 (2017).
62. Bergmann, T. J. & Molinari, M. Three branches to rule them all? UPR signalling in response to chemically versus misfolded proteins-induced ER stress. *Biol. Cell* **110**, 197–204 (2018).
63. Zhao, Q. et al. Systematic detection of putative tumor suppressor genes through the combined use of exome and transcriptome sequencing. *Genome Biol.* **11**, R114 (2010).
64. Olivieri, M. et al. A genetic map of the response to DNA damage in human cells. *Cell* **182**, 481–496 e21 (2020).
65. Ojha, R. & Amaravadi, R. K. Targeting the unfolded protein response in cancer. *Pharm. Res.* **120**, 258–266 (2017).
66. Fels, D. R. & Koumenis, C. The PERK/eIF2alpha/ATF4 module of the UPR in hypoxia resistance and tumor growth. *Cancer Biol. Ther.* **5**, 723–728 (2006).
67. Feldman, D. E., Chauhan, V. & Koong, A. C. The unfolded protein response: a novel component of the hypoxic stress response in tumors. *Mol. Cancer Res.* **3**, 597–605 (2005).
68. Teloni, F. et al. Efficient pre-mRNA cleavage prevents replication-stress-associated genome instability. *Mol. Cell* **73**, 670–683.e12 (2019).
69. Vohhodina, J. et al. The RNA processing factors THRAP3 and BCLAF1 promote the DNA damage response through selective mRNA splicing and nuclear export. *Nucleic Acids Res.* **45**, 12816–12833 (2017).
70. Andrews, S. FastQC: a quality control tool for high throughput sequence data. http://www.bioinformatics.babraham.ac.uk/projects/fastqc/ (2010).
71. Bolger, A. M., Lohse, M. & Usadel, B. Trimmomatic: a flexible trimmer for Illumina sequence data. *Bioinformatics* **30**, 2114–2120 (2014).
72. Langmead, B. & Salzberg, S. L. Fast gapped-read alignment with Bowtie 2. *Nat. Methods* **9**, 357–359 (2012).
73. Trapnell, C., Pachter, L. & Salzberg, S. L. TopHat: discovering splice junctions with RNA-Seq. *Bioinformatics* **25**, 1105–1111 (2009).
74. Trapnell, C. Cufflinks and Cuffdiff Documentation, v6, Open Module on GenePattern Public Server. GenePattern. http://www.broadinstitute.org/cancer/software/genepattern/modules/docs/Cufflinks.cuffdiff/6 (2013).
75. Breitling, R. et al. Rank products: a simple, yet powerful, new method to detect differentially regulated genes in replicated microarray experiments. *FEBS Lett.* **573**, 83–92 (2004).
76. Quinlan, A. R. & Hall, I. M. BEDTools: a flexible suite of utilities for comparing genomic features. *Bioinformatics* **26**, 841–842 (2010).
77. Durinck, S. et al. Mapping identifiers for the integration of genomic datasets with the R/Bioconductor package biomaRt. *Nat. Protoc.* **4**, 1184–1191 (2009).
78. Foskolou, I. P. et al. Measuring DNA replication in hypoxic conditions. *Adv. Exp. Med. Biol.* **899**, 11–25 (2016).

Acknowledgements

We thank Monica Olcina and Kienan Savage for their helpful comments on the manuscript. We would like to acknowledge the skills and expertise of the staff in the Microscopy Scientific Research Facility at the Department of Oncology, University of Oxford. SR, KBL, PV and MH were supported by a CRUK grant C5255/A23755 (awarded to E.M.H.). N.N. was supported by an MRC studentship (MC_ST_U16007). I. P.F. was supported by CRUK Oxford Centre Prize DPhil Studentship C38302/A12981. N.G. was supported by a Royal Society University Research fellowship. W.-C.C. was funded by CRUK grant 23969 (awarded to F.M.B.). S.F.E.-K. was supported by a Wellcome Trust Investigator Award (103844) and a Lister Institute of Preventative Medicine Fellowship (137661). J.G. was supported by a Jean Shanks Foundation/Pathological Society of Great Britain and Ireland Clinical PhD Fellowship (JSPS CPhD 2018 01).

Author contributions

S.R. and T.M. designed, conducted, and interpreted the experiments and wrote the paper, N.N., I.P.F., and M.-S.H. conducted experiments, J.G., P.V., W.-C.C., and F.M.B. carried out the RNA-seq bioinformatics, K.B.L. performed the TCGA analysis and advised on experiments, N.G. and S.F.E.-K. advised on the project, E.M.H. conceived the project, designed/interpreted experiments and wrote the paper. All authors commented on the manuscript.

Competing interests

The authors declare no competing interests.

Additional information

Supplementary information The online version contains supplementary material available at https://doi.org/10.1038/s41467-021-24066-z.

Correspondence and requests for materials should be addressed to E.M.H.

Peer review information *Nature Communications* thanks Domenico Maiorano and the other, anonymous, reviewer(s) for their contribution to the peer review of this work. Peer reviewer reports are available.

Reprints and permission information is available at http://www.nature.com/reprints

Publisher's note Springer Nature remains neutral with regard to jurisdictional claims in published maps and institutional affiliations.

Open Access This article is licensed under a Creative Commons Attribution 4.0 International License, which permits use, sharing, adaptation, distribution and reproduction in any medium or format, as long as you give appropriate credit to the original author(s) and the source, provide a link to the Creative Commons license, and indicate if changes were made. The images or other third party material in this article are included in the article's Creative Commons license, unless indicated otherwise in a credit line to the material. If material is not included in the article's Creative Commons license and your intended use is not permitted by statutory regulation or exceeds the permitted use, you will need to obtain permission directly from the copyright holder. To view a copy of this license, visit http://creativecommons.org/licenses/by/4.0/.

© The Author(s) 2021

Check for updates

Biochemical Society Transactions (2021) **49** 1251–1263
https://doi.org/10.1042/BST20200861

PORTLAND PRESS

Review Article

Links between the unfolded protein response and the DNA damage response in hypoxia: a systematic review

Hannah Bolland*, Tiffany S. Ma*, Syafiq Ramlee, Kristijan Ramadan and Ester M. Hammond

MRC Oxford Institute for Radiation Oncology, Department of Oncology, University of Oxford, Old Road Campus Research Building, Oxford OX3 7DQ, U.K.

Correspondence: Ester M. Hammond (Ester.hammond@oncology.ox.ac.uk)

OPEN ACCESS

Hypoxia is a feature of most solid tumours and predicts for poor prognosis. In radiobiological hypoxia (<0.1% O_2) cells become up to three times more resistant to radiation. The biological response to radiobiological hypoxia is one of few physiologically relevant stresses that activates both the unfolded protein and DNA damage responses (UPR and DDR). Links between these pathways have been identified in studies carried out in normoxia. Based in part on these previous studies and recent work from our laboratory, we hypothesised that the biological response to hypoxia likely includes overlap between the DDR and UPR. While inhibition of the DDR is a recognised strategy for improving radiation response, the possibility of achieving this through targeting the UPR has not been realised. We carried out a systematic review to identify links between the DDR and UPR, in human cell lines exposed to <2% O_2. Following PRISMA guidance, literature from January 2010 to October 2020 were retrieved via Ovid MEDLINE and evaluated. A total of 202 studies were included. LAMP3, ULK1, TRIB3, CHOP, NOXA, NORAD, SIAH1/2, DYRK2, HIPK2, CREB, NUPR1, JMJD2B, NRF2, GSK-3B, GADD45a, GADD45b, STAU1, C-SRC, HK2, CAV1, CypB, CLU, IGFBP-3 and SP1 were highlighted as potential links between the hypoxic DDR and UPR. Overall, we identified very few studies which demonstrate a molecular link between the DDR and UPR in hypoxia, however, it is clear that many of the molecules highlighted warrant further investigation under radiobiological hypoxia as these may include novel therapeutic targets to improve radiotherapy response.

Introduction

Oxygen homeostasis in eukaryotes is essential in order to maintain aerobic metabolism and intracellular bioenergetics. Due to the high proliferative and metabolic rates observed in malignant cells, tumours rapidly outgrow their oxygen supply leading to regions of hypoxia (insufficient oxygen) [1]. Typically, the following terms are used to define cellular oxygen concentration: normoxia (21% O_2), tissue normoxia or physoxia (4–7.5% O_2), hypoxia (1–2% O_2) and radiobiological hypoxia (<0.1% O_2) [2–4]. Both hypoxia and radiobiological hypoxia are associated with the stabilisation of the hypoxia-inducible factors (HIF-1/2) [5]. The hypoxic tumour microenvironment drives genomic instability, down-regulates DNA repair and is associated with therapy resistance. Importantly, hypoxic tumours are associated with more aggressive disease, metastasis and poor patient prognosis [6,7].

The biological response to radiobiological hypoxia includes the DNA damage response (DDR) (Figure 1). Deregulation of the DDR is frequent and occurs early in cancer and drives genomic instability [8–10]. Radiobiological hypoxia leads to a replication stress-induced DDR, which is demonstrated by an increase in stalled replication forks, decreased origin firing and significant reduction in DNA replication rates [11,12]. The hypoxia-induced DDR includes the activation of the ATM and ATR

*These authors contributed equally to this work.

Received: 4 March 2021
Revised: 22 April 2021
Accepted: 23 April 2021

Version of Record published: 18 May 2021

Downloaded from http://portlandpress.com/biochemsoctrans/article-pdf/49/3/1251/916214/bst-2020-0861c.pdf by UK user on 19 September 2022

© 2021 The Author(s). This is an open access article published by Portland Press Limited on behalf of the Biochemical Society and distributed under the Creative Commons Attribution License 4.0 (CC BY).

Biochemical Society Transactions (2021) 49 1251–1263
https://doi.org/10.1042/BST20200861

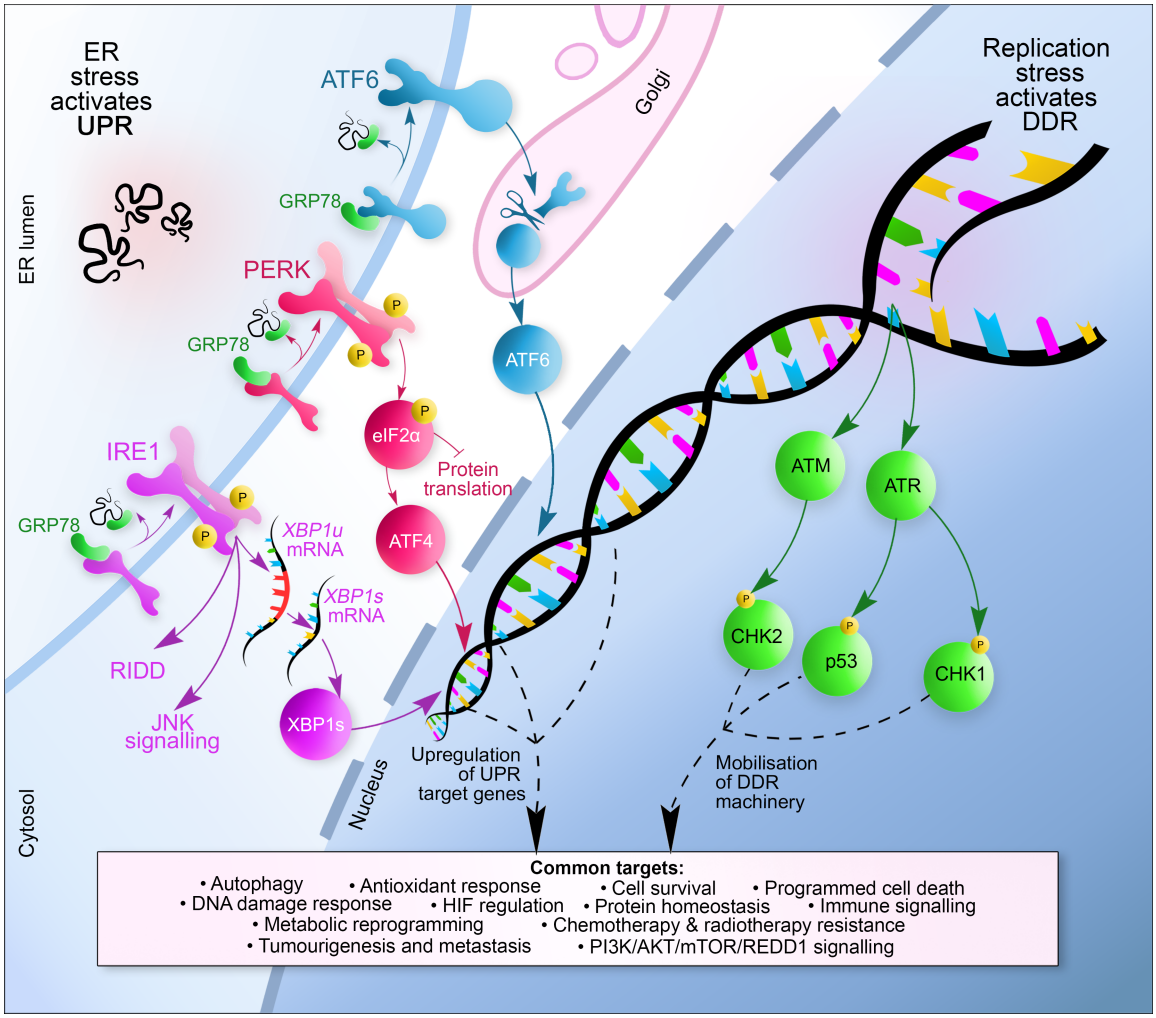


Figure 1. Overview of the hypoxia activated UPR and DDR pathways.

The UPR sensors, PERK, IRE1 and ATF4 are held in an inactive state via the binding of GRP78, a chaperone protein and the master regulator of the UPR. Hypoxia-induced ER stress leads to the dissociation of GRP78 from these sensors as GRP78 detects and binds to unfolded proteins. Following activation, PERK phosphorylates eIF2α to inhibit protein synthesis and allows for the transcription of ATF4 which leads to the transcriptional induction of genes associated with apoptosis, autophagy and amino acid metabolism. Activation of IRE1 followed by autophosphorylation activates its RNase activity leading to the alternative splicing of XBP1u to form XBP1s, a transcription factor that controls the transcription of genes encoding proteins involved in protein folding. ATF6 is transported to the Golgi upon activation where it is processed by S1P and S2P generating a cytosolic fragment (ATF6f) which up-regulates the transcription of genes involved in ERAD. Simultaneously, in the cells in S-phase, hypoxia leads to replication stress, manifested by stalled replication forks, decreased origin firing and an accumulation of single-stranded DNA. Hypoxia-induced replication stress activates the DDR pathway which includes both the ATM and ATR kinases. ATM and ATR phosphorylate their target transducers including, but not limited to, Chk1, Chk2 and p53. The transducers then up-regulate effectors, including genes that play a role in cell cycle arrest, apoptosis and DNA repair. The biological endpoints of UPR and DDR signalling are shared and focus on resolving the stress, allowing the cell time to repair and recover or, in the case of extreme stress and irreparable damage inducing cell death.

kinases, and phosphorylation of their downstream targets (Chk2, KAP1, Chk1, RPA, p53 and H2AX) [13]. Importantly, this DDR occurs in the apparent absence of detectable DNA damage (SSBs or DSBs) [13]. Hypoxia mediated changes to the chromatin also play a critical role in the induction of the DDR, for example ATM activation in hypoxia is linked to both replication stress and trimethylation of histone 3 at lysine 9 (H3K9me3) [14,15].

© 2021 The Author(s). This is an open access article published by Portland Press Limited on behalf of the Biochemical Society and distributed under the Creative Commons Attribution License 4.0 (CC BY).

Downloaded from http://portlandpress.com/biochemsoctrans/article-pdf/49/3/1251/916214/bst-2020-0861c.pdf by UK user on 19 September 2022

The unfolded protein response (UPR) is a cyto-protective, adaptive mechanism that maintains protein homeostasis (Figure 1). The UPR is activated upon the detection of misfolded proteins in the endoplasmic reticulum (ER), the main site of folding and maturation for transmembrane, secretory and ER-resident proteins in the cell [16]. Stressors such as hypoxia, viral infection, starvation, calcium depletion, hyper- or hypothermia and acidosis are all known to activate the UPR [17]. Experimentally, thapsigargin and tunicamycin, which cause ER stress by blocking the SERCA calcium pump on the ER membrane or by blocking N-linked glycosylation, respectively are commonly used to pharmacologically induce a UPR [18,19]. Once activated, the UPR inhibits protein synthesis, increases the folding capacity of chaperones, and transcriptionally activates UPR genes that lead to a myriad of outcomes (cell death through apoptosis, pro-survival pathways, autophagy, degradation of permanently misfolded proteins through endoplasmic reticulum-associated degradation (ERAD), amino acid and lipid biosynthesis, and redox homeostasis) [20]. Disulfide bonds occur in a significant proportion of membrane and secreted proteins, through an oxygen-dependent process including ER oxidoreductin (Ero1), and the soluble thiol-disulfide oxireductase protein disulfide isomerase (PDI) [21–23]. Therefore, radiobiological hypoxia leads to an accumulation of misfolded proteins within the ER lumen as a result of an inability to form disulfide bonds [24,25].

Notably, both the DDR and UPR are induced in response to hypoxia; however, most importantly this occurs with the same oxygen dependency. Radiobiological hypoxia (<0.1% O_2) is required to activate both the DDR and UPR. This suggests that the most therapy resistant fraction of solid tumours has active DNA damage and unfolded protein responses and raises the possibility that the two pathways may interact to lead to biological outcomes that promote tumour survival.

In support of this hypothesis, we recently demonstrated that hypoxia induces expression of the RNA/DNA helicase, senataxin (SETX), through the PERK/ATF4 arm of the UPR. Hypoxia-induced SETX reduces replication stress potentially through the resolution of DNA/RNA hybrids (R-loops) and prevents the accumulation of DNA damage [26]. SETX was also identified through RNA-sequencing as part of an XBP1-dependent gene signature [27]. To our knowledge, this is the most explicit link between the DDR and UPR that has been described in hypoxic conditions.

Direct links between the UPR and DDR under normoxic conditions have been described (recently reviewed in [28]). Indeed, the UPR may play a role in protecting the genome from DNA damage in normoxia. For example, IRE1 has an evolutionarily conserved role in protecting cells exposed to genotoxic stress through controlling the mRNA stability of DDR genes which impacts DNA repair, cell cycle arrest and apoptosis [29]. PERK deficiency leads to an accumulation of ROS and oxidative DNA damage in tumour cells and a Chk2-dependent cell cycle arrest [30]. Thapsigargin-induced UPR leads to the phosphorylation of Chk1 via Claspin1 and slowing of replication forks [31].

Importantly, like hypoxia, exposure to radiation has been shown to lead to both a DDR and UPR [32,33]. While a number of DDR inhibitors have been shown to increase radiosensitivity in both normoxic and hypoxic conditions, the links between the UPR and radiation response are less clear [34]. Studies have shown that inhibiting the UPR can increase radiosensitivity. Specifically, inhibition of PERK or knockdown of ATF4 reduces survival of glioblastoma cells exposed to ionising radiation (IR) [35]. The UPR can activate pro-survival autophagy through the PERK and IRE1 arms following irradiation [33,36]. Exposure to ionising radiation (1 Gy) has been shown to up-regulate UPR gene expression including GRP78, ATF4, CHOP and XP1 in blood samples collected from cancer patients [37]. However, studies also exist which demonstrate that activating the UPR can sensitise cells to ionising radiation. For example, the UPR can suppress DSB repair and sensitise tumour cells to ionising radiation through the proteasomal degradation of Rad51, an essential factor for homologous recombination [38]. Activation of the UPR using the HIV protease inhibitor, nelfinavir, was shown to radiosensitise head and neck cancer cells [39]. UPR activation through the inhibition of the protein disulfide isomerase, PDIA1, decreases DNA repair capacity after irradiation through the down-regulation of DNA repair genes and leads to increased radiosensitivity [40]. This evidence linking the UPR to radiosensitivity highlights an additional example of where the DDR and UPR co-exist.

The DDR and UPR direct a coordinated response to cellular stress that is particularly relevant in hypoxic conditions which induce both replication and ER stress leading to the DDR and UPR, respectively. Moreover, these hypoxic conditions provide the ideal context to uncover UPR-DDR links as it is one of the few physiologically relevant stresses that induces both pathways. This systematic review presents an analysis of published literature in the last decade, for potential links between the DDR and UPR specifically in hypoxic conditions.

Downloaded from http://portlandpress.com/biochemsoctrans/article-pdf/49/3/1251/916214/bst-2020-0861c.pdf by UK user on 19 September 2022

© 2021 The Author(s). This is an open access article published by Portland Press Limited on behalf of the Biochemical Society and distributed under the Creative Commons Attribution License 4.0 (CC BY).

PORTLAND PRESS

Biochemical Society Transactions (2021) **49** 1251–1263
https://doi.org/10.1042/BST20200861

Methods

This systematic review was conducted following the standards set by the PRISMA (Preferred Reporting Items for Systematic Reviews and Meta-Analyses) statement. Literature containing experimental evidence were retrieved via Ovid MEDLINE, following an electronic search restricted to publications between January 1, 2010 and October 9, 2020. This period was chosen to ensure the most recent publications were reviewed but to also limit the number of publications to allow thorough review. To increase the sensitivity of our search, relevant and closely related terms were determined and appropriately truncated to account for derivational affixes (Figure 2). Shortlisted records were initially reviewed for duplicates; remaining materials were then evaluated for suitability at the title, abstract and full-text levels. Study selection was based on eligibility criteria designed around the SPIDER (Sample, Phenomenon of Interest, Design, Evaluation and Research type) framework (Supplementary Table S1). Any paper with hypoxic conditions of <2% O_2 was included in the screen. We

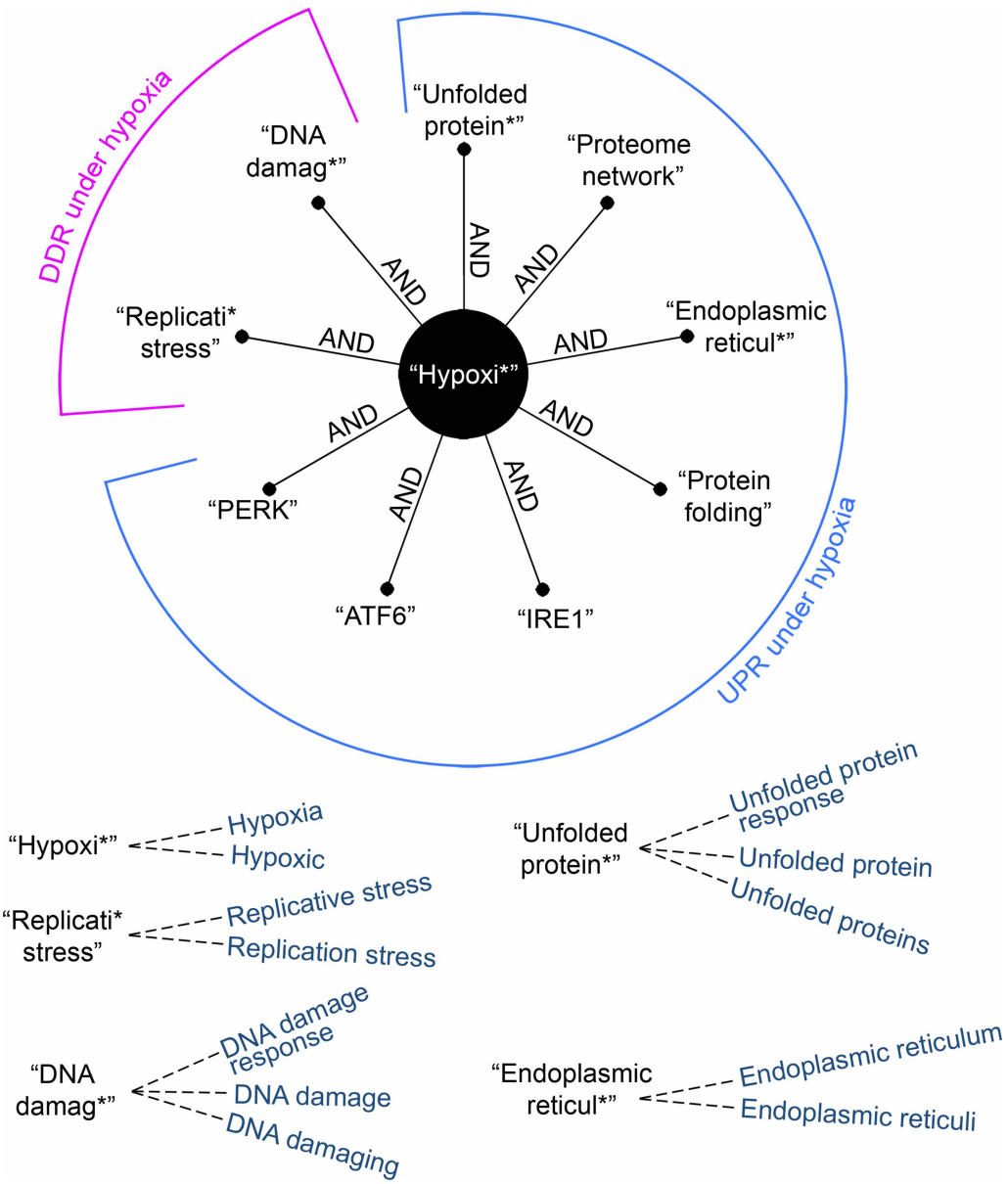


Figure 2. Boolean search strategy used.

Relevant and closely related terms were determined and appropriately truncated to account for derivational affixes.

Downloaded from http://portlandpress.com/biochemsoctrans/article-pdf/49/3/1251/916214/bst-2020-0861c.pdf by UK user on 19 September 2022

© 2021 The Author(s). This is an open access article published by Portland Press Limited on behalf of the Biochemical Society and distributed under the Creative Commons Attribution License 4.0 (CC BY).

chose to include this broad range of hypoxic conditions because the reported O_2 level rarely reflects the actual O_2 concentration in the cell culture dish and in some cases (e.g. after prolonged exposure), the O_2 concentration may be significantly lower than reported and therefore lead to a DDR/UPR. Large variations in methodology for hypoxia induction were found and include differences in duration, glucose levels in the medium, and surface area of the dish. To reduce subjectivity, the screening was conducted independently by two reviewers (Bolland, H. and Ma, T.), checked by a third reviewer (Ramlee, S.), and any discrepancies between the results of the screens were resolved. The search yielded 2,490 articles for review and, following exclusion, 202 articles remained for further analysis (Figure 3 and Supplementary Table S2).

Data extraction was then carried out to assess study methodology (oxygen concentration and cell lines used), reported observations and identified biological regulators. Papers which were identified as being part of the hypoxic DDR or the hypoxic UPR but not both, were further investigated to determine if by including studies carried out in normoxic conditions links between the UPR and DDR could be determined. One limitation of this methodology is that papers that include experiments carried out in hypoxia but do not contain the key terms in the title or abstract will have not been included in this screen (for example [41]).

Results

Our systematic approach identified no published studies that have explicitly investigated the links between the DDR and the UPR in hypoxia (<2% O_2). However, it was clear that the DDR and the UPR interact with many of the same pathways in hypoxia, including: autophagy, HIF regulation, immune signalling, metabolic reprogramming, antioxidant response and PI3K/AKT/mTOR signalling. Through systematic review, we have identified several genes, which although not linked directly to both the hypoxia-induced DDR and UPR, represent credible links between these two pathways. Specifically, we identified genes which have been described to play roles in the hypoxic DDR or UPR but by including some studies in normoxic conditions we found evidence that the genes play roles in both stress response pathways (Supplementary Table S3). The majority of the factors identified are discussed in brief below, organised by the stage/arm of the UPR they are linked to.

General ER stress induced

Specificity protein 1 (Sp1) is a transcription factor that is overexpressed in several cancers and regulates genes involved in cell cycle and proliferation [42]. Sp1 has been shown to have a dual role in regulating the UPR in Panc-1 cells; it is required for GRP78 activation by ER stress and, in the same cell line, is required for the induction of UPR genes via binding to ER stress response elements (ERSEs) in target gene promoters [43]. Sp1 and HIFs collaborate upon exposure to 1% O_2 to activate genes needed to adapt to the hypoxic microenvironment [44]. Sp1 knockdown leads to lysosomal membrane permeabilisation, chronic ER stress and cell death due to the inability of cells to activate GRP78 and the UPR [45]. In response to ionising radiation, Sp1 is phosphorylated by ATM and localises with the MRN complex at sites of DNA damage to facilitate DNA repair [46]. Together, these data suggest that inhibition of Sp1 would represent a strategy to radiosensitise hypoxic tumours via inhibition of both the cytoprotective UPR and DDR.

Clusterin (CLU), is a pro-survival, chaperone-like protein, that stabilises unfolded proteins and has been demonstrated to play a role in DNA repair and cell cycle regulation [47,48]. CLU is induced upon genotoxic stress; siRNA inhibition of CLU was found to sensitise cells to a variety of DNA damaging agents including ionising radiation [49–51]. CLU has previously been shown to be induced under 1% O_2 via direct binding of HIF1α to hypoxic response elements in the CLU promoter [52]. CLU was found to be required for the activation of pro-survival autophagy in human proximal tubular epithelial cells induced by exposure to 1% O_2. Furthermore, CLU knockdown led to a reduction in UPR related gene expression in hypoxic kidney cells [53]. Given that loss of CLU has been shown to radiosensitise and that it is induced in hypoxia (1% O_2), it seems likely that inhibition of CLU could be an effective strategy to improve radiation response of hypoxic tumours.

PERK signalling

Lysosome-associated membrane glycoprotein 3 (LAMP3) expression is controlled by the PERK/ATF4 arm of the UPR. In response to ionising radiation, LAMP3 knockdown was found to reduce the formation of γH2AX foci and the expression of DDR proteins (DNAPK, phosphorylated ATM and ATR) leading to increased radiosensitivity [54]. The LAMP3-dependent impact on the DDR was proposed to be through an autophagy-dependent mechanism. Autophagy has previously been implicated in cellular radiosensitivity through multiple mechanisms including ATM/AMPK/TSC2 signalling (recently reviewed [55]). Our analysis highlighted that

Downloaded from http://portlandpress.com/biochemsoctrans/article-pdf/49/3/1251/916214/bst-2020-0861c.pdf by UK user on 19 September 2022

© 2021 The Author(s). This is an open access article published by Portland Press Limited on behalf of the Biochemical Society and distributed under the Creative Commons Attribution License 4.0 (CC BY).

Biochemical Society Transactions (2021) **49** 1251–1263
https://doi.org/10.1042/BST20200861

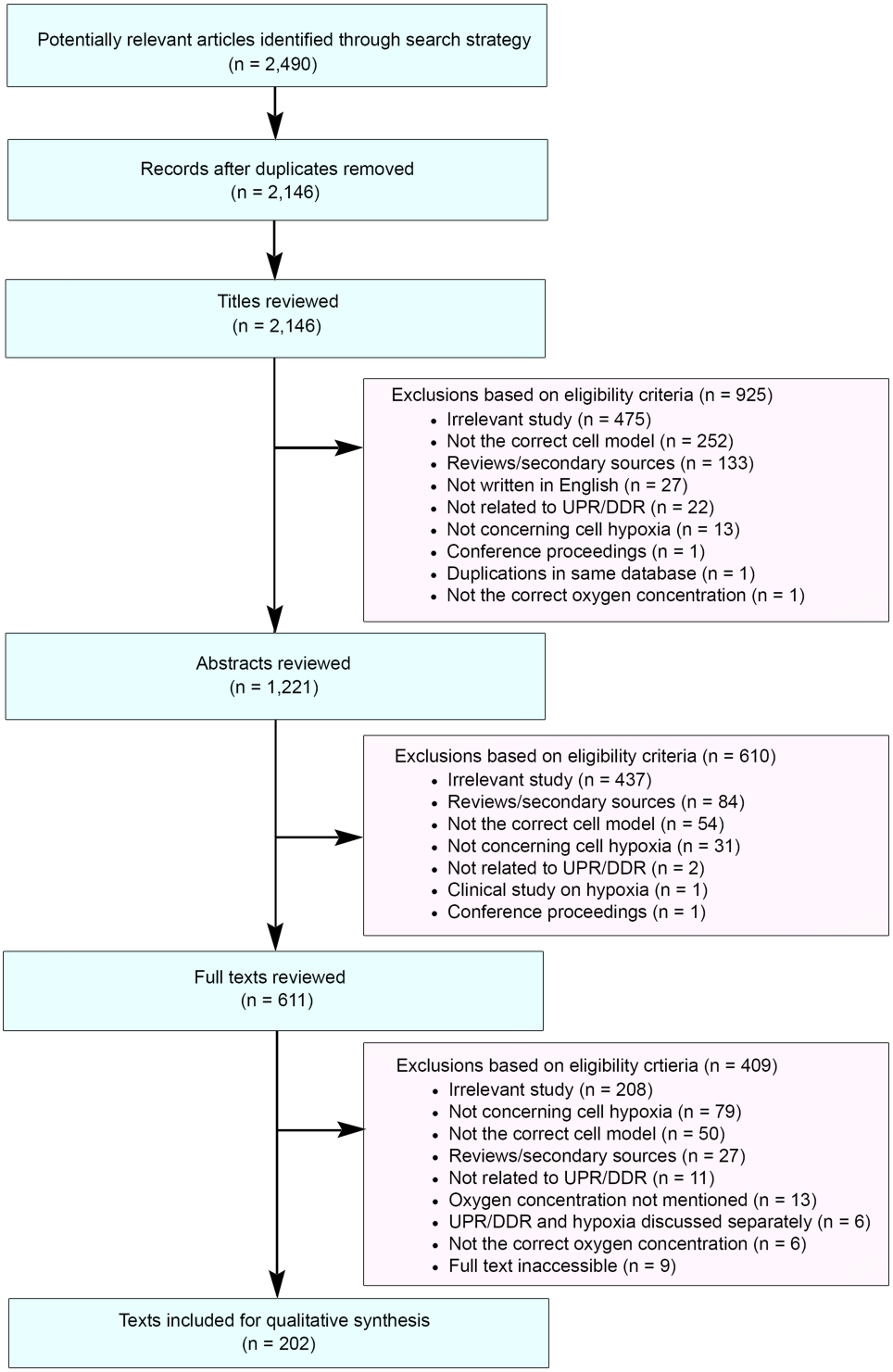


Figure 3. PRISMA flow diagram of the systematic literature exclusion process.
Ovid MEDLINE database was used to identify potentially relevant studies published between January 1, 2010 and October 9, 2020.

LAMP3 was also induced following treatment with tunicamycin and, in a cell line-dependent manner, in hypoxia (0.1% O_2) [56]. Knockdown of PERK, ATF4 and LAMP3 led to a reduction in breast cancer cell migration, with more pronounced effects observed at 0.1% O_2 compared with 1% O_2. LAMP3 knockdown also

Downloaded from http://portlandpress.com/biochemsoctrans/article-pdf/49/3/1251/916214/bst-2020-0861c.pdf by UK user on 19 September 2022

© 2021 The Author(s). This is an open access article published by Portland Press Limited on behalf of the Biochemical Society and distributed under the Creative Commons Attribution License 4.0 (CC BY).

reduced spheroid invasion in a breast cancer cell line [57]. It seems likely that LAMP3 knockdown may impact the hypoxic DDR and UPR and affect radiosensitivity.

Unc-51 like autophagy activating kinase 1 (ULK1) is a serine-threonine kinase that regulates autophagic flux [58]. In response to DNA damage, ULK1, is a transcriptional target of p53 and enhances the activity of the chromatin-associated enzyme PARP1 leading to sustained autophagy and cell death [59,60]. ULK1 is rapidly induced following exposure to hypoxia (<0.02% O_2) and is under the control of the PERK arm of the UPR [61]. ULK1 knockdown significantly reduced clonogenic survival of human colorectal and breast cancer cell lines in hypoxia (<0.02% O_2) but not in normoxic conditions [61]. Given the evidence that ULK1 plays a role in the UPR in hypoxia and is linked to the DDR in normoxia, it seems likely that perturbing ULK1 in hypoxia would impact both the UPR and DDR.

TRIB3 is a pseudo kinase protein, which lacks kinase activity and is overexpressed in several human cancers [62,63]. TRIB3 has been shown to protect HeLa cells from DSBs induced as the result of APOBEC3A-mediated deamination and is part of the CtIP-BRCA1-ATM network regulating the cell cycle, DNA repair and genome stability [64]. TRIB3 has been shown to be induced by both thapsigargin and hypoxia (0.1–0.5% O_2) in breast cancer cells and was found to co-localise with Pimonidazole (a marker of hypoxia) in breast cancer tissue. In hypoxic conditions, TRIB3 induction was found to be dependent on the PERK/ATF4/CHOP pathway and depletion of TRIB3 reduced cell survival under hypoxic conditions [65]. Interestingly, mass spectrometry has revealed that TRIB3 binds to DNA damage related proteins HMG1, TOP1, Ku80 and multiple members of the DDX family of RNA/DNA helicases [66]. This raises the question of whether inhibition of TRIB3, a UPR induced protein, leads to changes in genomic stability via its interactions with DDR proteins in hypoxia and therefore links the UPR to the protection of the genome in hypoxia.

DNA damage-inducible transcript 3 (DDIT3 or CHOP) was originally identified as a transcription factor responding to UV radiation and has since been shown to be a key effector of the UPR [67,68]. CHOP activity leads to cell cycle arrest and apoptosis following chronic UPR activation through transactivation of targets including BIM, NOXA PUMA, BAD and GADD34 [69,70]. CHOP depletion through siRNA knockdown reduces cell viability in hypoxic (1% O_2) prostate stromal cells via the inhibition of hypoxia-induced autophagy [71]. NOXA, a CHOP target gene, is responsible for apoptosis and hypoxia-induced cell death, and responds to DNA damage-induced p53 activation [72]. The lncRNA NORAD (non-coding RNA activated by DNA damage) is needed for the assembly of a topoisomerase complex for maintaining genome stability [73]. NORAD has been demonstrated to be hypoxia-inducible (1% O_2) and is required for full activation of the UPR including CHOP expression [74]. Disruption of CHOP may lead to a reduction in cell death but promote genomic instability; this warrants further investigation under radiobiological hypoxia to determine if this enhances radiosensitivity or otherwise.

SIAH proteins are E3 ubiquitin ligases that modulate the hypoxic response via their degradation of the prolyl hydroxylase, PHD3, leading to HIF1α stabilisation [75]. In addition, SIAH1/2 have been shown to play a role in the DDR via its interactions with p53, HIPK2, ATM and ATR [76]. SIAH1/2 are stress responsive; after DNA damage, SIAH1 expression is induced by p53 and the protein is phosphorylated by ATM/ATR [77]. SIAH1/2 are also part of the UPR, the transcription of SIAH1/2 is dependent on PERK/ATF4 and IRE1α/XBP1 in response to tunicamycin [78]. The induction of SIAH proteins by both the UPR and DDR suggests possible links in hypoxic conditions. For example, in hypoxia (1% O_2) the dual-specificity protein kinase, DYRK2, is a target of SIAH2-dependent degradation. The consequence of SIAH2-dependent degradation of DYRK2, includes reduced phosphorylation of p53 at residue serine 45 in response to doxorubicin-induced DNA damage in hypoxia [79]. An interesting hypothesis is that the hypoxia (<0.1% O_2) induced UPR may modulate the balance between SIAH2 and DYRK2 altering p53 dependent apoptosis in hypoxia. SIAH2 was also found to regulate the DDR through Chk2 turnover; inhibition of SIAH2 under 1% O_2 led to an increase in Chk2 expression [80].

The transcription factor, CREB is overexpressed in many human cancers and regulates the control of genes that function in cell cycle control, DNA repair and metabolism [81]. CREB has previously been demonstrated to regulate the expression of key DDR genes including ATM, ATR and RAD51; for example overexpression of CREB led to an increase in DDR signalling following etoposide treatment [82]. This systematic review highlights that phosphorylation and activation of CREB occurred in response to treatment with either thapsigargin or tunicamycin [83]. The same report described an induction of CREB in response to prolonged treatment (48 hours) at 1% O_2, although the authors noted the induction of the UPR in response to 1% O_2 was only moderate in comparison with Thapsigargin or Tunicamycin treatment [83]. These data suggest that CREB

Downloaded from http://portlandpress.com/biochemsoctrans/article-pdf/49/3/1251/916214/bst-2020-0861c.pdf by UK user on 19 September 2022

© 2021 The Author(s). This is an open access article published by Portland Press Limited on behalf of the Biochemical Society and distributed under the Creative Commons Attribution License 4.0 (CC BY).

Biochemical Society Transactions (2021) **49** 1251–1263
https://doi.org/10.1042/BST20200861

activity is induced in response to an UPR and that this would be more evident in radiobiological levels of hypoxia.

NRF2 is the master transcriptional regulator of the antioxidant response [84]. NRF2 has been shown to protect epithelial cells from ionising radiation by enhancing DDR signalling, reducing chromosomal aberrations and releasing DNA replication block [85]. Specifically, after irradiation, NRF2 was found to directly bind to antioxidant response elements (AREs) within the promoter region of the DNA damage sensor, 53BP1 [85]. Results from our analysis found that NRF2 was activated following exposure to hypoxia (24 hours at 1% O_2) in HepG2 cells. NRF2 was also found to activate ABCB1 mediated chemoresistance via an increase in drug efflux in hypoxia. Indeed, siRNA knockdown of NRF2 increased doxorubicin-induced apoptosis in HepG2 cells exposed to 1% O_2 [86]. NRF2 has also been shown to be up-regulated in response to anoxia and thapsigargin treatment in retinal pigment epithelial cells and concomitantly with the UPR under severe hypoxia but not mild hypoxia (4% O_2) in human lens epithelial cells [87,88]. Hypoxia, somewhat paradoxically, leads to an increase in mitochondrial ROS, leading to dissociation of NRF2 from its negative regulator Keap1, allowing it to translocate to the nucleus to regulate the transcription of antioxidant response genes [89,90]. Disruption of NRF2 signalling in radiobiological hypoxia may radiosensitise cells through its interaction with both the DDR and UPR.

The serine-threonine kinase, GSK-3β, contributes to the hypoxia-induced UPR (<1% O_2) through down-regulation of γ-Taxilin, an inhibitor of ATF4 activity [91]. GSK-3β has been shown to contribute to UPR-induced apoptosis via PP2A/AKT-dependent GSK-3β activation. This interaction occurs on a cytoplasmic ATM platform. Exposure to 1% O_2 was found to increase the expression of PP2A in ATM precipitates in 293T cells [41]. In addition, GSK-3β has been shown to translocate from the cytoplasm to the nucleus to induce DNA DSB repair by phosphorylating 53BP1 after irradiation and has been described as indispensable for DNA DSB repair [92]. The role of GSK-3β in the radiation response in hypoxic conditions which also lead to repression of the main DNA repair pathways is likely to yield interesting findings.

IRE1α signalling

SRC is a protein-tyrosine kinase that is overexpressed in a variety of cancers and induced in hypoxia [93,94]. Inhibition of c-SRC radiosensitised glioblastoma cells exposed to 1% O_2 and this was attributed to comprised DNA repair as indicated by sustained γH2AX staining [95]. SRC is activated by the UPR, forms a complex with IRE1α and acts to relocate ER chaperones to the cell surface [96]. In addition, SRC has also been implemented in regulation of the DDR via termination of the ATR-Chk1 dependent G2 DNA damage checkpoint [97]. Together, these findings suggest that inhibition of c-SRC may have profound impact on the radiosensitivity of cells experiencing radiobiological hypoxia i.e. the most therapy resistant tumour fraction.

Hexokinase 2 (HK2) the rate limiting enzyme in glycolysis is often overexpressed in cancers [98]. HK2 is induced following exposure to 1% O_2 and treatment with tunicamycin in an XBP1-dependent manner [99]. Loss of HK2 expression led to a reduction in glioma cell viability in hypoxia [99]. Furthermore, loss of HK2 led to increased DNA damage measured via comet assay in response to IR in U87 and GS2 cells [100]. These data suggest that HK2 would likely also be induced under radiobiological hypoxia and its inhibition could radiosensitise through increased DNA damage.

Caveolin-1 (Cav1) is a membrane protein and the main component of caveolae which are cholesterol enriched invaginations of the plasma membrane that are important for endocytosis, cell transport and cell signalling. Cav1 is overexpressed in a variety of cancers [101]. Cav1 expression suppresses UPR activation in melanoma cells following exposure to hypoxia (1% O_2) via direct binding to and repression of IRE1α [102]. Knockdown of Cav1 increased UPR activation and led to an increase in IR-induced ssDNA and γH2AX alongside a reduction in phospho-ATM and DSB repair by HR [103].

ATF6 signalling

Cyclophilin B (CypB) is a molecular chaperone that acts to fold and process newly synthesised proteins [104]. CypB is up-regulated in hypoxia by ATF6 (0.1% O_2) and cooperates with p300 to modulate the ubiquitination and degradation of CHOP under hypoxic conditions [105,106]. Knockdown of CypB led to an increase in hypoxia induced apoptosis at 0.1% O_2 [106]. CypB knockdown supressed p53 induction and sensitised cells to daunorubicin [104].

Downloaded from http://portlandpress.com/biochemsoctrans/article-pdf/49/3/1251/916214/bst-2020-0861c.pdf by UK user on 19 September 2022

© 2021 The Author(s). This is an open access article published by Portland Press Limited on behalf of the Biochemical Society and distributed under the Creative Commons Attribution License 4.0 (CC BY).

Conclusion

There are clear mechanistic and functional links between the DDR and UPR [28]. Hypoxia is one of few physiologically relevant stresses to lead to both a UPR and DDR and yet, surprisingly, there are only isolated reports of links between these two pathways. Furthermore, in those that have been investigated in hypoxia, there is a lack of consensus regarding the appropriate oxygen concentration to be used for the study of the DDR and UPR. Of note, the majority of the papers identified in this review focus on cancer, however, many reports identified in the initial screen investigated ischemia-reperfusion injury, stroke, obstructive sleep apnoea and hypertension. Due to exclusion criteria used in this review, these papers were not included as they were predominantly carried out in mouse or rat cell lines. It is likely that further links between the hypoxic DDR and UPR could be identified by also considering these pathophysiological conditions. Overall, the genes and proteins that have been identified from this review demonstrate that significant links between the hypoxic UPR and DRR are likely and warrant further investigation in this context. Most importantly, research in this area could identify therapeutic strategies which could be used to target the most therapy-resistant fraction of solid tumours.

Perspectives

- Both the UPR and DDR pathways have a significant impact on the cellular response to hypoxia.
- Links between the two pathways are emerging using pharmacological induction of either pathway.
- Further research is highly likely to identify mechanistic and functional links between the UPR and DDR which are important in hypoxia.

Competing Interests

The authors declare that there are no competing interests associated with the manuscript.

Open Access

Open access for this article was enabled by the participation of University of Oxford in an all-inclusive *Read & Publish* pilot with Portland Press and the Biochemical Society under a transformative agreement with JISC.

Author Contributions

Author contributions to the systematic screen are described in the methods section. H.B./T.S.M. wrote the manuscript which was edited by EMH and KR. SR drew Figures 1 and 2.

Acknowledgements

H.B. was funded by an EPSRC programme grant (EP/S019901/1) awarded to E.M.H. K.R. is supported by MRC Programme grant MC_PC 12001/1 (MC_UU_00001/1).

Abbreviations

AREs, antioxidant response elements; CLU, Clusterin; ER, endoplasmic reticulum; ERAD, endoplasmic reticulum associated degradation; HIF, hypoxia inducible factors; HK2, hexokinase 2; LAMP3, Lysosome-associated membrane glycoprotein 3; SETX, senataxin; ULK1, autophagy activating kinase 1; UPR, unfolded protein response.

References

1 Vaupel, P. and Harrison, L. (2004) Tumor hypoxia: causative factors, compensatory mechanisms, and cellular response. *Oncologist* **9**, 4–9 https://doi.org/10.1634/theoncologist.9-90005-4

2 Soni, S. and Padwad, Y.S. (2017) HIF-1 in cancer therapy: two decade long story of a transcription factor. *Acta Oncol.* **56**, 503–515 https://doi.org/10.1080/0284186X.2017.1301680

© 2021 The Author(s). This is an open access article published by Portland Press Limited on behalf of the Biochemical Society and distributed under the Creative Commons Attribution License 4.0 (CC BY).

Downloaded from http://portlandpress.com/biochemsoctrans/article-pdf/49/3/1251/916214/bst-2020-0861c.pdf by UK user on 19 September 2022

3 McKeown, S.R. (2014) Defining normoxia, physoxia and hypoxia in tumours—implications for treatment response. *Br. J. Radiol.* **87**, 20130676 https://doi.org/10.1259/bjr.20130676
4 Hammond, E.M., Asselin, M.-C., Forster, D., O'Connor, J.P.B., Senra, J.M. and Williams, K.J. (2014) The meaning, measurement and modification of hypoxia in the laboratory and the clinic. *Clin. Oncol.* **26**, 277–288 https://doi.org/10.1016/j.clon.2014.02.002
5 Semenza, G.L. (2012) Hypoxia-inducible factors in physiology and medicine. *Cell* **148**, 399–408 https://doi.org/10.1016/j.cell.2012.01.021
6 Horsman, M.R. and Overgaard, J. (2016) The impact of hypoxia and its modification of the outcome of radiotherapy. *J. Radiat. Res.* **57**, i90–i98 https://doi.org/10.1093/jrr/rrw007
7 Kim, J.-Y. and Lee, J.-Y. (2017) Targeting tumor adaption to chronic hypoxia: implications for drug resistance, and How It Can Be overcome. *Int. J. Mol. Sci.* **18**, 1854 https://doi.org/10.3390/ijms18091854
8 Blackford, A.N. and Jackson, S.P. (2017) ATM, ATR, and DNA-PK: the trinity at the heart of the DNA damage response. *Mol. Cell* **66**, 801–817 https://doi.org/10.1016/j.molcel.2017.05.015
9 Bartkova, J., Horejsí, Z., Koed, K., Krämer, A., Tort, F., Zieger, K. et al. (2005) DNA damage response as a candidate anti-cancer barrier in early human tumorigenesis. *Nature* **434**, 864–870 https://doi.org/10.1038/nature03482
10 Gorgoulis, V.G., Vassiliou, L.-V.F., Karakaidos, P., Zacharatos, P., Kotsinas, A., Liloglou, T. et al. (2005) Activation of the DNA damage checkpoint and genomic instability in human precancerous lesions. *Nature* **434**, 907–913 https://doi.org/10.1038/nature03485
11 Pires, I.M., Bencokova, Z., Milani, M., Folkes, L.K., Li, J.-L., Stratford, M.R. et al. (2010) Effects of acute versus chronic hypoxia on DNA damage responses and genomic instability. *Cancer Res.* **70**, 925–935 https://doi.org/10.1158/0008-5472.CAN-09-2715
12 Foskolou, I.P., Jorgensen, C., Leszczynska, K.B., Olcina, M.M., Tarhonskaya, H., Haisma, B. et al. (2017) Ribonucleotide reductase requires subunit switching in hypoxia to maintain DNA replication. *Mol. Cell* **66**, 206–220.e9 https://doi.org/10.1016/j.molcel.2017.03.005
13 Bencokova, Z., Kaufmann, M.R., Pires, I.M., Lecane, P.S., Giaccia, A.J. and Hammond, E.M. (2009) ATM activation and signaling under hypoxic conditions. *Mol. Cell. Biol.* **29**, 526–537 https://doi.org/10.1128/MCB.01301-08
14 Olcina, M.M., Foskolou, I.P., Anbalagan, S., Senra, J.M., Pires, I.M., Jiang, Y. et al. (2013) Replication stress and chromatin context link ATM activation to a role in DNA replication. *Mol. Cell* **52**, 758–766 https://doi.org/10.1016/j.molcel.2013.10.019
15 Olcina, M.M., Leszczynska, K.B., Senra, J.M., Isa, N.F., Harada, H. and Hammond, E.M. (2016) H3k9me3 facilitates hypoxia-induced p53-dependent apoptosis through repression of APAK. *Oncogene* **35**, 793–799 https://doi.org/10.1038/onc.2015.134
16 Hetz, C. (2012) The unfolded protein response: controlling cell fate decisions under ER stress and beyond. *Nat. Rev. Mol. Cell Biol.* **13**, 89–102 https://doi.org/10.1038/nrm3270
17 Walter, P. and Ron, D. (2011) The unfolded protein response: from stress pathway to homeostatic regulation. *Science* **334**, 1081–1086 https://doi.org/10.1126/science.1209038
18 Doan, N.T.Q., Paulsen, E.S., Sehgal, P., Møller, J.V., Nissen, P., Denmeade, S.R. et al. (2015) Targeting thapsigargin towards tumors. *Steroids* **97**, 2–7 https://doi.org/10.1016/j.steroids.2014.07.009
19 Wyszynski, F.J., Lee, S.S., Yabe, T., Wang, H., Gomez-Escribano, J.P., Bibb, M.J. et al. (2012) Biosynthesis of the tunicamycin antibiotics proceeds via unique exo-glycal intermediates. *Nat. Chem.* **4**, 539–546 https://doi.org/10.1038/nchem.1351
20 Bravo, R., Parra, V., Gatica, D., Rodriguez, A.E., Torrealba, N., Paredes, F. et al. (2013) Endoplasmic reticulum and the unfolded protein response: dynamics and metabolic integration. *Int. Rev. Cell Mol. Biol.* **301**, 215–290 https://doi.org/10.1016/B978-0-12-407704-1.00005-1
21 Wouters, B.G. and Koritzinsky, M. (2008) Hypoxia signalling through mTOR and the unfolded protein response in cancer. *Nat. Rev. Cancer* **8**, 851–864 https://doi.org/10.1038/nrc2501
22 Bartoszewska, S. and Collawn, J.F. (2020) Unfolded protein response (UPR) integrated signaling networks determine cell fate during hypoxia. *Cell. Mol. Biol. Lett.* **25**, 18 https://doi.org/10.1186/s11658-020-00212-1
23 Díaz-Bulnes, P., Saiz, M.L., López-Larrea, C. and Rodríguez, R.M. (2019) Crosstalk between hypoxia and ER stress response: a Key regulator of macrophage polarization. *Front. Immunol.* **10**, 2951 https://doi.org/10.3389/fimmu.2019.02951
24 Rzymski, T. and Harris, A.L. (2007) The unfolded protein response and integrated stress response to anoxia. *Clin. Cancer Res.* **13**, 2537–2540 https://doi.org/10.1158/1078-0432.CCR-06-2126
25 Koritzinsky, M., Levitin, F., van den Beucken, T., Rumantir, R.A., Harding, N.J., Chu, K.C. et al. (2013) Two phases of disulfide bond formation have differing requirements for oxygen. *J. Cell Biol.* **203**, 615–627 https://doi.org/10.1083/jcb.201307185
26 Ramachandran, S., Ma, T., Ng, N., Foskolou, I.P., Hwang, M.-S., Victori, P. et al. (2020) Hypoxia-induced SETX links replication stress with the unfolded protein response. *Cancer Biol*
27 Chen, X., Iliopoulos, D., Zhang, Q., Tang, Q., Greenblatt, M.B., Hatziapostolou, M. et al. (2014) XBP1 promotes triple-negative breast cancer by controlling the HIF1α pathway. *Nature* **508**, 103–107 https://doi.org/10.1038/nature13119
28 González-Quiroz, M., Blondel, A., Sagredo, A., Hetz, C., Chevet, E. and Pedeux, R. (2020) When endoplasmic reticulum proteostasis meets the DNA damage response. *Trends Cell Biol.* **30**, 881–891 https://doi.org/10.1016/j.tcb.2020.09.002
29 Dufey, E., Bravo-San Pedro, J.M., Eggers, C., González-Quiroz, M., Urra, H., Sagredo, A.I. et al. (2020) Genotoxic stress triggers the activation of IRE1α-dependent RNA decay to modulate the DNA damage response. *Nat. Commun.* **11**, 2401 https://doi.org/10.1038/s41467-020-15694-y
30 Bobrovnikova-Marjon, E., Grigoriadou, C., Pytel, D., Zhang, F., Ye, J., Koumenis, C. et al. (2010) PERK promotes cancer cell proliferation and tumor growth by limiting oxidative DNA damage. *Oncogene.* **29**, 3881–3895 https://doi.org/10.1038/onc.2010.153
31 Cabrera, E., Hernández-Pérez, S., Koundrioukoff, S., Debatisse, M., Kim, D., Smolka, M.B. et al. (2017) PERK inhibits DNA replication during the unfolded protein response via claspin and Chk1. *Oncogene* **36**, 678–686 https://doi.org/10.1038/onc.2016.239
32 Jeggo, P. and Löbrich, M. (2006) Radiation-induced DNA damage responses. *Radiat. Prot. Dosimetry* **122**, 124–127 https://doi.org/10.1093/rpd/ncl495
33 Chaurasia, M., Gupta, S., Das, A., Dwarakanath, B.S., Simonsen, A. and Sharma, K. (2019) Radiation induces EIF2AK3/PERK and ERN1/IRE1 mediated pro-survival autophagy. *Autophagy* **15**, 1391–1406 https://doi.org/10.1080/15548627.2019.1582973
34 Olcina, M., Lecane, P.S. and Hammond, E.M. (2010) Targeting hypoxic cells through the DNA damage response. *Clin. Cancer Res.* **16**, 5624–5629 https://doi.org/10.1158/1078-0432.CCR-10-0286

Downloaded from http://portlandpress.com/biochemsoctrans/article-pdf/49/3/1251/916214/bst-2020-0861c.pdf by UK user on 19 September 2022

© 2021 The Author(s). This is an open access article published by Portland Press Limited on behalf of the Biochemical Society and distributed under the Creative Commons Attribution License 4.0 (CC BY).

35 Dadey, D.Y.A., Kapoor, V., Khudanyan, A., Thotala, D. and Hallahan, D.E. (2018) PERK regulates glioblastoma sensitivity to ER stress although promoting radiation resistance. *Mol. Cancer Res.* **16**, 1447–1453 https://doi.org/10.1158/1541-7786.MCR-18-0224
36 Kim, K.W., Moretti, L., Mitchell, L.R., Jung, D.K. and Lu, B. (2010) Endoplasmic reticulum stress mediates radiation-induced autophagy via PERK-eIF2α in caspase-3/7 deficient cells. *Oncogene* **29**, 3241–3251 https://doi.org/10.1038/onc.2010.74
37 Saglar, E., Unlu, S., Babalioglu, I., Gokce, S.C. and Mergen, H. (2014) Assessment of ER stress and autophagy induced by ionizing radiation in both radiotherapy patients and Ex vivo irradiated samples. *J. Biochem. Mol. Toxicol.* **28**, 413–417 https://doi.org/10.1002/jbt.21579
38 Yamamori, T., Meike, S., Nagane, M., Yasui, H. and Inanami, O. (2013) ER stress suppresses DNA double-strand break repair and sensitizes tumor cells to ionizing radiation by stimulating proteasomal degradation of Rad51. *FEBS Lett.* **587**, 3348–3353 https://doi.org/10.1016/j.febslet.2013.08.030
39 Gupta, A.K., Li, B., Cerniglia, G.J., Ahmed, M.S., Hahn, S.M. and Maity, A. (2007) The HIV protease inhibitor nelfinavir downregulates Akt phosphorylation by inhibiting proteasomal activity and inducing the unfolded protein response. *Neoplasia* **9**, 271–278 https://doi.org/10.1593/neo.07124
40 Liu, Y., Ji, W., Shergalis, A., Xu, J., Delaney, A.M., Calcaterra, A. et al. (2019) Activation of the unfolded protein response via inhibition of protein disulfide isomerase decreases the capacity for DNA repair to sensitize glioblastoma to radiotherapy. *Cancer Res.* **79**, 2923–2932 https://doi.org/10.1158/0008-5472.CAN-18-2540
41 Hotokezaka, Y., Katayama, I. and Nakamura, T. (2020) ATM-associated signalling triggers the unfolded protein response and cell death in response to stress. *Commun. Biol.* **3**, 378 https://doi.org/10.1038/s42003-020-1102-2
42 Hedrick, E., Cheng, Y., Jin, U.-H., Kim, K. and Safe, S. (2016) Specificity protein (Sp) transcription factors Sp1, Sp3 and Sp4 are non-oncogene addiction genes in cancer cells. *Oncotarget* **7**, 22245–22256 https://doi.org/10.18632/oncotarget.7925
43 Abdelrahim, M., Liu, S. and Safe, S. (2005) Induction of endoplasmic reticulum-induced stress genes in Panc-1 pancreatic cancer cells is dependent on Sp proteins. *J. Biol. Chem.* **280**, 16508–16513 https://doi.org/10.1074/jbc.C500030200
44 Koizume, S., Ito, S., Nakamura, Y., Yoshihara, M., Furuya, M., Yamada, R. et al. (2015) Lipid starvation and hypoxia synergistically activate ICAM1 and multiple genes in an Sp1-dependent manner to promote the growth of ovarian cancer. *Mol. Cancer* **14**, 77 https://doi.org/10.1186/s12943-015-0351-z
45 Dauer, P., Gupta, V.K., McGinn, O., Nomura, A., Sharma, N.S., Arora, N. et al. (2017) Inhibition of Sp1 prevents ER homeostasis and causes cell death by lysosomal membrane permeabilization in pancreatic cancer. *Sci. Rep.* **7**, 1564 https://doi.org/10.1038/s41598-017-01696-2
46 Beishline, K., Kelly, C.M., Olofsson, B.A., Koduri, S., Emrich, J., Greenberg, R.A. et al. (2012) Sp1 facilitates DNA double-strand break repair through a nontranscriptional mechanism. *Mol. Cell. Biol.* **32**, 3790–3799 https://doi.org/10.1128/MCB.00049-12
47 Trougakos, I.P. and Gonos, E.S. (2002) Clusterin/apolipoprotein J in human aging and cancer. *Int. J. Biochem. Cell Biol.* **34**, 1430–1448 https://doi.org/10.1016/S1357-2725(02)00041-9
48 Shannan, B., Seifert, M., Leskov, K., Willis, J., Boothman, D., Tilgen, W. et al. (2006) Challenge and promise: roles for clusterin in pathogenesis, progression and therapy of cancer. *Cell Death Differ.* **13**, 12–19 https://doi.org/10.1038/sj.cdd.4401779
49 Trougakos, I.P., So, A., Jansen, B., Gleave, M.E. and Gonos, E.S. (2004) Silencing expression of the clusterin/Apolipoprotein J gene in human cancer cells using small interfering RNA induces spontaneous apoptosis, reduced growth ability, and cell sensitization to genotoxic and oxidative stress. *Cancer Res.* **64**, 1834–1842 https://doi.org/10.1158/0008-5472.CAN-03-2664
50 Criswell, T., Beman, M., Araki, S., Leskov, K., Cataldo, E., Mayo, L.D. et al. (2005) Delayed activation of insulin-like growth factor-1 receptor/Src/MAPK/Egr-1 signaling regulates clusterin expression, a pro-survival factor. *J. Biol. Chem.* **280**, 14212–14221 https://doi.org/10.1074/jbc.M412569200
51 Ming, X., Bao, C., Hong, T., Yang, Y., Chen, X., Jung, Y.-S. et al. (2018) Clusterin, a novel DEC1 target, modulates DNA damage–Mediated cell death. *Mol Cancer Res.* **16**, 1641–1651 https://doi.org/10.1158/1541-7786.MCR-18-0070
52 Park, J., Park, S.Y., Shin, E., Lee, S.H., Kim, Y.S., Lee, D.H. et al. (2014) Hypoxia inducible factor-1α directly regulates nuclear clusterin transcription by interacting with hypoxia response elements in the clusterin promoter. *Mol. Cells* **37**, 178–186 https://doi.org/10.14348/molcells.2014.2349
53 Alnasser, H.A., Guan, Q., Zhang, F., Gleave, M.E., Nguan, C.Y.C. and Du, C. (2015) Requirement of clusterin expression for prosurvival autophagy in hypoxic kidney tubular epithelial cells. *Am. J. Physiol. Renal Physiol.* **310**, F160–F173 https://doi.org/10.1152/ajprenal.00304.2015
54 Nagelkerke, A., Bussink, J., van der Kogel, A.J., Sweep, F.C.G.J. and Span, P.N. (2013) The PERK/ATF4/LAMP3-arm of the unfolded protein response affects radioresistance by interfering with the DNA damage response. *Radiother. Oncol.* **108**, 415–421 https://doi.org/10.1016/j.radonc.2013.06.037
55 Eliopoulos, A.G., Havaki, S. and Gorgoulis, V.G. (2016) DNA damage response and autophagy: a meaningful partnership. *Front. Genet.* **7**, 204 https://doi.org/10.3389/fgene.2016.00204
56 Nagelkerke, A., Sweep, F.C.G.J., Stegeman, H., Grénman, R., Kaanders, J.H.A.M., Bussink, J. et al. (2015) Hypoxic regulation of the PERK/ATF4/LAMP3-arm of the unfolded protein response in head and neck squamous cell carcinoma. *Head Neck* **37**, 896–905 https://doi.org/10.1002/hed.23693
57 Nagelkerke, A., Bussink, J., Mujcic, H., Wouters, B.G., Lehmann, S., Sweep, F.C.G.J. et al. (2013) Hypoxia stimulates migration of breast cancer cells via the PERK/ATF4/LAMP3-arm of the unfolded protein response. *Breast Cancer Res.* **15**, R2 https://doi.org/10.1186/bcr3373
58 Liu, L., Yan, L., Liao, N., Wu, W.-Q. and Shi, J.-L. (2020) A review of ULK1-mediated autophagy in drug resistance of cancer. *Cancers* **12**, 352 https://doi.org/10.3390/cancers12020352
59 Gao, W., Shen, Z., Shang, L. and Wang, X. (2011) Upregulation of human autophagy-initiation kinase ULK1 by tumor suppressor p53 contributes to DNA-damage-induced cell death. *Cell Death Differ.* **18**, 1598–1607 https://doi.org/10.1038/cdd.2011.33
60 Joshi, A., Iyengar, R., Joo, J.H., Li-Harms, X.J., Wright, C., Marino, R. et al. (2016) Nuclear ULK1 promotes cell death in response to oxidative stress through PARP1. *Cell Death Differ.* **23**, 216–230 https://doi.org/10.1038/cdd.2015.88
61 Schaaf, M.B.E., Cojocari, D., Keulers, T.G., Jutten, B., Starmans, M.H., de Jong, M.C. et al. (2013) The autophagy associated gene, ULK1, promotes tolerance to chronic and acute hypoxia. *Radiother. Oncol.* **108**, 529–534 https://doi.org/10.1016/j.radonc.2013.06.015
62 Wennemers, M., Bussink, J., van den Beucken, T., Sweep, F.C.G.J. and Span, P.N. (2012) Regulation of TRIB3 mRNA and protein in breast cancer. *PLoS ONE* **7**, e49439 https://doi.org/10.1371/journal.pone.0049439
63 Miyoshi, N., Ishii, H., Mimori, K., Takatsuno, Y., Kim, H., Hirose, H. et al. (2009) Abnormal expression of TRIB3 in colorectal cancer: a novel marker for prognosis. *Br. J. Cancer* **101**, 1664–1670 https://doi.org/10.1038/sj.bjc.6605361
64 Aynaud, M.-M., Suspène, R., Vidalain, P.-O., Mussil, B., Guétard, D., Tangy, F. et al. (2012) Human tribbles 3 protects nuclear DNA from cytidine deamination by APOBEC3A. *J. Biol. Chem.* **287**, 39182–39192 https://doi.org/10.1074/jbc.M112.372722

Downloaded from http://portlandpress.com/biochemsoctrans/article-pdf/49/3/1251/916214/bst-2020-0861c.pdf by UK user on 19 September 2022

© 2021 The Author(s). This is an open access article published by Portland Press Limited on behalf of the Biochemical Society and distributed under the Creative Commons Attribution License 4.0 (CC BY).

65 Wennemers, M., Bussink, J., Scheijen, B., Nagtegaal, I.D., van Laarhoven, H.W., Raleigh, J.A. et al. (2011) Tribbles homolog 3 denotes a poor prognosis in breast cancer and is involved in hypoxia response. *Breast Cancer Res.* **13**, R82 https://doi.org/10.1186/bcr2934
66 Lee, Y.-C., Wang, W.-L., Chang, W.-C., Huang, Y.-H., Hong, G.-C., Wang, H.-L. et al. (2019) Tribbles homolog 3 involved in radiation response of triple negative breast cancer cells by regulating Notch1 activation. *Cancers (Basel)* **11**, 127 https://doi.org/10.3390/cancers11020127
67 Fornace, A.J., Alamo, I. and Hollander, M.C. (1988) DNA damage-inducible transcripts in mammalian cells. *Proc. Natl Acad. Sci. U.S.A.* **85**, 8800–8804 https://doi.org/10.1073/pnas.85.23.8800
68 Nishitoh, H. (2012) CHOP is a multifunctional transcription factor in the ER stress response. *J. Biochem.* **151**, 217–219 https://doi.org/10.1093/jb/mvr143
69 Tabas, I. and Ron, D. (2011) Integrating the mechanisms of apoptosis induced by endoplasmic reticulum stress. *Nat. Cell Biol.* **13**, 184–190 https://doi.org/10.1038/ncb0311-184
70 Lafont, E. (2020) Stress management: death receptor signalling and cross-talks with the unfolded protein response in cancer. *Cancers (Basel)* **12**, 1113 https://doi.org/10.3390/cancers12051113
71 Zhang, N., Ji, N., Jiang, W.-M., Li, Z.-Y., Wang, M., Wen, J.-M. et al. (2015) Hypoxia-induced autophagy promotes human prostate stromal cells survival and ER-stress. *Biochem. Biophys. Res. Commun.* **464**, 1107–1112 https://doi.org/10.1016/j.bbrc.2015.07.086
72 Sermeus, A., Genin, M., Maincent, A., Fransolet, M., Notte, A., Leclere, L. et al. (2012) Hypoxia-induced modulation of apoptosis and BCL-2 family proteins in different cancer cell types. *PLoS ONE* **7**, e47519 https://doi.org/10.1371/journal.pone.0047519
73 Munschauer, M., Nguyen, C.T., Sirokman, K., Hartigan, C.R., Hogstrom, L., Engreitz, J.M. et al. (2018) The NORAD lncRNA assembles a topoisomerase complex critical for genome stability. *Nature* **561**, 132–136 https://doi.org/10.1038/s41586-018-0453-z
74 Zhao, X., Wei, X., Wang, X. and Qi, G. (2020) Long non-coding RNA NORAD regulates angiogenesis of human umbilical vein endothelial cells via miR-590-3p under hypoxic conditions. *Mol. Med. Rep.* **21**, 2560–2570 https://doi.org/10.3892/mmr.2020.11064
75 Simon, M.C. (2004) Siah proteins, HIF prolyl hydroxylases, and the physiological response to hypoxia. *Cell* **117**, 851–853 https://doi.org/10.1016/j.cell.2004.06.010
76 House, C.M., Möller, A. and Bowtell, D.D.L. (2009) Siah proteins: novel drug targets in the Ras and hypoxia pathways. *Cancer Res.* **69**, 8835–8838 https://doi.org/10.1158/0008-5472.CAN-09-1676
77 Winter, M., Sombroek, D., Dauth, I., Moehlenbrink, J., Scheuermann, K., Crone, J. et al. (2008) Control of HIPK2 stability by ubiquitin ligase Siah-1 and checkpoint kinases ATM and ATR. *Nat. Cell Biol.* **10**, 812–824 https://doi.org/10.1038/ncb1743
78 Scortegagna, M., Kim, H., Li, J.-L., Yao, H., Brill, L.M., Han, J. et al. (2014) Fine tuning of the UPR by the ubiquitin ligases Siah1/2. *PLoS Genet.* **10**, e1004348 https://doi.org/10.1371/journal.pgen.1004348
79 Pérez, M., García-Limones, C., Zapico, I., Marina, A., Schmitz, M.L., Muñoz, E. et al. (2012) Mutual regulation between SIAH2 and DYRK2 controls hypoxic and genotoxic signaling pathways. *J. Mol Cell Biol.* **4**, 316–330 https://doi.org/10.1093/jmcb/mjs047
80 García-Limones, C., Lara-Chica, M., Jiménez-Jiménez, C., Pérez, M., Moreno, P., Muñoz, E. et al. (2016) CHK2 stability is regulated by the E3 ubiquitin ligase SIAH2. *Oncogene* **35**, 4289–4301 https://doi.org/10.1038/onc.2015.495
81 Sakamoto, K.M. and Frank, D.A. (2009) CREB in the pathophysiology of cancer: implications for targeting transcription factors for cancer therapy. *Clin. Cancer Res.* **15**, 2583–2587 https://doi.org/10.1158/1078-0432.CCR-08-1137
82 Dutta, R., Tiu, B., Kaul, A., Mitton, B. and Sakamoto, K.M. (2015) CREB increases chemotherapy resistance through regulation of the DNA damage repair pathway in AML cells. *Blood* **126**, 1390–1390 https://doi.org/10.1182/blood.V126.23.1390.1390
83 Kikuchi, D., Tanimoto, K. and Nakayama, K. (2016) CREB is activated by ER stress and modulates the unfolded protein response by regulating the expression of IRE1α and PERK. *Biochem. Biophys Res. Commun.* **469**, 243–250 https://doi.org/10.1016/j.bbrc.2015.11.113
84 Nguyen, T., Nioi, P. and Pickett, C.B. (2009) The Nrf2-antioxidant response element signaling pathway and its activation by oxidative stress. *J. Biol. Chem.* **284**, 13291–5 https://doi.org/10.1074/jbc.R900010200
85 Kim, S.B., Pandita, R.K., Eskiocak, U., Ly, P., Kaisani, A., Kumar, R. et al. (2012) Targeting of Nrf2 induces DNA damage signaling and protects colonic epithelial cells from ionizing radiation. *Proc. Natl Acad. Sci. U.S.A.* **109**, E2949–E2955 https://doi.org/10.1073/pnas.1207718109
86 Xia, X., Wang, Q., Ye, T., Liu, Y., Liu, D., Song, S. et al. (2020) NRF2/ABCB1-mediated efflux and PARP1-mediated dampening of DNA damage contribute to doxorubicin resistance in chronic hypoxic HepG2 cells. *Fundam. Clin. Pharmacol.* **34**, 41–50 https://doi.org/10.1111/fcp.12505
87 Elanchezhian, R., Palsamy, P., Madson, C.J., Mulhern, M.L., Lynch, D.W., Troia, A.M. et al. (2012) Low glucose under hypoxic conditions induces unfolded protein response and produces reactive oxygen species in lens epithelial cells. *Cell Death Dis.* **3**, e301 https://doi.org/10.1038/cddis.2012.40
88 Miyamoto, N., Izumi, H., Miyamoto, R., Bin, H., Kondo, H., Tawara, A. et al. (2011) Transcriptional regulation of activating transcription factor 4 under oxidative stress in retinal pigment epithelial ARPE-19/HPV-16 cells. *Invest. Ophthalmol. Vis. Sci.* **52**, 1226–1234 https://doi.org/10.1167/iovs.10-5775
89 Chandel, N.S., McClintock, D.S., Feliciano, C.E., Wood, T.M., Melendez, J.A., Rodriguez, A.M. et al. (2000) Reactive oxygen species generated at mitochondrial complex III stabilize hypoxia-inducible factor-1alpha during hypoxia: a mechanism of O_2 sensing. *J. Biol. Chem.* **275**, 25130–8 https://doi.org/10.1074/jbc.M001914200
90 Guzy, R.D., Hoyos, B., Robin, E., Chen, H., Liu, L., Mansfield, K.D. et al. (2005) Mitochondrial complex III is required for hypoxia-induced ROS production and cellular oxygen sensing. *Cell Metab.* **1**, 401–408 https://doi.org/10.1016/j.cmet.2005.05.001
91 Hotokezaka, Y., Katayama, I., van Leyen, K. and Nakamura, T. (2015) GSK-3β-dependent downregulation of γ-taxilin and αNAC merge to regulate ER stress responses. *Cell Death Dis.* **6**, e1719–e1719 https://doi.org/10.1038/cddis.2015.90
92 Yang, Y., Lei, T., Du, S., Tong, R., Wang, H., Yang, J. et al. (2018) Nuclear GSK3β induces DNA double-strand break repair by phosphorylating 53BP1 in glioblastoma. *Int. J. Oncol.* **52**, 709–720 https://doi.org/10.3892/ijo.2018.4237
93 Suwaki, N., Vanhecke, E., Atkins, K.M., Graf, M., Swabey, K., Huang, P. et al. (2011) A HIF-regulated VHL-PTP1B-Src signaling axis identifies a therapeutic target in renal cell carcinoma. *Sci. Transl. Med.* **3**, 85ra47 https://doi.org/10.1126/scitranslmed.3002004
94 Dai, Y. and Siemann, D. (2019) c-Src is required for hypoxia-induced metastasis-associated functions in prostate cancer cells. *Onco Targets Ther.* **12**, 3519–3529 https://doi.org/10.2147/OTT.S201320
95 Torrisi, F., Minafra, L., Cammarata, F.P., Savoca, G., Calvaruso, M., Vicario, N. et al. (2020) SRC tyrosine kinase inhibitor and X-rays combined effect on glioblastoma cell lines. *Int. J. Mol. Sci.* **21**, 3917 https://doi.org/10.3390/ijms21113917

Downloaded from http://portlandpress.com/biochemsoctrans/article-pdf/49/3/1251/916214/bst-2020-0861c.pdf by UK user on 19 September 2022

© 2021 The Author(s). This is an open access article published by Portland Press Limited on behalf of the Biochemical Society and distributed under the Creative Commons Attribution License 4.0 (CC BY).

96 Tsai, Y.-L., Ha, D.P., Zhao, H., Carlos, A.J., Wei, S., Pun, T.K. et al. (2018) Endoplasmic reticulum stress activates SRC, relocating chaperones to the cell surface where GRP78/CD109 blocks TGF-β signaling. *Proc. Natl Acad. Sci. U.S.A.* **115**, E4245–E4254 https://doi.org/10.1073/pnas.1714866115
97 Fukumoto, Y., Morii, M., Miura, T., Kubota, S., Ishibashi, K., Honda, T. et al. (2014) Src family kinases promote silencing of ATR-Chk1 signaling in termination of DNA damage checkpoint. *J. Biol. Chem.* **289**, 12313–12329 https://doi.org/10.1074/jbc.M113.533752
98 Garcia, S.N., Guedes, R.C. and Marques, M.M. (2019) Unlocking the potential of HK2 in cancer metabolism and therapeutics. *Curr. Med. Chem.* **26**, 7285–7322 https://doi.org/10.2174/0929867326666181213092652
99 Liu, Y., Hou, X., Liu, M., Yang, Z., Bi, Y., Zou, H. et al. (2016) XBP1 silencing decreases glioma cell viability and glycolysis possibly by inhibiting HK2 expression. *J. Neurooncol.* **126**, 455–462 https://doi.org/10.1007/s11060-015-2003-y
100 Vartanian, A., Agnihotri, S., Wilson, M.R., Burrell, K.E., Tonge, P.D., Alamsahebpour, A. et al. (2016) Targeting hexokinase 2 enhances response to radio-chemotherapy in glioblastoma. *Oncotarget* **7**, 69518–69535 https://doi.org/10.18632/oncotarget.11680
101 Ketteler, J. and Klein, D. (2018) Caveolin-1, cancer and therapy resistance. *Int. J. Cancer* **143**, 2092–2104 https://doi.org/10.1002/ijc.31369
102 Díaz, M.I., Díaz, P., Bennett, J.C., Urra, H., Ortiz, R., Orellana, P.C. et al. (2020) Caveolin-1 suppresses tumor formation through the inhibition of the unfolded protein response. *Cell Death Dis.* **11**, 648 https://doi.org/10.1038/s41419-020-02792-4
103 Zhu, H., Yue, J., Pan, Z., Wu, H., Cheng, Y., Lu, H. et al. (2010) Involvement of caveolin-1 in repair of DNA damage through both homologous recombination and non-homologous end joining. *PLoS ONE* **5**, e12055 https://doi.org/10.1371/journal.pone.0012055
104 Choi, J.W., Schroeder, M.A., Sarkaria, J.N. and Bram, R.J. (2014) Cyclophilin B supports Myc and mutant p53-dependent survival of glioblastoma multiforme cells. *Cancer Res.* **74**, 484–496 https://doi.org/10.1158/0008-5472.CAN-13-0771
105 Jeong, K., Kim, K., Kim, H., Oh, Y., Kim, S.-J., Jo, Y. et al. (2015) Hypoxia induces cyclophilin B through the activation of transcription factor 6 in gastric adenocarcinoma cells. *Oncol. Lett.* **9**, 2854–2858 https://doi.org/10.3892/ol.2015.3102
106 Jeong, K., Kim, H., Kim, K., Kim, S.-J., Hahn, B.-S., Jahng, G.-H. et al. (2014) Cyclophilin B is involved in p300-mediated degradation of CHOP in tumor cell adaptation to hypoxia. *Cell Death Differ.* **21**, 438–450 https://doi.org/10.1038/cdd.2013.164

Downloaded from http://portlandpress.com/biochemsoctrans/article-pdf/49/3/1251/916214/bst-2020-0861c.pdf by UK user on 19 September 2022

© 2021 The Author(s). This is an open access article published by Portland Press Limited on behalf of the Biochemical Society and distributed under the Creative Commons Attribution License 4.0 (CC BY).

7492–7506 *Nucleic Acids Research, 2021, Vol. 49, No. 13* *Published online 1 July 2021*
https://doi.org/10.1093/nar/gkab551

Replication catastrophe induced by cyclic hypoxia leads to increased APOBEC3B activity

Samuel B. Bader, Tiffany S. Ma, Charlotte J. Simpson, Jiachen Liang, Sakura Eri B. Maezono, Monica M. Olcina, Francesca M. Buffa and Ester M. Hammond*

Oxford Institute for Radiation Oncology, Department of Oncology, The University of Oxford, Oxford, OX3 7DQ, UK

Received November 20, 2020; Revised June 07, 2021; Editorial Decision June 08, 2021; Accepted June 11, 2021

ABSTRACT

Tumor heterogeneity includes variable and fluctuating oxygen concentrations, which result in the accumulation of hypoxic regions in most solid tumors. Tumor hypoxia leads to increased therapy resistance and has been linked to genomic instability. Here, we tested the hypothesis that exposure to levels of hypoxia that cause replication stress could increase APOBEC activity and the accumulation of APOBEC-mediated mutations. APOBEC-dependent mutational signatures have been well-characterized, although the physiological conditions which underpin them have not been described. We demonstrate that fluctuating/cyclic hypoxic conditions which lead to replication catastrophe induce the expression and activity of APOBEC3B. In contrast, stable/chronic hypoxic conditions which induce replication stress in the absence of DNA damage are not sufficient to induce APOBEC3B. Most importantly, the number of APOBEC-mediated mutations in patient tumors correlated with a hypoxia signature. Together, our data support the conclusion that hypoxia-induced replication catastrophe drives genomic instability in tumors, specifically through increasing the activity of APOBEC3B.

INTRODUCTION

Hypoxia, which is defined as conditions of insufficient oxygen, is associated with the resistance of tumors to standard therapies and poor patient prognosis (1,2). Tumor hypoxia has been described as chronic or acute but is also cyclic/intermittent. Regions of chronic hypoxia occur at distances beyond the diffusion distance of oxygen in tissue, whilst acute hypoxia can occur near to vessels as a result of the inefficient and malformed vasculature. Cyclic or intermittent hypoxia in tumors is characterized by fluctuating oxygen levels due to both angiogenesis and red blood cell flux (3–6).

The extreme levels of hypoxia (<0.1% O_2) most associated with therapy resistance, referred to as radiobiological hypoxia, lead to replication stress (7). Replication stress is highly complex and can be broadly defined as situations where DNA replication fork dynamics are abnormal. Our studies have shown that radiobiological hypoxia induced replication stress, which includes the rapid accumulation of single stranded DNA (ssDNA), leads to a DNA damage response (DDR) (8). Importantly, radiobiological hypoxia is unusual in that the induction of replication stress does not lead to an apparent accumulation of DNA damage, which suggests that the level of replication stress is transient or mitigated by other factors (9,10). This lack of associated DNA damage observed in hypoxia, even after prolonged exposures, might indicate that despite a robust replication stress response, damage is avoided potentially by reduced DNA replication/transcription rates (10,11). In contrast, a number of commonly used pharmacological agents, which lead to replication fork stalling, have been shown to lead to DNA damage and this has been attributed to RPA exhaustion resulting in replication catastrophe (12).

The apolipoprotein B mRNA-editing enzyme, catalytic polypeptide-like (APOBEC) proteins are a family of conserved cytidine deaminases that play a critical role in viral immunity (13,14). APOBEC-mediated cytosine deamination to uracil can occur in RNA but primarily occurs in regions of ssDNA including at R-loops, stalled replication forks, transcription bubbles, and during end resection of damaged DNA (15–19). Many C to T and C to G mutations within the APOBEC consensus deamination sequence (TCW) have been observed in the genomic sequences of patient tumors and attributed to APOBEC enzymatic activity. This observation has led to the characterization of an APOBEC mutational signature (20,21). The frequency of the APOBEC signature in cancers is second only to the ageing signature and the majority of APOBEC-induced mutations in human cancers have been attributed to either APOBEC3A (A3A) or 3B (A3B) expression (20–24). Notably, A3B activity has been shown to increase in response to hydroxyurea (HU)-induced replication stress in an ATR-dependent manner (25). The current paradigm is that cancers where this mutational signature predominates have

*To whom correspondence should be addressed. Tel: +44 1865 617320; Email: ester.hammond@oncology.ox.ac.uk

© The Author(s) 2021. Published by Oxford University Press on behalf of Nucleic Acids Research.
This is an Open Access article distributed under the terms of the Creative Commons Attribution License (http://creativecommons.org/licenses/by/4.0/), which permits unrestricted reuse, distribution, and reproduction in any medium, provided the original work is properly cited.

Downloaded from https://academic.oup.com/nar/article/49/13/7492/6312757 by guest on 19 September 2022

deregulated APOBEC activity, and this contributes to cancer progression by increasing genomic instability and treatment resistance through an elevated mutation rate. Correspondingly, an increase in A3B expression can be seen in many of the cancers that possess an APOBEC mutational signature (22,26). In contrast to the pro-tumorigenic consequences of A3B overexpression, it has recently been shown that A3B overexpression can increase the sensitivity of tumor cells to immune checkpoint blockade therapy through an increase in the presentation of novel neoepitopes on the surface of cancer cells (27). It is currently unclear whether increasing or ablating APOBEC activity in tumors would be beneficial therapeutically. Importantly, the mechanism by which A3B initially becomes deregulated in human cancer has not been described. It is crucial that we understand how APOBECs are regulated in tumors and particularly as specific inhibitors become available. Hypoxia-induced replication stress, which includes the significant accumulation of the APOBEC substrate, ssDNA, suggests that hypoxia could be a critical factor in regulating APOBEC expression and activity in tumors.

MATERIALS AND METHODS

Cell lines and reagents

Colorectal RKO (ATCC), RKO$^{HIF1a+/+}$ and RKO$^{HIF1a-/-}$ (28), HCT116, Breast MCF7, MDA-MB231, Bladder T24, VMCUB1 (provided by Prof Anne Kiltie, Oxford University) and HCT116 p53+/+ and p53−/− (provided by Prof Bert Vogelstein, Johns Hopkins Medicine) cells were grown in DMEM media. Non-tumorigenic breast MCF10A (provided by Prof Paul Span, Nijmegen University) cells were grown in MEGM media. Non-transformed lung MRC5 cells (ATCC) were grown in EMEM media. Esophageal OE21 cells (PHE) were grown in RPMI media. All cell media was supplemented with 10% FBS, except MEGM media which was supplemented with 20% FBS, and cells were maintained in an incubator set at 37°C and 5% CO_2. All cell lines were verified mycoplasma free using a HEK-Blue™ detection kit (Invivogen). Inhibitors/drugs used were: VX-970 (M6620) (MedChemExpress), AZD6738 (MedChemExpress), Gö6976 (Sigma Aldrich), MK-8776 (Selleckchem), Bay11-7085 (Tocris Biosciences), PHA-767491 (Selleckchem), *N*' acetylcysteine (NAC) (Sigma Aldrich), and roscovitine (Ros) (Selleckchem). For siRNA-mediated knockdowns, RKO cells were transfected with siRNA to a final concentration of 50 nM using DharmaFECT 1 (T-2001-03; Horizon Discovery, Cambridge, UK) following manufacturer's protocols. Sequences of siRNAs used: siA3B (CCUGAUGGAUCCAGACACA[dT][dT]), sip53 (GUAAUCUACUGGGACGGAA[dT][dT]), and siATR (CAG GCA CTA ATT GTT CTT CAAd[T]d[T]).

Hypoxia exposure

Hypoxia treatments at <0.1% O_2 were carried out in a Bactron II anaerobic chamber (Shel Labs) while all cyclic treatments were carried out in an M35 variable atmosphere workstation (Don Whitley Scientific). Oxygen concentrations were periodically validated using anaerobic oxygen indicator strips (Thermo Fisher) and an Oxylite oxygen probe (Oxford Optronix). Cells were seeded on glass dishes and harvested in the chamber with equilibrated solutions.

RT-qPCR

Total RNA was isolated from cells with Trizol (Invitrogen/Life Technologies) and was reverse transcribed into cDNA with Verso enzyme kit (Thermo Scientific). SYBR Green PCR Master Mix kit (Applied Biosystems) was mixed with gene specific primers and the reaction was run on a StepOne Real-Time PCR System (Thermo Scientific). Fold change values relative to normoxia (21% O_2) were determined using the ΔΔct method using 18S as an endogenous control. Graphs were plotted using the mean of three biological replicates ± SEM. Primers sequences are given in Supplementary Table S1.

Deamination assay

Cells were lysed in HED lysis buffer (25 mM HEPES, 5 mM EDTA, 10% glycerol, 0.2% NP-40, 1 mM DTT (added fresh), 1X protease inhibitor (Roche) (added fresh), homogenized with a 25 G needle, and sonicated briefly in a Biorupter plus sonicator (Diagenode) before pre-clearing by centrifugation for 10 min. A deamination mix was made consisting of 8.25 ml of 5 μg/μl protein lysate, 0.625 μl RNaseA, 0.625 μl TE buffer, and 0.5 μl of 200 μM ssDNA oligo (5′-ATTATTATTANTCAAATGGATTTATT TATTTATTTATTTATTT'FAM3′) and incubated at 37°C for 3 h. Samples were then treated with 100 mM NaOH at 95°C for 30 min. Samples were mixed with Gel loading buffer II (Invitrogen) and incubated at 70°C for 3 min before being run on a 15% TBE-urea gel (Novex). Bands were analyzed with a Chemi-doc touch imaging system (Bio-Rad). Product bands were quantified using the analyze gels tool in ImageJ.

Western blotting

Cells were lysed in HED lysis buffer and treated as with the deamination assay. Proteins were separated on a 4–20% polyacrylamide gel (Bio-Rad) and blotted onto a nitrocellulose membrane (Bio-Rad). Bands were imaged using Odyssey Infrared Imaging (LI-COR Biosciences). Experiments were carried out in triplicate and a representative blot is shown for each experiment. Antibodies used; Cell Signaling: p53-S15 (9284), RPA32 (2208), Chk1-S345 (2341), Chk1-S296 (90178), H3 (3638), H3-S10 (9701), p65 (3033), p65-S536 (93H1), cGAS (15102); Santa Cruz: p53 (sc-126), β-Actin (sc-69879), Chk1 (sc-8408), ATR (sc-515173); Bethyl: KAP1 (A300-274A), KAP1-S824 (A300-767A); Millipore: γH2AX (05–636), H2AX (07–627); Abcam: A3B (ab184990), Cyclin A (ab181591); BD Biosciences: HIF-1α (610958), GRP78 (610979).

Fluorescence activated cell sorting (FACS)

For BrdU incorporation plots, freshly made up BrdU (20 μM) was added in the dark to cells for 1 h before fixation in ice-cold 70% ethanol. Samples were treated with

Downloaded from https://academic.oup.com/nar/article/49/13/7492/6312757 by guest on 19 September 2022

2 M HCl and blocked in 2% FBS PBS solution. Propidium Iodide (Sigma Aldrich) was added to samples to determine total DNA content. Antibodies used were: BrdU (BD biosciences #347580), H3-S10 (Cell Signaling #9701) and Alexa Fluoro 488 (Invitrogen). Samples were run on a BD FACSCaliber machine (BD biosciences) and plots were analyzed with FloJo software.

Immunofluorescence

Cells were seeded onto autoclaved cover slips (Menzel-Glaser) before treatment. Cells were fixed with 4% fixation buffer (4% (w/v) paraformaldehyde in PBS). Samples were permeabilized with 1% PBS-Triton X-100 (Thermo Fisher) and blocked in 2% (w/v) BSA (Thermo Fisher) in 0.1% PBS-tween. For A3B staining, samples were permeabilized with 0.1% PBS–Triton X-100 (Thermo Fisher) and blocked in 5% (w/v) BSA (Thermo Fisher) in PBS. For EdU staining, cells were incubated with EdU (10 μM) (Thermo Fisher) and Click-iT Alexa Fluor 657 labelling kit (Thermo Fisher) was used for staining. Proteins were visualized with an LSM710 confocal microscope (Carl Zeiss Microscopy Ltd) and at least 150 cells were counted per condition. DNA damage and replication stress were quantified by counting cells with >5 53BP1 foci or >6 RPA foci respectively. Antibodies used: 53BP1 (Novus Biologicals #NB100-904), A3B (Origene TA349029), RPA (Cell Signaling #2208), RPA-S4/S8 (Abcam ab243866), Alexa Fluoro 488 (Invitrogen), and Alexa Fluoro 594 (Invitrogen).

TCGA data analysis

Raw expression data from 51 genes within a validated hypoxia signature (29) and data from 6 hypoxia inducible p53 response genes (BTG2, CYFIP2, INPP5D, KANK3, PHLDA3 and SULF2) (30) were taken from TCGA datasets downloaded from the GDC data portal (https://portal.gdc.cancer.gov/) to represent hypsig and p53genes respectively. The harmonized TCGA data were considered (31). The mean value of hypsig and p53genes within a tumor sample was then calculated as a summary score of their expression (32). Mutational data for TCGA datasets considered in this study were obtained from a previous study (21). Datasets were selected where there were >100 samples with available mutational data, these were BRCA and LUAD (21). APOBEC mutations were defined as the number of C to T or C to G mutations occurring in the TCW sequence context in a given sample. Mutation values were logged base 10 and shifted by 0.5 for visual reason so to display data from tumors with no observed APOBEC mutations. Summary scores for expression signatures, APOBEC gene expression and the number of APOBEC mutations contained in tumor samples were correlated using non-parametric Spearman's rank-order correlation test to avoid issues from non-normality of the data distributions and the effect of outliers.

Other statistical analysis

A two-tailed, paired Student's *t*-test was used for the comparison of two means and a one-way analysis of variance (ANOVA) was used for the comparison of more than two means. Statistical significance was assumed if $P < 0.05$. Error bars represent mean ± standard error of the mean (SEM).

RESULTS

Hypoxia-induced replication stress leads to increased APOBEC expression but decreased deamination

To confirm the induction of replication stress, RKO cells were exposed to hypoxia (<0.1% O_2) and changes to RPA and Chk1 were determined. Both RPA and Chk1 phosphorylation increased in hypoxia (<0.1% O_2) but, as previously described, returned to near normoxic levels after longer exposure (20 hours) (8). Importantly, the induction of replication stress in response to hypoxia was found to be oxygen dependent, with no replication stress observed at 2% O_2 (Figure 1A). Here, we investigated the APOBEC3 family members and their response to hypoxia. RKO cells were exposed to <0.1 or 2% O_2 followed by RT-qPCR. HU was used as a positive control to induce APOBEC expression (25) and the levels of the p53 target gene, *INPP5D*, and a target of the unfolded protein response, *CHOP*, were determined to demonstrate an oxygen-dependent hypoxia response (Supplementary Figure S1A, B) (30,33). All APOBEC3 mRNA transcripts except for APOBEC3A (A3A) and APOBEC3G (A3G) could be detected in the RKO cell line. Of the 5 APOBEC3s detected (A3B, APOBEC3D (A3D), APOBEC3H (A3H), APOBEC3F (A3F) and APOBEC3C (A3C)), A3D and A3H were significantly induced in hypoxia in an oxygen-dependent manner (Figure 1B, C). A similar pattern of expression was observed for A3C and A3F although this failed to reach statistical significance (Supplementary Figure S1C, D). To verify that this was not restricted to the RKO cell line we determined the expression of A3H in the MCF-7 cell line and again observed a significant increase in response to hypoxia (Figure S1E). The induction of A3D and A3H at <0.1 but not at 2% O_2 suggests that the hypoxia induced factor (HIF1) is not involved in APOBEC expression as HIF1 is stabilized at both <0.1 and 2% O_2. However, to confirm this, RKO cells with and without HIF1α were treated with hypoxia (<0.1% O_2) and the levels of A3D and A3H determined. Induction of A3D in response to hypoxia was not changed by the lack of HIF1α while the induction of A3H in response to hypoxia increased further. These data demonstrate that neither A3D nor A3H were induced in a HIF1 dependent manner in hypoxia (<0.1% O_2) (Supplementary Figure S1F, G). Both A3D and A3H have been described previously as targets of the p53 transcription factor, suggesting that hypoxia-induced p53 could transactivate A3D/A3H (34). In support of this, the induction of p53 in hypoxia shows the same oxygen dependency as observed for A3D/A3H induction (Figure 1D). Using siRNA specific for p53, expression of p53 was reduced in normoxic (21% O_2) and hypoxic (<0.1% O_2) conditions. Successful p53 knockdown was verified by the decrease in mRNA expression of *INPP5D*, a validated hypoxia-inducible p53 target gene (Supplementary Figure S1H) (30). As expected, in the absence of p53 the hypoxia-induced expression of both A3D and A3H was abrogated, demonstrating they

Downloaded from https://academic.oup.com/nar/article/49/13/7492/6312757 by guest on 19 September 2022

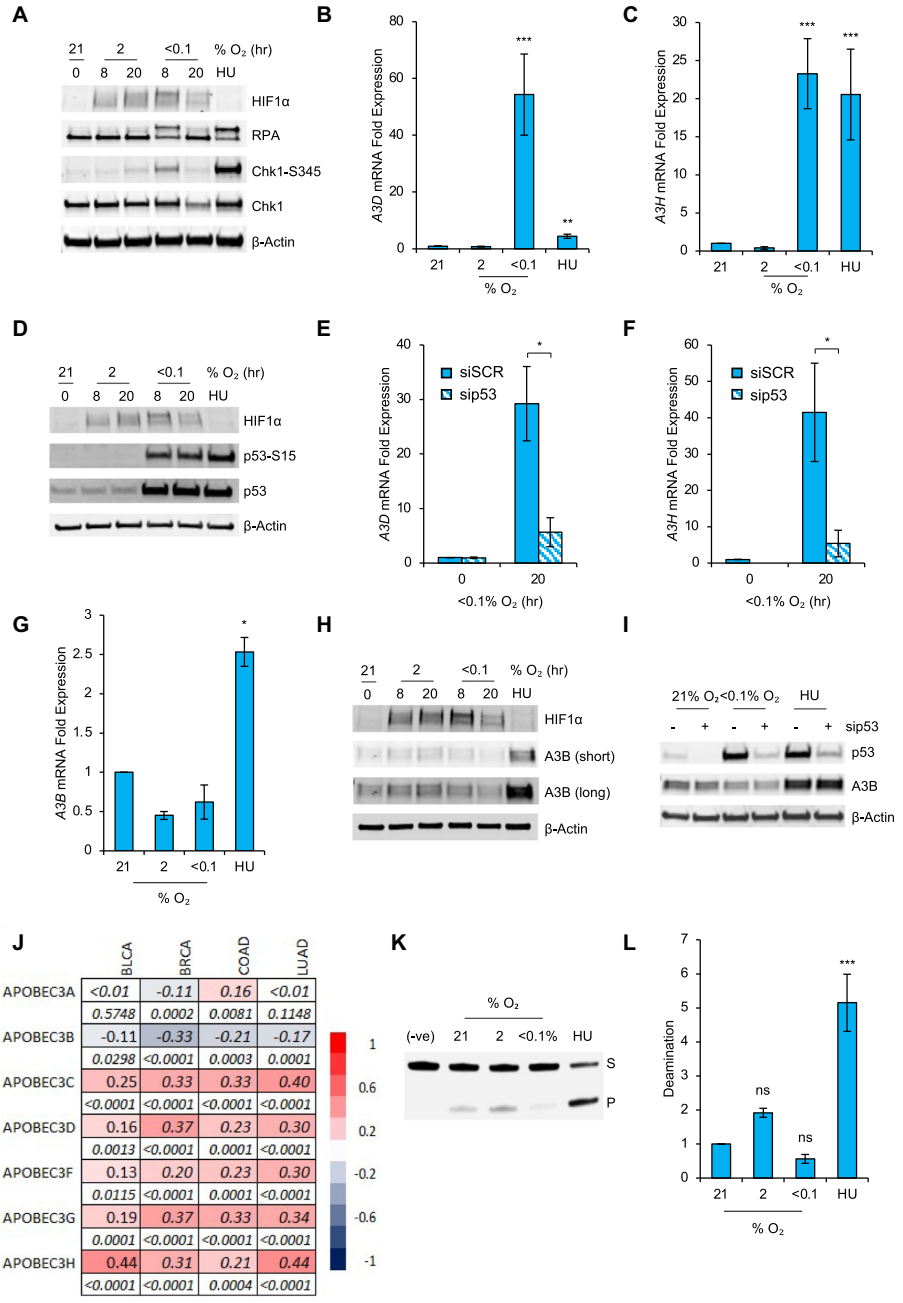


Figure 1. Hypoxia-induced replication stress leads to increased APOBEC expression but decreased deamination. (**A**) RKO cells were exposed to the indicated oxygen concentration or HU (2 mM, 20 h) for the indicated times and western blotting was carried out; β-actin was used as a loading control. (**B, C**) RKO cells were exposed to the oxygen concentrations indicated or HU (2 mM) for 20 h. The mRNA levels of the indicated APOBECs, *A3D* (B) and *A3H* (C), as a relative fold change to normoxic (21% O_2) levels are shown. (**D**) RKO cells were exposed to the oxygen concentrations indicated for the times shown or HU (2 mM, 20 h) followed by western blotting as indicated. (**E, F**) RKO cells were treated with siRNA to p53 (sip53), or a scramble control (siSCR) followed by exposure to <0.1% O_2 for 20 h. mRNA levels of *A3D* (E) and *A3H* (F) are shown relative to the normoxic control. (**G**) RKO cells were exposed to the oxygen concentrations indicated for 20 h or HU (2 mM, 20 h). The mRNA level of *A3B* as a relative fold change to normoxic (21% O_2) level is shown. (**H**) RKO cells were exposed to the conditions indicated or HU (2 mM, 20 h) followed by western blotting. For clarity, long and short exposures of A3B blot are shown. (**I**) RKO cells were treated with siRNA to p53 (sip53) or a scramble control (siSCR) (indicated as -) followed by exposure to the indicated oxygen concentration or HU (2 mM) for 20 h. Western blotting was carried out. (**J**) Spearman rank-order correlation between a signature of hypoxia-induced p53 response genes and APOBEC mRNA expression in Bladder Urothelial Carcinoma (BLCA), Breast Invasive Carcinoma (BRCA), Colorectal Adenocarcinoma (COAD), and Lung Adenocarcinoma (LUAD) from the TCGA harmonized dataset (see methods). For each gene the correlation values (top raw) and *P* values (bottom raw) are given. Color scale of correlation values is shown on the right of the heatmap. (**K**) RKO cells were exposed to the indicated oxygen concentrations or HU (2 mM) for 20 h followed by a deamination assay. The top band (S) is the substrate band and the bottom band (P) is the product band. (**L**) Quantification of data shown in part K where the average intensity of the product band (P) across three biological repeats is plotted relative to the intensity of the normoxic product band. Data from three separate experiments ($n = 3$) are displayed ± standard error of the mean (SEM) unless specified otherwise. $*P < 0.05$, $**P < 0.01$, $***P < 0.001$.

Downloaded from https://academic.oup.com/nar/article/49/13/7492/6312757 by guest on 19 September 2022

are induced in a p53-dependent manner in hypoxia (<0.1% O_2) (Figure 1E, F). However, in contrast to A3D, A3H, A3C and A3F, the expression of A3B mRNA did not increase in response to hypoxia (<0.1% O_2) (Figure 1G). To confirm that the decrease in A3B in response to hypoxia was not restricted to RKO cells, we measured the levels of A3B mRNA in response to hypoxia in seven additional cells lines and saw a reduction in each (Supplementary Figure S1I). Next, we investigated the level of A3B protein in response to hypoxia and found that A3B expression was moderately reduced while a clear induction was observed in HU treated cells (Figure 1H). Previous reports have suggested that p53 represses the expression of A3B mRNA (34,35). Repression of A3B by p53 in hypoxia seemed unlikely as decreased expression of A3B was observed in several p53 mutant cell lines (Supplementary Figure S1I, J). However, to formally verify this we depleted p53 in RKO cells and used the genetically matched $p53^{+/+}$ and $p53^{-/-}$ HCT116 cell lines and demonstrated that loss of p53 had no impact on A3B expression in hypoxic conditions (Figure 1I, Supplementary Figure S1K). The p53-mediated response to hypoxia is both oxygen-dependent and extremely stress specific with only select p53-target genes being induced. We have previously characterized a group of six genes induced in hypoxia in a p53-dependent manner, which showed coherent expression in clinical samples (30), and so asked if there was a correlation between these genes and members of the APOBEC3 family. Using TCGA datasets, specifically, Bladder Urothelial Carcinoma (BLCA), Breast Invasive Carcinoma (BRCA), Colorectal Adenocarcinoma (COAD), and Lung Adenocarcinoma (LUAD), a highly significant positive correlation ($P \leq 0.0001$ in 17 cases, $P \leq 0.001$ in two cases, $P = 0.01$ in one case) was found between A3C, A3D, A3F, A3G, A3H and the mean score of the six hypoxia-induced p53-dependent genes in all these cancers (Figure 1J). At a single gene level, we observed differences in the degree of correlation and loss of correlation for specific genes in specific cancer types. While this is expected, the overall results were similar (Table S2). Interestingly, the expression of A3C and A3F positively correlated with the 6 gene signature, supporting our observation of a trend to increased expression in response to hypoxia *in vitro*, for these two genes (Supplementary Figure S1C, D). As predicted by our *in vitro* data, a negative correlation was seen between A3B and the mean expression of the 6 p53-dependent genes in all datasets, furthering the evidence for the decrease in A3B in hypoxia (<0.1% O_2). However, as all members of the APOBEC3 family have deamination activity, we hypothesized that deamination could increase in response to replication stress in hypoxia as a result of increased expression of A3C, A3D, A3F and A3H, despite unchanged A3B levels. Using an *in vitro* deamination assay, we observed the expected increase in deamination in response to HU, however deamination was unchanged in both of the hypoxic conditions tested (2 and <0.1% O_2) (Figure 1K, L). These data suggested that the expression of A3B, which has been reported to be one of the two APOBEC3 proteins primarily responsible for the generation of the APOBEC mutational signature, might also dictate the level of deamination in hypoxic conditions. Most interestingly, these data highlight a difference in the biological response to hypoxia and HU-induced replication stress and demonstrate that APOBEC activity is not induced in response to all conditions which lead to replication stress.

Hypoxia-induced replication stress is distinct to the response to HU

To explain the contrasting biological responses to hypoxia and HU, we began with further investigation of the impact of both HU and hypoxia (<0.1% O_2) on DNA replication. RKO cells were exposed to HU or hypoxia and both propidium iodide (PI) and bromodeoxyuridine (BrdU) incorporation was analyzed (Figure 2A, B and Supplementary Figure S2A). The most noticeable difference between the two treatments was the presence of a sub-G1 population indicative of apoptosis in the hypoxic cells but not the HU treated cells, which was surprising given that the induction of p53 is similar in both cases (Figure 1D, Supplementary Figure S2B). As expected, hypoxia (<0.1% O_2) lead to a significant decrease in the mean fluorescence intensity (MFI) of the BrdU staining indicating decreased DNA replication. However, it was notable that the HU treated cells were incorporating significantly more BrdU compared to the hypoxic cells (Figure 2B). We predicted that the residual DNA replication in HU treated cells included origin firing, and therefore we used an inhibitor of CDK1, 2, 5 and 7 (roscovitine) to block origin firing and determined the impact on BrdU incorporation. As expected, inhibiting origin firing significantly decreased BrdU incorporation in the HU treated cells compared to control cells (Figure 2C, Supplementary Figure S2C). We hypothesized that on-going replication in HU treated cells would lead to RPA exhaustion and ultimately replication catastrophe (12,36,37). In contrast, we know that hypoxic cells do not experience replication catastrophe, as evidenced by a lack of DNA damage, and attribute this to the extremely limited replication/origin firing (7). To definitively confirm replication catastrophe in response to HU but not hypoxia, we co-stained treated cells for a marker of DNA damage (53BP1) and replication stress (RPA) and measured the proportion of cells that contained both 53BP1 and RPA foci (Figure 2D, E; foci count per cell are also shown Supplementary Figures S2D–F). Together, these data demonstrate that HU-induced replication stress, which leads to APOBEC activity, includes replication catastrophe, while replication catastrophe does not occur in response to hypoxia (<0.1% O_2).

Cyclic hypoxia leads to replication catastrophe

These data led us to refine our original hypothesis and consider that APOBEC activity is induced by replication catastrophe as opposed to replication stress. To test this hypothesis, we considered hypoxic conditions which might include some origin firing and thus could maintain active DNA replication potentially leading to replication catastrophe. Specifically, we asked if including periods of milder hypoxia (2% O_2), which alone do not induce replication stress, might lead to increased replication and the DNA damage associated with replication catastrophe. Using a hypoxia chamber capable of rapidly switching between multiple oxygen concentrations, we investigated cyclic hypoxia conditions consisting of periods of <0.1% O_2, which induce replication

Downloaded from https://academic.oup.com/nar/article/49/13/7492/6312757 by guest on 19 September 2022

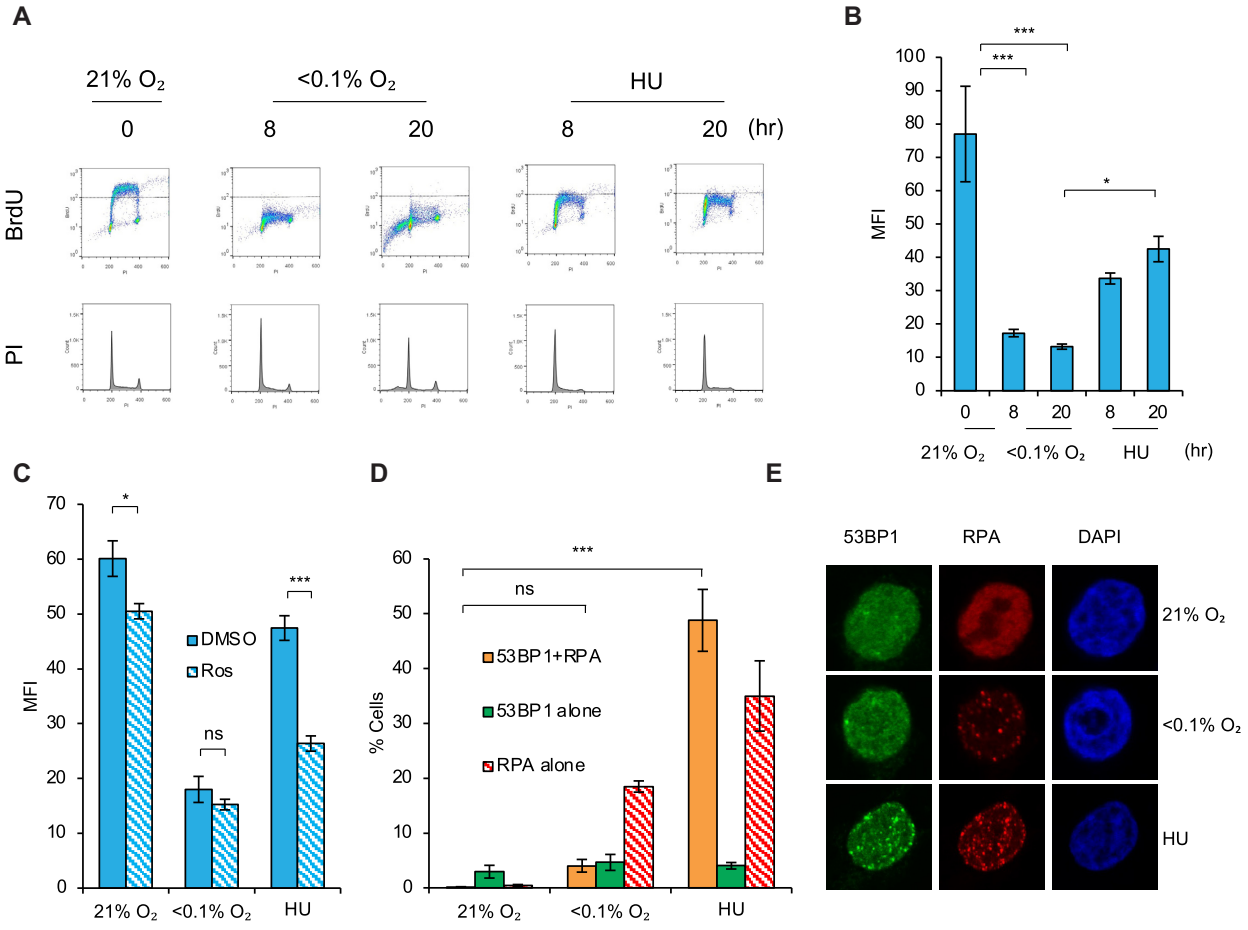


Figure 2. Hypoxia-induced replication stress is distinct to the response to HU. (**A**) RKO cells were exposed to the indicated oxygen concentrations or HU (2 mM) for the indicated times. Cells were labeled with BrdU (20 μM) 1 h prior to collection and analyzed by FACS. (**B**) Quantification of data in A. showing the mean fluorescence intensity (MFI) of cells in each condition. (**C**) RKO cells were pre-treated with DMSO or roscovitine (20 μM) for 30 min and exposed to normoxia (21% O_2), <0.1% O_2 or HU (2 mM) for 20 h. Cells were pulsed with BrdU (20 μM) 1 h prior to collection and analyzed by FACS. Mean fluorescence intensity (MFI) in each condition is shown. Exemplar FACs plots are shown in Figure S2C. (**D**) RKO cells were exposed to the indicated oxygen concentration or HU (2 mM) for 20 h. 53BP1 and RPA foci were visualized by immunofluorescence. The percentages of cells with >5 53BP1 and >6 RPA foci are shown. (**E**) Representative images of data shown in part D. Data from three separate experiments ($n = 3$) are displayed ± standard error of the mean (SEM). * $P < 0.05$, *** $P < 0.001$.

stress, and 2% O_2 which leads to HIF stabilization but no replication stress (Figure 3A). The choice of these cycling conditions is further supported by studies which have measured the periodicity and magnitude of oxygen fluctuations in xenograft tumors (38). Measurements of oxygen concentrations were taken using a built-in oxygen probe over the course of all cyclic experiments (Supplementary Figure S3A). We confirmed that the addition of these periods of milder hypoxia (2% O_2) still led to replication stress by showing that Chk1 and RPA were phosphorylated in cyclic hypoxia (Figure 3B). As seen previously both RPA and Chk1 phosphorylation was reduced after 20 hours in stable hypoxia (<0.1% O_2), however these phosphorylations appeared to be maintained in cyclic hypoxia. To investigate further, we determined the number of cells with RPA foci in each condition and found that the percentage of cells with RPA foci increased over time in cyclic hypoxia, while in stable hypoxia they formed and decreased over time (Figure 3C, D). Interestingly, when we determined the number of RPA foci per cell, we saw that this number remained constant in cyclic conditions while it decreased over time in stable hypoxia (Supplementary Figure S3B). Together, these data suggested that replication stress persists in cyclic hypoxia compared to stable/chronic conditions. Supportively, cells in cyclic hypoxia incorporated BrdU at a similar rate as those in normoxia, demonstrating on-going DNA replication (Figure 3E, F). An increase in the sub-G1 population was not observed in the cycling conditions in contrast to the stable/chronic hypoxia shown previously (compare Figure 3E to Figure 2A). Interestingly, we found that p53 was phosphorylated and stabilized in cyclic conditions suggesting that while p53 induced in response to stable hypoxia (<0.1% O_2) leads to apoptosis this is not evident in cycling conditions (Supplementary Figure S3C) (30). Furthermore, cells in cyclic hypoxia accumulated in S-phase before eventually arresting in G2 (Figure 3G). A G2 arrest was con-

Downloaded from https://academic.oup.com/nar/article/49/13/7492/6312757 by guest on 19 September 2022

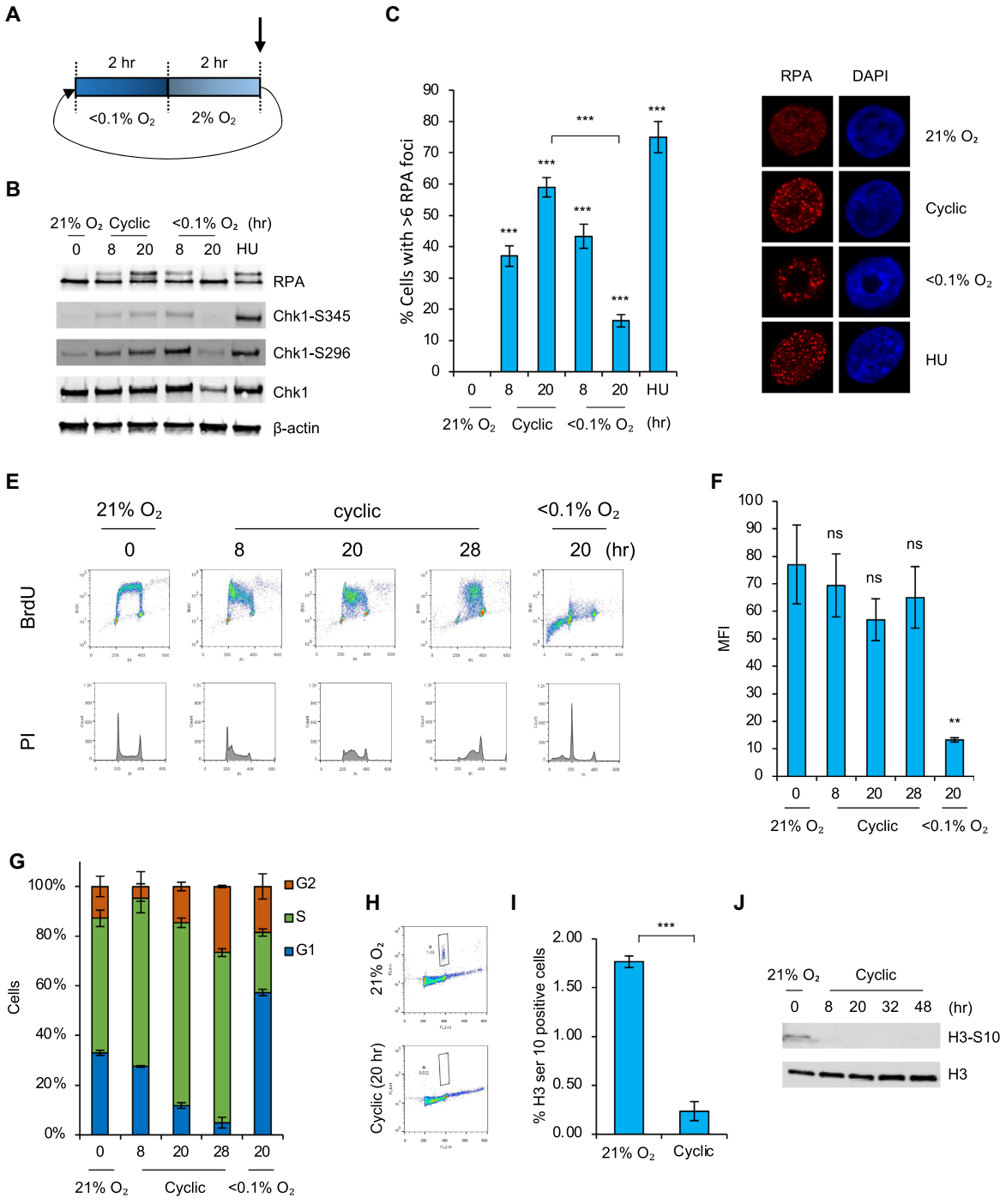


Figure 3. Cyclic hypoxia causes replication stress and a G2 cell cycle arrest. (**A**) A schematic representation of the cyclic hypoxia treatment schedule. Cells were treated with <0.1% O_2 for 2 h followed by 2% O_2 for 2 h. This cycle then repeated. The actual O_2 concentration inside the chamber over a period of 5 cycles is shown in Figure S3A. The arrow indicates the point at which samples were harvested i.e., within the last 5 min of the 2% O_2 segment. (**B**) RKO cells were exposed to the oxygen concentrations indicated for the times shown or HU (2 mM, 20 h). Western blotting was carried out. (**C**) RPA foci were visualized by immunofluorescence in RKO cells treated with cyclic hypoxia, hypoxia (<0.1% O_2), or normoxia (21% O_2) for the indicated times, or HU (2 mM, 20 h). The percentage of cells with >6 RPA foci is shown. (**D**) Representative images from data shown in part C. (**E**) RKO cells were exposed to cyclic hypoxia, hypoxia (<0.1% O_2), or normoxia (21% O_2) for the indicated times. Cells were labeled with BrdU (20 μM) 1 h prior to collection and analyzed by FACS. The 21 and <0.1% O_2 treated conditions are the same data shown in Figure 2A as these experiments were conducted at the same time. (**F**) Quantification of the data in part E showing the MFI of cells in each condition is shown. (**G**) Quantification of the data in part E showing the percentage of cells in each phase of the cell cycle. (**H**) RKO cells were exposed to cyclic hypoxia or normoxia (21% O_2) for 20 h. FACS was carried out to assess the percentage of cells with H3 ser 10 positive staining. (**I**) Quantification of data shown in H. (**J**) RKO cells were exposed to cyclic hypoxia for the indicated timepoints. Western blotting was carried out. $n = 1$ Data from three separate experiments ($n = 3$) are displayed ± standard error of the mean (SEM) unless specified otherwise. *** $P < 0.001$.

Downloaded from https://academic.oup.com/nar/article/49/13/7492/6312757 by guest on 19 September 2022

firmed by staining for the absence of the mitotic marker H3 serine 10 detected by both FACS and western blotting (Figure 3H, I, J).

Importantly, the BrdU MFI of cells in cyclic hypoxia decreased when cells were treated with roscovitine, suggesting that on-going replication in these conditions included origin firing (Figure 4A, B). Having characterized the cellular response to cyclic hypoxia, we asked if DNA damage accumulated in the cyclic conditions. We began by co-staining cells in cyclic hypoxia for RPA and γH2AX and determined a significant correlation between these two markers (Supplementary Figure S3D). However, because chronic hypoxia leads to an increase in pan-nuclear γH2AX staining we investigated changes in 53BP1 foci in cyclic hypoxia. Cells exposed to cyclic hypoxia accumulated 53BP1 and this occurred predominantly in the S-phase population (Supplementary Figure S3E). Furthermore, co-staining for 53BP1 and RPA demonstrated that >50% of cells in cyclic hypoxia were positive for both 53BP1 and RPA foci demonstrating that these conditions induced replication catastrophe (Figure 4C). In addition, to determine the kinetics of DNA repair after exposure to cyclic conditions, cells were also exposed to cyclic hypoxia followed by a period at 2% O_2. Interestingly, when the cyclic hypoxic cells were released into 2% O_2, a significant number of cells with 53BP1 and RPA foci remained 24 h later (Figure 4C, D). This approach also highlighted that cells retaining DNA damage appeared larger than non-damaged comparators (Figure 4E). Notably, the cells released into 2% O_2 after cyclic treatment further accumulated DNA damage over time as measured by the absolute number of 53BP1 foci per cell compared to those treated in cyclic alone or with HU (Supplementary Figure S3F–I). Further analysis of cell size determined that the mean nuclear size of cells positive for both RPA and 53BP1 foci i.e. experiencing replication catastrophe, was significantly larger than undamaged cells and this was further increased after reoxygenation to 2% O_2 (Figure 4F). As an additional measure of DNA damage, the protein expression of the cytoplasmic DNA sensor, cGAS was determined in stable (<0.1% O_2) and cyclic hypoxia. A robust increase in cGAS protein was seen in response to cyclic hypoxia while no increase was observed in stable hypoxia (Figure 4G). Together, these data are supportive of cyclic hypoxia-inducing replication catastrophe as cells that experience replication catastrophe have been shown to demonstrate persistent replication stress, DNA damage, and an increase in nuclear size after the stress is removed (12).

Cyclic hypoxia increases the expression and activity of A3B

To determine if cyclic hypoxia would lead to increased APOBEC activity, RKO cells were exposed to either stable (<0.1% O_2) or cyclic hypoxic conditions and western blotting was carried out for A3B. A 4-fold induction of A3B was seen in the cycling conditions but not stable hypoxia (Figure 5A, Supplementary Figure S4A). Using an antibody previously validated for immunofluorescent staining of A3B (39), we also determine a significant increase in A3B nuclear intensity in response to cyclic hypoxia and HU but not stable hypoxia (Figure 5B, C). Deamination assays demonstrated that, as before, deamination did not increase in stable hypoxia but was significantly increased in response to cyclic hypoxia (Figure 5D, E). We also found that reoxygenating cells to 21% O_2 after exposure to hypoxia (<0.1% O_2) lead to increased deamination suggesting that this is not dependent on the specific cyclic conditions used (Supplementary Figure S4B, C). Importantly, we show that the increased deamination in cyclic hypoxia is dependent on A3B as siRNA mediated knock down of A3B abrogated deamination (Figure 5F–H). Previous reports have demonstrated that overexpression of A3B impacts cell cycle distribution as well as the activation of various DDR effector proteins (40,41). In contrast, we found no A3B-dependent changes in the cell cycle in cyclic hypoxia (Figure 5I, Supplementary Figure S4D, E). Furthermore, no change was observed in RPA, Chk1 or KAP1 phosphorylation in cyclic hypoxia when A3B was depleted (Figure 5J). Increased APOBEC expression, including A3B, has been linked to the NF-κB transcription factor, which is also known to be active in hypoxic conditions (42,43). Induction of A3B protein in cyclic hypoxia was partially abrogated by treatment with a NF-κB inhibitor (Bay11-7085) (Supplementary Figure S4F). This finding raised the possibility that cyclic hypoxia-induced cGAS could lead to NF-κB activity and consequent A3B expression (44). However, RKO cells lack STING expression and siRNA mediated depletion of cGAS had no impact on A3B induction (Supplementary Figure S4G) (45).

To investigate whether the increased A3B seen in cyclic hypoxia was a result of replication catastrophe, we began by co-staining for A3B and RPA. In response to both HU and cyclic hypoxia the nuclear intensity of A3B and the number of nuclear RPA foci increased. In contrast in stable hypoxia, only the number of cells with RPA foci increased (Figure 6A, B). Next, we treated cells with roscovitine to block origin firing. The addition of roscovitine in cyclic hypoxia decreased the number of cells experiencing replication catastrophe as determined by co-staining for 53BP1 and RPA foci (Figure 6C, D, foci count per cell are also shown Supplementary Figure S5A–F). Most importantly and in support of our hypothesis, when roscovitine was used, A3B no longer accumulated in cyclic hypoxia (Figure 6E). In further support of A3B induction depending on origin firing in cyclic hypoxia, addition of the cdc7 inhibitor (PHA-767491), another commonly used method to inhibit origin firing, also blocked A3B accumulation in cyclic hypoxia (Supplementary Figure S5G). These data demonstrate that the expression and activity of A3B is increased in response to cyclic hypoxia and that this activity correlates with replication catastrophe. We hypothesized that the activity of reactive oxygen species (ROS) would also likely contribute to replication catastrophe in cyclic hypoxia and the subsequent A3B activity. Supportive of this hypothesis, treatment with the ROS scavenger N' acetylcysteine (NAC) in cyclic hypoxia significantly decreased the proportion of cells experiencing replication catastrophe and decreased A3B expression (Supplementary Figure S6A–C, foci numbers per cell are also shown S6D–I).

Having demonstrated that blocking origin firing reduces A3B induction in cyclic hypoxia, we predicted that inhibition of ATR-mediated signaling in cyclic hypoxia would lead to increased origin firing, and therefore could potentially increase A3B accumulation/activity. Cells in cyclic

Downloaded from https://academic.oup.com/nar/article/49/13/7492/6312757 by guest on 19 September 2022

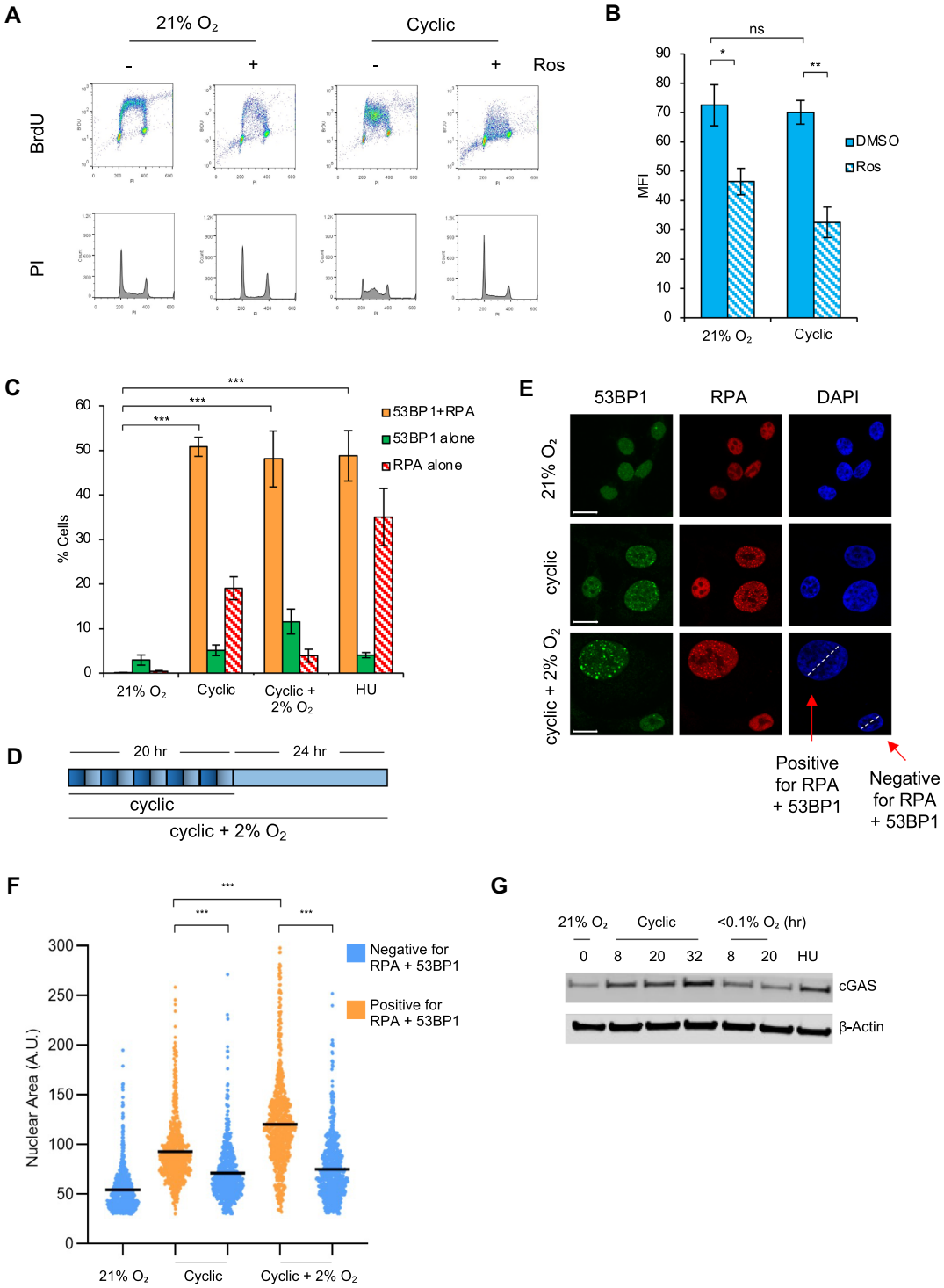


Figure 4. Cyclic hypoxia causes replication catastrophe. (**A**) RKO cells were pretreated with DMSO or roscovitine (Ros) (20 μM) for 30 min and exposed to 21% O_2 or cyclic hypoxia for 20 h. Cells were labeled with BrdU (20 μM) 1 h prior to collection and analyzed by FACS. (**B**) Quantification of the data in part A showing the mean fluorescence intensity (MFI) in each condition. (**C**) RKO cells were treated with the indicated oxygen treatments or HU (2 mM, 20 h) and co-stained for 53BP1, RPA, and DAPI. Foci were visualized by immunofluorescence. The 21% O_2 and HU treated conditions are the same data shown in Figure 2D as these experiments were conducted at the same time. (**D**) Schematic representation of the cyclic and cyclic + 2% O_2 conditions used in part C, E, F. Dark blue represents <0.1% O_2 and light blue represents 2% O_2. (**E**) Representative pictures of data in C. The dashed white line demonstrates the difference in cell size. Scale bar = 10 μm. (**F**) Cells were divided into two groups; negative for >5 53BP1 + >6 RPA foci and positive for > 5 53BP1 and >6 RPA. The mean nuclear area of cells in both groups in E were calculated using Fiji software and the nuclear size of individual cells plotted for each condition. (**G**) RKO cells were exposed to the indicated oxygen concentrations for the times shown or HU (2 mM, 20 h), followed by western blotting. Data from three separate experiments (n = 3) are displayed ± standard error of the mean (SEM). * $P < 0.05$, ** $P < 0.01$, *** $P < 0.001$.

Downloaded from https://academic.oup.com/nar/article/49/13/7492/6312757 by guest on 19 September 2022

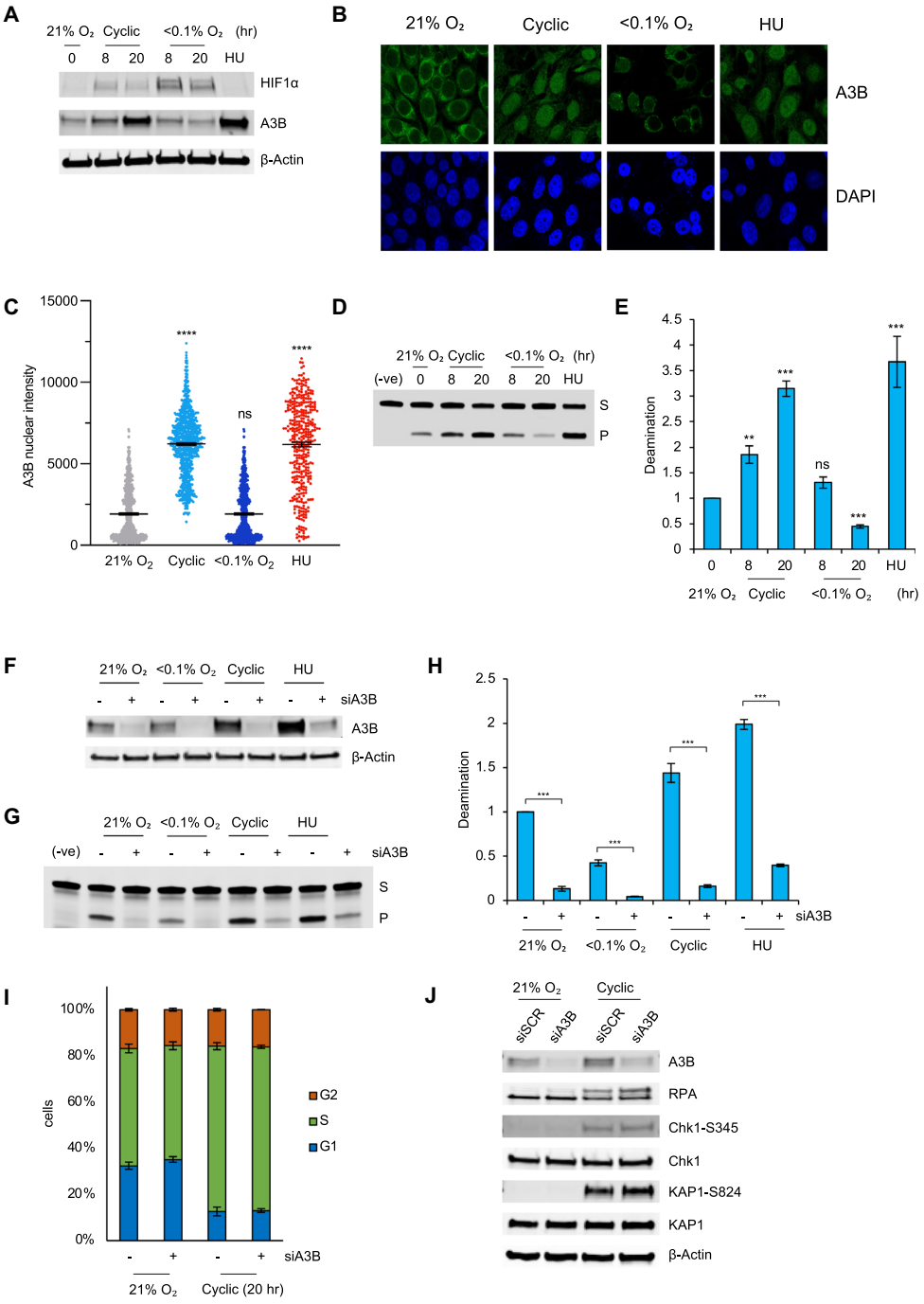


Figure 5. Cyclic hypoxia increases the expression and activity of A3B. (**A**) RKO cells were exposed to the oxygen concentrations indicated for the times shown or HU (2 mM, 20 h). Western blotting was carried out. (**B**) RKO cells were exposed to the indicated oxygen treatments for 20 h or HU (2 mM, 20 h) and co-stained for A3B and DAPI. The cells were visualized by immunofluorescence. (**C**) Quantification of A3B nuclear intensity from part B. (**D**) *In vitro* deamination assay measuring deamination activity in samples collected in the indicated hypoxic treatments for the indicated times or HU (2 mM, 20 h). The top band is the substrate band (S) and the bottom band is the product band (P). (**E**) Quantification of deamination in D. where the average intensity of the product band (P) (bottom) across 3 biological repeats is plotted relative to the intensity of the normoxic product band. (**F**) RKO cells were treated with an siRNA to A3B (siA3B) or a scramble (siSCR) (indicated by –) and then exposed to the hypoxic conditions indicated or HU (2 mM) for 20 h, followed by western blotting. (**G**) The samples from F. were also analyzed by deamination assay. The top band (S) is the substrate band and the bottom band (P) is the product band. (**H**) Quantification of data shown in part G where the average intensity of the product band (P) across 3 biological repeats is plotted relative to the intensity of the normoxic product band. (**I**) RKO cells were treated with siRNA to A3B (siA3B) or a a scramble control (siSCR) followed by exposure to cyclic hypoxia for 20 h. Cells were labeled with BrdU (20 μM) 1 h prior to collection and analyzed by FACS. Quantification of the data shows the percentage of cells in each phase of the cell cycle is shown. Exemplar FACs plots are shown in Figure S4D. (**J**) RKO cells were treated with siRNA to A3B (siA3B), or a scramble control (siSCR) followed by exposure to cyclic hypoxia or normoxia (21% O_2) for 20 h. Western blotting was carried out. Data from three separate experiments ($n = 3$) are displayed ± standard error of the mean (SEM) unless specified otherwise. ** $P < 0.01$, *** $P < 0.001$.

Downloaded from https://academic.oup.com/nar/article/49/13/7492/6312757 by guest on 19 September 2022

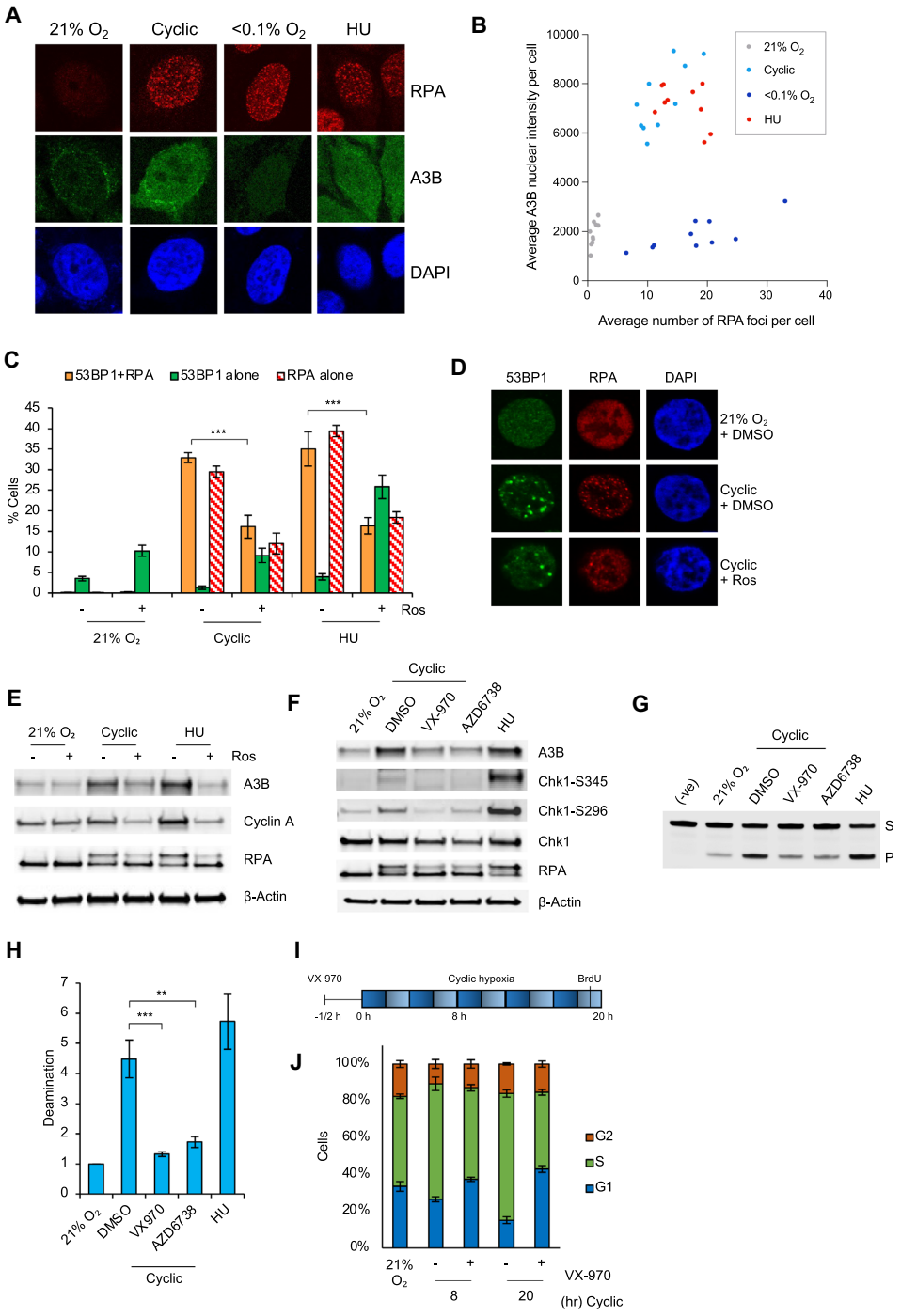


Figure 6. Replication catastrophe leads to increased A3B. (**A**) RKO cells were exposed to the indicated oxygen treatments for 20 h or HU (2 mM, 20 h) and co-stained for RPA, A3B and DAPI. The cells were visualized by immunofluorescence and representative images are shown. (**B**) Quantification of average A3B nuclear intensity and average number of RPA foci per cell. Each dot represents a field of view containing at least 20 cells, a minimum of 200 cells were quantified per condition. (**C**) RKO cells were pretreated with DMSO or roscovitine (Ros) for 30 min (20 μM) and exposed to 21% O_2, cyclic hypoxia, or HU (2 mM) for 20 h. Cells were stained by immunofluorescence to detect cells with >5 53BP1 and >6 RPA foci and mounted in DAPI. (**D**) Representative images of data shown in C. (**E**) Cells were treated as in C. and western blotting was carried out. (**F**) RKO cells were pre-treated with VX-970 (1 μM), AZD6738 (5 μM), or DMSO for 30 min and then exposed to 20 h cyclic hypoxia or HU alone (2 mM, 20 h). Western blotting was carried out. (**G**) *In vitro* deamination assay on RKO cells pre-treated with VX-970 (1 μM), AZD6738 (5 μM) or DMSO for 30 min and then exposed to 20 h cyclic hypoxia or HU alone (2 mM, 20 h). S = substrate band, P = product band. (**H**) Quantification of the bottom band (P) intensity in samples from part G. (**I**) A schematic showing how cells are treated in part J. (**J**) RKO cells were pre-treated with VX-970 for 30 min (1 μM) or DMSO and then exposed to cyclic hypoxia (8 or 20 h) Cells were labeled with BrdU (20 μM) 1 h prior to collection and analyzed by FACS. Quantification of the percentages of cells in each cycle phase. Data from three separate experiments ($n = 3$) are displayed ± standard error of the mean (SEM) unless specified otherwise. ** $P < 0.01$, *** $P < 0.001$.

Downloaded from https://academic.oup.com/nar/article/49/13/7492/6312757 by guest on 19 September 2022

hypoxia were treated with inhibitors to ATR (VX-970, AZD6738) followed by western blotting for A3B. Surprisingly, inhibition of ATR abrogated the induction of A3B in cyclic hypoxia (Figure 6F). This was further confirmed using siRNA to knock down ATR (Supplementary Figure S7A). Treatment with both ATR inhibitors also abrogated APOBEC activity in cyclic hypoxia as assayed by the *in vitro* deamination assay (Figure 6G, H). These data were surprising as they suggest A3B is induced in cyclic hypoxia through an ATR-dependent mechanism, although this is in agreement with the mechanism previously described for HU-induced APOBEC activity (25). However, it was important to consider the impact of ATR inhibition on the cell cycle as replication catastrophe cannot occur outside of S-phase. Cells were exposed to cycling hypoxia in the presence of an ATR inhibitor (VX-970) and the cell cycle analyzed. Inhibition of ATR during cycling conditions prevented the accumulation of cells in S-phase leading instead to an accumulation in the G1 phase (Figure 6I, J, Supplementary Figure S7B). To further support this finding, cells were treated with Chk1 inhibitors (MK-8776 or Gö6976) and exposed to cyclic hypoxia. As observed after ATR inhibition, treatment with the Chk1 inhibitors in cyclic hypoxia led to a G1 accumulation and abrogated the induction of A3B (Supplementary Figure S7C, D). Together, these data suggest that inhibition of ATR/Chk1 in cyclic hypoxia leads to a reduced S-phase population and therefore reduced replication catastrophe and most importantly, link A3B expression/activity with replication catastrophe.

APOBEC expression and activity correlates with hypoxia in patient samples

Finally, we sought to identify a link between tumor hypoxia and APOBEC expression/activity in patient samples. We have shown that hypoxic conditions which include cyclic variations between <0.1% and 2% O_2 lead to the induction of A3B expression and activity. Cyclic hypoxia is a physiologically relevant condition, although detailed study of this phenomenon has been hampered by difficulties in measuring the periodicity in patients. As of yet, there are no clinically useful markers of cyclic hypoxia in routine use (6,46,47). Therefore, we used a validated hypoxia signature, which is primarily made up of HIF target genes to determine a link between hypoxia and A3B expression in patient tumors (29). Our rationale to support the use of the hypoxia signature is that cells experiencing fluctuating/cyclic hypoxic conditions also stabilize HIF1α (Figure 5A) and therefore expression of associated HIF-target genes will be increased. To support this rationale, we verified that genes included in the hypoxia signature were induced in response to cyclic hypoxia (Figure 7A-D). Next, using the TCGA patient cohort, and the cancer types where there were more than 100 samples with available APOBEC mutational data (BRCA and LUAD), we found a significant correlation between the number of APOBEC mutations present and the hypoxic signature in both datasets (Figure 7E, F). In further support of our conclusions, we found a significant positive correlation between the hypoxia signature and the expression of A3A and A3B in all datasets for A3A, and three out of four datasets for A3B, but not the other A3s (Figure 7G).

DISCUSSION

We have demonstrated that the biological response to replication stress is determined by the level of accompanying DNA damage (replication catastrophe). Exposure to hypoxia (<0.1% O_2) induces significant replication stress but this occurs in the apparent absence of DNA damage and does not lead to APOBEC expression/activity. In contrast, replication stress induced by either HU or cycling hypoxia leads to replication catastrophe and results in APOBEC expression/activity. The significance of our finding is highlighted by evidence suggesting that cycling hypoxia leads to increased APOBEC activity in patient samples.

Though it has yet to be measured routinely in human tumors, a wealth of evidence from *in vivo* experiments suggest that cyclic hypoxia is commonplace in solid tumors (5,46,48–51). Though much study has been done to date on the effects of cyclic hypoxia on treatment modalities such as radiotherapy and chemotherapy, this has seldomly been done at oxygen concentrations that have been detected *in vivo.* The vast majority of studies utilize ambient air (21% O_2) as the reoxygenation portion of their cyclic schedule (52), while the maximum oxygen concentration predicted to occur in xenografts is closer to 5% O_2 (5). Our cyclic hypoxia schedule represents a more physiological relevant condition and the first description of an endogenous source of replication catastrophe that likely occurs in human tumors. Therefore, the link between replication stress and APOBEC expression/activity is a plausible mechanism by which the APOBEC signature can manifest in human cancer. Notably, we found that the significance of the correlations between A3B and the hypoxia metagene differs between the cancer types we investigated. However, this is not surprising given that the presence of the APOBEC-mediated mutational signature has also been shown to be cancer type specific (20,26).

Our study showed an upregulation of A3D, and A3H and to a lesser extent A3C and A3F in stable hypoxia (<0.1% O_2). As APOBECs can also bind RNA as a substrate, mRNA editing has been proposed as a possible function of the family. Recently, a limited number of studies have implicated both A3A and A3G in mRNA editing (53–55). Interestingly, while there was overlap between the transcripts edited by A3A and A3G, many were specifically edited by one or the other. These observations raise two interesting questions; Firstly, whether the APOBECs upregulated in hypoxia can contribute to gene regulation through mRNA editing and secondly, if so, do they influence overlapping or distinct sets of genes? Furthermore, A3A was shown to edit the mRNA of a specific gene, succinate dehydrogenase B (SDHB), and this activity increased in response to mild levels of hypoxia (1% O_2) (55). Further study would be required to determine whether hypoxic regulation of APOBEC mRNA editing by A3A is a global phenomenon or restricted to specific genes such as SDHB.

A number of previous reports have described increased replication stress signaling and a G2/M phase cell cycle arrest following A3B overexpression (40,41). In contrast, we did not find an A3B-dependent effect on either replication stress or cell cycle profile. A notable difference between the previous studies and ours is the method of A3B induction, cyclic hypoxia induces the endogenous expression of

Downloaded from https://academic.oup.com/nar/article/49/13/7492/6312757 by guest on 19 September 2022

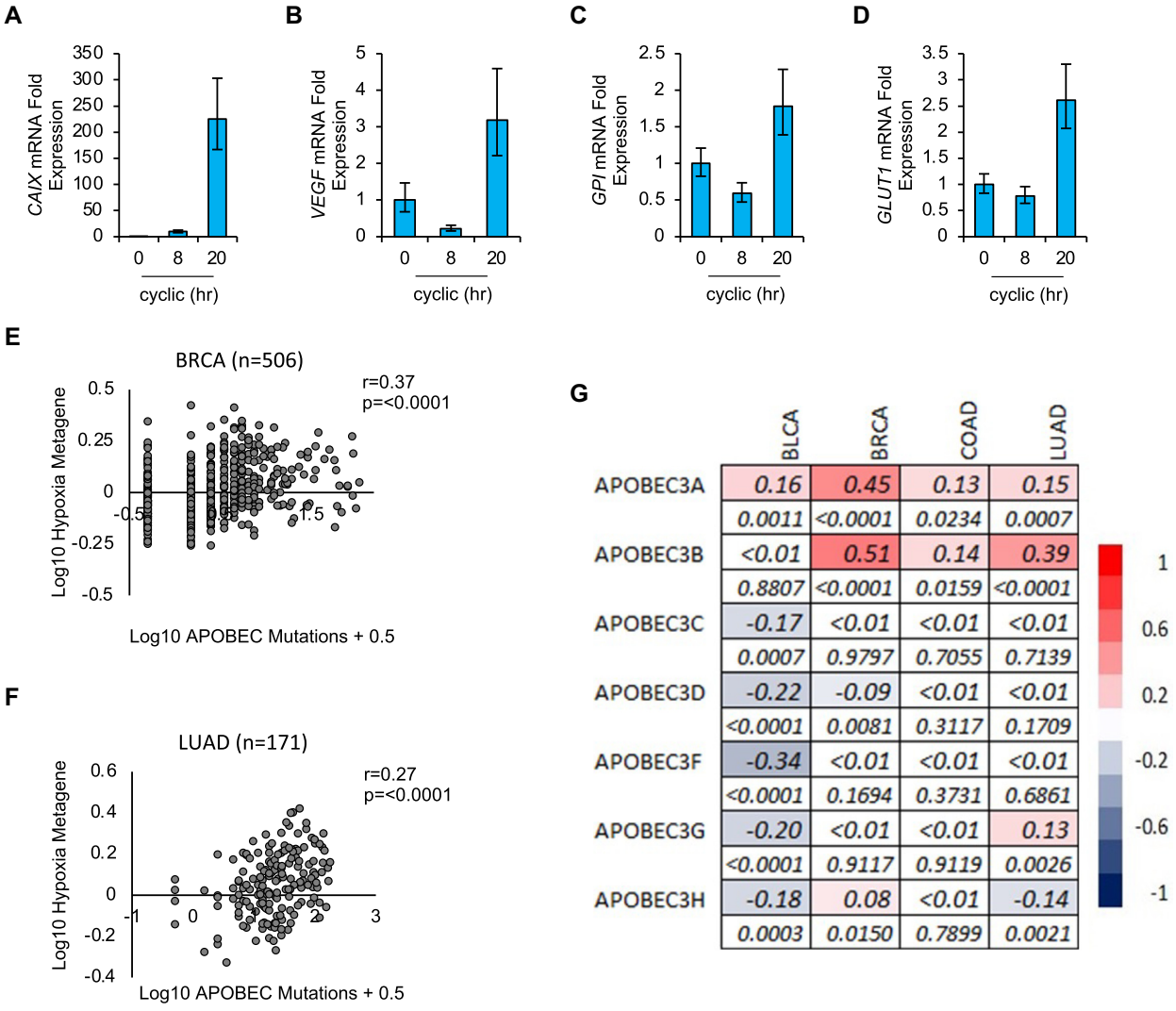


Figure 7. APOBEC activity correlates with hypoxia in patient samples. (**A–D**) RKO cells were exposed to cyclic hypoxia (20 h) followed by qPCR analysis for the hypoxia-inducible genes indicated (CAIX, VEGF, GPI and GLUT1). $n = 1$. (**E, F**) Correlation between the hypoxia metagene and the number of APOBEC mutations in the two TCGA datasets where mutational data were available for >100 cases. APOBEC mutations refers to the number of tCw to tTw and tCw to tGw changes. The log mean expression of the hypoxia signature for each cancer dataset is shown compared to the scaled number of APOBEC mutations (see methods). The Spearman's rank-order correlation coefficient (rho), and p value are displayed. (**G**) Spearman's rank-order correlation between the hypoxia metagene and APOBEC mRNA expression in TCGA datasets, correlation and significance are shown. For each gene the correlation values (top raw) and *P* values (bottom raw) are given. Color scale of correlation values is shown on the right of the heatmap.

A3B whereas previous reports rely on levels of A3B resulting from exogenous overexpression. Differences in the overall quantity and localization of A3B in the cell could potentially explain the discrepancy. Interestingly, the effects of both endogenously interferon-stimulated A3A and ectopically expressed A3A on cell viability has been investigated and found that while ectopically expressed A3A significantly decreased cell viability, endogenously expressed A3A did not (56).

A limitation of our study is that A3A expression could not be detected in the RKO cell line which is significant as the generation of the APOBEC mutational signature in human cancers has been attributed to A3B and A3A (20–24). However, A3A expression is generally restricted to immune cells and is seldomly detected in cancer cell lines derived from other tissues (26,57,58). Further study in alternative models would be required to determine the effect of hypoxia on A3A expression/activity. It is possible that the increases in A3B-mediated deamination we have observed in cyclic hypoxia would be further increased in cells also expressing A3A.

Further investigation is required to determine the fate of cells that experience replication catastrophe due to cyclic hypoxia. Interestingly, our data clearly demonstrate that in contrast to stable hypoxia (<0.1% O_2), cyclic hypoxia-induced p53 does not lead to apoptosis. Our findings demonstrating an increase in cell size and a G2 cell cycle arrest (Figures 3G–J and 4E, F), as well as previous reports investigating replication catastrophe, suggest that senescence is a possible outcome (12). However, it is im-

Downloaded from https://academic.oup.com/nar/article/49/13/7492/6312757 by guest on 19 September 2022

portant to note that our study was carried out in a p53 proficient cell line, which we predict will significantly impact the cellular response to cyclic hypoxia. It is plausible that in the presence of wild type p53, cyclic hypoxia contributes to tumourigenesis through senescence. However, in the absence of p53 cells which experience non-lethal levels of cyclic hypoxia-induced replication catastrophe/DNA damage could increase genomic instability through elevated APOBEC expression/activity.

Targeting APOBECs is an emerging clinical strategy. Decreasing APOBEC expression could be used as an enhanced treatment strategy to limit tumorigenesis and the development of treatment resistance through a decreased mutation rate. Supportively, a study investigating the development of tamoxifen resistance *in vivo* showed a significant A3B dependent effect on the speed at which tumors developed treatment resistance (59). Strategies to inhibit APOBEC activity include, the development of a modified oligonucleotide that can be used to selectively inhibit A3B *in vitro* (60). The development of inhibitory compounds and preclinical testing will be required to determine if these strategies will prove efficacious in a clinical setting. Somewhat controversially, it is worth considering that increasing APOBEC activity in cancers could be beneficial and particularly in the immunosuppressive hypoxic regions of tumors. Increasing APOBEC expression has been shown to increase the efficacy of immune checkpoint blockade therapy due to increased neoepitope presentation (27). Overall, our study provides the first mechanistic insight into the mechanism of increased APOBEC activity and links this mechanism to the presence of APOBEC-mediated mutations in human cancers.

DATA AVAILABILITY

All data is available from the corresponding author upon request.

SUPPLEMENTARY DATA

Supplementary Data are available at NAR Online.

ACKNOWLEDGEMENTS

We are grateful to Prof. Adrian Harris and Amato Giaccia (University of Oxford) for feedback and advice. We would like to acknowledge the skills and expertise of Dr Rhodri Wilson in the Microscopy Scientific Research Facility at the Department of Oncology, University of Oxford.

FUNDING

CRUK [C5255/A23755 awarded to E.M.H.]; MRC [4050620859 to M.O.]; European Research Council project microC [772970 to F.M.B.]. Funding for open access charge: The University of Oxford.
Conflict of interest statement. None declared.

REFERENCES

1. Begg,A.C., Stewart,F.A. and Vens,C. (2011) Strategies to improve radiotherapy with targeted drugs. *Nat. Rev. Cancer*, **11**, 239–253.
2. Hockel,M. and Vaupel,P. (2001) Tumor hypoxia: definitions and current clinical, biologic, and molecular aspects. *J. Natl. Cancer Inst.*, **93**, 266–276.
3. Dewhirst,M.W., Cao,Y. and Moeller,B. (2008) Cycling hypoxia and free radicals regulate angiogenesis and radiotherapy response. *Nat. Rev. Cancer*, **8**, 425–437.
4. Dewhirst,M.W. (2009) Relationships between cycling hypoxia, HIF-1, angiogenesis and oxidative stress. *Radiat. Res.*, **172**, 653–665.
5. Yasui,H., Matsumoto,S., Devasahayam,N., Munasinghe,J.P., Choudhuri,R., Saito,K., Subramanian,S., Mitchell,J.B. and Krishna,M.C. (2010) Low-field magnetic resonance imaging to visualize chronic and cycling hypoxia in tumor-bearing mice. *Cancer Res.*, **70**, 6427–6436.
6. Bader,S.B., Dewhirst,M.W. and Hammond,E.M. (2020) Cyclic hypoxia: an update on its characteristics, methods to measure it and biological implications in cancer. *Cancers (Basel)*, **13**, 23.
7. Foskolou,I.P., Jorgensen,C., Leszczynska,K.B., Olcina,M.M., Tarhonskaya,H., Haisma,B., D'Angiolella,V., Myers,W.K., Domene,C., Flashman,E. *et al.* (2017) Ribonucleotide reductase requires subunit switching in hypoxia to maintain DNA replication. *Mol. Cell*, **66**, 206–220.
8. Pires,I.M., Bencokova,Z., Milani,M., Folkes,L.K., Li,J.L., Stratford,M.R., Harris,A.L. and Hammond,E.M. (2010) Effects of acute versus chronic hypoxia on DNA damage responses and genomic instability. *Cancer Res.*, **70**, 925–935.
9. Olcina,M.M., Foskolou,I.P., Anbalagan,S., Senra,J.M., Pires,I.M., Jiang,Y., Ryan,A.J. and Hammond,E.M. (2013) Replication stress and chromatin context link ATM activation to a role in DNA replication. *Mol. Cell*, **52**, 758–766.
10. Bencokova,Z., Kaufmann,M.R., Pires,I.M., Lecane,P.S., Giaccia,A.J. and Hammond,E.M. (2009) ATM activation and signaling under hypoxic conditions. *Mol. Cell. Biol.*, **29**, 526–537.
11. Pires,I.M., Bencokova,Z., McGurk,C. and Hammond,E.M. (2010) Exposure to acute hypoxia induces a transient DNA damage response which includes Chk1 and TLK1. *Cell Cycle*, **9**, 2502–2507.
12. Toledo,L.I., Altmeyer,M., Rask,M.B., Lukas,C., Larsen,D.H., Povlsen,L.K., Bekker-Jensen,S., Mailand,N., Bartek,J. and Lukas,J. (2013) ATR prohibits replication catastrophe by preventing global exhaustion of RPA. *Cell*, **155**, 1088–1103.
13. Rebhandl,S., Huemer,M., Greil,R. and Geisberger,R. (2015) AID/APOBEC deaminases and cancer. *Oncoscience*, **2**, 320–333.
14. Smith,H.C., Bennett,R.P., Kizilyer,A., McDougall,W.M. and Prohaska,K.M. (2012) Functions and regulation of the APOBEC family of proteins. *Semin. Cell Dev. Biol.*, **23**, 258–268.
15. Muramatsu,M., Kinoshita,K., Fagarasan,S., Yamada,S., Shinkai,Y. and Honjo,T. (2000) Class switch recombination and hypermutation require activation-induced cytidine deaminase (AID), a potential RNA editing enzyme. *Cell*, **102**, 553–563.
16. Haradhvala,N.J., Polak,P., Stojanov,P., Covington,K.R., Shinbrot,E., Hess,J.M., Rheinbay,E., Kim,J., Maruvka,Y.E., Braunstein,L.Z. *et al.* (2016) Mutational strand asymmetries in cancer genomes reveal mechanisms of DNA damage and repair. *Cell*, **164**, 538–549.
17. Hoopes,J.I., Cortez,L.M., Mertz,T.M., Malc,E.P., Mieczkowski,P.A. and Roberts,S.A. (2016) APOBEC3A and APOBEC3B preferentially deaminate the lagging strand template during DNA replication. *Cell Rep.*, **14**, 1273–1282.
18. Seplyarskiy,V.B., Soldatov,R.A., Popadin,K.Y., Antonarakis,S.E., Bazykin,G.A. and Nikolaev,S.I. (2016) APOBEC-induced mutations in human cancers are strongly enriched on the lagging DNA strand during replication. *Genome Res.*, **26**, 174–182.
19. Roberts,S.A., Lawrence,M.S., Klimczak,L.J., Grimm,S.A., Fargo,D., Stojanov,P., Kiezun,A., Kryukov,G.V., Carter,S.L., Saksena,G. *et al.* (2013) An APOBEC cytidine deaminase mutagenesis pattern is widespread in human cancers. *Nat. Genet.*, **45**, 970–976.
20. Alexandrov,L.B., Nik-Zainal,S., Wedge,D.C., Aparicio,S.A., Behjati,S., Biankin,A.V., Bignell,G.R., Bolli,N., Borg,A., Borresen-Dale,A.L. *et al.* (2013) Signatures of mutational processes in human cancer. *Nature*, **500**, 415–421.
21. Roberts,S.A., Lawrence,M.S., Klimczak,L.J., Grimm,S.A., Fargo,D., Stojanov,P., Kiezun,A., Kryukov,G.V., Carter,S.L., Saksena,G. *et al.* (2013) An APOBEC cytidine deaminase mutagenesis pattern is widespread in human cancers. *Nat. Genet.*, **45**, 970–976.
22. Burns,M.B., Lackey,L., Carpenter,M.A., Rathore,A., Land,A.M., Leonard,B., Refsland,E.W., Kotandeniya,D., Tretyakova,N.,

Downloaded from https://academic.oup.com/nar/article/49/13/7492/6312757 by guest on 19 September 2022

Nikas,J.B. *et al.* (2013) APOBEC3B is an enzymatic source of mutation in breast cancer. *Nature*, **494**, 366–370.
23. Burns,M.B., Leonard,B. and Harris,R.S. (2015) APOBEC3B: pathological consequences of an innate immune DNA mutator. *Biomed J*, **38**, 102–110.
24. Harris,R.S. (2015) Molecular mechanism and clinical impact of APOBEC3B-catalyzed mutagenesis in breast cancer. *Breast Cancer Res.*, **17**, 8.
25. Kanu,N., Cerone,M.A., Goh,G., Zalmas,L.P., Bartkova,J., Dietzen,M., McGranahan,N., Rogers,R., Law,E.K., Gromova,I. *et al.* (2016) DNA replication stress mediates APOBEC3 family mutagenesis in breast cancer. *Genome Biol.*, **17**, 185.
26. Burns,M.B., Temiz,N.A. and Harris,R.S. (2013) Evidence for APOBEC3B mutagenesis in multiple human cancers. *Nat. Genet.*, **45**, 977–983.
27. Driscoll,C.B., Schuelke,M.R., Kottke,T., Thompson,J.M., Wongthida,P., Tonne,J.M., Huff,A.L., Miller,A., Shim,K.G., Molan,A. *et al.* (2020) APOBEC3B-mediated corruption of the tumor cell immunopeptidome induces heteroclitic neoepitopes for cancer immunotherapy. *Nat. Commun.*, **11**, 790.
28. Dang,D.T., Chen,F., Gardner,L.B., Cummins,J.M., Rago,C., Bunz,F., Kantsevoy,S.V. and Dang,L.H. (2006) Hypoxia-inducible factor-1alpha promotes nonhypoxia-mediated proliferation in colon cancer cells and xenografts. *Cancer Res.*, **66**, 1684–1936.
29. Buffa,F.M., Harris,A.L., West,C.M. and Miller,C.J. (2010) Large meta-analysis of multiple cancers reveals a common, compact and highly prognostic hypoxia metagene. *Br. J. Cancer*, **102**, 428–435.
30. Leszczynska,K.B., Foskolou,I.P., Abraham,A.G., Anbalagan,S., Tellier,C., Haider,S., Span,P.N., O'Neill,E.E., Buffa,F.M. and Hammond,E.M. (2015) Hypoxia-induced p53 modulates both apoptosis and radiosensitivity via AKT. *J. Clin. Invest.*, **125**, 2385–2398.
31. Gao,G.F., Parker,J.S., Reynolds,S.M., Silva,T.C., Wang,L.B., Zhou,W., Akbani,R., Bailey,M., Balu,S., Berman,B.P. *et al.* (2019) Before and After: comparison of Legacy and Harmonized TCGA Genomic Data Commons' Data. *Cell Syst.*, **9**, 24–34.
32. Dhawan,A., Barberis,A., Cheng,W.C., Domingo,E., West,C., Maughan,T., Scott,J.G., Harris,A.L. and Buffa,F.M. (2019) Guidelines for using sigQC for systematic evaluation of gene signatures. *Nat. Protoc.*, **14**, 1377–1400.
33. Rouschop,K.M., Dubois,L.J., Keulers,T.G., van den Beucken,T., Lambin,P., Bussink,J., van der Kogel,A.J., Koritzinsky,M. and Wouters,B.G. (2013) PERK/eIF2alpha signaling protects therapy resistant hypoxic cells through induction of glutathione synthesis and protection against ROS. *Proc. Natl. Acad. Sci. U.S.A.*, **110**, 4622–4627.
34. Menendez,D., Nguyen,T.A., Snipe,J. and Resnick,M.A. (2017) The Cytidine Deaminase APOBEC3 Family Is Subject to Transcriptional Regulation by p53. *Mol. Cancer Res.*, **15**, 735–743.
35. Periyasamy,M., Singh,A.K., Gemma,C., Kranjec,C., Farzan,R., Leach,D.A., Navaratnam,N., Palinkas,H.L., Vertessy,B.G., Fenton,T.R. *et al.* (2017) p53 controls expression of the DNA deaminase APOBEC3B to limit its potential mutagenic activity in cancer cells. *Nucleic Acids Res.*, **45**, 11056–11069.
36. Toledo,L., Neelsen,K.J. and Lukas,J. (2017) Replication catastrophe: when a checkpoint fails because of exhaustion. *Mol. Cell*, **66**, 735–749.
37. King,C., Diaz,H.B., McNeely,S., Barnard,D., Dempsey,J., Blosser,W., Beckmann,R., Barda,D. and Marshall,M.S. (2015) LY2606368 causes replication catastrophe and antitumor effects through CHK1-dependent mechanisms. *Mol. Cancer Ther.*, **14**, 2004–2013.
38. Matsumoto,S., Yasui,H., Mitchell,J.B. and Krishna,M.C. (2010) Imaging cycling tumor hypoxia. *Cancer Res.*, **70**, 10019–10023.
39. Schmitt,C., Lucius,R., Synowitz,M., Held-Feindt,J. and Hattermann,K. (2018) APOBEC3B is expressed in human glioma, and influences cell proliferation and temozolomide resistance. *Oncol. Rep.*, **40**, 2742–2749.
40. Nikkila,J., Kumar,R., Campbell,J., Brandsma,I., Pemberton,H.N., Wallberg,F., Nagy,K., Scheer,I., Vertessy,B.G., Serebrenik,A.A. *et al.* (2017) Elevated APOBEC3B expression drives a kataegic-like mutation signature and replication stress-related therapeutic vulnerabilities in p53-defective cells. *Br. J. Cancer*, **117**, 113–123.
41. Serebrenik,A.A., Starrett,G.J., Leenen,S., Jarvis,M.C., Shaban,N.M., Salamango,D.J., Nilsen,H., Brown,W.L. and Harris,R.S. (2019) The deaminase APOBEC3B triggers the death of cells lacking uracil DNA glycosylase. *Proc. Natl. Acad. Sci. U.S.A.*, **116**, 22158–22163.
42. Leonard,B., McCann,J.L., Starrett,G.J., Kosyakovsky,L., Luengas,E.M., Molan,A.M., Burns,M.B., McDougle,R.M., Parker,P.J., Brown,W.L. *et al.* (2015) The PKC/NF-kappaB signaling pathway induces APOBEC3B expression in multiple human cancers. *Cancer Res.*, **75**, 4538–4547.
43. Culver,C., Sundqvist,A., Mudie,S., Melvin,A., Xirodimas,D. and Rocha,S. (2010) Mechanism of hypoxia-induced NF-kappaB. *Mol. Cell. Biol.*, **30**, 4901–4921.
44. Bakhoum,S.F., Ngo,B., Laughney,A.M., Cavallo,J.A., Murphy,C.J., Ly,P., Shah,P., Sriram,R.K., Watkins,T.B.K., Taunk,N.K. *et al.* (2018) Chromosomal instability drives metastasis through a cytosolic DNA response. *Nature*, **553**, 467–472.
45. Pepin,G. and Gantier,M.P. (2018) Assessing the cGAS-cGAMP-STING activity of cancer cells. *Methods Mol. Biol.*, **1725**, 257–266.
46. O'Connor,J.P.B., Robinson,S.P. and Waterton,J.C. (2019) Imaging tumour hypoxia with oxygen-enhanced MRI and BOLD MRI. *Br. J. Radiol.*, **92**, 20180642.
47. Horsman,M.R., Mortensen,L.S., Petersen,J.B., Busk,M. and Overgaard,J. (2012) Imaging hypoxia to improve radiotherapy outcome. *Nat. Rev. Clin. Oncol.*, **9**, 674–687.
48. Hillestad,T., Hompland,T., Fjeldbo,C.S., Skingen,V.E., Salberg,U.B., Aarnes,E.K., Nilsen,A., Lund,K.V., Evensen,T.S., Kristensen,G.B. *et al.* (2020) MRIdistinguishes tumor hypoxia levels of different prognostic and biological significance in cervical cancer. *Cancer Res.*, **80**, 3993–4003.
49. Ron,A., Dean-Ben,X.L., Gottschalk,S. and Razansky,D. (2019) Volumetric optoacoustic imaging unveils high-resolution patterns of acute and cyclic hypoxia in a murine model of breast cancer. *Cancer Res.*, **79**, 4767–4775.
50. Cao,Y., Li,C.Y., Moeller,B.J., Yu,D., Zhao,Y., Dreher,M.R., Shan,S. and Dewhirst,M.W. (2005) Observation of incipient tumor angiogenesis that is independent of hypoxia and hypoxia inducible factor-1 activation. *Cancer Res.*, **65**, 5498–5505.
51. Nehmeh,S.A., Lee,N.Y., Schroder,H., Squire,O., Zanzonico,P.B., Erdi,Y.E., Greco,C., Mageras,G., Pham,H.S., Larson,S.M. *et al.* (2008) Reproducibility of intratumor distribution of (18)F-fluoromisonidazole in head and neck cancer. *Int. J. Radiat. Oncol. Biol. Phys.*, **70**, 235–242.
52. Saxena,K. and Jolly,M.K. (2019) Acute vs. chronic vs. cyclic hypoxia: their differential dynamics, molecular mechanisms, and effects on tumor progression. *Biomolecules*, **9**, 339.
53. Sharma,S., Patnaik,S.K., Kemer,Z. and Baysal,B.E. (2017) Transient overexpression of exogenous APOBEC3A causes C-to-U RNA editing of thousands of genes. *RNA Biol*, **14**, 603–610.
54. Sharma,S., Patnaik,S.K., Taggart,R.T. and Baysal,B.E. (2016) The double-domain cytidine deaminase APOBEC3G is a cellular site-specific RNA editing enzyme. *Sci. Rep.*, **6**, 39100.
55. Sharma,S., Patnaik,S.K., Taggart,R.T., Kannisto,E.D., Enriquez,S.M., Gollnick,P. and Baysal,B.E. (2015) APOBEC3A cytidine deaminase induces RNA editing in monocytes and macrophages. *Nat. Commun.*, **6**, 6881.
56. Land,A.M., Law,E.K., Carpenter,M.A., Lackey,L., Brown,W.L. and Harris,R.S. (2013) Endogenous APOBEC3A DNA cytosine deaminase is cytoplasmic and nongenotoxic. *J. Biol. Chem.*, **288**, 17253–17260.
57. Ng,J.C.F., Quist,J., Grigoriadis,A., Malim,M.H. and Fraternali,F. (2019) Pan-cancer transcriptomic analysis dissects immune and proliferative functions of APOBEC3 cytidine deaminases. *Nucleic Acids Res.*, **47**, 1178–1194.
58. Koning,F.A., Newman,E.N., Kim,E.Y., Kunstman,K.J., Wolinsky,S.M. and Malim,M.H. (2009) Defining APOBEC3 expression patterns in human tissues and hematopoietic cell subsets. *J. Virol.*, **83**, 9474–9485.
59. Law,E.K., Sieuwerts,A.M., LaPara,K., Leonard,B., Starrett,G.J., Molan,A.M., Temiz,N.A., Vogel,R.I., Meijer-van Gelder,M.E., Sweep,F.C. *et al.* (2016) The DNA cytosine deaminase APOBEC3B promotes tamoxifen resistance in ER-positive breast cancer. *Sci. Adv.*, **2**, e1601737.
60. Barzak,F.M., Harjes,S., Kvach,M.V., Kurup,H.M., Jameson,G.B., Filichev,V.V. and Harjes,E. (2019) Selective inhibition of APOBEC3 enzymes by single-stranded DNAs containing 2'-deoxyzebularine. *Org. Biomol. Chem.*, **17**, 9435–9441.

Downloaded from https://academic.oup.com/nar/article/49/13/7492/6312757 by guest on 19 September 2022